Transactions of the ASME

Convective Heat Transfer for Mixed, Free, and Forced Flow Through Tubes . . . . . *E. R. G. Eckert and A. J. Diaguila* 497

Heat Transfer to Mercury in Turbulent Pipe Flow . . . . . *H. A. Johnson, W. J. Clabaugh, and J. P. Hartnett* 505

Heat Transfer to Lead-Bismuth and Mercury in Laminar and Transition Pipe Flow . . . . . *H. A. Johnson, J. P. Hartnett, and W. J. Clabaugh* 513

Effect of Single Roughness Elements on the Heat Transfer From a 1:3 Elliptical Cylinder . . . . . *R. A. Seban, S. Levy, D. L. Doughty, and R. M. Drake, Jr.* 519

Heat Transfer in a Gas-Fired Furnace . . . . . *S. J. Gemma, E. J. Nolan, and A. A. Purczyk* 527

A Review of Thermal-Radiation Constants . . . . . *N. W. Snyder* 537

Radiation in Metals . . . . . *N. W. Snyder* 541

Thermal-Radiation Tables and Applications . . . . . *R. V. Dunkle* 549

Local Boiling Heat Transfer to Water at Low Reynolds Numbers and High Pressures . . . . . *J. A. Clark and W. M. Rohsenow* 553

Tube Expanding and Related Subjects . . . . . *F. F. Fisher and G. J. Brown* 563

Electronic-Control Method for the Precision Expanding of Tubes. . . . . *F. E. Dudley* 577

Application of Quality-Control Requirements in Manufacture of Components for a Coaxial-Carrier System . . . . . *A. T. Chapman* 585

On the Theory of Regenerative Chatter in Precision-Grinding Operations . . . . *R. S. Hahn* 593

An Experimental Study of Metal Extrusions at Various Strain Rates . *J. Frisch and E. G. Thomsen* 599

Cutter Life for Face-Milling Cast Iron . . . . *W. W. Gilbert, O. W. Boston, and H. J. Siekmann* 607

Measurement of Stresses Imposed on Wheels in Diesel-Locomotive Service. . . . *L. L. Olson* 613

1.5 Per Cent Carbon Cast-Steel Railroad-Car Wheels. . . . . *N. A. Matthews and R. A. Flinn* 617

Better Yield Through Dimensional Control in Small-Sawmill Operation . . . . *J. S. Bethel* 623

A Concept of Fatigue Damage . . . . . *S. M. Marco and W. L. Starkey* 627

Linkage Design—A Note on One Method . . . . . *A. S. Hall, Jr., and D. C. Tao* 633

Thermal-Shocking Austenitic Stainless Steels With Molten Metals . *R. A. Tidball and M. M. Shrut* 639

Heat-Treatments of Welded Structures for Relief of Residual Stresses With Particular Reference to Type 347 Stainless-Steel Weldments . . . . . *W. L. Fleischmann* 645

Thermal Checking of Wrought-Steel Railway Wheel Material . . . . . *H. R. Wetenhamp* 649

A Short Method for the Evaluation of the Effect of Some Thermal-Cycle Variations on Steam-Turbine Heat Rates . . . . . *S. D. Fulton* 655

Experimental Superheater for Steam at 2000 Psi and 1250 F—Progress Report After 12,000 Hours of Operation . . . . . *F. Eberle, F. G. Ely, and J. A. Dillon* 665

Interface Extension Versus Upper Limiting Time-Mean Energy-Release Rates of Constant-Pressure Steady-State Combustion Process . . . . . *W. J. Woblenberg* 679

Pulverized-Coal-Fired Gasifier for Production of Carbon Monoxide and Hydrogen . . . . . *P. R. Grossman and R. W. Curtis* 689

TRANSACTIONS OF THE AMERICAN SOCIETY OF MECHANICAL ENGINEERS

VOLUME 76 MAY 1954 NUMBER 4

Transactions

of The American Society of Mechanical Engineers

Published on the tenth of every month, except March, June, September, and December

OFFICERS OF THE SOCIETY:

LEWIS K. SILLCOX, *President*

JOSEPH L. KOPF, *Treasurer* — C. E. DAVIES, *Secretary*

EDGAR J. KATES, *Ass't Treasurer*

COMMITTEE ON PUBLICATIONS:

PAUL T. NORTON, JR., *Chairman*

OTTO DE LORENZI — W. E. REASER

COLIN CARMICHAEL — KERR ATKINSON

JOSEPH SCHMERLER, PETER WALLACE } *Junior Advisory Members*

GEORGE A. STETSON, *Editor* — K. W. CLEMENDINNING, *Managing Editor*

REGIONAL ADVISORY BOARD OF THE PUBLICATIONS COMMITTEE:

RICHARD L. ANTHONY—I
JOHN DE S. COUTINHO—II
WILLIAM N. RICHARDS—III
FRANCIS C. SMITH—IV
H. M. CATHER—V
J RUSSELL PARRISH—VI
J. KENNETH SALISBURY—VII
JOHN H. KEYES—VIII

Published monthly by The American Society of Mechanical Engineers. Publication office at 20th and Northampton Streets, Easton, Pa. The editorial department is located at the headquarters of the Society, 29 West Thirty-Ninth Street, New York 18, N. Y. Cable address, "Dynamic," New York. Price $1.50 a copy, $12.00 a year for Transactions and the *Journal of Applied Mechanics* to members and affiliates, $1.00 a copy, $6.00 a year. Changes of address must be received at Society headquarters seven weeks before they are to be effective on the mailing list. Please send old as well as new address.... By-Law: The Society shall not be responsible for statements or opinions advanced in papers or...printed in its publications (B13, Par. 4) ....Entered as second-class matter March 2, 1928, at the Post Office at Easton, Pa., under the Act of August 24, 1912....Copyrighted, 1954, by The American Society of Mechanical Engineers. Reprints from this publication may be made on condition that full credit be given the Transactions of the ASME and the author, and that date of publication be stated.

Convective Heat Transfer for Mixed, Free, and Forced Flow Through Tubes

By E. R. G. ECKERT[1] and A. J. DIAGUILA[2]

This paper presents current knowledge on heat transfer caused by simultaneously occurring free and forced convection in tubes. It discusses the results of experiments that have been conducted by the NACA on mixed, free, and forced-convection heat transfer in turbulent flow through a vertical tube with a length-to-diameter ratio of 5. In these studies, forced air flow was directed parallel or opposite to the flow direction which free-convection flow alone would have under the same temperature conditions. Results of experiments made by other investigators, when analyzed in the same way as the NACA experiments, make it possible to generalize and extend the heat-transfer relations established. A calculation by R. C. Martinelli and L. M. K. Boelter for laminar mixed, free, and forced flow in parallel direction, and its extension to flow in opposite direction furnish information on heat transfer in the laminar-flow range.

Nomenclature

The following nomenclature is used in the paper:

A = inside area of section of tube surrounded by condensate chamber, sq ft
c_p = specific heat of fluid at constant pressure, Btu/(lb) (deg F)
d = inside diameter of tube, ft
Gr = Grashof number, $\mathrm{Gr}_x = x^3 \beta g (t_w - t_a)/\nu^2$, $\mathrm{Gr}_\xi = \xi^3 \beta g (t_w - t_a)/\nu^2$, and $\mathrm{Gr}_d = d^3 \beta g (t_w - t_a)/\nu^2$
Gz = Graetz number $(\pi/4\ \mathrm{Re}_d\ \mathrm{Pr}\ d/L)$
g = acceleration due to gravity, 32.2 ft/sec²
h = local heat-transfer coefficient, $Q_c/A\ (t_w - t_a)$, Btu/(deg F) (sq ft) (sec)
k = thermal conductivity of fluid, Btu/(deg F)(ft) (sec)
L = length of tube, ft
Nu = local Nusselt number, $\mathrm{Nu}_x = hx/k$, $\mathrm{Nu}_\xi = h\xi/k$, and $\mathrm{Nu}_d = hd/k$
Pr = Prandtl number, $c_p\ \mu/k$
Q_c = convective heat flow, Btu/sec
Re = Reynolds number, $\mathrm{Re}_x = \rho v x/\mu$, $\mathrm{Re}_\xi = \rho v \xi/\mu$, and $\mathrm{Re}_d = \rho v d/\mu$
t = temperature, deg F
v = average velocity, $4W/\pi\rho d^2$
W = forced air flow, lb/sec
x = characteristic dimension measured from lower heated edge, ft
β = coefficient of thermal expansion of fluid, 1/deg R
μ = dynamic viscosity of fluid, lb/(sec) (ft)
ν = kinematic viscosity of fluid, μ/ρ, sq ft/sec
ξ = characteristic dimension measured downward from upper heated edge, ft
ρ = density of fluid, lb/cu ft

Subscripts:

a = air
c = convective
w = wall
f = fluid

Superscript:

Barred symbols indicate average values

Introduction

In calculations of convective heat-transfer problems, the flow usually is classified as forced flow in which the flow is caused by external means like pumps, or free-convection flow in which buoyancy forces connected with temperature differences in the fluid create the flow. Actually, such buoyancy forces always are present in forced-flow heat transfer as well. Usually they are of a smaller order of magnitude than the external forces and may be neglected. In certain engineering applications, however, this cannot be done. It was, for instance, realized at an early date that the heat exchange in oil coolers is affected markedly by the free-convection currents superposed to the forced flow. Free-convection effects in this case cannot be neglected because of the low flow velocities employed in such coolers.

More recently applications have become important in which such large free-convection forces are present that they change the flow pattern even at high velocities. Forced flow through rotating components always is subject to centrifugal forces and Coriolis forces. In the presence of temperature differences these forces create strong free-convection flows. Cooling of rotating parts such as rotor blades of gas turbines and ramjets attached to the rotors of helicopters are examples in which very large free-convection forces exist.

This paper is concerned with heat transfer under the simultaneous influence of free and forced convection for flow through circular tubes. A limited number of papers has been published on this subject. In all of these investigations the free-convection forces are created by the gravitational field of the earth. Reference (1)[3] presents experimental information on heat transfer in laminar flow of oils through tubes which includes the free-convection effect. Reference (2) describes experiments on heat transfer in the transition region between laminar and turbulent flow with water flowing through a cooled vertical tube with an L/d ratio of 20.

An analysis of laminar mixed, free, and forced heat transfer in a vertical tube is given in reference (3). The results of this calculation are compared with experimental results on oil and water in reference (4). Measurements of heat transfer in turbulent flow of water through a tube with $L/d = 52$ reported in reference (5) show a considerable effect of free-convection currents on heat transfer. References (6) and (7) present calculations of laminar free and mixed flow for different configurations and wall-temperature distributions. An investigation on free and forced-

[1] Professor of Mechanical Engineering, University of Minnesota, Minneapolis, Minn., and Consultant, Lewis Flight Propulsion Laboratory, NACA, Cleveland, Ohio. Mem. ASME.

[2] Aeronautical Research Scientist, Lewis Flight Propulsion Laboratory, NACA, Cleveland, Ohio.

Contributed by the Heat Transfer Division and presented at the Annual Meeting, New York, N. Y., November 29–December 4, 1953, of The American Society of Mechanical Engineers.

Note: Statements and opinions advanced in papers are to be understood as individual expressions of their authors and not those of the Society. Manuscript received at ASME Headquarters, September 2, 1953. Paper No. 53—A-191.

[3] Numbers in parentheses refer to the Bibliography at the end of the paper.

convection heat transfer in a heated tube with forced air flowing parallel or opposite in direction to the free-convection flow is presented in reference (8). This is the only experimental investigation which obtained local heat-transfer coefficients in mixed flow through tubes.

This paper will discuss in detail the last-mentioned investigation. The results obtained from it are combined with analytical and experimental results of the previously mentioned investigations to form a survey in which the free, forced, and mixed-flow regimes are established and the available information on convective heat transfer in the mixed-flow regime is collected.

Experiments on Turbulent Flow Through Short Tubes

Before presenting the results on mixed flow through short tubes contained in reference (8), it appears necessary to describe briefly the test setup and the procedure by which this information was obtained. For a more detailed discussion the reader is referred to the original paper.

Apparatus and Procedure. The apparatus used in this investigation is shown in Fig. 1. It consists essentially of a vertical steel tube and two covers, A. The tube is $13\frac{1}{2}$ ft high and has a 24-in. OD. It is surrounded by a steam jacket on a length of 10 ft. By proper adjustment of valves in the lines B_t, B_b, C_t, C_b, or D, air at approximately 80 deg F and with pressures from atmospheric to 125 psia could be introduced into the tube through the bottom cover or the top cover to produce different flow conditions. Upward flow of the air through the tube was obtained by admitting the air through the line B_b into the bottom cover and discharging through the exhaust line C_t. To obtain downward flow in the tube, air was admitted through the line B_t into the top cover and was discharged from the bottom cover through the exhaust line C_b. Air could also be admitted into the top cover through line B_t and removed from the upper portion of the tube through lines D. In this way cool air was supplied continuously to the upper portion of the tube. Circulation of the air within the tube proper was accomplished by the free-convection currents. To assure that the air entered the tube proper with a constant velocity, dense screens E were installed at the top and bottom of the tube. The surface of the tube was uniformly heated with low-pressure steam superheated by 2 or 3 deg F.

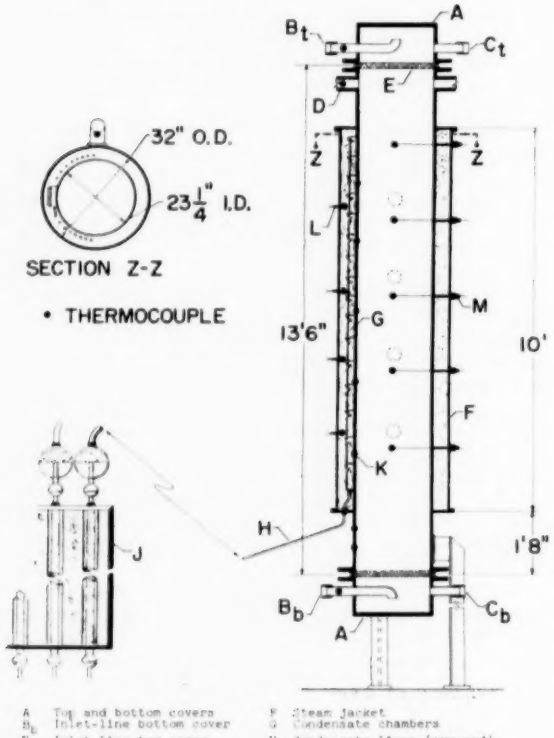

A	Top and bottom covers	F	Steam jacket
B_b	Inlet-line bottom cover	G	Condensate chambers
B_t	Inlet-line top cover	H	Condensate lines (exposed)
C_t	Exhaust-line bottom cover	J	Burette board
C_t	Exhaust-line top cover	K	5 Heated-wall thermocouples
D	Exhaust line on tube	L	4 Steam thermocouples
E	Screening	M	Probes

Fig. 1 Mixed, Free, and Forced-Convection Tube

Sixteen condensate chambers G were arranged along the length of the heated section of the tube. The chambers trapped the condensate which developed on the section of the tube wall enclosed by these chambers. From each chamber the condensate was carried through the steam jacket to the condensate-measuring apparatus. The exposed portion of these lines H was insulated heavily to reduce heat losses. From a volumetric measurement J of the rate of condensation in the individual chambers, the local convective heat flow into the tube surface could be determined after corrections for radiant-heat exchange within the tube arrangement and for heat losses in the lines H had been applied.

Local heat-transfer coefficients were obtained by dividing the local heat flow by the tube surface area which was covered by the individual chamber and by the difference between tube-wall temperature (measured at K) and the air temperature at the tube axis in the same tube cross section as the condensate chamber under consideration. The thermocouple probes which measured the air temperature also were used to investigate the entire temperature field in the tube interior.

Discussion of Results. Dimensional analysis shows that in the mixed, free, and forced-convection regime, the average heat-transfer coefficients can be expressed in a dimensionless form as a relation between Nusselt number (Nu), Reynolds (Re), Grashof (Gr), and Prandtl (Pr)

$$\mathrm{Nu} = f(\mathrm{Re}, \mathrm{Gr}, \mathrm{Pr}) \quad [1]$$

for a fluid with constant property values and for geometrically similar configurations. In the present investigation the variation of the property values is sufficiently small to permit them to be considered constant. For flow through tubes, geometric similarity restricts the relation given by Equation [1] to tubes with a certain ratio of length to diameter or, generally, this ratio L/d appears as an additional parameter in the foregoing dimensionless relation. The local heat-transfer coefficient depends also on the location expressed in dimensionless co-ordinates. In addition to the described parameters, the heat-transfer coefficient is determined by the boundary conditions, that is, by the velocity and temperature profile in the entrance cross section and by how the temperature varies over the heat-transferring area. In the present case the temperatures were constant across the inlet section and along the heated-wall portion. Special efforts were made to obtain a uniform velocity over the inlet cross section.

Parallel Flow. Fig. 2 shows the results of the experiments with the free-convection force being parallel to the forced-flow velocity (upward flow). The local Nusselt number Nu_x is plotted against the product of Grashof and Prandtl numbers $\mathrm{Gr}_x\mathrm{Pr}$, with the Reynolds number Re_d as parameter. The length parameter used in the Nusselt and Grashof numbers is the distance x from the lower end of the heated tube section to the desired point on the surface. The difference between the tube-wall temperature t_w and that of the air along the tube axis, t_a, is used throughout the report to calculate the Grashof number. Physical properties of the air were based on a film temperature $(t_w + t_a)/2$

for all parameters except Re_d, which was based on the average air temperature along the tube axis $\bar{t}_a$. The diameter of the tube and the average velocity of the forced flow were used to obtain the Re_d. The air pressure in the tube, which in turn affects the Grashof number range, appears as parameter for the different diagrams in the figure. Lines of constant Re_d are drawn through the experimental points. The significance of the solid points, identified as Re_x, will be explained later in the paper.

As a limiting case, free-convection flow alone was investigated in the manner described in the previous section. The results of these runs are shown in Fig. 3. The dashed line in this figure constitutes the mean line through the experimental points. Also inserted in the figure as solid lines are two correlations derived in reference (8) from literature for free convection on a vertical plate. The dashed mean-data line in Fig. 3 is on the average located 20 per cent below the turbulent correlation for the flat plate. In a tube of small length-to-diameter ratio the boundary-layer thickness will be small as compared to the tube diameter and the conditions should be quite similar to those on a flat plate. Under these conditions it is also to be expected that the distance from the starting point of the boundary layer will be the main-length parameter on which the flow and the heat transfer depend. Therefore a diagram in which the Reynolds number based on this distance is used as parameter should give more information than the presentation in Fig. 2.

Fig. 4 shows such a diagram which reveals the transition process between forced and free-convection flow very clearly. To obtain

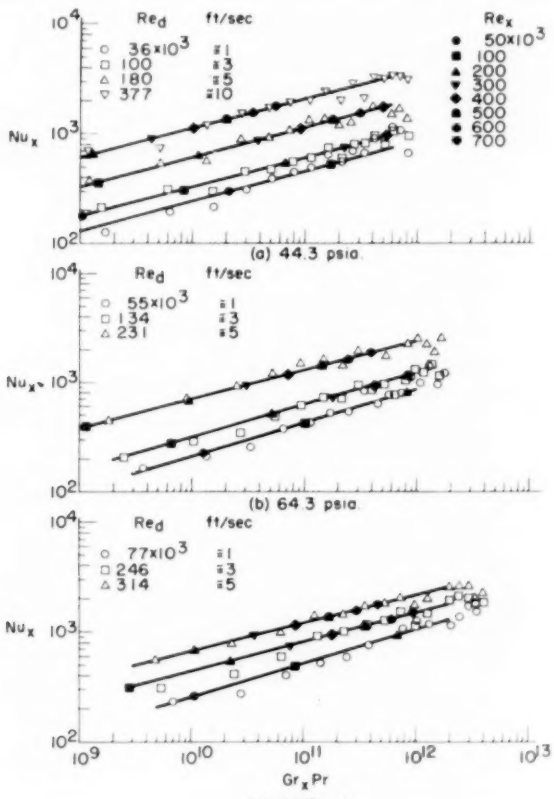

Fig. 2 Dimensionless Correlation of Local Heat-Transfer Coefficients for Turbulent Parallel Flow at Several Air Pressures

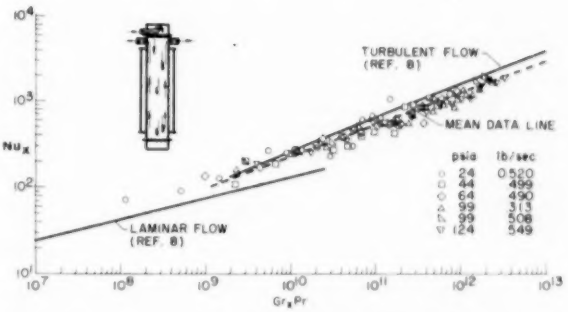

Fig. 3 Dimensionless Correlation of Local Heat-Transfer Coefficients for Turbulent Free-Convection Flow and Comparison With Known Equations for Vertical Flat Plate

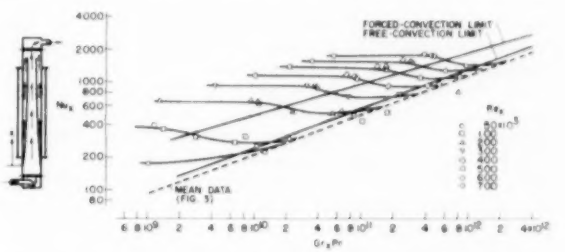

Fig. 4 Dimensionless Correlation of Local Mixed, Free, and Forced-Convection Heat-Transfer Coefficients for Turbulent Parallel Flow

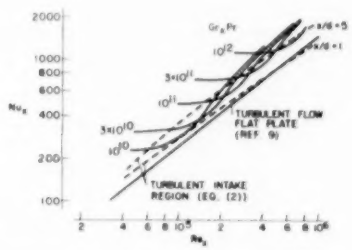

Fig. 5 Dimensionless Correlation of Mixed, Free, and Forced-Convection Heat-Transfer Coefficients for Turbulent Parallel Flow

this figure, points of constant Re_x were calculated on the Re_d-curves in Fig. 2 (shown as black points) and transferred into this figure. Averaging lines are drawn through these points. It may be recognized that for large Grashof numbers all constant Re_x-curves converge into the mean-data line (dashed line) for the free-convection data presented in Fig. 3 (free-convection regime). On the other hand, each of the lines for constant Reynolds number becomes more and more horizontal with decreasing Grashof number, indicating the fact that for each Reynolds number the Nusselt number becomes independent of the Grashof number in this region (forced-flow regime). Noticeable is a dip on all Re_x-curves.

Fig. 5 shows a cross plot of Fig. 4 with Nusselt numbers plotted against Reynolds numbers and with the Grashof times Prandtl numbers appearing as parameter. The regions which may be termed pure free and forced-convection regions may be recognized again in this figure by the horizontal trend of the curves toward the lower Reynolds number and by the fact that all

curves tend to converge asymptotically into a single line at the higher Reynolds number. This asymptotic line should be the relation for pure forced-convection flow. Available correlations for turbulent forced flow are shown in the figure. The solid line is the correlation for a turbulent boundary layer along a flat plate (9). The two dashed curves for two x/d-ratios are obtained from the following equation

$$\mathrm{Nu}_x = 0.116\left[\left(\mathrm{Re}_x\frac{d}{x}\right)^{2/3} - 125\right](\mathrm{Pr})^{1/3}\left(\frac{x}{d}\right)\left[1 + \frac{1}{3}\left(\frac{d}{x}\right)^{2/3}\right] \quad \ldots\ldots\ldots\ldots [2]$$

This equation for local Nusselt numbers was derived from an empirical relation for average heat-transfer coefficients determined by H. Hausen from experiments in the entrance region of a circular tube (8). The curve for the smaller x/d-ratio agrees reasonably well with the relation for a flat plate as would be expected. The values given by the curve for $x/d = 5$, however, are already higher than the flat-plate values, indicating the fact that the development of the boundary layer in a tube is already different from the one on a flat plate for this length-to-diameter ratio. The length-to-diameter ratio increases along the curves of constant $\mathrm{Gr}_x\mathrm{Pr}$ from left to right, ending with the ratio $x/d = 5$. Therefore it can be stated that the measured heat-transfer coefficients in the forced-flow regime fall within the values predicted by Hausen at the lower Re_x-values. At higher values of Re_x, the measured heat-transfer coefficients are somewhat higher. The dip in the curves of constant $\mathrm{Gr}_x\mathrm{Pr}$ is also explained by the fact that the x/d-ratio along the curves increases from smaller to larger values toward the right.

Of primary interest for the investigated problem is the question in which range of Reynolds and Grashof numbers the heat transfer may be considered as pure forced convective, as pure free convective, or as mixed, forced, and free convective. The determination of the limits between these regimes requires some arbitrary definition since actually the transition of the mixed-flow region into the other two regimes is asymptotic as can be seen in Figs. 4 and 5. Therefore the forced-flow regime is defined as that part in which the influence of the Grashof number changes the heat-transfer coefficient by not more than 10 per cent. A corresponding definition will be applied to the limit of the free-convection regime. The limiting lines were determined in this way in Fig. 4. These lines may be used to determine in any special case whether the heat-transfer coefficients should be calculated from forced-flow equations or from free-convection equations or whether they will be in the mixed-flow regime. The limit curves as determined in Fig. 4 can be represented by the following equations:

between free and mixed flow

$$\mathrm{Re}_x = 8.25\,(\mathrm{Gr}_x\mathrm{Pr})^{0.40} \quad \ldots\ldots\ldots\ldots [3]$$

between forced and mixed flow

$$\mathrm{Re}_x = 15.0\,(\mathrm{Gr}_x\mathrm{Pr})^{0.40} \quad \ldots\ldots\ldots\ldots [4]$$

These limits also are inserted together with information which will be obtained later in a Reynolds-Grashof diagram, Fig. 12.[4]

The Grashof times Prandtl numbers in the investigation under discussion varied between 10^9 and 10^{13}. Free-convection flow in this range is turbulent. The Reynolds numbers Re_x varied between 5×10^4 and 10^6. Forced flow in this range may be laminar or turbulent. It was, however, observed that mixed flow is more unstable than forced flow and it is, therefore, assumed that the flow was turbulent in the whole range covered by this investigation.

McAdams[5] proposed the following rule: In cases where it is doubtful whether forced or free-convection flow applies, the heat-transfer coefficient should be calculated using both the forced and the free-convective relation and the larger one should be used. An investigation of Fig. 4 shows that in the mixed-flow regime the actual heat-transfer coefficient was always somewhat smaller than the one determined by this rule, the largest deviation being approximately 25 per cent so that the rule by McAdams gives correct values within this degree of accuracy.

Counterflow. Fig. 6 shows the results of the runs in which the forced flow was in a direction opposite to the free-convection forces. The presentation is the same as in Fig. 2. The use of the Reynolds number based on the distance x from the lower end of the heated section converts Fig. 6 into Fig. 7. Also inserted in Fig. 7 is the dashed line which averages the results of the experiments with free-convection flow, Fig. 3. It may be observed that the curves with constant Reynolds number Re_x again tend to converge for large Grashof numbers asymptotically toward the free-convection mean-data line from Fig. 3. However, the approach is much more gradual in this case than in the case of parallel flow. The limit of the pure free-convection regime can be found as before by a line located 10 per cent above the free-convection mean-data line into which the curves for constant Re_x

[5] Reference (10), p. 207.

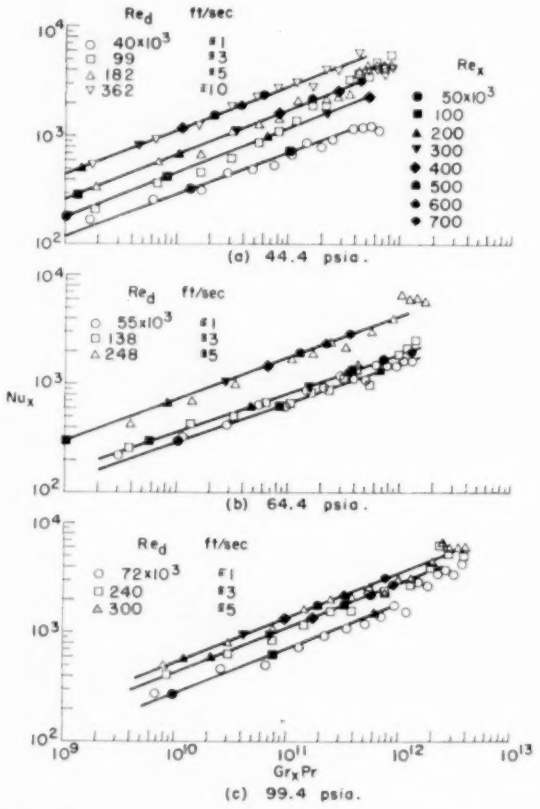

FIG. 6 DIMENSIONLESS CORRELATION OF LOCAL HEAT-TRANSFER COEFFICIENTS FOR TURBULENT COUNTERFLOW AT SEVERAL AIR PRESSURES

[4] The accuracy to which these equations could be determined did not warrant the use of different exponents for both equations.

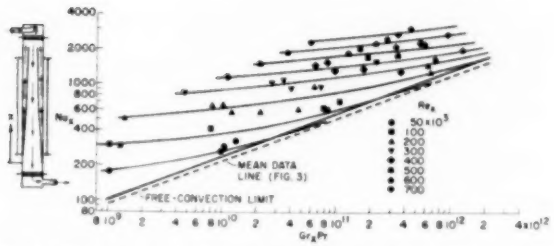

FIG. 7 DIMENSIONLESS CORRELATION OF LOCAL MIXED, FREE, AND FORCED-CONVECTION HEAT-TRANSFER COEFFICIENTS FOR TURBULENT COUNTERFLOW

are assumed to converge. The following equation represents this limit between free and mixed flow

$$Re_x = 18.15\ (Gr_x Pr)^{0.33} \quad \ldots\ldots [5]$$

The accuracy with which this limit could be determined was less than for parallel flow and Equation [5] can be considered only as tentative.

In determining the corresponding limit for pure forced flow, however, the following difficulty is encountered: For pure forced flow in a downward direction, it has to be expected that the boundary layers which determine the heat transfer start at the upper end of the heated tube section and increase in thickness in the downward direction. Accordingly, the length parameter which mainly determines the magnitude of the heat-transfer coefficient is expected to be the distance from the upper end of the heated section. In Fig. 7, however, all the parameters are based on the distance x from the lower end of the heated section. Therefore all parameters were converted to the ones which use the distance ξ measured from the upper end of the heated section as characteristic length.

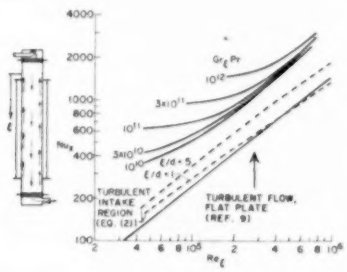

FIG. 8 DIMENSIONLESS CORRELATION OF MIXED, FREE, AND FORCED-CONVECTION HEAT-TRANSFER COEFFICIENTS FOR TURBULENT COUNTERFLOW

Fig. 8 shows the result with the Reynolds number Re_ξ as abscissa and the product of Grashof number Gr_ξ and Prandtl number Pr as parameter. Again, the curves for pure forced flow, which already were presented in Fig. 5, are inserted as dashed lines. It is indicated that the constant Grashof times Prandtl-number curves have the tendency to approach these lines asymptotically; however, in the investigated range they are a considerable distance away from the forced-convection limits. Accordingly, it can be concluded that the mixed-flow regime approaches the pure forced-flow conditions much more gradually in the case of counterflow than for parallel flow. The velocity range of the investigation was not sufficient to determine the 10 per cent limit between the mixed and the forced-flow regimes. The available facilities prevented a further increase in the forced-flow velocities. A plot analogous to Fig. 8, but with all parameters based on the distance x from the downward end, also was prepared. Correlation obtained from this plot and its interpretation was unsatisfactory.

In accordance with the more gradual transition from free to forced convection, the heat-transfer coefficients found in the counterflow experiments are up to twice as large as the higher one of the values calculated for pure forced or free-convection flow. This is astonishing since it might be expected that the free and forced-convection forces acting in opposite directions tend to cancel each other partially and in this way reduce the heat-transfer coefficients to values even below the pure free or forced-flow conditions. The large heat-transfer coefficients which actually were found probably result from an increased turbulence which is very likely under the condition where the flow in the central core of the tube tends to move in a direction opposite to the flow in the heated boundary layers near the wall. This increased large-scale turbulence actually could be observed with hot-wire anemometers.

CALCULATIONS BY MARTINELLI AND BOELTER FOR LAMINAR PARALLEL FLOW IN SHORT TUBES AND EXTENSION TO COUNTERFLOW

Reference (3) presents a method by which heat transfer in a tube for the mixed regime of free and forced convection under the condition of laminar flow could be calculated. The model used for this calculation is different from the one investigated in the previous section in that it has an unheated starting section and that the velocity profile already is established at the entrance to the heated part of the tube. The wall temperature is assumed uniform over the heated section. For the calculation it was postulated also that the free-convection forces are parallel to the forced-flow velocities and that the heat transfer primarily is determined by the conditions near the tube wall. Accordingly, the velocity profile in the flow was approximated by a linear-velocity increase with distance from the wall. The density was assumed to be a linear function of temperature. The first step in this calculation, called first approximation, neglects free convection and is identical with Leveque's solution.

In another step, which is called second approximation in the referenced report, the temperature in the bulk of the fluid was assumed constant and equal to the entrance temperature restricting this analysis to short tubes. The following equation for the average Nusselt number in the tube of the length L, was obtained

$$\overline{Nu}_d = 1.75 \sqrt[3]{Gz_d + 0.0722 \left(Gr_d Pr \frac{d}{L}\right)^{0.7}} \quad \ldots\ldots [6]$$

The Graetz number Gz_d in this equation is connected with the Reynolds and Prandtl numbers by the following relation

$$Gz_d = \frac{\pi}{4} Re_d Pr \frac{d}{L} \quad \ldots\ldots [7]$$

The dimensionless parameters, Nusselt, Graetz, and Grashof, are all based on the tube diameter as characteristic length.

The Nusselt numbers as determined by Equation [6] are shown in Fig. 9 as the lines identified as parallel flow. It can be observed that the general behavior of the lines, $GrPr\ (d/L) = \text{const}$, is the same as in Figs. 5 and 8. In the same way as before, limits between the forced, mixed, and free-convection regimes can be determined. The following equations describe these limits

$$\text{Forced-flow limit: } Gz_d = 0.217 \left(Gr_d Pr \frac{d}{L}\right)^{0.75} \quad \ldots\ldots [8]$$

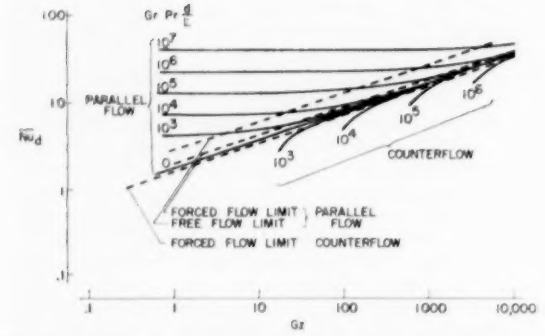

FIG. 9 DIMENSIONLESS CORRELATION OF MIXED, FREE, AND FORCED-CONVECTION HEAT-TRANSFER COEFFICIENTS FOR LAMINAR FLOW IN VERTICAL TUBE AS PREDICTED BY MARTINELLI AND BOELTER'S SECOND APPROXIMATION, (3)

$$\text{Free-flow limit: } Gz_d = 0.0241 \left(Gr_d Pr \frac{d}{L} \right)^{0.75} \quad \ldots\ldots [9]$$

Expressed in Reynolds numbers instead of Graetz numbers, the limits become

$$\text{Forced-flow limit: } Re_d = 0.276\, Gr_d^{3/4} Pr^{-1/4} \left(\frac{L}{d} \right)^{1/4} \quad \ldots [10]$$

$$\text{Free-flow limit: } Re_d = 0.0307\, Gr_d^{3/4} Pr^{-1/4} \left(\frac{L}{d} \right)^{1/4} \quad \ldots [11]$$

Also, it can be determined easily from Fig. 9 that in the mixed-flow regime the actual Nusselt number is up to 25 per cent larger than the larger one of either the forced-flow coefficient determined at the same Graetz number or the free-flow coefficient determined for the same $GrPr(d/L)$-parameter.

The calculation in reference (3) can be repeated for the case in which the free-convection forces act in a direction opposite to the forced flow. The only difference is a change in sign of the term in the hydrodynamic equation which describes the free-convection force.[6] The calculation with this change leads to the equation

$$\overline{Nu}_d = 1.75 \sqrt[3]{Gz_d - 0.0722 \left(Gr_d Pr \frac{d}{L} \right)^{0.75}} \quad \ldots\ldots [12]$$

describing the average Nusselt number for laminar-mixed counterflow. The calculation procedure, however, gives no real solutions for the condition

$$GrPr \frac{d}{L} < 7\, (Gz_d)^{4/3} \quad \ldots\ldots [13]$$

Equation [12] should not be used outside this range. The Nusselt numbers obtained from Equation [12] are inserted also in Fig. 9 as solid lines.

From the physics of the process it is expected that in laminar counterflow the Nusselt numbers drop with decreasing Graetz number to a minimum which is reached when, on the average, the free-convection forces balance the forces set up in the forced-flow field. With further decrease of the Graetz number, the Nusselt numbers will rise again and finally assume the values indicated in Fig. 9 for low Graetz numbers and parallel flow. From the experience collected in reference (8) it is expected that for counterflow conditions laminar flow is maintained only at very low Reynolds and Grashof numbers.

The limit between forced and mixed flow as derived from Equation [12] by the stipulation that at this limit the mixed-flow Nusselt numbers exceed the forced-flow values by 10 per cent is

$$Gz_d = 0.289 \left(Gr_d Pr \frac{d}{L} \right)^{0.75} \quad \ldots\ldots [14]$$

or

$$Re_d = 0.368\, Gr_d^{3/4} Pr^{-1/4} \left(\frac{L}{d} \right)^{1/4} \quad \ldots\ldots [15]$$

In reference (3) the calculation is carried further by accounting for the fact that in longer tubes the temperature increases in the core of the fluid in flow direction. In reference (8), however, indications were pointed out that this solution, called third approximation, is valid only in a range within which it does not differ appreciably from the second approximation. Hence the third approximation will not be used here.

EXPERIMENTS ON MIXED FLOW IN LONG TUBES

In reference (2) the results of an experimental investigation on a vertical tube with a ratio $L/d = 20$ are presented. Warm water was directed in most of the tests in a downward direction through the tube which had walls externally cooled by water in counterflow. Velocities and temperatures were practically constant over the entrance cross section and the wall temperature probably varied along the tube lengths. The conditions investigated employed free-convection forces parallel to the direction of the forced flow. The Prandtl number based on the film temperature was within the limits 2 to 5. The length used in the Nu_d, Re_d, and Gr_d parameters was the diameter d of the tube. It seems reasonable to expect that for the comparatively large length-to-diameter ratio, heat transfer should be determined mainly by this length parameter.

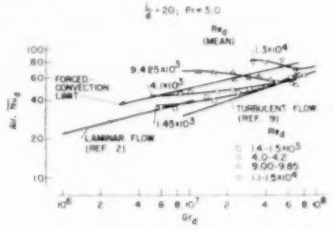

FIG. 10 DIMENSIONLESS CORRELATION OF EXPERIMENTAL HEAT-TRANSFER DATA IN VERTICAL TUBE
(Length-to-diameter ratio, 20; Prandtl number, approximately 3.0; obtained by Watzinger and Johnson, reference 2.)

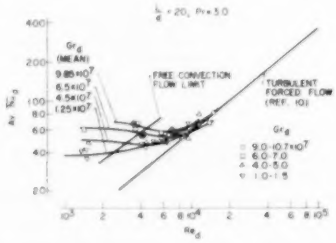

FIG. 11 DIMENSIONLESS CORRELATION OF EXPERIMENTAL HEAT-TRANSFER DATA IN VERTICAL TUBE
(Length-to-diameter ratio, 20; Prandtl number, approximately 3.0; obtained by Watzinger and Johnson, reference 2.)

[6] Reference (3), equation [24].

From the data in this report Figs. 10 and 11 could be obtained. They exhibit, in general, qualitatively the same behavior of the Nusselt number in function of Re_d and Gr_d as the data obtained on turbulent flow through short tubes and presented in Figs. 4 and 5. However, some differences are apparent. In the Nu_d-Gr_d plot only the curves for the larger Re_d-numbers show a dip in Fig. 10, whereas all of them have the dip in Fig. 4. On the other hand, the dip found on the curves for the higher Gr_d-parameters in Fig. 11 is missing on the curves in Fig. 5. These differences may be connected with the fact that both Re_d and Gr_d-values were considerably lower in the experiments reported in reference (2) than in the tests with the short tube. From the values of both parameters it is expected that the flow in the experiments on the long tube was in the transition range between laminar and turbulent flow. The limit between the free and mixed-flow regime can be determined as before and represented by the equation[7]

$$Re_d = 7.39\ (Gr_d)^{0.35} \quad [16]$$

and the one between the forced and mixed-flow regime by the equation

$$Re_d = 19.64\ (Gr_d)^{0.35} \quad [17]$$

Nusselt numbers in the forced-flow regime followed the well-known relations for developed turbulent flow in a tube. In the free-convection regime the values agree with the relation for turbulent free-convection flow on a vertical plate when the tube diameter is used as length parameter in the Nusselt and Grashof numbers. In the mixed-flow regime the actual Nusselt numbers are up to 30 per cent larger or 20 per cent smaller than the larger one of either the values expected for forced flow at the same Reynolds number or the value expected for free-convection flow at the same Grashof number.

A few experiments were done in the same apparatus also under the condition of counterflow. The counterflow heat-transfer coefficients were found to be larger than those of the parallel-flow experiments over the entire investigated range. The differences between both values were between 6 and 20 per cent with the largest difference found at high Reynolds and Grashof numbers. This fact is in qualitative agreement with the results of the investigation presented in this paper. The data were not sufficient to establish limits for the different flow regimes.

Experiments with water ($Pr \cong 1.65$) flowing through a vertical tube with $L/d = 126$, with Reynolds numbers between 500 and 2700, with Grashof numbers near 10^7, and for parallel-flow conditions have been made by E. B. Weinberg (4). This reference also contains the results of tests by E. B. Weinberg, G. Alves, and C. J. Southwell with oil ($Pr \cong 49.0$) flowing through a tube with $L/d = 300$ and 600, with Reynolds numbers between 1 and 2300, and Grashof numbers near 10^9. These results were compared in reference (4) with the calculated results in reference (3) after a correction had been made on the latter for an effect of turbulence which was assumed to be present to some degree in the experiments. Reasonable agreement was obtained. The data, however, cannot be used for a more detailed evaluation as presented in this paper since the range of parameters covered in the experiments is insufficient for this purpose.

Significant effects of free convection on heat transfer from the walls of a vertical tube under parallel-flow conditions are indicated in reference (5). No quantitative check with the results reported herein is possible, however, since the published data are not sufficient to calculate the Grashof numbers. The length-to-diameter ratio of the tube used in these experiments was 52.

At an early date Colburn (1) offered the following equation obtained from experimental information on vertical and horizontal tubes available at that time

$$\overline{Nu_d} = 1.65\ (Gz_d)^{1/3} \left(\frac{\mu_w}{\mu_f}\right)^{1/3} \left[1 + 0.015\ (Gr_d)^{1/3}\right] \quad [18]$$

In this equation the ratio of viscosities based on the wall and film temperatures accounts for the dependence of the heat-transfer coefficient on the variation of the property values. The limit at which the mixed-flow Nusselt number exceeds the pure forced-flow value by 10 per cent is found from this equation as $Gr_d = 300$. This means that the onset of free-convection effects would be independent of the Graetz or Reynolds number. This is in disagreement with all the results presented in this paper. The reason for this deviation is due probably to the small amount of experimental data available at the time when reference (1) was published.

Survey of Flow Regimes

By combining the information which has been collected, it is possible to obtain a tentative survey over the different regimes in the whole range of Reynolds and Grashof numbers for a tube with parallel flow. Fig. 12 presents such a survey. For Reynolds and Grashof numbers which are expected to characterize laminar flow conditions, the Equations [10] and [11] were used to determine the limits between the different flow regimes. The limits are calculated for two L/d-ratios (5 and 20) and for two values of the Prandtl number (0.7 and 3). From the way in which the limits appear in Fig. 12 it can be concluded that the limits between the different flow regimes are, at least in the laminar range, not greatly affected by a change in either parameter. Information on the limits in the turbulent-flow regime can be obtained from the experimental results presented in the first section of this paper. However, the following difficulty arises in this connection: The experiments on the short tube described in this paper determined the limits for the local heat-transfer coefficients, whereas all the previous information was concerned only with average heat-transfer values. In order to be able to introduce the limits for the turbulent range into Fig. 12 it was assumed that the local conditions at the exit cross section $x = L$ are identical with the conditions for the average heat transfer in the tube length L. The parameters Re_x and Gr_x in Equations [3], [4], and [5] were converted to the ones used in Fig. 12 and the limits were inserted in this figure. To get initial information on the position of the different regimes in the transitional region between laminar and turbulent flow, the limits obtained in Watzinger and Johnson's

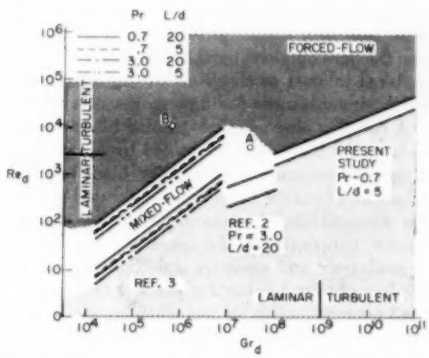

Fig. 12 Summary of Available Data on Free, Forced, and Mixed-Flow Regimes in Parallel Flow

[7] See footnote 4.

investigation (2) have been inserted also. It has to be kept in mind that these limits were obtained for tubes with a different L/d-ratio, 20, and with a different Prandtl number (approximately 3) than the limits in the turbulent regime.

For counterflow conditions, only two limits were determined, namely, the free-convection limit for turbulent flow and the forced-convection limit for laminar flow through short tubes. In addition, it is only known that the turbulent mixed-flow regime extends farther into the forced-flow regime for counterflow than for parallel flow. This information is not sufficient to construct even a tentative diagram similar to Fig. 12. In general, it may be expected that the location of the mixed-flow regime in the Grashof-Reynolds plot is approximately the same for counterflow and for parallel flow but that the width of the mixed-flow regime is larger for the first flow condition.

Heat-transfer coefficients can be calculated with the established relations in the forced-flow and in the free-flow regime. For the mixed-flow regime they can be obtained from the corresponding figures in this report. For parallel-flow conditions, McAdams' rule, to calculate the heat-transfer coefficients as if free or forced convection would be present alone and to use the larger one of the calculated values, can be used as a first approximation. Measured values deviated by not more than 25 per cent from the value determined with this rule. For turbulent counterflow, however, measured values were up to 100 per cent larger then the ones obtained by the same rule.

It may be of interest to check on an engineering application, under which circumstances the flow moves into the mixed-flow regime. A rotating air-cooled gas-turbine blade was selected as an example. The blade may be cooled by air moving radially outward through passages in the hollow blade interior. Reynolds numbers and Grashof numbers as generated by the centrifugal forces were calculated, assuming plausible values for passage diameter, temperatures, and amount of cooling air. For 1 per cent cooling-air and sea-level conditions the Reynolds and Grashof values obtained determine point A in Fig. 12. Point B represents 3 per cent cooling air and altitude conditions ($\approx$ 30,000 ft). It can be seen that the flow of the cooling air through such a turbine blade may be well in the mixed-flow regime, especially when it is remembered that counterflow conditions prevail in this application and that the mixed-flow range is wider for counterflow then the one shown in Fig. 12.

Summary

Convective heat transfer has been discussed as it is connected with flow through circular tubes under the combined effect of free and forced convection. The investigations reported were made under the condition that free and forced-flow forces were parallel or opposite in direction.

Local heat-transfer coefficients were measured on a short tube, $L/d = 5$. The results of the tests revealed that the whole flow regime as characterized by its Reynolds and Grashof number could be divided into a forced-flow, a free-convection, and a mixed-flow regime. The limits between these regimes are determined by Equations [3] to [5]. Heat-transfer coefficients in the forced and free-flow regime can be calculated with established relations; for the mixed-flow regime they are presented in Figs. 4, 5, 7, and 8.

Corresponding information for laminar flow through short tubes was obtained from a calculation by Martinelli and Boelter. Equations [8] to [11], [14], and [15] give the limits for the different flow regimes, and Fig. 9 presents the average Nusselt numbers to be expected in the mixed-flow regime.

Experiments on turbulent flow in long tubes, $L/d = 20$, were made by Watzinger and Johnson. They were evaluated to obtain information on the limits between the different regimes. Equations [16] and [17] express these limits, and Nusselt numbers for the mixed-flow range can be taken from Figs. 10 and 11.

Fig. 12 summarizes the information on the location of the different regimes in a Reynolds-Grashof number plot and for parallel-flow conditions. For counterflow conditions the available information is more restricted and only one limit for laminar and one for turbulent flow through short tubes could be established.

BIBLIOGRAPHY

1 "A Method of Correlating Forced Convection Heat Transfer Data and a Comparison With Fluid Friction," by A. P. Colburn, Trans. AIChE, vol. 26, 1933, pp. 174–210.

2 "Wärmeübertragung von Wasser on Rohrwand bei senkrechter Strömung im Übergangsgebiet zwischen laminarer und turbulenter Strömung," by A. Watzinger and D. H. Johnson, *Forschung auf dem Gebiete des Ingenieurwesens*, vol. 10, 1939, p. 182.

3 "The Analytical Prediction of Superposed Free and Forced Viscous Convection in a Vertical Pipe," by R. C. Martinelli and L. M. K. Boelter, University of California Press, Berkeley and Los Angeles, Calif., 1942.

4 "Heat Transfer and Pressure Drop for a Fluid Flowing in the Viscous Region Through a Vertical Pipe. Part 1—Heat Transfer Data," by R. C. Martinelli, C. J. Southwell, G. Alves, H. L. Craigh, E. B. Weinberg, N. F. Lansing, and L. M. K. Boelter, Trans. AIChE, vol. 38, 1942, pp. 493–530.

5 "Local Boiling Heat Transfer to Water at Low Reynolds Numbers and High Pressure," by J. A. Clark and W. M. Rohsenow, Division Industrial Cooperation, M.I.T., July 1, 1952. (For Office Naval Research Contract N5ori-078270 NR-035-267; DIC Project No. 6627.)

6 "Mathematical Theory of the Steady Heat Transfer in a Circular Vertical Hole With Superposition of Forced and Free Laminar Convection," by G. A. Ostroumov, *Journal of Technical Physics*, vol. 20, no. 6, 1950, pp. 750–757.

7 "Laminar Natural-Convection Flow and Heat Transfer of Fluids With and Without Heat Sources in Channels With Constant Wall Temperatures," by Simon Ostrach, NACA TN 2863, 1952.

8 "Experiments on Mixed-Free- and Forced-Convective Heat Transfer Connected With Turbulent Flow Through a Short Tube," by E. R. G. Eckert, A. J. Diaguila, and A. N. Curren, NACA TN 2974, 1953.

9 "Introduction to the Transfer of Heat and Mass," by E. R. G. Eckert, McGraw-Hill Book Company, Inc., New York, N. Y., 1950.

10 "Heat Transmission," by W. H. McAdams, second edition, McGraw-Hill Book Company, Inc., New York, N. Y., 1942, pp. 237–251.

11 "Laminar-Flow Heat-Transfer Coefficients for Ducts," by R. H. Norris and D. D. Streid, Trans. ASME, vol. 62, 1940, p. 525.

Heat Transfer to Mercury in Turbulent Pipe Flow

By H. A. JOHNSON,[1] W. J. CLABAUGH,[2] AND J. P. HARTNETT[3]

Experimental heat-transfer results are presented for turbulent flow of nonwetting mercury in a ³/₄-in., 18-gage mild-steel tube with constant heat flux. The identical test heat exchanger developed for the previously reported investigation of molten lead-bismuth eutectic (10, 11, 12)[4] was used. This present investigation also includes a series of short-duration tests for possible effects due to secondary flow, the use of argon as an alternate for a helium-gas atmosphere, and the addition of magnesium-titanium amalgam as a wetting agent. Heat-transfer tests with water preceded and followed those for mercury to establish continuing reliable performance of the test exchanger and its instrumentation. The results are correlated for the Peclet modulus range from 200 to 10,000 and are 4 to 10 per cent lower than the previously reported values for lead-bismuth and 35 to 40 per cent lower than the Martinelli-Lyon momentum theory (15, 17). No difference in heat-transfer performance was noted for upward versus downward flow or for the use of argon as a replacement for the helium atmosphere. No visible evidence of wetting occurred on the addition of the magnesium-titanium amalgam and no effect was found in the heat transfer.

Nomenclature

The following nomenclature is used in the paper:

A = heat-transfer area, sq ft
a = thermal diffusivity of fluid, sq ft/sec
c_p = specific heat of fluid evaluated at t_m, Btu/lb-deg F
D = inside diameter of test section, ft
g = acceleration of gravity, ft/sec²
h = average heat-transfer coefficient, Btu/hr sq ft deg F
h_L = local heat-transfer coefficient at entrance, Btu/hr sq ft deg F
k = thermal conductivity of fluid at t_m, Btu/hr sq ft deg F/ft
k_{al} = thermal conductivity of aluminum jacket, Btu/hr sq ft deg F/ft
k_s = thermal conductivity of steel-tube wall, Btu/hr sq ft deg F/ft
L = heat-transfer length of exchanger, ft
q_e = net electrical input, Btu/hr
q_f = heat gain indicated by flow rate and temperature rise of fluid, Btu/hr
r_i = radius to inner steel-pipe-wall surface, ft
r_o = radius to outer steel-pipe-wall surface, ft
r_t = radius to thermocouple position in aluminum jacket, ft
t_I = fluid temperature at test-section inlet, deg F
t_{II} = fluid temperature at test-section exit, deg F
t_f = local mixed mean fluid temperature, deg F
t_m = mean fluid temperature in test section $(t_I + t_{II})/2$, deg F
t_t = aluminum-jacket temperature at r_t, deg F
t_w = temperature at inner wall of steel pipe, deg F
u = mean bulk velocity, ft/sec
W = weight rate of flow, lb/hr
x = distance along test section, ft
μ = viscosity evaluated at t_m, lb/hr ft
ν = kinematic viscosity evaluated at t_m, sq ft/hr
ρ = weight density, fluid flowing, lb/cu ft

Dimensionless ratios:

Nu = Nusselt number, hD/k
Re = Reynolds number, uD/ν
Pe = Peclet number, Re × Pr, uD/a
Pr = Prandtl number, $c_p \mu/k$

Introduction

With the publication of the AEC "Liquid Metals Handbook," edited by R. N. Lyon (16), current information concerning theory, experiment, and experience in heat transfer to liquid metals has become readily available to those interested in the subject. This source reveals, however, that there are serious and unexplained differences between experiment and theory, particularly for the nonalkali metals, mercury and molten lead-bismuth. With the exception of results reported by Isakoff and Drew (9) and Untermyer (29), which compare favorably with the Martinelli-Lyon momentum theory (15, 17), all others report heat-transfer performance for these fluids to be substantially lower. Suggestions as to cause for the differences include possible faults in testing technique, phenomena of surface wetting, gas entrainment in the flow circuit, fouling of the heat-transfer surface, and separation or detached flow at the surface (26).

Since the test heat exchanger and technique previously used for lead-bismuth and water (10, 11, 12) demonstrated consistent and reproducible performance, this extension, with the identical heat exchanger, to include mercury appeared desirable.

Apparatus

A completely new flow system and safety enclosure for the mercury heat-transfer tests were built by the Mechanical Engineering Division of the University of California. The test section, Fig. 1, used in an earlier lead-bismuth investigation (10) was disassembled and new heaters, thermocouples, mixing chamber, and end fittings were installed and this unit used in the mercury tests.

As shown in Fig. 2, the system contains a centrifugal pump driven by an enclosed motor, a reservoir tank, a double-pipe water cooler, orifice meter, flow-control valves, and the necessary piping. Two additional sections of pipe, flanged on the ends, allow inversion of the test section. The materials in contact with the mercury are limited to glass, iron, mild and stainless steels, and Teflon. Provisions are made for evacuating the internal sys-

[1] Professor of Mechanical Engineering, University of California, Berkeley, Calif., Mem. ASME.
[2] Engineer, Knolls Atomic Power Laboratory, Schenectady, N. Y. Formerly at University of California. Assoc. Mem. ASME.
[3] Assistant Professor of Mechanical Engineering, University of Minnesota, Minneapolis, Minn. Formerly at University of California.
[4] Numbers in parentheses refer to Bibliography at end of paper.
Contributed by the Heat Transfer Division and presented at the Annual Meeting, New York, N. Y., November 29–December 4, 1953, of The American Society of Mechanical Engineers.
Note: Statements and opinions advanced in papers are to be understood as individual expressions of their authors and not those of the Society. Manuscript received at ASME Headquarters, September 2, 1953. Paper No. 53—A-189.

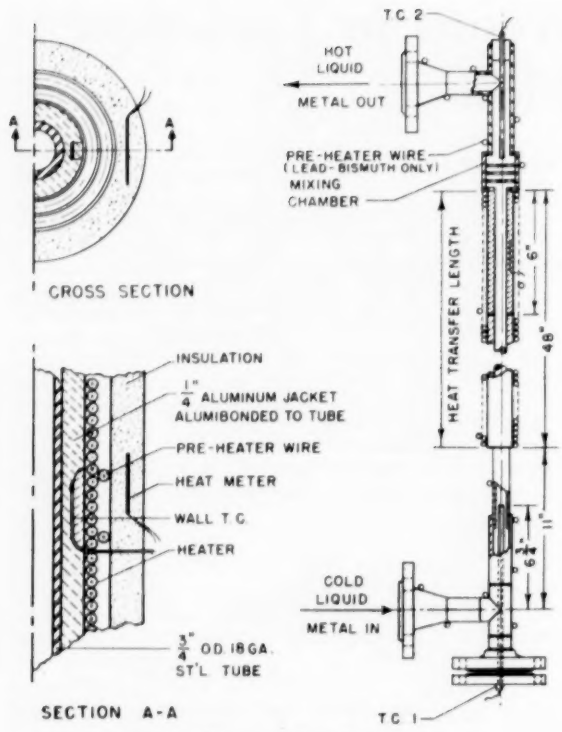

FIG. 1 HEAT-TRANSFER TEST-SECTION DETAIL

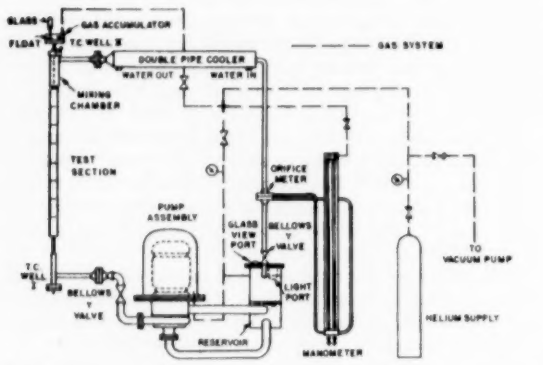

FIG. 2 SCHEMATIC DIAGRAM OF MERCURY HEAT-TRANSFER SYSTEM

tem and for introducing an atmosphere of helium which is maintained at 3 psig throughout the heat-transfer tests.

The test section, shown in Fig. 1, is a 4-ft-long, 0.750-in-OD, 0.652-in-ID mild-steel tube with a 0.25-in-thick aluminum jacket attached to the tube by the "Alumibond" casting process. Axial heat flow is minimized by circumferential grooves dividing the jacket into eight sections, each 6 in. in length. The high thermal conductivity of the aluminum provides a region of moderate radial temperature gradient in which thermocouples can be located with sufficient precision to assure an acceptable tube-wall temperature measurement. A thermocouple is located in each section, permitting eight separate determinations of the heat-transfer coefficient. Each iron-constantan thermocouple is positioned at one end of a $1^1/_2$-in-long, $^1/_8$-in-deep, $^3/_{32}$-in-wide axial slot, cemented in with Ames Technical B copper-oxide cement and capped with an aluminum bar.

Fluid temperatures are measured by single-junction iron-constantan thermocouples in steel wells installed in pairs at the entrance and exit sections; additional thermocouples also were spot-welded to the pipe walls at these locations as a further check. A mixing chamber at the exit of the exchanger assures a mixed mean temperature measurement.

Four test-section heaters of 19-gage insulated nichrome wire are wound uniformly over the aluminum jacket. A 5-kw motor-generator set used for the power source assures voltage stability. The electrical input to the heater is determined from wattmeter readings corrected for line losses. External losses are measured with four thermopile heat meters imbedded in the external insulation.

Complete details of the mercury and lead-bismuth systems have been reported (1, 10).

Spectrographic analyses of mercury samples taken during the test program showed the following range of values of contamination in parts per million:

Silver	Copper	Gold	Iron
0.09 to 1.0	0.02 to 0.25	0 to 0.5	nil

The magnesium and titanium used in the last test series were supplied by the General Electric Company as a standard-stock amalgam content of 2 lb titanium, $^1/_2$ lb magnesium, and 40 lb mercury. This was added to the test system to provide the amount of 0.012 per cent magnesium and 0.048 per cent titanium.

TEST AND ANALYSIS PROCEDURE

Details of the test and analysis procedure were substantially as reported in earlier work with lead-bismuth (10, 11, 12). The reliability of the results is established indirectly by heat-transfer tests with water before and after each series of liquid-metals tests using, of course, the same test section.

The heat-transfer-test sequence is given in Table 1, and range of variables is given in Table 2. This program was preceded by 430 hr of operation with lead-bismuth previously reported (10, 11, 12).

TABLE 1 HEAT-TRANSFER TEST SEQUENCE

1	First water tests	
2	First mercury series by Clabaugh (1) (normal operation[a] 70 hr)	70 hr
3	Second water tests	
4	Second mercury series	186 hr
	(a) Downward flow—98 hr	
	(b) Normal operation—50 hr	
	(c) Argon atmosphere—29 hr	
	(d) Normal operation—9 hr	
5	Third water tests	
6	Magnesium-titanium additive tests	56 hr
	(a) Normal operation—19 hr	
	(b) With additive—37 hr	
	Total mercury operating time	312 hr

[a] "Normal operation" signifies a vertical upward flow in test section, a helium-gas atmosphere, and no wetting-agent additive.

TABLE 2 RANGE OF VARIABLES FOR MERCURY TESTS

Flow rate, lb/hr	1400	67000
Velocity, ft/sec	0.2	10
Heat-transfer coefficient, Btu/sq ft-hr deg F	630	2600
Mean fluid temperature, deg F	100	350
Fluid-temperature rise, deg F	5	175
Wall to fluid temperature difference, deg F	4	22
Net electrical-heat flux, Btu/sq ft hr	3900	15300
Reynolds modulus	11000	450000
Prandtl modulus	0.012	0.022
Peclet modulus	170	10000
Nusselt modulus	5.7	26

ANALYSIS OF DATA

The flow of heat through the composite aluminum-steel wall to

the fluid in the pipe is expressed in terms of the individual thermal resistances by

$$q_e/A = \frac{t_t - t_f}{\frac{r_i \ln r_i/r_o}{k_{al}} + \frac{r_i \ln r_o/r_i}{k_s} + \frac{1}{h}}$$

where h is defined in the usual manner by

$$h = \frac{q_e/A}{t_w - t_f}$$

The first expression is rearranged to yield the final formulation used in the calculation of the heat-transfer coefficient

$$h = \frac{1}{\frac{t_t - t_f}{q_e/A} - \frac{r_i \ln r_i/r_o}{k_{al}} - \frac{r_i \ln r_o/r_i}{k_s}}$$

$$= \frac{1}{\frac{t_t - t_f}{q_e/A} - 2.36 \times 10^{-4}}$$

The calculation thus involves the measured aluminum-jacket and fluid temperatures, the net electrical-heat input and the calculated thermal resistance of the composite wall. The reliability of the calculated resistance value of 2.36×10^{-4} is verified by the water heat-transfer tests in the Reynolds-modulus region of 10^4 to 10^5 where good agreement (less than ± 10 per cent) with McAdams' equation [4c] (18) was found.

The heat input per unit length of exchanger is constant, imposing a linear increase of the bulk fluid temperature through the test section. Local fluid temperatures, therefore, may be interpolated from those measured at the entrance and exit. The calculated mean heat-transfer coefficient is based on the arithmetic average of the temperature differences $(t_t - t_f)$ in the last five sections. Fig. 3 illustrates two measured-temperature distributions; one distribution, indicated by open circles, is not typical since the variations from the mean line are substantially greater than for the majority of runs.

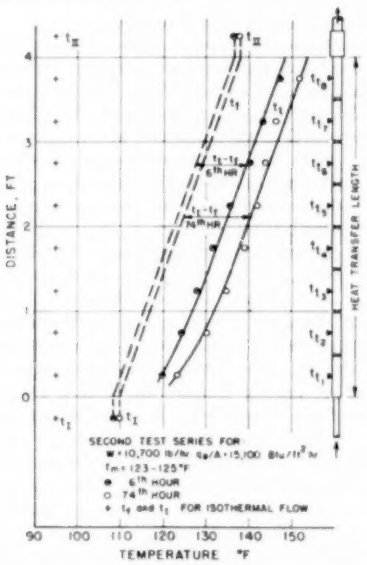

FIG. 3 MERCURY AND WALL THERMOCOUPLE TEMPERATURE DISTRIBUTION

The rate of heat transfer q_e is determined from the measured gross electrical input corrected for lead losses and external heat losses through the insulation. The external insulation losses are measured by calibrated thermopile heat meters.

The flow rate is obtained from an orifice-metering section made to ASME specifications and calibrated with water. The flow coefficients for the 0.358 diameter-ratio orifice in the 1-in. standard pipe are approximately 3 per cent higher than the ASME predicted values for the same orifice-diameter ratio but with a 2-in. pipe.

Based on the orifice-meter flow rates, 143 of 154 values for the heat balances average 0.96 ± 0.04, and the average for all 154 values is 0.96 ± 0.06.

The experimental accuracy, based on the precision of the instrumentation, is estimated to be as shown in Table 3.

TABLE 3 ESTIMATE OF EXPERIMENTAL ACCURACY BASED ON PRECISION OF INSTRUMENTATION

Quantity	Fluid	Probable error, per cent		Maximum error, per cent	
		High flow rate	Low flow rate	High flow rate	Low flow rate
h	mercury	6	3	17	8
h	water	9	3	25	6
q_f/q_e	mercury	4	5	9	10
q_f/q_e	water	4	2	8	5

PRESENTATION AND DISCUSSION OF RESULTS

This investigation of heat transfer to mercury in turbulent pipe flow with Reynolds modulus ranging from 14,000 to 400,000 was conducted in the same 0.652-in-ID mild-steel-tube test exchanger as was used for a previously reported lead-bismuth investigation (10, 11, 12). In addition to the "reference" or "normal" operation, defined as vertically upward flow of nonwetting mercury with a system internal atmosphere of helium, tests of limited duration were performed to investigate the possible influence (*a*) of flow direction, (*b*) lower thermal conductivity gas for the internal atmosphere, and (*c*) magnesium-titanium as a wetting agent.

Although heated downward flow is more favorable for secondary-flow effects as compared to thermally stable heated upward flow, this effect should only influence the heat-transfer performance at low Reynolds moduli and should not be evident at the high Reynolds values of this investigation. To confirm this, the heat exchanger was inverted and 13 values of the heat-transfer coefficient were obtained over a 30-hr period. The average ratio of these downward-flow heat-transfer coefficients compared to the upward-flow results is 1.03 ± 0.01. Since this deviation is less than the experimental accuracy it is concluded that the effects of flow direction are negligible.

It has been postulated that the discrepancy between reported experimental and theoretical results for nonwetting liquid metals may be due to an insulating gas layer at the fluid-wall interface (21). For previously reported lead-bismuth results (12), a thickness of approximately 3×10^{-4} in. would be sufficient to account for the observed low coefficients. Although the roughness of the exchanger surface is quantitatively unknown, the value of 3×10^{-4} is probably of the same order of magnitude as the asperities, in which the gas layer might be retained. If argon gas with $^1/_9$ the thermal conductivity replaced this same thickness of helium this effect would be magnified greatly and would result in coefficients 25 to 50 per cent of those obtained with helium. To investigate this postulate the system was evacuated, purged with argon several times, filled with argon and a 30-hr test run undertaken. For 14 values of the heat-transfer coefficient with an argon internal atmosphere the average ratio compared with those obtained with helium is 1.01 ± 0.04. Since this deviation is less than the experimental accuracy, no effect is found. In view of this result and the agreement among other nonwetting liquid-metal investigations using other seal-gas atmospheres, the postulate apparently is discredited.

The experimental investigations of the effect of wetting on heat-transfer performance reveal conflicting results. Untermyer (29), Seban (21), and Doody and Younger (2) offer evidence of increased heat transfer with wetting, and this also is noted in mercury-boiler experience (6, 13, 23) where the color of the boiler-tube surface changes markedly with the onset of effective wetting. Several major investigators of mercury and lead-bismuth (14, 26, 28) who either added magnesium or sodium or changed to a suitable tube material to promote wetting report no significant change in heat transfer although the exchanger surface was observed to have been "tinned." These mercury and lead-bismuth results, however, are considerably below the Lyon-Martinelli momentum theory whereas the wetting results of Lyon (15) and Werner, et al. (30) for sodium potassium are in good agreement with the prediction; this comparison raises the question as to whether the visual indication of "tinning" in the nonalkali metals was a sufficient criterion of "thermal wetting."

Although it was realized that the addition of magnesium-titanium amalgam to the mercury charge would not guarantee wetting, such an amalgam was purchased from the General Electric Company and added in amounts of 0.012 per cent magnesium and 0.048 per cent titanium as recommended for mercury-boiler practice. The heat-transfer-coefficients ratio for 17 values obtained with the additive during a 35-hr period as compared to those obtained with no additive is 1.00 ± 0.03 and, therefore, no change in performance is noted. During the early period of the test there appeared a slight tendency for the heat-transfer performance to decrease with time, as shown in Fig. 4, but this was

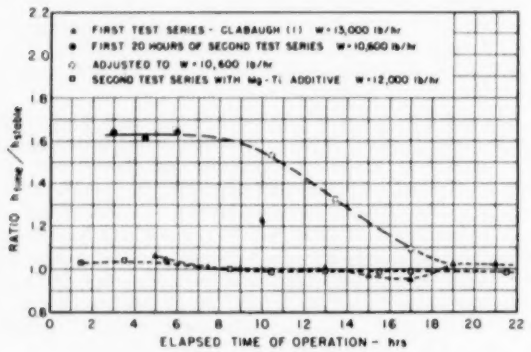
FIRST TEST SERIES - CLABAUGH (1) W = 13,000 lb/hr
FIRST 20 HOURS OF SECOND TEST SERIES W = 10,600 lb/hr
ADJUSTED TO W = 10,600 lb/hr
SECOND TEST SERIES WITH Mg - Ti ADDITIVE W = 12,000 lb/hr
RATIO h time / h cycle
ELAPSED TIME OF OPERATION - hrs

FIG. 4 MERCURY HEAT-TRANSFER-COEFFICIENT RATIO FOR FIRST 20 HR

accompanied by a comparable decrease in flow rate. On inspection of the test-exchanger surface at the completion of the test no visual evidence of wetting was observed. The only surface which appeared tinned was the surface on which the return flow impinged in the reservoir tank as could be witnessed through the glass view port, Fig. 2. Since mercury-boiler practice recommends circulation at 1000 F and since Stromquist (26) found fluxing necessary to obtain wetting with sodium additive, it is apparent that the low-temperature (115 F) short period (35 hr) and the simple, direct additive technique used in this investigation was not adequate to assure wetting.

As there were no effects due to secondary flow, type of seal gas, or magnesium-titanium wetting agent, all such results are presented in Figs. 5 and 6 and are not separately identified. Figs. 5 and 6 do, however, distinguish chronologically between the first test series and the second test series, each preceded and followed by reference tests with water to verify that no significant change had occurred in the test exchanger or its instrumentation.

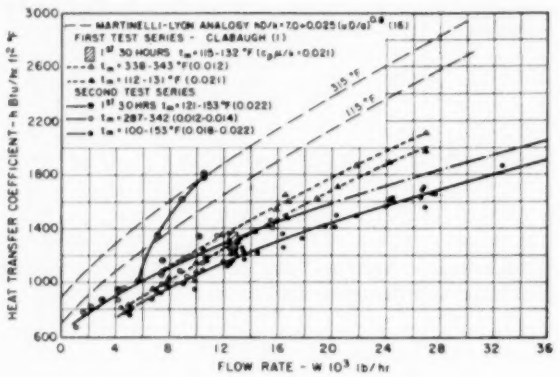
MARTINELLI-LYON ANALOGY
FIRST TEST SERIES - CLABAUGH (1)
SECOND TEST SERIES
HEAT TRANSFER COEFFICIENT - h Btu/hr ft² °F
FLOW RATE - W 10³ lb/hr

FIG. 5 MERCURY HEAT-TRANSFER COEFFICIENTS

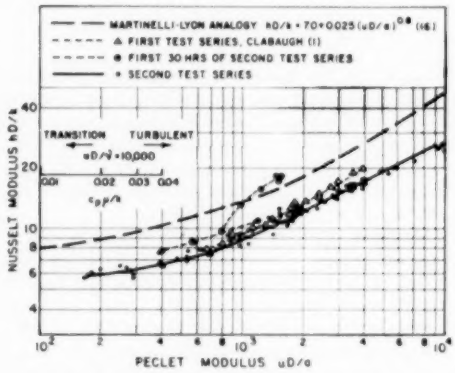

FIG. 6 MERCURY HEAT-TRANSFER CORRELATION

The results of the water heat-transfer reference tests before and after the first mercury test series, as revealed in Fig. 7, show good agreement with McAdams' equation [4c] (18). The results obtained after the second mercury series, however, are somewhat lower than predicted, which may indicate that the aluminum-steel bond may be beginning to fail. Since the maximum coefficients measured with mercury are approximately 2000 Btu/hr sq ft deg F, which value was obtained in the water tests at a Reynolds modulus of 60,000, where reasonable agreement is still demonstrated, it is felt that the second mercury series are reliable.

Except for the first 30 hours of each test series, comparison with the Lyon-Martinelli analogy theory (15, 17) in Fig. 5 reveals that the results of the first series reported by Clabaugh (1) are 30 and 24 per cent low at flow rates of 5000 and 28,000 lb/hr, respectively, while the corresponding deviations for the second series are 30 and 35 per cent. Since control of the temperature level was best during the first series, less scatter is demonstrated in the first series results. The analogy prediction of increasing heat transfer with increasing temperature level is revealed in both series, although the temperature effect shown by the first series is appreciably less than predicted by the theory. Considering that the average heat balance is 0.96 ± 0.04 and that there were no significant differences in the operation or testing procedure, the discrepancies between the first and second test series may be due either to a partial deterioration of the aluminum-steel bond or to obscure differences at the fluid-wall interface. Evidence of such obscure and irrational surface effects are demonstrated in the early periods of each test series.

With lead-bismuth in this same exchanger the heat-transfer coefficients uniformly decreased with time during the first 10 to 30 hr of each test series, but the opposite is true for the present mercury results. Figs. 4 and 5 reveal only a minor indication of decreasing values for the first test series, whereas the decrease for the second test series is striking. During the first 6 hr, after steady-state operation was established, three determinations at 1½-hr intervals, a flow rate of 10,600 lb/hr, a mean fluid temperature of 125 deg F and a heat-balance ratio of 0.96, gave heat-transfer coefficient values of 1810, 1780, and 1810 Btu/sq ft hr deg F, which values are 14 per cent greater than the analogy theory predicts and 43 per cent greater than a comparable normal value of 1260 Btu/sq ft hr deg F obtained during the 74th hr of operation. The difference is demonstrated clearly by the observed temperatures, shown in Fig. 3, where the fluid to thermocouple temperature differences are 12.0 deg F and 16.1 deg F, respectively. Corresponding fluid to inner-wall surface-temperature differences, i.e., thermocouple temperatures corrected for wall resistance, are 8.2 deg F and 12.0 deg F. A detailed review indicated that the same mercury charge was used and there were no differences in operating technique except that after the first test series the exchanger was cleaned as previously described (10) and stored for five months after which time it was inspected and installed for the second test series. There was no evidence of gas entrainment, as previously reported by Johnson, Hartnett, and Clabaugh (10, 12) for lead-bismuth and Quittenton (20) for sodium, during this period. This result (i.e., no entrained gas) had been demonstrated previously in the first test series when the gas accumulator, Fig. 2, was in the flow circuit. The Euler modulus ($2g\,p/\rho\,u_m^2$) considered by Stromquist (26) to be of importance for values less than 15, was 320 for this series, and subsequent tests revealed no effect when a minimum value of 20 for this modulus was varied by changing the system pressure level. The cause for this high performance, therefore, is not known but it is conceivable, based on reported boiler experience (6, 23, 31), that for some obscure reason the tube surface did become and remain for 6 hours "thermally wet" and that the results called here "normal operation" represent a thermally nonwetted heat-transfer surface. If such thermal wetting did occur it would indicate that visual evidence of wetting reported by Trefethen (28), Lubarsky (14), and Stromquist (25) is not sufficient to assure thermal wetting; furthermore, a surface which is thermally wetted may not necessarily remain so wetted.

A comparison of the present mercury results with those previously reported for lead-bismuth in the same test section is shown in Figs. 8 and 9. Fig. 8 reveals that the effect of temperature level predicted by the momentum theory is demonstrated by both the lead-bismuth and mercury results and that the relative position of the lead-bismuth experimental heat-transfer coefficients at 345 F (Curve 5-5) compared to those for mercury at 115 F (Curve 3-3) is in agreement with the theory. However, the 575 F lead-bismuth results (Curve 4-4) are slightly above the 315 F mercury values (Curve 2-2) while the analogy predicts the opposite to be true; since the predicted deviation of these results is of the same order of magnitude as the experimental accuracy, the instrumentation is probably not sufficiently sensitive to detect it.

These same lead-bismuth and mercury results are presented on a Nusselt-Peclet comparison in Fig. 9, where it is revealed that the first mercury-test-series results gradually increase from 10 per cent below those for lead-bismuth at a Peclet modulus of 600, to 10 per cent above at a Peclet value of 4000. The results of the more extensive second mercury series remain below those for lead-bismuth by from 4 to 10 per cent over the entire experimental range. Although this disagreement between the first mercury series, second mercury series, and the lead-bismuth results is not

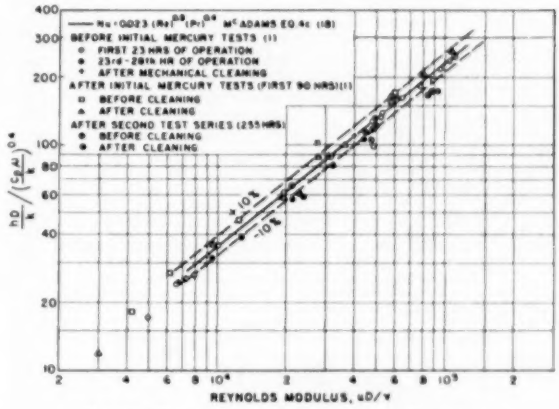

FIG. 7 WATER HEAT-TRANSFER TEST RESULTS

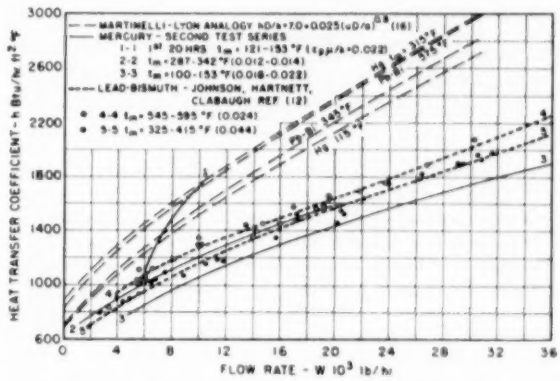

FIG. 8 LEAD-BISMUTH HEAT-TRANSFER COEFFICIENTS

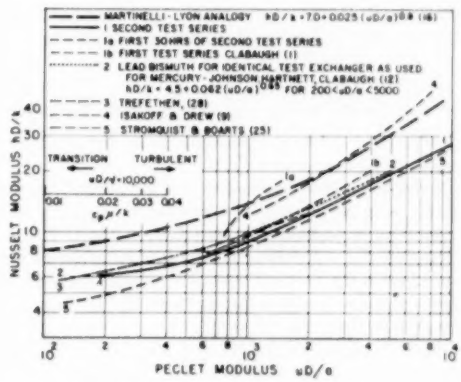

FIG. 9 COMPARISON OF HEAT-TRANSFER INVESTIGATIONS

great, it is, nevertheless, more than is anticipated if the estimated experimental accuracy and the basic assumptions of the momentum theory are valid. The noted discrepancies cannot be rationalized at this time but may be due to a variation of conditions at the fluid-wall interface. It is noteworthy that the results of the majority of the more recent lead-bismuth and mercury investigations can be represented by a line approximately 38 per cent below the Martinelli-Lyon theory.

An accurate specification of the thermal entry length for this

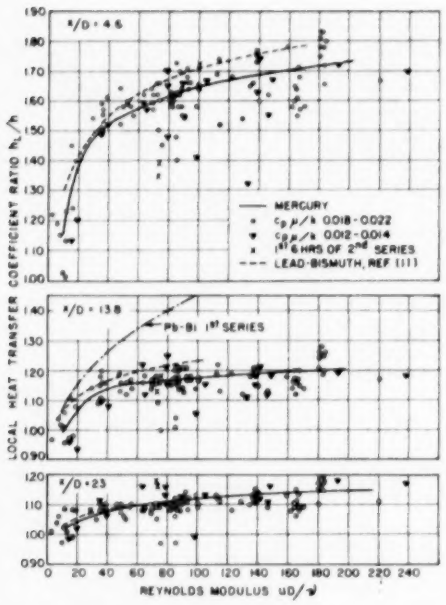

FIG. 10 LOCAL HEAT-TRANSFER COEFFICIENTS IN ENTRY LENGTHS

entrance geometry, Fig. 1, is difficult in view of the scatter of the entry length heat-transfer ratios, h_L/h, as may be seen in Fig. 10. The values for the first 6 hr of the second test series, where heat-transfer coefficients exceeded the momentum prediction, are separately identified. Mean lines are drawn through all data and similar curves are shown for previous lead-bismuth tests (10, 11, 12). Two lines for lead-bismuth are shown in Fig. 10 for x/D at 13.8 which distinguish between the first and second series. However, for some unknown reason, this was not observed for the other values of x/D. Based on these arbitrary lines an entry length of the order of 30 diameters, probably increasing with Reynolds modulus, is indicated for both lead-bismuth and mercury.

CONCLUSIONS

As a result of this investigation these conclusions are presented:

1 The direction of flow, upward or downward, had no noticeable effect on the heat transfer.

2 The heat-transfer performance was not affected by changing the internal inert-gas atmosphere from helium to argon, although the thermal conductivities differ by a ratio of 9 to 1.

3 The addition of a wetting agent of magnesium and titanium did not influence the heat-transfer performance in this investigation, nor was there visual evidence that any wetting of the exchanger surface had occurred.

4 When compared on the basis of the Nusselt versus Peclet modulus correlation, the bulk of mercury heat-transfer data for this investigation are 4 to 10 per cent lower than the lead-bismuth results obtained in the identical test-section heat exchanger.

5 There are indications that a distinction may exist between thermal and visual wetting.

6 Within ±15 per cent, the results of the majority of investigations for nonwetting lead-bismuth and mercury are represented by a mean Nusselt versus Peclet line which is 38 per cent below the Lyon equation.

7 A thermal entry length of approximately 30 diam, increasing slightly with Reynolds modulus and apparently insensitive to the Prandtl number over the range tested, is indicated.

ACKNOWLEDGMENTS

The authors gratefully acknowledge the sponsorship of the Atomic Energy Commission and permission to present this work which is a summary of the report "Heat Transfer to Mercury in Turbulent Pipe Flow," by H. A. Johnson, W. J. Clabaugh, and J. P. Hartnett, Institute of Engineering Research, University of California, Berkeley, Calif., July, 1953.

Appreciation also is expressed to Dr. R. A. Seban for his assistance and suggestions during the investigation.

BIBLIOGRAPHY

1 "Heat Transfer to Mercury in Turbulent Pipe Flow," by W. J. Clabaugh, MS thesis, University of California, Berkeley, Calif., 1953.

2 "Heat Transfer Coefficients for Liquid Mercury and Dilute Solutions of Sodium in Mercury in Forced Convection," by T. C. Doody and A. H. Younger, Preprints for Heat Transfer Symposium at the Forty-Fourth Annual Meeting, American Institute of Chemical Engineers, December, 1951.

3 "Heat Transfer Measurements With Mercury," by D. Elser, Translation by Ronald Kay and William Shrank, Forced Convection Engineering Research Project, University of California, Berkeley, Calif., May, 1949.

4 "Heat Transfer Properties of Mercury," by D. English and T. Barrett, Atomic Energy Research Establishment Report ER 547, Harwell, Berks, England, June, 1950.

5 "Physical Properties of Heat Transfer Fluids," by "Genie" Report GI 401, General Engineering and Consulting Laboratory, General Electric Company, Schenectady, N. Y., November, 1947.

6 "Mercury for the Generation of Light, Heat, and Power," by H. N. Hackett, Trans. ASME, vol. 64, 1942, pp. 647–653.

7 "The Thermal Conductivities of Mercury, Sodium, and Sodium Amalgams in the Liquid State," by W. C. Hall, *Physical Review*, vol. 53, 1938, pp. 1004–1009.

8 "Handbook of Chemistry and Physics," by C. D. Hodgman, Chemical Rubber Company, thirty-third edition, 1951.

9 "Heat and Momentum Transfer in Turbulent Flow of Mercury," by S. E. Isakoff and T. B. Drew, Preprint for Heat Transfer Discussions, London, England, September, 1951.

10 "Heat Transfer to Molten Lead-Bismuth Eutectic in Turbulent Pipe Flow," by H. A. Johnson, J. P. Hartnett, and W. J. Clabaugh, Institute of Engineering Research Division Report, University of California, Berkeley, Calif., November, 1951.

11 "Heat Transfer to Molten Lead-Bismuth Eutectic in Turbulent Pipe Flow," by H. A. Johnson, J. P. Hartnett, and W. J. Clabaugh, Institute of Engineering Research Division Report, University of California, Berkeley, Calif., February, 1952.

12 "Heat Transfer to Molten Lead-Bismuth Eutectic in Turbulent Pipe Flow," by H. A. Johnson, J. P. Hartnett, and W. J. Clabaugh, Preprint for Heat Transfer and Fluid Mechanics Institute, Stanford University Press, Stanford, Calif., June, 1952.

13 "Mercury for the Generation of Light, Heat, and Power," by H. N. Hackett, Trans. ASME, vol. 64, 1942, pp. 647–653; discussion by H. J. Kerr, pp. 654–655.

14 "Experimental Investigation of Forced-Convection Heat-Transfer Characteristics of Lead-Bismuth Eutectic," by B. Lubarsky, NACA Research Memorandum E51G02, September, 1951.

15 "Forced Convection Heat Transfer Theory and Experiments With Liquid Metals," by R. N. Lyon, Report ORNL-361, Oakridge National Laboratory, 1949.

16 "Liquid Metals Handbook," by R. N. Lyon, Atomic Energy Commission and Bureau of Ships, Navy Department, June, 1952.

17 "Heat Transfer to Molten Metals," by R. C. Martinelli, Trans. ASME, vol. 69, 1947, pp. 947–959.

18 "Heat Transmission," by W. H. McAdams, second edition, McGraw-Hill Book Company, Inc., New York, N. Y., 1942.

19 "Heat Transfer to Mercury," by R. J. Musser and W. R. Page, MS thesis, Massachusetts Institute of Technology, Cambridge, Mass., May, 1947.

20 "The Direct Measurement of the Film Coefficient of Heat Transfer to Molten Sodium Metal in Forced Convection," by R. C. Quittenton, PhD thesis, University of Toronto, Can., March, 1953.

21 "Heat Transfer Measurements on Lead-Bismuth Eutectic in Turbulent Pipe Flow," by R. A. Seban, Institute of Engineering Research Division Report, University of California, Berkeley, Calif., June, 1950.

22 "Flow Metering of Molten Lead-Bismuth Eutectic," by R. A. Seban, W. T. Shrank, and D. Bartz, Institute of Engineering Re-

search Division Report, University of California, Berkeley, Calif., May, 1949.

23 "The Mercury-Vapor Process," by A. R. Smith and E. S. Thompson, Trans. ASME, vol. 64, 1942, pp. 625–646.

24 "Smithsonian Physical Tables," Smithsonian Institution, Washington, D. C., vol. 88, 1934.

25 "Effect of Wetting on Liquid Heat Transfer," by W. K. Stromquist and R. M. Boarts, Progress Report, Department of Chemical Engineering, The University of Tennessee, Knoxville, Tenn., September, 1952.

26 "Effect of Wetting on Heat Transfer Characteristics of Liquid Metals," by W. K. Stromquist, Department of Chemical Engineering, The University of Tennessee, Knoxville, Tenn., AEC Contract At-(40-1)-1310 Report, March, 1953.

27 "Heat Exchange at Very Low Prandtl Numbers," by M. A. Styrikovitch and K. H. Semenovker (in Russian), Ja Tech. Phys. USSR, vol. 10, 1940, pp. 1324–1330.

28 "Heat Transfer Properties of Liquid Metals," by L. M. Trefethen, Oakridge National Laboratory NP1788, July, 1950.

29 "Heat Transfer Experiments With Bismuth Alloys," by S. Untermyer, Personal Communication, Argonne National Laboratory, Bailey & Lamont, Chicago, Ill., June, 1949.

30 "Forced Convection Heat Transfer With Liquid Metals," by R. C. Werner, E. C. King, and R. A. Tidball, Presented at the Forty-Second Annual Meeting, American Institute of Chemical Engineers, Pittsburgh, Pa., December, 1949.

31 "South Meadow—First Post-War Mercury Power Unit," by O. L. Wood, *Power Engineering*, vol. 54, March, 1950, pp. 62–67, 75.

Heat Transfer to Lead-Bismuth and Mercury in Laminar and Transition Pipe Flow

By H. A. JOHNSON,[1] J. P. HARTNETT,[2] AND W. J. CLABAUGH[3]

Experimental heat-transfer results in the low Reynolds modulus range of 1000 to 10,000 are reported for two different liquid metals, lead-bismuth eutectic and mercury. The single heat exchanger used in both series of tests was a $^3/_4$-in., 18-gage, 4-ft-long mild-steel tube. Similar heat-transfer tests with water in laminar and turbulent flow were performed with this same tube before and after each liquid-metal series, and the agreement of the turbulent-water tests with previous published results supports the liquid-metals test procedure. The data for both liquid metals, including flow in the upward and downward directions, are correlated on a Nusselt-Peclet basis with a single curve representing all experimental results with a maximum deviation of 20 per cent. The experimental Nusselt values decrease from approximately 6 at Reynolds number of 10,000 down to 1 at a Reynolds number of 1200, and consequently are considerably lower than the theoretical constant heat-rate laminar-flow Nusselt value of 4.36 (6).[4] Possible causes for this behavior which have been investigated and found to be inadequate when considered independently include: (a) Insulating gas-layer or oxide-film fouling at the heated surface; (b) nonwetting; (c) uncertainties in property values; (d) axial-conduction effects. Although no supporting data are available, a distortion of the velocity profile from the parabolic distribution appears to be the most plausible explanation.

Introduction

FOR the case of a fluid flowing in laminar motion through a circular pipe with a constant heat input per unit length, theoretical considerations, with appropriate assumptions, yield a Nusselt modulus of 4.36 (6). Since experience with nonmetal fluids (15) reveals a heat-transfer performance substantially higher than this theoretical value, it has been assumed that that Nusselt value 4.36 represents a lower limit for all fluids with a constant heat input per unit length. The "Liquid Metals Handbook" (14), therefore, states, "In the cases of laminar flow of liquid metals through tubes or natural convection around tubes, the heat-transfer coefficient, or unit thermal conductance, can be predicted with reasonable assurance using the same relationships which apply to other types of fluids."

In view of these considerations the available meager heat-transfer data in the laminar and transition-flow ranges were discounted since they demonstrated values near and below the "limiting" value. When similar low heat-transfer performance was observed first in the present lead-bismuth investigation, the results were regarded with suspicion and although briefly described (10) were not presented. Subsequently, the mercury tests results using the identical test exchanger in a new flow system were found to be in good agreement with the earlier lead-bismuth values and also to compare favorably with several other mercury investigations in transition flow. For this reason the results now are presented.

Apparatus, Test Procedure, and Data Analysis

The apparatus, test procedure, and data analysis have been described previously (11), but the following is pertinent to this paper.

Heat-transfer tests with water also were made before and after each series of liquid-metal tests and served to validate the technique and to establish continuing satisfactory operation of the test section. The program included the following sequence of tests and range of variables (Table 1):

Test Sequence:

1 Initial water heat-transfer tests.
2 Lead-bismuth heat-transfer tests.
3 Water heat-transfer tests.

After this step, the test section was disassembled and new heaters and thermocouples were installed and the test program continued as follows:

4 Water heat-transfer tests.
5 Mercury heat-transfer tests.
6 Water heat-transfer tests.

TABLE 1 RANGE OF VARIABLES FOR LIQUID-METAL INVESTIGATIONS

Lead-bismuth (flow direction upward):	
Flow rate, lb/hr	230– 2100
Velocity, fps	0.04– 0.4
Heat-transfer coefficient, Btu/hr sq ft deg F	140– 815
Mean fluid temperature, deg F	415– 550
Fluid temperature rise, deg F	15– 250
Wall-to-fluid temperature difference, deg F	6– 25
Net electrical heat flux, Btu/sq ft hr	1700–16,000
Reynolds modulus	1100–10,000
Prandtl modulus	0.026–0.035
Peclet modulus	30– 300
Nusselt modulus	1.3– 7.2
Mercury (flow direction upward for 6 runs, flow direction downward for 7 runs):	
Flow rate, lb/hr	150– 2300
Velocity, fps	0.02– 0.38
Heat-transfer coefficient, Btu/hr sq ft deg F	100– 700
Mean fluid temperature, deg F	180– 350
Fluid-temperature rise, deg F	60– 300
Wall-to-fluid temperature difference, deg F	6– 25
Net electrical heat flux, Btu/sq ft hr	1200–14,000
Reynolds modulus	1100–17,500
Prandtl modulus	0.012–0.017
Peclet modulus	20– 300
Nusselt modulus	1.0– 5.9

The heat-transfer coefficient is calculated as an average value for the five downstream thermocouple sections, Fig. 1, following the data-analysis procedure previously described except for the flow-rate determinations which are based on an energy or heat-balance-ratio value of unity. This was necessary since a satis-

[1] Professor of Mechanical Engineering, University of California, Berkeley, Calif. Mem. ASME.

[2] Asst. Professor of Mechanical Engineering, University of Minnesota, Minneapolis, Minn. Formerly at University of California.

[3] Engineer, Knolls Atomic Power Laboratory, Schenectady, N. Y. Formerly at University of California. Assoc. Mem. ASME.

[4] Numbers in parentheses refer to the Bibliography at the end of the paper.

Contributed by the Heat Transfer Division and presented at the Annual Meeting, New York, N. Y., November 29–December 4, 1953, of The American Society of Mechanical Engineers.

Note: Statements and opinions advanced in papers are to be understood as individual expressions of their authors and not those of the Society. Manuscript received at ASME Headquarters, September 2, 1953. Paper No. 53—A-188.

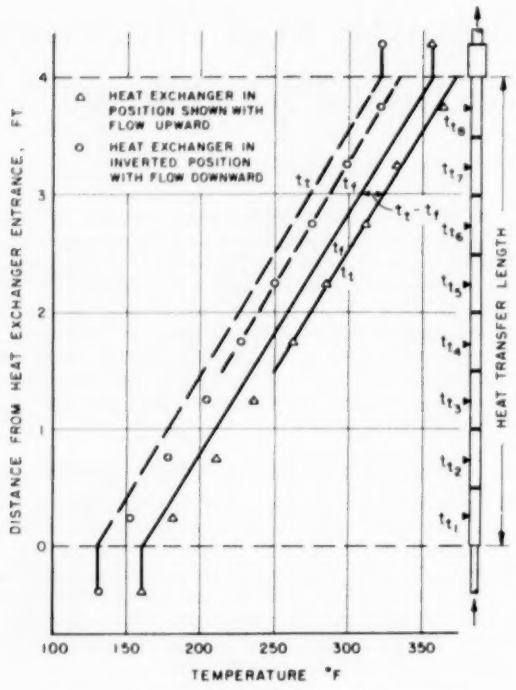
HEAT EXCHANGER IN POSITION SHOWN WITH FLOW UPWARD
HEAT EXCHANGER IN INVERTED POSITION WITH FLOW DOWNWARD
DISTANCE FROM HEAT EXCHANGER ENTRANCE, FT.
HEAT TRANSFER LENGTH
TEMPERATURE °F

FIG. 1 TEMPERATURE DISTRIBUTION FOR MERCURY

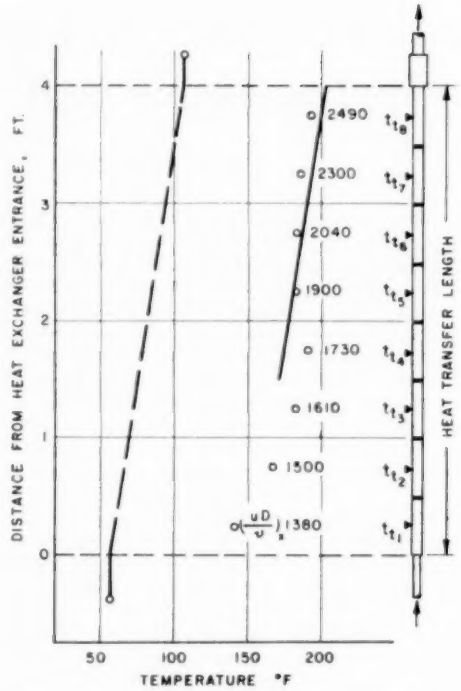

FIG. 2 TEMPERATURE DISTRIBUTION FOR WATER

factory orifice meter could not be designed for these extremely low flow rates. The assumption of a heat balance of unity is justified since high flow-rate tests where metering was possible yielded heat-balance ratios of 0.94 ± 0.03 for lead-bismuth and 0.96 ± 0.04 for mercury, while present water tests produced a value of 0.96 ± 0.02.

WATER HEAT-TRANSFER RESULTS

The water heat-transfer tests utilizing the same heat-exchanger unit were performed before and after each liquid-metal test series to demonstrate the reliability of the technique. The heat-transfer coefficients for these tests were calculated by the same procedure as those for the liquid-metal investigations, and for turbulent flow demonstrated good agreement with McAdams' Equation [4c] (17) up to a Reynolds modulus of 100,000.

A typical low flow-rate temperature distribution, which is representative of those tests near the critical Reynolds number, is shown in Fig. 2. That the flow begins as laminar in the initial section of the pipe and becomes turbulent at some distance from the entrance is demonstrated in Fig. 2 by the shape of the wall-temperature curve and the local Reynolds modulus posted at each thermocouple position.

The experimental water heat-transfer results up to a Reynolds number of 10^4 are presented in Fig. 3, with separate representation given to the four series of water tests. Fig. 3 reveals that the results of the four series of water tests are consistent above a Reynolds modulus of 5000 and in good agreement with McAdams' Equation [4c]. For Reynolds modulus below 5000 a departure from the latter is indicated as predicted by McAdams for the transition region (17). In the laminar-flow region, the Hausen approximation of the constant wall temperature, Graetz solution (3), and the unpublished results of a constant heat rate-finite difference solution are shown. The analysis of Klein and Tribus (25) was not used since it yields an incorrect answer ap-

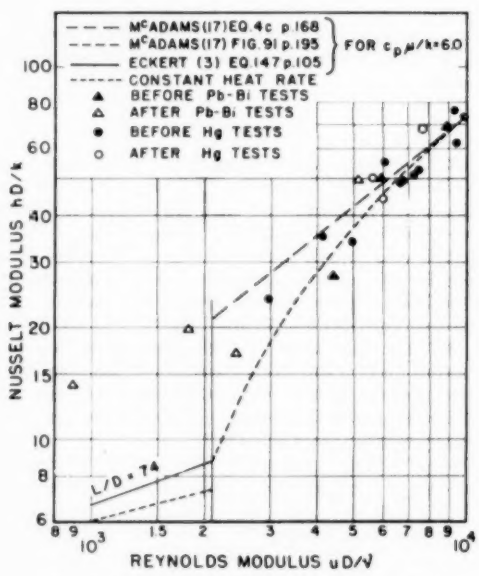

FIG. 3 WATER HEAT-TRANSFER CORRELATION

parently due to an insufficient number of eigenvalues (26). The two experimental points in this report are approximately 150 per cent higher than the prediction, which is consistent with other laminar-flow results for heating (15, 17). Although it is realized that the laminar and transition water-test results are a minimum and subject to excessive temperature rises, it is, however, suggested that the results do indicate predicted trends of performance

in these flow regions and that, therefore, the test technique is sound and should be reliable for liquid metals.

Liquid-Metals Heat-Transfer Results

The heat-transfer results reported here are for lead-bismuth eutectic and mercury in the laminar and transition range ($1000 < uD/\nu < 10{,}000$) as measured in the same 0.652-in-ID mild-steel tube test heat exchanger as previously used to obtain turbulent-flow liquid-metal heat-transfer data (10, 11). Periodic visual inspection revealed no evidence to indicate that either liquid metal had "wetted" the tube-wall surface of the test section.

The average heat-transfer coefficients for all runs of both liquid metals are shown in Fig. 4 to be represented by a mean line with a maximum deviation of 20 per cent. This also is indicated by the predicted heat-transfer coefficients as shown for laminar and turbulent flow, the latter assumed representative in the transition range. Although the fluid temperature rise is excessive for the low flow rates, the local Reynolds modulus (see Fig. 2 for water) for all runs shown in the laminar-flow region, with one exception, was less than 2100 throughout the entire tube length. Contrary to performance with normal fluids, no evidence of a basic change in the character of flow was reflected in the heat transfer, but rather a continuous decrease is noted on passing through the transition to the laminar region. The experimental accuracy is estimated at 10 per cent due to uncertainties caused by observed temperature fluctuations.

This continuous decrease in the performance also is demonstrated in Fig. 5, where the Nusselt-Reynolds correlation is shown

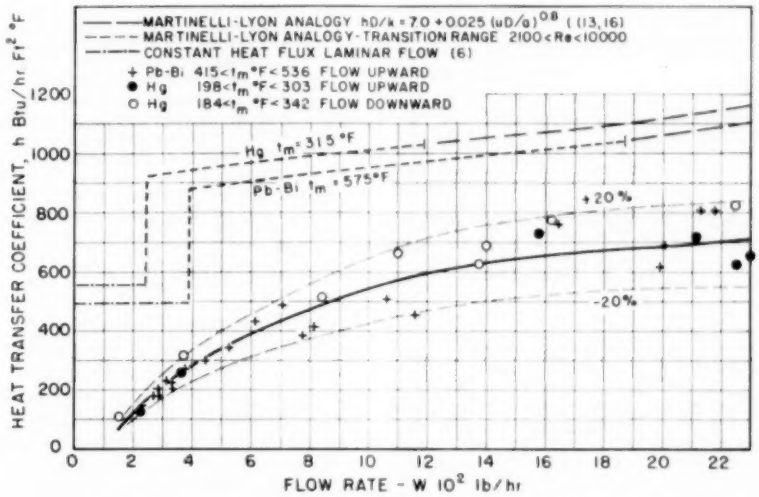
MARTINELLI-LYON ANALOGY hD/k = 7.0 + 0.025 (uD/a)^0.8 (13,16)
MARTINELLI-LYON ANALOGY-TRANSITION RANGE 2100<Re<10000
CONSTANT HEAT FLUX LAMINAR FLOW (6)
+ Pb-Bi 415<t_m °F<536 FLOW UPWARD
● Hg 198<t_m °F<303 FLOW UPWARD
○ Hg 184<t_m °F<342 FLOW DOWNWARD
Hg t_m = 315 °F
Pb-Bi t_m = 575°F
+20%
-20%
HEAT TRANSFER COEFFICIENT, h Btu/hr Ft² °F
FLOW RATE - W 10² lb/hr

Fig. 4 Mercury and Lead-Bismuth Heat-Transfer Coefficients

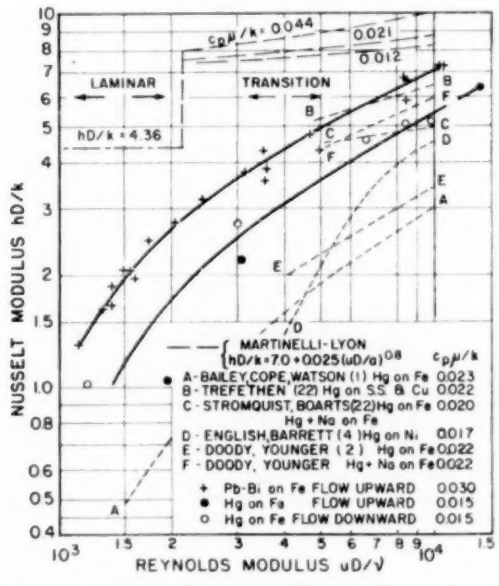
LAMINAR
TRANSITION
hD/k = 4.36
cpμ/k = 0.044
0.021
0.012
MARTINELLI-LYON
{hD/k = 7.0 + 0.025(uD/a)^0.8 cpμ/k
A - BAILEY, COPE, WATSON (1) Hg on Fe 0.023
B - TREFETHEN (22) Hg on S.S. & Cu 0.022
C - STROMQUIST, BOARTS (22) Hg on Fe 0.020
Hg + Na on Fe
D - ENGLISH, BARRETT (4) Hg on Ni 0.017
E - DOODY, YOUNGER (2) Hg on Fe 0.022
F - DOODY, YOUNGER Hg + Na on Fe 0.022
+ Pb-Bi on Fe FLOW UPWARD 0.030
● Hg on Fe FLOW UPWARD 0.015
○ Hg on Fe FLOW DOWNWARD 0.015
NUSSELT MODULUS hD/k
REYNOLDS MODULUS uD/ν

Fig. 5 Liquid-Metals Comparison, Nusselt Versus Reynolds

Although it is recognized that the data shown are limited in quantity, subject to large differences in terminal fluid temperatures, and exhibit as of doubtful influence the downward flows (in the case of some mercury runs), mean lines are drawn through the lead-bismuth and mercury data. The results reveal a Prandtl effect, not only in the transition range where this is anticipated, but also in the laminar range where no such dependency is predicted. If such a Prandtl-modulus effect in the laminar-flow region eventually should be supported by other investigators, then a simple or direct explanation may be difficult since the 4.36 value of the Nusselt modulus is independent of both Reynolds and Prandtl moduli. The performance indicated by Bailey, Cope, and Watson (1), English and Barrett (4), and Doody and Younger (2) is even more difficult to rationalize than the present results, unless their flow systems were subject to gas entrainment (9, 18), or flow-separation problems (21) previously reported.

The usual liquid-metals Nusselt-Peclet modulus correlation, wherein fluid-property effects are minimized, is presented in Fig. 6. This correlation reveals that a mean line with a maximum deviation of 20 per cent representing all present results also includes a majority of those previously reported for mercury by other investigators. Although it generally is anticipated from results with nonmetal fluids that downward flow is more favorable for secondary flows and, consequently, higher heat-transfer performance (17), the present results, as shown in Fig. 6, reveal no marked effect on inverting the heat exchanger. Although

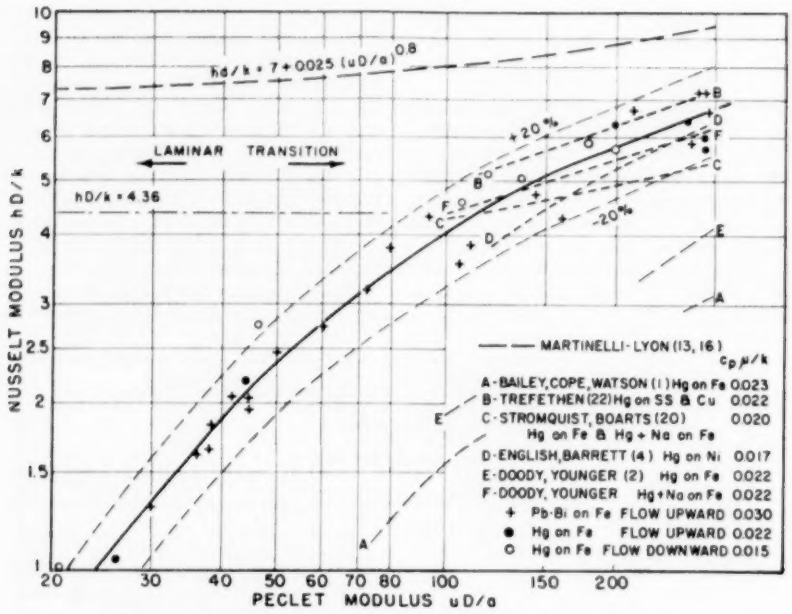
NUSSELT MODULUS hD/k
PECLET MODULUS uD/a
hd/k = 7+0.025 (uD/a)^0.8
hD/k = 4.36
LAMINAR
TRANSITION
+20%
-20%
MARTINELLI-LYON (13, 16)
A-BAILEY, COPE, WATSON (1) Hg on Fe 0.023
B-TREFETHEN (22) Hg on SS & Cu 0.022
C-STROMQUIST, BOARTS (20) 0.020
Hg on Fe & Hg + Na on Fe
D-ENGLISH, BARRETT (4) Hg on Ni 0.017
E-DOODY, YOUNGER (2) Hg on Fe 0.022
F-DOODY, YOUNGER Hg + Na on Fe 0.022
Pb-Bi on Fe FLOW UPWARD 0.030
Hg on Fe FLOW UPWARD 0.022
Hg on Fe FLOW DOWNWARD 0.015

FIG. 6 LIQUID-METALS COMPARISON, NUSSELT VERSUS PECLET

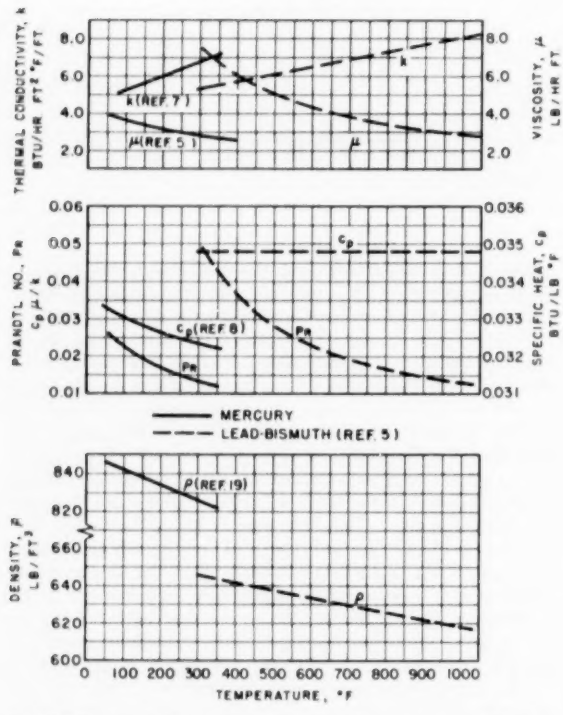

FIG. 7 PHYSICAL PROPERTIES OF LEAD-BISMUTH AND MERCURY

the liquid-metal Grashof moduli are large compared to normal types of fluids, reference to the work of Bonilla, et al. (14) indicates that both the product of the Grashof and Prandtl moduli, an important free-convection parameter, and the experimental Nusselt moduli, are nominally low compared to other fluids. It is, therefore, possible that natural convection effects may not be significant for liquid metals in pipe flow.

Since the heat-transfer performance is appreciably lower than expected such possible factors as an insulating gas layer or oxide film, gas entrapment, nonwetting, uncertainty of physical properties, and axial-conduction effects now will be considered.

The postulate of an insulating gas layer has been discredited previously by tests with argon (11) and satisfactory water-test results indicate the presence of an oxide film as unlikely. Gas entrapment also appears unlikely since two separate flow loops with different types of centrifugal pumps were used, and it is extremely doubtful, in view of the correlation obtained, that exactly the proper proportion of gas necessary to yield such results would be entrapped and circulated in both the lead-bismuth and in the mercury systems. Another check on possible gas entrapment was made in the mercury system where a small chamber was installed at the highest part of the flow circuit, where any circulated gas could be accumulated by displacing the free surface of the liquid in this chamber. The liquid-level indicator, which consisted of a steel float with a glass-enclosed stem, revealed no change in the liquid level. It is reasonably certain, therefore, that no gas was entrapped in flowing liquid.

If "visual wetting" is a sufficient criterion of "thermal wetting," the agreement of the wetting result of Trefethen (22), Stromquist and Boarts (20), and Doody and Younger (2) with the present nonwetting investigation indicates that the low performance is not necessarily due to lack of wetting. If a difference between visual and thermal wetting is acknowledged and a surface resistance assumed characteristic of thermal nonwetting, this resistance estimated in the turbulent region (i.e., resistance necessary to bring experimental data up to theoretical prediction) would have to be three to tenfold greater for laminar flow. Thus this postulate appears inadequate. It is unfortunate that data for the alkali metals which are in agreement with theory for turbulent flow (13, 23) are not reported for laminar and transition flows.

The possible errors associated with the available property values are insufficient to account for the discrepancy between the

test results and theory. Changes in the property values owing to the temperature rise of the fluid through the test section are not considered in the theoretical analysis; however, even if the Nusselt modulus is based on the thermal conductivity at the fluid entrance temperature, where the thermal conductivity is a minimum, the resulting Nusselt moduli are not significantly different.

The effect of axial conduction is shown to be important only in the entrance region in the constant wall-temperature analysis of Wilson (24). This same result can be demonstrated for the constant heat-rate rise. Since the experimental heat-transfer performance was evaluated at a considerable distance from the entrance, the influence of axial conduction is, therefore, negligible.

Having investigated these possibilities, there yet remains the question of the validity of the parabolic velocity distribution, which is a basic assumption in obtaining the theoretical Nusselt modulus of 4.36. Since analytical constant heat-rate solutions reveal a significant change in the heat-transfer rate when the velocity profile changes from a uniform distribution (slug-flow solution with a resulting Nusselt modulus of 8.0) to the parabolic distribution, it is conceivable that a distortion of the velocity profile could be a contributing factor in the observed low heat-transfer performance.

It is apparent that more experimental work on liquid-metal heat transfer in the laminar and transition region is essential and that studies of the velocity distribution and pressure drop should be undertaken to explain the apparent discrepancy between the theory and existing experimental results.

Conclusions

1 When correlated on a Nusselt-Peclet modulus basis, the lead-bismuth and mercury heat-transfer results of this investigation for the range of Reynolds modulus, from 1000 to 10,000, are represented by a mean line with a maximum deviation of 20 per cent which also includes a majority of the results of other mercury investigations.

2 In the laminar-flow region the heat-transfer performance is as low as one-fourth that predicted as a theoretical lower limit.

3 Contrary to results obtained with normal fluids (such as air, oil, water) no evidence of a basic change in the character of flow is reflected in the heat-transfer performance of liquid metals in the laminar-transition region.

4 When considered individually, an insulating gas layer, an oxide film, gas entrainment, nonwetting (if visual evidence is adequate), uncertainty in the physical properties or axial conduction do not account for the low heat-transfer performance observed here.

5 Additional heat-transfer studies, including velocity distribution and pressure-drop measurements, are recommended for the laminar and transition-flow regions.

Acknowledgments

The authors gratefully acknowledge the sponsorship of the Atomic Energy Commission and permission to present this work which is a summary of the report "Heat Transfer to Lead-Bismuth and Mercury in Laminar and Transition Pipe Flow," by H. A. Johnson, J. P. Hartnett, and W. J. Clabaugh, Institute of Engineering Research, University of California, Berkeley, August, 1953. Appreciation is also expressed to Dr. R. A. Seban for his assistance and suggestions during the investigation.

Bibliography

1 "Heat Transfer to Mercury," by D. L. R. Bailey, W. F. Cope, and G. G. Watson, National Physical Laboratory, Engineering Division, N. O., 379/48, 1949.

2 "Heat Transfer Coefficients for Liquid Mercury and Dilute Solutions of Sodium in Mercury in Forced Convection," by T. C. Doody and A. H. Younger, Preprints for Heat Transfer Symposium at the Forty-Fourth Annual Meeting, American Institute of Chemical Engineers, December, 1951.

3 "Introduction to the Transfer of Heat and Mass," by E. R. G. Eckert, McGraw-Hill Book Company, Inc., New York, N. Y., 1950, pp. 98–105.

4 "Heat Transfer Properties of Mercury," by D. English and T. Barrett, Atomic Energy Research Establishment Report ER 547, Harwell, Berks., England, June, 1950.

5 "Genie" Report GI 401, "Physical Properties of Heat Transfer Fluids," General Engineering and Consulting Laboratory, General Electric Company, Schenectady, N. Y., November, 1947.

6 "Modern Developments in Fluid Dynamics," by S. Goldstein, Oxford University Press, London, England, vol. 2, pp. 622–623.

7 "The Thermal Conductivities of Mercury, Sodium, and Sodium Amalgams in the Liquid State," by W. C. Hall, *Physical Review*, vol. 53, 1938, pp. 1004–1009.

8 Handbook of Chemistry and Physics," by C. D. Hodgman, Chemical Rubber Company, thirty-third edition, 1951.

9 "Heat Transfer to Molten Lead-Bismuth Eutectic in Turbulent Pipe Flow," by H. A. Johnson, J. P. Hartnett, and W. J. Clabaugh, Institute of Engineering Research Division Report, University of California, Berkeley, Calif., November, 1951.

10 "Heat Transfer to Molten Lead-Bismuth Eutectic in Turbulent Pipe Flow," by H. A. Johnson, J. P. Hartnett, and W. J. Clabaugh, Preprints for Heat Transfer and Fluid Mechanics Institute, Stanford University Press, Stanford, Calif., June, 1952.

11 "Heat Transfer to Mercury in Turbulent Pipe Flow," by H. A Johnson, W. J. Clabaugh, and J. P. Hartnett, published in this issue, pp. 505–511.

12 "Experimental Investigation of Forced-Convection Heat-Transfer Characteristics of Lead-Bismuth Eutectic," by B. Lubarsky, NACA Research Memorandum E51GO2, September, 1951.

13 "Forced Convection Heat Transfer Theory and Experiments With Liquid Metals," by R. N. Lyon, Report ORNL-361, Oakridge National Laboratory, 1949.

14 "Liquid Metals Handbook," by R. N. Lyon, Atomic Energy Commission and Bureau of Ships, Navy Department, June, 1952.

15 "Heat Transfer and Pressure Drop for a Fluid Flowing in the Viscous Region Through a Vertical Pipe," by R. C. Martinelli, et al., Trans. AICE, vol. 38, June 25, 1942.

16 "Heat Transfer to Molten Metals," by R. C. Martinelli, Trans. ASME, vol. 69, 1947, pp. 947–959.

17 "Heat Transmission," by W. H. McAdams, second edition, McGraw-Hill Book Company, Inc., New York, N. Y., 1942.

18 "The Direct Measurement of the Film Coefficient of Heat Transfer to Molten Sodium Metal in Forced Convection," by R. C. Quittenton, Ph.D. Thesis, University of Toronto, Canada, March, 1953.

19 Smithsonian Physical Tables, Smithsonian Institution, Washington, D. C., vol. 88, 1934.

20 "Effect of Wetting on Liquid Heat Transfer," by W. K. Stromquist and R. M. Boarts, Progress Report, Department of Chemical Engineering, The University of Tennessee, Knoxville, Tenn., September, 1952.

21 "Effect of Wetting on Heat Transfer Characteristics of Liquid Metals," by W. K. Stromquist, Department of Chemical Engineering, The University of Tennessee, Knoxville, Tenn., March, 1953.

22 "Heat Transfer Properties of Liquid Metals," by L. M. Trefethen, Oakridge National Laboratory NP1788, July, 1950.

23 "Forced Convection Heat Transfer With Liquid Metals," by R. C. Werner, E. C. King, and R. A. Tidball, presented at the Forty-Second Annual Meeting, American Institute of Chemical Engineers, Pittsburgh, Pa., December, 1949.

24 H. A. Wilson, Proceedings, Cambridge Philosophical Society, vol. 12, 1904, p. 406.

25 "Forced Convection From Nonisothermal Surfaces," by J. Klein and M. Tribus, University of Michigan Engineering Research Institute Report, August,1952.

26 Personal Communication, by J. Klein, September, 1953.

Effect of Single Roughness Elements on the Heat Transfer From a 1:3 Elliptical Cylinder

By R. A. SEBAN,[1] S. LEVY,[2] D. L. DOUGHTY,[3] and R. M. DRAKE, JR.[1]

The effect of single roughness elements on the heat transfer from the surface of a 1:3 elliptical cylinder to an air stream has been investigated by placing single spanwise nylon filaments on the surface of the cylinder. The results are compared with those for the smooth surface of the same cylinder which have already been presented and, as before, these results are given in terms of the pressure coefficient, recovery factor, and local heat-transfer coefficient. On-stream air speeds ranged from 184 to 423 fps giving Reynolds numbers, based on the 6-in. chord of the cylinder, from 531,000 to 1,200,000. The roughness element produced an effect in all cases and in the majority there was an apparent transition to turbulent flow either at or downstream of the element. In those cases in which the roughness element was not too large compared to the thickness of the laminar boundary layer, the heat-transfer coefficients after the point of transition were in good accord with those predicted from the Colburn equation. The point of transition itself was in approximate agreement with values found by other experimenters.

Nomenclature

The following nomenclature is used in the paper:

c_f	=	skin-friction coefficient, dimensionless
C_p	=	pressure coefficient, defined by Equation [1]
c_p	=	specific heat at constant temperature, Btu/slug deg F
D	=	major axis of elliptical cylinder, ft
d	=	nylon-filament diameter, ft
H	=	form parameter, ratio of displacement to momentum thickness of boundary layer
h	=	local heat-transfer coefficient, Btu/hr sq ft deg F
J	=	energy conversion factor, 778 ft-lb/Btu
k	=	thermal conductivity of fluid, Btu/hr ft deg F
p	=	local static pressure on model surface, psf
p_a	=	static pressure just upstream of model, psf
q	=	local heat flux, Btu/hr sq ft
S	=	meridional distance along cylinder from stagnation point, ft
T_{aw}	=	local adiabatic wall temperature, deg F
T_0	=	surface temperature at point, deg F
T_s	=	stagnation temperature of stream, deg F
u_a	=	free-stream velocity just upstream of model, fps
u'	=	velocity fluctuation in u_a, fps
u_1	=	local free-stream velocity at edge of boundary layer, fps
x	=	distance measured from initiation of boundary layer, ft
x_0	=	distance of corrugation behind leading edge, ft
x_t	=	distance corresponding to start of transition, ft
θ	=	momentum thickness, ft
ρ	=	density of fluid, slugs per cu ft
ρ_a	=	density of fluid just upstream of model, slugs per cu ft
ν	=	kinematic viscosity of fluid, sq ft per sec

Introduction

In a previous paper (1)[4] the local heat-transfer coefficients for the smooth surface of an elliptical cylinder of axis ratio 1:3 were presented. These coefficients were determined by measuring the temperature of the surface of the cylinder, which dissipated heat at a constant rate to the boundary layer formed by the air stream which passed over the surface at moderately high speeds. For the most part the boundary layers were laminar and it was possible to correlate results for different air-stream velocities by the use of parameters indicated by the theory for laminar boundary-layer flows. Moreover, the actual values of the local heat-transfer coefficient were found to be in general accord with those which were predicted by approximate analytical methods.

This paper deals with the effect of single roughness elements, placed on the surface of this same cylinder, on the value of the local heat-transfer coefficient. The elements were nylon filaments of circular cross section affixed along a cylinder generator in locations at which the previous results for the smooth surface had indicated the boundary layer to be laminar. Sizes larger and smaller than the minimum size indicated as necessary to disturb the laminar layer were used, and the results indicate some effect of the roughness element in all cases. Flow conditions were the same as those for which the results for the smooth surface have been presented, except that this investigation emphasized the zero angle-of-attack position. As before, the results are given in terms of the pressure coefficient, recovery factor, and local heat-transfer coefficient.

These investigations dealt with the possibility of producing turbulent boundary layers on this cylinder by means of single roughness elements, rather than a detailed study of the characteristics of flow produced by the elements, hence the range of sizes and positions of the elements is not so great as might be desired. The results, however, are of general interest in design and represent heat transfer under conditions which, heretofore, have been little investigated.

Apparatus and Procedure

The apparatus and procedure were the same as in the experiments with a smooth surface as already reported (1). The elliptical cylinder, 6 in. in chord length and 6 in. wide, spanned the 6-in. width of the 6-in. × 9-in. throat of the wind tunnel in which it was located. Fig. 1 shows the cylinder with the side of the tunnel removed. Three nichrome ribbons, each 1 in. wide, are heated by an electric current passing through them in series. Thermocouples located immediately below the center ribbon serve to indicate, very closely, the surface temperature of that

[1] Associate Professor, Mechanical Engineering, University of California. Mem. ASME.

[2] Research Engineer, University of California.

[3] Research Engineer, University of California. Assoc. Mem. ASME.

Contributed by the Heat Transfer Division and presented at the Annual Meeting, New York, N. Y., November 29–December 4, 1953, of The American Society of Mechanical Engineers.

Note: Statements and opinions advanced in papers are to be understood as individual expressions of their authors, and not those of the Society. Manuscript received at ASME Headquarters, August 12, 1953. Paper No. 53—A-86.

[4] Numbers in parentheses refer to the Bibliography at the end of the paper.

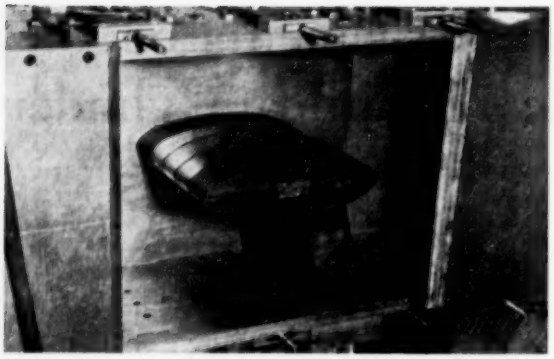

FIG. 1 ELLIPTICAL CYLINDER AS INSTALLED IN WIND TUNNEL

ribbon. Pressure taps are located between the center test ribbon and the side ribbons, which guard heat the center ribbon. The locations of the thermocouples and pressure taps are given in Fig. 2 and its associated table.

Approximate observations of the turbulence level u'/u_a were made after the tests on the cylinder with a smooth surface and prior to the series of tests with the roughness elements. These observations were made with a conventional hot-wire anemometer at a single location, 3 in. upstream from the model and 3 in. below the top of the test section. There, the turbulence level u'/u_a ranged from 0.002 to 0.003 in the range of Reynolds numbers

$$5.3 \times 10^5 < \frac{u_a D}{\nu} < 1.20 \times 10^6$$

The roughness elements were single-filament nylon, of diameters from 0.0008 to 0.021 in., stretched across the model sur-

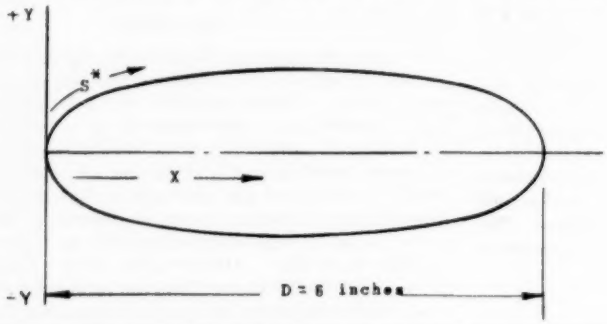

THERMOCOUPLES				PRESSURE TAPS				
STATION	X INCHES	Y INCHES	S/D	ROW NO.	STATION	X INCHES	Y INCHES	S/D
1	2.584	-1.000	-0.488	1	1	2.584	-1.000	-0.488
2	2.157	-0.972	-0.418	1	2	1.755	-0.927	-0.351
3	1.755	-0.927	-0.351	1	3	0.928	-0.743	-0.212
4	1.327	-0.850	-0.280	1	4	0.355	-0.480	-0.104
5	0.928	-0.743	-0.212	1	5	0.055	-0.204	-0.036
6	0.538	-0.585	-0.141	1	6	0.038	0.192	0.033
7	0.183	-0.352	-0.069	1	7	0.328	0.468	0.100
8	0.000	0.000	0.000	1	8	0.900	0.734	0.207
9	0.038	0.192	0.033	1	9	1.728	0.923	0.347
10	0.175	0.345	0.067	1	10	2.583	0.998	0.488
11	0.328	0.468	0.100	1	11	3.403	0.995	0.625
12	0.533	0.584	0.140	1	12	4.237	0.918	0.753
13	0.900	0.734	0.207	1	13	5.054	0.735	0.903
14	1.325	0.849	0.280	1	14	5.804	0.365	1.043
15	1.728	0.923	0.347	1	15	5.826	-0.350	-1.047
16	2.155	0.971	0.417	2	16	2.157	-0.972	-0.418
17	2.583	0.998	0.488	2	17	1.327	-0.850	-0.280
18	2.996	1.005	0.557	2	18	0.538	-0.585	-0.141
19	3.403	0.995	0.625	2	19	0.183	-0.352	-0.069
20	3.830	0.977	0.694	2	20	0.000	0.000	0.000
21	4.237	0.918	0.753	2	21	0.175	0.345	0.067
22	4.648	0.847	0.832	2	22	0.533	0.584	0.140
23	5.054	0.735	0.903	2	23	1.325	0.849	0.280
24	5.453	0.575	0.976	2	24	2.155	0.971	0.417
25	5.804	0.365	1.043	2	25	2.996	1.005	0.557
26	6.000	0.000	1.115	2	26	3.830	0.977	0.694
27	5.826	-0.350	-1.047	2	27	4.648	0.847	0.832
				2	28	5.453	0.575	0.976
				2	29	6.000	0.000	1.115

* DISTANCE FROM X = 0, Y = 0

FIG. 2 LOCATION OF THERMOCOUPLES AND PRESSURE TAPS ON 1:3 ELLIPTICAL CYLINDER

TABLE 1 SUMMARY OF TEST CONDITIONS

Filament diam., in.	Location S/D	Angle of attack, deg	$\frac{u_\infty D}{\nu}$	$\frac{\theta}{D} \times 10^3$	$\frac{\theta}{d}$	Symbol on heat-transfer representation
0.021	0.33	0	932000	0.259	0.074	△
0.021	0.33	0	781000	0.283	0.081	△
0.021	0.21	0	776000	0.219	0.062	▽
0.0065	0.21	0	963000	0.198	0.183	○
0.0065	0.21	0	766000	0.222	0.205	○
0.0065	0.33	0	1180000	0.232	0.214	○
0.0065	0.33	0	981000	0.252	0.232	○
0.0065	0.33	0	766000	0.286	0.264	○
0.0065	0.33	0	629000	0.315	0.290	○
0.0065	0.48	0	963000	0.316	0.292	○
0.0065	0.48	0	757000	0.356	0.329	○
0.0065	0.48	0	531000	0.425	0.392	○
0.005	0.33	0	1200000	0.228	0.274	×
0.002	0.53	0	763000	0.286	0.860	□
0.0008	0.21	0	1060000	0.188	1.41	◇
0.0008	0.21	0	967000	0.196	1.48	◇
0.0008	0.21	0	760000	0.221	1.66	◇
0.0008	0.33	0	1040000	0.245	1.84	◇
0.0008	0.33	0	962000	0.255	1.91	◇
0.0008	0.33	0	756000	0.288	2.16	◇
0.0065	-0-	6	814000	0.066	0.063	○
0.0065	0.33	6	966000	0.290	0.268	○
0.0065	0.33	6	817000	0.315	0.291	○
0.0065	0.33	6	641000	0.356	0.329	○

face and cemented to it to prevent vibration. Table 1 gives the filament sizes and positions and the Reynolds numbers for which tests were made.

The observations made were those necessary for the determination of the pressure coefficient, recovery factor, and heat-transfer coefficient. These are defined by the equations

$$C_p = \frac{p - p_\infty}{\frac{\rho_\infty u_\infty^2}{2}} \quad \ldots\ldots [1]$$

$$r = 1 - \frac{T_\infty - T_{aw}}{u_1^2/2\,Jc_p} \quad \ldots\ldots [2]$$

$$h = \frac{q}{T_w - T_\infty + (1-r)(u_1^2/2\,Jc_p)} \quad \ldots\ldots [3]$$

Adiabatic wall temperatures T_{aw} were taken to be the temperatures indicated with operation without any heating current. At higher speeds, the effects of internal heat conduction in the model and external heat radiation were small enough to make these temperatures a fair approximation to the temperatures which would exist for a truly adiabatic condition. As noted in the previous paper (1) the expected accuracy in the recovery factor is from 2 to 3 per cent.

The maximum error in the heat-transfer coefficient, as evaluated from the data by Equation [3], was estimated previously at about 6 per cent. The consistency and reproducibility of the results are superior to this, but such deviations may still obtain because of heat-conduction effects in the model, particularly in regions where the surface temperature changes rapidly.

During, and at the end of, experiments with the roughness elements, experiments with the surface smooth indicated the performance to remain as previously reported.

Table 2 gives the range of some of the important variables as they occurred in these experiments.

TABLE 2 RANGE OF VARIABLES

On-stream velocity, u_∞, fps	184–423
Free-stream stagnation pressure, in. Hg	30.0
Reynolds number	5.31 (10⁵)–1.20 (10)⁶
Local Mach number	0–0.6
Free-stream stagnation temperature, deg F	75–87
Temperature difference, model surface to stagnation temperature:	
(a) Heated, deg F	4–26
(b) Adiabatic, deg F	0–7.6
Surface pressure, in. H_2O	0.7–77
Electric current, amp	5–8.5

Results

The results, most of which refer to the position of zero angle of attack, are presented in terms of the pressure coefficient, recovery factor, and local heat-transfer coefficient. In the presentation, the heat-transfer coefficient is incorporated into the group

$$\frac{hD}{k}\sqrt{\frac{\nu}{u_\infty D}}$$

which serves to correlate the local heat-transfer coefficients at any point for

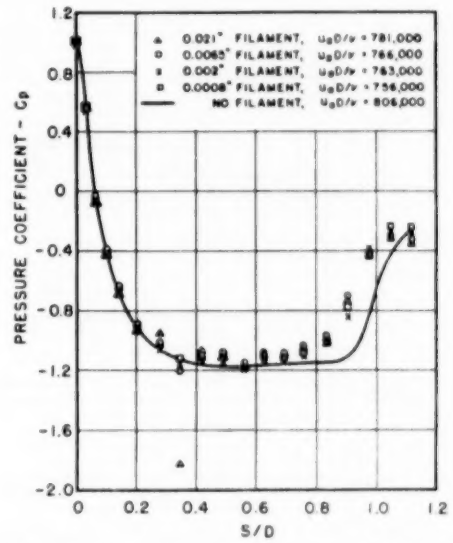
PRESSURE COEFFICIENT - C_p
S/D
0.021" FILAMENT, $u_\infty D/\nu$ = 781,000
0.0065" FILAMENT, $u_\infty D/\nu$ = 766,000
0.002" FILAMENT, $u_\infty D/\nu$ = 763,000
0.0008" FILAMENT, $u_\infty D/\nu$ = 756,000
NO FILAMENT, $u_\infty D/\nu$ = 806,000

FIG. 3 TYPICAL PRESSURE COEFFICIENT DISTRIBUTION FOR VARIOUS NYLON FILAMENTS LOCATED AT $S/D = 0.33$

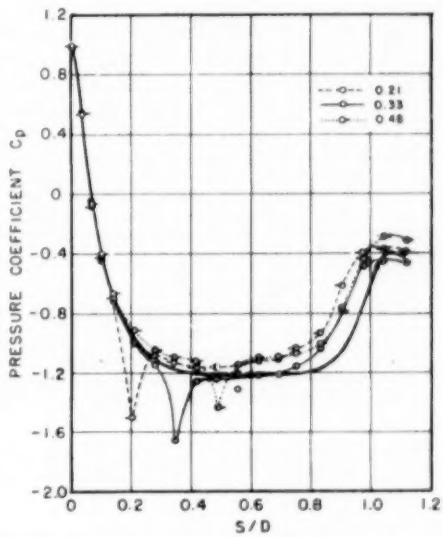

FIG. 4 TYPICAL PRESSURE COEFFICIENT DISTRIBUTION FOR 0.0065-IN. NYLON FILAMENT LOCATED AT VARIOUS POSITIONS

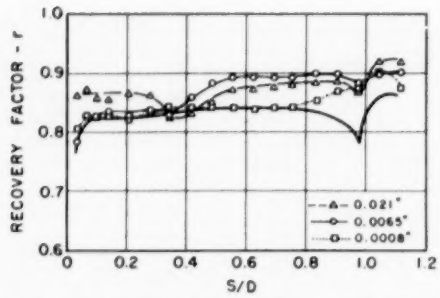

FIG. 5 TYPICAL LOCAL RECOVERY FACTOR DISTRIBUTION FOR VARIOUS NYLON FILAMENTS LOCATED AT $S/D = 0.33$

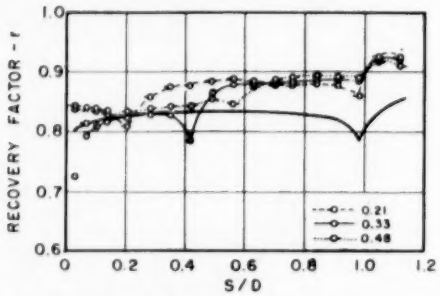

FIG. 6 TYPICAL LOCAL RECOVERY FACTOR DISTRIBUTION FOR 0.0065-IN. NYLON FILAMENT LOCATED AT VARIOUS POSITIONS

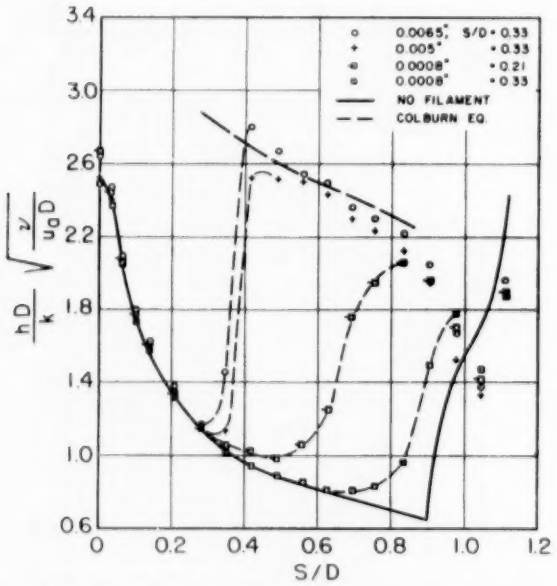

FIG. 7 LOCAL HEAT-TRANSFER COEFFICIENT OVER ELLIPTICAL CYLINDER AT ZERO ANGLE OF ATTACK FOR $1{,}040{,}000 < u_0D/\nu < 1{,}200{,}000$ AND VARIOUS NYLON FILAMENTS

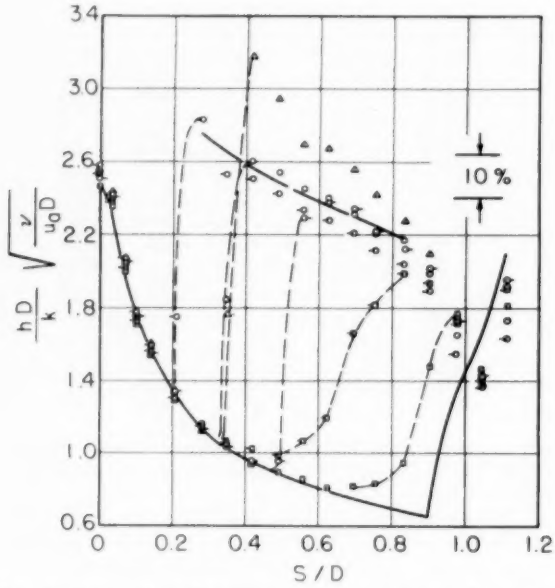

FIG. 8 LOCAL HEAT-TRANSFER COEFFICIENT OVER ELLIPTICAL CYLINDER AT ZERO ANGLE OF ATTACK FOR $932{,}000 < u_0D/\nu < 981{,}000$ AND VARIOUS NYLON FILAMENTS

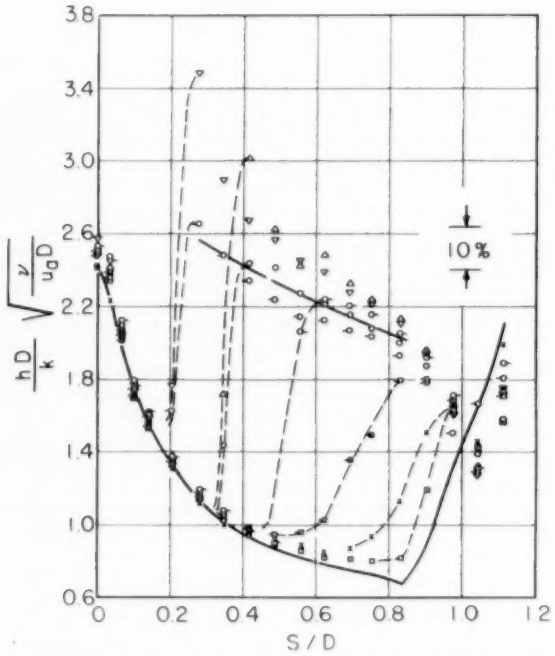

FIG. 9 LOCAL HEAT-TRANSFER COEFFICIENT OVER ELLIPTICAL CYLINDER AT ZERO ANGLE OF ATTACK FOR $756{,}000 < u_0D/\nu < 781{,}000$ AND VARIOUS NYLON FILAMENTS

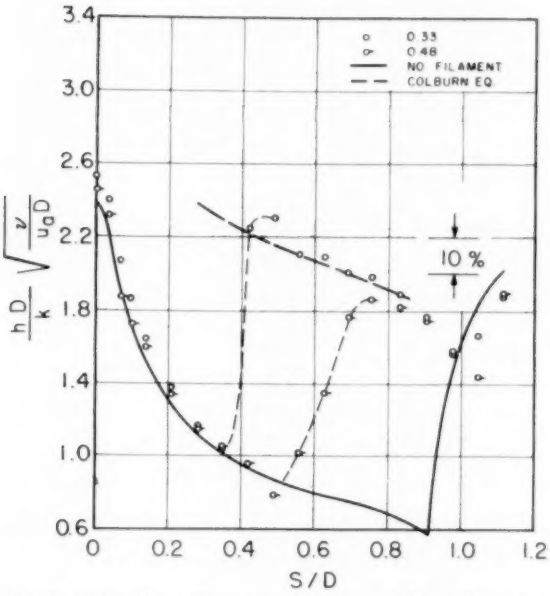

FIG. 10 LOCAL HEAT-TRANSFER COEFFICIENT OVER ELLIPTICAL CYLINDER AT ZERO ANGLE OF ATTACK FOR $531{,}000 < u_a D/\nu < 629{,}000$ AND 0.0065-IN. NYLON FILAMENTS

which the boundary layer is laminar. In this group and in the Reynolds number $u_a D/\nu$ occurring separately, all properties have been evaluated at the stagnation temperature of the air stream.

Some typical results for the pressure coefficient are shown in Figs. 3 and 4. These are representative and illustrate the effect of the roughness element as obtained in these experiments. Two effects are notable, a depression of the local pressure immediately downstream of the roughness element and a change in the behavior of the pressure coefficient over the rear portion of the cylinder. Both effects depend on the relative size and position of the roughness element.

Figs. 5 and 6 reveal results for the recovery factor for the highest air speeds, where the reliability of this quantity is greatest. The presence of the roughness element produces a rise in the recovery factor contrasted to that which obtains for equivalent test conditions and a smooth surface.

Figs. 7, 8, 9, and 10 give the values of the local heat-transfer coefficient for all of the conditions indicated in Table 1 for zero angle of attack. Each of the figures refers to an almost constant Reynolds number and demonstrates the effect of different wire sizes and positions. The curve, shown for the corresponding results with a smooth surface, indicates that in all cases the heat-transfer behavior upstream of the roughness element was unaltered by its presence, and the alteration produced downstream depends on the relative size of the wire. As an aid to the consideration of this effect, Table 1 contains values of the ratio of the size of the element to the momentum thickness at the element position as predicted from the approximate laminar boundary-layer theory (2).

As indicated in Table 1, the effect of a roughness element on the cylinder at a 6-deg angle of attack also was investigated. Fig. 11 reveals a typical set of results for the pressure coefficient, recovery factor, and heat-transfer coefficient for the 0.0065-in. filament at $S/D = 0.33$ for $u_a D/\nu = 817{,}000$. The results at other Reynolds numbers were similar.

When this element was placed at $S/D = 0$, with the 6-deg angle of attack, a substantial increase in the heat transfer took place at

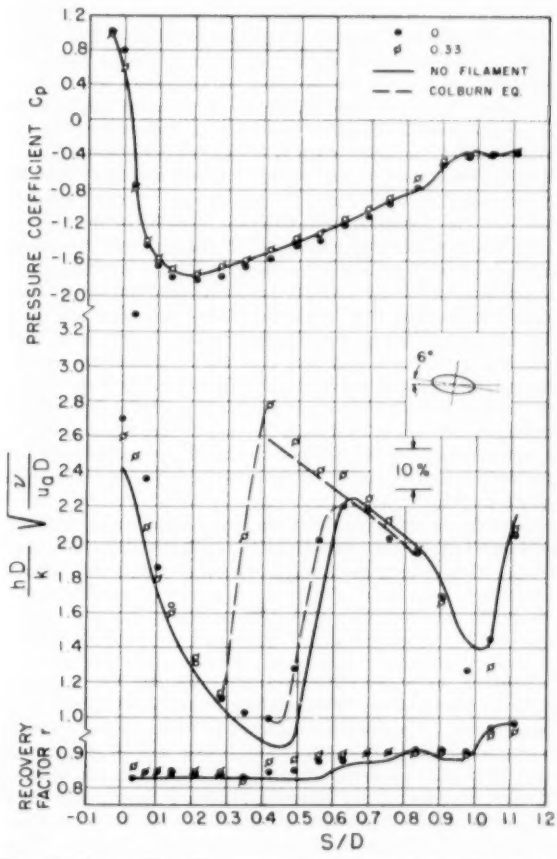

FIG. 11 LOCAL HEAT-TRANSFER COEFFICIENT OVER ELLIPTICAL CYLINDER AT 6-DEG ANGLE OF ATTACK FOR $814{,}000 < u_a D/\nu < 817{,}000$ AND 0.0065-IN. NYLON FILAMENT

the wire. The rise is, however, rapidly damped out and the results coincide with those obtained for the smooth model. The correspondence between the heat-transfer coefficients with and without the nylon filament indicates possible laminar reattachment caused by the large favorable pressure gradient at the filament location. The results for this case are shown in Fig. 11.

DISCUSSION

The most significant effect of the roughness element in the results is the increase in the heat-transfer coefficient which occurs either at or somewhat downstream of the roughness element. This increase is presumably due to a transition to turbulence in the boundary layer, and this presumption is supported by the behavior of the recovery factor, which increases in magnitude in the same region. In cases in which a transition to turbulent flow occurs, the usual design recommendation regarding the prediction of the local heat-transfer coefficient is the use of the Colburn equation, which, for a fluid of Prandtl number equal to 0.70, is

$$\frac{h}{\rho u_1 c_p} = \frac{0.037}{\left(\frac{u_1 x}{\nu}\right)^{1/5}} \qquad [4]$$

This equation is normally construed as being definitely applicable to the case of flow over a flat plate at zero incidence to the stream, with an isothermal wall, but even with this condition it has not

received extensive experimental confirmation, particularly in regard to the constant factor. If Equation [4] is applied to the elliptical cylinder with the velocity u_i taken on a local basis, and distance x taken as the distance from the stagnation point, which is S in the case of zero angle of attack, the predicted values of the heat-transfer coefficient are as shown on the figures containing the results. These predictions are in fair correspondence with most of the results from the point at which transition seems to end up to about $S/D = 0.85$, where the free-stream velocity decreases rapidly. The correspondence obtained is probably due, in the main, to the relative insensitivity of the heat-transfer coefficient as predicted by Equation [4] to the local Reynolds number.

The correspondence between predicted and measured heat-transfer coefficients that is obtained here, and that which was demonstrated in the previous report for the region of laminar boundary-layer flows, indicates that the local heat-transfer coefficient for at least a good portion of bodies of this type can be predicted quite well if the point of transition can be determined. In the present case, at least for all cases with zero angle of attack, transition was influenced by the roughness element, and the point of transition can be compared with available predictions in this regard.

Early suggestions regarding the effect of a single roughness element on a laminar boundary-layer flow indicated that if the magnitude of a Reynolds number for the roughness element

$$\frac{u_i d}{\nu}\sqrt{\frac{c_f}{2}}$$

exceeded a value in the range of 7 to 20, the character of the boundary-layer flow would be affected by its passage over the element. Experiments by Fage (3), dealing primarily with roughness elements of length B and height h, with B generally much larger than h, indicated the roughness element to produce an effect even though the Reynolds number in the foregoing was of a lower value. Fage's results, with the transition point specified mostly from the relative response of surface tubes, were given in the generalized forms

$$\frac{h}{x_t} = 9\,(10^6)\left(\frac{u_i x_t}{\nu}\right)^{-1/3}\left(\frac{B}{x_t}\right)^{1/3};\quad \left(\frac{x_0}{x_t}\right)\left(\frac{B}{x_t}\right)^{1/3} > 0.09 \quad [5]$$

$$\frac{h}{x_t} = 13.5\,(10^6)\left(\frac{u_i x_t}{\nu}\right)^{-1/3}\left(\frac{x_0}{x_t}\right)^{1/3}\left(\frac{B}{x_t}\right);$$

$$\left(\frac{x_0}{x_t}\right)\left(\frac{B}{x_t}\right)^{1/3} < 0.09 \quad [6]$$

In the present experiments, using round filaments as the roughness elements, $d = h = B$, and the circumstances of the experiment were such that Equation [6] would best apply, although the values of length to transition as obtained from either equation would be about the same.

Gazley (4), in a recent review of the effect of roughness elements on transition, presented a figure similar to Fig. 12, which contains lines for the criterion

$$\frac{du_i}{\nu}\sqrt{\frac{c_f}{2}} = \text{const}$$

with line B-B corresponding to a constant of 7 and D-D to a constant of 20. Equation [5] is also shown. The results assembled by Gazley, largely those of Fage, generally confirmed Fage's curve below line D-D and were located in the area between lines B-B and D-D when above line D-D. Most of these latter results were for immediate transition at the wire. Fig. 12 contains results from the present experiments with the point of transition

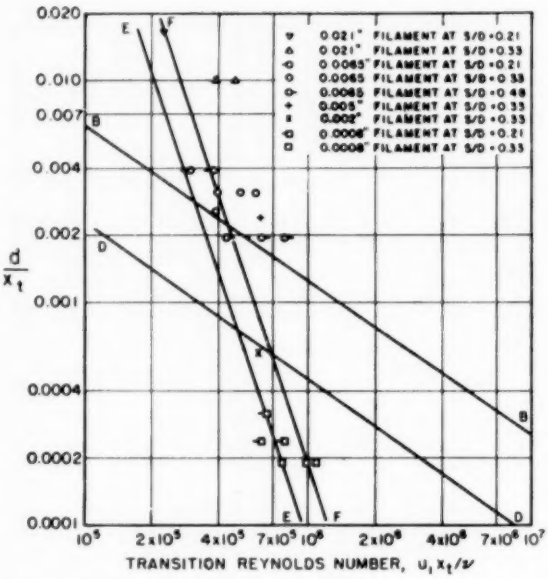

FIG. 12 EFFECT OF NYLON FILAMENT ON BOUNDARY-LAYER TRANSITION

taken where the heat-transfer coefficient first deviates from the trend typical of laminar flow. For these the distances x and S were taken as the same. Alternatively, the distance could have been taken as the distance on a flat plate which would have produced a momentum thickness equal to that predicted for the point considered by the approximate laminar boundary-layer theory. This value is about 60 to 70 per cent of S and, if used, would shift the points on Fig. 12 upward and to the left on a 45-deg line, by this percentage. The experimental scatter and the size of the scale of Fig. 12 are such that this would not have changed the degree of correspondence between the results and Fage's line.

The present results agree with Fage's result to the effect that roughness elements smaller than those specified by line D-D will affect the laminar boundary layer. All the points above line B-B are associated with almost immediate transition and are located in the region of Fage's line. In that connection, line F-F represents Equation [6] with $x_0 = x_t$, and this line may have some utility in indicating immediate transition.

Conversely, had Fage's line been used to predict the point of transition, values reasonable in terms of the experiment would have been obtained, provided that a prediction of transition slightly ahead of the wire would have been construed to mean at the wire. Thus, for most of the cases presented here, the use of the laminar-flow prediction, together with Fage's equation and the use of Equation [4], would have enabled a rather satisfactory prediction of the local heat-transfer coefficient up to the point $S/D = 0.85$.

While Equation [4] predicts the magnitude of the heat-transfer coefficient in the turbulent region, further examination of the behavior of this quantity in this region is dictated by the systematic deviations of the experimental values from the values given by Equation [4]. Further, this additional consideration enables the presentation of some results for the case of a 6-deg angle of attack which have only been alluded to before.

Fig. 13 represents the local Stanton number in terms of the local Reynolds number and presents the line corresponding to Equation [4]. The results shown refer to the region from the

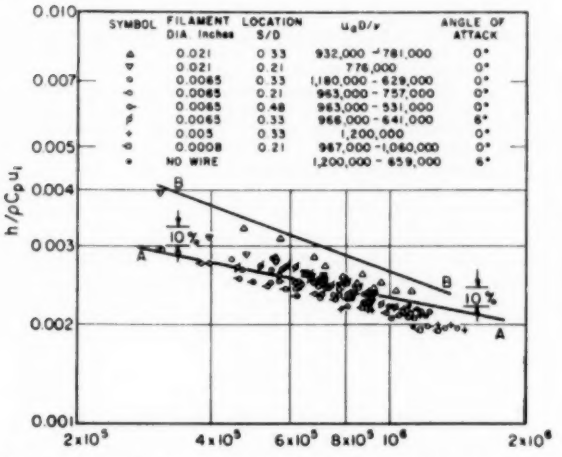

FIG. 13 LOCAL STANTON NUMBER OVER ELLIPTICAL CYLINDER AT 0-DEG AND 6-DEG ANGLE OF ATTACK FOR $x_t/D < S/D < 0.85$ WITH AND WITHOUT NYLON FILAMENT

(A-A, Colburn Equation $h/\rho u_i C_p = 0.037 \left(\frac{u_i x}{\nu}\right)^{-1/5}$; B-B, same, with x taken to make energy content of laminar and turbulent boundary layers the same at the transition point, for case indicated in discussion.)

first point behind the apparent completion of transition, as shown on Figs. 7 through 11, up to $S/D = 0.85$ for zero angle-of-attack runs. For these runs, Fig. 13 reveals the same correspondence as shown in the previous figures. Points for the runs at a 6-deg angle of attack differ from those associated with 0-deg angle of attack in one respect; at zero angle of attack the free-stream velocity is almost constant in the region of S/D considered, while at a 6-deg angle of attack the region of S/D for which points are presented experiences a free-stream velocity decrease of about 10 per cent. The correspondence between these points and Equation [4] is, however, as good as for the case of zero angle of attack.

The position of the points in Fig. 13, in general, depends on the ratio of wire thickness to the momentum thickness of the laminar boundary layer at the wire, with the lowest Stanton number at a given Reynolds number being associated with a small value of this ratio. Improved correspondence between points would be sought in terms of an improved specification of distance S, but such an adjustment involves a number of factors which are not clear individually: (*a*) It already has been noted that the effective "flat-plate" length of the undisturbed laminar boundary layer is less than S. (*b*) The momentum thickness of the boundary layer must increase after the roughness element to account for the drag of the element. This effect is hard to contrast with natural transition, for the change in momentum thickness which occurs in a natural transition is not known. (*c*) While the skin-friction coefficient is expected to be related quite directly to a momentum-thickness Reynolds number, the Stanton number in addition depends on the thermal-energy content of the layer. This has been demonstrated analytically by Rubesin (5) and experimentally by Scesa and Sauer (6) for cases of unheated starting lengths, to the effect that under such conditions Equation [4] satisfactorily approximates the Stanton number when the distance x is measured from the point where heating begins, rather than from that at which the momentum boundary layer begins.

In relation to the data as presented, effect (*a*) is small, (*b*) substantial, and (*c*) substantial, with the (*b*) and (*c*) tending to compensate each other. Curve *B-B* in Fig. 13 reveals the third effect, and is the prediction according to Equation [4] and the postulate that, with instantaneous transition at $S/D = 0.33$ at a Reynolds number $U_\infty D/\nu$ of the order of 1,170,000, the initial value of x in Equation [4] is that which makes the thermal-energy content of the laminar and turbulent layers identical at transition.

Hypothetically, when the roughness element becomes large and the transition becomes more abrupt, the effect of the relative energy content of the boundary layers becomes larger. Such a hypothesis would tend to explain the increased heat transfer under those conditions wherein the momentum thickness must be increased substantially. This is in itself dubious, however, since large heat-transfer coefficients, as obtained with the 0.021-in. filament, do not follow the trend of the other results and produce, in the region behind the wire, recovery factors of continuously fluctuating magnitudes. This suggests a long separation of the flow, with reattachment at a considerable distance downstream.

Finally, the relation between the experimental results and Equation [4] is dependent on the degree to which a flat-plate type of flow is attained downstream of the roughness elements of the type employed. Klebanoff and Diehl (7) found that circular rods were less effective in producing thickened turbulent boundary layers than were roughened surfaces, and that distances of the order of 500 rod diameters might be required to develop a stabilized turbulent flow. Within this region the form parameter H exceeded slightly the final value of 1.40, so that within it the flow was not completely comparable to the "flat-plate" type of flow.

Only very general comments are possible relative to the region downstream of $S/D = 0.85$ at the zero angle-of-attack position, in which the flow decelerates rapidly and eventually separates from the surface. Figs. 3 and 4 reveal that when the boundary layer is turbulent, the pressure recovery begins earlier but the base pressure remains substantially unaltered. In the region of the pressure rise, the prediction of Equation [4] has been continued by methods proposed previously (7) for flows with variable free-stream velocity. Values of the heat-transfer coefficient so predicted are within 8 per cent of the experimental values in the region from $S/D = 0.85$ to the point of the minimum heat-transfer coefficient. This is an improvement over the use of Equation [4] in this region of pressure rise. However, the predicted variation of the form parameter was from the flat-plate value to $H = 1.86$ at $S/D = 1.01$ and this is much lower than the value of $H = 2.8$ indicated by the theory for the point of separation. Since the behavior of the heat-transfer coefficient seems to indicate separation soon after this point, the theory used appears to fail in regard to separation despite the satisfactory prediction regarding the local heat-transfer coefficient.

CONCLUSIONS

The introduction of single spanwise surface-roughness elements into the laminar boundary layer of the 1:3 elliptical cylinder produced an apparent transition to turbulent flow for which, in almost all cases, the local heat-transfer coefficient could be predicted from the Colburn equation as long as the variation in free-stream velocity was not severe. When the ratio θ/d was less than about unity, transition occurred practically at the roughness element and for greater ratios, transition occurred at some downstream point, which could in turn be approximated from Fage's equation. When θ/d was less than 0.10, an extended flow separation appears to have occurred and the local heat-transfer coefficient was substantially higher than that given by Colburn equation.

ACKNOWLEDGMENT

The work reported in this paper was sponsored by the Flight Research Laboratory, Wright Field, Ohio, under Contract AF

33 (038) - 12941 and Contract 33 (616) - 348, and is a part of the program of boundary-layer research being carried out at the University of California, Berkeley, Calif. The authors greatly appreciate this support.

BIBLIOGRAPHY

1 "Local Heat-Transfer Coefficients on the Surface of an Elliptical Cylinder, Axis Ratio 1:3, in a High-Speed Air Stream," by R. M. Drake, Jr., R. A. Seban, D. L. Doughty, and S. Levy, Trans. ASME, vol. 75, 1953, pp. 1291–1302.

2 "Calculation Method for Two-Dimensional Laminar Boundary Layers With Arbitrary Free-Stream Velocity Variation and Arbitrary Wall-Temperature Variations," by R. A. Seban, Institute of Engineering Research, Report 2–12, University of California, 1950.

3 "The Smallest Size of a Spanwise Surface Corrugation Which Affects Boundary-Layer Transition on an Aerofoil," by A. Fage, Great Britain Aeronautical Research Council, Reports and Memoranda No. 2120, 1943.

4 "Boundary-Layer Stability and Transition in Subsonic and Supersonic Flow: A Review of Available Information and New Data in the Supersonic Range," by Carl Gazley, Jr., *Journal of the Aeronautical Sciences*, vol. 20, 1943, pp. 19–28.

5 "The Effect of an Arbitrary Surface-Temperature Variation Along a Flat Plate on the Convective Heat Transfer in an Incompressible Turbulent Boundary Layer," by M. W. Rubesin, NACA TN 2345, 1951.

6 "An Experimental Investigation of Convective Heat Transfer to Air From a Flat Plate With a Stepwise Discontinuous Surface Temperature," by S. Seesa and F. M. Sauer, Trans. ASME, vol. 74, 1952, pp. 1251–1255.

7 "Some Features of Artificially Thickened Fully Developed Turbulent Boundary-Layers With Zero Pressure Gradient," by P. S. Klebanoff and Z. W. Diehl, NACA TN 2475, 1951.

8 "A Calculation Method for the Skin Friction and Heat Transfer of a Turbulent Boundary-Layer With Variable Free-Stream Velocity," by S. Levy and R. A. Seban, Institute of Engineering Research, Report 41-4, University of California, 1951.

Heat Transfer in a Gas-Fired Furnace

By S. J. GENNA,[1] E. J. NOLAN,[2] and A. A. FURCZYK[3]

The general problem of heat transfer in a gas-fired furnace is examined. A method of analysis is introduced for determining the contributions of the various modes of heat transfer. A particular furnace, gas-fired with nonluminous flames, is investigated in the temperature range of 1750 to 2110 F. The results indicate that approximately 80 per cent of the heat is transferred by radiation from the furnace walls to the charge being heated and the remainder by gas convection and gas radiation.

Nomenclature

The following nomenclature is used in the paper:

A_c = projected area of Duradiant burners, sq ft
A = surface area of charge, sq ft
A_w = furnace-wall area, sq ft
C_p = specific heat, Btu, lb_m^{-1}, deg F^{-1}
h_c = convection-heat-transfer coefficient, Btu ft^{-2} hr^{-1} deg F^{-1}
k = thermal conductivity of 347 S.S. Btu ft^{-2} hr^{-1} deg F^{-1} ft
M = mass of charge, lb
Q = heat-transfer rate Btu hr^{-1}
T_c = average Duradiant cup temperature, deg R
T_f = instantaneous temperature of products of combustion, deg R
T_f = average temperature of products of combustion, deg R
$\Delta T_f'$ = deviation of instantaneous flame temperature from mean temperature as a measurable drift, deg F
T_s = instantaneous average temperature of charge, deg R
T_{ss} = instantaneous surface temperature of charge, deg R
T_{sc} = instantaneous center temperature of charge, deg R
T_w = instantaneous wall temperature, deg R
T_w = instantaneous average wall temperature, deg R
$(T_w)_{avg}$ = time average wall temperature, deg R
$\Delta T_w'$ = deviation of instantaneous wall temperature from mean temperature as a measurable drift
χ = distance along cylindrical axis, ft
α_f = absorptivity of products of combustion
θ = time, min
ξ = effective emissivity of charge defined by Equation [10]. (Figs. 4 and 6)
ϵ_f = emissivity of products of combustion
ϵ_s = emissivity of charge defined by Equation [7]
σ = Stefan-Boltzmann constant = 1.71×10^{-8} Btu ft^{-2} hr^{-1} deg R^{-4}
ψ = absorptivity of charge for total effective combustion-products radiation
α_s = absorptivity of charge for black-body radiation
α_s' = absorptivity of charge for combustion-products radiation
α_{ss}'' = absorptivity of charge for wall radiation absorbed by combustion products

Introduction

In a fuel-fired furnace, heat is transferred to the charged material by wall radiation, gas radiation, gas convection, and sometimes by conduction. Although methods for calculation of the foregoing terms while working alone are available in the literature, few quantitative data have been presented to show the relative effect of each when all are present together. Even though the relative importance of the various modes of heat transfer depends upon the furnace temperature employed and the particular furnace design, the designer is helped greatly if in a given case, there is some indication as to what mode of heat transfer predominates.

Sinnott and Siebert (1)[4] published results of forced-convection-heating experiments performed in a furnace 27 × 12 × 14 in. In this furnace a steel plate was heated to temperatures ranging from 600 F to 1200 F, using air at velocities up to 8 fps. By subtracting the computed refractory radiation from measured values of the over-all heat-transfer coefficient, the convection coefficient was obtained. In a particular case, these values showed that at steel-plate temperatures ranging from 150 to 750 F, radiation from the refractory wall was 59 to 73 per cent of the total heat transfer, convection then being 41 to 27 per cent, respectively.

Recently, Hulse (2) pointed out some apparent discrepancies in the convection coefficients of the foregoing authors and suggests the possibility of errors arising in the calculated radiant-heat transmission. If the convection data of Sinnott and Siebert are high, as Hulse suggests, then the percentage of total heat transfer by wall radiation presumably would be even higher than that mentioned before.

Furnaces fired with nonluminous flames can be designed such that the greatest percentage of heat transfer is obtained from the furnace wall.

With the advance of high-speed precision heating under mass-production schedules and high uniformity of quality standards, more emphasis is being placed on methods to increase the heat-transfer rate during industrial heating.

Since the radiant-heat-transfer rate is proportional to the fourth power of the absolute temperature, one would expect that at temperatures encountered in the common production furnace, improved radiation methods would result in increased heat-transfer rates.

It is the object of this investigation to explore the heat-transfer mechanism and to determine the relative percentages of heat transfer by wall radiation, gas radiation, and convection in a furnace to be described, and fired with city gas.

Theory

An equation relating transfer of radiant heat to a charge in an enclosure surrounded by radiating gases, such as a furnace, may be derived with the aid of the following assumptions; these assumptions will be analyzed and corrections made for deviation from optimum experimental conditions:

[1] Research Physicist, Sloan Kettering Cancer Research Institute, New York, N. Y.
[2] Research Engineer, Selas Corporation of America, Philadelphia, Pa.
[3] Chief Development Engineer, Selas Corporation of America.
Contributed by the Heat Transfer Division and presented at the Annual Meeting, New York, N. Y., November 29–December 4, 1953, of The American Society of Mechanical Engineers.
Note: Statements and opinions advanced in papers are to be understood as individual expressions of their authors and not those of the Society. Manuscript received at ASME Headquarters, September 2, 1953. Paper No. 53—A-190.

[4] Numbers in parentheses refer to the Bibliography at the end of the paper.

(*a*) The furnace-wall area is large compared to the charge area and the furnace completely encloses the charge.

(*b*) The radiating surface of the furnace is at a uniform and constant temperature.

(*c*) The combustion products (or furnace gases) are at a uniform and constant temperature.

The net instantaneous radiation heat-transfer rate to a charge in a furnace is given by the difference between the incident radiant flux density (Btu hr^{-1} ft^{-2}) absorbed by the charge and the radiant flux density emitted by the charge. Consequently, the radiant heat-transfer equation takes the form

$$\frac{(Q)}{(A)}\text{ net} = \frac{(Q)}{(A)}\text{ absorbed} - \frac{(Q)}{(A)}\text{ emitted} \quad [1]$$

In the absence of an absorbing gas atmosphere the radiant flux density on the surface of the charge is given by the Stefan-Boltzmann law

$$\sigma T_w^4 \quad [2]$$

since it is assumed, (*a*) and (*b*), that black-body conditions prevail. In an absorbing gas atmosphere, however, a fraction of this radiation, α_f, will be absorbed before reaching the charge. The amount absorbed is

$$\sigma \alpha_f T_w^4 \quad [3]$$

where α_f is a function of the combustion-products-wall-charge geometry and the combustion products and wall temperatures.

In addition to the radiation received from the wall, the charge also receives radiation from the combustion products, carbon dioxide, and water vapor. Denote this by

$$\sigma \epsilon_f T_f^4 \quad [4]$$

where ϵ_f is a function of the combustion-products-wall-charge geometry and the combustion-products temperature. Consequently, the total radiant flux density on the charge is

$$[\sigma T_w^4 - \sigma \alpha_f T_w^4] + \sigma \epsilon_f T_f^4 \quad [5]$$

Only a fraction of the radiant flux density impinging on the charge will be absorbed by it. Generally, assuming nongray-body conditions for the charge, the fraction of the radiation absorbed by the charge will depend upon the spectral distribution of the radiant flux density and upon the temperature of the charge. Denoting by α_s, α_s', and α_s'' the charge absorptivity for black-body radiation, the combustion-products radiation, and the radiation absorbed by the combustion products, respectively, the radiation absorbed by the charge per unit area, per unit time is

$$\underset{\text{absorbed}}{}\left(\frac{Q}{A}\right) = \sigma \alpha_s T_w^4 + \sigma \alpha_s' \epsilon_f T_f^4 - \sigma \alpha_s'' \alpha_f T_w^4 \quad [6]$$

The charge radiates according to the equation

$$\underset{\text{emitted}}{}\left(\frac{Q}{A}\right) = \sigma \epsilon_s T_{ss}^4 \quad [7]$$

Consequently Equation [1] becomes

$$\underset{\text{radiation}}{\text{Net}}\left(\frac{Q}{A}\right) = \sigma[\alpha_s T_w^4 - \epsilon_s T_{ss}^4] + \sigma[\alpha_s' \epsilon_f T_f^4 - \alpha_s'' \alpha_f T_w^4] \quad [8]$$

Equation [8] represents a general instantaneous radiation heat-transfer equation subject to the conditions given previously. Here we note that T_w and T_f are assumed constant. Therefore α_f and ϵ_f are constant for a given combustion-products-wall-charge geometry.

Some simplification of Equation [8] is necessary if any analysis is to be made. Under gray-body conditions for the charge, we would have $\epsilon_s = \alpha_s = \alpha_s' = \alpha_s''$ equals a constant, and Equation [8] would reduce to

$$\underset{\text{radiation}}{\text{Net}}\left(\frac{Q}{A}\right) = \sigma \epsilon_s[T_w^4 - T_{ss}^4] + \sigma \epsilon_s[\epsilon_f T_f^4 - \alpha_f T_w^4] \quad [9]$$

This would offer a considerable simplification of the original equation and an analysis could be performed. Unfortunately, however, deviations from gray-body conditions generally are too large to enable one to employ the foregoing equation as it stands. An equation of this form can be utilized, however, with certain restrictions on the terms.

Consider the first term in Equation [8]; suppose we wish to write this in the form

$$[\alpha_s T_w^4 - \epsilon_s T_{ss}^4] = \xi[T_w^4 - T_{ss}^4] \quad [10]$$

To do this, we note that ξ is a function of T_w and T_{ss}

$$\xi = f(T_w, T_{ss})$$

However, if T_w remains constant then

$$\xi = f(T_{ss})$$

Hereafter, ξ will be referred to as the effective emissivity of the charge.

Similarly one can write

$$[\alpha_s' \epsilon_f T_f^4 - \alpha_s'' \alpha_f T_w^4] = \psi[\epsilon_f T_f^4 - \alpha_f T_w^4] \quad [11]$$

and imposing the conditions that ϵ_f, T_f, α_f, and T_w remain constant we note

$$\psi = f(T_{ss})$$

Consequently, Equation [8] can be written

$$\underset{\text{radiation}}{\text{Net}}\left(\frac{Q}{A}\right) = \sigma \xi[T_w^4 - T_{ss}^4] + \sigma \psi[\epsilon_f T_f^4 - \alpha_f T_w^4] \quad [12]$$

The first term of Equation [12] represents the ordinary heat-transfer equation for radiation to a charge in an enclosure in the absence of radiating and absorbing gases. The second term represents the effect of interposing an absorbing and radiating-gas atmosphere in the furnace. When the furnace-wall temperature and the temperature of the combustion products are identical, the second expression vanishes since $\epsilon_f T_f^4 = \alpha_f T_w^4$. For combustion-products temperatures lower than the wall temperature, the combustion products would absorb more radiant energy from the walls than they radiate, since in this case $\epsilon_f T_f^4 < \alpha_f T_w^4$. Ordinarily the combustion-products temperature is higher than the wall temperature and more radiation is emitted from the gases than is absorbed.

In addition to the total radiation received by the charge, the combustion-products transfer heat by convection according to Newton's law

$$\underset{\text{convection}}{\text{Net}}\left(\frac{Q}{A}\right) = h_c(T_f - T_{ss})$$

The total net heat transfer to the charge by radiation and gas convection now becomes

$$\underset{\text{total}}{\text{Net}}\left(\frac{Q}{A}\right) = \sigma \xi[T_w^4 - T_{ss}^4] + \sigma \psi[\epsilon_f T_f^4 - \alpha_f T_w^4] + h_c[T_f - T_{ss}] \quad [13]$$

In retrospect it will be noted that Equation [13] represents a general furnace-heat-transfer equation. Only assumptions (*a*),

(*b*) and (*c*) have been employed in its derivation. No inquiry need be made into the nature of the combustion-products absorption or emission as long as the combustion products and wall satisfy conditions (*b*) and (*c*) previously given. Consequently, if we neglect the small variation of h_s with charge temperature, the only variables remaining are ξ, ψ, and T_{ss}. The expression written in the foregoing form will permit analysis. Each of the terms can be evaluated quantitatively. As will be shown later, the accuracy of the evaluation necessarily will depend upon the relative magnitude of the individual terms.

Experimental Equipment and Temperature Measurements

All the total-heat-transfer experiments described in this investigation were performed using the sample (charge) shown in Fig. 1 and the furnace illustrated in Fig. 2. The charge was suspended as shown in Fig. 2.

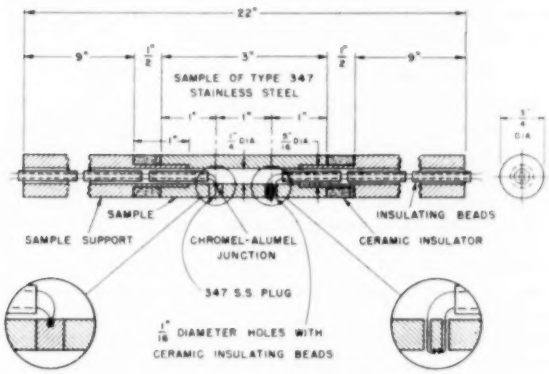

Fig. 1 Diagram of Sample

This furnace was constructed of K-30 Babcock & Wilcox refractory brick and fired with a slightly rich fuel mixture, as explained later, of Philadelphia city gas[5] and air, employing three Selas "Duradiant" burners. The gas and air were premixed in a Selas combustion controller, set at the appropriate gas-air mixture ratio and delivered to the burners at a constant flow rate. No humidification of the combustion air was attempted.

The steady-state furnace-wall temperature was determined by ten 18-gage chromel-alumel calibrated thermocouples, two each in the side walls, end walls, and bottom, as indicated in Fig. 2. These thermocouples were embedded in the furnace walls with their junctions flush with the furnace-wall surface. Each thermocouple junction was covered with approximately $^1/_{64}$-in. layer of milled zircon paste, to protect the junction from the furnace gases and to maintain the thermocouple junction at essentially the same rate of heat transfer that is being received by the flat furnace walls; otherwise the protruding sharp edge of the thermocouple junction would experience a higher heat-transfer rate.

For a furnace fired with the burners mentioned, the temperature of the burner cup is always higher than the furnace-wall temperature. For the purpose of this investigation it was necessary to compensate for the higher cup temperature by evaluating a mean effective wall temperature. Several tests were conducted in which the cup and wall temperature were compared at thermal equilibrium. The cup temperature as a function of the wall

[5] Gross heating value, 700 Btu per cu ft (volume measured at 60 F and 1 atm). A typical analysis of this gas in per cent is as follows: 0.4 illuminants; 3.1 CO; 17.8 H_2; 57.7 CH_4; 1.7 C_2H_6; 2.8 CO_2; 2.3 O_2; 14.2 N_2; therefore the stoichiometric percentage in air = 13.8 per cent.

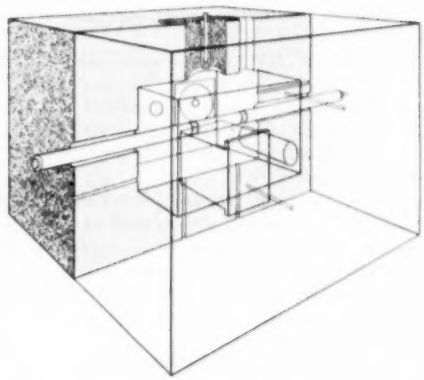

SECTIONAL PERSPECTIVE VIEW OF EXPERIMENTAL GAS-FIRED FURNACE

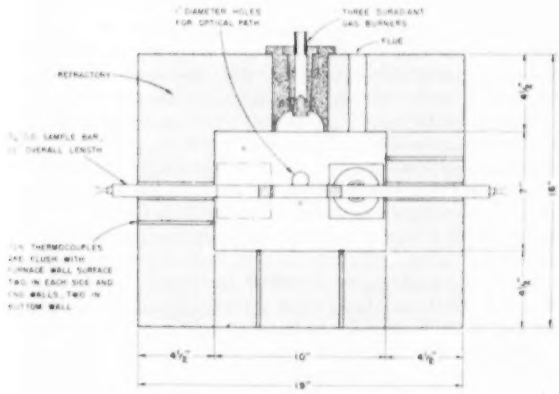

Fig. 2 View of Furnace Showing Sample Placement

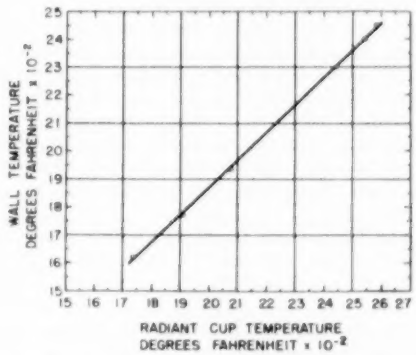

Fig. 3 Variation of Wall Temperature With Cup Temperature

temperature is given in Fig. 3. The instantaneous average wall temperature was then approximated as

$$T_w = \left[\frac{A_w T_w^4 + A_c T_c^4}{A_w + A_c}\right]^{1/4} \quad \ldots\ldots\ldots\ldots [14]$$

A fourth-power average was employed because the heat is

transferred from the wall to the charge according to the Stefan-Boltzmann law.

Since the temperature of the furnace walls dropped significantly when the charge was placed within the furnace, the instantaneous furnace-wall temperature had to be measured. It was found that the thermocouples as employed lagged considerably behind the surface wall temperature, and consequently could not be used for instantaneous readings.

To measure the instantaneous wall temperature a phototube, sensitive in the infrared region, was focused on the wall surface by an appropriate lens system. The phototube response was found to be influenced by the gas-air flow within the chamber. Consequently, independent calibrations were obtained for different gas-air flows in order to compensate for changes in gas-layer density from one test to another.

Because of the fatigue factor influencing the response of the photocell, it was calibrated immediately preceding each test with the appropriate gas-air flow. This was accomplished by establishing equilibrium at various wall temperatures with an air-cooled tube inserted through the furnace. The calibration was obtained by determining millivolt readings in the phototube circuit as compared to the steady-state wall temperature given in Equation [14], under equilibrium conditions for a given gas-air flow. The wall temperature could then be recorded continuously by using an electronic potentiometer in conjunction with the phototube.

The temperature of the combustion products in the furnace (or furnace-gas temperature) was determined by employing the sodium line-reversal method. This method has been described in detail by Jones, Lewis, Friauf, and Perrott (3). The tungsten-comparison radiator was calibrated at the Nela Park Laboratory of the General Electric Company, as brightness temperature in the red versus current. Corrections were made for lens absorption and yellow brightness as described previously (3). The salt (NaCl) was introduced as a spray through a small flue opening in the roof of the furnace as the furnace readings were taken.

When the salt used is not easily dissociated, the emission is localized in the hotter regions of the flame which then alone determines the measured value. If the salt used is dissociated easily, it also will radiate in the lower-temperature regions of the flame. Consequently, as noted by Ribaud, Laure, and Gaudry (4), a certain mean temperature of the different portions of the gases interposed in the path of the radiation from the lamp is obtained. It was observed that a higher D-line intensity could be obtained when using a fuel-rich instead of a fuel-lean mixture. Therefore the fuel-rich mixture would give a higher degree of dissociation. Hence a slightly fuel-rich mixture was used to facilitate readings and obtain a mean temperature.

In determining temperatures of natural gas-oxygen flames, Kaveler and Lewis (5) noticed a similar effect. They attribute the suppression of the sodium-atom concentration to the excess of oxygen in the gases.

The sample (charge) was constructed from a piece of type 347 stainless steel.[6] Fig. 1 illustrates the method of sample support. Both the sample and the sample supports were constructed from identical steel, with the support junction press-fitted into the sample. Ceramic was used to insulate the ends of the sample against longitudinal heat flow.

A special test sample constructed as described, with two 22-gage chromel-alumel thermocouples placed before and after the support junction, was used to determine the heat lost through the sample supports. A negligible longitudinal temperature gradient across the sample support was indicated as noted in the Discussion of Results. The technique employed yielded a sample with negligible heat loss through the ends, such that the heat flow was essentially radial.

Two 22-gage chromel-alumel thermocouples were used in measuring the temperature of the sample. The surface thermocouple was inserted through two $^1/_{16}$-in-diam holes drilled radially so as to minimize any distortion of heat flow. Ceramic beads were used as insulation to prevent the thermocouples from contacting the walls of these holes. The thermocouple leads were attached, the chromel and alumel separately, to the surface by welding them to the sample by the Heliare process.

A space of about $^1/_{16}$ in. separated the two welded chromel-alumel wires at the junction. Thus the temperature measured was essentially that of the surface segment separating the chromel-alumel wires. The center thermocouple was attached to a small plug of identical metal which was press-fitted into the sample.

To insure a constant tight oxide coating on the sample surface, the sample was oxidized at a temperature of 2200 F before any tests were conducted.

Procedure for Determining Emissivity

The first term in Equation [13], $\sigma\xi[T_w^4 - T_{ss}^4]$ represents the heat transfer per unit area to a specimen receiving black-body radiation from the walls, as assumed previously in (*a*). This assumption is more accurate the larger the ratio of furnace-wall area to charge area.

For a given wall charge-area ratio, geometric considerations would give a shape factor which would multiply the term just mentioned, according to the evaluation of the net interchange of energy. Since the geometry of the system employed makes an exact evaluation of the configuration factor prohibitive, the effective emissivity of the charge was determined under experimental conditions. Hence the value of ξ determined in this investigation is the effective emissivity.

Emissivity tests were conducted in a muffle furnace having the exact inside dimensions as the total-heat-transfer furnace illustrated in Fig. 2. The furnace-wall temperatures were determined by two 22-gage chromel-alumel thermocouples suspended in the chamber. Continuous furnace and sample temperatures were obtained using an "Electronik" potentiometer, which recorded the temperature every 2 sec. With time-temperature curves es-

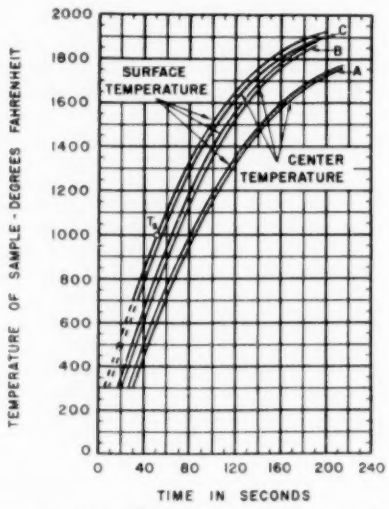

Fig. 4 Radiation Heat Transfer—Time Temperature Curves Used for Emissivity Determination of 347 Stainless-Steel Sample

[6] Analysis, per cent: 0.062 C; 1.11 Mn; 0.12 P; 0.017 S; 0.64 Si; 17.6 Cr; 9.55 Ni; 0.15 Ta; 0.16 Mo; 0.21 Cu; 0.75 Cb; 0.19 Sn; 0.004 Pb; 0.15 W; 0.11 Co; 0.26 Se.

tablished, the effective emissivity is computed by equating the sensible-heat gain per unit time to the radiation loss by the walls as follows

$$MC_p \frac{dT_s}{d\theta} = \sigma A \xi [T_w^4 - T_{ss}^4] \quad \ldots\ldots\ldots\ldots [15]$$

In Equation [15], $dT_s/d\theta$ represents the slope of the average time-temperature curve at the instantaneous mean sample temperature. The slope $dT_s/d\theta$ is taken using the average curve at a time corresponding to a given surface temperature T_s. This is illustrated in Figs. 4 and 5.

For example, the slope corresponding to a surface temperature T_s, Fig. 4, was determined at point P, Fig. 5. When the slope was determined, the equation was solved for ξ and ξ plotted as a function of surface temperature. This is shown in Fig. 6. The specific-heat data used were supplied by the National Bureau of Standards. These data are listed in Table 1.

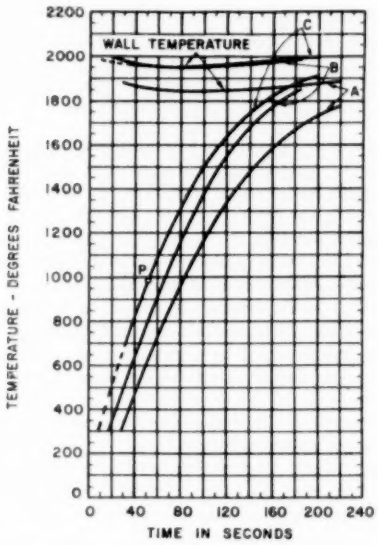

FIG. 5 RADIATION HEAT TRANSFER—AVERAGE SAMPLE TEMPERATURE FROM FIG. 4 AND WALL TEMPERATURE IN TESTS A, B, AND C

TABLE 1 MEAN SPECIFIC HEAT OF STAINLESS-STEEL TYPE 347 (6)

Temperature, deg F	Specific heat, Btu lb^{-1} deg F^{-1}
32	0.110
212	0.118
392	0.123
572	0.128
752	0.133
932	0.137
1112	0.141
1292	0.145
1472	0.149
1652	0.152

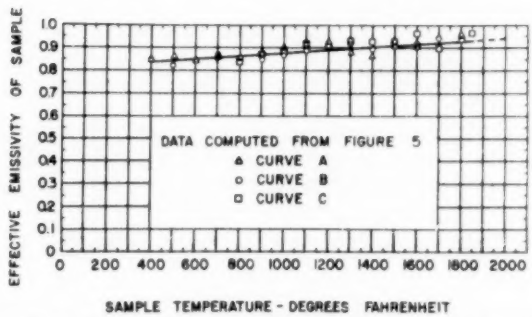

FIG. 6 EFFECTIVE EMISSIVITY OF 347 STAINLESS STEEL; OXIDIZED INITIALLY AT 2200 F

PROCEDURE FOR DETERMINING TOTAL INSTANTANEOUS HEAT-TRANSFER RATE

To evaluate total instantaneous heat-transfer rates, time-temperature curves for the sample were obtained for various gas-fired furnace temperatures. The time-temperature curves are illustrated in Figs. 7 and 8. For each experiment the sample and instantaneous average furnace-wall temperatures were recorded continuously and the flame temperature was noted immediately before and after each run. The methods used to determine these variables were described previously.

The total instantaneous heat-transfer rate to the sample is given by the average sensible-heat change of the sample per unit time

$$\frac{Q}{A} = \frac{M}{A} C_p \frac{dT_s}{d\theta} \quad \ldots\ldots\ldots\ldots [16]$$

Hence the rate of heat transfer at any instant may be determined by differentiating the average time-temperature curve and multiplying by the appropriate factors, as shown previously. The average time-temperature curve was graphically differentiated at time increments corresponding to 100-deg F increments of the surface temperature of the sample. A discrete number of instantaneous heat-transfer rates as a function of the surface temperature of the sample were thus obtained.

It was noted that the furnace-wall temperature dropped significantly as the sample was introduced into the furnace. In addition to the furnace-wall temperature varying with time, the temperature of the combustion products also varied.

Independent tests were conducted to determine the magnitude of the flame-temperature variation. A cold bar of 347 SS, pretreated in the same manner as the sample bar, with the same dimensions as the sample was introduced into the furnace and the average temperature of the combustion products in the furnace was determined every 20 sec. During this time, the furnace-wall temperature was recorded continuously. The results of these tests show that for the experiments conducted herein, the average temperature of the combustion products varies by an amount which is approximately 80 per cent of the variation in the average furnace-wall temperature.

The heat-transfer rates obtained by Equation [16] represent the rates at instantaneous sample, wall, and combustion-products temperature. In order to obtain more easily interpreted data, it is desirable to simplify the results by obtaining heat-transfer rates for a given set of steady-state wall and temperatures. Heat-transfer rates for a constant wall temperature can be approximated by adding to both sides of the total-heat-transfer equation the correction term

$$\frac{\Delta}{A} = \sigma \xi [(T_w)_{avg}^4 - T_w^4] \quad \ldots\ldots\ldots\ldots [17]$$

where

$(T_w)_{avg}$ = time average furnace-wall temperature; i.e., the average of T_w, taken over a finite time period.

Equation [13] now becomes

$$\frac{M}{A} C_p \frac{dT_s}{d\theta} + \frac{\Delta}{A} = \sigma \xi [(T_w)_{avg}^4 - T_{ss}^4]$$

$$+ \sigma \psi [\epsilon_f T_f^4 - \alpha_f \bar{T}_w^4] + h_c (T_f - T_w) \quad \ldots [18]$$

Equation [18] contains a constant wall temperature in the first term on the right while the last two terms still contain the instantaneous furnace-wall and combustion-products temperatures, respectively.

Although the reduction to a given state of static conditions is not complete, it will be shown that a negligible error is introduced due to neglecting the variable wall and combustion-products temperatures in the last two terms. For the present, therefore, we shall consider the combustion products and wall temperature as constant and defer a discussion of the errors introduced by this assumption until later in the paper. The furnace-wall temperature used is the arithmetic average of the instantaneous average wall temperatures. The combustion-products temperatures correspond to the average of readings taken before and after each test.

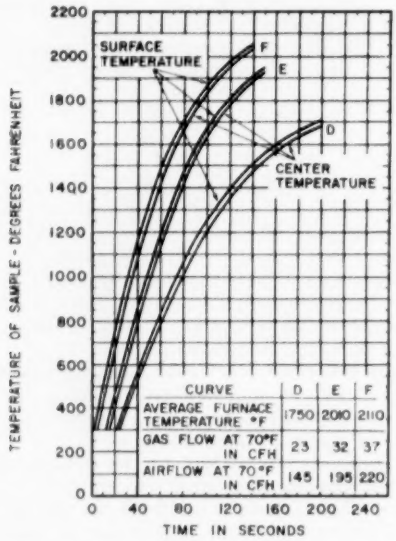
SURFACE TEMPERATURE
CENTER TEMPERATURE
F
E
D
TEMPERATURE OF SAMPLE - DEGREES FAHRENHEIT
TIME IN SECONDS
CURVE | D | E | F
AVERAGE FURNACE TEMPERATURE °F | 1750 | 2080 | 2110
GAS FLOW AT 70°F IN CFH | 23 | 32 | 37
AIRFLOW AT 70°F IN CFH | 145 | 195 | 220

FIG. 7 TOTAL HEAT TRANSFER—TIME TEMPERATURE CURVES OF 347 STAINLESS-STEEL SAMPLE

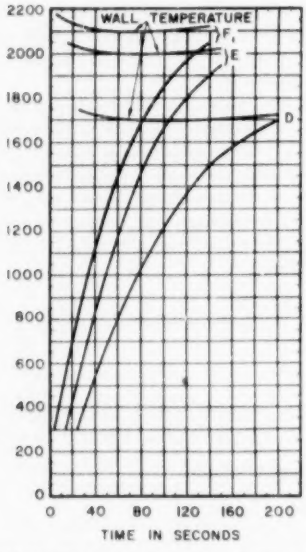

FIG. 8 TOTAL HEAT TRANSFER; AVERAGE SAMPLE TEMPERATURE FROM FIG. 7, AND WALL TEMPERATURES IN TESTS D, E, AND F

DISCUSSION OF RESULTS

Figs. 9, 10, and 11 show the results of three independent experiments. The total heat-transfer rates were obtained in the manner previously described. The wall radiation heat transfer was computed by using the results obtained in the emissivity investigation, Fig. 5, and the average wall temperature for each experiment. The difference between the two curves yields the net heat transferred by combined gas radiation and convection. The latter curve approximated a straight line.

Although a straight line is not actually expected for the net heat-transfer rate by gas radiation and convection, it was felt by the authors that the inherent experimental errors did not permit a more accurate determination of the shape of the curve. The straight line represents an approximation to the equation

$$\frac{Q}{A} = \sigma\psi[\epsilon_f T_f^4 - \alpha_f \bar{T}_w^4] + h_c(T_f - T_{as}) \ldots\ldots [19]$$

If we neglect the variation in this equation due to the variation of $\psi(T_{as})$ and h_c with the sample temperature, the first term represents a constant heat-transfer rate, since T_f and $\bar{T}_w$ are taken as constants; while the second term is a straight line, of slope $-h_c$, intersecting the abscissa at $T_{as} = T_f$. Consequently, the line drawn parallel to the line obtained as the difference between the total and wall-radiation heat-transfer rates, and intersecting the abscissa at $T_{as} = T_f$, represents the average convection-heat-transfer rate. The difference between the two parallel lines yields the average gas-radiation heat-transfer rate. This method of approximation is justified in view of the magnitude of the experimental errors.

Fair agreement is found between measured and computed values of the gas-radiation term.

Both experimental errors and errors due to the approximations made in the experiment will be considered. The former includes errors in temperature measurements, error due to heat lost through the sample supports, and errors in graphical differentiation. Since the curves for the convection plus gas-radiation heat transfer were obtained from the total and wall-radiation heat-transfer curves, an estimate of the probable error in both curves will be made. Later, results will be interpreted in terms of the probable error in convection and gas-radiation heat-transfer data.

It is assumed that no correction need be applied to the total heat transfer due to the variation of wall and combustion-products temperature in the last two terms of Equation [18]. The variation of the average instantaneous wall temperature with time is shown in Fig. 8. The combustion-products-temperature variation was approximately 80 per cent of the wall-temperature variation, as noted earlier. Therefore the errors due to the assumptions made in the experiment can be summed up as

$$\frac{\Delta Q}{Q} = \frac{4\sigma\psi[\epsilon_f T_f^3 \Delta T_f' - \alpha_f (T_w)_{avg}^3 \Delta T_w'] + h_c \Delta T_f'}{Q/A} \ldots [20]$$

where the primes indicate a deviation from the mean as a measurable drift; while unprimed Δ terms indicate a probable spread.

Therefore, using the foregoing probable errors, and making the approximation $\epsilon_f \approx \alpha_f$, the error can be approximated as

$$\frac{\Delta Q}{Q} = \frac{4\sigma\psi\alpha_f[0.8\bar{T}_f^3 - (\bar{T}_w)_{avg}^3]\Delta T_w' + 0.8h_c \Delta T_w'}{Q/A} \ldots [21]$$

Actually, $\epsilon_f < \alpha_f$ since the combustion-products temperature is higher than the wall temperature. The assumption that they are equal yields a more conservative approximation of error.

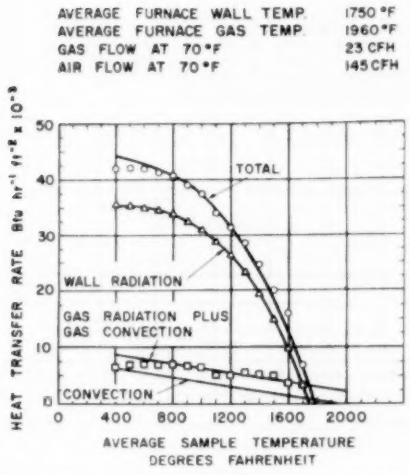
AVERAGE FURNACE WALL TEMP. 1750 °F
AVERAGE FURNACE GAS TEMP. 1960 °F
GAS FLOW AT 70 °F 23 CFH
AIR FLOW AT 70 °F 145 CFH
HEAT TRANSFER RATE Btu hr⁻¹ ft⁻² x 10⁻³
TOTAL
WALL RADIATION
GAS RADIATION PLUS GAS CONVECTION
CONVECTION
AVERAGE SAMPLE TEMPERATURE DEGREES FAHRENHEIT

FIG. 9 TEST D ANALYSIS OF HEAT TRANSFER IN A GAS-FIRED FURNACE; AVERAGE FURNACE TEMPERATURE, 1750 F

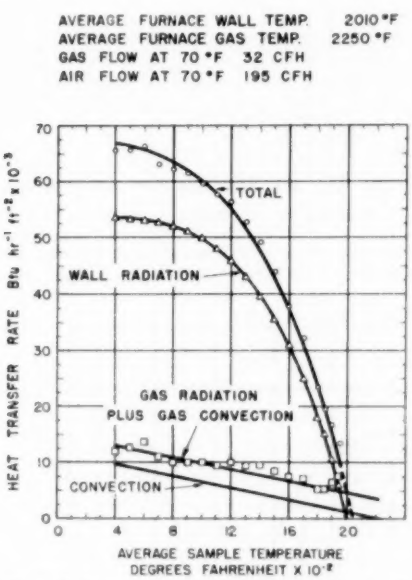
AVERAGE FURNACE WALL TEMP. 2010 °F
AVERAGE FURNACE GAS TEMP. 2250 °F
GAS FLOW AT 70 °F 32 CFH
AIR FLOW AT 70 °F 195 CFH
HEAT TRANSFER RATE Btu hr⁻¹ ft⁻² x 10⁻³
TOTAL
WALL RADIATION
GAS RADIATION PLUS GAS CONVECTION
CONVECTION
AVERAGE SAMPLE TEMPERATURE DEGREES FAHRENHEIT X 10⁻²

FIG. 10 TEST E ANALYSIS OF HEAT TRANSFER IN A GAS-FIRED FURNACE; AVERAGE FURNACE TEMPERATURE, 2010 F

The probable error in wall-temperature measurement as computed for Fig. 8, test F, is 6 deg F. The combustion-products-temperature measurement, is assumed correct to within 10 deg F, since the current through the standard lamp circuit could be read to within that degree of accuracy. Assuming the errors are additive

$$\frac{\Delta Q}{Q} = \frac{4\sigma\xi(\bar{T}_w)_{avg}^3\Delta T_w + 4\sigma\psi\alpha_f[\bar{T}_f^3\Delta T_f + (\bar{T}_w)_{avg}^3\Delta T_w] + h_c\Delta T_f}{Q/A} \quad \ldots\ldots [22]$$

In addition to the foregoing temperature errors, errors are encountered in sample temperature measurement

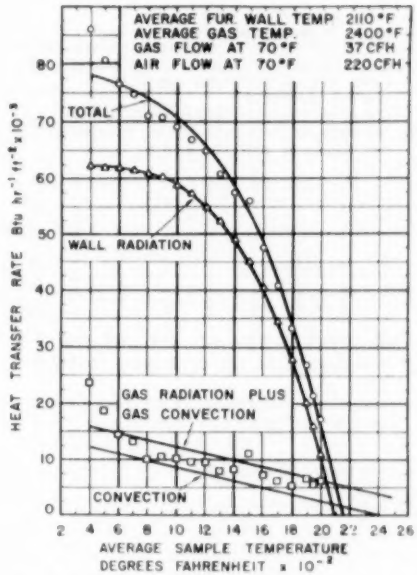
AVERAGE FUR. WALL TEMP. 2110 °F
AVERAGE GAS TEMP. 2400 °F
GAS FLOW AT 70 °F 37 CFH
AIR FLOW AT 70 °F 220 CFH
HEAT TRANSFER RATE Btu hr⁻¹ ft⁻² x 10⁻³
TOTAL
WALL RADIATION
GAS RADIATION PLUS GAS CONVECTION
CONVECTION
AVERAGE SAMPLE TEMPERATURE DEGREES FAHRENHEIT x 10⁻²

FIG. 11 TEST F ANALYSIS OF HEAT TRANSFER IN A GAS-FIRED FURNACE; AVERAGE FURNACE TEMPERATURE, 2110 F

$$\frac{\Delta Q}{Q} = \frac{4\sigma\xi T_{av}^3\Delta T_{av} + h_c\Delta T_{av}}{Q/A} \quad \ldots\ldots [23]$$

The error in sample temperature measurement is approximated as 3 deg F.

The longitudinal heat flow through the supports was determined by using a sample with thermocouples placed immediately before and after the thin supporting tube. The resulting error in heat-transfer determination is given by

$$\frac{\Delta Q}{Q} = \frac{2kA\dfrac{dT_s}{dx}}{Q} \quad \ldots\ldots [24]$$

The maximum difference was measured to be 20 F at a sample temperature of 700 F, becoming less at higher and lower sample temperatures. Using the maximum temperature difference, the conduction heat lost is approximately 130 Btu hr^{-1} ft^{-2}.

The method of graphical differentiation introduces an error due to the difficulty in judging the slopes accurately. Although this error cannot be computed, an approximate error estimation based on the deviations in slope measurements taken at different times can be used. This per cent error is larger for the smaller slopes, ranging from approximately 0.5 per cent to 3 per cent in order of increasing sample temperatures.

The probable error in the total heat-transfer curve is summarized in Fig. 12. The errors were computed from the foregoing analysis using the data obtained from test F.

The accuracy of the emissivity results depends primarily on the error in the specific-heat determination, and the experimental errors of temperature measurements and slope determinations. The error in the specific heat is believed to be less than 3 per cent by the National Bureau of Standards. The error introduced through graphical differentiation varies from about 0.5 per cent to 3.5 per cent. Wall-temperature and sample-temperature measurements are believed to be accurate to within 3 deg F. Consequently, assuming fractional errors are additive, the error

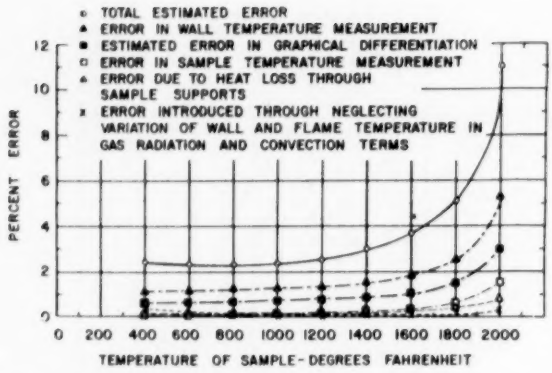
TOTAL ESTIMATED ERROR
ERROR IN WALL TEMPERATURE MEASUREMENT
ESTIMATED ERROR IN GRAPHICAL DIFFERENTIATION
ERROR IN SAMPLE TEMPERATURE MEASUREMENT
ERROR DUE TO HEAT LOSS THROUGH SAMPLE SUPPORTS
ERROR INTRODUCED THROUGH NEGLECTING VARIATION OF WALL AND FLAME TEMPERATURE IN GAS RADIATION AND CONVECTION TERMS
PERCENT ERROR
TEMPERATURE OF SAMPLE - DEGREES FAHRENHEIT

FIG. 12 ESTIMATION OF THE INSTANTANEOUS ERROR IN THE TOTAL HEAT-TRANSFER CURVE IN TEST F OF FIG. 11

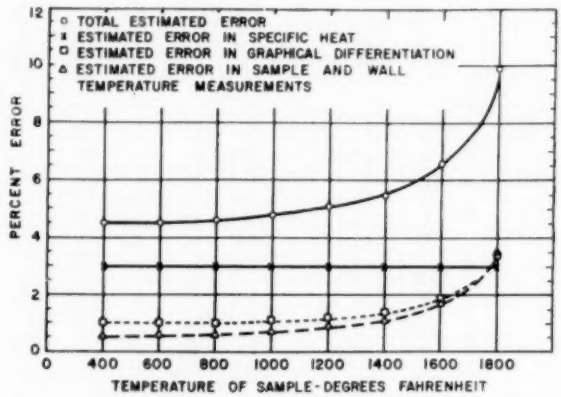
TOTAL ESTIMATED ERROR
ESTIMATED ERROR IN SPECIFIC HEAT
ESTIMATED ERROR IN GRAPHICAL DIFFERENTIATION
ESTIMATED ERROR IN SAMPLE AND WALL TEMPERATURE MEASUREMENTS
PERCENT ERROR
TEMPERATURE OF SAMPLE - DEGREES FAHRENHEIT

FIG. 13 TEST C ESTIMATION OF THE INSTANTANEOUS ERROR IN THE EMISSIVITY DETERMINATION OF FIG. 6

in temperature measurements introduces a fractional error in the emissivity given by

$$\frac{\Delta\xi}{\xi} = \frac{4[(T_w)_{avg}^3 + T_{as}^3]\Delta T}{(T_w)^4 - T_{as}^4} \qquad [25]$$

The numerator of the term on the right side contains a sum, since the errors are assumed to be additive

The combined probable error in emissivity data obtained from Fig. 5, curve C, is compiled in Fig. 13.

Figs. 12 and 13 give the maximum possible error in the total heat-transfer and radiation heat-transfer curves. Each total error curve is subdivided in the foregoing manner. In all the error computations it has been assumed that the errors are additive in order to arrive at a more conservative estimate.

The probable error in convection plus gas-radiation heat trans-

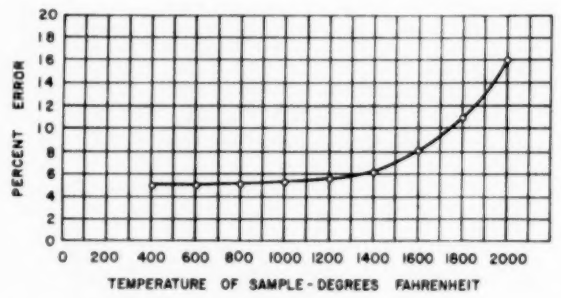

FIG. 14 ESTIMATION OF THE INSTANTANEOUS ERROR IN THE GAS RADIATION AND CONVECTION TERMS, TESTS F AND C

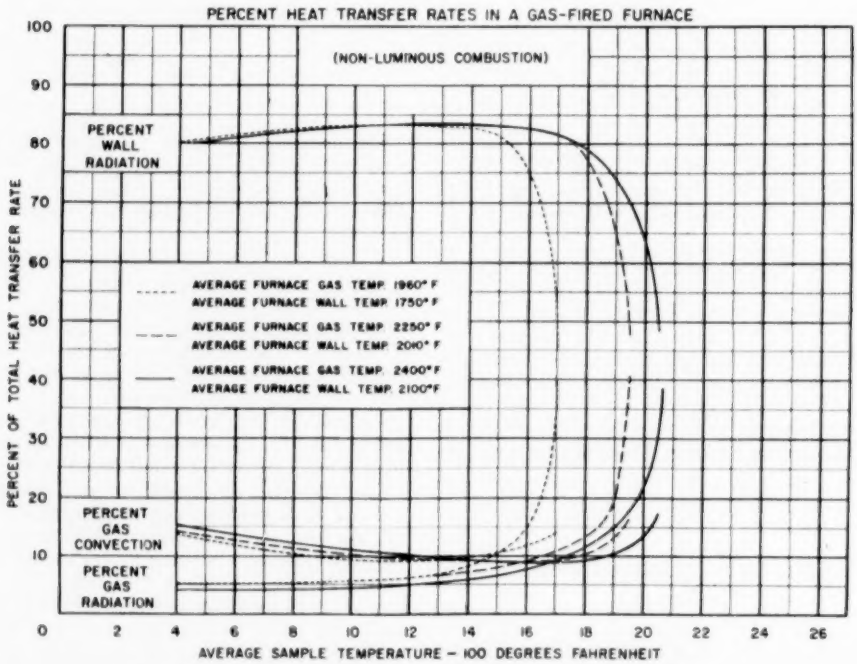
PERCENT HEAT TRANSFER RATES IN A GAS-FIRED FURNACE
(NON-LUMINOUS COMBUSTION)
PERCENT WALL RADIATION
AVERAGE FURNACE GAS TEMP. 1960° F
AVERAGE FURNACE WALL TEMP. 1750° F
AVERAGE FURNACE GAS TEMP. 2250° F
AVERAGE FURNACE WALL TEMP. 2040° F
AVERAGE FURNACE GAS TEMP. 2400° F
AVERAGE FURNACE WALL TEMP. 2100° F
PERCENT GAS CONVECTION
PERCENT GAS RADIATION
PERCENT OF TOTAL HEAT TRANSFER RATE
AVERAGE SAMPLE TEMPERATURE – 100 DEGREES FAHRENHEIT

FIG. 15 PER CENT HEAT-TRANSFER RATES IN A GAS-FIRED FURNACE

fer of test F, Fig. 11, is given in Fig. 14 as a function of the sample temperature. This was obtained using the root mean square of the errors in Figs. 12 and 13.

The per cent error, in the convection plus gas-radiation heat-transfer curves, varies from 5 per cent at a sample temperature of 400 F, to an estimated 16 per cent for a sample temperature of 2000 F. Consequently, the results obtained for higher temperatures are inconclusive. An approximation to the convection and gas-radiation heat transfer has been made by assuming that h_c is independent of the sample temperature T_s, and neglecting the variation in the gas-radiation term due to the variation of ξ. This method of approximation should yield the correct values for the convection and gas-radiation terms to within 10 per cent.

Conclusions

The results of three independent experiments conducted at furnace-wall temperatures of 1750 F, 2010 F, and 2110 F are summarized in Fig. 15 in terms of the percentage of the total heat-transfer rates contributed by the various modes of heat transfer. It is seen from these curves that wall radiation is the predominant mode of heat transfer.

The relative percentage of the various modes of heat-transfer rates essentially is constant at the three furnace temperatures. It is reasonable to believe, therefore, that higher furnace temperatures would not alter the results materially. Since the relative gas-input rates are equivalent to what might be expected in industrial furnaces, the relative percentage of the heat-transfer rates should not be altered greatly in a totally enclosed though larger industrial furnace of similar geometry.

The analysis presented is not intended to supersede any method that is used primarily to evaluate radiation, convection, and gas-radiation heat-transfer rates independently. Its usefulness is felt only when a combination of the foregoing modes of heat transfer is present and independent evaluation would be forbidden.

Obviously, the per cent errors obtained in the evaluation of the convection and the gas-radiation heat-transfer curves will be high when their contribution to the total heat transfer is small. In the present experiments the wall radiation contributed approximately 80 per cent of the total heat-transfer rate. Furthermore, since the convection and gas-radiation heat-transfer rates were obtained by a method of differences, a large probable error should be expected.

In ordinary applications, one is not necessarily interested in high accuracy in the determination of relatively small percentages of heat transfer. The method of analysis should prove valuable where one is primarily interested in the per cent accuracy of the finished product, namely, total heat-transfer rates; and for gaining further insight into the relative importance of the three modes of heat transfer.

BIBLIOGRAPHY

1 "Heat Transfer in a Recirculating Furnace," by M. J. Sinnott and C. A. Siebert, *Industrial and Engineering Chemistry*, vol. 40, 1948, pp. 1039-1044.

2 "Convection and Non-Luminous Gas Radiation in Furnace Heating," by C. Hulse, *Sheffield University Fuel Society Journal*, vol. 3, 1952, pp. 32–38.

3 "Flame Temperatures of Hydrocarbon Gases," by G. W. Jones, B. Lewis, J. B. Friauf, and G. St. J. Perrott, *Journal of the American Chemical Society*, vol. 53, 1931, pp. 869–883.

4 "The Measurement of Flame Temperatures," by G. Ribaud, Y. Laure, and H. Gaudry, *Journal of the Institute of Fuel*, Symposium on Gas Temperature Measurement, vol. 12, March, 1939, pp. S-18–S-30.

5 "Flame Temperatures and Vertical Gradients in Natural-Gas Flames," by H. H. Kaveler and B. Lewis, *Chemical Reviews*, vol. 21, 1937, pp. 421–429.

6 "National Bureau of Standards, Private Communication."

Discussion

Victor Paschkis.[7] This paper is so well designed logically that each step is of importance. With this in mind, two questions arise regarding Equation [14] and Fig. 3.

In the figure, the wall temperature is directly related to the cup temperature. It would appear to the writer as if this relationship would change with the heat output of the burners; the relationship determined in an empty furnace should not hold for a furnace with high heat demand.

Similarly, a different curve must be expected for furnaces of different design, with either more cups per unit area, or different sizes.

How significant these changes would be for the final results depends on the relative magnitudes in Equation [14]. If they are significant, the conclusion that the results of the work can be directly applied to industrial furnaces would be doubtful.

Authors' Closure

The authors wish to thank Dr. Paschkis for his discussion of their paper.

The questions raised by Dr. Paschkis are well taken and are somewhat pertinent in the extrapolation of the results given in the paper to other similar furnace designs.

It should be noted that Equation [14] represents instantaneous average furnace wall temperature values, while the temperature used as a basis for calculation is the time average furnace wall temperature, noted in Equation [18]. The instantaneous average furnace wall temperature and the time average furnace wall temperature are, of course, inter-related and this relationship is given by Equation [17].

In the experiments reported herein, the maximum deviation between the instantaneous average furnace wall temperature as given by Equation [14] and the time average furnace wall temperature, as noted in Equation [18], was 45 deg F. This deviation took place during Test F, Fig. 8, at the moment the cold test sample was introduced into the furnace; the equilibrium furnace temperature before introduction of the test sample being considerably in excess of 2100 F.

As implied in the paper, the relationship between burner cup and wall temperature shown in Fig. 3 was determined by varying the heat output of the burners, waiting until equilibrium was established, then noting the pertinent experimental data.

In this instance, Fig. 3 shows a linear relationship between cup and wall temperature. Whether this exact relationship exists under non-equilibrium conditions could not be determined because of experimental difficulties.

Substitution of the proper quantities into Equation [14] will show that the contribution of the cup temperature to the instantaneous average wall temperature is small (about 10 to 15 deg F) because the cup area is small compared to the total wall surface area. Nevertheless, the contribution of the cup temperature should be considered because the instantaneous average wall temperature is finally raised to the fourth power. In properly designed furnaces the ratio of furnace wall to charge area is most important and the ratio of cup area to furnace wall area must exceed a certain value, according to the dictates of general heat transfer principles, among which is configuration factor geometry.

Data taken in the field indicate that under controlled operating conditions, a difference of about 100 to 150 deg F exists between wall and cup temperature. Since in the normal furnace the cup area is small compared to the total wall area, one would not expect a large dependence of cup temperature on the instantaneous average temperature defined by Equation [14]. In a particu-

[7] Technical Director, Heat and Mass Flow Analyzer Laboratory, Columbia University, New York, N. Y. Mem. ASME.

lar case, which is also a severe one, a 300 deg F difference in temperature existed between the cup temperature and the wall temperature. This large difference in temperature between the cup and the wall increased the instantaneous average temperature T_w of Equation [14] only 30 deg F above its initial equilibrium value. This would change the error curve in Fig. 12 about $1^1/_2$ per cent.

In summarizing, it may be said that in the design of the usual furnace the ratio of burner cup area to wall area is small enough so that even a substantial temperature difference between burner cup and wall does not change the instantaneous average temperature appreciably. Based on experiences in the field and the results of the present experiment, the authors believe that the changes mentioned by Dr. Paschkis are not significant and therefore the conclusions reached as to the projection of results found herein into other furnaces of similar design would be substantiated.

A Review of Thermal-Radiation Constants

By N. W. SNYDER,[1] BERKELEY, CALIF.

A survey of engineering literature and some of the recent textbooks in heat transfer indicates a lack of knowledge by the authors that the various radiation constants used are no longer valid. The various radiation constants, as reported in the CGS system of units by Birge (3),[2] have been ignored, as well as the recent work of Dumond and Cohen (13) who have further refined the constants reported by Birge. The one particular constant which seems to vary from reference to reference is the Stefan-Boltzmann constant, σ. Values appear to range from 1723×10^{-12} Btu/hr ft² deg R⁴ to 1740×10^{-12}. An investigation by the author of the atomic constants presented by Birge, and Dumond and Cohen indicates that this constant should be 1714×10^{-12}. A complete discussion concerning the various constants is given in the paper.

Introduction

COMPUTATION of the radiant energy emitted by a surface requires a knowledge of several constants which have been determined experimentally, directly, or indirectly. The basic equation used for determining the emission is that developed by Planck for the emission of radiant energy from an ideal radiator at a given temperature T and wave length λ. It is written as

$$E_{\lambda,T} = \frac{C_1}{\lambda^5} \frac{1}{e^{\frac{C_2}{\lambda T}} - 1} \quad \ldots\ldots\ldots\ldots\ldots\ldots [1]$$

where

$E_{\lambda,T}$ = monochromatic radiosity or monochromatic emissive power from an ideal radiator at temperature T, ergs/sec cm²(cm)
λ = wave length of radiation, cm
C_1 = first radiation constant erg cm²/sec
C_2 = second radiation constant, cm deg K

A precise determination of $E_{\lambda,T}$ for a Planckian (ideal) radiator requires a precise knowledge of C_1 and C_2 with λ and T given.

Values of the Temperature

For experimental work, the value of T is obtained by means of some temperature-measuring device, for instance, a thermocouple. This thermocouple may be calibrated according to the International Temperature Scale of 1948 (11) (see Table 1) which would yield temperatures in deg C. By knowing the ice point in deg K all determinations made with the thermocouple in deg C could then be reduced to Kelvin's thermodynamic scale. The value of the ice point in deg C has been designated by the 1948 International Temperature Scale as zero. However, the NBS has designated that the triple point of water is more reproducible and is used for great precision. The value is given as 0.0100 deg C at the triple point (12). In terms of the thermodynamic scale, Beattie (1) has indicated a value of 273.165 ± 0.02 deg K and Birge (3) has reported a value of 273.16 ± 0.01 deg K for the ice point.

TABLE 1 FUNDAMENTAL AND PRIMARY FIXED POINTS AT A PRESSURE OF 1,013,250 DYNES/CM² PRESSURE (14.696 PSIA)

Fixed point	Temperature, deg C
(a) Oxygen point (boiling point)	182.97
(b) Ice point (fundamental fixed point) (equilibrium between ice and air-saturated water)	0.00
(c) Steam point (fundamental fixed point) (boiling point)	100.00
(d) Sulphur point (boiling point)	444.60
(e) Silver point (freezing point)	960.80
(f) Gold point (freezing point)	1063.00

NOTE: Standard instruments to be used are platinum-resistance thermometer (−182.97 → 630.5 C range); platinum-platinum-10 per cent rhodium alloy (630.5 → 1063 C range); and above 1063 C an optical pyrometer.

The International Temperature Scale of 1948 has set several basic calibration points using different substances at their freezing points or boiling points. The highest of these is the gold point at 1063 C determined by Day and Sosman (9). (See Table 1.)

Above the gold point, the temperature scale is extended by making use of Planck's equation. By comparing the brightness at a given wave length of an ideal radiator at the freezing point t deg C of a substance with the brightness of an ideal radiator at the gold point one can determine the ratio of $E_{\lambda,T}/E_{\lambda,Au}$. Using Planck's equation

$$\frac{E_{\lambda,(t+273.16)}}{E_{\lambda,T_{Au}}} = \frac{\frac{C_2}{e^{\lambda T_{Au}} - 1}}{\frac{C_2}{e^{\lambda(t+273.16)} - 1}} \quad \ldots\ldots\ldots [2]$$

One can solve for t by knowing C_2 and T_{Au} when measurements are taken at a given wave length. An approximate expression of Equation [2] is valid for $T \ll c_2/\lambda$ and is given by

$$\log_e \frac{E_t}{E_{Au}} = \frac{C_2}{\lambda}\left(\frac{1}{1336} + \frac{1}{t+273}\right) \quad \ldots\ldots\ldots [3]$$

where 1336 is the gold point plus 273. The value of C_2 is somewhat controversial but seems to be more firmly established, as indicated by the following discussion.

Because the thermodynamic scale is employed by most users of precise temperatures, it appears that the International Temperature Scale should be based upon the thermodynamic scale. For instance, Giauque (4) has noted that 273 K should be the ice point with 0 K as the basic datum.

First and Second Radiation Constants

Value of C_1. C_1 may be determined from established physical constants (13) by using the equation

$$C_1 = 2\pi hc^2 \quad \ldots\ldots\ldots\ldots\ldots [4]$$

where

c = velocity of light in a vacuum = 2.997902 ± 0.0000009 × 10^{10} cm/sec
h = Planck's constant = 6.62377 ± 0.00018 × 10^{-27} erg-sec

Therefore

$$C_1 = 2\pi\,(2.997902 \times 10^{10})^2\,(6.62377 \times 10^{-27})$$
$$= 374.041 \times 10^{-7} \text{ erg cm}^2\text{/sec}$$

[1] University of California.

[2] Numbers in parentheses refer to the Bibliography at the end of the paper.

Contributed by the Heat Transfer Division and presented at the Annual Meeting, New York, N. Y., November 29–December 4, 1953, of THE AMERICAN SOCIETY OF MECHANICAL ENGINEERS.

NOTE: Statements and opinions advanced in papers are to be understood as individual expressions of their authors and not those of the Society. Manuscript received at ASME Headquarters, September 3, 1953. Paper No. 53—A-176.

The Optical Society of America Colorimetry Committee adopted Birge's value of 374.02 as of 1944 (5). The value just given results from Dumond and Cohen's recent revision of Atomic Constants (13).

Value of C_2. C_2 was adopted as 1.4320 cm deg K by the 1927 International Temperature Scale for determining high temperatures by the use of Wien's Equation [3]. Since that time various other values have been used. Birge indicated a value of 1.432 ± 0.003 in 1929 (6) but revaluated it as $1.4384_3 \pm 0.0003_4$ in 1941 (3) by means of physical constants. Dumond and Cohen (13) refined Birge's value also using the atomic constants. From the definition of C_2 given as

$$C_2 = \frac{ch}{k} \quad [5]$$

then

$$C_2 = \frac{(2.99790 \times 10^{10})(6.62377 \times 10^{-27})}{(1.38026 \times 10^{-16})} = 1.43868 \text{ cm deg K}$$

where

k = Boltzmann's constant = 1.38026×10^{-16} erg deg K^{-1}

In 1939 Wensel (2) reviewed the various methods of determining C_2 and concluded that the most probable value was 1.4362 ± 0.001 with the greatest weight on the method by means of atomic constants. This occurred before Birge had published his research in 1941, and would, therefore, favor C_2 as determined in the foregoing through the use of atomic constants. Harding (7) employed Birge's value in his colorimetric table and the Optical Society of America Colorimetry Committee of 1944 recommends 1.4385.

Recent work by Van Dusen and Dahl (8) at the Bureau of Standards in the determination of the freezing point of cobalt and nickel yielded a value of $C_2 = 1.438$. They utilized Wien's Equation [3] with brightness comparisons between nickel and gold and cobalt and gold at their freezing points. It is interesting to note that they used the gold point of 1063 C as determined by Day and Sosman (9) in their monumental work in gas thermometry in 1911.

It was concluded that the validity of the value of C_2 as determined by atomic constants had been strengthened considerably by the experimental work of Van Dusen and Dahl. Since 1927 the value of C_2 has crept upward from 1.432 until today it appears that the most probable value is that determined by atomic constants. Thus the value of 1.43868 is used in computations which follow.

The Stefan-Boltzmann Constant (σ)

An integration of Equation [1] over the entire spectrum for a particular temperature yields

$$\int_0^\infty E_{\lambda,T}\,d\lambda = E_T = \left[\frac{C_1}{15}\left(\frac{\pi}{C_2}\right)^4\right] T^4 \quad [6]$$

With

$$\sigma = \frac{C_1}{15}\left(\frac{\pi}{C_2}\right)^4$$

then

$$E_T = \sigma T^4 \quad [7]$$

From the values of C_1 and C_2 just given

$$\sigma = \frac{374.041 \times 10^{-7}}{15}\left(\frac{\pi}{1.43868}\right)^4$$

or

$$\sigma = 5.6699 \times 10^{-5} \text{ erg/sec cm}^2 \text{ deg K}^4$$

Wien's Displacement Law

An equation for the location of the maximum point of the spectral distribution may be determined from Equation [1] yielding the expression

$$(\lambda T)_{E_{max}} = (\lambda T)^* = \frac{C_2}{4.965114}$$

The constant 4.965114 is a root of the equation

$$e^{-\beta} + \beta/5 - 1 = 0$$

which results from the differentiation of Equation [1]. Then

$$(\lambda T)_{E_{max}} = \frac{1.43868}{4.96511} = 0.289757 \text{ cm deg K} \quad [8]$$

Table 2 gives values of the different constants used in radiation calculations.

In a paper by Moon (10), a table of values for $E_{\lambda,T}$ were given as computed by means of Equation [1] over the visible range from 0.38μ to 0.76μ. Moon employed a value of $C_1 = 369.70 \times 10^{-7}$ erg cm^2/sec and the "old" value of $C_2 = 1.432$ cm deg K. In his paper he indicates an awareness that more precise values of C_2 were available but preferred to use the old value. Since 1927, when the value of 1.432 for C_2 was established, thermometry and radiation measurements have become more precise. Thus the value of $C_2 = 1.4385$ cm deg K, as given by Birge and later refined to 1.43868 by Dumond and Cohen, was found to be in agreement to four significant figures (1.438) with the experimental value of Van Dusen and Dahl (8).

A computation of $E_{\lambda,T}$ using the constants from Table 2 in Equation [1] at 0.76μ and 3000 deg K yields

$$E_{0.75\mu,\ 3000 \text{ deg K}} = 268.49 \text{ watts/cm}^2\mu$$

From the tables presented by Moon (10)

$$E_{0.76\mu,\ 3000 \text{ deg K}} = 273.47723 \text{ watts/cm}^2\mu$$

Suffice to say that Moon's results may be considered correct in the second significant figure only. Furthermore, he reported values of $E_{\lambda,T}$ to eight significant figures based upon constants which were known to be, at best, only good to four figures.

The conversion of the constants to U. S. engineering units required the use of conversion factors to be found in the International Critical Tables. The mean British thermal unit was employed for the constants where it appeared. Inasmuch as the Btu conversion factor appears to only five significant numbers, the values of constants affected are shown with only five significant figures.

In making radiation computations it is usually unnecessary to carry the accuracy of the emissive powers to greater than three significant figures. For cases where a greater accuracy is desired, the limitations usually will lie in the accuracy of the temperature.

The accuracy of the temperature cannot be any greater than those reported in the International Temperature Scale and that of the ice point in degrees Kelvin. The ice point reported by Birge was 273.16 ±.01 deg K indicating five-place accuracy. The "primary" temperatures of the ITS as shown in Table 1 vary from 5 to 6 significant figures. The "secondary" temperatures of the ITS (11) are given to four significant figures. It is recommended that radiation computations should yield results to no more than five significant figures in any case because of the limitations of the primary temperature scale as well as the ice point which is used

TABLE 2 CONSTANTS TO BE USED FOR EVALUATING PLANCK'S AND THE STEFAN-BOLTZMANN EQUATION IN CGS AND U. S. ENGINEERING UNITS

Quantity	CGS_1	CGS_2	U. S. Engineering
E	$\frac{\text{erg}}{\text{sec cm}^2(\text{cm})}$	$\frac{\text{watts}}{\text{cm}^2\mu}$	$\frac{\text{Btu}}{\text{hr ft}^2(\mu)}$
E	$\frac{\text{erg}}{\text{sec cm}^2}$	$\frac{\text{watts}}{\text{cm}^2}$	$\frac{\text{Btu}}{\text{hr ft}^2}$
λ	cm	μ(microns)	μ
C_1	$3.74041 \times 10^{-5} \frac{\text{erg cm}^2}{\text{sec}}$	$37{,}404.1 \frac{\text{watt} \times \mu^4}{\text{cm}^2}$	$1.1870 \times 10^8 \frac{\text{Btu}}{\text{hr ft}^2} \mu^4$
C_2	1.43868 cm°K (±0.00006)[a]	14386.8μ °K (±0.6)	25896μ °R
σ	$5.6699 \times 10^{-5} \frac{\text{erg}}{\text{sec cm}^2\text{°K}^4}$ (±0.0009)	$5.6699 \times 10^{-12} \frac{\text{watts}}{\text{cm}^2\text{°K}^4}$ (±0.0009)	$1714.0 \times 10^{-12} \frac{\text{Btu}}{\text{hr ft}^2\text{°R}^4}$
$\lambda T)_{E_{max}}$	0.289757 cm °K (±0.000012)	2897.57μ°K (±0.12)	5215.6μ°R

[a] Deviations shown are those evaluated by Dumond and Cohen (13).

to convert temperature to the absolute scale. The work of Van Dusen and Dahl in high-temperature thermometry showed results of C_2 to four significant figures, which is an indication that experimental work at high temperatures should be limited to four figures.

The measurement of radiation is far from being simple because of the extraneous radiation present, the difficulty of measuring surface temperatures for use in computing emissivities, and the nonuniformity of temperatures of sample surfaces or experimental ideal radiators. To be able to control all variables and protect against errors in experimentation to five significant figures is virtually impossible.

Acknowledgment

This work was part of the Thermal Radiation Project supported by the Office of Naval Research under Contract No. N7-onr-295, Task I, with J. T. Gier and L. Possner as Project Supervisor and Engineer, respectively.

BIBLIOGRAPHY

1 "The Thermodynamic Temperature of the Ice Point," by J. A. Beattie, Temperature, American Institute of Physics, Reinhold Publishing Company, 1941, p. 74.

2 "International Temperature Scale and Some Related Constants," by H. T. Wensel, Journal of Research, Bureau of Standards, vol. 22, 1939, p. 375.

3 "A New Table of the General Physical Constants," by R. T. Birge, *Review of Modern Physics*, vol. 13, 1941, p. 233.

4 "A Proposal to Redefine the Thermodynamic Temperature Scale," by W. F. Giauque, *Nature*, vol. 143, 1939, p. 623, and private communication at the University of California, 1948.

5 "Quantitative Data and Methods for Colorimetry," Optical Society of America Colorimetry Committee, *Journal of the Optical Society of America* (JOSA), vol. 34, 1944, p. 633.

6 "Probable Values of the General Physical Constants," by R. T. Birge, *Review of Modern Physics*, vol. 1, 1929, p. 1.

7 "Colors of Total Radiators as Expressed in the C.I.E. Trichromatic System," by H. G. W. Harding, Proceedings of the Physical Society, London, England, vol. 58, 1946, p. 1.

8 "Freezing Points of Cobalt and Nickel," by M. S. Van Dusen, and A. I. Dahl, *Journal of Research*, National Bureau of Standards, vol. 39, 1947, p. 281, R.P. 1828.

9 "High Temperature Gas Thermometry," by A. Day and R. B. Sosman, Carnegie Institute, Wash., Pub. 157, 1911.

10 "A Table of Planckian Radiation," by P. Moon, JOSA, vol. 38, 1948, p. 291.

11 "The International Temperature Scale," by H. F. Stimson, *Journal of Research*, National Bureau of Standards, vol. 42, 1949, p. 211, R.P. 1962.

12 "Basic Temperature Scales," by R. E. Wilson, *Instrumentation*, vol. 5, 1950, p. 27.

13 "Least Square Adjusted Values of the Atomic Constants as of December, 1950," by J. W. M. Dumond and R. E. Cohen, *Physical Review*, vol. 82, 1951, p. 555.

Radiation in Metals

By N. W. SNYDER,[1] BERKELEY, CALIF.

This paper presents a résumé on the electromagnetic theory of radiation in metals.

Nomenclature

The following nomenclature is used in the paper:

A = absorptivity
B = magnetic induction
c = velocity of light
D = dielectric displacement
e = base of natural logarithms
ϵ = dielectric constant
e_λ = spectral emissivity at wave length λ
E = electric field strength
E_x, E_y, E_z = components of electric field strength in x, y, z-directions, respectively
H = magnetic-field strength
H_x, H_y, H_z = components of magnetic field strength in x, y, z-directions
i = $\sqrt{-1}$
I = current
k = extinction coefficient
λ = wave length of radiation in vacuum
λ_τ = wave length of radiation of period τ in vacuum
m = mass of electron
μ = permeability
n = refractive index
N = number of free electrons per cm³ of material
N_{eff} = number of effective free electrons per cc of material
ν = frequency of radiation
ν_τ = frequency of radiation of period
q = charge of electron
q_v = charge density
r = resistive force acting on an electron whose velocity is unity in a metal
R = spectral reflectivity
ρ = specific volume resistivity
σ = specific conductivity
t = time
τ = period of radiation
ω = $2\pi\nu$ = circular frequency
x = displacement of electron in metal from the position it would be in without an applied field

Classification of Solids

Most solids can be classified according to their optical and electrical properties. The two main groups are metals and dielectrics. According to modern theories of solids, both metallic and dielectric solids are crystals. A substance such as glass which does not have a definite lattice structure is classified as a liquid of very high viscosity.

Metals are materials of high electrical and thermal conductivity. At the same time they have a low emissivity, a high reflectivity, and a high extinction coefficient for infrared rdaiation, and are therefore opaque.[2] For very long waves, i.e., in the far infrared, the optical behavior of metals is determined completely by their conductivity and they have no characteristic absorption lines in that region.

Dielectrics are materials of low electrical conductivity. They usually have a higher emissivity and lower reflectivity than metals. In most regions of the spectrum they also possess a smaller absorption coefficient and are therefore much more transparent than metals. They do have absorption lines in the infrared; near these lines they behave similarly to metals, (i.e., they have a high reflectivity).

Use is made of this fact to produce monochromatic infrared radiation by the so-called "residual-ray" method. Radiation containing a broad band of wave lengths is reflected several times from a dielectric crystal (for instance, quartz). Since the crystal has a low reflectivity everywhere except near its absorption band, a monochromatic beam is thus produced with a wave length corresponding approximately to the characteristic absorption line of the crystal.[3] The optical properties of a dielectric crystal are determined by the lattice vibrations of its crystal structure. Its properties, therefore, usually change for different directions in the crystal. Thus it is more important to use polarized light for experiments in the infrared with dielectric crystals, than it is for experiments with metals. In this way, the anisotropic characteristics of the crystals to radiation may be determined.

When the atoms of the solid are arranged in groups or molecules, additional spectral lines result. The atoms constituting the group will vibrate with respect to each other, keeping the center of gravity of the group fixed. These vibrational spectra also will lie in the infrared, and the effect of the binding of the solid is to displace and slightly spread the spectral lines which the molecules of that material would have in gaseous form. As an example, we might take the carbonates, all of which show three reflection maxima at approximately 7, 11, and 14 microns (1).[4] Therefore it may be concluded that these are the characteristic frequencies of the CO_3 ion.

Qualitative Description of Classical Theory of Metals and Dielectrics

Such phenomena as absorption, emission, reflection, and refraction of light, and electric properties of matter, such as electrical conductivity and dielectric constant, can be explained from an atomistic point of view. We shall give here a classical interpretation of these phenomena. The radiation emitted in the infrared, in most cases, is associated with nearly simple harmonic vibrations of charged particles and the classical frequency (by classical frequency we mean the resonant-frequency determined with the atomic arrangement the same as a spring-mass-undamped sys-

[1] University of California.

Contributed by the Heat Transfer Division and presented at the Annual Meeting, New York, N. Y., November 29–December 4, 1953, of The American Society of Mechanical Engineers.

Note: Statements and opinions advanced in papers are to be understood as individual expressions of their authors and not those of the Society. Manuscript received at ASME Headquarters, September 9 1953. Paper No. 53—A-132.

[2] The extinction coefficient characterizes the ability of the material to absorb radiation which has entered the metal through the surface. We do not mean absorptivity, i.e., the fraction of the radiation incident upon the surface, which enters the material and is not reflected. For instance, since metals have a high reflectivity, they have a low absorptivity; but they still possess a high absorption or extinction coefficient.

[3] The maximum of the absorption line and the maximum of the reflective power do not coincide exactly, but they are very near to each other.

[4] Numbers in parentheses refer to the Bibliography at the end of the paper.

tem) of a simple harmonic oscillator is identical to the quantum mechanical frequency. Therefore a classical treatment, in many cases, can give a good qualitative and sometimes even a good quantitative picture. Let us first consider metals.

Metals. The first to develop a theory for the properties of metals were P. Drude (2) and H. A. Lorentz (3). Although in the meantime, quantum theory and the application of Fermi Dirac statistics to the free electrons of metals have brought many refinements into the theory, many of the basic concepts of Drude's and Lorentz's theory still hold.

Drude and Lorentz assumed that metals contain electrons which are essentially free to move under the influence of an electric field. (These are the electrons of the outer shells of the atoms constituting the metal.) When the electrons are accelerated by an electric field, only collisions with the atoms of the metal deter them from their straight accelerated paths. It can be shown that the effect of these collisions is equivalent to a resistive force, proportional to the velocity of the electrons. In the case of a steady electric field, such a resistive force leads to a constant final velocity of the electrons proportional to the applied field.[6] This is Ohm's law which states the current is proportional to the applied electric field for a given metal.

Every monochromatic light wave carries with it an electric and magnetic field which vary like a simple harmonic oscillator with the frequency of the light. These fields are always perpendicular to the direction of propagation of the light. When such an electromagnetic wave is normally incident upon a metallic surface, an oscillating electric field is therefore set up in the metal, parallel to its surface. The free electrons in the metal will vibrate under the influence of this field, with the same frequency as the radiation itself. (The resistive force only causes a phase difference between the two vibrations.) Thus the radiation sets up an oscillating current, parallel to the surface of the metal. This current will have two effects. Owing to the collisions of the electrons with the atoms of the material, part of the energy of the electrons is converted into lattice vibrations of the atoms of the substance, or, in other words, into heat energy. This is essentially the same effect as the heat produced by a current in a wire. We say in this case, that part of the energy of the incident light is absorbed by the material. This absorption effect is therefore produced solely by the free electrons of the metal, explaining why most metals are opaque to visible and infrared light, while most dielectrics, which contain no free electrons, are most transparent.

The other effect of the current produced by the incident radiation is that the vibrating electrons will radiate electromagnetic radiation. (It is known that an electron which is accelerated or decelerated radiates. The electrons of the metal are constantly changing their velocity since they vibrate like harmonic oscillators.) As the electrons vibrate with the same frequency as the incident light, the light which they reradiate also will have this same frequency. The individual electrons will reradiate in all directions. It can be shown that when the effect of all the electrons is taken into account, the light radiated from them will interfere in such a way that only one wave in the forward and one in the backward direction will remain. Thus we get a transmitted and reflected wave (4).

As will be shown later, there exists an equation for the reflectivity of a metal for long waves, the so-called "Hagen-Rubens" equation. This equation expresses the reflectivity for a certain wave length entirely in terms of the conductivity of the metal. (It has been proved experimentally that this equation holds for waves above approximately 10 microns.) In the derivation of this formula it is assumed that the current produced in the metal by the electric field of the incident radiation obeys Ohm's law: $I = \sigma E$ (I = current density; σ = conductivity; E = electric field strength). As indicated previously, Ohm's law presupposes that the electron has a chance to collide with the atoms of the substance during a time which is longer than the mean time between collisions but shorter than the period of the light. This specification is one of the reasons why the Hagen-Rubens formula is accurate only for long waves.

The foregoing treatment holds qualitatively in the quantum theory. A quantitative change will occur when one takes into account the fact that the free electrons of the metal are not completely free but are subject to the electric field of the atoms constituting the crystal lattice of the material. We then must substitute for the number N of free electrons per unit volume of the material a number N_{eff} which is a certain fraction of N. ($N_{eff} = Nn_{eff}$ where n_{eff} has values between 0.5 and 1 for monovalent metals and about 0.2–0.4 for divalent metals.) Any computations making use of the number of free electrons will be effected accordingly and one must use the effective number.

Light also may be much more strongly absorbed in the body of the metal, either by ejecting an electron from a closed shell of an atom of the material or by causing a conduction electron to jump from one energy zone to another. (It has been proved by the quantum theory (5) that such energy zones exist.) In neither case can a quantum of radiation be absorbed for a frequency less than a certain critical frequency. It is therefore to be expected that a decrease in wave length will cause a sudden increase in the absorption coefficient (5). However, this will not occur in the far infrared.

Dielectrics. It is impossible to obtain quantitative results for the optical constants of dielectrics without the use of the quantum theory. When the quantum theory is used the equations developed become complicated and can be solved for very few cases and then only by making many approximations. Since some of the qualitative properties of dielectrics can be explained by the classical theory an outline of this will be given.

Unlike metals, dielectrics do not contain free electrons. Lorentz showed that it is possible to account for the behavior of insulators by a simple atomic model. He postulated that insulating materials contain electrons that are bound to equilibrium positions by Hooke's law forces. These electrons have certain natural frequencies of vibration with respect to the atoms, to which they are bound. We can see qualitatively that if such a material is struck by light whose frequency is not near any of the natural frequencies of the dielectric, only a small part of the energy will increase the vibrations of the electrons. This occurs in the region of "normal behavior" of the dielectric in which it is transparent, has a refractive index n greater than 1, and the relation $n^2 = \epsilon$ holds approximately for most substances (ϵ = dielectric constant).

If, on the other hand, the frequency of the incident light is near one of the natural frequencies of vibration of the crystal, we have what is called an "absorption band." Here resonance occurs; i.e., the incident light increases the amplitude of the natural vibrations of the crystal to a high degree. Therefore a great part of the energy of the incident light will be absorbed; and the dielectric behaves in this region in a similar way to a metal. Its refractive index is smaller than 1.

The greater the mass of a particle bound to a fixed center by a force obeying Hooke's law, the smaller its frequency of vibration. It has been stated that the extinction or absorption bands of dielectrics are due to vibrations of electrons at the resonant frequencies. However, since electrons have such a small mass, these absorption bands will lie mainly in the high-frequency ultraviolet region. The absorption bands of dielectrics in the low-frequency infrared region are, therefore, due to vibrations of

[6] Just as rain drops attain a constant final velocity due to the resistance of the air although they are subjected to a constant force due to the gravitational field of the earth.

heavier particles. As indicated, they may be due to vibrations of the atoms or ions constituting the crystal lattice of the dielectric about their equilibrium positions in the lattice. Absorption bands found for molecular crystal also may be due to vibrations of the atoms of each molecule with respect to the fixed center of mass of the molecule. This, however, does not change the foregoing classical treatment because the only assumption made was that there were charged particles which vibrated about a fixed center to which they were bound by a Hooke's law of force.

The Hagen-Rubens Equation for Reflectivity of Metals in the Infrared

For radiation incident normally upon a smooth conducting surface, the reflectivity can be calculated from Maxwell's equations. It is shown in the Appendix that for normally incident light the following formula is obtained for the reflectivity

$$R = \frac{2\tau/\rho - 2\sqrt{\tau/\rho} + 1}{2\tau/\rho + 2\sqrt{\tau/\rho} + 1} \quad [1]$$

where

ρ = specific volume resistivity of metal
τ = period of incident radiation = 1/frequency

It is assumed in the derivation of Equation [1] that

$$\epsilon \ll \frac{2\tau}{\rho} = \frac{2\lambda}{\rho c} = \frac{2\lambda}{3 \times 10^{10}\rho}$$

where

λ = wave length of radiation
ϵ = dielectric constant of metal
c = velocity of light

This will hold for practically all metals in the infrared since even for metals with lower conductivities, ρ is of the order of 10^{-4} ohm-cm = $10^{-16}/9$ = 10^{-17} esu (statohm-cm) and the infrared wave lengths are approximately 10^{-4} cm. It is also assumed for the derivation of Equation [1] that the permeability $\mu = 1$.

In deriving the formula from Maxwell's equations, it was assumed that Ohm's law, $I = \sigma E$, holds for the current I, developed by the changing electric field E of the incident radiation. But Ohm's law will hold only if the period of the incident radiation is not small as compared to the time between collisions of an electron with atoms inside the metal. Therefore the Hagen-Rubens equation holds only for long waves. Experimental results show that the equation begins to hold in the region between 1 and 10 microns, depending on the metal and the temperature.

Assuming again that $\sigma\tau \gg 1$, Equation [1] can be developed into a power series, resulting in a first approximation of the reflectivity

$$R_\lambda = 1 - 2\sqrt{\frac{\rho}{\tau}} \quad [2]$$

This is the Hagen-Rubens equation for the reflectivity of a smooth metallic surface. The reflectivity R is related to the absorptivity A for opaque bodies by the expression

$$R_\lambda = 1 - A_\lambda$$

(Even thin layers of metals whose thickness is of the order of a few wave lengths are opaque because metals have a high extinction coefficient.)

By Kirchhoff's law the absorptivity A_λ and the emissivity are numerically equal, so that the emissivity is

$$e_\lambda = 2\sqrt{\frac{\rho}{\tau}} \quad [2a]$$

Note that the emissivity decreases with decreasing resistivity and with increasing wave length.

If instead of τ the wave length λ is introduced and if ρ is measured in ohm-cm instead of esu the following formula results

$$R_\lambda = 1 - 36.05\sqrt{\frac{\rho}{\lambda}} \quad [2b]$$

where

ρ = specific volume resistivity, ohm-cm
λ = wave length, microns

Equation [2a] is quite accurate for metals over the entire spectrum for temperatures of radiation below 400 C or 700 F. This equation may be combined with Planck's equation (Aschkinass (12)

$$E_{p,\lambda,T} = \frac{C_1}{\lambda^5}\left[\frac{1}{e^{\frac{c_2}{\lambda T}} - 1}\right] \quad [2c]$$

where

$E_{p,\lambda,T}$ = monochromatic emissive power for an ideal (or planckian) radiator, watts/cm^2 μ
C_1 = Planck's first radiation constant watts/cm^2 $(\mu)^4$
C_2 = Planck's second radiation constant, μ deg K
λ = wave length, microns, μ

by using the fact that

$$e_\lambda = \frac{E_{m,\lambda,T}}{E_{p,\lambda,T}} \quad [2d]$$

where

$$e_\lambda = 36.05\sqrt{\frac{\rho}{\lambda}}$$

$E_{m,\lambda,T}$ = monochromatic emissive power of metal surface watts/cm$^2\mu$

then

$$E_{m,\lambda,T} = 36.05 C_1\sqrt{\rho}\left[\frac{\lambda^{-5.5}}{e^{\frac{c_2}{\lambda T}} - 1}\right] \quad [2e]$$

By differentiating Equation [2e] one arrives at the maximum of radiation

$$(\lambda T)(E_{m,\lambda,T} = \max) = (\lambda T)^* = 2660\mu \text{ deg K}$$

as compared to $(\lambda T)^* = 2897\mu$ deg K for an ideal radiator.

The total emissive power is obtained by integrating Equation [2e] over the entire spectrum

$$E_{m,T} = \int_{\lambda=0}^{\lambda=\infty} E_{m,\lambda,T}\, d\lambda$$

Let $x = C_2/(\lambda T)$ in Equation [2e] and

$$E_{m,T} = 36.05\, C_1\sqrt{\rho}\left(\frac{T}{C_2}\right)^{4.5}\int_0^\infty \frac{x^{3.5}}{e^x - 1}\, dx$$

yielding

$$E_m = 36.05\, C_1\sqrt{\rho}\left(\frac{T}{C_2}\right)^{4.5}(12.27) \quad [2f]$$

for pure metals

$$\rho = \rho_m \left(\frac{T}{273}\right) \quad \ldots\ldots\ldots\ldots\ldots\ldots [2g]$$

ρ_m = specific volume resistivity of metal at 0 C, ohm-cm

and

$$E_m = \left(36.05 \frac{C_1}{C_2^{4.5}} \sqrt{\rho_m}\right) T^5 \quad \ldots\ldots\ldots\ldots [2h]$$

For pure metals then, the total radiation is proportional to the absolute temperature to the 5th power instead of the 4th power as in the case of ideal radiators, this provided that the radiation is in the longer wave lengths, say, $>4\mu$ or 5μ or temperatures less than 400 C.

Experiments of Lummer and Kurlbaum (13) and Lummer and Pringsheim (14), however, showed that for platinum the $E_{m,T}$ was proportional to T^5 in the range 700 to 1800 K. Thus the results presented by Aschkinass appear to be valid up to much higher temperatures than expected. For alloys with low-temperature coefficients for ρ, the deviations from Equation [2h] occur at the lower temperatures.

Figs. 1 to 4 show some measurements of emissivity and reflectivity of smooth metallic surfaces which should indicate how well and in what wave length region the Hagen-Rubens equation holds. The solid curves in all these figures give the values calculated according to the Hagen-Rubens equation. The dots are experimental points obtained by Hagen and Rubens. Figs. 1 to 3 show the emissivity of different metals as a function of the wave length at room temperature. The crosses in Figs. 1 and 2 are experimental points obtained in this project (6). Fig. 4 shows the dependence of the emissivity upon the temperature for a constant wave length. This also can be calculated from the Hagen-Rubens equation provided the dependence of the resistivity upon temperature is known.

For Hagen and Rubens' experiments see reference (7). For summaries on the infrared spectrum, see references (8) and (9).

Acknowledgment

The author would like to thank Ellen Grunwald for the work which she performed in helping make this paper possible. This work was supported by the Office of Naval Research under Contract No. N4-onr-295, Task I. Prof. J. T. Gier was the supervisor of this project and encouraged having this paper written.

Bibliography

1 "Kurzwellige ultrarote Eigenfrequenzen der Sulfate und Karbonate," by C. Schaefer and M. Schubert, *Annalen der Physik*, vol. 50, 1916, pp. 283–338.

2 "Zur Elektronentheorie der Metalle," by P. Drude, *Annalen der Physik*, vol. 1, 1900, pp. 566–613; vol. 3, 1900, pp. 369–402.

3 "Theory of Electrons," by H. A. Lorentz, B. G. Tuebner, Leipzig, Germany, 1909.

4 "Optik," by M. Born, J. Springer, Berlin, Germany, 1933, Edwards Bros., Ann Arbor, Michigan, 1943, p. 313.

5 "Theory of the Properties of Metals and Alloys," by N. F. Mott and H. Jones, Clarendon Press, London, England, 1936, p. 115.

6 "The Absolute Spectral Reflectivity of Certain Pigments and Metals in the Wave Length Range Between 2 and 15 Microns," by J. T. Gier, L. Possner, A. J. Test, R. V. Dunkle, and J. T. Bevans, Thermal Radiation Project, ONR Contract N7-onr-295, Take I, February 18, 1949.

7 "Das Reflexionsvermögen von Metallen und belegten Glasspiegeln," by E. Hagen and H. Rubens, *Annalen der Physik*, vol. 1, 1900, pp. 352–375.

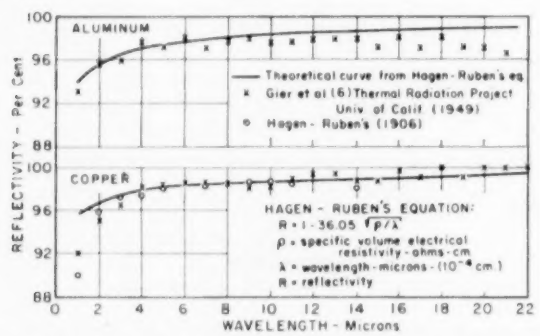
ALUMINUM
COPPER
Theoretical curve from Hagen-Ruben's eq.
Gier et al (6) Thermal Radiation Project Univ. of Calif. (1949)
Hagen-Ruben's (1906)
HAGEN-RUBEN'S EQUATION:
R = 1 - 36.05 √(ρ/λ)
ρ = specific volume electrical resistivity - ohms - cm.
λ = wavelength - microns - (10⁻⁴ cm.)
R = reflectivity
REFLECTIVITY - Per Cent
WAVELENGTH - Microns

Fig. 1 Spectral Reflectivity of Polished Metals at Room Temperature—Aluminum and Copper

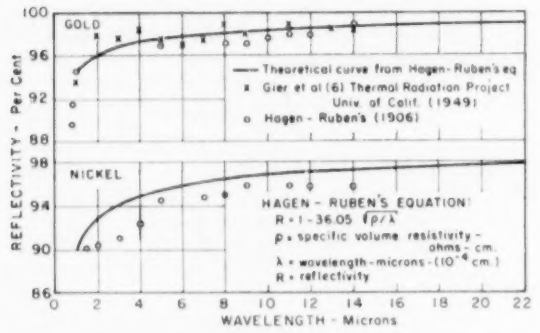
GOLD
NICKEL
Theoretical curve from Hagen-Ruben's eq.
Gier et al (6) Thermal Radiation Project Univ. of Calif. (1949)
Hagen-Ruben's (1906)
HAGEN-RUBEN'S EQUATION:
R = 1 - 36.05 √(ρ/λ)
ρ = specific volume resistivity - ohms - cm.
λ = wavelength - microns - (10⁻⁴ cm.)
R = reflectivity
REFLECTIVITY - Per Cent
WAVELENGTH - Microns

Fig. 2 Spectral Reflectivity of Polished Metals at Room Temperature—Gold and Nickel

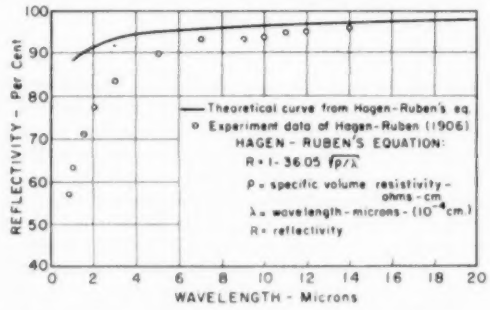
Theoretical curve from Hagen-Ruben's eq.
Experiment data of Hagen-Ruben (1906)
HAGEN-RUBEN'S EQUATION:
R = 1 - 36.05 √(ρ/λ)
ρ = specific volume resistivity - ohms - cm.
λ = wavelength - microns - (10⁻⁴ cm.)
R = reflectivity
REFLECTIVITY - Per Cent
WAVELENGTH - Microns

Fig. 3 Reflectivity of Polished Steel at Room Temperature

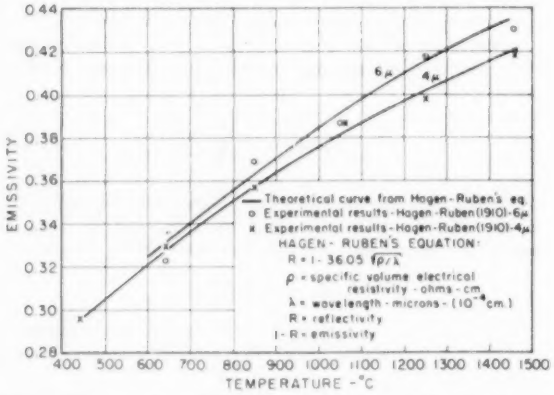

Fig. 4 Spectral Emissivity of Platinum at $\lambda = 6\mu$ and 4μ as a Function of Temperature

"Das Reflexionsvermögen einiger Metalle für ultraviolette und ultrarote Strahlen," by E. Hagen and H. Rubens, *Annalen der Physik*, vol. 8, 1902, pp. 1–21.

"Über Beziehungen des Reflexions und Emissionsvermögens der Metalle zu ihren elektrischen Leitvermögen," by E. Hagen and H. Rubens, *Annalen der Physik*, vol. 11, 1903, pp. 873–901.

"Emissionsvermögen und elektrische Leitfähigkeit der Metall-Legierungen," by E. Hagen and H. Rubens, *Verhandlungen der Deutschen Physikalischen Gesellschaft*, vol. 1, 1899, pp. 215–235.

8 "Handbuch der Physik," vol. 21, p. 207.

9 "Das Ultrarote Spektrum," by C. Schaefer and F. Matossi, Julius Springer, Berlin, Germany, 1930.

10 Reference (7), vol. 11, 1903, p. 873.

11 Akademie der Wissenschaften, Sitzungsberichte, Berlin, Germany, vol. 1, 1910, p. 477.

12 "Die Wärmestrahlung der Metalle," by E. Aschkinass, *Annalen der Physik*, vol. 17, 1905, pp. 960–976.

13 "Der electrisch geglühte 'absolut schwarze' Körper und seine Temperaturmessung," by O. Lummer and E. Kurlbaum, *Verhandlungen der Physikalischen Gesellschaft* in Berlin, Germany, vol. 17, 1898, pp. 106–111.

14 "Die Verteilung der Energie im Spektrum des schwarzen Körpers und des blanken Platins. 2. Temperaturbestimmung fester glühender Körper," by O. Lummer and E. Pringsheim, *Verhandlungen der Deutschen Physikalischen Gesellschaft*, vol. 1, 1899, pp. 215–235.

Summarizing Literature

Books:

"Le spectre infrarouge," by J. Lecomte, Paris, France, 1928.

"Infrared Analysis of Molecular Structure," by F. I. G. Rawline and A. M. Taylor, Cambridge University Press, London, England, 1929.

"Das Ultrarote Spektrum," by C. Schaefer and F. Matossi, Berlin, Germany, 1930.

Short Summarizing Representations:

"Le spectre infrarouge," by H. Rubens, Rapports du Congr. intern. de Phys., 1900.

"Das ultrarote Spektrum und seine Bedeutung für die Bestaetigung der elekromagnetischen Lichttheorie," by H. Rubens, Berliner Berichte über Leder Hänte Felle, 1917, p. 47.

"Ultrarotforschung. Ergebnisse der exakt.," by G. Laski, *Naturwissenschaften*, vol. 3, 1924, p. 86.

"Die Eigenschwingungen der Kristalle," by C. Schaefer, Forsch. d. Min. Krist. u. Petrogr. vol. 9, 1924, p. 31.

"Handbuch der Physik," vol. 21, p. 207 (Licht und Materie) and other articles in same handbook.

"Handbuch der physikalischen Optik," vol. 2, 1928, pp. 851 and 879, and other articles in same handbook.

A very detailed bibliography is contained in: "Infrared Spectroscopy, Industrial Applications and Bibliography," by R. B. Barnes, R. C. Gore, Urner Liddel, and Van Zandt Williams, Stamford Research Laboratories, American Cynamid Company, Stamford, Conn., 1944.

"Wärmestrahlung Technischer Oberflächen bei gewöhnlicher Temperatur," by E. Schmidt, *Gesundheits-Ingenieur Beihefte*, Series 1, no. 20, 1927.

"Über die Richtungsverteilung der Wärmestrahlung von Oberflächen," by E. Schmidt and E. Eckert, *Forschung auf dem Gebiete des Ingenieurwesens*, vol. 6, 1935, pp. 175–183.

On Theories of Metals:

"The Theory of Electrons and Its Applications to the Phenomena of Light and Radiant Heat," by H. A. Lorentz, Leipzig, Germany, 1909.

"The Theory of the Properties of Metals and Alloys," by N. F. Mott and H. Jones, Oxford University Press, London, England, 1936.

"Elektronentheorie der Metalle," by H. Froehlich, Berlin, Germany, 1936.

"The Electronic Structure of Metals," by J. C. Slater, *Review of Modern Physics*, vol. 6, 1934, p. 209.

Hagen-Rubens Equation and Its Experimental Confirmation:

"Optical Properties of Metals for Long Waves," by M. Planck, *Sitzungsberichte der koeniglichen Akademie der Wissenschaften*, March, 1903, pp. 278–280.

"Change of Emissivity of Metals With Temperature in the Short-Wave Infrared," by E. Hagen and H. Rubens (translated title of 1910 reference), *Sitzungsberichte der koeniglichen Akademie der Wissenschaften*, Berlin, Germany, 1910, pp. 467–487; also reference (7).

"Radiometric Investigations of Infra-Red Absorption and Reflection Spectra. II. Reflection Spectra; Reflecting Power of Metals," by W. W. Coblentz, Bulletin of the U. S. Bureau of Standards, vol. 2, 1906, pp. 470–477.

"The Reflecting Power of Various Metals," by W. W. Coblentz, Bulletin of the U. S. Bureau of Standards, vol. 7, 1911, pp. 197–225.

"Reflecting Power of Monel Metal, Stellite, and Zinc," by W. W. Coblentz, Bulletin of the U. S. Bureau of Standards, vol. 16, 1920, pp. 249–252.

"Reflecting Power of Tungsten and Stellite," by W. W. Coblentz and W. B. Emerson, Bulletin of the U. S. Bureau of Standards, vol. 14, 1917, pp. 307–316.

"Reflecting Power of Stellite and Lacquered Silver," by W. W. Coblentz and H. Kahler, Bulletin of the U. S. Bureau of Standards, vol. 15, 1919, pp. 215–217.

"Preparation and Reflective Properties of Some Alloys of Aluminum With Magnesium and With Zinc," by R. G. Waltenberg and W. W. Coblentz, Bulletin of the U. S. Bureau of Standards, vol. 15, 1920, pp. 653–657.

"Bestimmung des selectiven Reflexionsvermögens einiger Planspiegel," by F. Paschen, *Annalen der Physik*, vol. 4, 1901, pp. 304–306.

Appendix

Maxwell's Equations

The following are Maxwell's equations

$$\text{div } \underline{D} = 4\pi q_v \quad [3]$$

$$\text{div } \underline{B} = 0 \quad [4]$$

$$\text{curl } \underline{H} = \frac{4\pi}{c}\underline{I} + \frac{1}{c}\frac{\partial \underline{D}}{\partial t} \quad [5]$$

$$\text{curl } \underline{E} = -\frac{1}{c}\frac{\partial B}{\partial t} \quad [6]$$

(See Harnwell, "Principles of Electricity and Electromagnetism," equations 2.21, 9.14, 10.7, 10.3. Except for different units which Harnwell uses, these are the same equations.)

$\underline{D} = \epsilon \underline{E}$ = displacement vector, ϵ = dielectric constant
q_v = charge density
$\underline{B}$ = induction = μH, μ = permeability
$\underline{H}$ = magnetic-field intensity
$\underline{I}$ = current density
$\underline{E}$ = electric-field intensity
c = velocity of light

Equation [3] is derived from Coulomb's law of force between two charges. When true charges are not present, it follows from Equation [3] that div $D = 0$. If ϵ = const in all directions, it follows that ϵ div $\underline{E}$ is 0 or div $\underline{E}$ is 0, which signifies that the number of lines of electric force entering a volume equals the number of lines leaving it. From div $\epsilon \underline{E} = 0$, one can derive the condition that at the boundary between two media 1 and 2, the normal component of the electric field E_n satisfies

$$\epsilon_1 E_{1n} = \epsilon_2 E_{2n} \quad [7]$$

Equation [4] for the magnetic induction is analogous to Equation [4] for the electric displacement, but since no true magnetic charges exist, div $\underline{B} = 0$ always. This signifies that the number of lines of induction entering a volume equals the number leaving it, or it can be said that the magnetic lines of induction are always closed curves. From this, the boundary condition which can be derived is

$$\mu_1 H_{1n} = \mu_2 H_{2n} \quad [8]$$

In Equation [5] the first term on the right side, $(4\pi/c)\underline{I}$, is derived from Ampere's law which states that the work in taking a magnetic charge of magnitude one around a current of magnitude I is $(4\pi/c)I$.

The second term

$$\frac{1}{c}\frac{\partial \underline{D}}{\partial t}$$

represents Maxwell's displacement current signifiying that even the displacement of charges in a dielectric (e.g., a dielectric between two charged condenser plates) gives rise to a magnetic field.

Equation [6] is derived from an extension of Faraday's law which states that the electromotive force induced in a circuit is proportional to the change of the number of lines of induction through this circuit. Since an electromotive force is caused by an electric field, Maxwell assumed that every change in magnetic induction is accompanied by electric lines of force, even if a loop of wire is not present.

For a conducting medium Ohm's law is valid: $\underline{I} = \sigma \underline{E}$, where σ is the conductivity. Also, if the medium is homogeneous, ϵ = const and μ = const

$$\frac{\partial \underline{D}}{\partial t} = \frac{\partial(\epsilon \underline{E})}{\partial t} = \epsilon \frac{\partial \underline{E}}{\partial t}$$

$$\frac{\partial \underline{B}}{\partial t} = \frac{\partial(\mu \underline{H})}{\partial t} = \mu \frac{\partial \underline{H}}{\partial t}$$

$$\text{div } \underline{D} = \text{div } (\epsilon \underline{E}) = \epsilon \text{ div } \underline{E}$$

$$\text{div } \underline{B} = \text{div } (\mu \underline{H}) = \mu \text{ div } \underline{H}$$

Assume also that true charges are not present in the conductor so that $q_v = 0$. Maxwell's equations therefore become

$$\text{div } \underline{E} = 0 \quad [9]$$

$$\text{div } \underline{H} = 0 \quad [10]$$

$$\text{curl } \underline{H} = \frac{\epsilon}{c} \frac{\partial \underline{E}}{\partial t} + \frac{4\pi\sigma}{c} \underline{E} \quad [11]$$

$$\text{curl } \underline{E} = -\frac{\mu}{c} \frac{\partial \underline{H}}{\partial t} \quad [12]$$

At the boundary between two media possessing the same ϵ, it can be concluded from Equation [3] that the normal component of the electric field vector is continuous (see Equation [7]). If the media have the same μ, Equation [4] indicates that the normal component of the magnetic vector is continuous (see Equation [8]).

Ohm's law, $\underline{I} = \sigma \underline{E}$ is rigorously valid for stationary electric fields and currents only. For the case of radiation incident upon the metal, $\underline{E}$ is a periodic function of time and $\underline{I} = \sigma \underline{E}$ will be accurate for long waves only (i.e., for waves whose period of vibration is large compared with the mean time between two collisions of the free electrons of the metal).

Propagation of Electromagnetic Waves in Conducting Media[6]

Maxwell's equations for a conducting medium, see Equations [9 to 12], are

$$\text{curl } \underline{H} = \frac{\epsilon}{c} \frac{\partial \underline{E}}{\partial t} + \frac{4\pi\sigma}{c} \underline{E} \quad [11]$$

$$\text{curl } \underline{E} = -\frac{\mu}{c} \frac{\partial \underline{H}}{\partial t} \quad [12]$$

$$\text{div } \underline{E} = 0 \quad [9]$$

$$\text{div } \underline{H} = 0 \quad [10]$$

Eliminating $\underline{H}$ from Equations [11] and [12] by taking $\partial/\partial t$ of Equation [11] and the curl of Equation [12]

$$\Delta^2 \underline{E} = \frac{\epsilon\mu}{c^2} \frac{\partial^2 \underline{E}}{\partial t^2} + \frac{4\pi\sigma\mu}{c^2} \frac{\partial \underline{E}}{\partial t} \quad [13]$$

Now find a solution of this equation in the form of a plane wave in the x-direction. Such a wave is defined by the fact that all quantities connected with it are constant over a y-z-plane, or

$$\frac{\partial}{\partial y} = \frac{\partial}{\partial z} = 0$$

Substituting this into Equations [9] and [10]

$$E_x = H_x = 0$$

Assume now that we can find a solution for $\underline{E}$ which is a periodic function of time

$$E_y = f(x)e^{i\omega t}; \quad E_z = g(x)e^{i\omega t} \quad [14]$$

For simplicity of notation the discussion will be restricted to plane polarized waves whose electric vector $\underline{E}$ is in the X-Y-plane; hence

$$E_z = 0$$

Substituting into Equation [13]

$$\frac{d^2 f}{dx^2} + \left[\frac{(\epsilon\mu)\omega^2}{c^2} - i\frac{4\pi\sigma\mu\omega}{c^2}\right] f = 0$$

This is a differential equation for the point function for which the solution is

$$f(x) = Ae^{\pm i\left(\sqrt{\epsilon\mu\omega^2 - i4\pi\sigma\mu\omega}\right)\frac{x}{c}} \quad [15]$$

(Negative sign in the exponential is for wave propagated in positive x-direction.)

For $\sigma = 0$, Equation [15] yields an undamped wave because it reduces to an imaginary exponential only.

In order to separate the exponential into real and imaginary parts, the real variables n and k are introduced which are defined by the following equation

$$\sqrt{\epsilon\mu\omega^2 - i4\pi\sigma\mu\omega} = \omega(n - ik) \quad [16]$$

Squaring and equating the real and imaginary parts

$$n^2 - k^2 = \epsilon\mu$$

$$nk = \frac{2\pi\mu\sigma}{\omega} \quad [17]$$

but

$$\omega = 2\pi\nu = \frac{2\pi}{\tau}$$

and therefore

$$nk = \frac{\mu\sigma}{\nu} \quad \text{or} \quad nk = \mu\sigma\tau \quad [18]$$

where $1/\nu = \tau$ = period of vibration.

By solving the simultaneous Equations [17] and [18] for n and k the following result is obtained

$$n = \sqrt{\frac{\mu}{2}\left(\sqrt{\epsilon^2 + 4\sigma^2\tau^2} + \epsilon\right)} \quad [19]$$

$$k = \sqrt{\frac{\mu}{2}\left(\sqrt{\epsilon^2 + 4\sigma^2\tau^2} - \epsilon\right)} \quad [20]$$

[6] The treatment here is taken from "Theoretical Physics," by G. Joos, page 320.

Substituting these into Equation [14] using $f(x)$ from Equation [15]

$$E_y = Ae^{i\omega t}e^{-i\omega n\frac{x}{c}}e^{-\omega k\frac{x}{c}}$$

or

$$E_y = Ae^{-\omega k\frac{x}{c}}e^{i\omega t-\frac{n x}{c}}$$

Thus the imaginary term $-ik$ in Equation [16] furnishes a real negative exponential function (i.e., a damping factor) while the velocity of propagation v of the phase is determined by n ($v = c/n$ as in dielectrics). Therefore n, defined by Equation [16], is called the index of refraction.

The meaning of k can be found as follows

First, $$\frac{\omega}{c} = \frac{2\pi\nu}{c} = \frac{2\pi}{\nu}$$

where

λ = wave length of the radiation in vacuum. Thus the damping factor is

$$e^{-2\pi k\frac{x}{\lambda}}$$

For $x = \lambda$ this factor becomes $e^{-2\pi k}$. Thus, in traveling a distance equal to the wave length in vacuum, the amplitude of the radiation diminishes by a factor $e^{-2\pi k}$ and k is called the extinction coefficient.

Calculating H from Equation [12]

$$H_x = H_y = 0$$

$$\frac{\partial H_z}{\partial t} = -\frac{c}{\mu}\frac{\partial E_y}{\partial x}$$

and substituting for E_y

$$\frac{\partial H_z}{\partial t} = \frac{\omega}{\mu}(k + in)Ae^{-\omega k\frac{x}{c}}e^{i\omega\left(t - n\frac{x}{c}\right)}$$

Upon integration with respect to t

$$H_z = \frac{1}{\mu}(n - ik)Ae^{-\omega k\frac{x}{c}}e^{-i\omega\left(t - n\frac{x}{c}\right)}$$

or

$$H_z = \frac{1}{\mu}(n - ik)E_y \qquad [21]$$

Now, from the relationship in the complex plane

$$n - ik = \sqrt{n^2 + k^2}\,e^{-i\gamma}$$

where

$$\tan\gamma = \frac{k}{n}$$

Then

$$H_z = \frac{1}{\mu}\sqrt{n^2 + k^2}E_y e^{-i\gamma}$$

or

$$H_z = \frac{1}{\mu}\sqrt{n^2 + k^2}Ae^{-\omega k\frac{x}{c}}e^{i\omega\left(t - n\frac{x}{c}\right) - i\gamma} \qquad [21a]$$

Therefore, H lags behind E by a phase difference γ for conducting media.

According to this discussion, all conductors should internally absorb electromagnetic waves while insulators should transmit them. However, examples can be given at once, which contradict this: A solution of NaCl, in spite of high electric conductivity, is perfectly transparent, while vulcanite, which is a good insulator, is opaque. The explanation is variation of the conductivity with frequency. It was assumed in this discussion that the conductivity is a constant independent of frequency and equal to the conductivity for steady currents.

Reflectivity of a Smooth Metallic Surface for Normally Incident Radiation

Let the surface of the separation between two media be in the Y-Z-plane, and let the incident ray propagate in the x-direction (normal incidence).

Define:

A, amplitude of electric vector of incident ray
A', amplitude of electric vector of reflected ray
A'', amplitude of electric vector of refracted ray

From Equation [21] the amplitude of the magnetic vector will be given by

$$\frac{n - ik}{\mu}A$$

It is assumed that in the first medium $\epsilon = \mu = 1$, and in the second medium (the metal) $\mu = 1$. In the first medium, therefore, $n = 1$, $k = 0$, and the magnetic vector is equal in magnitude to the electric vector.

Thus from Equation [21] the magnetic vector of the incident ray is

$$H_z = E_y; \quad H_y = -E_z$$

For the reflected ray, since the direction of the ray and E and H must form a right-handed co-ordinate system, the magnetic vector is

$$H_z' = -E_y'; \quad H_y' = -E_z'$$

For the refracted ray

$$H_z'' = (n - ik)E_y''; \quad H_y'' = -(n - ik)E_z''$$

The boundary conditions are such that the tangential components of the electric and magnetic vectors are continuous. The boundary conditions for the electric vector therefore yield the relationships

$$A_y + A_y' = A_y'' \qquad [22]$$

$$A_z + A_z' = A_z'' \qquad [23]$$

and from the boundary conditions for the magnetic vector

$$A_y - A_y' = (n - ik)A_y'' \qquad [24]$$

$$-A_z + A_z' = -(n - ik)A_z'' \qquad [25]$$

Eliminating A_y'' from Equations [22] and [24]

$$(n - ik - 1)A_y + (n - ik + 1)A_y' = 0$$

or

$$\frac{A_y'}{A_y} = -\frac{n - ik - 1}{n - ik + 1}$$

and a similar equation can be written for A_z by eliminating A_z'' in Equations [23] and [25]

$$\frac{A_z'}{A_z} = \frac{n - ik - 1}{n - ik + 1}$$

The reflectivity which is the ratio of the intensities or the square of the amplitudes is given by

$$R = \frac{A'^2}{A^2} = \frac{|n - ik - 1|^2}{|n - ik + 1|^2}$$

or

$$R = \frac{(n-1)^2 + k^2}{(n+1)^2 + k^2}$$

or

$$R = \frac{n^2 + k^2 + 1 - 2n}{n^2 + k^2 + 1 + 2n} \quad \ldots\ldots [26]$$

Note that when k is large $R \to 1$. Therefore radiant energy of a particular wave length which is strongly absorbed internally is strongly reflected. Hence the colors of such substances by transmitted and by reflected light are complementary, and a thin film of gold, for example, appears blue by transmitted light.

The values of n and k when $\mu = 1$ are, according to Equations [19] and [20]

$$n = \sqrt{\frac{1}{2}\left(\sqrt{\epsilon^2 + 4\sigma^2\tau^2} + \epsilon\right)} \quad \ldots\ldots [27]$$

$$k = \sqrt{\frac{1}{2}\left(\sqrt{\epsilon^2 + 4\sigma^2\tau^2} - \epsilon\right)} \quad \ldots\ldots [28]$$

and therefore

$$n^2 + k^2 = \sqrt{\epsilon^2 + 4\sigma^2\tau^2} \quad \ldots\ldots [29]$$

Thus the reflectivity becomes by substituting Equations [29] and [27] into Equation [26]

$$R = \frac{\sqrt{4\sigma^2\tau^2 + \epsilon^2} + 1 - \sqrt{2\left(\sqrt{4\sigma^2\tau^2 + \epsilon^2} + \epsilon\right)}}{\sqrt{4\sigma^2\tau^2 + \epsilon^2} + 1 + \sqrt{2\left(\sqrt{4\sigma^2\tau^2 + \epsilon^2} + \epsilon\right)}} \quad \ldots [30]$$

For $\epsilon \ll \sigma\tau$ the reflectivity becomes

$$R = \frac{2\sigma\tau + 1 - 2\sqrt{\sigma\tau}}{2\sigma\tau + 1 + 2\sqrt{\sigma\tau}} \quad \ldots\ldots [31]$$

Substituting the specific volume resistivity, $\rho = \frac{1}{\sigma}$

$$R = \frac{\frac{2\tau}{\rho} - 2\sqrt{\frac{\tau}{\rho}} + 1}{\frac{2\tau}{\rho} + 2\sqrt{\frac{\tau}{\rho}} + 1} \quad \ldots\ldots [32]$$

Thermal-Radiation Tables and Applications

By R. V. DUNKLE,[1] BERKELEY, CALIF.

In this paper the properties of ideal thermal radiators are tabulated in a generalized form for use with ideal sources at any temperature. These tables are presented in a form which simplifies the computation of total radiant properties from spectral properties for nonideal sources and receivers, and examples of their utilization are included. The values of the thermal-radiation constants utilized in the preparation of the tables were the latest available.[2] Conventional engineering units are employed in this paper, conversion to other systems of units being accomplished readily. These tables were prepared from the tables computed by the Federal Works Agency, Work Projects Administration,[3] after converting to engineering units and correcting for the revised values of the radiation constants.

Nomenclature

The following nomenclature is used in the paper:

C_1 = first radiation constant = 1.1860×10^8 Btu μ^4/hr sq ft
C_2 = second radiation constant = $25{,}896\mu$ deg R
e = total emissivity
e_λ = spectral emissivity
$e_{\lambda T-\infty}$ = average emissivity from λT to ∞
E = total emissive power, ideal radiator Btu/hr sq ft
E_λ = spectral emissive power, Btu/hr sq ft μ
$E_{0-\lambda}$ = emissive power from $\lambda = 0$ to given wave length λ, Btu/hr sq ft
$E_{0-\lambda T}$ = emissive power from $\lambda T = 0$ to given λT, Btu/hr sq ft
F = shape factor of source with respect to receiver
G = total irradiation of receiver, Btu/hr sq ft
G_λ = spectral irradiation of receiver, Btu/hr sq ft μ
r = total reflectivity
r_λ = spectral reflectivity
T = temperature, deg R
λ = wave length, microns
σ = Stefan-Boltzmann constant 1713×10^{-12} Btu/hr sq ft deg R^4
μ = micron = 10^{-6}

Discussion

The basic equations will be reviewed and then some specific applications will be presented. Planck's well-known equation describing the spectral distribution of the monochromatic emissive power emitted by an ideal thermal radiator is

$$E_\lambda = \frac{C_1}{\lambda^5 \left(e^{\frac{C_2}{\lambda T}} - 1\right)} \quad \ldots\ldots [1]$$

It is found convenient to rewrite this equation with λT as the independent variable. This is accomplished by dividing Equation [1] by σT^5. This gives Planck's equation in the following form

$$\frac{E_\lambda}{\sigma T^5} = \frac{C_1}{\sigma(\lambda T)^5 \left(e^{\frac{C_2}{\lambda T}} - 1\right)} \quad \ldots\ldots [2]$$

This equation illustrates that $E_\lambda/\sigma T^5$ is a function of λT only, as C_1, C_2, and σ are all constants. This function is tabulated in Table 1 and is also plotted in Fig. 1.

If Equation [2] is differentiated with respect to λT at constant temperature, the peak in the curve is located at a value of $\lambda_{max} T = 5214.9\mu$ deg R at which point

$$\frac{E_\lambda}{\sigma T^5} = 12.607 \times 10^{-4} (\mu \text{ deg R})^{-1}$$

Integration of Equation [2] at constant temperature will give the power emitted in any spectral region. The total power emitted by an ideal radiator from zero wave length out to any wave length λ is expressed by

$$E_{0-\lambda} = \int_0^\lambda E_\lambda d\lambda \quad \ldots\ldots [3]$$

Again, the equation can be written in terms of λT as the independent variable

$$E_{0-\lambda T} = \frac{1}{T} \int_0^{\lambda T} E_\lambda d(\lambda T) \quad \ldots\ldots [4]$$

and upon substitution of E_λ from Equation [2]

$$\frac{E_{0-\lambda T}}{\sigma T^4} = \int_0^{\lambda T} \frac{C_1 d(\lambda T)}{\sigma(\lambda T)^5 \left(e^{\frac{C_2}{\lambda T}} - 1\right)} \quad \ldots\ldots [5]$$

This integral can be expressed as a series, which was the method used in the computation of the radiation tables.[3] This integral is tabulated in Table 1 as a function of (λT) and gives the fraction of the total power emitted by an ideal radiator below the wave length corresponding to the value of (λT) or, by difference, the fraction of the emitted power between any two wave lengths.

It is to be noted that

$$\int_0^\infty \frac{C_1 d(\lambda T)}{\sigma(\lambda T)^5 \left(e^{\frac{C_2}{\lambda T}} - 1\right)} = 1.0000 \quad \ldots\ldots [6]$$

Computation of total radiant properties from spectral properties readily is accomplished with the aid of column 2 of Table 1. Taking reflectivity as an example, suppose that the reflectivity of a material is desired for radiation from an ideal source. The equation for the total reflectivity is

$$r = \frac{\int_0^\infty r_\lambda G_\lambda d_\lambda}{\int_0^\infty G_\lambda d_\lambda} \quad \ldots\ldots [7]$$

where spectral irradiation of the material from the source is

$$G_\lambda = F E_\lambda \quad \ldots\ldots [8]$$

---

[1] Associate Professor, University of California.

[2] "Recent Advances in Our Knowledge of the Numerical Values of the Fundamental Atomic Constants," by J. W. M. Du Mond and R. E. Cohn, *American Scientist*, vol. 40, 1952, p. 447.

[3] Planck's Radiation Functions and Electronic Functions, Federal Works Agency, Work Projects Administration, 1941.

Contributed by the Heat Transfer Division and presented at the Annual Meeting, New York, N. Y., November 29–December 4, 1953, of The American Society of Mechanical Engineers.

Note: Statements and opinions advanced in papers are to be understood as individual expressions of their authors and not those of the Society. Manuscript received at ASME Headquarters, September 15, 1953. Paper No. 53—A-220.

TABLE 1 PLANCK'S RADIATION FUNCTIONS

λT	$\frac{E_\lambda \times 10^5}{\sigma T^5}$	$\frac{E_{0-\lambda T}}{\sigma T^4}$	λT	$\frac{E_\lambda \times 10^5}{\sigma T^5}$	$\frac{E_{0-\lambda T}}{\sigma T^4}$	λT	$\frac{E_\lambda \times 10^5}{\sigma T^5}$	$\frac{E_{0-\lambda T}}{\sigma T^4}$
1000	.0000394	0	9400	6.411	.6606	29000	.234	.9742
1200	.001184	0	9600	6.136	.6731	30000	.208	.9765
1400	.01194	0	9800	5.872	.6851	40000	.0741	.9881
1600	.0618	.0001	10000	5.619	.6966	50000	.0326	.9941
1800	.2070	.0003	10200	5.378	.7076	60000	.0165	.9965
2000	.5151	.0009	10400	5.146	.7181	70000	.0919	.9981
2200	1.0384	.0025	10600	4.925	.7282	80000	.0055	.9987
2400	1.791	.0053	10800	4.714	.7378	90000	.0035	.9990
2600	2.753	.0098	11000	4.512	.7474	100000	.0023	.9992
2800	3.872	.0164	11200	4.320	.7559	∞	0	1.0000
3000	5.081	.0254	11400	4.137	.7645			
3200	6.312	.0368	11600	3.962	.7724			
3400	7.506	.0506	11800	3.796	.7802			
3600	8.613	.0667	12000	3.637	.7876			
3800	9.601	.0850	12200	3.485	.7947			
4000	10.450	.1051	12400	3.341	.8015			
4200	11.151	.1267	12600	3.203	.8081			
4400	11.704	.1496	12800	3.071	.8144			
4600	12.114	.1734	13000	2.947	.8204			
4800	12.392	.1979	13200	2.827	.8262			
5000	12.556	.2229	13400	2.714	.8317			
5200	12.607	.2481	13600	2.606	.8370			
5400	12.571	.2733	13800	2.502	.8421			
5600	12.458	.2983	14000	2.416	.8470			
5800	12.282	.3230	14200	2.309	.8517			
6000	12.053	.3474	14400	2.219	.8563			
6200	11.783	.3712	14600	2.134	.8606			
6400	11.480	.3945	14800	2.052	.8648			
6600	11.152	.4171	15000	1.972	.8688			
6800	10.808	.4391	16000	1.633	.8868			
7000	10.451	.4604	17000	1.360	.9017			
7200	10.089	.4809	18000	1.140	.9142			
7400	9.725	.5007	19000	.962	.9247			
7600	9.357	.5199	20000	.817	.9335			
7800	8.997	.5381	21000	.702	.9411			
8000	8.642	.5558	22000	.599	.9475			
8200	8.293	.5727	23000	.516	.9531			
8400	7.954	.5890	24000	.448	.9580			
8600	7.624	.6045	25000	.390	.9621			
8800	7.304	.6195	26000	.341	.9657			
9000	6.995	.6337	27000	.300	.9689			
9200	6.697	.6474	28000	.265	.9718			

Substitution of Equation [8] into Equation [7] gives

$$r = \frac{\int_0^\infty r_\lambda F E_\lambda d_\lambda}{\int_0^\infty F E_\lambda d_\lambda} = \frac{\int_0^\infty r_\lambda \left(\frac{E_\lambda}{\sigma T^5}\right) d(\lambda T)}{\int_0^\infty \left(\frac{E_\lambda}{\sigma T^5}\right) d(\lambda T)} \quad \ldots\ldots [9]$$

Since the integral in the denominator of the right-hand term is equal to unity

$$r = \int_0^\infty r_\lambda \left(\frac{E_\lambda}{\sigma T^5}\right) d(\lambda T) \quad \ldots\ldots [10]$$

In most cases the integral in Equation [10] is replaced by a simple summation, use of small intervals insuring satisfactory accuracy. The method can be outlined as follows:

An increment in (λT) is decided upon, the size of the increment depending in part upon the character of the spectral-reflectivity curve. If the curve is very irregular, or if a high degree of accuracy is desired, smaller increments are chosen. Values of λT are then tabulated and λ is calculated for each value of λT by dividing by source temperature. Values of r_λ from the spectral-reflectivity curve are tabulated for those wave lengths, multiplied by $E_\lambda/\sigma T^5$, summed, and multiplied by the increment in (λT). This gives the reflectivity. For opaque bodies this enables the absorptivity to be found since the reflectivity plus the absorptivity is equal to unity. If the source and the material are at the same temperature, the absorptivity is equal to the emissivity. If the spectral characteristics of the material do not change appreciably with temperature, the room-temperature spectral properties can be used to calculate the emissivity at higher temperatures. The same methods apply with any other spectral property, such as transmissivity.

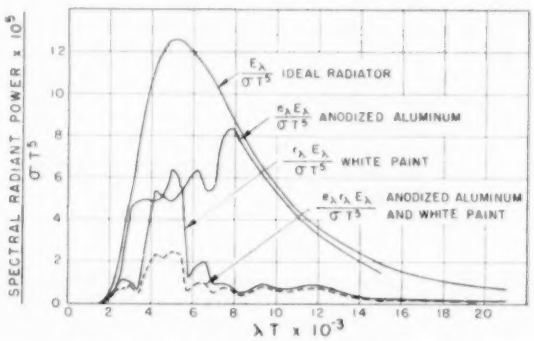
SPECTRAL RADIANT POWER x 10^5 / σT^5
E_λ / σT^5 IDEAL RADIATOR
ε_λ E_λ / σT^5 ANODIZED ALUMINUM
r_λ E_λ / σT^5 WHITE PAINT
ε_λ r_λ E_λ / σT^5 ANODIZED ALUMINUM AND WHITE PAINT
λT x 10^-3
0 2 4 6 8 10 12 14 16 18 20
0 2 4 6 8 10 12

FIG. 1 SPECTRAL EMISSIVE POWER FOR IDEAL RADIATOR; SPECTRAL EMISSIVE POWER, ANODIZED ALUMINUM AT 1000 R; REFLECTED SPECTRAL RADIANT POWER FROM WHITE PAINT IDEAL SOURCE AT 1000 R; ANODIZED ALUMINUM SOURCE AT 1000 R

This method is extended easily to include the calculation of the reflectivity of a material for a nonideal source at a different temperature. Referring to Equation [7] the spectral irradiation of the sample by the source becomes

$$G_\lambda = F \epsilon_\lambda E_\lambda \quad \ldots\ldots [11]$$

and upon substitution of Equation [11] into Equation [7]

$$r = \frac{\int_0^\infty r_\lambda e_\lambda \left(\frac{E_\lambda}{\sigma T^5}\right) d(\lambda T)}{\int_0^\infty e_\lambda \left(\frac{E_\lambda}{\sigma T^5}\right) d(\lambda T)} \quad \ldots\ldots\ldots [12]$$

In this equation the reflectivities refer to the receiver at the receiver temperature, while e_λ and E_λ refer to the source at the source temperature. The term in the denominator of Equation [12] is recognized to be the emissivity of the source, hence

$$r = \frac{1}{e} \int_0^\infty r_\lambda e_\lambda \left(\frac{E_\lambda}{\sigma T^5}\right) d(\lambda T) \quad \ldots\ldots\ldots [13]$$

The same method of numerical integration is used with Equation [13] as with Equation [10]. It is to be noted that for a black-body source, $e = e_\lambda = 1.0$, and Equation [13] reduces to Equation [10].

It is seen from Equation [12] that if r_λ is constant, the total reflectivity is equal to the spectral reflectivity. If the source is a gray body (e_λ = const) then the reflectivity is the same as for a black-body source.

These same methods also can be extended to include the spectral response of measuring instruments, or in illumination calculations where the visibility function would be included.

Use of Tables

As a first example, it is desired to know the wave length below which 90 per cent of the emitted power lies, for a body at 70 F. From Table 1 this is found to be approximately at $\lambda T = 17{,}000$ and hence $\lambda = 17{,}000/530 = 32$ microns. That is, for a source at room temperature, 90 per cent of the total emissive power lies at wave lengths less than 32 microns.

As another example, what fraction of the sun's radiation lies in the ultraviolet, visible, and in the infrared spectrum below 2.5μ? The temperature of the sun is taken as 10,800 R, and the limits of the visible as 0.4μ and 0.75μ. Multiplying the wave lengths by the absolute temperature of the sun, the respective values of λT are found to be 4300, 8100, and 27,000, giving the fraction of the total emissive power below these wave lengths from Table 1 as 0.138, 0.563, and 0.969. This indicates that 13.8 per cent of the solar emission lies in the ultraviolet, 56.3 — 13.8 = 42.5 per cent lies in the visible, and the remainder lies in the infrared. Ninety-six and nine-tenths per cent of the energy is at wave lengths less than 2.5 microns.

Computation of Total Properties From Spectral Properties

As examples, the emissivity of anodized aluminum at 1000 R, the reflectivity of white paint (flat white enamel undercoater, Pittsburgh LA 404) for black-body radiation from a 1000 F source, and the reflectivity of the same paint for radiation from anodized aluminum at 1000 R will be computed. The spectral reflectivity of anodized aluminum at room temperature is given in Fig. 2. The spectral emissivity is equal to 1 minus the reflectivity. In the computations it is assumed that the spectral emissivities do not change in the range from 530 R to 1000 R. The spectral reflectivity of flat white paint is given in Fig. 2.[4,5]

[4] "The Absolute Spectral Reflectivity of Certain Pigments and Metals in the Wave-Length Range Between 2 and 15 Microns," by J. T. Gier, L. Possner, A. J. Test, R. V. Dunkle, and J. T. Bevans, Report No. 7, Report Code NR-015-202.

[5] "Final Report," by R. V. Dunkle, N. Snyder, L. Possner, A. J. Test, E. Hisdal, and J. T. Gier, Thermal Radiation Project, Report No. 10, Report Code NR-015-202.

Referring to Table 2, the calculation procedure is as follows: Increments of λT of 400μ R are used, corresponding to 0.4 microns for a 1000 R source. The lowest value of λT tabulated in Table 2 is 1800, as it is seen from Table 1 that only 0.03 per cent of the total emissive power lies at shorter wave lengths. Values of $E_\lambda/\sigma T^5$ are read from Table 1 and tabulated in column 2 of Table 2. Values of λ for $T = 1000$ R are tabulated in column 3, corresponding to the values of λT in column 1. Values of the spectral emissivity of anodized aluminum were read from Fig. 2

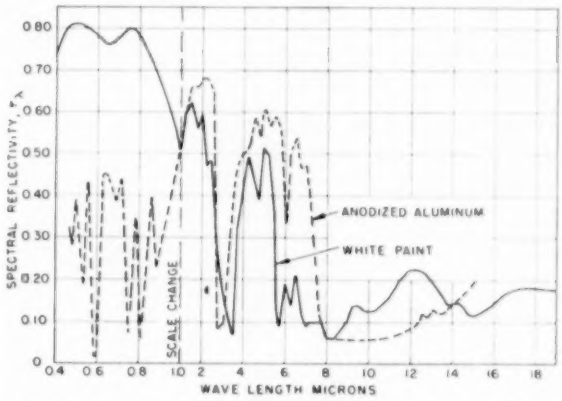

Fig. 2 Spectral Reflectivity, Flat White Enamel Undercoater, Pittsburgh LA 404; Anodized Aluminum, Heavy Coating

and tabulated in column 4. The product of columns 3 and 4 is tabulated in column 5 and is also plotted in Fig. 1.

Since spectral-emissivity data for anodized aluminum are only available out to 15μ an additional complication arises. It is necessary to extrapolate the spectral emissivity curve beyond 15 microns. It is assumed that the value of 0.8 will be a good approximation of the emissivity beyond 15μ. (The emissivity at 15μ = 0.80.) The fraction of the total emissive power beyond 15μ(λT = 15,000) is 0.132 from Table 1. An error of 0.10 in the extrapolated values would only result in an error of 0.013 in the total emissivity. The sum of column 5 to $\lambda T = 15{,}000$ is 68.73×10^{-6}. (Note that the last tabular value was multiplied by 1/2 owing to the use of the trapezoidal rule in summation.) The emissivity is then obtained by multiplying by the increment in λT and adding the fraction of the total emissive power beyond the long wave limit of the spectrum multiplied by the estimated spectral emissivity in this region. Hence

$$e = \Delta(\lambda T) \left[\sum_0^{\lambda T} \frac{e_\lambda E_\lambda}{\sigma T^5}\right] + e_{\lambda T - \infty} \left(1 - \frac{E_{0-\lambda T}}{\sigma T^4}\right)$$

or

$$e = 400 \times 147.8 \times 10^{-6} + 0.80 \times 0.132 = 0.697$$

Reflectivity of White Paint at Room Temperature for Black-Body Source at 1000 R

In column 6 of Table 2 is tabulated the reflectivity of the flat white paint. In this case data were available out to 21μ, so the tabulation is carried out to $\lambda T = 21{,}000$, the fraction of the total emissive power beyond this point being 0.059. In column 7 is the product of columns 2 and 6; this product is also plotted in Fig. 1. Using an estimated reflectivity of 0.15 beyond 21μ the reflectivity of white paint for a black-body source at 1000 R is

$$r = 400 \times 50.45 \times 10^{-6} + 0.15 \times 0.059 = 0.211$$

TABLE 2 WORKSHEET FOR COMPUTATION FROM SPECTRAL DATA OF TOTAL EMISSIVITY OF ANODIZED ALUMINUM AT 1000 R; REFLECTIVITY OF WHITE PAINT FOR RADIATION FROM AN IDEAL OR GRAY-BODY SOURCE AT 1000 R; AND REFLECTIVITY OF WHITE PAINT FOR RADIATION FROM ANODIZED ALUMINUM AT 1000 R

	Anodized Aluminum					White Paint		
	$E_\lambda \times 10^5$			$\epsilon_\lambda E_\lambda \times 10^5$		$r_\lambda E_\lambda \times 10^5$	$r_\lambda \epsilon_\lambda E_\lambda \times 10^5$
λT	σT^5	λ	ϵ_λ	σT^5	E_λ	σT^5	σT^5
1800	.21	1.8	.34	.07	.57	.12	.04
2200	1.04	2.2	.32	.33	.50	.52	.17
2600	2.75	2.6	.60	1.65	.40	1.10	.66
3000	5.08	3.0	.90	4.57	.19	.97	.87
3400	7.50	3.4	.65	4.88	.10	.75	.48
3800	9.59	3.8	.52	4.99	.34	3.26	1.69
4200	11.14	4.2	.44	4.90	.48	5.35	2.35
4600	12.10	4.6	.42	5.08	.42	5.08	2.13
5000	12.53	5.0	.39	4.89	.51	6.39	2.49
5400	12.55	5.4	.42	5.27	.44	5.52	2.32
5800	12.26	5.8	.48	5.88	.10	1.22	.59
6200	11.77	6.2	.54	6.36	.15	1.77	.96
6600	11.13	6.6	.48	5.34	.18	2.00	.96
7000	10.43	7.0	.52	5.42	.09	.94	.49
7400	9.71	7.4	.80	7.77	.10	.97	.78
7800	8.98	7.8	.93	8.35	.09	.81	.75
8200	8.28	8.2	.945	7.82	.06	.50	.47
8600	7.61	8.6	.945	7.19	.07	.53	.50
9000	6.98	9.0	.940	6.56	.10	.70	.66
9400	6.40	9.4	.945	6.05	.14	.90	.85
9800	5.86	9.8	.940	5.51	.13	.76	.71
10200	5.37	10.2	.94	5.05	.13	.70	.66
10600	4.92	10.6	.94	4.62	.14	.69	.65
11000	4.50	11.0	.935	4.21	.16	.72	.67
11400	4.13	11.4	.93	3.84	.19	.78	.73
11800	3.79	11.8	.92	3.49	.22	.83	.76
12200	3.48	12.2	.92	3.20	.225	.78	.72
12600	3.20	12.6	.885	2.83	.22	.70	.62
13000	2.94	13.0	.885	2.60	.20	.59	.52
13400	2.71	13.4	.890	2.41	.17	.46	.41
13800	2.50	13.8	.86	2.15	.14	.35	.30
14200	2.31	14.2	.85	1.96	.14	.32	.27
14600	2.13	14.6	.825	1.76	.13	.23	.23
15000	1.97	15.0	.80 x 1/2	.79	.115	.23	.18
15400	1.83	15.4			.12	.22	.18
15800	1.69	15.8			.135	.23	.18
16200	1.57	16.2			.15	.24	.19
16600	1.46	16.6			.17	.25	.20
17000	1.36	17.0			.18	.24	.19
17400	1.26	17.4			.18	.23	.18
17800	1.18	17.8			.18	.21	.17
18200	1.10	18.2			.18	.20	.16
18600	1.03	18.6			.18	.19	.15
19000	.96	19.0			.20	.19	.15
19400	.90	19.4			.19	.17	.14
19800	.84	19.8			.18	.15	.12
20200	.79	20.2			.17	.13	.10
20600	.75	20.6			.15	.11	.09
21000	.70	21.0			.15 x 1/2	.05	.04
SUM				147.80		50.45	29.88

Reflectivity of White Paint for Anodized Aluminum Source at 1000 R

In column 8 of Table 2 is tabulated the product of columns 7 and 4, which is also plotted in Fig. 1. The sum of this column using the same extrapolated properties as before, divided by the emissivity of the anodized aluminum, gives the reflectivity of the white paint for radiation from anodized aluminum at 1000 R to be 0.181.

This compares with the reflectivity of 0.211 for radiation from a black-body source, a difference of roughly 15 per cent. It is well to point out that the difference in the reflectivity for real and ideal sources is often less than this but in some cases can be considerably greater.

Conclusion

These tables were computed for two reasons: (1) To make use of the latest information on the radiation constants, and (2) to put this information in a readily usable form for engineers. Unfortunately, there is a great dearth of published information on spectral characteristics of materials, particularly with regard to the effect of temperature upon the spectral properties. It is hoped that this paper will stimulate more interest in obtaining additional information on spectral properties.

Local Boiling Heat Transfer to Water at Low Reynolds Numbers and High Pressures

By J. A. CLARK[1] and W. M. ROHSENOW[2]

Local surface coefficients of heat transfer and maximum heat-flux density are presented for degassed, distilled water flowing upward in a vertical L-nickel tube under the following conditions: Mass velocities in the range 2.6 to 73 lb_m/ft^2 sec (or inlet velocities in the range 0.05 to 1.4 fps), absolute pressures up to 2000 psia, and liquid subcooling between 0 to 300 F. The effects of natural convection on the nonboiling heat-transfer process were found to be significant, causing the transition from laminar to turbulent flow at the surface to occur at length Reynolds number in the range 60,000–100,000. Emphasis is placed on data in the region of surface boiling. The test section dimensions were 0.180 in. ID and 9.4 in. long.

Nomenclature

The following nomenclature is used in the paper:

A = heat-transfer area, sq ft
c_p = specific heat, Btu/lb deg F
D_i = inner diameter of test section, ft
E = test-section voltage, volts
G = mass velocity, lb/hr ft^2
h = surface coefficient of heat transfer, Btu/hr ft^2 deg F
I = test-section current, amp
k = thermal conductivity of fluid, Btu/hr ft deg F
k_o = thermal conductivity of tube wall at t_o, Btu/hr ft deg F
L_p = test-section heated length, ft
$N_{Re} = \dfrac{D_i G}{\mu}$
q/A = heat-flux density, Btu/hr ft^2
$(q/A)_{n-(n-1)} = \frac{1}{2}[(q/A)_n + (q/A)_{(n-1)}]$
$j = \dfrac{h}{c_p G}\left(\dfrac{c_p \mu}{k}\right)^{2/3}$
r_o = outer radius of test section, ft
r_i = inner radius of test section, ft
R = resistance, ohms
τ_b = test water bulk temperature, deg F
τ_{in} = test water-inlet bulk temperature, deg F
τ_{out} = test water-outlet bulk temperature, deg F
t_w = test-section inner-wall temperature, deg F
t_{sat} = saturation temperature, deg F
T_s = wall temperature minus saturation temperature, $t_w - t_{sat}$, deg F
V = flow velocity, fps
w = flow rate, lb/hr
$\Delta X = (r_o - r_i)$
X = distance between thermocouple stations, 1.4 in.
t_o = test-section outer-wall temperature, deg F
x = bulk quality of liquid-vapor mixture, mass fraction vapor
β = temperature coefficient of electrical resistivity, deg F^{-1}
α = temperature coefficient of thermal conductivity, deg F^{-1}
ρ_o = electrical resistivity at t_o, ohm-ft
ρ_m = electrical resistivity at temperature $t_m = \dfrac{1}{\Delta X}\displaystyle\int_{r_i}^{r_o} (t - t_w)\,dr$
ρ = mass density of fluid at fluid temperature, lb_m/cu ft
μ_F = viscosity at film temperature, $\dfrac{\tau_b + t_w}{2}$, lb/hr ft
μ_b = viscosity at average bulk-fluid temperature
μ_w = viscosity at wall temperature
σ = standard deviation

Introduction

This work is an extension of the region reported in reference (1)[3] into the very low velocity and very low liquid-subcooling range. It represents some of the initial data available for these conditions of very low flow rates with surface boiling, including maximum heat-flux densities. The particular type of heat-transfer process studied is encountered in liquid-cooled rocket motors and in the more recent steam power-plant equipment.

Apparatus

A schematic arrangement of the test circuit is shown in Fig. 1. Power was supplied by two 36-kw 12-volt d-c generators driven by 440-volt, 3-phase, a-c 600-rpm synchronous motors. For the low flow-rates small-size "pin-hole" orifices of 0.018, 0.024 in. diam were calibrated and installated. To prevent clogging of these small openings with dirt particles, it was found necessary to install a filter, consisting of stainless-steel wool, ahead of the flow-measuring orifice. A by-pass was installed around the orifice to permit high flow rates, as when preheating the test circuit water. Also, an ion-exchanger (1) was found to be necessary in order to prevent contamination of the test-section surface. The water was circulated by a Westinghouse type 30-A centrifugal stainless-steel canned-rotor pump cooled by transformer oil remotely circulated. A Hayward-Tyler centrifugal pump was used as stand-by equipment.

The test section, Fig. 2, consists of a pure L-nickel tube (International Nickel Company "L" nickel) of 0.1805 in. ID, 0.2101 in. OD, and a length of 9.4 in. The location of the thermocouples which measure outer tube-wall temperatures are shown in Fig. 3. All thermocouples were chromel-constantan, precalibrated. Also shown is the voltage-divider scheme used to determine the voltage difference between the potential taps.

The inner tube-wall temperature at each of the seven stations

---

[1] Assistant Professor, Department of Mechanical Engineering, Massachusetts Institute of Technology, Cambridge, Mass. Assoc. Mem. ASME.

[2] Associate Professor, Department of Mechanical Engineering, Massachusetts Institute of Technology. Assoc. Mem. ASME.

Contributed by the Heat Transfer Division and presented at the Annual Meeting, New York, N. Y., November 29–December 4, 1953, of The American Society of Mechanical Engineers.

Note: Statements and opinions advanced in papers are to be understood as individual expressions of their authors and not those of the Society. Manuscript received at ASME Headquarters, September 2, 1953. Paper No. 53—A-183.

[3] Numbers in parentheses refer to Bibliography at end of paper.

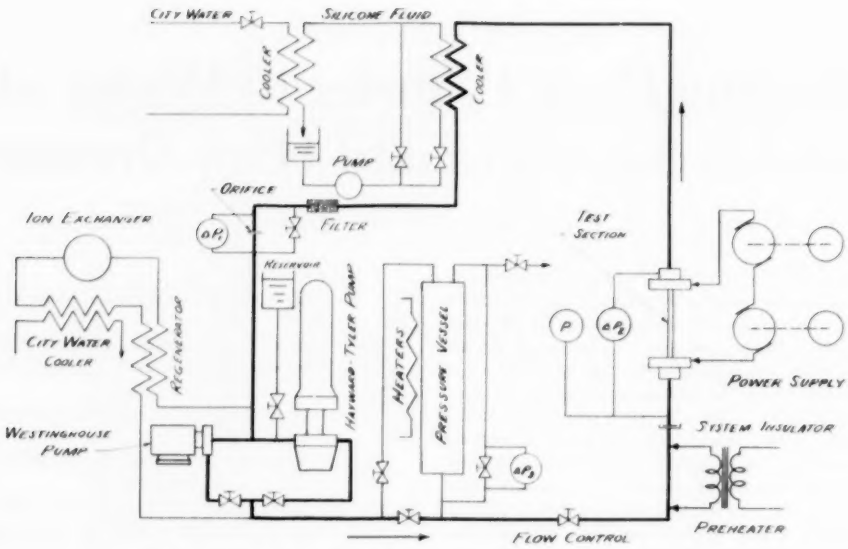

FIG. 1 SCHEMATIC DIAGRAM OF SYSTEM

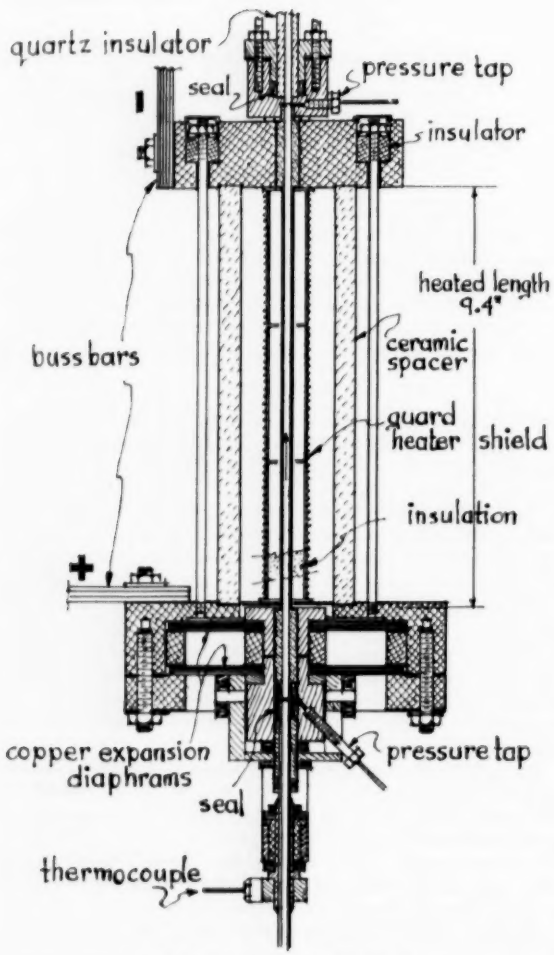

FIG. 2 TEST-SECTION ASSEMBLY

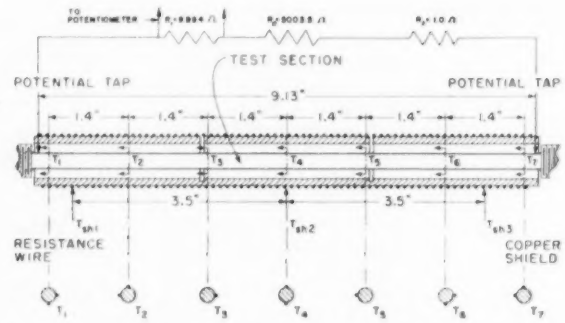

FIG. 3 LOCATION OF THERMOCOUPLES, POTENTIAL TAPS, AND VOLTAGE-DIVIDER NETWORK

along the tube was determined by measuring the outer-wall temperature and calculating the temperature difference across the tube wall from the electric current and tube properties. The thermocouples were insulated from the tube wall by a thin sheet of mica 0.0015 in. thick. The electrically heated shield, with insulation material between the test section and shield, provided an isothermal region by making the shield temperature equal the tube-wall thermocouple temperature. Then the tube-wall thermocouple temperature was equal to the outer tube-wall temperature. This method was proved to be very satisfactory in the work reported in reference (1).

The bulk temperature of the water entering and leaving the test section was determined by an inlet thermocouple located $5^1/_2$ in. upstream of the heated length and by an outlet thermocouple 9 in. downstream of the heated length. At very low velocities a considerable temperature drop of the water occurred between the thermocouples and the heated section. This heat loss to the atmosphere in the $5^1/_2$-in. section was minimized by packing a sizable quantity of 85 per cent magnesia insulation around it. Before each test run at a particular velocity and liquid subcooling, a calibration run was made by reducing the electric current to zero and determining the temperature drop in this inlet section. The bulk temperature at succeeding points along the tube was obtained by integrating a plot of q/A versus length to determine the enthalpy increase of the water to the particular location.

The inner-wall temperature was calculated from a Taylor series solution of the temperature distribution for heat conduction in an electrically heated tube with an adiabatic outer wall. This equation which is similar to that proposed by Kreith and Summerfield (2) is

$$t_o - t_w = \frac{m}{k_o \rho_o}\left\{\overline{\Delta x^2} + \frac{\overline{\Delta x^3}}{r_o} + \overline{\Delta x^4}\left[\frac{m}{6}\frac{(3\alpha + 4\alpha\beta t_o + \beta)}{(1+\beta t_o)(1+\alpha t_o)} + \frac{1}{4r_o^2}\right] + \ldots\right\} \ldots\ldots [1]$$

where

$$m = \frac{3.413\, I^2 \rho_m^2}{2\pi^2(r_o^2 - r_i^2)^2}$$

For accuracy within 0.5 per cent of $t_o - t_w$ the third term may be neglected, the working equation then becoming

$$t_o - t_w = \frac{m}{K_o \rho_o}\left\{\overline{\Delta x^2} + \frac{\overline{\Delta x^3}}{r_o} + \ldots\right\} \ldots\ldots [1a]$$

This relation includes allowance for variation of electrical resistivity and thermal conductivity with temperature and for electrical resistivity with radius.

Measurement of Heat-Flux Density

The power dissipated in any portion of the test section is dependent upon the electrical resistance, which, being a function of temperature, varies from point to point along the tube. The heat-flux density then varies along the test-section length and must be calculated to obtain accurate results. For a small element of length dx

$$q/A = \frac{3.413 I^2 \rho_m dx}{\pi D_i dx \pi (r_o^2 - r_i^2)} = 1.148 \times 10^9 I^2 \rho_m \ldots\ldots [2]$$

for the tube of 0.1805 in. ID and 0.2101 in. OD.

The electric current was determined from the measured voltage drop across a 0.00001667-ohm G-E manganic shunt calibrated by the National Bureau of Standards. The shunt was in series with the test section and its voltage drop was measured by a Rubicon potentiometer.

The voltage drop across the test section was measured by the potentiometer and a voltage-divider network as illustrated in Fig. 3. The resistors were General Radio Company resistors calibrated at the M.I.T. Electrical Instruments Laboratory. The potential taps were made of nichrome wire tied firmly to the tube with asbestos string. The voltage drop across the test section is then

$$E_{ts} = E_1\left(\frac{R_1 + R_2 + R_3}{R_1}\right) \ldots\ldots [3]$$

The method of determining the fluid temperature at any station along the tube consisted of integrating q/A from the inlet to the station in question and determining the fluid enthalpy rise from the inlet. Neglecting axial heat flow and neglecting the effect of vapor bubbles on the effective specific heat of the water, an energy balance results in

$$\int_{i_w}^{h_n} dh = \frac{\pi D_i}{w}\int_0^n (q/A)dx = h(\Delta\tau) \ldots\ldots [4]$$

In general, it was sufficiently accurate to make the actual calculation by a stepwise integration between any two stations n and $(n-1)$ in the form

$$h_n - h_{(n-1)} = \frac{\pi D_i}{w} x_{n-(n-1)}(q/A)_{n(n-1)} = h(\tau_n) - h(\tau_{n-1}) \ldots [5]$$

Accuracy of Results

The tube thickness varied ± 0.0003 in. Equation [2] with the values of m introduced shows the first and major term of the series to be proportional to the square of the tube diameter. For the high heat-flux tests the value of $(t_o - t_w)$ was about 6 deg F; then the maximum error of t_w attributable to tube-thickness variation was 0.02 deg F and decreases as the heat flux is lowered.

The thermal-conductivity data were obtained from the International Nickel Company and the electrical-resistivity data were determined experimentally to an estimated accuracy of ± 0.5 per cent.

It is expected that the inner-wall temperature has been determined within a ± 2 deg F error.

Experimental Procedure

The system was filled with freshly distilled water (0.70 ppm as NaCl and approximately 15 ml air/l) from a supply tank by means of gravity to an aspirator located at the top of the Hayward-Tyler pump. Although this pump was used infrequently, it was filled with water so as to be in readiness if its use was required. Also, the aspirator flow from this pump served as an indication that the system was full of water.

As soon as it was certain that the upper thrust bearing on the Hayward-Tyler pump was immersed in water and the system pressure was raised to approximately 100 psig by the pressure vessel, this pump or the Westinghouse pump was started and water was circulated through the test loop. Degassing was accomplished by circulating the test circuit water through the heated pressure vessel vented to the atmosphere for a period of 1/2 to 3/4 hr with the orifice by-pass open. This period was found to be of sufficient length to reduce the oxygen content to approximately 1.5 ml air/l, as determined by the Winkler technique. Subsequent to degassing, the system was sealed by closing the degassing vent and test water was circulated through the test section at high velocity. The bulk temperature of the water was increased by applying power to the test section and the system pressure was raised to the desired level by heating the water in the closed pressure vessel. The system pressure could be controlled to ± 2 psi by the chromolox strip heaters regulated by a variac. The inlet bulk temperature was controlled and maintained at the desired level by regulating the power to two 2-kva transformers connected to a section of the inlet tubing and forming an electrical resistance heater which transferred heat to the inlet water. Cooling-water flow to the ion-exchanger heat exchanger and the city-water heat exchanger was fixed at its maximum rate at the beginning of the run and not thereafter adjusted. The water at the discharge of the ion exchanger was consistently at approximately 0.1 ppm NaCl.

About 1/2 hr prior to a run, the generators were started and allowed to warm up. During a run, power was applied to the test section in small increments to obtain the desired conditions. At each collecting condition the temperature shields were balanced and readings taken of outer-wall temperatures, inlet and outlet-water temperatures, shield temperatures, test-section voltage and amperage, temperature of orifice and ion exchanger, system pressure, and orifice pressure drop. The flow rates were too small for test-section pressure drop to be indicated. Under conditions of local boiling, which was the principal sphere of interest in this investigation, the wall temperatures of the tube were constant except at the ends where cooling effects were encountered. This simplified the shield-balancing procedure.

Because of the cooling of the water from the inlet thermocouple to the beginning of the heated section it was necessary during each run, for each velocity and inlet bulk temperature, to perform a calibration and determine the magnitude of this cooling. This

was accomplished by reducing the test-section power to zero, balancing the shields, and taking readings at the inlet-water thermocouple and the test-section wall thermocouples. The difference was the magnitude of the cooling, thus allowing far more accurate determinations of the temperature of the water at the inlet to the heated section.

Experimental Results

Wall-Temperature Distribution. The typical wall-temperature-distribution curves of the test runs are shown as dotted curves in Fig. 4. In the nonboiling runs the wall temperature followed the general shape of the fluid-temperature curve since the film coefficient generally does not vary radically along the tube. In the boiling runs, the wall temperature was nearly constant along the tube.

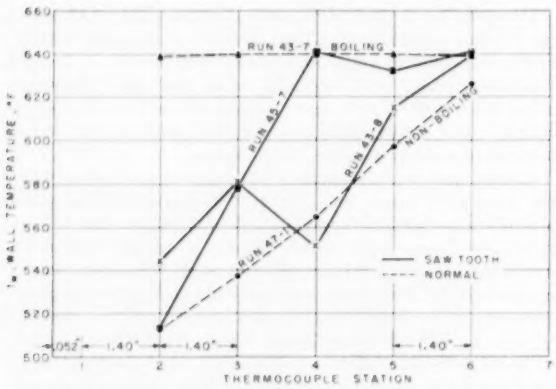

Fig. 4 "Sawtooth" Wall-Temperature Distribution

Under certain conditions of operation in the velocity range from 0.25 to 0.6 fps unusual wall-temperature-distribution curves resulted. Typical of these unusual curves are the solid lines in Fig. 4. These results could be repeated in subsequent runs, and the point of the "sawtooth" could be shifted along the tube by changing the fluid velocity or the heat flux.

This sawtooth curve has been explained by postulating laminar flow upstream of the break in the curve and turbulent flow downstream. This then becomes a transition region. Since the diameter Reynolds numbers of the flow existing when these unusual curves were encountered were in the range 1650–4800, this seems to be a reasonable explanation.

The sharp drop in wall temperature along the tube indicates a decrease in the temperature difference between wall and fluid. Since the electric current requires an almost uniform rate of heat transfer for each section of tube length, this decrease in wall temperature indicates a sharp rise in film coefficient of heat transfer which would be expected to accompany such a change from laminar to turbulent flow. This transition in the type of flow is probably a result of a predominating effect of free convection owing to the density gradient in the heated fluid. All nonboiling runs are plotted in Fig. 5 as hD/k versus Re_s. It is seen that a sharp increase in the Nusselt number occurs consistently in the length Reynolds-number range $60{,}000 \leqslant Re_s \leqslant 100{,}000$. This is the transition region, excited in the particular cases reported here by the effects of free convection in a vertical tube. These effects of superimposed free convection are clearly shown in Fig. 6 where low values of hD/k are plotted against diameter Reynolds numbers. At Reynolds numbers in the range 1000–3000 the data all lie considerably above the line of Norris and Sims (6) through the higher Reynolds-number points. Furthermore,

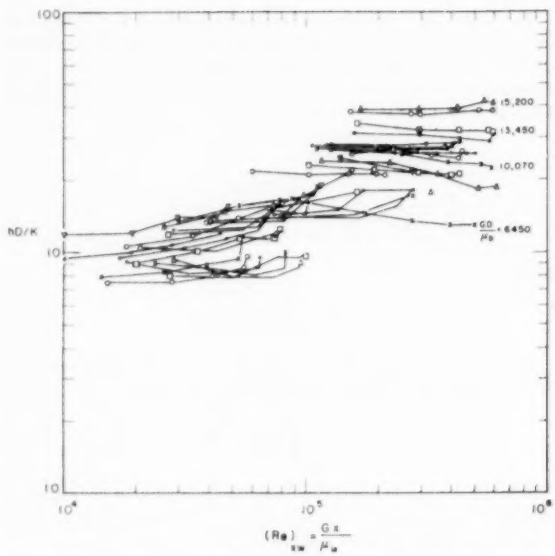

Fig. 5 Nusselt Number Versus Length Reynolds Number, Showing Transition From Laminar to Turbulent Flow for Nonboiling Heat Transfer

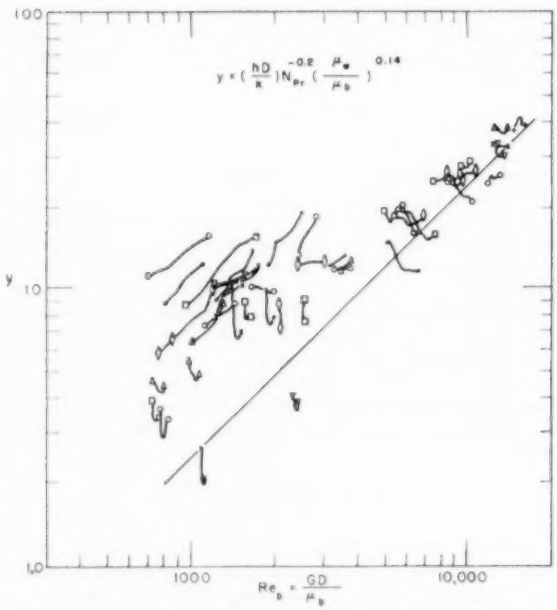

Fig. 6 Nusselt Number Versus Diameter Reynolds Number, Showing Effect of Superimposed Free Convection on Nonboiling Heat Transfer

the data for any one run (shown by connecting points) indicate an increasing Nusselt number with length, a phenomenon contrary to the usual entrance effects on heat-transfer processes. In all such runs reported here the turbulence level in the heated pipe is increasing significantly with length. The initial turbulence level was unknown.

One or two sets of nonboiling data were taken before each set of boiling data was gathered. These nonboiling data show that the

boiling data have been gathered for the cases in which boiling is superimposed on flow which normally would be laminar in the absence of bubble formation and agitation as well as for the case in which the flow normally would be turbulent in the absence of bubble formation and agitation.

Heat Transfer in Forced Convection With Surface Boiling. Heat-transfer data at various fluid velocities in the range 0.04–1.4 fps at 2000 psia were obtained. (Typical curves of q/A versus Δt for 2000 psia and 500 psia are presented in Figs. 11 and 12.) Tables of data are available in reference (7).

Representative data of boiling runs at 2000 psia for the various fluid velocities are shown in Fig. 7 along with the high-velocity (10–30 fps) data reported earlier in reference (1). The data for

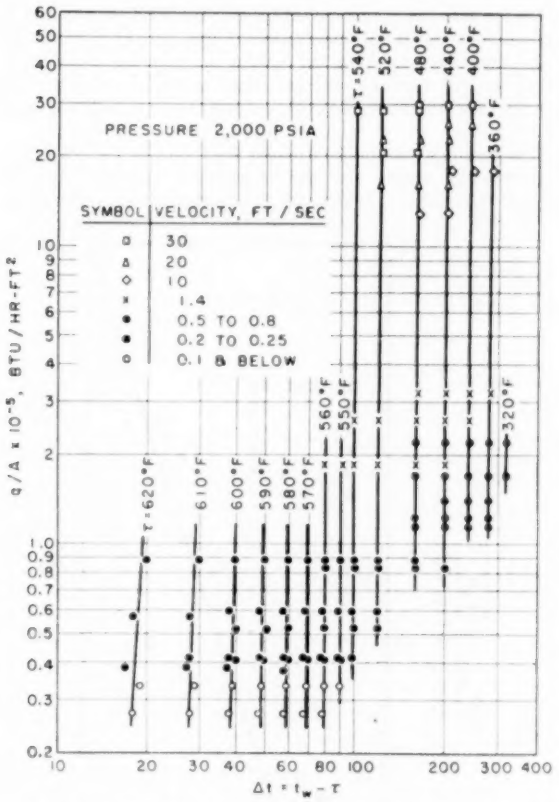

FIG. 7 HEAT FLUX VERSUS TEMPERATURE DIFFERENCE FOR FORCED CONVECTION WITH SURFACE BOILING OF WATER AT 2000 PSIA

this plot were selected so that maximum and minimum heat-flux densities obtained at any given velocity would appear; in some cases intermediate data also are shown. It is observed that the data for a particular fluid bulk temperature fall on a single line independent of the fluid velocity. The lines are nearly vertical showing that the wall temperature does not change much over a wide variation of heat-flux density.

The same data are replotted in Fig. 8 with an abscissa of wall temperature minus saturation temperature. This method of plotting aligns the points for a given fluid velocity along a single line independent of fluid bulk temperature. It must be remembered that the values of the abscissa of Fig. 8 are below 8 F. These values are obtained by subtracting the saturation temperature from the inner-wall temperature which in turn is calculated

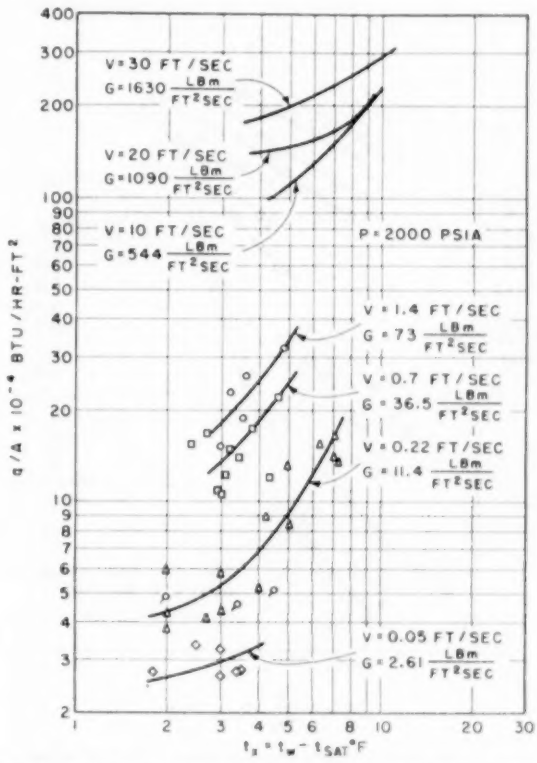
V = 30 FT / SEC
G = 1630 LBm / FT²SEC
V = 20 FT / SEC
G = 1090 LBm / FT²SEC
V = 10 FT / SEC
G = 544 LBm / FT²SEC
P = 2000 PSIA
V = 1.4 FT / SEC
G = 73 LBm / FT²SEC
V = 0.7 FT / SEC
G = 36.5 LBm / FT²SEC
V = 0.22 FT / SEC
G = 11.4 LBm / FT²SEC
V = 0.05 FT / SEC
G = 2.61 LBm / FT²SEC
q/A x 10⁻⁴ BTU / HR-FT²
t_s = t_w - t_SAT °F

FIG. 8 HEAT FLUX VERSUS T_s FOR FORCED CONVECTION WITH SURFACE BOILING OF WATER AT 2000 PSIA

from the measured outer-wall temperature and the magnitude of the electrical current. An error of only 1 deg F in the determination of the inner-wall temperature is greatly magnified on the plot of Fig. 8. In view of this, the scattering of points is remarkably small.

Observation of the curves of Fig. 8 shows a tendency for the curves associated with the various fluid velocities to merge into a single curve at the high values of T_s where the boiling becomes more vigorous. This supports the hypothesis that the motion of the bubbles in vigorous boiling controls the heat-transfer process by the resulting agitation of the fluid, and the fluid velocity or pipe Reynolds number has little influence (3), (4). The predominance of the effect of bubble agitation is shown in both cases where, in the absence of bubble motion (boiling), the flow would be either laminar or turbulent, Fig. 7.

For pool boiling it has been shown in reference (4) that the data for a particular clean surface-fluid combination could be correlated by the relation

$$\frac{c_l T_s}{h_{fg}} = C_{sf}\left[\frac{q/A}{\mu_l h_{fg}}\sqrt{\frac{g_c\sigma}{g(\rho_l-\rho_v)}}\right]^{0.33}\left(\frac{c_l\mu_l}{k_l}\right)^{1.7} \quad \ldots\ldots [6]$$

where the magnitude of C_{sf} is determined by the particular surface-fluid combination.

The local boiling data with forced convection shown in Figs. 7 and 8 were plotted in Fig. 9 in the same manner as the pool-boiling data, reference (4). Shown on the same graph is a line at a slope of 3, which might represent pool-boiling data for this surface-fluid combination. The line is arbitrarily placed to appear as an asymptote of the forced-convection boiling data. The vertical distance between the line representing the forced-con-

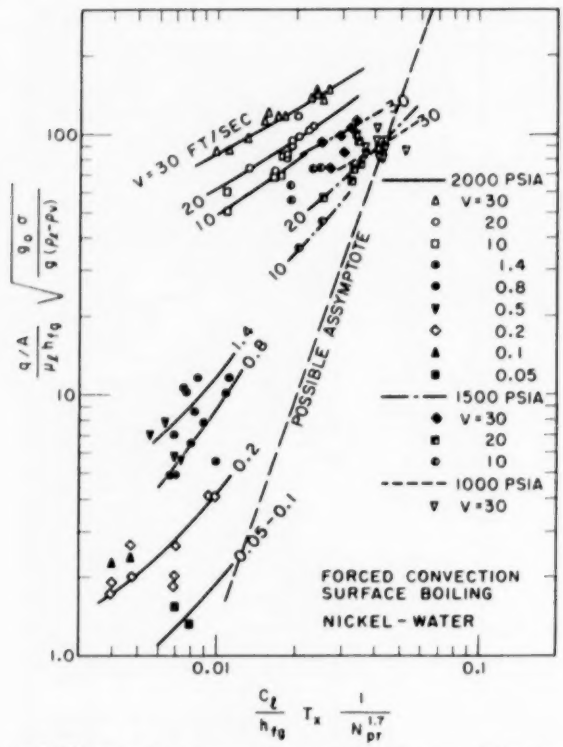

FIG. 9 FORCED-CONVECTION BOILING DATA PLOTTED WITH DIMENSIONLESS GROUPS SUGGESTED BY POOL BOILING CORRELATION OF REFERENCE (4)

vection boiling data and the asymptote (interpreted as a line for pool boiling) might be interpreted as the effect of nonboiling superimposed on the effect of boiling alone (pool boiling). Based on this superposition, hypothesis graphs were prepared and presented in reference (5) as shown here in Fig. 10 where

$$(q/A)_{boil} = (q/A) - (q/A)_{conv} \quad [7]$$

and

$$(q/A)_{conv} = h(t_w - t_{liq}) \quad [8]$$

and

$$\left(\frac{h}{c_p G}\right) N_{Pr}^{2/3} = 0.019 \left(\frac{GD_i}{\mu}\right)^{-0.2} \quad [9]$$

In Fig. 10 only the boiling data are plotted for which the nonboiling condition results in turbulent flow. Equation [9] was shown in an earlier paper (1) to correlate the nonboiling forced-convection heat-transfer data in turbulent flow.

From Fig. 10 all of the forced-convection boiling data in the range of pressures and velocities investigated has been reduced to a single line which has the equation

$$\frac{c_l T_x}{h_{fg}} = 0.006 \left[\frac{(Q/A)_{boil}}{\mu_l h_{fg}} \sqrt{\frac{g_o \sigma}{g(\rho_l - \rho_v)}}\right]^{0.33} \left(\frac{c_l \mu_l}{k_l}\right)^{1.7} \quad [10]$$

where C_{sf} of Equation [6] is 0.006. In the pool-boiling correlations (5) the value of C_{sf} ranged from 0.003 to 0.015; hence this value of 0.006 seems to be reasonable. It must be remembered that the magnitude of C_{sf} depends upon the kind of surface and fluid being boiled. For this case C_{sf} = 0.006 is for an L-nickel-water combination. The forced-convection data of Kreith and Summerfield (2) also were shown in reference (5) to be correlated by an equation of the form of Equation [10] but with C_{sf} = 0.014 for a 0.54-in-ID type 304 stainless-steel tube with water.

Maximum Heat Flux. The boiling curves in Figs. 7 and 8 have an upper limit of the nucleate boiling range when the (q/A) is increased sufficiently to cause a vapor "blanketing" of the heating surface. When vapor blanketing occurs the wall temperature rises rapidly for a particular heat flux since the heat-transfer resistance of the vapor is high compared with that of the agitated liquid. Usually the final steady-state wall temperature necessary to transfer the peak flux of the nucleate boiling range through the vapor blanket is above the melting point of the tube metal. At low velocities, below V = 1.4 fps, it was found that when the peak flux was exceeded the wall temperature rose slowly enough to permit the operator to reduce the electrical power input manually, thus preventing the melting or rupturing of the tube. At higher velocities the peak heat flux was so high that the wall temperature rose too rapidly to be arrested by manual reduction of the power.

The results of the peak-flux tests are shown in Fig. 13 where the discharge quality x of the liquid-vapor mixture is plotted against mass velocity G, for various conditions of inlet subcooling

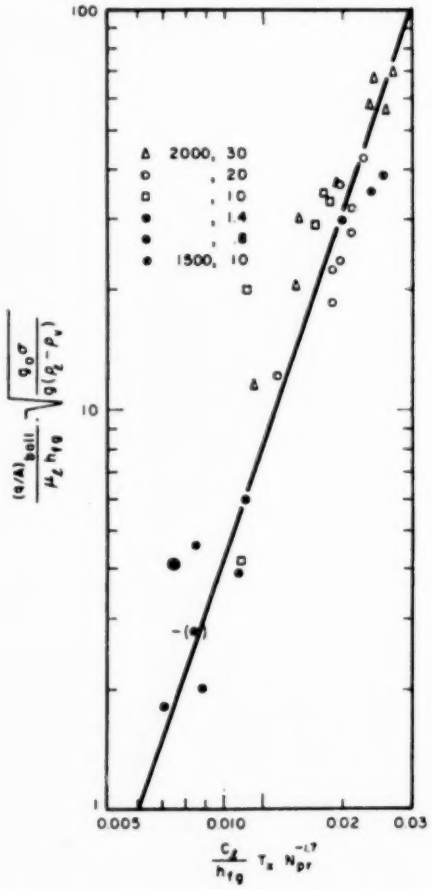

FIG. 10 CORRELATION FOR FORCED-CONVECTION BOILING DATA WITH SUPERIMPOSED NONBOILING PREDICTED HEAT-TRANSFER RATE SUBTRACTED

[Reproduced from Fig. 39 of reference (5).]

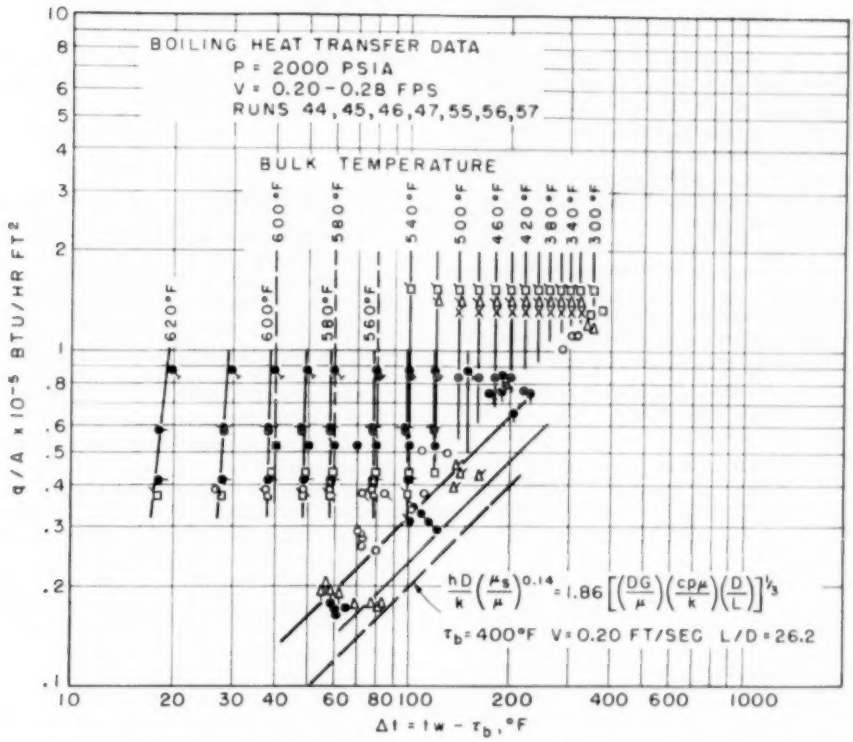

FIG. 11 q/A VERSUS ΔT FOR 2000 PSIA AND 0.20–0.28 FPS

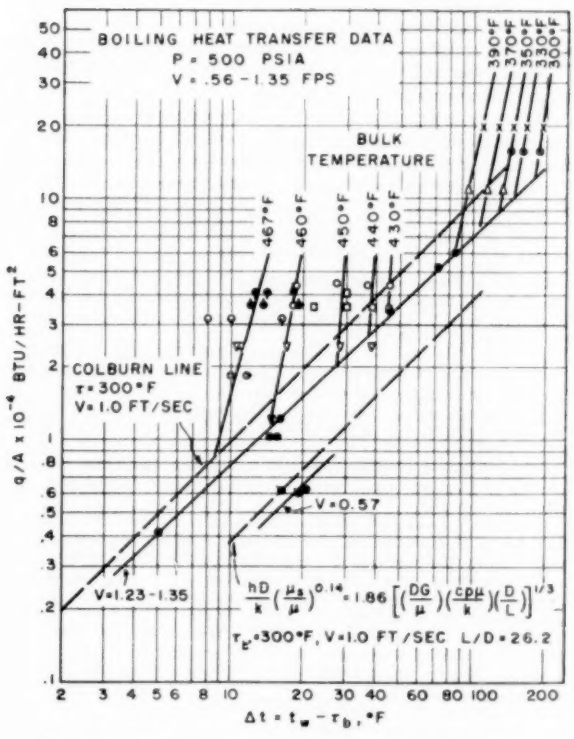

FIG. 12 q/A VERSUS ΔT FOR 500 PSIA AND 0.56–1.35 FPS

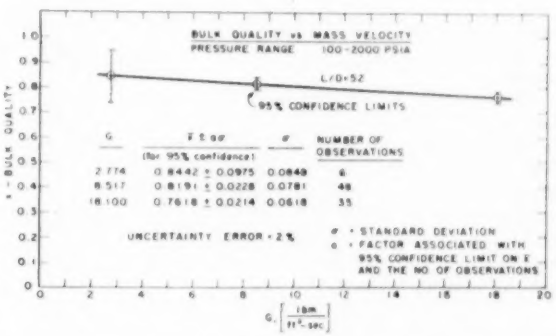

FIG. 13 PEAK HEAT-FLUX DATA FOR FORCED CONVECTION WITH SURFACE BOILING OF WATER AT 2000 PSIA

and pressure. Statistical analysis of the data for 95 per cent confidence indicates an average quality at the peak-flux condition of 0.80 ± 0.03 for the particular $L/D = 52$ and for the range of mass velocities investigated. A slight effect of mass velocity on x is suggested by the data, as would be expected; that is, at higher mass velocities the quality at burnout should decrease gradually, for a fixed L/D, finally passing through zero and ultimately becoming negative at great velocities. In all probability the value of $(q/A)_{max}$ increases at higher velocities for fixed L/D in spite of the presumed reduction in x. At constant mass velocity, the value of x at burnout also may be expected to decrease with decreased L/D. The value of $(q/A)_{max}$ would decrease also. For L/D larger than that tested in this study the opposite would be true.

It is important to make clear the limited applicability of these

burnout data, i.e., to tubular systems of approximately 50 L/D at mass velocities less than 20 lb_m/ft^2-sec and with net steam generation. The parameter x, the bulk quality, is probably not the best for representing burnout conditions in view of the wide range of its possible values as indicated in the foregoing. However, these results do suggest that burnout in subcooled systems is controlled by a liquid-vapor distribution, possibly the "quality" in the bubble boundary layer, which may be about 0.80 at burnout. At the moment more work needs to be done on these boundary layers before any definite answers are to be given to this important problem.

Fig. 14 shows the effect of pressure on the bulk quality at burnout. This effect is not large but seems to have a definite trend, reaching a maximum value between 500 to 1000 psia.

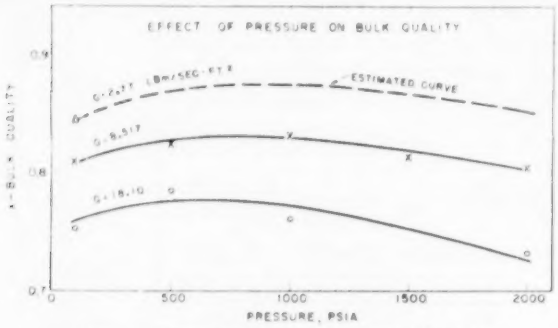

FIG. 14 EFFECT OF PRESSURE ON BULK QUALITY

The data including their statistical treatment are given in reference (7). An uncertainty analysis of experimental errors according to the method of Kline and McClintock (8) indicates an approximate uncertainty of 2 per cent on the mean for 20:1 odds, or 95 per cent confidence in the specified error of the individual measurements.

Results similar to these on an entirely different system have been reported by Witzig, Penny, and Cyphers (9). These workers tested Freon-12 at low pressures in a horizontal $^3/_8$-in-OD copper tube. Under conditions of net steam generation they found a sharp increase in tube-wall temperature when the Freon quality was approximately 70 per cent. The L/D at burnout was about 60 at a mass velocity of roughly 7.5 lb_m/sec-ft^2. Their Fig. 4 could be interpreted to result in a bulk quality of about 75 per cent at burnout, however.

The fairly constant value of x at peak flux for these conditions greatly simplifies the prediction of $(q/A)_{max}$ for design as a function of mass velocity, pressure, and inlet subcooling for heat transfer in a tube whose length is under the condition of local boiling and with net steam generation; that is, the first law of thermodynamics applied to such a flow shows that

$$\left[\frac{4(L/D)(q/A)_{max}}{G(h_f - h_i)} - 1\right] = x\left(\frac{h_{fg}}{h_f}\right)\left[1 - \frac{h_i}{h_f}\right]^{-1} \quad \ldots [11]$$

In all probability, for flows with net vapor generation at discharge the bulk quality x at peak heat flux is a function of L/D. For $L/D = 52$, as employed in this study, Equation [11] becomes

$$\left[\frac{208(q/A)_{max}}{G(h_f - h_i)} - 1\right] = 0.80\left(\frac{h_{fg}}{h_f}\right)\left[1 - \frac{h_i}{h_f}\right]^{-1} \quad \ldots [12]$$

and for heat transfer to water, Equation [12] is

$$\left[\frac{208(q/A)_{max}}{G(h_f - h_i)} - 1\right]\left[1 + \frac{p}{p_{crit}}\right]^{2.635} = 1.96\left[1 - \frac{h_i}{h_f}\right]^{-1} \quad [13]$$

since

$$0.80\,\frac{h_{fg}}{h_f} = 1.96\left[1 + \frac{p}{p_{crit}}\right]^{-2.635} \quad \ldots [14]$$

CONCLUSIONS

From this study the following conclusions are drawn:

1 A transition from laminar to turbulent type of flow occurs at a length Reynolds number (viscosity based on wall temperature) between 60,000 and 100,000 for upward (heating) flow in a vertical tube. The initial turbulence level was unknown.

2 This transition is excited by the effects of superimposed free convection, increasing the heat-transfer coefficient by as much as 600 per cent.

3 As previously observed at higher velocities, the wall temperature is essentially constant for local boiling heat transfer at lower velocities, this being the result of vigorous bubble agitation at the heated surface.

4 Forced-convection-boiling heat-transfer data may be correlated by means of a modified bubble Reynolds number leading to an equation of the form of Equation [10] where $(q/A)_{boil}$ is calculated from Equations [7 to 9].

5 Maximum (burnout) heat flux under conditions of local boiling with net vapor generation occurs at a bulk quality of approximately 0.80, for a boiling L/D of 52, and is independent of pressure and initial subcooling.

ACKNOWLEDGMENTS

The work reported here was sponsored by the Office of Naval Research, Contract N5-ori-07827, NR-035-267. The authors gratefully acknowledge this aid and also the help of the following: The many problems associated with the design of the high-pressure apparatus were for the most part solved by Milton W. Raymond, project design engineer, who also originally conceived and successfully built the ion exchanger with very little design data. The maintenance and operation of the equipment and the gathering of the test data were accomplished by Frank Mullin and P. J. Malherbe, graduate students in the Department of Mechanical Engineering, Massachusetts Institute of Technology. Calculated results for preparing Fig. 10 were compiled by Carl E. Lenngren of Bofors, Sweden, who was temporarily in the United States.

BIBLIOGRAPHY

1 "Heat Transfer and Pressure Drop Data for High Heat Flux Densities to Water at High Sub-Critical Pressures," by W. M. Rohsenow and J. A. Clark, Heat Transfer and Fluid Mech. Inst., Stanford, Calif., 1951.

2 "Heat Transfer to Water at High Flux Densities, With and Without Surface Boiling," by F. J. Kreith and M. J. Summerfield, Trans. ASME, vol. 71, 1949, pp. 805–815.

3 "A Study of the Mechanism of Boiling Heat Transfer," by W. M. Rohsenow and J. A. Clark, Trans. ASME, vol. 73, 1951, pp. 609–620.

4 "A Method of Correlating Heat-Transfer Data for Surface Boiling of Liquids," by W. M. Rohsenow, Trans. ASME, vol. 75, 1952, pp. 969–976.

5 "Heat Transfer With Evaporations," by W. M. Rohsenow, Lectures at Symposium on Heat Transfer, University of Michigan, published by University of Michigan Press, July 18–19, 1952.

6 "Simplified Heat Transfer Correlation for Semi-Turbulent Flow of Liquids in Pipes," by R. H. Norris and M. W. Sims, Trans. American Institute of Chemical Engineers, vol. 38, 1942.

7 "Local Boiling Heat Transfer to Water, at Low Reynolds Numbers and High Pressures," by J. A. Clark and W. M. Rohsenow, Technical Report No. 4, DIC Project 6627, Massachusetts Institute of Technology, July 1, 1952.

8 "Describing Uncertainties in Single-Sample Experiments," by S. J. Kline and F. A. McClintock, *Mechanical Engineering*, vol. 75, 1953, pp. 3–8.

9 "Heat Transfer Rates to Evaporating Freon-12 in a Horizontal Tube Evaporator," by W. F. Witzig, G. W. Penny, and J. A. Cyphers, Refrigerating Engineering, February, 1948.

Discussion

C. F. Bonilla.[4] Our experience in predicting local boiling at lower pressures in tubes of small size from curves in McAdams' original paper[5] indicates that below reasonably high values of q/A no local boiling can be obtained. If the Δt in forced-convection heating is below the minimum required for local boiling, the water will heat up to the boiling point and enter saturated boiling with no intermediate local boiling. It might be helpful for the authors to present their results also in one or more curves showing the regions in which local boiling is and is not obtainable at these high pressures.

W. H. Jens.[6] Many investigators have found that reproducible and predictable data are difficult to obtain for maximum heat flux in nucleate boiling within a heated tube in a forced-flow system. This difficulty appears to result in part from the simultaneous occurrence of an increase in pressure drop at the outlet section of the heated tube together with the critical conditions of flow, fluid temperature, and heat flux, commonly called burnout. If the increase in pressure drop is sufficiently large compared to the over-all system pressure drop the flow in the tube tends to decrease. Since the heat input is obtained by electrical resistance heating it remains practically constant and the temperature of the fluid at the outlet end of the heated tube increases, resulting in conditions more critical than before. The pressure drop continues to increase and the flow continues to decrease until the heated tube is devoid of liquid and it overheats and burns out.

This autocatalytic effect has a greater tendency to occur in experimental systems which use a centrifugal pump and in which a large part of the total available pressure drop occurs along the heated tube. In many cases the flow instrumentation does not have a sufficiently fast response to detect a sudden decrease in flow at burnout. The flow before the autocatalytic event occurs is probably what is recorded.

In systems in which a special effort is made to insure positive flow, the data become more predictable and reproducible. Higher heat fluxes are then obtainable with the same flow rate and temperature at the inlet of the heated tube. Constant heat-input data indicate a rise in pressure drop with a decrease in flow. Positive flow can be insured by reducing the ratio of the pressure drop along the heated tube to the total pressure drop. This can be accomplished by the installation of a larger head pump in which most of the pressure drop is used in a throttling valve or orifice before the inlet to the heated tube.

Many of the applications of nucleate boiling are in systems in which pressure drop remains constant, such as in heated parallel-flow channels. Without knowledge of the pressure drop the data obtained in a constant-flow system are not generally applicable. For this reason, and because of the seriousness of a burnout prediction, the data should be used with caution.

Authors' Closure

We wish to thank Drs. Bonilla and Jens for their discussions of our paper.

Concerning Dr. Bonilla's comment, we would state that we have always been able to obtain local boiling at certain locations in our tube (ID 0.1805 in.) providing the inlet water was subcooled. Boiling, of any nature, never took place until the tube-wall temperature was a few degrees above the saturation temperature. In these instances, the fluid bulk temperature was always below the saturation temperature and local boiling would set in and persist downstream until the bulk temperature of the fluid increased to the saturation temperature. Once saturation conditions were reached the boiling was not of the "localized" type as the vapor bubbles did not condense in the fluid bulk. Otherwise, the boiling action appeared similar to local boiling, that is, the wall temperatures did not show any noticeable change.

It would seem possible to us that systems using small-diameter tubes at moderate q/A in the nonboiling region could have such high rates of change of fluid bulk temperature that the length of tube from the onset of local boiling to the point where the fluid bulk temperature is equal to saturation temperature (i.e., saturation boiling) could be quite small and difficult to detect. The effect of tube size on bubble diameters at breakoff from the tube wall might conceivably be important here as large bubbles could control the enthalpy distribution across the tube. So far as we are aware, however, no information is yet available on this problem.

All of the data presented in Figs. 7, 8, 9, 10, 11, and 12 are for local boiling.

Dr. Jens has raised a very significant point and we are in complete agreement with him. Early in our burnout studies we encountered what he has called the autocatalytic effect. At that time we were unable to obtain any reproducibility in our burnout data. The overheating of the tube was observed to occur not always at the discharge end, where we would normally expect, but at upstream locations. This difficulty was overcome, at the suggestion of Dr. Jens and his associates at the Argonne National Laboratory, by placing both the flow-control valve and the flow-measuring orifice immediately before the test-section inlet and using the Hayward-Tyler pump to circulate the water. By such an arrangement (not shown in Fig. 1) the test-section pressure drop was a small percentage of the total pressure drop available. Thereafter the data became more reproducible as shown by the confidence limits on Fig. 13.

The autocatalytic process in boiling systems is of considerable importance to a designer and can bear further development. It is a result of an unstable combination of pump and system caused by the unusually large pressure drop across a tube which discharges net vapor and which is fed with liquid. We have recently made measurements of this on a small tube (0.18 inch ID and 18 in. long) at atmospheric pressure. The results are shown in Fig. 15. This pressure drop-flow characteristic is typical for boiling systems, the large increase at low flows being principally a result of the great change in momentum in going from liquid to vapor. The data in Fig. 15 were obtained on a system having a total available pressure drop about 10 times that required by the test section.

The role played by instability in flow can be seen only by examining the combined characteristic of the pump and the system including valves, test section, and piping. The burnout data reported in this paper were gathered by setting the q/A at a fixed value and reducing the flow by closing down on the flow-control valve until burnout occurred. A system which becomes unstable is shown in Fig. 16. Here the pressure drop produced by the pump and that demanded by the system for four control-valve positions is plotted against the flow rate. The test-section pressure drop is also shown and for this example is purposely taken to be a large percentage of total-system pressure drop. As the flow rate is reduced by closing down on the valve at constant q/A the system passes successively from point A to point D, Fig. 16. It will be noticed that points A, B, and C are stable

[4] Professor, Columbia University, New York, N. Y.

[5] "Heat Transfer at High Rates to Water With Surface Boiling," by W. H. McAdams, et al., *Industrial and Engineering Chemistry*, vol. 41, 1949, pp. 1945–1953.

[6] Engineer, Nuclear Development Associates, White Plains, N. Y. Mem. ASME.

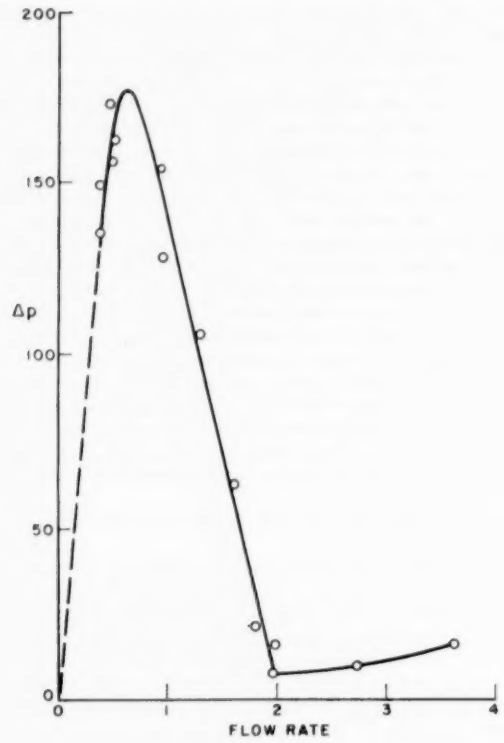

Fig. 15

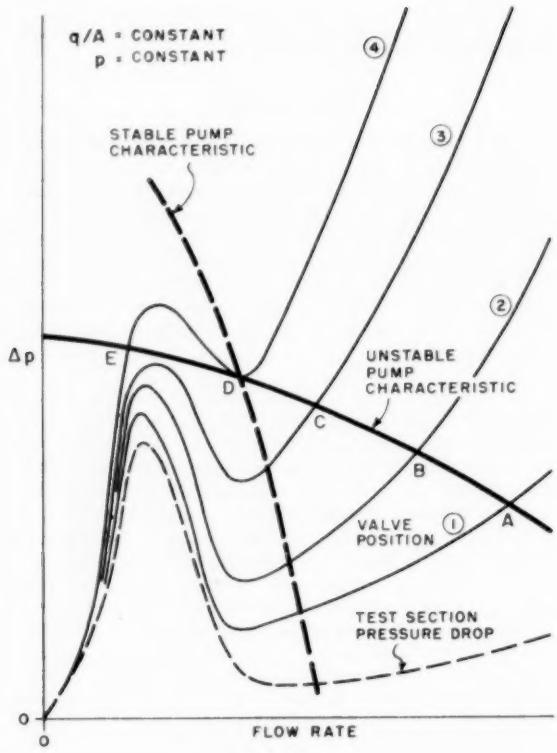

Fig. 16

operating points. However, there will be some point D for any such system where it is stable for increases in flow rate but unstable for decreases in flow rate. It is at such points as D that the autocatalytic effect is produced, since any momentary decrease in flow rate at constant q/A results in greater volume of vapor produced, which causes greater pressure drop and a further decrease in flow rate, etc. The system will finally come to equilibrium at point E (a stable point) provided that at this point the concentration of vapor is such as not to blanket and insulate the heat-transfer surface. Otherwise, point E will never be obtained as somewhere between D and E the tube surface becomes insulated with vapor and burnout and rupture rapidly ensue. For such a system as just described, there will always be some q/A at which instability occurs at D and will burn out before E is reached. In such a system, D is, in effect, the burnout point even though the heat-transfer surface is not insulated and may be capable of transferring considerably more heat than actually passing through it. A pump characteristic such as that shown dotted, Fig. 16, would result in a point of stable operation at D.

The design of boiling systems which are stable requires the use of a pump which puts out a constant-flow rate, or if a centrifugal pump is used, that the boiling section pressure drop be a small proportion of total pressure drop. This is suggested by Dr. Jens. The resulting system would be as shown in Fig. 17. The significant point here is that nowhere does the system Δp-characteristic become tangent to the pump characteristic. Dr. Jens is correct that to use boiling data properly in the design of apparatus, the pressure-drop characteristics of the boiling section must be known or calculable. We believe, however, that our burnout data were collected on a stable system and is the result of insulation of the heat-transfer surface reached through a succession of stable points and not precipitated by an autocatalytic process. Hence the resulting data represent those regions of thermal instability and not those of hydraulic instability on our particular system.

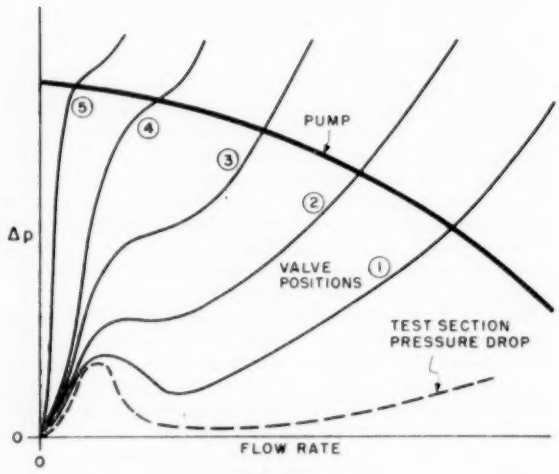

Fig. 17

We did not report our particular test-section pressure drop as it was too small for us to record. The numerical values themselves would provide little useful information.

Tube Expanding and Related Subjects

By F. F. FISHER[1] and G. J. BROWN,[2] DETROIT, MICH.

The paper summarizes experiences gained by expanding tubes into various types of powerhouse equipment and by the development of improved expanding tools and new rolling methods. Manual and controlled rolling methods are described and their relative merits discussed. Information is given relative to the making of rolled joints having optimum strength and stability. All subject matter is viewed and discussed from a practical standpoint and references are cited, if pertinent and available.

Introduction

TUBE expanding, known also as tube rolling or "rolling-in" of tubes, is the art of cold-working the ends of tubes into intimate contact with the metal of the containing tube holes. Properly executed, this rolling-in process produces pressure-tight joints of great strength and stability. The value and fitness of this method of fastening tubes to sheets or headers is attested by the fact that most utility services, factory outputs, and many material processes depend upon equipment or apparatus having expanded tube joints. In fact, in many cases, tube rolling is the only practical method of fastening tubes to headers.

ASME Codes establish definite design standards for boilers and unfired pressure vessels but do not cover the making and rolling of joints. Thus this important matter is left to the judgment of individuals who may be inexperienced, and in consequence, joints that are well designed may be rolled improperly and give unsatisfactory service. It is apparent, therefore, that in order to prevent costly service interruptions, expensive shutdowns and repairs, the rolling-in of tubes should proceed in the best possible manner.

Basic Rolling-In Process

When rolling tubes, an expander similar to those shown in Fig. 1 is inserted into the tube end and the tapered mandrel rotated. Feeding the mandrel inward causes the expander rollers to be forced apart and, by rolling over the inside tube surface, cold-work the tube metal. As shown in Fig. 2, the tube is enlarged and contacts the tube-hole surface; then, because the tube hole is a restraining barrier, further expanding deforms the tube metal and forces it into more intimate contact with the metal of the tube hole. Since all displaced tube metal cannot escape radially, it flows from the center to each end of the rolled joint. The tube-hole metal is, of course, also affected, and the hole is slightly enlarged. The net result of the expanding operation is a joint condition similar to a shrink-fitted shaft coupling.

Joint Assembly

Cleanliness is one of the basic requirements for making good joints. Both tube holes and tube ends should be well cleaned of scale, dust, and dirt before assembly, and care should be taken to keep oil, soap, and other lubricants out of the unrolled joint. Dirty tube ends or tube holes will produce joints that are inferior in strength and tightness. Tube holes in tube sheets, baffles, and support plates should be free from burrs in order to prevent longitudinal scratching of the tube ends, should the tubes be fed through such holes at assembly. Tube-end scratches and tube-hole toolmarks are a major cause of leaky joints.

Tube Expanders

There are several standard types of expanders, as well as expanders built for specific purposes, each of which may be of different size and roller length. All, however, work on the same principle and all have three essential parts, namely, a tapered central mandrel or pin, 3, 4, or 5 rollers of suitable length spaced equally around the mandrel, and a cylindrical roller cage that constrains the loosely held rollers in their respective positions.

Types of Expanders

Most expanders are of the self-feeding type; that is, they have rollers that are held at a slight angle to the center line of the tapered mandrel, instead of being parallel as in the nonfeeding type, Fig. 1(A). In the latter, the tapered mandrel is forced inward by hammer blows, which are repeated as rolling progresses. These so-called hand expanders are too slow for production purposes, but are good tools for small jobs and for rerolling.

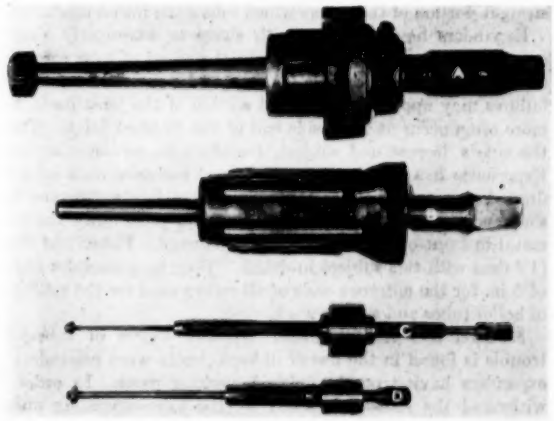

A	Three-roller manually operated expander	Use: Low-pressure boiler tubes
B	Five-roller expander with 2 belling rollers	Use: Rolling and flaring boiler and refinery tubes
C	Three-roller expander with adjustable, ball-bearing stop collar	Use: Controlled rolling for tubes up to 3 in. diam
D	Three-roller expander, motor or manually operated	Use: Conventional small-tube expanding

Fig. 1 Types of Expanders

On self-feeding expanders, Fig. 1(B, C, D), the angle of the roller causes a simultaneous feeding in the whole expander assembly as well as the tapered mandrel, thus speeding up the rolling-in process considerably. When equipped with belling rolls, Fig. 1(*b*), self-feeding expanders also make it possible to complete in one operation the rolling-in and forming of the flare specified by the ASME Boiler Code. Fig. 1(C) depicts an expander equipped

[1] Retired, The Detroit Edison Company.

[2] General Superintendent of Construction and Maintenance Department, The Detroit Edison Company. Mem. ASME.

Contributed by the Heat Transfer Division and presented at the Annual Meeting, New York, N. Y., November 29–December 4, 1953, of The American Society of Mechanical Engineers.

Note: Statements and opinions advanced in papers are to be understood as individual expressions of their authors and not those of the Society. Manuscript received at ASME Headquarters, September 3, 1953. Paper No. 53—A-174.

with a ball bearing, a type commonly used for controlled tube rolling. Fig. 1(D) may be used for conventional expanding, or, when the rolling diameter is limited by means of a stop placed on the mandrel, it can roll completely through any length of joint. Conventional mandrel tapers vary from 1/4 to 1/2 in-per-ft of mandrel depending on the size of the expander and the work to be performed.

Most expanders used today, especially on high-pressure work, are of the parallel rolling type. These expanders have rollers with tapers of one half that of the mandrel taper, but in the reverse direction. Such expanders are capable of rolling cylindrical holes in their respective tube ends, except when the rolling-in is carried past the point where the elastic limit of the joint metal is exceeded. In that case, a slightly tapered tube hole results, with the larger end usually being at the back of the joint. Parallel rolling expanders are preferable to other taper combinations because they insure a uniform cold-working of all tube and tube-sheet metals comprising the joint, and therefore tend to develop the maximum strength of rolled joints.

Expander Details

Entrance End of Rollers. The shape of the entrance end of expander rollers has a definite influence on the strength and stability of rolled joints. The term "entrance ends" applies to that portion of the roller end which actually contacts and rolls the tube metal. Should the entrance ends be square, or have sharp edges or angles that cut the tube metal when it is cold-worked by the expander rollers, the inside of the tube end may be damaged seriously. Unfortunately, these injuries are not visible in newly finished joints, excepting at the inner end because the other surface cuts are rolled down and hidden by the straight portion of the rollers which follow the initial track.

Expanders having rollers with sharp or improperly shaped entrance ends are, therefore, potential sources of tube corrosion and are believed responsible for many tube-end failures. These failures may appear in the rolled section of the joint itself, but more often occur at the inside end of the finished joint. There the cut is deepest and subject, therefore, to corrosion attacks. Experience has shown that streamlined entrance ends of teardrop design are ideal for the rolling-in of joints, because this shape causes the rollers to climb over and press down the tube metal in front of the rollers without damage. Fisher and Cope (1)[3] deal with this subject in detail. They recommend a radius of 5 in. for the entrance ends of all rollers used for the rolling-in of boiler tubes and similar work.

Mandrel and Roller Finish. Another source of tube-joint trouble is found in the use of ill-kept, badly worn expanders or expanders having poorly finished working parts. In order to withstand the stresses imposed by the tube-expanding operation, all working parts must be either hardened or case-hardened, depending on the material employed. However, during the hardening process many rollers and mandrels warp, bend, or lose their true cylindrical shape. This is especially true of the smaller expander sizes. Uneven or rough roller surfaces also tend to cut or mar the tube surface in contact with the rollers and may thus start the flaking off of the tube metal. Further, since all power applied to the mandrel for rolling-in purposes is transmitted to the rollers by line contact only, an irregular roller or mandrel surface tends to set up highly destructive local stresses at the line of contact. Therefore a consequent rapid deterioration of these vital expander parts can be expected.

It is evident that although such unfinished or inferior expanders may be low in first cost, they are expensive in the long run and are a handicap to good workmanship and the making of reliable expanded joints. Experience has demonstrated that it is good practice to discard all rollers and mandrels that do not roll smoothly on a level surface, and all expander parts that have worn or damaged surfaces. Well-made expanders having ground mandrels and rollers are the best tools for the making of good expanded joints.

Rolling Speed and Feed Angle. Thum and Jantscha (2) proved by test on over 5000 rolled joints that fast machine rolling gave superior results over slower-rolling methods. Improved holding strength and tightness were some of the advantages. However, it should be noted that, generally speaking, permanent tube-hole deformation was greater at high expander speeds, whereas slower rolling produced a greater reduction in the tube-wall thickness.

There is another expander detail which influences the quality of a rolled joint, namely, the feed angle of the rollers. With expanders of the same type and all other factors remaining the same, the feed angle controls the length of time and number of revolutions required for the tube-expanding operation. In joint assemblies consisting of elements having smooth contact surfaces, such as smooth Admiralty tubes in a reamed brass condenser-tube sheet, a full metal-to-metal contact is made readily and a good joint may be obtained without difficulty. Such joints, therefore, can be rolled quickly and a feed angle of 2 or 3 deg may be appropriate for such expander.

In joint assemblies having rough contact surfaces, an entirely different situation presents itself. The joint surfaces first must be pressed together and smoothed out before favorable conditions prevail for a good tight joint. In such cases a slower feeding expander may be selected in order to increase cold-working of the tube metal—and an expander having a lesser feed angle is indicated. An actual case will serve as an illustration: Tubes in a very large condenser were rolled with expanders having a 2 1/2-deg feed angle and the 4-hr water test disclosed quite a few leaky joints. When a rerolling of these joints did not stop the leaks, several tubes were removed in order to discover the cause of the leakage. An inspection showed that the tube holes were full of tiny scratches, apparently caused by cleaning the tube holes with too stiff a wire brush. After rerolling the joints with an expander having a 1 1/2-deg feed angle, the joints obtained were tight enough to pass even the most rigid of tests.

Three, Four, or Five Rollers. In sizes up to 7/8 in., expanders have only three rollers. Above this tube size, they may be had with 3, 4, or 5 rollers, those having an uneven number of rollers predominating. In an investigation made in 1945 to determine the relative merits of 3 and 4-roller expanders, the 3-roller type was proved to be better. The test results are given by Shannon, et al. in reference (3).[4] The reason given was "because the internal surface of the tube was freer from blemish and there was a more satisfactory extrusion of the tube metal into the seat groove." But the report goes on to caution that its use "may result in excessive deformation and permanent set of a tube hole having marked unequal rigidity around the periphery; for example, a relatively large diameter hole in a small diameter header." Maxwell (4) also recommends 3-roller expanders for use on tubes having nonuniform wall thickness.

Thum and Jantscha (2), from extensive and elaborate experiments with 3 and 5-roller expanders, concluded: "If the permanent deformation of header and tube caused by various methods of rolling are compared, we find that the deformations are smallest in case of the five-roller expander." Also: "The five-roller expander is, therefore, especially to be recommended where on account of a thin sheet, and on account of a material which does not work-harden much, the seat would give too much; it is also to be recommended wherever the hole has already been considerably expanded through frequent changes of boiler tubes."

[3] Numbers in parentheses refer to the Bibliography at the end of the paper.

[4] Pages 6, 7, and 21 of reference (3).

Thum and Jantscha's recommendations agree with the experience and opinion of the authors.

Belling Rolls. Modern self-feeding expanders, in one operation, can expand the tube and form the tube end into the flare or bell specified by the ASME Boiler Code. This Code calls for a bell, the diameter of which is not less than $^1/_8$ in. larger than the tube-hole diameter. These tube flares are formed by the rotary forward travel of the expander rollers and the containing expander cage. The actual flaring is accomplished by means of angular belling rollers mounted at the back of the expander rollers as shown in Fig. 1(B). (The Code specification does not, however, apply to heat exchangers, although some exchangers have tubes with flared ends.)

Many expander catalogs list expanders having one belling roller only. This type of expander may be cheaper than others having two or more belling rollers, but cannot be recommended because it does not produce flares of uniform height and leaves deep, conspicuous, and objectionable roller imprints in the face of the flares. However, when the forming of the flare is divided between two or more rollers, the objectionable roller imprints are greatly reduced.

Another but more serious disadvantage of expanders having a single belling roller on one side only is the fact that, while belling, the expander is unbalanced and tends to wobble in the rolled joint. In consequence, joints rolled thus may not be of the desired strength and serious joint or tube-hole distortion may result. This wobbling tendency increases with the increase in ratio between tube diameter and joint length. When retubing such distorted joints it is difficult to obtain stability and tightness. On the other hand, under like circumstances, expanders having two or more belling rollers are balanced and do not wobble.

Strength of Rolled Joints

During the rolling-in process, the tube and tube-hole metals are deformed permanently and the pressure and friction set up between the two contacting surfaces determine the strength and stability of the joints. Fig. 2 depicts the three stages of tube expanding, namely, assembly, tube contacting tube hole, and finished rolled joint. In this connection, attention is called to the fact that after a tube is removed from a rolled joint, providing this joint was not over-rolled, the metal surrounding the tube hole undergoes a gradual elastic recovery. When this recovery is completed, the tube hole will be smaller than it was when the joint was broken.

A belief that heavy rolling-in is necessary in order to obtain strong and tight joints has been proved to be erroneous. The contact pressure, and with it the joint strength, increase with the rolling imparted to the joint, only until they reach a definite maximum. Further rolling, because it tends to reduce or destroy the elasticity of metals comprising the joint, reduces its strength and stability as shown graphically in Fig. 3, which applies specifically to ferrous materials but is also applicable to other metals

Since rolled joints can be classed as friction joints, it is apparent that the holding strength of any joint increases as the roughness of the contacting surfaces of tube and tube hole increases. The extent of such roughness, however, must be kept within reasonable bounds because of the axial flow or elongation of tube metal, which is incident to all tube rolling. This elongation, or lengthening of the rolled tube, tends to shear or smooth off much of this roughness, Fig. 4. The shearing action in joints made up of different metals increases as the hardness of the tube material approaches that of the tube-hole metal. Thum and Mielentz (5) describe and illustrate joints having different tube-surface finishes. They come to the conclusion that tube ends having a fine thread-

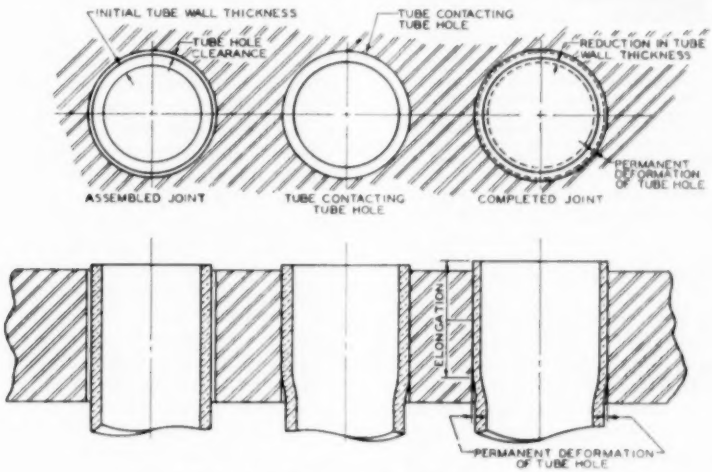

Fig. 2 Three Stages of Tube Expanding
(Joint shown is typical of feedwater heaters and similar equipment.)

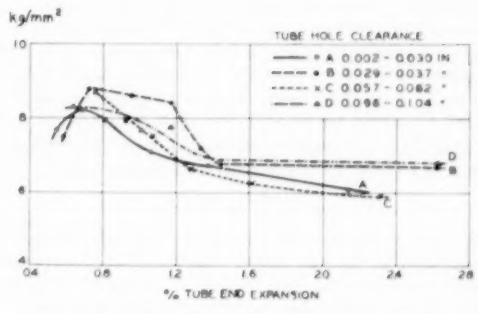

Fig. 3 Effect of Degree of Expanding on Strength and Stability of Rolled Joints
(Values shown are for ferrous tube joints having different tube-hole clearances. From A. Thum and J. W. Mielentz, reference 5.)

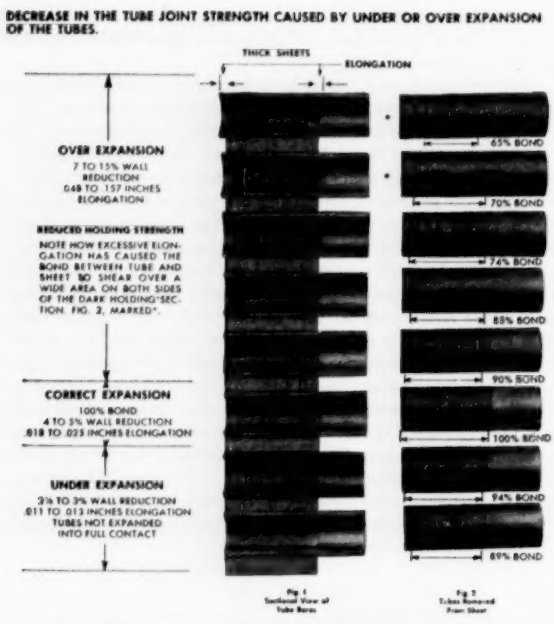
DECREASE IN THE TUBE JOINT STRENGTH CAUSED BY UNDER OR OVER EXPANSION OF THE TUBES.
THICK SHEETS
ELONGATION
OVER EXPANSION
7 TO 15% WALL REDUCTION
.049 TO .157 INCHES ELONGATION
REDUCED HOLDING STRENGTH
NOTE HOW EXCESSIVE ELONGATION HAS CAUSED THE BOND BETWEEN TUBE AND SHEET TO SHEAR OVER A WIDE AREA ON BOTH SIDES OF THE DARK HOLDING SECTION. FIG. 2, MARKED *.
CORRECT EXPANSION
100% BOND
4 TO 5% WALL REDUCTION
.018 TO .023 INCHES ELONGATION
UNDER EXPANSION
3% TO 3% WALL REDUCTION
.011 TO .013 INCHES ELONGATION
TUBES NOT EXPANDED INTO FULL CONTACT
65% BOND
70% BOND
74% BOND
83% BOND
90% BOND
100% BOND
94% BOND
89% BOND
Fig. 1 Sectional View of Tube Bores
Fig. 2 Tubes Removed From Sheet
¾ - 14 BWG ADMIRALTY TUBES EXPANDED IN 1½ INCH THICK STEEL SHEET. THE DARK SECTIONS OF THE TUBES, FIG. 2, ARE IN EXPANDED CONTACT WITH THE SHEET HOLE GIVING THE JOINT ITS STRENGTH. THE SECTIONS ON EITHER SIDE HAVE SHEARED THEIR BOND AND THE METAL SHOWS UP POLISHED. DRILL MARK IMPRESSIONS FROM THE TUBE SHEET HOLE APPEAR IN THE DARK BONDED SECTIONS BUT ARE OBLITERATED IN THE SHEARED AREAS.

FIG. 4 TUBE-EXPANSION CONTROL—FACT SHEET NO. 2
(Courtesy of The Airetool Manufacturing Company.)

like finish are best and could increase the strength of rolled joints by 35 per cent.

The strength of a rolled joint increases, all other factors remaining equal, with an increase (not proportional) in length and an increase in the thickness of the tube wall, but it decreases with an increase in tube size. Different materials also influence the strength of rolled joints. A tube and tube-sheet combination consisting of steel tube and steel sheet produces joints having a high holding strength, whereas a steel tube rolled into a copper-tube sheet would furnish a joint having but little strength and stability. Experience has shown that for the best over-all results, the hardness of the tube preferably should be somewhat less than that of the tube-sheet metal. A reversed condition usually results in distorted or greatly enlarged tube holes.

It must always be remembered that strength of joint alone is not enough to guarantee a good joint. Consideration must be given to joint tightness, which is influenced greatly by the degree of roughness of the joint materials. Generally speaking, a tight joint can be made much more easily if the contacting surfaces of tube and tube hole are smooth, but such a joint is, because of this smoothness, a minimum strength joint. The experiments of Thum and Mielentz (5) confirm these statements.

LENGTH OF JOINT

It has been stated and proved that the strength of rolled joints increases with an increase in seat length. However, it may be assumed safely that the code design thickness of a vessel also allows a joint length having the strength and stability necessary for its safe operation. An example of this may be found in boiler practice where, in most instances, shell thickness equals the joint length.

According to European sources, when design requirements call for thicker tube sheets, no appreciable gain is evident, either in strength or stability of joint, when rolled joints are made longer than $1^{3}/_{8}$ in. According to Thum and Mielentz (5), the stability values are as follows:

With plate thickness of 0.55 in. = 6.5 kg/mm²
With plate thickness of 1.18 in. = 10.5 kg/mm²
With plate thickness of 1.97 in. = 10.9 kg/mm²

a gain of only 0.4 kg/mm² for an increase of 0.79 in. in plate thickness. Maxwell (4) is a proponent of even shorter joints, $1^{1}/_{4}$ to $1^{1}/_{2}$ in. However, the authors believe that this minimum seems to be a little too low. If in heat exchangers the conditions and designs are similar to conventional boiler practice, a rolled joint $1^{3}/_{8}$ in. long should be of sufficient length to meet all purposes.

It is the authors' opinion that the use of rolled joints of excessive length in high-pressure feedwater heaters and other heat exchangers having small tubes cannot be justified. This was brought out in a paper (6) presented by the authors in 1950, which discussed in detail the aspects of making small-tube joints. Although the tube sheets of such vessels may vary in thickness from $2^{1}/_{2}$ to 12 in., the conventional practice has been to roll the tubes for a length equal to the thickness of the tube sheet. Numerous tests have shown that in many cases, rolled joints $2^{1}/_{2}$ in. long equal or exceed in strength either the elastic limit or the ultimate strength of the tube itself. Thus there seems to be no advantage in rolling joints longer than $2^{1}/_{2}$ in., Fig. 9. The validity of this claim is supported by the history of certain high-pressure heaters with tube joints reduced to a length of $2^{1}/_{2}$ in., which have operated satisfactorily for many years.

Joints of excessive length, besides being more expensive, may prove to be a liability if the materials comprising the joint have different coefficients of expansion, as, for example, copper tubes and steel tube sheets. The difference in linear expansion and contraction induced by operational or sudden changes in temperature may bring on premature joint failure. Short joints in thick tube sheets have another advantage because, in case of joint failure or leaks, the unrolled portion of the joint may be utilized. For instance, due to a sticking floating head, a number of tubes failed at the back end of the rolled joint in a high-pressure feedwater heater located in a larger power plant. It was apparent that many more tubes were damaged in the same manner and would soon fail in service. Therefore, instead of retubing this heater, the unrolled portion of the joint 1 in. in length was utilized to form a new, or in some joints, an additional joint.

On thick tube sheets having short rolled joints at one end, the open annular clearance between tube and tube hole at the other end may be closed by simply enlarging a portion of the tube by means of an expander having short rollers until this opening is sealed off against the intrusion of impurities, Fig. 9(*d*).

JOINT REINFORCEMENTS

When the expander rollers extend beyond the tube-sheet edges, some tube metal is squeezed out over one or both edges of the sheet. The tube then becomes larger at these points than the tube hole and this adds shearing strength to the joint in either one or both directions, Fig. 5. As a rule, tubes that are installed by passing through the tube holes are rolled by expanders having rollers extending over the face edge of the tube sheet only, Fig. 2. Thus the tube at the back of the sheet is not enlarged and the tube may be withdrawn in case of failure.

In boiler or similar work, the flared tube end specified by the ASME Boiler Code gives protection against the tubes pulling through the tube holes, Fig. 5. Because of the axial flow of tube metal incident to tube expanding, these flares do not abut against

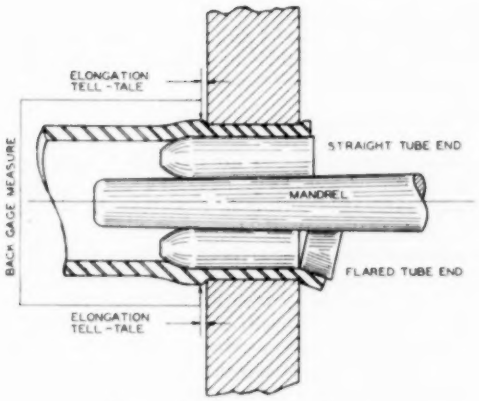

FIG. 5 TYPICAL BOILER JOINTS

the tube-hole edges and, therefore, do not prevent the initial slip of a rolled-in tube. The gap thus existing between flare and shell is, therefore, an ideal starting point for pitting and corrosion unless it is sealed off by a protective coating.

Since the conventional self-feeding tube expander rolls and flares at the same time, care and skill are required to form and place the flare properly. When improper belling places the flare too deep into the drum metal, the consequent excessive deformation of tube and tube hole sets the stage for caustic embrittlement or other troubles. The use of expanders equipped with loose stop collars that limit the flare size by contacting the tube end is a step in the right direction. It should improve the tube-flaring operations. The flaring difficulties increase, of course, with the thickness of the tube wall, and under certain conditions it is, therefore, advantageous to produce the flare by means of a separate belling operation. On thicker tubes, since conventional belling tends to loosen portions of the adjacent joint, an expander having a slight taper is used at times to "touch up" the joint before testing.

In order to meet the demands of higher pressures, most tube joints are strengthened by the machining of suitably shaped circumferential grooves into the walls of the tube hole. During the rolling-in process, a portion of the tube metal is extruded into these grooves. In this manner additional anchorage and shear strength is provided for the rolled joint. The grooves should be so placed in the tube hole that the elongation incident to tube rolling forces the extruded tube metal against the outside wall of the grooves. The intimate contacts thus formed eliminate any initial slippage of the joint proper and provide additional strength and extra pressure seals. Rectangular grooves are commonly used for reinforcement purposes, and they increase the holding strength and stability of rolled joints by more than 100 per cent, Fig. 6. Design particulars for the value and location of grooves may be found in (5).

Because the optimum degree of expanding fills these grooves only partially, the full potential shear strength is hardly ever realized, except in the case of thick tubes. There it is possible, by heavier rolling, to extrude additional tube metal into the grooves, and in this manner raise the shear strength without over-rolling and without injuring the tube metal. It is universally recognized that grooves or other methods of strengthening rolled joints are essential for the safe operation of high-pressure boilers and other pressure vessels. Fig. 6 shows a German groove design as depicted in reference (5), two English designs illustrated in reference (3), and the conventional rectangular grooves of the U. S. A. compared with a V-groove design. Also shown is a joint used for still fittings of oil refineries.

SIZE OF TUBE HOLES

The clearance between tube and tube hole has a definite influence on the tube-expanding operation. Primarily, excess clearance lengthens the expanding cycle considerably, although the actual joint-forming time remains the same. In reference (6) the case of $^3/_4$-in. condenser tubes is cited, where 0.030 in. excess clearance increased the rolling cycle from 3 to 10 sec, and one of 0.057 in. to 20 sec, or 7 times as long. Unless care is exercised by an experienced operator, the resulting joints are apt to be of poor quality. The curves shown in Fig. 3 represent the joint strength of rolled boiler tubes, and they demonstrate also the fact that oversize holes do not necessarily affect the joint strength, that is, if the joints are rolled according to the enlarged and over-

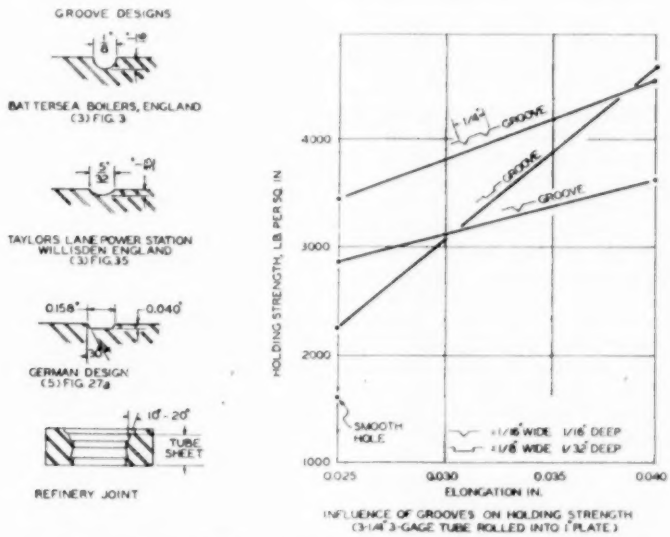

FIG. 6 INFLUENCE OF GROOVES ON HOLDING STRENGTH; GROOVE DESIGNS

sized tube hole and can be rolled without damaging the tube metal.

Rolling limitations due to tube-metal hardness, however, apply to all tube joints of whatever metal, size, or thickness. For instance, in a test conducted to determine the effect of oversized tube hole on $^3/_4$-in. Admiralty condenser tubes having different hardnesses, the first samples used were annealed and had a hardness of 62 Rockwell E. These tubes made a satisfactory joint in a hole 0.050 in. oversize. The next samples had a hardness of 72 Rockwell E, and when rolled into the same test piece and hole size, several tube ends split. The remaining tube samples tested 85 Rockwell E and, of these, every tube end split during the rolling-in operation.

The authors believe that tube-hole clearances should be as small as practical and for small seamless drawn tubes should be held between the limits of 0.005 and 0.008 in. This clearance could be increased to 0.010 in. for larger size tubes. The ASME Boiler Code prescribes that a clearance of $^1/_{32}$ in. be used for boilers and their components, and this clearance has proved to be quite satisfactory.

Tube-Hole Finish

As explained before, expanded joints are primarily friction joints. Thus, all other factors being equal, any feature capable of increasing friction or resistance to sliding will tend to increase the strength of a rolled joint. Because smooth contact surfaces will more readily form watertight joints, cold-drawn tubes in smoothly reamed holes are suitable for condensers and similar equipment in the low-pressure field. Although such a joint would be of minimum strength only, it would be ample for the purpose intended. For example, the pushout strength of $^3/_4$-in. condenser tubes in brass tube sheets, with joints $^7/_8$ in. long, is approximately 1800 lb. However, additional strength and seals may be provided by grooves or similar reinforcements.

At higher pressures, in equipment having tubes softer than the tube-hole metal, such as copper tubes in steel tube sheets, a rougher tube-hole finish may be utilized. This applies especially to the heavier tubes, for when rolling-in, the tube metal can fill the irregularities present in the tube-hole finish before full metal-to-metal contact occurs. In this manner the resistance to sliding is increased and the joint strength raised above the normal capacity. However, as stated before, when rolling-in proceeds past the optimum degree of expanding, the resulting elongation shears off the extruded tube metal at both ends of the rolled joint, Fig. 4, and, of course, causes a corresponding drop in joint strength.

For tubes whose hardness approaches or approximates that of the tube-hole metal, as in boiler and refinery work, the conventional "drill and ream" tube-hole finish is in order. In this case, however, the relation between tube and tube hole is reversed, because here the high points present in the tube-hole finish are pressed into the tube metal. The effect of over-rolling is the same, namely, a sudden drop in joint strength due to the shearing off at both ends of the joint of high points present in the tube-hole finish. Grimison and Lee describe this phenomenon (7).

At times, manufacturers preroll the tube holes of their equipment. This raises the hardness of the tube-hole metal and should result in stronger joints. However, it also smooths the tube-hole surface, and hot-rolled tubes having conventional tube finish usually require additional rolling in order to produce tight joints. Prerolling, however, is an excellent finish for the holes of support and baffle plates.

All tube holes, of whatever type or size, should be truly circular and of cylindrical shape. Under no circumstances should toolmarks or other blemishes be continuous or leave connecting marks, which would allow leakage from one end of the joint to the other. This applies especially to blemishes of any kind which parallel the tube axis. Should such marks occur, they should be interrupted or removed entirely by means of grinding wheels or other suitable tools.

Degree of Expanding

The most important task on any tube-rolling job is to determine the optimum degree of expanding for a particular tube-and-tube-sheet combination. Next in importance is to roll every joint uniformly to the optimum degree. Tube rolling in the days of low pressures was a simple matter. Rolled joints carried relatively light loads and rolling-in was carried on with manually operated expanders, usually until the mill scale cracked around the edges of the boiler-tube hole. With the advent of high pressures, thick tube sheets, power-driven expanders, and many new alloys, the matter of ascertaining the optimum degree of expanding is more complicated, and its duplication in every joint is of vital importance.

Figs. 3 and 4 illustrate the necessity for such procedures These charts show clearly the effect of different degrees of expanding on rolled joints. They demonstrate also that proper rolling-in produces joints having maximum strength and stability. Since the successful operation of much expensive equipment depends to a large degree upon the tightness and stability of its rolled joints, all guesswork pertaining to rolled joints should be eliminated.

Each tube-and-tube-sheet combination presents a different rolling problem. For example, thin tube sheets require heavier rolling than thicker sheets, other factors remaining the same. To be on the safe side, it is good practice first to roll several sample joints to various degrees of expanding, using tube and plate materials similar to the actual materials used on the job. The merits of each sample may then be ascertained by visual inspection or by using a testing machine.

This practice of pretesting rolled joints in order to gain definite information is rapidly placing tube rolling on a more positive and scientific basis. Tests on rolled joints formed in curved tube sheets are usually made on flat test plates. For the investigation of small tube joints, Fisher and Brown (6) describe several simple testing devices that may be used even on small jobs.

So far, there is no standard nomenclature to cover the evaluation of "joint strength" as disclosed by sample tests. The authors suggest that it could be as follows:

1 "Holding strength," expressed in pounds when joints are evaluated by a testing machine or similar apparatus.

2 "Hydraulic strength," expressed in pounds per square inch if internal fluid pressure is used to break the test joint.

3 "Stability," expressed in pounds per square inch when both internal pressure and external forces are applied to break the joint.

Rolling Methods Based on Change in Tube Dimensions

The methods employed for attaining or duplicating the desired degree of expanding may be treated under two classifications. One is based on the measuring of changes in tube dimensions brought about by tube expanding. The other involves methods that measure and control the power input to the expander, or measure other manifestations of the power used for making of rolled joints.

(*A*) *Reduction in Tube-Wall Thickness.* According to the Airetool Manufacturing Company, a firm having much experience in tube rolling, the optimum degree of expanding for nonferrous tubes is usually developed by expanding the tubes until the wall thickness is reduced by approximately 5 per cent Fig.

4 confirms the soundness of this suggestion. Their formula for obtaining this reduction is as follows:

$$\text{Rolled tube ID} = \text{tube ID} + \text{tube-hole clearance} + \frac{\text{tube-wall thickness}}{10}$$

For ferrous tubes, the same company recommends less reduction, and for ferrous tubes in refinery fittings having standard tolerances and limits, the recommendation is given in Table 1.

TABLE 1 RECOMMENDED REDUCTION FERROUS TUBES IN REFINERY FITTINGS

Tube-wall thickness, in.	Increase inside diameter, in.
1/4	8/64– 9/64
5/16	9/64–10/64
3/8	11/64–12/64
7/16	12/64–14/64
1/2	13/64–16/64
7/8	16/64–17/64

Instructions state specifically that these values are to be used on conventional limits only. This increase in inside tube diameter seems rather excessive and the smaller values would be preferred by the authors.

(*B*) *Tube-End Expansion.* For expanding ferrous tubes in boilers and similar work, the German "tube-end expansion" is much used in Europe. It is the relationship between the reduction of tube-wall thickness expressed as a percentage of the tube-hole diameter. This can be transposed to give

$$\text{Rolled tube ID} = \text{tube ID} + \text{tube-hole clearance} + \text{per cent of expansion} \times \text{tube-hole diameter}$$

Based on tests, Thum and Mielentz (5) state that this tube-end expansion, when used as a measure for tube expanding, should not exceed 1.2 per cent of the original tube-hole diameter. The authors conclude, and illustrate by Fig. 3, that any expanding beyond this limit decreases the strength and stability of rolled joints. However, they admit that this is but a guide and that tube expanding must be tailored to suit the job.

Rolling Methods A and B

In order to uniformly expand all tube joints of a pressure vessel by methods that utilize empirical formulas or other predetermined measurements, it must be presupposed that all tube and tube-hole dimensions are uniform and have similar characteristics. However, on account of high costs and manufacturing difficulties, such accuracy seldom prevails in commercial products. This statement applies equally to vessels having large or small tubes. For example, according to the Battersea report (3), the tube walls of many of the original 4-in. water crossover tubes were 1/16 in. thicker than others. In addition, although actual tube-hole measurements were not given, the tolerance specified for the machining of tube holes was 0.016 in., from 4.040 to 4.056 in., but probably was greater. It is obvious that under such conditions, any rolling method that calls for the rolling of tube ends to a predetermined inside tube diameter cannot produce rolled joints of a uniform character.

Conventional rolling methods that are based on this principle consist of methods that limit or measure the mandrel travel in order to attain a uniform rolling diameter of predetermined dimensions. This is called the "uniform mandrel entrance method," which produces the same size holes in all tube ends rolled with the same mandrel adjustment. This measure is also known, and often referred to, as "tube expansion" and is based and given in per cent of the tube-wall thickness, or in per cent of tube-hole diameter.

Another method employs expanders that automatically cease expanding after reaching the predetermined rolling diameter. Still another method utilizes a definite number of expander turns in order to gain the same result. The latter method has real merit if the expander turns were counted beginning with the full contact between tube and tube hole. This type of operation, however, requires great care, much time, and skill. One German expander accomplishes this task automatically.

On pressure vessels having smaller tubes, the tube-wall thickness usually does not vary an appreciable amount. Tube-hole dimensions, however, do vary. For instance, on commercial work it is considered good workmanship if the tube-hole sizes are kept within a tolerance of 0.005 in. Although such tolerance is seemingly small, it affects the strength of the rolled joints if they are rolled to a fixed tube expansion. For instance, according to the recommendation of the Airetool Manufacturing Company, 3/4-in. 18-gage tubes should be rolled to a tube expansion of only 0.010 in. Thus, if the expander is adjusted to the nominal tube-hole size, many tube ends could be underrolled and, if set to the upper tolerance limit, many could be overrolled.

It is evident that rolled joints of small tubes, when rolled to a fixed tube expansion, have but little chance of being uniform. Since the quality of rolled joints varies with the variations of the hole dimensions when rolled in this manner, it is important that the tolerances of tube-hole sizes should be kept at a minimum. This practice, unfortunately, is not always followed. On heat exchangers and feedwater heaters, especially on those having steel tube sheets, the authors have often encountered variations in tube-hole sizes of 0.020 in. or more. Also, on those having two tube sheets, the holes in one tube sheet are often larger than those of the other. When it comes to retubing jobs, the size of the tube holes may be unpredictable if a nonuniform rolling method was originally used. Especially on the thinner tube sheets, variations of 1/16 in. or even more are frequently encountered.

This, however, is not the whole story—variations in the hardness of tube and tube-hole metals have a distinct influence on the quality of rolled joints. For example, assuming that the expander is adjusted to suit a definite metal specification, then any variation from this specification calls for a readjustment of the expander setting. This is because softer tubes require a larger tube expansion in order to obtain the same joint-contact pressure. With a change in hardness of the tube-hole metals, such as differences that may exist between drums, headers, or still fittings, rolling results in the softer hole metal would be equally unsatisfactory. This is especially pronounced if the tube is harder than the tube-hole metal, a condition not at all uncommon. Experiments of Grimison and Lee (7) treat this subject in detail.

Back-Gage Measure. This method is used on boilers and similar work. In it the tubes are expanded until the bulge formed by rolling at the back of the tube sheet, Fig. 5, attains a predetermined size. The criterion of completed expanding is the "no go" of the back gage. This gage is handled by an extra man on the outside of the drum who signals the expander operator. The measure used is approximately 0.032 in. but has been increased to 0.020 in. per in. of tube diameter for the heavier tubes. It is claimed that in this method of rolling the degree of expanding may be ascertained or checked at any time after rolling-in is completed.

Because this method necessitates measuring at and access to the back of the rolled joint it can only be used on open work, such as watertube boilers. The Battersea boilers were of this type and were rolled according to this method by boilermen well versed in this type of rolling. Therefore, since these boilers are discussed in reference (3), which also describes and evaluates this rolling method impartially, pertinent facts disclosed by this report may be used safely as a criterion.

The back-gage measure used was approximately 0.032 in. larger than the tube-hole diameter. Considering that these tubes were almost 1/2 in. thick, this measure seems rather inade-

quate. An allowance of 0.020 in. for every inch of tube diameter would have been more appropriate.

After describing the poor rolling results obtained,[5] Shannon's and his associates' conclusions on the back-gage rolling method are as follows: "Trial expandings were effected both in the boiler drums and in experimental seat plates. Trials were also made with three roller expanders. These showed that the back gage as a measure of the amount of expanding was unreliable, unless accounts were taken of the particular expander equipment used, the length of the rollers, and their projection through the tube seat. The back gage measured circumferentially to the drum was 0.010–0.015 in. larger than that measured longitudinally."

In other words, on boilers, unless measured in one direction only, one half of the desired expansion may be lost in this manner. Since the back-gage measure may not be a reliable rolling measure, as demonstrated by the Battersea boilers, neither can it be a reliable record of the degree of expanding. All it does is to indicate the size of the back-gage measure used; but it is not a criterion of the rolled joint's condition. This is especially so in cases where the hardness of the tube metal approaches or exceeds that of the tube-hole metal. Under such conditions the tube-hole metal is apt to give way within the limits of the back-gage measure—this without building up the desired joint-contact pressure. Grimison and Lee (7) describe experiments on this subject.

Rolling Methods Based on Measure of Torque

In order to avoid the undesirable features inherent in rolling methods which employ empirical formulas or that measure changes induced by the tube-rolling process, many engineers prefer methods that disregard dimensional joint changes and depend upon procedures that, in one way or another, measure the torque applied to the expander mandrel. In the following discussion the advantages and disadvantages inherent to various rolling methods of this type will be pointed out under their respective headings.

"Feel" Method. Probably the most widely practiced rolling method is the manual feel method which usually is associated with manually operated expanders. Here, the operator simply guesses at the mandrel torque required for the making of a good joint. It is obvious that his guess may be either right or wrong, depending somewhat on his skill and experience. It is evident, also, that an operator's feel may vary considerably during a day's work, nor is it the same day after day. Further, the feel of different operators varies and it is not often that they agree on how much to roll. Thus many joints rolled in this manner are of questionable stability.

Some engineers apply this "manual feel" to power-driven expanders also, but this only complicates matters because the torque delivered to the expander mandrel varies with the power developed and the condition of the machines used; nor is the operator's feel a dependable factor. To illustrate the latter point: It has been the authors' experience that, should the feel of finish-rolling be left to the operator's discretion, the latter invariably will roll until the motor used gives indications of slowing down. This is done regardless of whether the motor is in good or bad working condition, whether it is suitable for the work at hand, or whether the motor is too large or too small for the making of reliable rolled joints.

In order to assist their operators in maintaining a uniform manual feel, some plants maintain a definite and uniform air pressure for the motors used. Although this practice eliminates one variable factor, it does not preclude inferior tube rolling because, aside from the operator's inability to feel the same at all times, it is the torque actually delivered to the expander mandrel that really matters. When checked, it is surprising indeed how much the motor output varies even in otherwise identical machines. The difference in the available motor torque may be, and often is, especially in the smaller tube sizes, the difference between good and badly rolled joints. One drawback common to the manual-feel methods enumerated is that this feel cannot be evaluated and used as a basic measure. It is difficult to transfer a manual feel from one motor to another even if they are the same make and model. It is doubly difficult if the motor makes are dissimilar.

"Mechanical-Feel" Method. In order to eliminate the undesirable features of the manual feel, some engineers substitute a mechanical feel, such as the friction clutches built into several types of portable commercial motors. Though the idea seems quite feasible, experience has shown that the clutch wear due to the rolling-in process and necessary reversal of the expander mandrel makes it extremely difficult to keep the machine in adjustment suitable for the rolling-in of tubes. Nor can the clutch setting be duplicated readily in another motor.

On the European market, several makes of automatic expanders can be found which contain calibrated springs that release the driving mechanism whenever the mandrel torque exceeds the spring setting. Such spring-actuated release mechanisms are somewhat better than the friction-clutch drive, but they cannot be checked readily, nor are they made in the smaller sizes. This is because they are too complicated to withstand the stresses imposed by the demands of present-day manufacturing methods. Today, an expander control must be simple, sturdy, and capable of turning out rolled joints of uniform quality at a high rate—all this with a minimum of effort by the operator, who may be of the unskilled or semiskilled type.

Controlled Rolling. Perhaps the most successful of the tube-rolling methods which meets this specification is the method originated by The Detroit Edison Company. In its design it was aimed to eliminate guesswork and consequent tube and joint troubles and, if possible, put the rolling-in of tubes on a sound engineering basis. After many years of experimenting and testing under operating conditions, a practical and reliable rolling method finally was developed which fully met the company's requirement for construction and maintenance purposes.

This method is based on the assumption that once the optimum degree of expanding and its power requirement have been established for any tube-and-tube-sheet combination, the expanding of any other joint having similar characteristics will produce, with the same power input or torque, joints having the same degree of expanding and, consequently, the same strength and stability. Tests and experience have proved this contention to be valid. It is confirmed by Dunkley (9). Unless abnormal conditions are encountered, such as greatly over-rolled tube sheets, the common commercial tolerances met with in everyday tube-rolling practice do not affect the rolling result to any appreciable extent.

In this method, the manual feel is replaced by an electrical feel consisting of an accurate and adjustable commercial control relay which shuts off the current to the driving motor whenever the power applied to the expander mandrel exceeds the expanding limit set by the control relay and rolling-in torque requirements. The relay setting may be changed readily by means of a rheostat included in the control circuit, a change in the cut-off setting and the power consumption of the driving motor being indicated by a built-in ammeter. For any given tube-and-tube-sheet combination, this relay setting consists of the idling current required for the operation of the driving motor, to which is added the desired degree of expansion, measured and expressed in amperes. Since the current consumption of the idling motor is in-

[5] Reference (3), p. 7.

dicated and can be read on the ammeter, the motor's condition or a change in condition can be seen at a glance.

The motor drive consists of portable commercial tapping machines having motors rotating clockwise only, but their tapping spindles, which drive the expander mandrels, may rotate in either direction. Through a clutch-and-gear arrangement their normal rotation is counterclockwise. However, when an expander is inserted into a tube to be rolled, a forward push on the motor will produce an axial movement of the driving spindle and change its rotation to the clockwise rotation necessary for the expander operation. At the same time a microswitch, mounted on the motor and actuated by the spindle movement, routes the motor current through the rheostat, ammeter, and the load-measuring control relay until rolling-in is completed and the motor current is cut off by the control relay. A pull on the motor will then change the spindle back to its counterclockwise rotation, while the microswitch cuts the motor back into the uncontrolled line current, thus furnishing the extra and ample power needed to reverse and back out the expander swiftly and safely. The expander may then be withdrawn by grasping its nonrotating cage with one hand while holding the motor with the other, and a new joint started by inserting the expander into the next tube end, thus completing the rolling cycle.

The various operations constituting a tube-rolling cycle are interlocked in such a manner that it is not possible to reverse or change the operating cycle. Thus every cycle rolled represents a finished joint of uniform quality, whether rolled by a novice or a man skilled in the art of tube rolling. To further simplify rolling and eliminate expensive skill, self-feeding, parallel rolling expanders are used, which are inserted into the tube end until a ball-thrust bearing fastened to the expander body contacts the tube sheet. This thrust bearing may be adjusted to obtain the joint length desired, and once adjusted eliminates any need for further checking or measuring. The tendency of a self-feeding expander to feed forward is counteracted by this thrust bearing, but because of its antifriction properties, it does not interfere with the proper function or accuracy of the control relay.

In this connection, attention is called to another item that affects the uniformity of controlled rolling. It has been found that an expander mandrel is subjected to severe side stresses when rigidly connected to the driving motor and operated out of line with the tube and tube hole. In consequence, such a condition tends to distort the joints, especially on thin sheets, and at the same time absorb a portion of the torque intended for tube-expanding purposes. This condition may be due to space restrictions, or to the operator's negligence. In the control described, this drawback is eliminated by the adoption of a simple nonslipping chuck, which has a positive mandrel drive, yet allows for considerable angular misalignment.

This method of controlling the degree of tube rolling was first brought to the public's attention in 1941 by F. Fisher through a McGraw-Price paper. A detailed account of its operation and the improvements made in its design can be found in a paper by Fisher and Cope (8). A London report by Dunkley (9) describes the favorable results obtained by this method in rolling-in the tubes of a new condenser. Originally designed for condenser work, the capacity of this rolling control has since been increased to handle tubes up to 3 in., and experiments are under way to increase its capacity still further. It is believed also that many tube joints having flared tube ends also can be brought within its range by simply resting the ball-bearing stop on the tube end instead of on the tube sheet.

Elongation Measure (Extrusion). In this method the optimum degree of expanding is ascertained and duplicated in the field by means of the elongation measure. As stated before, and clearly shown in Fig. 4, stable rolled joints cannot be made without causing an axial flow of tube metal. Also, since this axial flow is from the center of the joint, also shown in Fig. 4, it may be measured by means of a dial indicator in thousandths of an inch at either end of the joint. Further, since the elongation varies with the work performed, it may be considered to be an indication of the degree of expanding imparted to a joint. The appropriate elongation varies with each tube-and-tube-sheet combination. For instance, it may be 0.008 in. for a condenser or 0.065 in. for a high-pressure boiler tube. In a test made to determine the thrust caused by the elongation (1) and check the effectiveness of this measure against possible high resistance, such as when rolling-in boiler tubes 1 ft long, it was found that it indicated the degree of expanding correctly up to the point where the tube joint would be useless as a connecting medium. In a research report, Fig. 7, the average holding strength of three tubes is shown at each elongation increment.

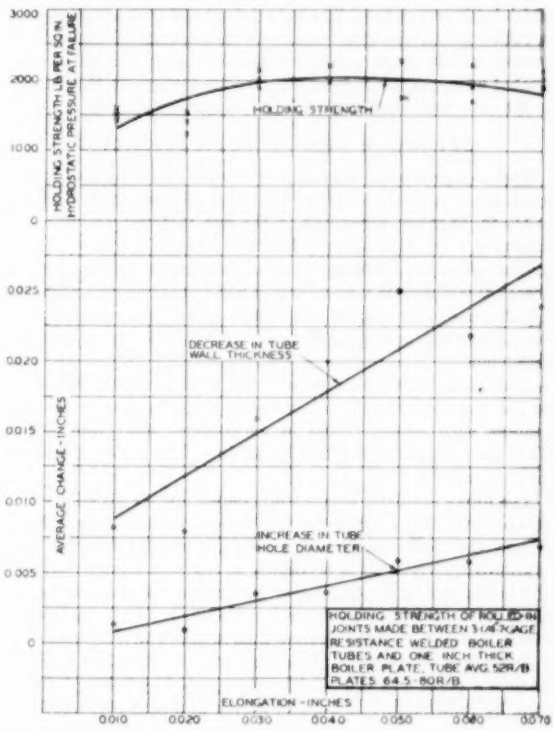

FIG. 7 ELONGATION AND DEGREE OF EXPANDING

This method was developed originally in the plants of The Detroit Edison Company for the purpose of rolling-in boiler tubes. It was described by Fisher and Cope (1) in 1935. Since then, this method has been used successfully for determining the optimum degree of expanding and to duplicate this in the field on all kind and sizes of tube joints having flared or straight tube ends. As it is of universal application, it is often used as a basic measure for checking expanding operations and to adjust rolling controls. For consistent results, however, it is necessary to use well-constructed, parallel rolling expanders and measure the same side of the joint, because expanders forming tapered holes and some expander types produce unequal elongation at the ends of the joint.

Grimison and Lee (7) state that the elongation is an "excellent indicator" of the degree of rolling. However, the authors con-

tend that it is the sum of both elongations which is the correct measure. This, however, does not agree with the findings of other investigators (1). John Van Brunt, New York, N. Y., in a communication to (3) stated that his company rolled the tubes of 63 large boilers ranging in pressures from 1350 to 2000 psi by the elongation method. The degree of expanding was arrived at by inspecting four sample joints rolled to different elongations. As a result, usually the boilers so rolled, when tested, disclosed from 3 to 10 leaky joints that required rerolling; others often passed the tests without any leakage whatever.

The main objection to the elongation method is that the dial indicators must be read by men not accustomed to fine measurements. Errors also could be caused by improper fastening of the indicators. However, promising experiments are now in progress that are expected to eliminate these objections, as well as improving this method by making it semiautomatic, the idea being to signal the expander operator automatically whenever rolling-in of a joint is completed. The actual degree of expanding imparted to rolled joints, old or new, may be ascertained by checking the beveled telltale mark resulting from the rolling operation. It is located adjacent to the tube sheet and is formed by the thinning of the tube wall combined with the elongation, Fig. 5.

Sequence of Tube-Expanding Procedures

The elongation phenomenon increases the length of rolled tubes by an amount varying from a few thousandths of an inch to $^1/_{16}$ in. or more, depending on the size, material, and tube-wall thickness, as well as the length of the joint to be rolled. When rolling tubes of a U-shape or tubes having sufficient flexibility to absorb this elongation, no difficulty will be experienced when rolling the second or closing end of the tubes. They should, however, be rolled uniformly in order to maintain the proper tube alignment.

Conditions, however, change entirely when rolling the second end of straight and stiff tubes that connect fixed tube sheets or headers such as are found in condensers, stills, and boilers. Here the elongation, due to lengthening of the tubes, becomes a major problem.

The forces involved vary widely, depending on the tube layout and purpose of the equipment. On 1-in. condenser tubes, for instance, the thrust exerted by a single, straight tube 24 in. long is approximately 1000 lb according to research reports; whereas the rolling-in of a $3^1/_4$-in., 7-gage boiler tube 1 ft long, into a tube sheet $1^7/_8$ in. thick, raises this value to 7000 lb (1). This does not mean, however, that the stresses thus imposed on a tube sheet are a multiple of all tubes rolled, because some of the rolled tubes will assume a portion of the total load generated by rolling. Therefore, by judiciously spacing and rolling-in a sufficient number of so-called "tack tubes," distortion of tube sheets and headers can be held at a minimum. By starting rolling between the tack-tube spacing and working toward the tack tubes or finished portion, the tube sheet will be stiffened still further. This recommended rolling sequence applies also to boilers and headers.

Fig. 8 depicts in a somewhat exaggerated form the effects of elongation created by various rolling sequences: Fig. 8(*a*) shows what will happen without tack tubes or other restraining means when rolling operations are carried on successively across the tube sheet or header. The rolling sequence is indicated by the numerals. It does not take very long before tube sheets or headers are gradually forced apart as shown, and the remaining tubes become too short for the job. On floating heads, this neglect manifests itself by cocked tube sheets. On fixed tube sheets of lighter construction, such as generator air-cooling equipment, the tube sheet may be distorted by one or more bows when following such rolling sequence. Clamping water boxes or similar connections to tube sheets thus distorted will set up excessive

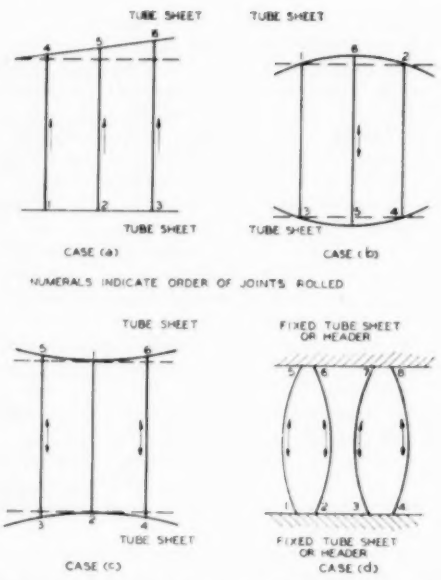

Fig. 8 Effect of Rolling Sequence on Tube Sheets and Tubes (Shown in exaggerated form.)

stresses that ultimately will lead to tube failures or other troubles.

Figs. 8 (*b*) and (*c*) illustrate the stress conditions created by the rolling sequence as enumerated. Both are common occurrences during erection or the replacement of tubes. However, by following practical rolling procedures, the resulting stresses usually are absorbed by the tubes or structure. Fig. 8 (*d*) depicts the behavior of slender tubes when rolled into two fixed headers or tube sheets. The bow shown, to a certain extent, relieves the pressure on the tube sheets. In fact, by using the "controlled tube-rolling method," with its expanders fully inserted into the tube end, it is quite possible to have straight tubes and to roll slender tubes without stressing the tube sheets; that is because the feeding action of the expander, being limited by the ball bearing resting on the tube sheet, tends to stretch the tube before rolling-in takes place. For instance, $^3/_4$-in. condenser tubes 24 ft long stretch approximately 0.008 in., which may be offset by an elongation of from 0.008 to 0.009 in. produced by the rolling-in process. This applies to stiff or well-stayed tube sheets. On others, this initial pull may lead to tube-sheet distortions unless counteracted by sufficient tack tubes, properly placed.

Long Tube Joints

The effects of elongation in smoothing off irregularities of the joint-contact surfaces have been discussed previously and shown in Fig. 4. So has the fact that reinforcing grooves should be placed near the center, but not at the center, of the rolled joint. This takes advantage of the elongation without incurring the chances of shearing the tube metal extruded into the grooves. On thicker tube sheets, however, that is, on joints too long for available expander rollers, this statement does not hold true because such joints are rolled in a different manner.

The conventional method is to step-roll the joint; that is, roll it in sections somewhat less than the length of the expander rollers, the shorter length, in order to insure an overlap in rolling. Also, this manner of rolling is started at the back of the joint as shown in Fig. 9(*a*), to keep the elongation at a minimum. Otherwise, if rolled in the opposite order, several elongations would accumulate, as is indicated in Fig. 9(*b*). This would cause

slender tubes to bend, and on stiffer tubes set up destructive stresses in the joints as well as the structure. These are also the objections to the use of one expander type, Fig. 1(D), if it is set to the desired rolling size and then fed through the joint in one operation, from the front to the back. It may be used in this manner on the first tube sheet rolled, but not on the second or closing joint.

In order to eliminate this cause of excessive stressing, expanding means have been devised that roll a joint in the reverse direction, the so-called "retractive" expanders. These are arranged to first roll up to the desired degree of expanding at the back of the joint and then roll forward at that setting until the joint is completed. They do not, as claimed, eliminate the elongation but may reduce it slightly, because expanders having short rollers usually are employed for this purpose, and the elongation is a function of the roller length. Their advantage lies in the fact that long joints having a multiplicity of reinforcing grooves can be rolled-in in one operation without running the risk of shearing tube metal extruded into these grooves, because the grooves fill progressively as rolling proceeds and the unrolled portion of the tube end is free to move in and through the tube hole.

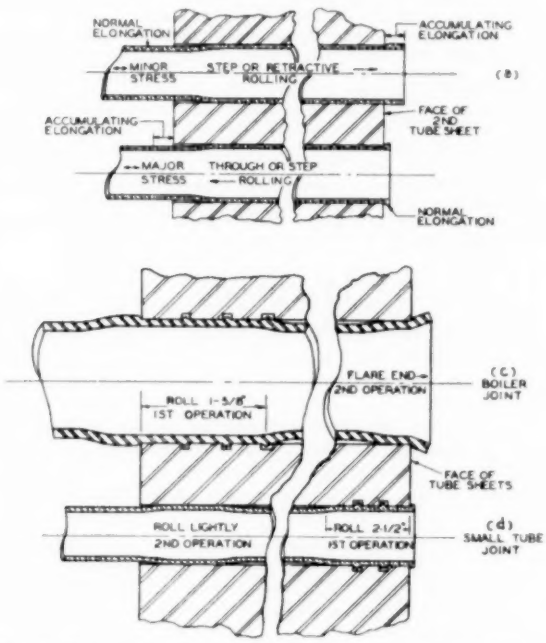

FIG. 9 COMPARISON OF ROLLING PROCEDURES; SHORT JOINTS IN THICK TUBE SHEETS

According to the best information available at present, the merits of long rolled joints seem rather problematical. Since there is no appreciable reduction in elongation when using retractive expanders and boiler joints thus rolled must be supplemented by a separate tube-end flaring process, there seems to be no reason why equal results cannot be obtained by conventional means.

In boiler work, a joint length of $1^{3}/_{4}$ in. is universally accepted as a safe and satisfactory length for all boiler tubes. Maxwell (4) is quite satisfied with joints $1^{1}/_{4}$ to $1^{1}/_{2}$ in. long. Thus conventional joints $1^{3}/_{4}$ in. long could be formed at the back of the joint and the tubes flared by a separate operation, the same as required for rolling with retractive expanders. It also would bring such joints within the range of controlled tube expanding. A joint of this type is shown in Fig. 9(*c*). The same reasoning applies to long joints in heat exchangers and similar equipment. Fisher and Brown (6) advocate a joint length of $2^{1}/_{2}$ in. for equipment of this type, this length having given satisfactory service in the plants of The Detroit Edison Company for 10 years or more. The annular gap at the other end may be closed by light rolling as indicated in Fig. 9(*d*).

REROLLING OF TUBES

If it becomes necessary to reroll rolled joints, it is good practice to do so lightly, assuming, of course, that the joints involved have been assembled initially and rolled in a workmanlike manner. Such joints may be lightly rolled several times without affecting the strength of the joint seriously or damaging tube or tube-sheet material. Heavy rolling, however, is apt to cause excessive deformation of the affected tube and tube-sheet material with a consequent reduction in the strength and stability of the joints rolled. Fig. 4 depicts clearly the effect of the difference between light and heavy rolling.

Leaks are not so likely to occur on step-rolled joints because each step roll forms an additional joint, that is, if it is made in a workmanlike manner. However, if necessary, rerolling can be done with the original tools used. This differs somewhat from long joints made with a retractive or ball-drift expander, where re-working of such joints by means of the original tools may not be practical on account of the accumulating elongation. This applies specifically to cases where tube and tube-sheet material are of approximately the same hardness. Here the resulting excessive elongation tends to loosen the original bond and may shear off tube metal extruded into the grooves. A safer procedure is to step-roll one or more sections of such joints using expanders having short rollers, say, about $1^{1}/_{2}$ in. long.

RETUBING

The first step in a retubing job is to cut off and remove the old tubes, and next dispose of the tube ends remaining in the tube hole in order to make room for the new tubes, and clean tube holes in preparation for rolling. Large ferrous tubes may be cut by using an oxyacetylene cutting torch. With it, the tube stubs may be split axially by careful handling of the torch. Or, if suitable, mechanical tube cutters may be used and the stubs split by means of gages or cape chisels, then bent inward and removed. This method is applicable to both flared or straight tube ends as well as tube holes with or without grooves.

For small tubes, such as found in condensers or similar equipment having smooth tube holes, motor-driven cutters may be had that cut off the tubes back of the tube sheet. The other rolled end and the tube itself may then be withdrawn by means of a hydraulic puller or other suitable means. The stub end may be pulled in the same manner, or an "Easy-Out" fastened to a rod having a sliding hammer weight also may be used for the same purpose.

On tube sheets having grooved tube holes, the tubes cannot be pulled in the same manner and different tactics are necessary. On the thinner tube sheets and thin tubes, after cutting off the tubes, the remaining stub end may be removed by driving a tapered tool between tube and tube sheet. This doubles up the tube end and permits its removal. However, this method, unless carefully executed, often results in damaged tube holes and consequent difficulties in obtaining tight joints for the new tubes.

For this reason many engineers prefer to dispose of the stub ends by means of drilling. This, however, does not remove the tube metal extruded into the grooves. To remove these remnants is an arduous, tedious, and time-consuming task. In many

cases the removal of the stub ends is the most expensive of all retubing operations. The authors have experimented with several ideas designed to eliminate this bottleneck. The most promising is one in which a helical gun tap of nominal tube size is utilized to relieve the contact pressure between tube and tube hole. Steel bolts are then inserted into the tapped tube end and the stub pulled by means of a small hydraulic jack. Twenty $^{3}/_{4}$-in. 16-gage admiralty tubes have been pulled by this means cleanly in 5 min from tube sheets 6 in. thick, but means to counteract the variations found in tube-hole sizes still remain to be developed.

Rolling-In of Replacement Tubes

It has been demonstrated that any tube-rolling operation is accompanied by a deformation of the joint components. Thus, if the initial rolling was of a nonuniform or over-rolled character, it safely may be assumed that replacement tubes go into nonuniform or oversized tube holes. Such conditions are especially prevalent in thin tube sheets and headers. It is apparent that in cases of this kind, any rolling method which is based on changes in tube dimensions is of little value.

For larger tubes, in consequence there are only two methods which give assurance of uniform rolling One is to expand the tube until it contacts the tube hole firmly. Then, noting the remaining length of the expander mandrel, rolling is continued until the mandrel has entered the expander an additional distance corresponding to the desired degree of expanding, or the expander revolutions may be counted. This type of rolling calls for a careful and experienced operator. The other method consists of rolling to the appropriate elongation. This can be done in safety because elongation does not begin, regardless of tube-hole size, until full contact has been made with the tube hole.

With smaller tubes, in order to obtain uniformly rolled joints, a good way is by means of a tube-rolling control. Here an appropriate control setting will produce good joints within a reasonable deviation from normal tube-hole size, say, 0.020 in. for smaller tubes. This leeway, of course, varies with the tube hardness and should be checked before proceeding. Tubes in holes exceeding safe rolling limits require more rolling at a higher control setting.

In order to disclose such oversize holes automatically, it is good practice to put a mark or stop corresponding to the maximum travel on the expander mandrel. Then, whenever during the rolling-in of the tubes, the mandrel enters the expander up to this mark and the control does not operate, these tube holes should be marked and rerolled at a higher control setting with an adjusted travel stop. This operation may be repeated. However, should this not suffice in rolling the tube, if necessary the tube should be removed and the ends annealed before further tube expanding is attempted.

Should the replacements consist of tubes having wide variations in hardness, the tubes that require rolling at a higher control setting can be spotted readily by observing the finish rolling position of the travel mark. If the mandrel protrudes from the expander much more than the usual distance, it is a sign that this tube is much harder than others and requires rerolling at a higher control setting—this in order to raise the joint strength equal to that of other joints having softer tubes.

At times it is desirable to replace or install short or straight tubes without stressing other portions of the structure. A simple procedure, which requires but a few minutes, is first to lengthen the tubes by the application of heat an amount corresponding to the elongation to be rolled on the closing joint. When cooled, these tubes should be in a state of neutral stress. Variations of such procedure may be used for other purposes, such as compressing gasket, and so on.

Conclusion

The material covered in the paper reflects many years of study and experience by the authors in the field of tube expanding—improvements to tools and development of new rolling methods. In addition, the authors have assembled all of the information available to them on the art of tube rolling and the combination of this information with their experience should be of assistance to the engineer faced with a problem in tube rolling.

BIBLIOGRAPHY

1 "Rolling-In of Boiler Tubes," by F. F. Fisher and E. T. Cope, Trans. ASME, vol. 57, 1935, pp. 145–152; discussion, vol. 58, 1936, pp. 66–72.

2 "The Beading of Boiler and Superheater Tubes by Means of Rolling Pressure, If Various Materials Are Used," by Dr. A. Thum and Dr. Ing. R. Jantscha; translated from Archives für Warmewirtschaften und Dampfkesselwesen, December, 1930, pp. 397–401.

3 "Expanded Tube Joints in Boiler Drums, With Special Reference to the Battersea High-Pressure Boilers," by W. B. Shannon, C. W. Pratt, T. B. Webb, and W. B. Carlson, The Institution of Mechanical Engineers and The Institution of Electrical Enginers, published in London, England, March 23, 1945.

4 "Practical Aspects of Making Expanded Tube Joints," by C. A. Maxwell, Trans. ASME, vol. 65, 1943, pp. 507–514.

5 "Das Verhalten von Einwalzstellen Bei Verschiedenen Ausbildungformen und Betriebsbedingungen," by A. Thum and J. W. Mielentz, Materialprufunganstalt, Darmstadt. Mitteilungen der V.G.B., Heft 55, 1935, pp. 258–290.

6 "Expanded Tube Joints in Feedwater Heaters and Heat Exchangers," by F. F. Fisher and G. J. Brown, Paper No. 50—A-130.

7 "Experimental Investigation of Tube Expanding," by E. D. Grimison and G. H. Lee, Trans. ASME, vol. 65, 1943, pp. 497–505.

8 "Automatic Uniform Rolling-In of Small Tubes," by F. F. Fisher and E. T. Cope, Trans. ASME, vol. 65, 1943, pp. 53–60.

9 "Steam Condensers With Rolled-In Tubes," by W. H. Dunkley, *Engineering*, London, England, December, 1947, pp. 592-593.

Discussion

W. E. Cooper.[6] At the 1953 Brown University Plasticity Symposium, Prof. Hugh Ford of the Imperial College, London, England, reported briefly on some work in this field which may be of interest.

The British Shipbuilding Research Association is sponsoring "An Experimental Investigation of the Process of Expanding Boiler Tubes Into the Shells of Tube Plates of High Pressure Boilers." This project is designated as BSRA Research Item No. 11.

In connection with this project, H. Ford and J. M. Alexander have prepared Interim Report No. 3 which is a theoretical treatment of the problem. This work includes the majority of the factors which have been neglected in previous work by Nadai and by Taylor and Hill.

It is their hope that as a result of this investigation, it will be possible to approach this problem on a theoretical basis rather than on a purely empirical basis.

Authors' Closure

It is indeed a pleasure to learn that the British Shipbuilding Research Association is sponsoring an experimental investigation of the process of expanding boiler tubes into the shells of tube plates of high-pressure boilers. As this investigation deals with boiler and tube materials produced according to definite specifications, we may expect an impartial evaluation of the tools and rolling methods now in use. It is also hoped that it will disclose improved means or methods for the production of uniformly rolled joints of optimum strength and stability. Whatever the

[6] General Electric Company, Schenectady, N. Y.

outcome, such investigation should make a valuable contribution to the art of tube expanding.

Viewed from a practical standpoint, it is desirable that this investigation also include the expanding of tubes into the small headers common to ship boilers. While, for example, tube joints in most boiler drums can readily be expanded by means of controlled tube-expanding equipment, and the flares formed later, the same technique cannot be used on the smaller headers that cannot be entered.

This is because many headers have tube holes that differ in plane or alignment from the handhole openings provided for access purposes. For the rolling-in of such joints it may be necessary to use mandrel extensions, knuckle joints, an appropriate train of gears, or right-angle gear drives. Often also, limited working space compels the use of several short taper mandrels of suitable length and diameter, before the tube can be fully expanded.

Attention is also called to the fact that a successful rolling method should be capable of compensating for an impediment to uniform tube rolling, namely, boiler tubes that are harder then their tube sheets. The consequences are expanded tube joints of inferior quality. Excess hardness may be caused by an improper annealing process; or it may be due to differences in hardness evaluations.

For instance: Some engineers prefer to take hardness readings on the median diameter of the tube end and may thus obtain values that are within the limits of the tube-sheet hardness. The outside of the tube, however, consisting of metal that contacts the side of the tube hole and forms the joint, may actually be harder than the tube-sheet metal. If this difference in hardness is too great, the resulting joints may not be satisfactory.

Although this investigation appears to deal primarily with marine boilers, any lesson learned therefrom applies equally well to boilers of the stationary type.

Electronic-Control Method for the Precision Expanding of Tubes

By F. E. DUDLEY,[1] WESTMONT, N. J.

As conditions of temperature and pressure become more severe in modern heat-transfer equipment, the art of expanding tubes must keep abreast of this progress in engineering. This is especially true with tubes being expanded at both ends where metal-to-metal fixed joints are required to maintain absolute leaktight integrity and mechanical stability for safe and efficient operation. Overexpanding imposes excessive cold-work stresses in tubes and sheets, resulting in early failures. Underexpanding carries its burden of leakage and added nonproductive hours for correction in the field. This paper relates to progress in the precision expanding of tubes during the past few years.

Introduction

RECORDS indicate that the expanded tube joint has been in use approximately 90 years.

In all probability the first joints were established by driving a tapered pin into the tube, thereby swedging or expanding the tube, with sufficient force to create leaktight joints for low-pressure and temperature operation.

The next tool, for expanding, was the three-roll, "nonself-feeding," "nonparallel" rolling expander. This tool was an improvement over the "drift pin," but was for hand operation only and not suitable for the production establishment of expanded joints. Later this nonparallel rolling tool was modified to create "self-feeding" qualities, but still inherent in its design was the nonparallel feature. This tool is still in use in some plants today and will remain until management discovers its detrimental features to the establishment of properly expanded tube joints.

There are applications in the industry such as the expanding of bimetal tubes whereby the nonparallel rolling expanders may be used to advantage. However, this tool should not be used for general expanding if expanded joints of mechanical and leaktight stability are to be expected.

From this tool evolved the "self-feeding," "parallel rolling" expander used throughout industry today, Fig. 1.

Controlled Rolling Investigated

In 1940, while employed by the United States Navy, the author was delegated to investigate the difficulties being encountered with the expanded tube joint. This was occasioned by the following:

The main condenser of a ship was retubed at a major base, the ship was loaded with high priority cargo and sailed for a foreign port. Twenty miles at sea, her condensers failed, necessitating return to port. An investigation disclosed the following:

1 The tubes had been over-rolled, resulting in cracking and splitting of the tubes.

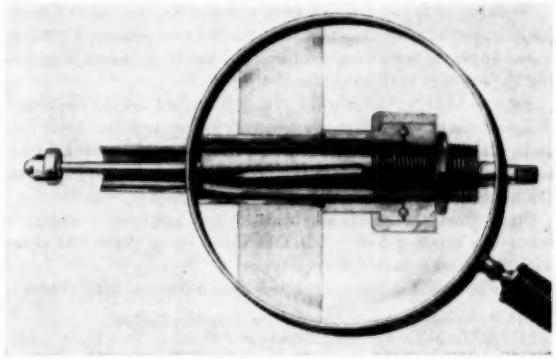

Fig. 1 Self-Feeding, Parallel Rolling, Ball-Bearing-Type Tube Expander, 1/16-In-Recess Collar

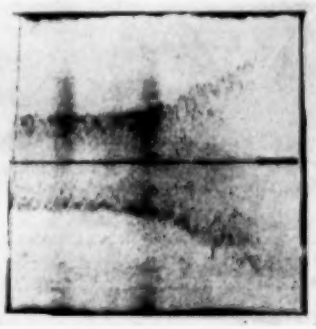

Fig. 2 Oscillogram of Electronic Control Showing Cut-Off at Pre-Determined Setting With No Lag or Relay Chatter

2 The tubes had been expanded using nonparallel rolling expanders.

Delving further into the expanded joint, we discovered that one of the large foreign producers[3] of condensers had experimented with controlled rolling of tubes in 1927. This work involved the placing of a watthour meter in the circuit with an electric-motor-driven expander to measure the power necessary to expand a given size tube.

Others in this country[3] had conducted tests of controlled rolling, utilizing an electromagnetic relay in series with the expander-drive motor. Also, experiments had been conducted by many in the industry, to provide adequate control for the air motor-driven expander. After an investigation into the possible application, for Navy use, of the foregoing methods of controlled rolling, we felt that features should be incorporated in the device to make it possible for unskilled personnel to operate the device with a minimum of training; it should be accurate, Fig. 2, with a minimum cost of operation.

[1] President, Franklin Manufacturing Company, Inc.

Contributed by the Heat Transfer Division and presented at the Annual Meeting, New York, N. Y., November 29–December 4, 1953, of The American Society of Mechanical Engineers.

Note: Statements and opinions advanced in this paper are to be understood as individual expressions of the author and not those of the Society, of the Navy Department, or the service at large. Manuscript received at ASME Headquarters, September 19, 1953. Paper No. 53—A-133.

[3] "Rolling Tubes in Boiler Plates," by P. H. Oppenheimer, *Power*, vol. 65, 1927, pp. 300–303.

[3] "Automatic Uniform Rolling-In of Small Tubes," by F. F. Fisher and E. T. Cope, Trans. ASME, vol. 65, 1943, pp. 53–60.

Electronic Control Developed

In 1944, after 2 years of experimentation at the Norfolk Naval Shipyard, the author was placed in charge of the development program to produce an electronic control for expanding condenser tubes. This program was presented to the Bureau of Ships in 1945; funds were made available to the Naval Research Laboratory, Anacostia, Washington, and the Engineering Experiment Station at Annapolis.

Working with Dr. J. E. Dinger[4] of the Naval Research Laboratory, a prototype of the electronic control was produced. Subsequent approval tests were conducted by the U. S. Naval Engineering Experiment Station at Annapolis.[5]

Further tests, at the Norfolk Naval Shipyard, on the condensers designed for the USS *Kentucky*, involving several thousand tube ends, all expanded by the electronic control, with no leaks, using unskilled personnel, assured the acceptance of the device by the United States Navy.

Since then the electronic control has been used widely in capacities ranging from 1/4-in-OD tubes up to 10-in-OD tubes. Figs. 3, 4, and 5 show different types.

Prior to this development, tubes were affixed to tube sheets by so-called "skilled" operators who utilized various means of determining when the joint had been established properly, such as, (*a*) listening for a particular sound of the expander-drive motor and (*b*) by feel, noting the counter torque imparted to the operator holding the expander-drive motor.

[4] U. S. Naval Research Laboratory Test No. C-2708.
[5] U. S. Naval Engineering Experiment Station, Test No. C-2179.

Tests of Electronic-Controlled Expanding

Tests were conducted, using an operator who had been expanding tubes for a period of 20 years. The tube-sheet plate was mounted in a vise, at workbench height, which afforded ideal conditions for consistency. Tests then were conducted to obtain push-out value in pounds of the tubes expanded into the test sheet, Fig. 6, from which it will be noted variations between 1750 up to 5880 lb were measured.

To determine the mechanical strength required for a given size and gage tubing, which would be necessary in an expanded joint, short sections of tubing, 2 in. long, were cut with ends parallel, and placed between the platens of an Olsen machine, Fig. 7. Pressure then was applied to determine the failing point of the tube sections in compression.

Of particular interest, owing to their wide use in surface condensers, we will analyze the curve, Fig. 8, showing the failure, resulting from column loading, in a 7/8-in. 18-gage Admiralty tube

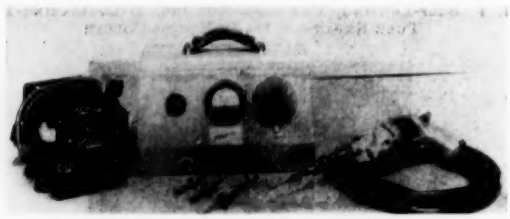

Fig. 3 Type "A-s" Electronic Tube-Expander Control for Expanding 1/8-In. Up to and Including 1/2-In-OD Nonferrous Tubes

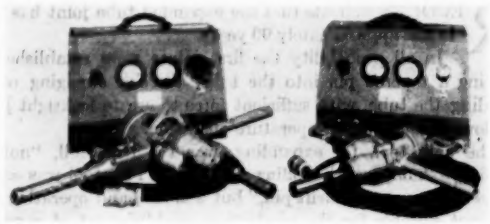

Fig. 4 *At left*, Type B-1 and *right*, Type B Electronic Tube-Expander Controls for Expanding 2-In. Up to and Including 4-In-OD Tubes and 1-In. Up to and Including 2-In-OD Tubes

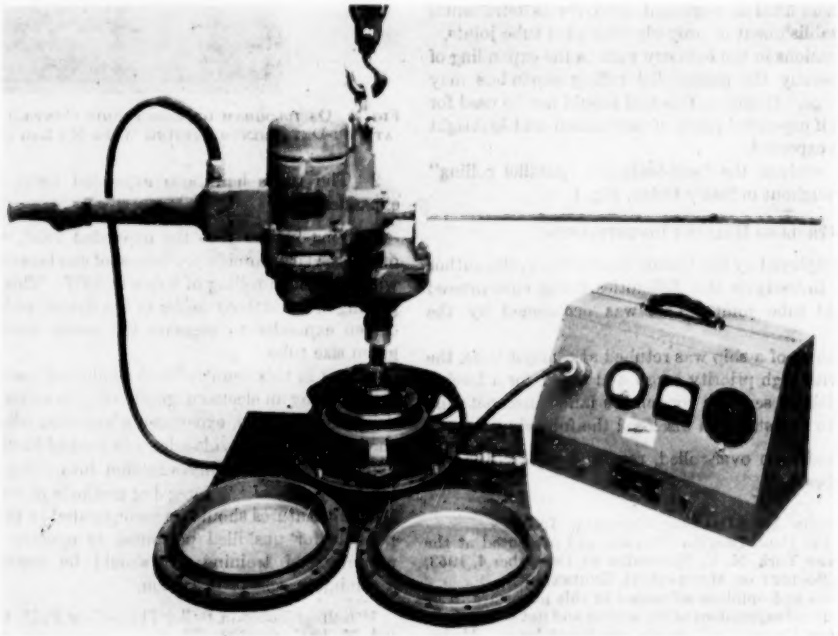

Fig. 5 Type "BX" Electronic Tube-Expander Control for Expanding 4-In. Up to and Including 10-In-OD Tubes

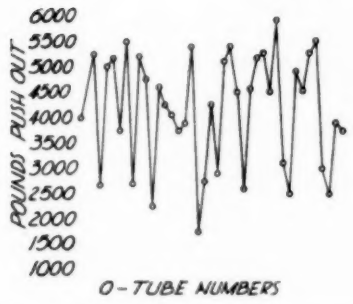

FIG. 6 CURVE SHOWING NONUNIFORM EXPANDING OF SO-CALLED EXPERIENCED OPERATORS

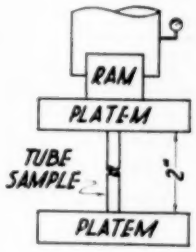

FIG. 7 METHOD OF OBTAINING COLUMN-LOADING TESTS OF 2-IN. TUBE SECTIONS

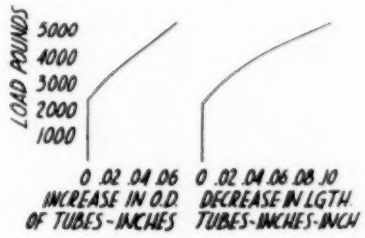

FIG. 8 COLUMN-LOADING TEST OF 7/8-IN. 18-GAGE ADMIRALTY TUBE

and a 1-in. 18-gage Admiralty tube, Fig. 9, with the same failure

The 7/8-in. 18-gage Admiralty tube started to fail by decrease in length with a column loading of 2000 lb, continuing to fail by increase in OD at 2500 lb. The 1-in. 18-gage Admiralty tube started to fail, by decrease in length, at 1000 lb and continued to fail, by increase in OD, at 3000 lb.

These tests would indicate that a mechanical joint of 2000 lb would be sufficient to give stability beyond the failing point of the tube itself. A 2000-lb joint may be obtained with either the 7/8-in. 18-gage or the 1-in-OD 18-gage tubing in a 1-in. sheet, with an expansion of 0.003 to 0.004 in., after metal-to-metal contact, in a standard commercially reamed hole, with no serrations. This tube joint will withstand hydrostatic tests up to 600 psig. This further indicates that the use of serrations are not warranted, since serrations do not contribute to leaktightness but tend to increase mechanical strength.

Generally speaking, the use of serrations varies with designers, for no particular reason. It is pointed out that careful thought should be given to the use of serrations such as the type and the number, since serrations make tube removal most difficult and are, of course, costly to put in. The results of the use of serrations are given in Table 1.

Referring to Fig. 10, a 5/8-in. 20-gage cupro-nickel tube starts to fail, under column-loading tests, by decrease in length of the tube at approximately 500 lb; also, failing by increase in OD of the tube, under column loading, at 1000 lb.

It will be noted from Table 1 that it was possible to obtain a

TABLE 1 DATA OF MECHANICAL STRENGTH, BASED ON NUMBER OF SERRATIONS USED—SERRATIONS OF STANDARD, NAVY V-TYPE

Push-Out Holding Power Tests of Tubes Expanded by "Rolotron" Method (5/8-in. 20 BWG C/N tubes—C/N sheet 1 in. thick.)

Test no.	Load, amp.	Amount of expansion, in. diam	Length of joint, in.	Sheet hole	No. of joints	Average holding power, lb
1	1.4	0.003	0.985	Reamed	13	2613
2	1.4	0.003	0.985	1 serration	14	2802
3	1.4	0.003	0.985	2 serrations	12	3063
4	1.4	0.003	0.985	3 serrations	12	3740

Range of Individual Holding-Power Tests, lb

Test 1	Test 2	Test 3	Test 4
2100	2410	2790	3425
2305	2640	2840	3425
2410	2650	2855	3500
2460	2675	2975	3540
2500	2710	3030	3580
2500	2775	3045	3645
2610	2815	3110	3810
2640	2835	3120	3900
2735	2845	3175	3930
2805	2855	3190	3955
2915	2925	3270	4085
2960	2970	3365	4090
3030	3030		
	3105		
Range: 930	695	575	665

NOTE: Amount of expansion measured on inside diameter of tube after metal-to-metal contact of tube and tube-sheet hole, after expansion.

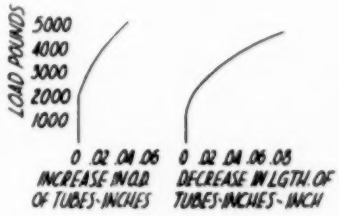

FIG. 9 COLUMN-LOADING TEST OF 1-IN. 18-GAGE ADMIRALTY TUBE

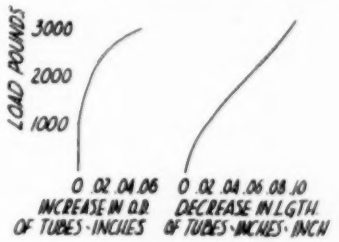

FIG. 10 COLUMN-LOADING TEST OF 5/8-IN. 20-GAGE CUPRO-NICKEL TUBES

2613-lb mechanical joint with a 5/8-in. 20-gage tube, in a reamed hole, with an expansion of 0.003 in. which far exceeds the mechanical strength of the tube itself. Hydrostatically, such a joint would withstand a 600-lb test, Table 2.

Figs. 11 and 12 cover column-loading tests for the 5/8-in. 18-gage and the 3/4-in. 18-gage Admiralty tubing.

TUBE-EXPANDING TECHNIQUES

Overexpanding creates longitudinal and radial stresses in the unit. During the expanding process, the tube increases in length. Measurements indicate that there is a 70 per cent flow of metal away from the operator and a 30 per cent flow toward the operator. During expanding of the inflow ends, which normally are expanded first, the tube is free to increase in length without restrictions. However, when the outflow end is expanded, compressive loading of the tube takes place, tending to separate the sheets, Fig. 13. This condition imposes longitudinal stresses in the entire unit, particularly if unequal expansion of the various tube joints has been made. Concentration of the stresses also are imposed in the area of joint termination.

It is interesting to note the following tests conducted by others (unknown): A 20-ft, 1-in. 18-gage tube expanded into fixed tube sheets with support plates located every 5 ft. The tube was expanded at A and E, temperature 70 F; by passing steam through

TABLE 2 PRESSURE AND TEMPERATURE TESTS ON SMALL MODEL CONDENSER

A model unit equipped with 1-in-thick copper-nickel tube sheets, with 30 $^{5}/_{8}$-in. reamed holes, was constructed for pressure and temperature tests.

30 $^{5}/_{8}$-in. 20 BWG copper-nickel tubes were selected for their minimum wall thickness of 0.035 in.

Tubes were expanded at both ends without provision for an expansion joint.

Expansion of Tube Ends as Follows:

No. of joints	Load amp	Length of joint, in.	Hole	No. of joints	Load amp	Length of joint, in.	Hole
4	1.2	$^{13}/_{16}$	Reamed	4	1.2	$^{5}/_{8}$	Reamed
4	1.3	$^{13}/_{16}$	Reamed	4	1.3	$^{5}/_{8}$	1 Serration
5	1.4	$^{13}/_{16}$	Reamed	3	1.4	$^{5}/_{8}$	1 Serration
6	1.5	$^{13}/_{16}$	Reamed	2	1.4	$^{5}/_{8}$	Reamed
6	1.6	$^{13}/_{16}$	Reamed	5	1.5	$^{5}/_{8}$	Reamed
5	1.7	$^{13}/_{16}$	Reamed	1	1.5	$^{5}/_{8}$	1 Serration
				1	1.6	$^{5}/_{8}$	1 Serration
				5	1.6	$^{5}/_{8}$	Reamed
				5	1.7	$^{5}/_{8}$	Reamed

RESULTS OF TESTS

Test 1, Cold water 50 psi—$^{1}/_{2}$ hr—no leaks.
Test 2, Water 212 F 50 psi—$^{1}/_{2}$ hr—no leaks.
Test 3, Hot and cold cycle tests 64 F to 212 F—50 psi—20 cycles—no leaks.
Test 4, [a] Cold-water pressure test—maximum pressure 600 psi—no leaks.

[a] Due to leakage of gaskets, maximum psi reached was 600 lb. Expansion after metal-to-metal contact varied from 0.0025 in. for 1.2 amp to 0.006 in. for 1.7 amp.

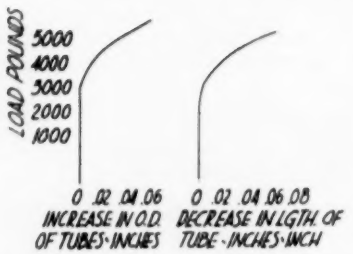

FIG. 11 COLUMN-LOADING TEST OF $^{5}/_{8}$-IN. 18-GAGE ADMIRALTY TUBE

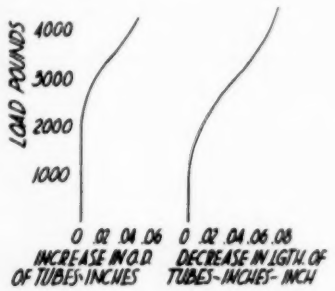

FIG. 12 COLUMN-LOADING TEST OF $^{3}/_{4}$-IN. 18-GAGE ADMIRALTY TUBE

FIG. 13 SHOWING DIRECTION OF FORCE, TENDING TO SEPARATE TUBE SHEETS AS A RESULT OF COMPRESSIVE LOADING OF TUBES DUR'NG EXPANDING

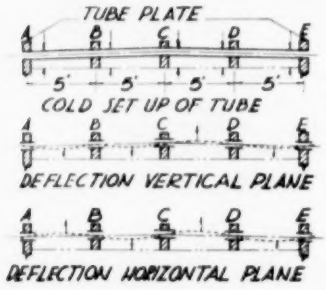

FIG. 14 METHOD OF DETERMINING REACTIVE EFFORT IMPARTED TO EXPANDED JOINT AT A AND E
(Also showing deflection in vertical and horizontal plane of tube as a result of thermal changes.)

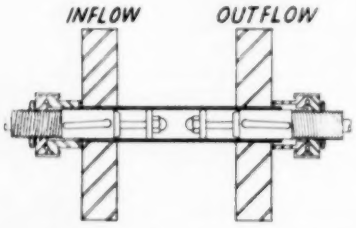

FIG. 15 SHOWING TECHNIQUE USING $^{1}/_{16}$-IN. RECESSED COLLAR FOR EXPANDING INFLOW ENDS AND DEEP RECESSED COLLAR FOR EXPANDING OUTFLOW ENDS TO REDUCE COMPRESSIVE LOADING OF TUBES

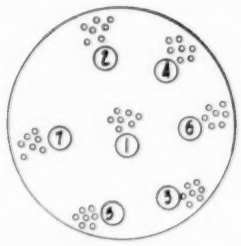

FIG. 16 SHOWING SEQUENCE OF EXPANDING OUTFLOW ENDS, PATTERN ROLLING, STARTING WITH NO. 1

the tube, the temperature of the tube was raised 212 F, resulting in deflection, in the horizontal plane, between the supports of $1^{3}/_{4}$ in. and deflection in the vertical plane, between the support plates, as much as 1 in., Fig. 14. The reactive effort was measured and found to be $301^{1}/_{2}$ lb. Such stresses can result in early failure of the entire unit.

The compressive loading of tubes, during expanding, may be reduced by the following technique, Fig. 15. The inflow ends of all exchangers should be expanded first. If the inflow ends are to be flared, utilize a recess collar, as shown, to position the tube, automatically, beyond the face of the sheet. The depth of recess, normally used in the industry, is $^{1}/_{16}$ in.; the bottom of the recess is knurled. This knurled face eliminates spinning of the tube, during expanding, as well as an assistant who normally would hold the tube at the opposite end.

The outflow ends of the unit are then expanded with a deep recess collar, as shown, which clears the end of the tubes during expanding. The self-feeding action of the expanding tool will cause the tube metal to flow into the recess, unrestricted.

Tests have been conducted, utilizing dial indicators across the expansion joint, showing that, with this technique, the expansion joint was closed by as much as 0.010 in. Therefore the tubes are placed in tension. This is most desirable for units operating above normal temperatures.

For units operating below normal temperatures, it is desirable to place the tube in compression. This may be accomplished by replacing the deep recess collar with a flush collar which will bear against the face of the tube during the expanding of the outflow end and restrict the outward flow of metal during expanding.

To alleviate longitudinal and radial stresses in the unit further, it is advisable to pattern-roll the outflow ends, starting with No. 1, as shown in Fig. 16.

Additional Tests

Tests also were conducted, by metallographic examination of the tube metal, at various degrees of expansion.

Fig. 17 shows a 70-30 cupro-nickel tube which has been expanded 0.009 in. on the diameter, after metal-to-metal contact, of the tube OD with the tube-hole wall. Note that the grain structure has become enlarged and distorted.

Fig. 18 is a metallographic section of the same cupro-nickel tube expanded 0.003 in., after metal-to-metal contact; the grain structure is uniform.

Hydrostatic and mechanical tests indicate that an expansion of 0.003 in., after metal-to-metal contact, of the cupro-nickel tube, was sufficient to give hydrostatic pressure of 600 lb and a mechanical strength joint in excess of 2000 lb in a reamed hole.

Fig. 19 shows a 3-S aluminum tube, $^3/_4$-in. OD 16-gage, annealed temper, which had been expanded into a $2^1/_2$-in. aluminum sheet of the same material. From the curve it will be noted that, with an expansion of 0.008 in., after metal-to-metal contact, the maximum mechanical strength joint was obtained. Expanding beyond this figure weakened the joint and, at an expansion of 0.012 in. on the diameter, after metal-to-metal contact, yielding of the ligament took place. Attempts to make the joint leak-tight, beyond this figure, were unsuccessful.

Table 3 shows hardness increase which may be expected at varying degrees of expansion.

TABLE 3 TUBE HARDNESS TEST—INTERIOR SURFACE BEFORE AND AFTER EXPANDING

Rockwell hardness tests, using 30-kg load and $^1/_{16}$-in. ball penetrator, were made on interior surface of tube sections in areas of various degrees of expansion and also on unexpanded tube section for comparison. These values were converted to Brinell hardness readings.

Tube size, in.	Amount of expansion, in.	Original tube hardness, Bhn	Expanded section, Bhn	Difference, Bhn
$^3/_4$-20 BWG C/N	1.4 amp-0.003	82	111	29
$^3/_4$-20 BWG C/N	1.5 amp-0.003	86	111	25
$^3/_4$-20 BWG C/N	1.6 amp-0.003	86	113	27
$^3/_4$-20 BWG C/N	1.7 amp-0.003	85	115	30
Average of 4 determinations				
20 BWG-0.035 in. wall thickness				
$^3/_8$-18 BWG C/N	1.5 amp-0.003	90	125	35
$^3/_8$-18 BWG C/N	... 0.012	93	145	52
Average of 4 determinations				
$^3/_4$-18 BWG Adm.	0.002	90	100	10
$^3/_4$-18 BWG Adm.	0.003	88	110	22
$^3/_4$-18 BWG Adm.	0.004	88	120	32
$^3/_4$-18 BWG Adm.	0.005	89	129	40
$^3/_4$-18 BWG Adm.	0.006	89	141	52
$^3/_4$-18 BWG Adm.	0.010	87	152	65
1-18 BWG Adm.	0.003	82	96	14
1-18 BWG Adm.	0.004	95	108	13
1-18 BWG Adm.	0.005	94	119	25
1-18 BWG Adm.	0.006	82	118	36
1-18 BWG Adm.	0.008	94	132	38

It is of prime importance to maintain cleanliness between the mating surfaces of the expanded joints. The surfaces should be free of grease, grit, oil, and the like. This is one of the primary causes of tube-joint failure and it cannot be overemphasized.

Expanding in Double-Sheet Exchangers

With the current trend toward double-sheet exchangers, it may be worth while to mention the following technique for expanding this type unit: In expanding the inner sheets, the rollers of the expander should be relieved at both ends. The effective roller length should be $^1/_4$ in. less than the sheet thickness with the expander collar adjusted, so that $^1/_8$ in. from either face of the tube sheet will not be expanded. This will make tube removal much easier and eliminate stress concentration at the sharp edges of the sheet face. Select the proper collar for the expander, depending upon whether the tube should be flared or whether the tube is to be held flush with the face of the sheet. Fig. 20 shows the proper sequence of expanding, beginning with No. 1. In expanding sheets Nos. 3 and 4, the deep recess collar should be utilized to reduce compressive loading of the tubes.

Fig. 17 Photomicrograph of Cupro-Nickel Tube Expanded 0.009 In. After Metal-to-Metal Contact

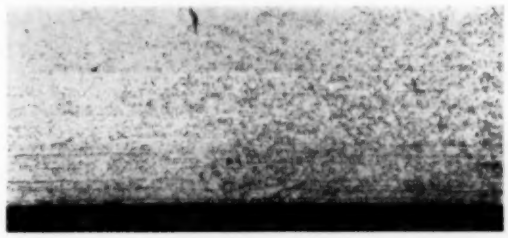

Fig. 18 Photomicrograph, From Same Piece of Tubing, as in Fig. 17, Expanded 0.003 In. After Metal-to-Metal Contact

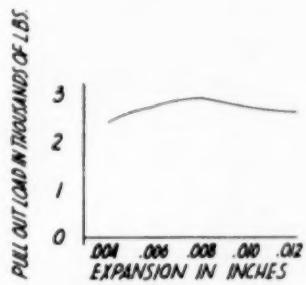

Fig. 19 Curve Showing Decrease in Mechanical Strength of Expanded Joint; 0.008-In. Expansion, After Metal-to-Metal Contact

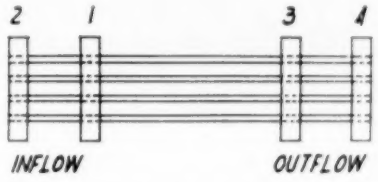

Fig. 20 Recommended Technique for Expanding Double-Sheet Exchangers, Starting With No. 1

The expanding of stainless steels has been of much concern in industry because of their cold-work phenomena. Stainless-steel tube ends which are to be expanded should be annealed fully. Hole clearance of the OD of the tube should be held to a minimum.

Lubrication for expanding the tubes should be of the water-soluble type. Considerable research has been made into the type of lubricants which are satisfactory and we find the water-soluble lubricant to have considerable merit over the petroleum or oil-base lubricant.

FIG. 23 MECHANICAL ASSEMBLY OF 2-IN. 11-GAGE COPPER TUBING OF DIESEL-ENGINE INJECTOR
(Courtesy of Baldwin-Lima-Hamilton Company, Essington, Pa.)

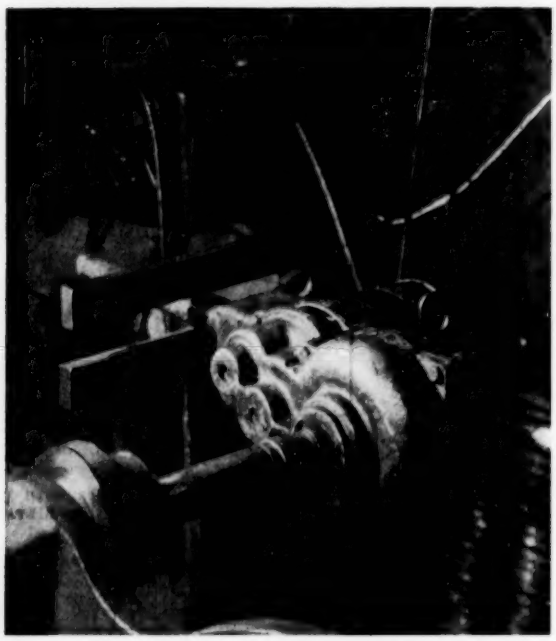

FIG. 21 MECHANICAL ASSEMBLY OF 4-IN-OD MECHANICAL TUBE HAVING 3/8-IN. WALL, EXPANDED INTO A 3 1/2-IN. JOINT TO ESTABLISH A 60,000-LB MECHANICAL JOINT; EXPANSION 0.031 IN. AFTER METAL-TO-METAL CONTACT
(Courtesy of the Budd Company, Philadelphia, Pa.)

EXPANDED JOINT FOR MECHANICAL ASSEMBLIES

Of interest to the engineering profession, in general, has been the development of applications of the expanded joint for mechanical assemblies. Fig. 21 shows the expanding of a 4-in-OD 3/8 in-wall mechanical tube which is being expanded into a joint 3 1/2 in. in length. This assembly is used to support the brake assembly of a self-propelled railway car.

The mechanical assembly, by expanding, of a bridge hand railing, Fig. 22, entails a 5-in-OD aluminum tubing as the top rail, a 3-in. aluminum channel as the base, and a 1 1/2-in-OD aluminum tube as the supporting upright. The expander was designed to expand both joints in one operation. The time required to expand both joints is 40 sec.

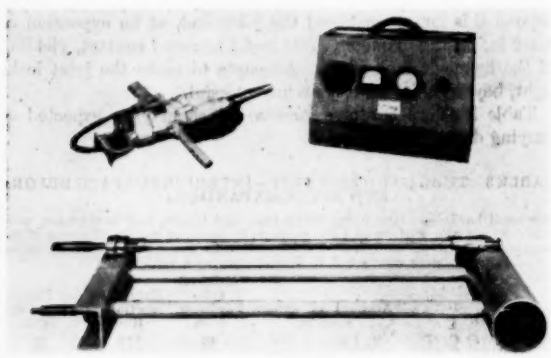

FIG. 22 MECHANICAL ASSEMBLY OF BRIDGE HAND RAILING
(Note expander design whereby both joints are expanded in one operation.)

Fig. 23 shows the mechanical assembly of a 2-in-OD 11-gage copper tube into the injector of a diesel engine.

The field of application for mechanical assemblies, by this process, is unlimited.

The electronic method of expanding tubes has found its place in industry, including the precision expanding of boiler tubes. Recently, a complete boiler was expanded by the electronic-control method. Preliminary reports of this test are most gratifying.

Discussion

R. M. ARMSTRONG.[6] What is the author's recommendation as to relative hardness of tube versus tube sheet for satisfactory rolling, and what maximum hardness of tube can be used and still give a satisfactory rolled joint?

E. L. FOWLER.[7] The author is to be congratulated on his informative discussion of a subject inadequately studied by the profession.

The author's reference to over-expanding and imposing excessive cold-work stresses in tubes and sheets, resulting in early failures, apparently encompasses the caution regarding stress-cracking.

Stress corrosion-cracking always involves some peculiar environment, the critical nature of which depends on the metal,

[6] Owner, Richard M. Armstrong Company, West Chester, Pa. Mem. ASME.

[7] Mechanical Engineer, The International Nickel Company, Inc., New York, N. Y. Mem. ASME.

such as ammonia with brasses and caustic soda with steels. Consequently, even though tubes may be stressed by the expanding operation, stress corrosion-cracking is not inevitable.

In the case of the high-nickel alloys, the number of critical environments is quite limited as is the need for special precautions in rolling operations in the absence of experience that has indicated the cracking potentialities of the corrosive medium involved, such as, handling nickel with fused caustic or monel with certain fluorine compounds.

Rolling-in tubing of nickel, monel, and inconel requires higher rolling pressures than lower strength materials. Considering the fact that often the tube-sheet material is of lower hardness than nickel, monel, and inconel tubing, there is always a possibility of over-rolling these tubes, with resulting flow of the metal in the tube-sheet ligament and thinning the wall of the tube at the rolled-in joint, than there is in the case of tubing having a lower hardness than the tube sheet. The high operating temperatures and pressures of present-day heat exchangers dictate exacting tight tube-to-tube sheet joints which cannot be produced consistently by guess-rolling technique. The fabrication of nickel, monel, and inconel heat-exchanger tubing by guess-rolling, on more than one occasion, has proved unsatisfactory and costly to fabricators. On the other hand, properly rolled, tight leakproof joints are attained by electronic-controlled rolling methods.

Comments of individuals pertaining to what constitutes the satisfactory clearance between the OD of the tube and the tube-sheet hole for the purpose of arriving at a yardstick for standardization might be in order. The writer feels the clearance should be held to the minimum in order to minimize the cold-working and subsequent wall-thinning of the tube into contact with the tube-sheet hole, as well as the resulting ridge at the tube-expander roller-nose termination.

Experience from rolling-in $^{5}/_{8}$-in-diam, 16-gage nickel tubing to a $^{3}/_{4}$-in-thick nickel tube sheet shows that after rolling the tube-to-metal contact with the tube-sheet hole, an additional rolling of 0.003 to 0.005 in. produces a tight leakproof mechanical joint of 2000 lb, withstanding hydrostatic test of 750 lb with failure of the gasket of the unit.

Care should be exercised not to drill bell-mouthed or oversized tube-sheet holes. Such hole conditions result from dog-tail motion of the drill, the drill ground off center, and drilling the tube sheets in packs.

The author's remarks regarding cleanliness of tube ends and tube-sheet holes are of particular importance with nickel and high-nickel alloy. Lubricants used for rolling should not contain sulphur or lead as those constituents will cause intergranular embrittlement to metals at elevated temperatures. Naturally, where the tube ends are to be welded, the use of such lubricants for rolling could not be tolerated.

With the higher temperatures and pressures that are used today in heat exchangers, the need for tubing of high strength is dictated; for example, on exchangers of hairpin tube design where the tubing is placed in tension by operating pressures. It is desirable to have the tubing of as light wall thickness as possible for heat-transfer qualities and still maintain mechanical strength; also with the use of tubing thinner than 18 gage, economies can be effected in the fabrication of the unit.

For the purpose of determining the suitability of tubing lighter than 18 gage, the writer's company looks forward to conducting tests of this possibility. When such information is available, it will, of course, be available to industry.

C. N. Overton.[8] Just what do we mean by electronic-control method for precision expanding of tubes? It is, in effect, the measure of the amount of torque required to roll a joint precisely and consistently after metal-to-metal contact.

With the introduction of new materials, higher pressures and temperatures, a control method for the rolling-in of tubes becomes more apparent.

Basically the need for such controls are numerous, such as the following:

1 Preventing over-rolling of tubes, thereby eliminating undue stresses, rupture, and cold-working of tubes.

2 Removing the human element from having to determine the amount of pressure or torque required by sound, feel, and so on.

3 To insure tight and stable joints consistently.

4 Saving in man-hours yearly both in shop and field service by eliminating rerolling, retesting, and down time from improper rolling.

The method of testing as outlined in this paper seems adequate and the joint pressures obtained are in line with our previous experiences. The writer believes a more realistic test for high-pressure, high-temperature heat-transfer apparatus would be the pull-out method. Jobs of this nature work under tension, especially the U-tube design. Inasmuch as these tests deal primarily with condenser work and that of low-pressure heat-transfer apparatus, 600 psi and under, we readily agree with the author that serrations and grooves, whichever the case may be, generally are not needed. However, design and operating conditions may dictate otherwise in certain cases.

We definitely feel that in the high-pressure high-temperature range grooves or serrations are a must both from a mechanical strength and leaktightness standpoint. It has been said that serrations or grooves do not add to leaktightness. This, it is believed, is in error as our experience has proved otherwise. The amount of serrations or grooves is questionable. We feel there is a limit to the number of serrations or grooves required in order to add the necessary holding and sealing power required and heartily agree with the author that variations do occur widely with different manufacturers. Careful thought should be given this item both from a cost and tube-removal standpoint.

Tube-expanding procedures vary within industry and are debatable items inasmuch as success in rolling-in of tubes may be achieved by the use of several methods. The pattern-rolling method has proved to be the most successful with the writer's company. This too can vary with different manufacturers.

The use of recessed collars is advantageous primarily from a cost standpoint. An additional man for holding or positioning tubes can be eliminated by their use. In rolling-in tubes, the tool used generally is the self-feeding-type expander. It should be so positioned that work is performed without the expander feeding in, that is, in a fixed position in relation to the depth of roll.

It has been our experience that tube walls having been reduced by rolling from 4 to 5 per cent produce favorable results where tube-hole preparation is consistent with that which is expected to be found in a commercially reamed hole. It is important to maintain clearances between mating surfaces of expanded joints. Also these surfaces should be free of grease, grit, oil, and the like. This is one of the primary causes of tube-joint failures and cannot be overemphasized.

By using the precision method of torque rolling-in of tubes, we eliminate the use of the so-called skilled operator. A short instruction period will qualify almost anyone for use of this type of apparatus. Much has been said with regard to holding pressure, leaktightness, and so on, in tube rolling. One very important point which it is felt has not been brought to light is, what tube-hole preparation is suitable for the rolling-in of the tube? By that is meant what finishes are required, how deep should we roll

[8] Westinghouse Electric Corporation, Essington, Pa.

a tube, number of grooves, serrations, and so on. There is an apparent need for standardization to cover this item pertaining to size, tubes, gages, tube-sheet thicknesses, and so on and we recommend that the heat transfer committee of the society give this considerable thought.

The use of precision method of torque rolling-in of tubes has opened up new fields and methods of manufacturing mechanical assemblies. A recent experience of the writer's was to roll an 8-in. commercially finished pipe into a flange of $1^{1}/_{8}$-in. thickness. This pipe has a wall thickness of $^{5}/_{16}$ in. and in rolling into the end flange the wall thickness was reduced by 4 per cent. After rolling, a hydrostatic test was placed on this job and tested to six times its normal designed working pressure. We made the necessary attachments and placed it on an Olsen testing machine to determine the amount of pull-out pressure required for breaking the joint. The results were very gratifying. We are not saying that this can be done on any or all jobs but we feel that on low-pressure work considerably larger barrels or shells may be rolled into flanges, and the like, and of sufficient strength to withstand design and operating conditions.

Author's Closure

The author wishes to express his sincere appreciation for the instructive discussions presented on the subject and to those who submitted many questions of interest to the industry at large.

In answer to Mr. Armstrong, considering the hardness increase of the tube material which invariably takes place during expanding or cold working, in the author's opinion, the tube sheet should be slightly harder than the tube, so that, after expanding, the sheet and expanded section would fall somewhere near the same hardness.

Experience indicates that cupro-nickel having a hardness of 80–88 Brinell; Admiralty with a hardness of 85–90 Brinell; nickel with a hardness of 78–110 Brinell; copper, $^{1}/_{4}$ hard; and, aluminum, $^{1}/_{4}$ hard, present no particular problem to expand. The ferrous metals with a Brinell hardness of 135–137, as well as stainless steel, in the same range, would also present no problem as long as the stainless steels are not unduly over-expanded.

Tubes having a hardness of 100 Rockwell "B" may be expanded; however, there is considerable danger of cracking or splitting the tube. Also, the possibility of upsetting the ligament while endeavoring to establish a leak-tight joint, not to mention a very high mortality rate of the expanding tools.

Mr. Fowler has commented on hole clearance standardization and Mr. Overton comments on hole preparation including standards for the use of serrations. The author concurs and hopes that the Society will follow through these suggestions with standards for the industry.

Application of Quality-Control Requirements in Manufacture of Components for a Coaxial-Carrier System

By A. T. CHAPMAN,[1] KEARNY, N. J.

Economic solution of transmission problems in a new coaxial-carrier system required limitation of excursions of sensitive characteristics from the design center. Basic quality-control techniques were utilized in developing a pattern of distribution requirements for the key characteristics of the critical electronic components. A description of the statistical techniques is presented with several illustrative factory applications.

Introduction

BASIC quality-control requirements have been used for electronic components in a new coaxial carrier system.[2,3] The aim of these requirements is to place a continuing limitation on the pattern and the spread of measured values around their average and to impose close limits on departures of the average from a desired nominal value. When this aim is attained, comparatively wide limits for the individual components are acceptable. Furthermore, the components may be selected on a random basis for the assembly and for subsequent maintenance of complex equipment.

The requirements are applied to one characteristic of any component. The characteristic selected for control necessarily is the most sensitive and, therefore, critical parameter in evaluating performance.

The New Coaxial System. A new long-distance carrier system, utilizing coaxial cables and providing in each direction either 1860 telephone channels or 600 telephone channels and a 4.2 megacycle broadcast television channel, has been designed by the Bell Telephone Laboratories. In a complete coast-to-coast system of 4000 miles, 1000 line and 200 office amplifiers are required. The amplification, equalization, and regulation equipment, and the associated components, are currently being manufactured by the author's company for a commercial installation from New York to Chicago. The New York to Philadelphia link has been in operation since early in 1953.

Reason for Applying Quality-Control Requirements. Before commercial manufacture of the new coaxial system could start it was apparent that (1) new and improved apparatus and equipment designs were required, and (2) more precise manufacturing machines, tools, processes, and techniques had to be developed. A review of the current status of the design and manufacturing art for electronic components for communications equipment showed that the best elements available would not be capable of achieving the design intent.

For example, amplifier equalization is based on the assumptions that the gain of the average line amplifier will match the loss of the preceding line section to within 0.15 decibel (db), and that the average amplifier gain will not vary from one lot of amplifiers to another by more than about 0.06 db. With the most precise components that can be made at present, it is possible that the gains of individual amplifiers would vary by about ±0.6 db Therefore, statistical quality control applied to the critical end-point characteristics of the components was introduced as the means by which the average gain of a group of amplifiers could be controlled economically to a greater precision than the individual amplifier.

Extent of Application. Quality-control requirements are being applied presently to 90 components used in the amplifiers and transmission networks of the new system. Not all components are subject to distribution requirements; for example, there are over 100 component elements in the amplifier of which about 40 have sensitivities which are sufficiently large to require application of quality-control requirements.

In addition, inspection records are being maintained for 60 characteristics of the completed line and office amplifiers with a view of establishing final design tolerances and as an aid in indicating manufacturing difficulties.

Basic Statistical Technique

Fundamental Concepts. The design engineer is accustomed to apply conventional quality-control techniques in order to specify tolerances consistent with design intent and manufacturing capabilities. Usually, data are obtained from tests on preproduction models or from a limited quantity of regular production. The manufacturing engineer uses statistical techniques for determining the process capabilities and for detecting assignable causes for significant manufacturing variations. In such cases, the application of these techniques is at the option of the manufacturing engineer; as the facilities and skills are improved, the number of control charts may be reduced.

In general, there is a reasonable margin between the ±3-sigma variation around the nominal value and the specification limits. Fig. 1[3] shows the customary limits as 1-1. The limits provide sufficient allowance for the process average to vary a reasonable amount around the nominal, a provision which permits the use of sampling and prevents frequent shutdown in production. When the specification limits are tightened to the 2-2 limits, small expected variations in the average will throw a percentage of the product out of limits and usually necessitate 100 per cent inspection. Further tightening of limits to 3-3 without concurrent improvement in manufacture techniques necessarily will require continuing 100 per cent inspection and will result in product shrinkage.

---

[1] Engineer, Inspection Development, Western Electric Company.

[2] "Quality Control Requirements," by H. F. Dodge, B. J. Kinsburg, and M. K. Kruger, *The Bell System Technical Journal*, July, 1953, pp. 943–967.

[3] "Application of Quality Control Requirements," by R. F. Garrett, T. L. Tufnell, and R. A. Waddell, *The Bell System Technical Journal*, July, 1953, pp. 969–1005.

Contributed by the Production Engineering Division and presented at a joint session with the Management Division at the Annual Meeting, New York, N. Y., November 29–December 4, 1953, of The American Society of Mechanical Engineers.

Note: Statements and opinions advanced in papers are to be understood as individual expressions of their authors and not those of the Society. Manuscript received at ASME Headquarters, November 27, 1953. This paper was not preprinted.

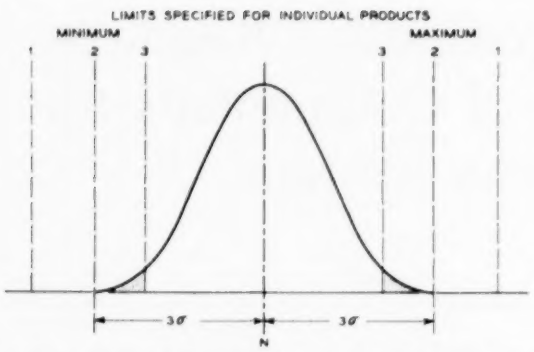

FIG. 1 RELATIONSHIP BETWEEN FREQUENCY DISTRIBUTION OF INDIVIDUAL UNITS AND VARIOUS SPECIFIED LIMITS

Distribution Requirements. Since the quality-control requirements were to become an integral part of the product specification, it was recognized that limits in terms of the usual ±3-sigma variation around the nominal would have to be increased to include a reasonable allowance for the process average to vary. A value of $\pm 1/3$-sigma was chosen for this variation as a balance between the end-use requirements of the product and manufacturing practicability. The over-all limits for individual units then become $N \pm 3\,1/3$-sigma. If the distance from the nominal to either limit is designated A, then the permissible variation in the process average becomes $\pm 0.1A$ ($\pm 1/3\sigma$) and the maximum standard deviation becomes $0.3A$. Fig. 2[2] illustrates the basis of the specified limits.

Accordingly, the product specification prescribes for each key characteristic a nominal value N, maximum and minimum limits for individual units, $N \pm A$, and adds the clause "subject to the distribution requirements." This supplementary specification primarily covers three inspection procedures for controlling component quality: (1) Control-chart method; (2) batch method; (3) three-cell method.

The control-chart or batch methods are used when the distribution of individual units maintains (*a*) an average within the band $N \pm 0.1A$, and (*b*) a standard deviation not greater than $0.3A$. The three-cell method assures conformity to requirements by packaging selected groups of five units chosen to meet a particular distribution pattern.

Control-Chart Method. The control-chart method is applied where production comprises a reasonably steady succession of individual units or small groups of units from a common source. This method requires maintenance of control charts for averages and ranges of samples of 5 units.

Fig. 3[2] shows the two acceptable distributions of individuals with their corresponding distribution of averages for samples of 5 units. The limits for process averages are $N \pm 0.1A$ (PA limits), and for individual averages, $N \pm 0.5A$ ($A5$ limits).[4] The limit for ranges is the customary upper 3-sigma control limit, which for samples of 5 becomes $1.48A$, maximum ($R5$ limits).[4]

A basis for establishing eligibility and a somewhat more lenient basis for maintaining eligibility are a necessary part of the control-chart method. The criteria for establishing eligibility for application of this method are (*a*) all averages and ranges for seven consecutive samples of 5 units meet the $A5$ and $R5$ limits, and (*b*) seven consecutive samples are not all outside the same process average limit (i.e., not all above the upper PA limit or all below the lower PA limit). Eligibility is maintained provided (*a*) seven consecutive averages (current sample and six preceding samples) do not all fall outside the same PA limit, and (*b*) the average either (1) meets the $A5$ limits; or (2) fails to meet the $A5$ limits but at the same time all of the six preceding consecutive averages meet the $A5$ limit, and (*c*) the range either (1) meets the $R5$ limit; or (2) fails to meet the $R5$ limit but at the same time all of the six preceding consecutive ranges meet the $R5$ limit and (*d*) no major change is made which may affect the product quality significantly.

Batch Method. Occasionally, the nature or economics of the

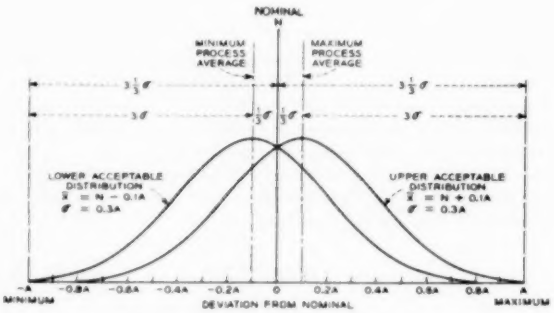

FIG. 2 BASIS OF SPECIFIED LIMITS

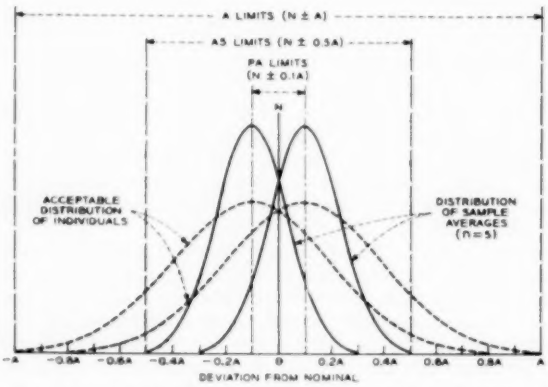
A LIMITS (N ± A)
A5 LIMITS (N ± 0.5A)
PA LIMITS (N ± 0.1A)
N
ACCEPTABLE DISTRIBUTION OF INDIVIDUALS
DISTRIBUTION OF SAMPLE AVERAGES (n = 5)
−A −0.8A −0.6A −0.4A −0.2A 0 0.2A 0.4A 0.6A 0.8A A
DEVIATION FROM NOMINAL

FIG. 3 BASIS OF *A5* LIMITS AND *PA* LIMITS FOR SAMPLE AVERAGES

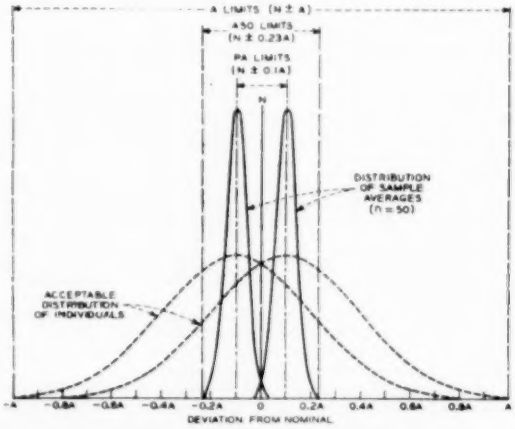
A LIMITS (N ± A)
A50 LIMITS (N ± 0.23A)
PA LIMITS (N ± 0.1A)
N
DISTRIBUTION OF SAMPLE AVERAGES (n = 50)
ACCEPTABLE DISTRIBUTION OF INDIVIDUALS
−A −0.8A −0.6A −0.4A −0.2A 0 0.2A 0.4A 0.6A 0.8A A
DEVIATION FROM NOMINAL

FIG. 4 BASIS OF *A50* LIMITS FOR SAMPLE AVERAGES

[4] Footnote 2, p. 954.

manufacturing process is such that relatively large batches are produced intermittently. The order of production is successive batches and the time sequence for individual units or small groups of units has no significance.

For the batch method, a sample normally of 50 units is selected at random from each batch. A batch is acceptable if the sample average and sample standard deviation fall within certain established limits. The limits for the average are $N \pm 0.23A$, shown in Fig. 4[3] as the $A50$ limits.[5]

To simplify calculation of the standard deviation, the values of the 50 units are divided randomly into 10 subgroups of 5 and the average range $\bar{R}$ is computed. The observed standard deviation, $S50 = 0.43\bar{R}$, is a statistic which is compared with the upper 3-sigma limit of the sampling distribution of $\bar{R}$ (for 10 samples of 5); namely, $S50$ limit $= 0.41A$ max.[5]

The batch is acceptable provided (*a*) the average meets the $A50$ limit, and (*b*) the standard deviation either meets the $S50$ limit, or fails to meet the $S50$ limit but at the same time all of the six preceding standard deviations meet the $S50$ limit.

Three-Cell Method. Under the three-cell method each unit of product is measured for the characteristic in question and conforming units are sorted into three cells: lower, middle, and upper, as shown in Fig. 5.[3] Either of the two distributions, 1-3-1 or 0-5-0, shown at the top of the figure, is acceptable for packaging units in groups of five prior to shipment.

The objective is to assure product shipment and at an outgoing quality equal to or slightly better than that provided by the control or batch method. The three-cell method permits

[5] Footnote 2, p. 957.

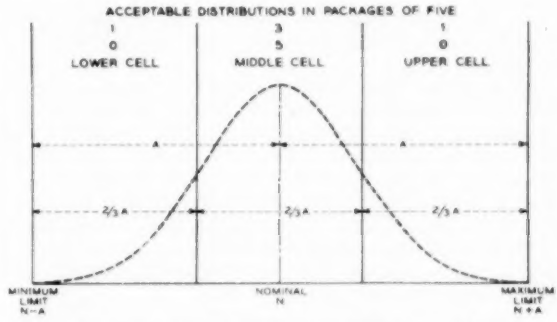

FIG. 5 ACCEPTABLE DISTRIBUTIONS—THREE-CELL METHOD

partial shipment when the product fails to meet the criteria for the control chart or batch methods or when production schedules or manufacturing difficulties prohibit the use of these methods.

Units in any cell which are in excess supply may be held in inventory, and subsequently packaged and shipped, as the process average shifts and units in the counterbalancing cell are produced.

APPLICATION OF QUALITY-CONTROL REQUIREMENTS

Selection of Method. The selection of the particular method depends on production levels, state of the design and manufacturing art, and the design tolerances. Since the control-chart and batch methods permit sampling inspection they are generally less expensive to apply than the three-cell method which re-

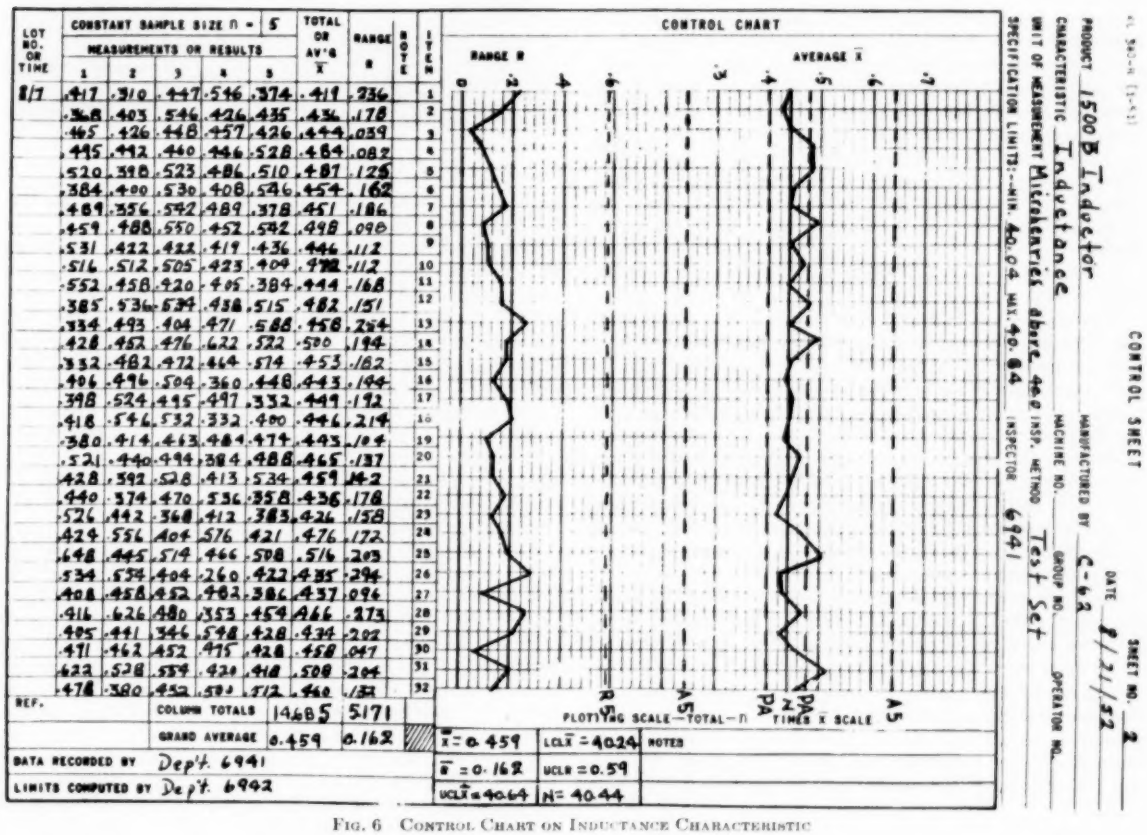

FIG. 6 CONTROL CHART ON INDUCTANCE CHARACTERISTIC

quires 100 per cent inspection. However, the three-cell method must be employed when the criteria of the first two methods are not met.

As mentioned before, distribution requirements are applied to the key characteristics. The key characteristic for precision components in electronic equipments is usually a severe electrical test requirement which is governed frequently by precise mechanical tolerances. For example, in the manufacture of inductors, a variation of ±0.0003 in. in wire diameter varies the inductance characteristic by ±0.15 per cent, a variation of ±0.0005 in. in core diameter varies the inductance by ±0.5 per cent, and a variation of ±0.001 in. in winding length varies the inductance by ±0.13 per cent.[6]

Ordinarily, to achieve maximum conformity with test requirements, there is a continuous flow of small groups of units carefully made in sequence rather than sequential batch lots, which occur more frequently in metal-finishing and chemical processes. Therefore, the control-chart method is used in the immediate application more extensively than the batch method.

Even to the present time, the new coaxial system continues to present design and manufacturing challenges. The manufacturing capabilities of the machines, tools, and processes are taxed to the utmost. In many cases characteristic limits could not be established until a reasonable quantity of production had been completed and the data analyzed; in certain cases, repeated changes in limits were brought about by the unusually tight mechanical and electrical requirements. Consequently, process average fluctuations in excess of $\pm^1/_3$ sigma were encountered frequently and shipment of product was achieved only through application of the three-cell method.

Through continuing engineering improvements and operator training, the various electrical components have been transferred gradually to the control-chart method to the point where today the key characteristics are controlled about one third by the control-chart and two thirds by the three-cell method. It probably will take several years for the state of the manufacturing art and changes in design to improve to the point where most components are controlled by the control-chart method. Without the three-cell method, it is likely that only a small part of the existing new coaxial-carrier system would be in service today.

Actual shop results in applying the control-chart, the three-cell, and the batch methods follow.

Single Layer-Type Inductor. One type of inductor used in the coaxial system is a small single layer-type coil with a circuit function of separating or splitting the winding capacitance from the input capacitance of the amplifier vacuum tube. The circuit requirements permit an estimated variation in inductance from the design center of approximately ±0.25 per cent, which includes manufacturing variations, aging and temperature effects. Since the 0.25 per cent tolerance is commercially impracticable, application of control-chart techniques, coupled with development of manufacturing methods and sources of uniform raw materials, permitted widening the A limit to ±1 per cent subject to the distribution requirements.[6]

Fig. 6 illustrates typical production results plotted on a control chart. During this period no point fell outside of the limits for averages and ranges, and the criteria for conformance to the distribution specification were maintained.

As a second example the inductor, Fig. 7, used in the input feedback network, combines resistance and inductance in a single product. The inductors are wound with resistance wire on close-dimensioned, low temperature-coefficient core tubes. To control the inductance, the number of turns and pitch are determined for each spool of resistance wire and the winding machine is adjusted accordingly.

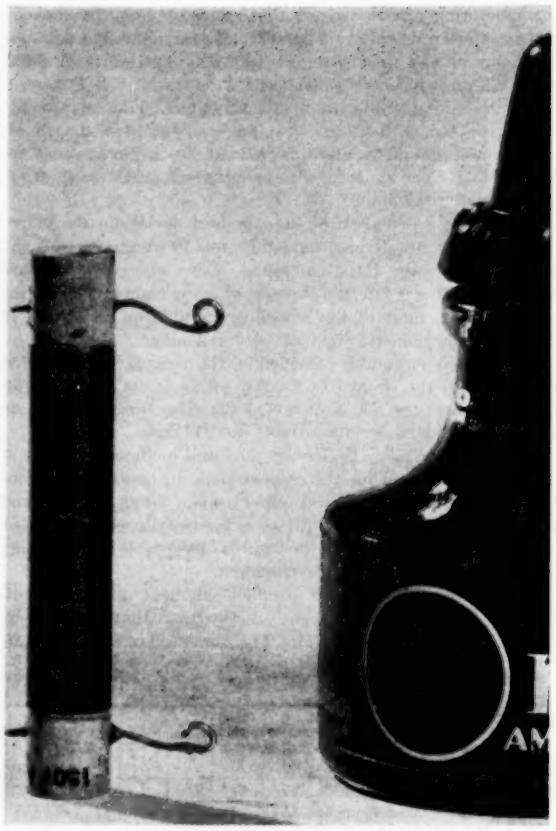

FIG. 7 INDUCTOR

The control chart, Fig. 8, shows that in general, the resistance characteristic maintains eligibility for application of the control-chart method. At sample No. 17 eligibility was lost because two successive averages exceeded the $N \pm 0.54$ limit. Eligibility was restored at sample No. 24 because seven consecutive groups of 5 units fell within limits. During the period of re-establishing eligibility the product was shipped by the three-cell method. Likewise, sample No. 39 shows loss of eligibility because of the process average of seven consecutive groups falling outside of the same PA limit. Subsequent regain of eligibility occurs at sample No. 46. A similar case where the range exceeded its criteria temporarily is shown by the loss and regain of eligibility occurring at samples Nos. 57 and 64, respectively.

Fused Quartz-Disk Capacitors. The quartz-disk capacitor, Fig. 9, is made by applying silver coating to small fused-quartz disks that have been lapped to the desired thickness. Final capacitance adjustment is made by mechanical removal of small areas of the silver coating. Design requirements were approximately $N \pm 0.025$ mmf which introduced acute measurement problems at the desired values near 10 mmf. By application of the distribution specification, it was possible to set the tolerance at ±0.1 mmf; accordingly, the product is divided into 3 cells of 0.067 mmf each. Reference standards are used to attain the desired precision.

Table 1 illustrates the results from the production of four codes of quartz capacitors differing only in capacitance value.

[6] Footnote 3, p. 982.

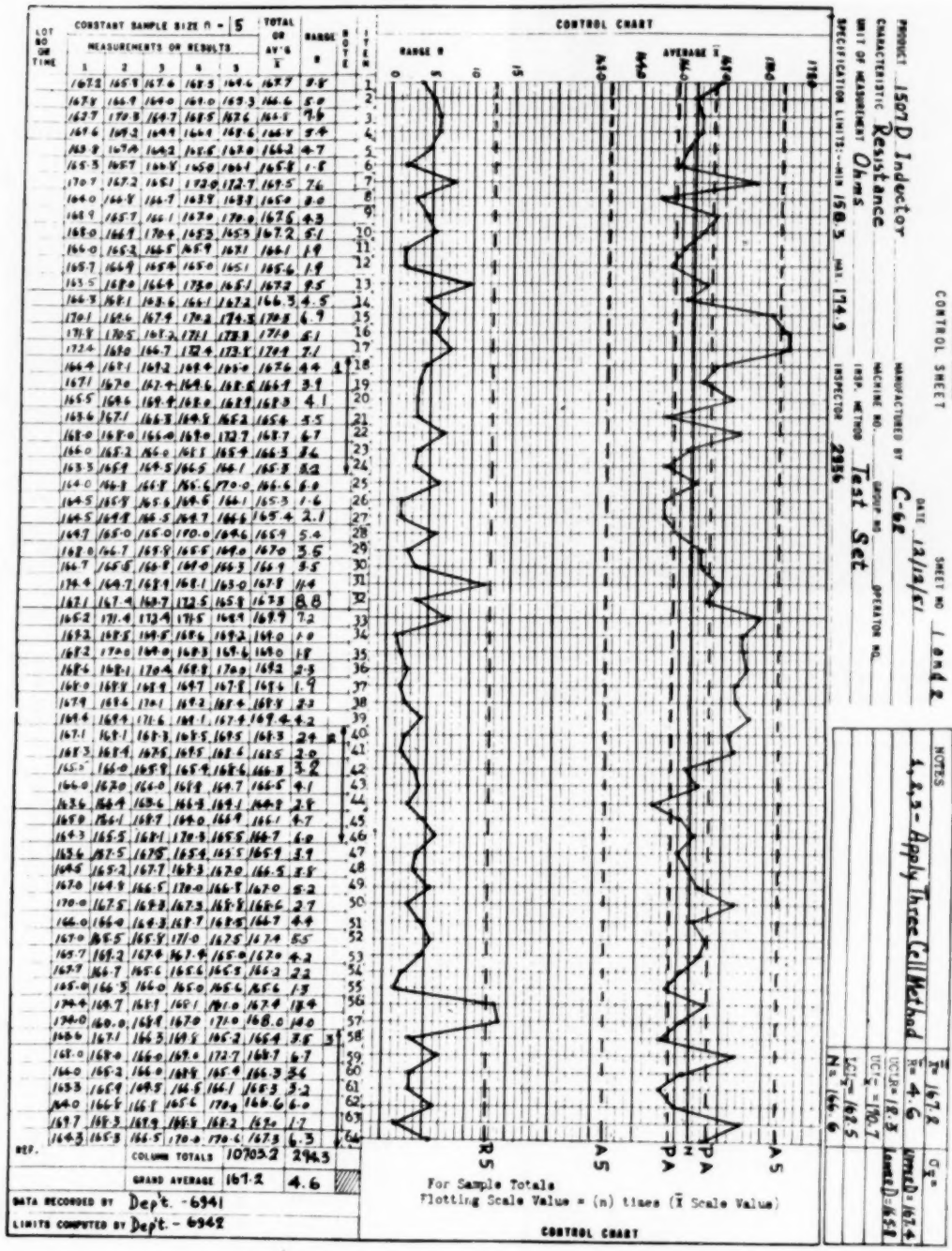

FIG. 8 CONTROL CHART ON RESISTANCE CHARACTERISTIC

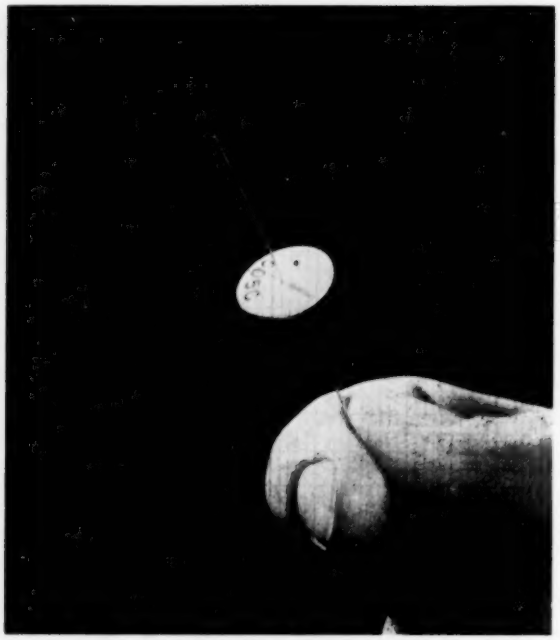

FIG. 9 QUARTZ-DISK CAPACITOR

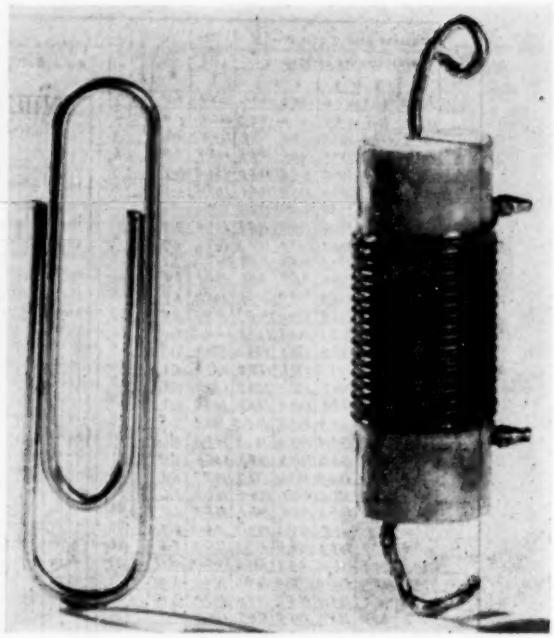

FIG. 10 RETARD COIL

CONTROL SHEET

PRODUCT 320P Retardation Coil MANUFACTURED BY 6926 DATE 1/14/53 SHEET NO. 2

CHARACTERISTIC Inductance MACHINE NO. GROUP NO. OPERATOR NO.

UNIT OF MEASUREMENT Microhenries INSP. METHOD Test Set

SPECIFICATION LIMITS:—MIN. 0.865 MAX 0.885 INSPECTOR

CONTROL CHART

Standard Dev. .004 .003 .002 .001 0

AVERAGE X̄ .870 .872 .874 .876 .878

PLOTTING SCALE—TOP—n TIMES SCALE

LOT NO. OR TIME	CONSTANT SAMPLE SIZE n = 50 MEASUREMENTS OR RESULTS 1	2	3	4	5	TOTAL OR AV'S X̄	RANGE R	NOTE	ITEM
1/17						.8721	.0028		1
						.8732	.0019		2
1/20						.8752	.0024		3
						.8740	.0022		4
1/21						.8720	.0027		5
1/30						.8724	.0017		6
						.8727	.0023		7
2/5						.8745	.0027		8
2/4						.8747	.0035		9
						.8754	.0028		10
4/10						.8746	.0022		11
4/16						.8732	.0024		12
4/20						.8726	.0030		13
4/24						.8739	.0012		14
5/1						.8735	.0021		15
5/4						.8750	.0026		16
5/6						.8746	.0025		17
5/12						.8744	.0019		18
5/14						.8753	.0015		19
5/18						.8738	.0022		20
5/19						.8760	.0024		21
5/22						.8734	.0018		22
5/25						.8733	.0024		23
						.8738	.0026		24
5/26						.8723	.0021		25
6/4						.8740	.0023		26
6/8						.8742	.0019		27
6/9						.8733	.0023		28
6/19						.8735	.0020		29
6/24						.8717	.0035	1	30
7/3						.8736	.0019	2	31
7/28						.8734	.0024		32
REF.									
				COLUMN TOTALS		27.9602	.0726		
				GRAND AVERAGE		.8738	.0023		

$\bar{\bar{X}}$ = .8738 LCL$_{\bar{X}}$ = .8719 NOTES 1-Lost eligibility for Batch

$\bar{R}$ UCL$_R$ method

UCL$_{\bar{X}}$ = .8761 UCL$_R$ = .0087 2-Eligibility reestablished

DATA RECORDED BY

LIMITS COMPUTED BY K. F. Wolf - 6942

FIG. 11 BATCH-CONTROL CHART

TABLE 1 FUSED QUARTZ-DISK CAPACITORS—PRODUCTION RESULTS

Codes	—Three-cell distribution— Lower cell	Middle cell	Upper cell	Total within *A*-limits	Out of *A*-limits	Production total
A	93	565	148	806	15	821
B	12	341	48	401	..	401
C	16	539	25	580	1	581
D	0	225	1	226	..	226
	121	1670	222	2013	16	2029

From a total of 2029 units produced, 1910 units or 94.1 per cent have been shipped, 103 or 5.1 per cent good units remain in inventory, and 16 or 0.8 per cent fell out of limits. The three-cell method is the most economical in this case, since production is intermittent and in small lots.

Retardation Coil. As mentioned previously, application of the batch method for controlling key electrical characteristics is limited because of the nature of the process and insufficient volume of production. However, as an illustration, the retardation coil, Fig. 10, used in the transmission equalizers is controlled by the batch method.

This retardation coil is wound at a rate of approximately 300 per 8-hr shift, a quantity which is treated as a batch. Considerable machine setup and operator skill is required; consequently, the production is discontinuous since the winding-machine setup and the operators are changed for other jobs between each batch.

The batch-control chart, Fig. 11, for the inductance characteristic covers the production of 12,500 retardation coils in batches varying from 100–700 units each. At one point, batch sample No. 30, eligibility was lost and it was necessary temporarily to ship the product under the three-cell criteria.

Conclusion

Inclusion of quality-control requirements as part of an electronic-component specification assures that any selected characteristic will be held within the desired distribution about the design center. The maintenance effort of collecting and computing the required statistical data is offset in large measure by (*a*) establishing compatibility between design tolerances and manufacturing process capabilities and (*b*) prompt determination and correction of assignable causes of variation.

The distribution requirements specification, as an integral part of the product specification, is just as much a tool to achieve the desired results as any of the more familiar manufacturing facilities. It is probable that the design of this tool will be refined with time. As soon as better components are designed and manufactured, new and better communications systems will be made at precisions one hesitates to contemplate today.

Production experience has not yet reached and probably will never quite reach the Utopian point where coaxial-line amplifiers automatically meet their end-point requirements when properly assembled from components controlled by the distribution requirements. However, substantial strides in this direction have been achieved, because the quality-control requirements have been developed and applied.

Acknowledgment

The author acknowledges the assistance of Mr. S. Panagakos of the inspection development department in the preparation of the control chart and tabular data and in the critical review of the manuscript. Material was drawn freely from the two referenced articles which had been reviewed by the author prior to their publication.

On the Theory of Regenerative Chatter in Precision-Grinding Operations

By R. S. HAHN,[1] WORCESTER, MASS.

The phenomenon of regenerative chatter is discussed. An analysis is made, based on the proportionality of the instantaneous wheel depth of cut to the instantaneous dynamic force existing between wheel and work, which yields two stability criteria from the Nyquist diagram. The grinding system will be unconditionally stable if one stability criterion is satisfied. If this criterion is not satisfied a second criterion may yet be satisfied by proper adjustment of the cycles of vibration per revolution of the workpiece. A qualitative check on the theory is given.

Nomenclature

The following nomenclature is used in the paper:

λ = wave length of chatter on workpiece
V = surface speed of workpiece
f = frequency
m = effective mass of vibrating system
c = effective damping in vibrating system
k = spring constant at wheel
$\tau \equiv \frac{1}{\eta}$ = time lag or period of work revolution
D = "grinding-rate factor," which is the radial component of wheel force required to produce a radial advance of one unit, of the wheel into the work, during a work revolution. It has the same dimensions as a spring constant (lb/in.)
v = feed rate of wheel carrier
$K \equiv k + D$ = "in contact" spring rate
$F(p) \equiv L\{y(t)\}$ = Laplace transform of $y(t)$
q = damped natural frequency
$\Omega \equiv \sqrt{\frac{K}{m}} \equiv 2\pi f$
$A \equiv D/K$
$\gamma \equiv f/\eta$ cycles of vibration per revolution of work (cpr)
η = work speed
n = an integer

Introduction

In precision-grinding operations a build-up of vibration during the grinding process frequently occurs. When precision parts are being ground, such as ball-bearing raceways and the like, any vibration of the grinding wheel relative to the workpiece is detrimental and interferes with the precision requirements of the part. Furthermore, these vibrations reduce the maximum permissible grinding rate and accordingly the rate of production.

It should be understood that all chatter marks found on workpieces do not necessarily come under the category of "regenerative chatter." In many instances sporadic chatter marks may be found which, often, are the result of vibrations produced by shocks or by forced vibrations originating in some associated equipment. On the other hand, vibration often occurs, which persists and spontaneously grows in amplitude and whose frequency is associated with some "natural frequency" of the machine. This self-excited type of vibration will be referred to as regenerative chatter. Since the frequency of vibration can be found readily from the relation

$$\lambda = \frac{V}{f}$$

as explained elsewhere (1),[2] it is relatively easy to determine the frequency of chatter from an examination of the workpiece and a knowledge of the work speed.

In the following analysis the internal-grinding process will be uppermost in mind, where the rigidity at the grinding wheel is, usually of necessity, considerably less than that in external grinding. However, the analysis applies equally well to external grinding.

Dynamics of Grinding Process

Fig. 1 shows a grinding wheel engaged with a workpiece. Suppose that at some moment during the grinding process, the

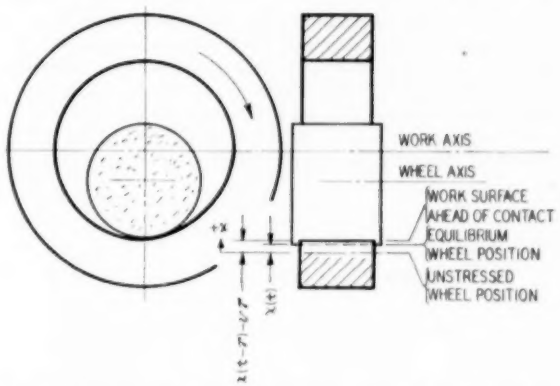

Fig. 1 Illustration Showing Instantaneous Wheel Depth of Cut

wheel be suddenly disturbed in a radial direction by a small amount, which in practice probably often occurs. The wheel on its nonrigid spindle would then execute some sort of transient vibration which presumably would die out. Fig. 2 shows the result of such a disturbance greatly exaggerated. The surface of the bore has a small "wave train" in some region as shown due to the vibratory disturbance. Fig. 2 is drawn for a time slightly later than the instant when the disturbance took place but in which a full work revolution has not yet occurred. As the work continues to rotate the wheel will engage the wave train, which

[1] Consulting Engineer, The Heald Machine Company. Mem. ASME.

Contributed by the Research Committee on Metal Processing and presented at the Annual Meeting, New York, N. Y., November 29–December 4, 1953, of The American Society of Mechanical Engineers.

Note: Statements and opinions advanced in papers are to be understood as individual expressions of their authors and not those of the Society. Manuscript received at ASME Headquarters, August 25, 1953. Paper No. 53—A-159.

[2] Numbers in parentheses refer to Bibliography at end of paper.

now will produce fluctuating forces on the wheel. Consequently, the wheel will again vibrate and will again generate another wave train. The question as to whether the wave train eventually will be ground out of the bore or whether it will grow on each successive work revolution until it more or less extends around the circumference is the objective of this paper.

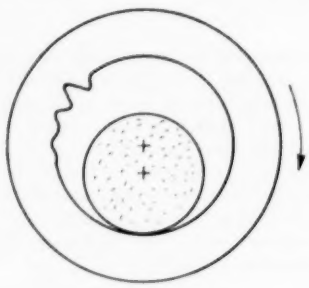

FIG. 2 ILLUSTRATION SHOWING UNDULATING GROUND SURFACE DUE TO A SMALL DISTURBANCE AND IMPLYING FEEDBACK OF ENERGY DURING NEXT REVOLUTION

It will be seen that the instantaneous forces acting on the wheel not only depend upon the present state of motion of the wheel but also on the motion of the wheel at an earlier time, i.e., one revolution preceding.

If the co-ordinate axis be taken at the unstressed wheel position shown in Fig. 1, and if we postulate—"The instantaneous depth of cut of the wheel into the work is proportional to the instantaneous normal force existing at the wheel-work contact"—the following differential equation is obtained, where the symbols are defined in the nomenclature

$$m\ddot{x}(t) + c\dot{x}(t) + kx(t) = D[x(t-\tau) - x(t) - v\tau] \quad [1]$$

where $x(t)$ is the displacement of the wheel at any time t, $x(t-\tau)$ is the displacement of the wheel which occurred one work revolution previously and now (at time t) behaves as an undulatory work surface which "forces" the wheel to vibrate. This type of phenomenon has been referred to as a retarded action (2).

If the term $x(t-\tau)$ be expanded in a Taylor series as suggested by Minorsky (2), and the following substitution be made

$$x = x_0 e^{zt} - \frac{Dv\tau}{k}$$

there results

$$m\ddot{y} + c\dot{y} + Ky - De^{-z\tau}\, y = 0 \quad [2]$$

where

$$y = x + \frac{Dv\tau}{k} \quad \text{and} \quad K = k + D$$

This equation is similar to those studied by Minorsky (2) and Ansoff (3) in connection with the stability of servomechanisms, differing only in the sign of the last term.

Following Ansoff we form the Laplace transform of Equation [2] obtaining

$$F(p) = \frac{my_0 p + cy_0 + m\dot{y}_0}{mp^2 + cp + K - De^{-p\tau}} \quad [3]$$

where $F(p)$ is the transform of $y(t)$.

Rewriting gives

$$F(p) = \frac{L(p)}{Y(p)} \cdot \frac{1}{1 - \dfrac{De^{-p\tau}}{mp^2 + cp + K}} \quad [4]$$

where

$$L(p) \equiv my_0 p + cy_0 + m\dot{y}_0$$
$$Y(p) \equiv mp^2 + cp + K$$

Then by the complex inversion integral and the theory of residues (4, 5, 6, 7)

$$y(t) = \frac{1}{2\pi i} \int_\Gamma \frac{L(p)}{Y(p)} \cdot \frac{1}{1 - \dfrac{De^{-p\tau}}{mp^2 + cp + K}}\, e^{pt}\, dt \quad [5]$$

where Γ is a contour enclosing all of the roots of the denominator in the p-plane. If the integrand has poles or the denominator is zero in the positive real half of the p-plane, solutions will be obtained containing an exponential factor with positive exponent and the motion will thus increase indefinitely.

Ansoff (3) shows that $Y(p)$ has no poles in the right-hand side of the p-plane and that we need only investigate

$$1 - \frac{De^{-p\tau}}{mp^2 + cp + K} \equiv 1 - q(p) \equiv w(p) \quad [6]$$

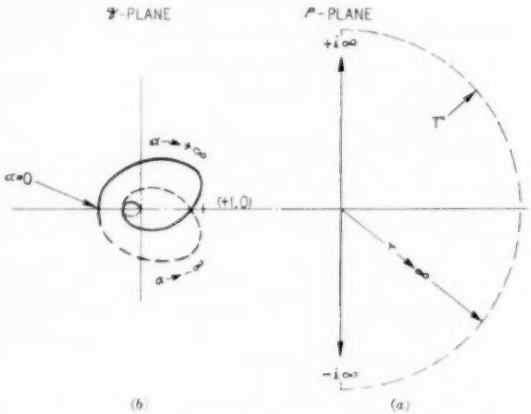

FIG. 3(a) CONTOUR OF INTEGRATION Γ IN p-PLANE

FIG. 3(b) TYPICAL NYQUIST CONTOUR IN q-PLANE CORRESPONDING TO Γ IN p-PLANE

Choosing the contour Γ shown in Fig. 3(a) it may be shown that $q(p) \to 0$ as $r \to \infty$ and that the only contribution to the Integral [5] occurs along the imaginary axis for $p = i\alpha$. It has also been shown that as p traverses the closed contour Γ in the p-plane, a corresponding closed contour is traced out in the w-plane and further the number of zeros enclosed in the p-plane is equal to the number of times the contour in the w-plane encircles the origin, or in the q-plane, the number of times the point $(+1, 0)$ is encircled.

Setting $p = i\alpha$ and dividing by K gives

$$q(i\alpha) = \frac{Ae^{-i\alpha\tau}}{(1 - a\alpha^2) + ib\alpha}$$

where

$$A \equiv \frac{D}{K}, \quad a \equiv \frac{m}{K}, \quad b \equiv \frac{c}{K}$$

Simplifying gives

$$q(i\alpha) = \frac{Ae^{-i(\alpha\tau + \varphi)}}{\sqrt{(1 - a\alpha^2)^2 + (b\alpha)^2}} \quad [7]$$

where

$$\tan \varphi = \frac{b\alpha}{1 - a\alpha^2}$$

As α varies between $+\infty$ and $-\infty$ in the p-plane Equation [7] generates spiral-like figures of the type shown in Fig. 3(b), for which $\varphi = \pi$ was chosen for $\alpha = 0$. The dotted branch corresponds to $-\infty < \alpha < 0$. As long as these figures do not encircle the point $(+1, 0)$ the system will be stable.

Stability Criteria

In view of the foregoing we may adjust conditions so that the lobes in Fig. 3(b) are of a magnitude less than unity, in which case they would never encircle the point $(+1, 0)$ regardless of their angular position. On the other hand, the lobes may be larger than unity but by proper angular positioning they again may be made to exclude the point $(+1, 0)$. In the first case one obtains the conditions for unconditional stability and in the second, the condition for conditional stability.

Unconditional Stability. The position vector for any point on the spiral of Equation [7] has a magnitude of

$$\rho = \frac{A}{\sqrt{(1 - a\alpha^2)^2 + (b\alpha)^2}} \quad \ldots\ldots\ldots\ldots [8]$$

By differentiating this with respect to α and setting to zero one finds the value of α for which the position vector is maximum, thus

$$\alpha_{max} = \pm \sqrt{\frac{2a - b^2}{2a^2}}$$

Substituting this into Equation [8] and setting $\rho = 1$ gives, after inserting the original parameters

$$c^2 \geq 2mK\left[1 \pm \sqrt{1 - \left(\frac{D}{K}\right)^2}\right] \quad \ldots\ldots\ldots [9]$$

as the criterion for unconditional stability. From physical reasoning we choose the negative sign before the radical since for $D \to 0$ smaller values of c would naturally be required to maintain stability.

Since the dashpot strength c is not directly measurable on a grinding machine it may be replaced by the logarithmic decrement δ, a more readily observable quantity, by using

$$\delta = \frac{\pi c}{mq} = \frac{\pi c}{\sqrt{mK}} \quad \text{or} \quad \frac{\delta\Omega}{\pi} = \frac{c}{m} \quad \ldots\ldots\ldots [10]$$

In this way one obtains

$$\delta^2 \geq 2\pi^2\left[1 - \sqrt{1 - \left(\frac{D}{K}\right)^2}\right] \quad \ldots\ldots\ldots [11]$$

This relation, determining unconditional stability, is plotted in Fig. 4.

Conditional Stability. If ρ be set to unity in Equation [8] and the resulting equation solved for α, one gets after using the approximation of Equation [10]

$$\frac{\alpha^2}{\Omega^2} = 1 - \frac{\delta^2}{2\pi^2} \pm \sqrt{\left(1 - \frac{\delta^2}{2\pi^2}\right)^2 - (1 - A^2)} \quad \ldots [12]$$

The values α_+^2/Ω^2 and α_-^2/Ω^2 are plotted in Fig. 5 for several values of A.

The position vectors of the points on the spiral which have a magnitude of unity are illustrated in Fig. 6 by O-A and O-B.

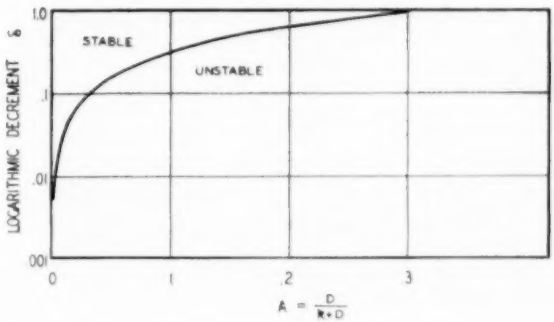

Fig. 4 Unconditional Stability Criterion

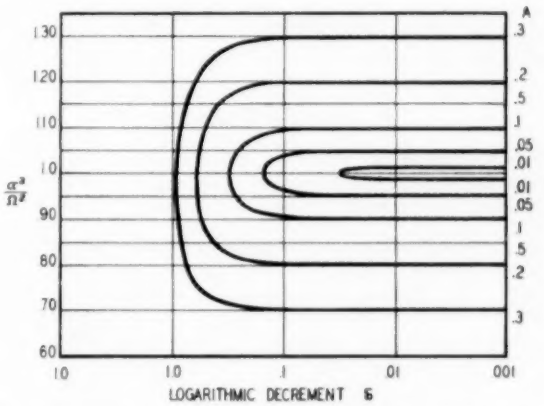

Fig. 5 Chart Giving Angles α_+ and α_- for Which Position Vector of Equation [7] Equals Unity

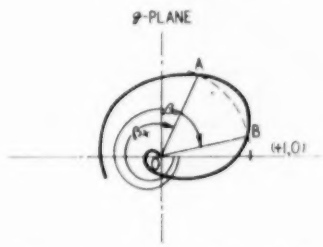

Fig. 6 Nyquist Contour in q-Plane Showing Typical Case of Conditional Stability

These vectors occur at the angles β_+ and β_- where

$$\beta_\pm = \alpha_\pm \tau + \varphi_\pm \quad \ldots\ldots\ldots\ldots [13]$$

From the expression for φ in Equation [7] one obtains after using the Relation [10]

$$\varphi_\pm = \tan^{-1} \frac{\frac{\delta}{\pi}\frac{\alpha_\pm}{\Omega}}{1 - \left(\frac{\alpha_\pm}{\Omega}\right)^2} \quad \ldots\ldots\ldots\ldots [14]$$

which may be used in computing Relation [13] with the aid of Fig. 5. If the values found, for a specific case, from Fig. 5 are

$$\frac{\alpha_{\pm}^2}{\Omega^2} = \mu_{\pm}^2$$

then

$$\left.\begin{aligned} \beta_{\pm} &= \mu_{\pm}\Omega\tau + \varphi_{\pm} \\ \text{or} \quad \beta_{\pm} &= \mu_{\pm}2\pi\gamma + \varphi_{\pm} \end{aligned}\right\} \quad \ldots\ldots\ldots\ldots [15]$$

Probably the simplest way of obtaining the position angles $\beta_{\pm}$ is to plot Equation [15] against γ for any specific set of conditions.

For example, taking $A = 0.1$, $\delta = 0.25$, $\Omega = 3141$ which lie in the unstable region of Fig. 4, one gets from Fig. 5

$$\mu_+^2 = 1.057, \quad \mu_-^2 = 0.937$$

The corresponding values of $\varphi_{\pm}$ from Equation [14] are

$$\varphi_+ = -0.305\pi, \quad \varphi_- = 0.282\pi$$

Equations [15] become

$$\begin{aligned} \beta_+ &= 1.028\,(2\pi\gamma) - 0.305\pi \\ \beta_- &= 0.97\,(2\pi\gamma) + 0.282\pi \end{aligned}$$

If these are plotted in the range $6 < \gamma < 10$, Fig. 7 results. The regions, where the lobe subtended by the angle $(\beta_+ - \beta_-)$ does not contain the positive real axis, are crosshatched. However,

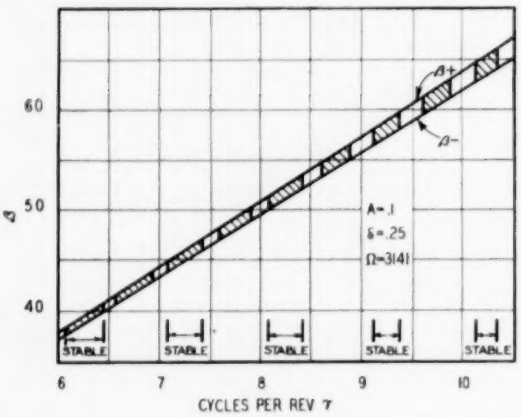

Fig. 7 Chart Showing Regions of Conditional Stability for Specific Values of $A = 0.1$, $\delta = 0.25$, $\Omega = 3141$

from elementary considerations concerning the work done on a periodic motion by a periodic force of the same frequency, which is given by

$$W = \pi P_0 x_0 \sin \psi$$

we see that work is only done on the system when the sin ψ is positive and abstracted when the sin ψ is negative. This corresponds in Fig. 8 to the region where γ equals $n - 1/4$ and $n + 1/4$. Consequently, only alternate crosshatched regions in Fig. 7 are stable. It will be noticed that as γ becomes large the stable regions shrink to zero. This corresponds to $|\beta_+ - \beta_-| \to \pi$.

Correlation With Practical Grinding

Although, at present, there are no detailed measured values of k, c, m, and D which are known experimentally to be stable or unstable, the foregoing theory can be checked in a qualitative manner in the light of general grinding experience.

It is known, for instance, that grinding wheels with wide faces are more apt to chatter than narrow ones. Since the grinding-rate factor D increases in proportion to the width of wheel thereby tending toward the unstable region of Fig. 4, qualitative agreement with the theory exists.

It is also known that as a grinding wheel becomes dull it becomes more likely to chatter. Here again a dull wheel means an increased grinding-rate factor D. Furthermore, it has been observed that chatter is more likely to occur at high work speeds.

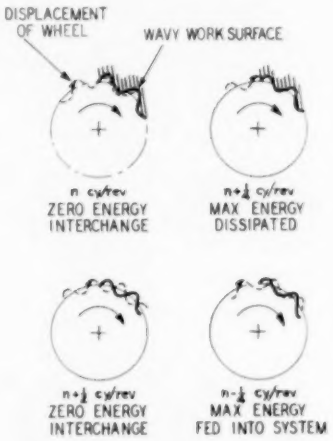

Fig. 8 Chart Illustrating Elementary Nature of Feedback

In the region of high work speeds it has been found that the rate of stock removal is nearly independent of work speed and, consequently, the radial advance of the wheel per revolution of the work becomes smaller as the work speed increases; i.e., D again tends to be large. This again confirms the theory.

Long flexible spindles have relatively low spring constants k, so that K, in Equation [11], tends to be smaller and therefore A larger, again confirming the theory.

Conclusions

By considering a grinding wheel to be mounted on an elastic structure and by making the simple proposition that the instantaneous depth of penetration of the wheel into the work is proportional to the instantaneous dynamic force existing between wheel and work, there results a theory capable of explaining the frequently observed phenomenon of chatter. Furthermore, the theory predicts a spectrum of values of γ for which stability should exist. Qualitatively, the theory appears to agree with practice with respect to changes in rigidity, changes in grinding-rate factor D, and changes in damping.

Acknowledgment

The author wishes to acknowledge the generous support of the management of The Heald Machine Company for making it possible to carry out this work.

BIBLIOGRAPHY

1 "Metal-Cutting Chatter and Its Elimination," by R. S. Hahn, Trans. ASME, vol. 75, 1953, pp. 1073–1080.

2 "Self-Excited Oscillations in Dynamical Systems Possessing Retarded Actions," by Nicholas Minorsky, *Journal of Applied Mechanics*, Trans. ASME, vol. 64, 1942, pp. A-65–A-71.

3 "Stability of Linear Oscillating Systems With Constant Time Lag," by H. I. Ansoff, *Journal of Applied Mechanics*, Trans. ASME, vol. 71, 1949, pp. 158–164.

4 "Modern Operational Mathematics in Engineering," by R. V. Churchill, McGraw-Hill Book Company, Inc., New York, N. Y., 1944.
5 "Complex Variable and Operational Calculus," by N. W. McLachlan, The Macmillan Company, New York, N. Y., 1942.
6 "Principles of Servo-Mechanisms," by G. S. Brown and D. T. Campbell, John Wiley & Sons, Inc., New York, N. Y., 1948.
7 "Network Analysis and Feedback Amplifier Design," by H. W. Bode, D. Van Nostrand Company, Inc., New York, N. Y., 1945.

Discussion

T. A. Hunter.[3] One of the principal difficulties in the analysis of regenerative chatter is the retarded-action feature. The author is to be commended for his success in overcoming these difficulties, and for his analysis of the solution obtained. It must be pointed out, however, that there are certain limitations on the use of the author's work.

Perhaps the most serious limitation is that the chatter is supposed to consist of one frequency. This will be approximately true in many cases and probably would be a good rule of thumb to follow, but for any instance where the chatter is of sufficient amplitude to cause the wheel to leave the work, then the wheel vibration will not be simple harmonic any longer. Certain frequencies higher than the fundamental will be introduced. As Fig. 7 of the paper shows, these higher frequencies may tend to be unstable since the bands of stability become narrower as the frequency increases.

The assumption of a simple proportion for the ratio of the depth of cut to the wheel-contact force is a widely useful one and usually will be met in practice. However, if there is a hard spot in the material, then the value of the proportionality constant k would have to be changed. This, of course, will introduce some nonlinearity into the problem, and thus increase the difficulty of the solution tremendously. It is the writer's opinion that hard spots and other such nonuniformities are primary causes of chatter.

E. G. Loewen.[4] One of the most difficult problems to analyze in metal cutting is that of vibrations which occur frequently and prevent precision-machining or at best give rise to unpleasant noise. The literature of this field is a limited one and the author's novel approach to the study of regenerative chatter is bound to stimulate further work in this direction.

In solving most differential equations, such as Equation [1] of the paper, it is necessary to assume constant coefficients, even if we know that this represents an approximation. Only experiment can show whether the approximations are justified. The author has concerned himself chiefly with the establishment of stability criteria, Equation [11] being the most interesting result. Since the grinding-rate factor D can be measured experimentally an assumed amount of damping would lead directly to the minimum stiffness k, required for stability. For a $^1/_2$-in-wide wheel a typical value for D has been measured to be 20,000 lb/in. Even if we assume an extremely high value of 1 for δ, the logarithmic decrement, the minimum stiffness k needed to avoid chatter would be 46,000 lb/in. Yet we know that grinding spindles having stiffnesses only a fraction of this figure are in common use. From this we may conclude that either linear coefficients do not represent the system accurately enough or that regenerative chatter is always present but usually with amplitudes too small to be of concern.

One of the interesting points brought out by Minorsky (author's reference 2) is that regenerative chatter always should take place at a frequency above the natural frequency of the simple system without the delayed-action forces. The difference between these frequencies is also a measure of the phase lag which is needed to supply the energy that sustains vibrations, as represented in his Fig. 8. In other words, these readily measured frequencies might prove to be a valuable tool when analyzing vibrations from an energy point of view.

That some sort of regenerative effect can also exist in lathe turning was shown by Saljé[5] who noted that when cutting with a tool having an appreciable overhang, so that it was prone to chatter, it took much less time to build up full vibration amplitude when the workpiece had previous chatter marks than when the workpiece was smooth.

Author's Closure

The comments of Professors Hunter and Loewen are greatly appreciated.

In answer to Professor Hunter's remarks it should be pointed out that the theory developed here applies only to the stability of a simple one-degree-of-freedom elastic system supporting the wheel in contact with the work. In considering only stability criteria it is not necessary to contemplate any finite amplitude of vibration but only infinitesimal displacements. The computation of amplitude as a function of time appears to be very complex indeed. In a practical setup, which usually has several modes of vibration, each with a characteristic frequency, one would investigate the stability in each mode separately. Different effective values of K, c, and m would have to be determined for each mode. In this way the stability conditions for the several modes of vibration may be investigated.

Fig. 7 is not to be interpreted as indicating that, as the frequency increases the stable regions are reduced, as Professor Hunter implies in his discussion. In developing Fig. 7 the frequency, i.e., Ω, is held constant as a fixed parameter. The cycles of vibration per revolution of the workpiece γ appearing along the abscissa vary as a consequence of changing work speed.

Professor Loewen correctly notes that a stiffness of 46,000 lb/in. is required for stability when the grinding factor D is 20,000 lb/in. Values of stiffness often occur in practice both above and below this value, especially in internal grinding. Also, chatter occurs more frequently than commonly believed, especially as more precise gaging means are applied to the workpiece. Equation [11] may demand greater decrements and stiffnesses than are actually required but it should be remembered that the decrement in Equation [11] is that corresponding to the wheel in contact and not the free decrement, and also under conditions of rotation and in the presence of cutting fluids. Under these conditions the decrement may be greater than when at rest and out of contact.

[3] University of Michigan, Ann Arbor, Mich.
[4] Assistant Professor of Mechanical Engineering, Massachusetts Institute of Technology, Cambridge, Mass. Assoc. Mem. ASME.
[5] "Ursachen und Minderung von Werkzeugschwingungen," by E. Saljé, *Industrie Anzeiger*, vol. 80, 1953, p. 1023.

An Experimental Study of Metal Extrusions at Various Strain Rates

By J. FRISCH[1] and E. G. THOMSEN,[2] BERKELEY, CALIF.

A 4.3-in-diam cylindrical commercially pure lead billet was extruded at room temperature into a 1.5-in-diam solid bar at three extrusion rates of 0.1, 0.74, and 5.15 ipm. Particle velocities, magnitude, and direction, for the inverted extrusion process using a sharp-edged die, were determined on a meridian plane by a stepwise extrusion method. It was found that for the extrusion rates investigated the flow pattern was invariable with respect to the extrusion rates. Measured wall pressures were found to increase approximately linearly with the extrusion speed in a similar manner as the extrusion load, such that the ratio of applied pressure to the wall pressure remained constant. Theoretical considerations appear to agree with the experimental observations. The mean pressure within the metal differed from the measured wall pressure by the condition necessary to establish plastic flow. The predicted mean pressure obtained from a graphical analysis of the velocity pattern of the billet agreed approximately with the measured mean pressure.

Nomenclature

The following nomenclature is used in the paper:

$\sigma_z, \sigma_\theta, \sigma_r$ = normal true stresses at a point in cylindrical co-ordinates, psi

$\dot{\epsilon}_z, \dot{\epsilon}_\theta, \dot{\epsilon}_r$ = normal plastic strain rate components associated with the normal stresses

$\tau_{zr}, \tau_{r\theta}, \tau_{\theta z}$ = shearing stresses perpendicular to co-ordinate direction of first subscript and in direction of second subscript, psi

$\dot{\gamma}_{zr}, \dot{\gamma}_{r\theta}, \dot{\gamma}_{\theta z}$ = plastic shearing strain rate components associated with shearing stresses

$$\bar{\sigma} = \begin{cases} \text{. . . . effective stress, psi} \\ \sqrt{\dfrac{(\sigma_z - \sigma_r)^2 + (\sigma_r - \sigma_\theta)^2 + (\sigma_\theta - \sigma_z)^2}{2} + 3(\tau_{zr}^2 + \tau_{r\theta}^2 + \tau_{\theta z}^2)} \end{cases}$$

$$\bar{\dot{\epsilon}} = \begin{cases} \text{. . . . effective plastic strain rate} \\ \dfrac{2}{3}\sqrt{\dfrac{(\dot{\epsilon}_z - \dot{\epsilon}_r)^2 + (\dot{\epsilon}_r - \dot{\epsilon}_\theta)^2 + (\dot{\epsilon}_\theta - \dot{\epsilon}_z)^2}{2} + \dfrac{3}{4}(\dot{\gamma}_{zr}^2 + \dot{\gamma}_{r\theta}^2 + \dot{\gamma}_{\theta z}^2)} \end{cases}$$

L = applied load, lb

A = cross-sectional area of billet, sq in.

p_w = wall pressure measured with SR-4 gages, psi

p = mean pressure, psi $= -\frac{1}{3}(\sigma_z + \sigma_\theta + \sigma_r)$

z = instantaneous axial distance from die opening to center line of pressure gage, in.

Introduction

From a technological as well as a scientific point of view it is of interest to know the details of plastic motion within a metal during a metal-forming operation and the resulting stress and strain distribution. Such information is readily obtainable, if the deformation process is homogeneous, since in this case, knowledge of the initial and final geometry of the metallic part together with its mechanical properties will often suffice. In most metal-forming operations, however, such as rolling, drawing, extrusion, or even the chip formation in metal cutting, the final geometrical shape of the part is obtained through a heterogeneous deformation process. Hence, a knowledge of the initial and final geometry of the part is insufficient to know or infer the actual details of the plastic-flow mechanism during the forming process. In fact, assumption of homogeneous deformation, in most cases, will lead to a wrong concept of the deformation process and the calculated deformation stresses may be in error by a factor of two or more when compared with the required external forming loads.

The application of theories of plasticity to the solution of certain forming problems has aided in giving some hint as to the possible detailed deformation processes involved. The theory most usually used for the solutions of forming problems is based on Hencky's (1)[3] plastic sector method. Hill (2) has given an excellent account of this theory and has developed further the necessary conditions which must be satisfied in any particular solution and has solved a number of interesting forming problems. For a quick review of the basic ideas involved in this theory, the reader may also consult an article by Lee (3).

There are some objections to accepting solutions to forming problems obtained by the application of the foregoing theory. These lie principally in the fact that the mathematical solutions require idealization of the flow properties of the metal under consideration and that solutions must be restricted to plane-strain problems, which are said to be statically determinate. Of these, the requirement that the material is ideal, i.e., it will flow when a constant stress has been exceeded and the metal can be separated by a definite boundary into a plastic and plastic-rigid part, may not be too severe. The further restriction, however, that only plane straining is involved, leaves a large number of practical forming problems out of reach of the purely mathematical attack, since it is dangerous to extrapolate to the general three-dimensional case. Furthermore the literature is practically void of experimental proof of the validity of theoretical solutions and hence general acceptance must be postponed until experimental data become available.

If the deformation mechanism in a metal being plastically deformed cannot be ascertained from the initial and final geometry of the metallic body, then it becomes necessary to know the instan-

[1] Assistant Professor of Engineering Design, University of California. Assoc. Mem. ASME.

[2] Associate Professor of Mechanical Engineering, University of California.

Contributed by the Research Committee on Metal Processing and the Applied Mechanics and Production Engineering Divisions and presented at the Annual Meeting, New York, N. Y., November 29–December 4, 1953, of The American Society of Mechanical Engineers.

Note: Statements and opinions advanced in papers are to be understood as individual expressions of their authors and not those of the Society. Manuscript received at ASME Headquarters, September 25, 1953. Paper No. 53—A-154.

[3] Numbers in parentheses refer to the Bibliography at the end of the paper.

taneous motion of particles making up the body. Such motion in the interior of the metallic body cannot be made visual directly. Tracer methods with radioactive isotopes can possibly be used for such visualization of particle motion, but the authors are not aware of investigations along this line having been reported in the literature. The separation of the metal along a plane on which no normal tensile stresses and across which no shear stresses exist, and tagging points on this plane for visual observation, is a practical way for visualizing plastic flow. This method involves subjecting the metallic body to a small step in a deformation process and observing the small displacements of marked points on the separation plane. Yang and Thomsen (4) used this method and obtained particle-flow directions in a lead billet during an inverted extrusion process. These investigators considered the intersection of originally square grid lines as their particles and thus were able to ascertain particle movement. Thomsen and Lapsley (5) showed that it is possible to obtain the internal stress distribution from a graphical analysis if the particle motion, direction and velocity, is obtainable on a separation plane

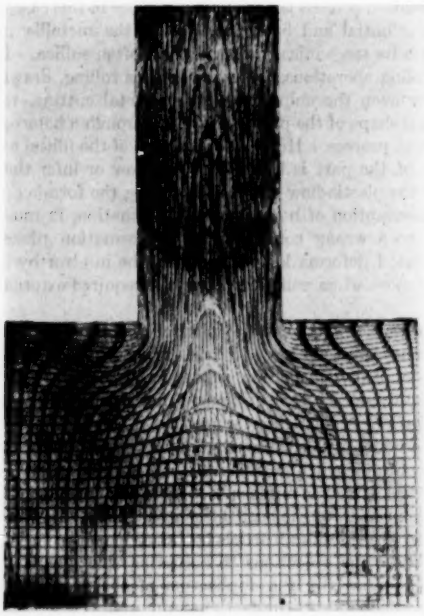

FIG. 1 PARTIALLY EXTRUDED LEAD BILLET SHOWING DEFORMED GRID LINES

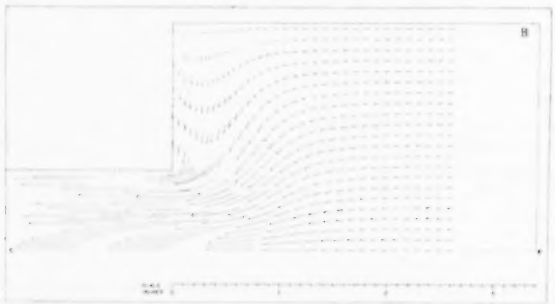

FIG. 2 PARTICLE FLOW DIRECTION DURING STEADY-STATE DEFORMATION AT A CONSTANT EXTRUSION RATE OF 1.0 IPM FOR A 1.5-IN-DIAM SOLID CYLINDRICAL BAR; BILLET REDUCTION = 8.2:1

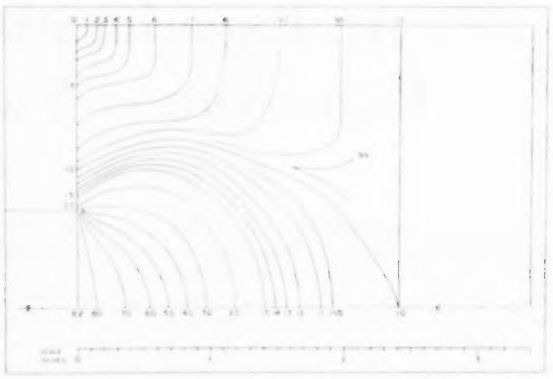

FIG. 3 DIMENSIONLESS ISO-VELOCITY TRAJECTORIES FOR STEADY-STATE DEFORMATION

(Identical for all extrusion rates given in Figs. 3 to 5, inclusive. Dimensionless velocity is given by the ratio of particle velocity to velocity of base end of billet.)

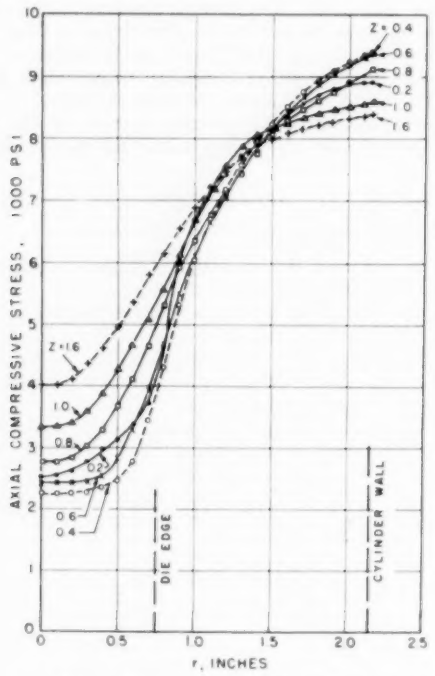

FIG. 4 AXIAL STRESS DISTRIBUTION IN A LEAD BILLET FOR SEVERAL DISTANCES z FROM THE ORIFICE

(Curves are the result of a graphical stress analysis using experimental flow patterns for an inverted extrusion process.)

from experimental observations. The experimental technique has been described and a graphical solution of stress and strain-rate distribution for a lead billet extruded in an inverted extrusion process has been given in detail in a recent series of three articles (6). A sample photograph from these articles of an originally square grid network on a meridian separation plane for a commercially pure lead billet during extrusion is shown in Fig. 1. One or more small additional deformation steps permitted determination of direction and magnitude of particle velocity during steady-state deformation. The particle directions during steady-state motion from experimental observation are given in

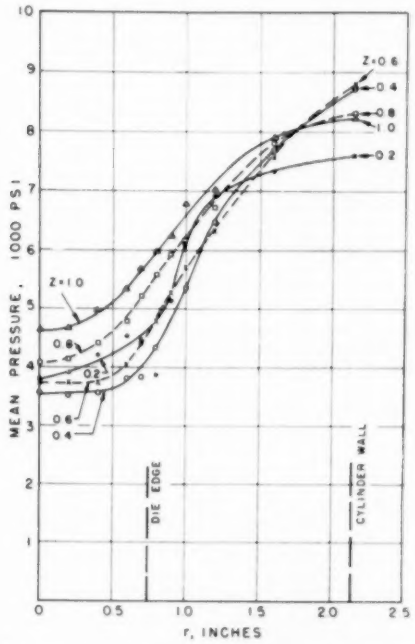

FIG. 5 DISTRIBUTION OF MEAN PRESSURE IN A LEAD BILLET FOR SEVERAL DISTANCES z FROM THE ORIFICE
(Curves are the result of a graphical stress analysis using experimental flow patterns for an inverted extrusion process.)

Fig. 2, and constant-velocity-ratio trajectories are given in Fig. 3. Using the Lévy-Mises criterion for flow, the measured applied load and the flow properties for lead, as determined from a compression test, permitted the calculation of axial stress, Fig. 4, and mean-pressure distribution, Fig. 5, in the billet. While it was ascertained that the metal of the billet was in steady-state motion at the time of determining velocities, no check on the calculated pressures was available. The present article, therefore, presents a comparison of measured pressures with calculated pressures. In addition the effect of extrusion speed on the flow pattern, forming load, and pressures will be evaluated.

EXPERIMENTAL TECHNIQUE

Fig. 6 shows the extrusion apparatus. The marked billet halves are assembled in this apparatus and all surfaces are lubricated with white lead in oil. The extrusion load is applied by a 200,000-lb hydraulic testing machine. The extrusion speeds were kept constant at 0.1, 0.74, and 5.15 ipm, giving a maximum speed ratio of more than 50:1, with the highest speed approaching some commercial extrusion rates. The extrusion temperature was atmospheric temperature. The wall pressure was measured with a special pressure gage also shown in Fig. 6. The pressure-sensitive element of the gage is a small piston having a reduced $^1/_{16} \times {}^1/_4$-in. section on which SR-4 strain gages are mounted. This piston is in contact with a $^1/_8$-in-diam load pin, which is guided in the extrusion chamber wall and kept flush during testing with the inner wall surface of the chamber. A dead-weight calibration with the gage in place gave a linear response. The calibration and the characteristic quantity that such a gage measures will be discussed in a later section. The sensitivity of this gage, assuming uniform pressure over the $^1/_8$-in-diam gage pin, is 30 psi per microinch indicator reading. Hence, this gage has low accuracy at small pressures but gives reasonable accuracy for pressures above 5000 psi, which is the pressure range encountered in the present investigation. The indicator has a least count of 10 microinches but can be estimated to 5 microinches or better. Thus the accuracy of pressure determination, estimating to the nearest 5-microinch indicator reading, may be in error by 3 per cent at 5000 psi and $1^1/_2$ per cent at 10,000 psi.

The experimental tests were divided into two parts: (*a*) Determination of flow pattern and (*b*) determination of load and pressures during extrusion. The determination of the flow pattern was the same as previously used (6). It consisted of extruding the 1.5-in-diam solid bar in the sharp-edged circular die at the desired extrusion rate in small steps. The cylindrical billet had a diameter of 4.3 in. and hence the reduction was equal to the area ratio of the bar to billet or 8.2/1. The small extrusion

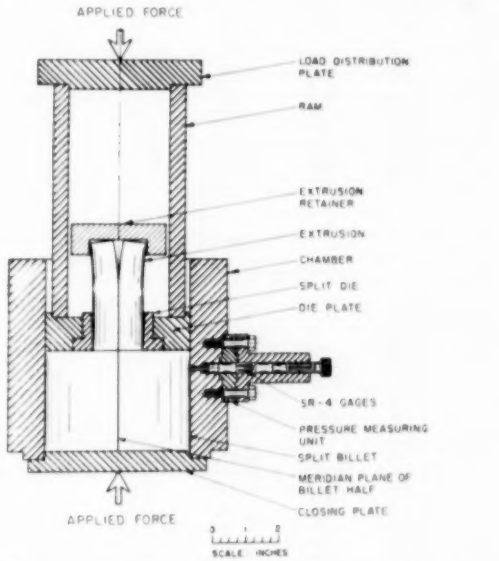

FIG. 6 DIAGRAMMATIC VIEW OF INDIRECT EXTRUSION APPARATUS AND PRESSURE-MEASURING DEVICE

steps as referred to the extrusion die motion or billet contraction were varied from approximately 0.030 to 0.100 in. in each step and were measured with a dial indicator with a least count of 0.001 in. The extrusion time was measured with a stop watch. The extrusion rate was held constant by adjusting the valves of the testing machine manually. After each extrusion step the billet was disassembled from the apparatus and the deformed grids were photographed at $^1/_2$ natural size in a fixed photographic setup. The films were later mounted between glass plates and projected on a screen to 10 times the original billet size. The instantaneous particle positions during each step were plotted on cross-section paper as represented by intersection of the images of the grid lines. A different billet was used for each extrusion rate and only steady-state-particle movements were recorded. The second part of the experiment consisted of extruding a different set of billets continuously at the several extrusion rates under investigation. The experimental data for three extrusion rates are given in Tables 1 to 3, inclusive.

RESULTS

Figs. 7 and 8 show the particle flow direction for extrusion rates of 0.1 ipm and 5.15 ipm, respectively, as determined from the stepwise extrusion processes. These two flow patterns are identical if superimposed one upon the other and in fact also agree with

TABLE 1

Extrusion rate: Die 0.0002 in. per sec
Bar 0.1 in. per min

Die movement, in.	Time, sec	s, in.	Load L, lb	p_w, psi	$\frac{L}{A p_w}$
0.000	0	0.783	30000	...	...
0.010	60	0.773	76000	4480	1.17
0.035	180	0.748	94800	5540	1.18
0.063	300	0.720	96000	5630	1.18
0.086	420	0.697	96100	5630	1.18
0.110	540	0.673	96100	5700	1.16
0.137	660	0.646	96000	5780	1.15
0.166	780	0.617	95000	5780	1.14
0.194	900	0.589	93900	5820	1.11
0.221	1020	0.562	92900	5780	1.11
0.246	1140	0.537	92900	5780	1.11
0.270	1260	0.513	92700	5780	1.11
0.295	1380	0.488	92700	5780	1.11
0.319	1500	0.464	92100	5780	1.10
0.343	1620	0.440	92200	5780	1.10
0.367	1740	0.416	92300	5780	1.10
0.391	1860	0.391	92400	5780	1.10
0.415	1980	0.368	92300	5780	1.10
0.439	2100	0.343	92300	5780	1.10
0.461	2220	0.322	92300	5700	1.11
0.484	2340	0.299	92700	5700	1.12
0.506	2460	0.277	93200	5700	1.13
0.528	2580	0.255	93400	5700	1.13
0.550	2700	0.233	94000	5700	1.14
0.574	2820	0.209	94500	5780	1.13
0.597	2940	0.186	94600	5820	1.12
0.621	3060	0.162	94700	5910	1.11
0.645	3180	0.138	94900	6030	1.09
0.669	3300	0.114	94900	6030	1.09
0.694	3420	0.089	95000	6150	1.07
0.706	3480	0.077	95000	6150	1.07

TABLE 2

Extrusion rate: Die 0.0015 in. per sec
Bar 0.740 in. per min

Die movement, in.	Time, sec	s, in.	Load L, lb	p_w, psi	$\frac{L}{A p_w}$
0.000	0	0.940	40000	...	...
0.040	20	0.900	91000	5870	1.07
0.070	40	0.870	100000	6200	1.10
0.095	60	0.845	105000	6400	1.13
0.120	80	0.820	106400	6470	1.13
0.150	100	0.790	107200	6930	1.07
0.180	120	0.760	106200	6930	1.06
0.210	140	0.730	104400	6810	1.06
0.240	160	0.700	103500	6810	1.05
0.270	180	0.670	105100	6810	1.05
0.300	200	0.640	103000	6810	1.04
0.330	220	0.610	102900	6650	1.06
0.360	240	0.580	102900	6600	1.07
0.390	260	0.550	102900	6600	1.07
0.420	280	0.520	102900	6600	1.07
0.450	300	0.490	103100	6600	1.08
0.480	320	0.460	103300	6600	1.08
0.510	340	0.430	103700	6600	1.08
0.540	360	0.400	103700	6600	1.08
0.570	380	0.370	103800	6600	1.08
0.600	400	0.340	103800	6600	1.08
0.635	420	0.305	103800	6600	1.08
0.665	440	0.275	104000	6480	1.10
0.700	460	0.240	104400	6480	1.11
0.730	480	0.210	104700	6480	1.11
0.760	500	0.180	104800	6480	1.11
0.795	520	0.145	104900	6520	1.11
0.825	540	0.115	105000	6680	1.08
0.860	560	0.080	105100	6810	1.06

TABLE 3

Extrusion rate: Die 0.01045 in. per sec
Bar 5.15 in. per min.

Die movement, in.	Time, sec	s, in.	Load L, lb	p_w, psi	$\frac{L}{A p_w}$
0.000	0	0.620	30000	...	...
0.120	10	0.500	144000	8810	1.12
0.230	20	0.390	149000	9140	1.12
0.320	30	0.300	147000	9140	1.11
0.438	40	0.182	142500	8650	1.13
0.535	50	0.085	143500	9140	1.09

that shown in Fig. 2, which was determined previously at an extrusion rate of approximately 1 ipm. If the velocity ratios are also compared it is found that they check with those of Fig. 3 within approximately 10 per cent, which is also the approximate accuracy with which the original velocity trajectories were established. The actual experimental values for magnitude of particle velocity are not shown, but the authors have examined various regions in the flow field and have found that the foregoing statement is substantiated. It appears, therefore, that at least

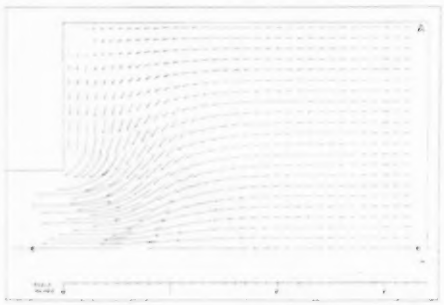

FIG. 7 PARTICLE FLOW DIRECTION DURING STEADY-STATE DEFORMATION, AT A CONSTANT EXTRUSION RATE OF 0.1 IPM FOR A 1.5-IN-DIAM SOLID CYLINDRICAL BAR; BILLET REDUCTION = 8.2:1

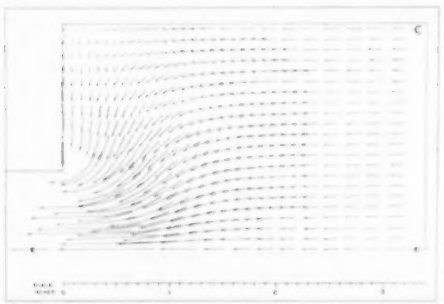

FIG. 8 PARTICLE FLOW DIRECTION DURING STEADY-STATE DEFORMATION AT A CONSTANT EXTRUSION RATE OF 5.15 IPM FOR A 1.5-IN-DIAM SOLID CYLINDRICAL BAR; BILLET REDUCTION = 8.2:1

for the present extrusion process and extrusion rates using lead, no strain-rate effect exists. This fact may be of practical importance, because a flow pattern determined at one strain rate may be used for other strain rates. This observation, however, should not be used as a general criterion until more experimental data are available, because work hardening or a nonuniform temperature distribution in the metal may yield different results.

Examining the results from the continuous extrusion tests at different strain rates it is found that the axial load and wall pressure at different extrusion rates vary with extrusion time, as given in Fig. 9 and Tables 1 to 3, inclusive. It is seen that load and wall pressure, except at the start of each test, are approximately constant during the entire extrusion process. A plot of die movement versus extrusion time has been included to show that the rate was constant for each individual test. Fig. 10 shows the applied axial extrusion load and measured wall pressure as functions of extrusion rates. While insufficient data are available it appears that the load and pressure increase approximately linearly with extrusion rate. It may also be of interest to note that the actual measured wall pressure is lower than an average pressure, p_{avg}, as calculated from the applied load divided by the billet cross-section area. This may have significance in the design of extrusion chambers since the wall pressure is less than p_{avg} and hence p_{avg} would be a safe pressure for calculating hoop stresses. No extrapolation should be made at this time, however, until more experimental data become available. Fig. 11 shows the ratio $(L/A)/p_w$, which is equal to

$$\frac{p_{avg}}{p_w}\left(\frac{\text{average pressure}}{\text{wall pressure}}\right)$$

as a function of gage position. Referring to Fig. 6, it is seen that

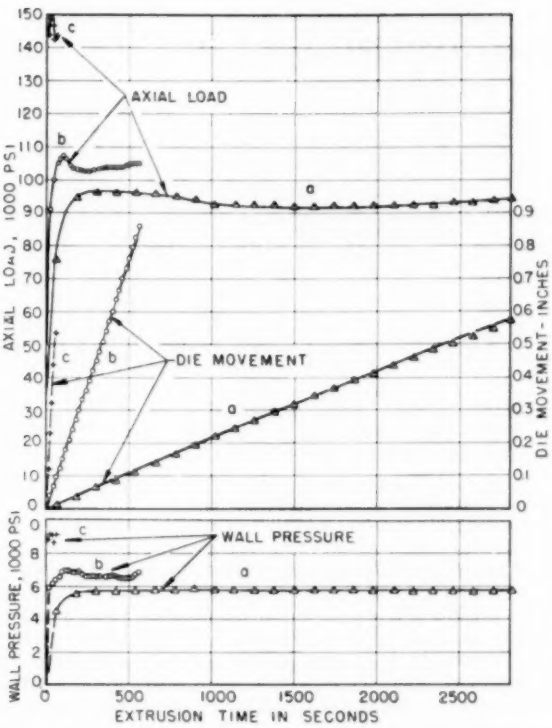

FIG. 9 AXIAL LOAD, DIE MOVEMENT, AND WALL PRESSURE AS FUNCTIONS OF EXTRUSION TIME

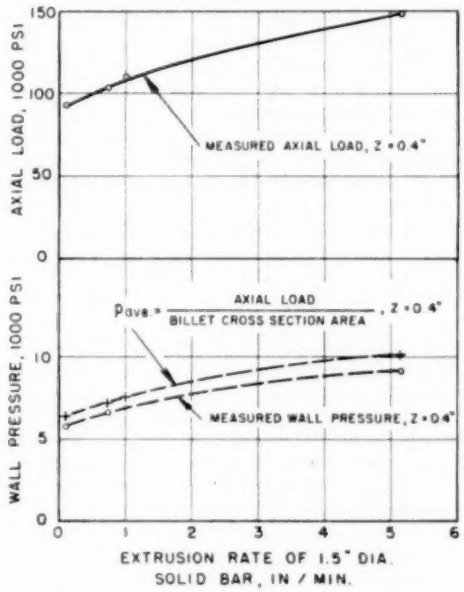
MEASURED AXIAL LOAD, Z = 0.4"
AXIAL LOAD, 1000 PSI
$P_{ave} = \frac{\text{AXIAL LOAD}}{\text{BILLET CROSS SECTION AREA}}$, Z = 0.4"
MEASURED WALL PRESSURE, Z = 0.4"
WALL PRESSURE, 1000 PSI
EXTRUSION RATE OF 1.5" DIA. SOLID BAR, IN / MIN.

FIG. 10 AXIAL LOAD AND PRESSURES AS FUNCTIONS OF EXTRUSION RATE
(Distance between pressure gage and die is 0.4 in.)

the pressure gage is at a constant location from the base end of the billet but at variable distance from the movable die. Thus the abscissa of Fig. 11 is given as the distance between die and gage and the experimental points give the instantaneous pressure ratios as functions of gage position from the die. From this figure it is seen, therefore, that the pressure ratio $\frac{p_{ave}}{p_w}$ is approximately constant for the three extrusion rates investigated and the conclusion that strain rate has no effect, except in raising load and wall pressure, is the same as reached earlier in examining the flow pattern.

It is now of interest to examine the theoretical validity for the foregoing conclusions. If the metal were an ideal metal with a constant-flow stress, then the flow pattern for plane strain should be identical for all strain rates as predicted by the Hencky theory. Even if the flow stress differs, as for other metals, the flow pattern is unique and only depends on the geometry. Hill (2) has given several solutions for extrusions in terms of slip lines, which can be converted to constant velocity fields. Lee (3) suggests that the same solution for one geometric shape is still applicable if the flow stress is a function of strain rate, if one assumes an average flow stress for the particular solution. Hence it appears that the present results for a real metal are in qualitative agreement with predictions based on the Hencky theory.

Let us now examine the Lévy-Mises equations, normally believed to apply for a general state of stress in a real isotropic metal, which were used in the calculation of axial stress and mean-pressure distribution in the billet under discussion and are shown in Figs. 4 and 5. The necessary development of this method is fully described in the previously mentioned articles (6). The stress-strain rate equations are

$$\left.\begin{aligned} \dot{\epsilon}_z &= \dot{\lambda}(\sigma_z + p),\ \dot{\gamma}_{zr} = 2\dot{\lambda}\tau_{zr} \\ \dot{\epsilon}_r &= \dot{\lambda}(\sigma_r + p),\ \dot{\gamma}_{r\theta} = 2\dot{\lambda}\tau_{r\theta} \\ \dot{\epsilon}_\theta &= \dot{\lambda}(\sigma_\theta + p),\ \dot{\gamma}_{\theta z} = 2\dot{\lambda}\tau_{\theta z} \end{aligned}\right\} \quad \ldots\ldots\ldots\ldots [1]$$

where

$$\dot{\lambda} = \frac{3}{2}\frac{\dot{\bar{\epsilon}}}{\bar{\sigma}} \quad \ldots\ldots\ldots\ldots [2]$$

$$\dot{\bar{\epsilon}} = \frac{2}{3}\sqrt{\frac{(\dot{\epsilon}_z - \dot{\epsilon}_r)^2 + (\dot{\epsilon}_r - \dot{\epsilon}_\theta)^2 + (\dot{\epsilon}_\theta - \dot{\epsilon}_z)^2}{2} + \frac{3}{4}(\dot{\gamma}_{zr}^2 + \dot{\gamma}_{r\theta}^2 + \dot{\gamma}_{\theta z}^2)} \quad \ldots\ldots [3]$$

and

$$\bar{\sigma} = \sqrt{\frac{(\sigma_z - \sigma_r)^2 + (\sigma_r - \sigma_\theta)^2 + (\sigma_\theta - \sigma_z)^2}{2} + 3(\tau_{zr}^2 + \tau_{r\theta}^2 + \tau_{\theta z}^2)} \quad \ldots\ldots [4]$$

The ratio $\dot{\lambda} = \frac{3}{2}\frac{\dot{\bar{\epsilon}}}{\bar{\sigma}}$ may vary from point to point in the plastic metal and is known as the plastic modulus. The functional relationship of the effective strain rate, $\dot{\bar{\epsilon}}$, and the effective stress, $\bar{\sigma}$, can be obtained from a mechanical test such as a compression test. For commercially pure lead it was found that the following linear equation is approximately applicable

$$\bar{\sigma} = \bar{\sigma}_o + m\dot{\bar{\epsilon}} \quad \ldots\ldots\ldots\ldots [5]$$

where $\bar{\sigma}_o$ is the effective yield stress and m is the slope of the stress-strain rate curve.

If inertial effects are absent, as is the case with a relatively slow-moving plastic metal, then the static equilibrium equations must be satisfied. For the extrusion problem under discussion, axial

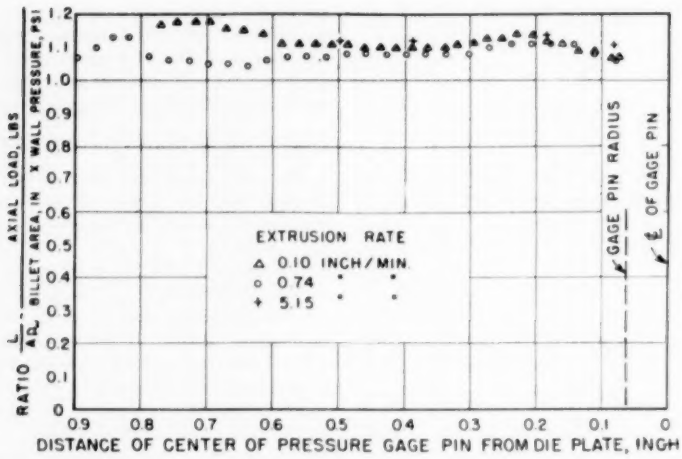

FIG. 11 RATIOS OF AVERAGE PRESSURE TO WALL PRESSURE AS FUNCTIONS OF THE DISTANCE BETWEEN PRESSURE GAGE AND DIE PLATE FOR VARIOUS EXTRUSION RATES

symmetry exists, and the static equilibrium equations take the following form

$$\left.\begin{aligned} \frac{\partial \sigma_z}{\partial z} + \frac{\partial \tau_{zr}}{\partial r} + \frac{\tau_{zr}}{r} &= 0 \\ \frac{\partial \sigma_r}{\partial r} + \frac{\partial \tau_{zr}}{\partial z} + \frac{\sigma_r - \sigma_\theta}{r} &= 0 \\ \frac{1}{r}\frac{\partial \sigma_\theta}{\partial \theta} &= 0 \end{aligned}\right\} \quad \ldots\ldots\ldots\ldots [6]$$

In the axial symmetrical extrusion problem $\dot{\epsilon}_z$, $\dot{\epsilon}_r$, $\dot{\gamma}_{zr}$, and $\dot{\bar{\epsilon}}$ can be obtained from the experimentally determined particle velocity pattern. For a complete analysis the reader is referred to the previously mentioned articles (6). The shear-strain rates $\dot{\gamma}_{r\theta}$ and $\dot{\gamma}_{\theta z}$ are zero on a meridian separation plane and the normal strain rate $\dot{\epsilon}_\theta$ can be obtained from the condition of constancy of volume, namely

$$\dot{\epsilon}_z + \dot{\epsilon}_r + \dot{\epsilon}_\theta = 0 \quad \ldots\ldots\ldots\ldots\ldots [7]$$

Hence, introducing the experimentally determined strain rates into the first of the three equilibrium Equations [6] by substitution of the plasticity Equations [1] and the stress-strain rate Equation [5], the following results

$$\left[2\frac{\partial}{\partial z}\left(\frac{\dot{\epsilon}_z}{\dot{\bar{\epsilon}}}\right) + \frac{\partial}{\partial r}\left(\frac{\dot{\gamma}_{zr}}{\dot{\bar{\epsilon}}}\right) + \frac{1}{r}\left(\frac{\dot{\gamma}_{zr}}{\dot{\bar{\epsilon}}}\right)\right] = \frac{3}{\sigma_o}\left[\frac{\partial p}{\partial z} - \frac{m}{3}\left(2\frac{\partial \dot{\epsilon}_z}{\partial z} + \frac{\partial \dot{\gamma}_{zr}}{\partial r} + \frac{\dot{\gamma}_{zr}}{r}\right)\right] \quad \ldots\ldots [8]$$

If the flow pattern is constant, the left-hand square bracketed term, which is composed of strain ratios, is constant at any given point but varies from point to point throughout the metal in plastic motion. Thus the right-hand term must also be constant for any given point, and $\frac{\partial p}{\partial z}$ must increase by a factor of $\frac{m}{3}$ times the increase in the strain rates. If the second equilibrium equation of Equations [6] is examined the conclusion that $\frac{\partial p}{\partial r}$ varies linearly with the extrusion speed is also confirmed. Thus the approximate linear relationship between pressure and extrusion speed observed experimentally is confirmed by an investigation of the plasticity equations, normally believed to be applicable to real isotropic metals.

While no distinction has been made between the measured wall pressure p_w and the mean pressure p used in the plasticity equations, it should be pointed out that these pressures are not identical. The wall pressure p_w is the stress per unit area experienced by the gage pin and also approximately by the chamber wall, while the mean pressure p is only experienced by the metal internally and not directly measurable with a pressure gage. It will be shown, however, that the foregoing observation of approximate linear mean-pressure rise p with extrusion speed is applicable.

Fig. 12 gives pressures as functions of SR-4 strain indicator readings in microinches. The straight line f is the gage pressure obtained from a dead-weight calibration referred to previously. If a lead billet is now placed in the chamber and the die is replaced with a flat plate a statical calibration can be obtained by loading the billet under condition of zero plastic flow. The mean pressure p is now constant in the billet and is given by the applied load divided by the cross-sectional area. Curves a, b, c, d, e are the mean-pressure variations during loading and unloading as recorded by the strain indicator. It is seen that at the beginning of the test, curve a, the pressure gage does not record at once until a substantial load has been applied. After a critical mean pressure has been exceeded the gage responds approximately linearly at nearly the same slope as given by the original dead-weight calibration curve. If the load is relaxed the pressure falls along b and upon reloading takes the new path along c. Further reloading and unloading along curves d and e has been achieved several times without appreciable deviation. The question now arises as to what pressure measurements are recorded by the pressure gage. Inasmuch as the gage experiences only the thrust that the metal exerts on the pin, it must be concluded that the straight-line calibration is approximately applicable for determination of the wall pressure. Since a metal does not flow plastically until a critical stress is exceeded it must, therefore, also be concluded that the pressure gage does not respond until the metal is at this particular state of stress. Hill (2) has analyzed the plane-strain problem of a flat punch penetrating a flat metallic surface. Since the gage pin may be thought of as a

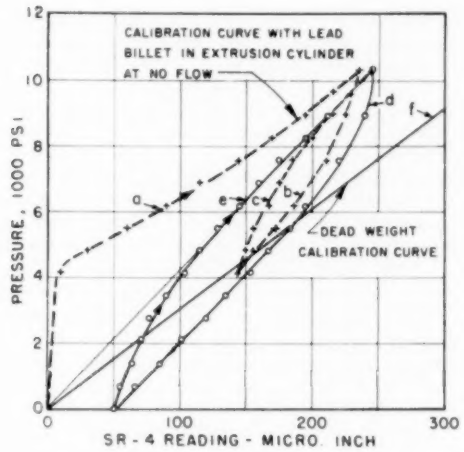

FIG. 12 PRESSURE GAGE CALIBRATION CURVES

flat punch it is evident that the two situations are analogous. He has found that plastic flow will be initiated for a semi-infinite metallic body when the punch pressure becomes approximately $5k$, where k is the critical shear stress for initiating flow. The critical shear stress for lead is approximately 1000 psi and hence the punch pressure becomes 5000 psi. It may be noted that the gage initially begins to respond at a pressure roughly in agreement with this prediction. Upon further loading and unloading, however, the pressure gage responds differently as pointed out previously. It may be noted that the difference of the ordinate between the curves d and e, giving the appearance of a hysteresis loop, is approximately 2000 psi when measured between the parallel portions of these curves. Also the intercept of these curves on the abscissa corresponds to approximately 2000 psi on the dead-weight calibration curve. These values seem to be in agreement with predictions when based on the previously discussed Lévy-Mises equations as will be shown in the following. If the gage is to respond, metal must flow in the radial direction and displace the pin an infinitesimal amount. Hence the principal strain is in the r direction. The strains in the other two co-ordinate directions are equal and because of constancy of volume equal to one half of the radial strain but opposite in sign. Replacing the strain rates of Equation [3] by infinitesimal principal strains, the shear strains are equal to zero, and the infinitesimal effective strain becomes

$$d\bar{\epsilon} = \frac{2}{3}\sqrt{\frac{d\epsilon_r^2\left(-\frac{1}{2}-1\right)^2 + d\epsilon_r^2\left(+1+\frac{1}{2}\right)^2}{2}} = \frac{2}{3}\,d\epsilon_r \times \frac{3}{2} = d\epsilon_r \quad [9]$$

The effective stress $\bar{\sigma}$ of Equation [4] is equal to the yield stress in tension or equal to

$$\bar{\sigma} = \bar{\sigma}_o \approx 2000 \text{ psi} \quad [10]$$

Substituting Equations [9] and [10] in the plasticity equation

$$d\epsilon_r = \lambda(\sigma_r + p) \quad [11]$$

and rearranging, Equation [11] becomes

$$\frac{d\epsilon_r}{d\bar{\epsilon}} = 1 = \frac{3}{2}\left(\frac{\sigma_r + p}{\bar{\sigma}_o}\right)$$

or

$$\sigma_r + p = \frac{2}{3}\,\bar{\sigma}_o = 1330 \text{ psi} \quad [12]$$

Since σ_r is a compressive stress, Equation [12] states that plastic flow is initiated when the difference between the radial stress and the mean pressure is 1330 psi. Hence, the pressure gage will record a pressure p_m, which is 1330 psi smaller than p upon loading but by the same amount greater when unloading. It may be seen that the difference in the curves d and e of Fig. 12 are in qualitative agreement with this prediction. The fact that the slope of the curves d and e are not constant and differ from the dead-weight calibration curves may be attributed to friction between the gage pin and chamber wall when some lead is extruded into the clearance space and possibly due to a rate of loading effect. The exact causes have not been determined, but further experiments are underway and results will be reported when they become available.

A choice must now be made as to which calibration curve should be used in estimating the mean pressure p. When first loading the billet, Hill's criterion appears in approximate agreement with the observations as given by curve a. However, at the beginning of the test the applied load must first expand the billet to fill the chamber; it is evident, therefore, that the gage will not respond at once. If this expansion has been accomplished, however, the gage will upon loading appear to follow the curve a. Since the billet has completely filled the chamber during a steady-state extrusion process, it appears that curve e is the more likely curve which measures the mean pressure, since it is also in substantial agreement with the Lévy-Mises equations.

For the present it was, therefore, decided to use curve e, as the most probable calibration curve in estimating the mean pressure p. Fig. 13 accordingly shows the mean pressures for a gage position of 0.4 in. from the die as a function of extrusion rate. It is seen that the mean pressure rises roughly linearly with extrusion speed and that the ratio of average pressure to mean pressure is again constant. The calculated pressure from the stress analysis, as shown in Fig. 5, has been included and appears to be in substantial agreement with the measured pressure, if the foregoing choice of gage calibration curve is accepted as reasonable.

CONCLUSIONS

1 The flow patterns on the meridian plane of a lead billet extruded into a 1.5-in-diam solid bar with an 8.2/1 reduction ratio at room temperature were identical for rates of 0.1, 0.74, and 5.15 ipm.

2 The wall pressure, as measured by a pressure gage, increased almost linearly with the extrusion rate. The applied load increased in a similar manner, such that the ratio of average extrusion load per unit area to the wall pressure remained constant.

3 The mean pressure within the metal cannot be recorded by a simple wall pressure gage whose response depends on elastic deformation of a pressure-sensitive element.

4 It was shown that the difference in the mean pressure in the metal and the pressure recorded by the gage differ by the magnitude of a critical flow stress.

5 The mean pressure calculated from a stress analysis using the experimental flow pattern agrees approximately with the measured mean pressure.

ACKNOWLEDGMENTS

The authors wish to thank the University of California for the use of the facilities and providing research grants for the investigation, as well as the Division of Mechanical Engineering for pre-

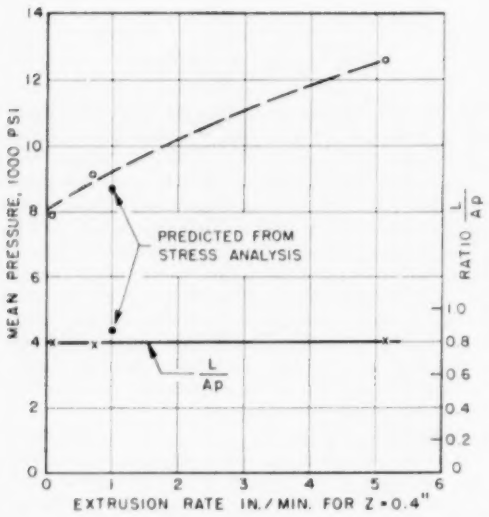

FIG. 13 PREDICTED AND EXPERIMENTAL VALUES OF MEAN PRESSURES AND PRESSURE RATIOS AS FUNCTIONS OF EXTRUSION RATE (Distance between pressure gage and die is 0.4 in.)

paring the lead billets in its shop facilities. They also wish to thank Mr. C. Lockrem, Senior Mechanician of the Production Laboratory, for the valuable aid rendered and the numerous constructive suggestions offered during the experimental phase of the work.

BIBLIOGRAPHY

1 "Über einige statisch bestimmte Fälle des Gleichgewichts in Plastischen Körpern," by H. Hencky, *Zeitschrift für Angewandte Mathematik und Mechanik*, vol. 3, 1923, p. 241.

2 "The Mathematical Theory of Plasticity," by R. Hill, Clarendon Press, Oxford, England, 1950.

3 "The Theoretical Analysis of Metal-Forming Problems in Plane Strain," by E. H. Lee, *Journal of Applied Mechanics*, Trans. ASME, vol. 74, 1952, pp. 97–103.

4 "Plastic Flow in a Lead Extrusion," by C. T. Yang and E. G. Thomsen, Trans. ASME, vol. 75, 1953, pp. 575–579.

5 "Experimental Stress Determination Within a Metal," by E. G. Thomsen and J. T. Lapsley, Jr., SESA Paper No. 235, presented in New York, N. Y., December, 1952.

6 "An Experimental Investigation of the Mechanics of Plastic Deformation of Metals" in three parts: "Visualization of Plastic Flow," by J. B. Bierbower and E. G. Thomsen, part 1; "Strain Analysis," by E. G. Thomsen and C. T. Yang, part 2; "Stress Analysis," by E. G. Thomsen and C. T. Yang, part 3; University of California, Berkeley, Calif. (to be published).

Discussion

C. T. YANG.[4] The authors state in their "Results and Discussion" of the paper that the axial load and extrusion pressure increase approximately linearly with the extrusion rate. This is not quite so. Pearson[5] did extensive investigation on the same problem with different materials. For pure lead he found the relationship between the extrusion pressure and extrusion speed is as follows:

$$p = 4v^{1/m}$$

where p is the extrusion pressure in tons per sq in., and v is the extrusion rate in ipm.

Therefore the relationship of extrusion pressure and rate is not linear. However, the range of the extrusion speed Pearson used in his experiment was much higher than that with which the authors worked. The deviation might be due to the thermal effect.

From the effective stress and effective strain-rate relationship, $\bar{\sigma} = \bar{\sigma}_o + m\dot{\epsilon}$, it is clear that the work material has a strain-hardening effect. Thereby Equation [10] of the paper, $\bar{\sigma} = \bar{\sigma}_o =$ 2000 psi, holds only at the yielding point. So with Equation [12] $\sigma_r + p = 1330$ which is true at yielding only.

The writer fails to see that the gage pin can be considered analogous to a flat punch. The problem is more nearly similar to extrusion than to a flat punch, because lead comes out (at least tends to) of the chamber into the gage tube against the gage pin. It is not the case that the pin goes into the chamber and makes a depression on the lead. These two cases are completely different.

Hill found in lead extrusion with a 50 per cent reduction the relationship, $p = 1.29Y$, holds, where P = extrusion pressure and Y = yielding compressive stress. Now in the authors' work the gage-pin hole is very small in comparison with the billet size, in other words, the percentage reduction is extremely high, thereby the value 1.29 in the foregoing equation is not true any more. It must be much higher.

AUTHORS' CLOSURE

The authors wish to thank Professor Yang for the discussion submitted to their paper but do not fully agree with the various conclusions drawn by him.

The authors have consulted Pearson's work with lead extrusions and were aware of the fact that an apparent power law exists between average extrusion pressure and extrusion speed. Inasmuch as the range of speeds in Pearson's tests were considerably above the highest speed of 5 ipm employed in the present investigation it was felt that a direct comparison was inadvisable.

The relationship given in Equation [5] was interpreted incorrectly by Professor Yang since it gives an approximate relationship between stress and strain rate and not between stress and total strain. Thus $\bar{\sigma}_o$ of Equation [5] is an equivalent flow stress at zero strain rate and therefore the argument presented by Professor Yang is invalid.

In view of the fact that the elastic deformation of the gage pin is due to a displacement of lead into the gage-pin hole of less than 0.0005 in., it is felt it cannot be interpreted as an extrusion process. This view is further strengthened by the fact that the displaced lead is subjected to a compressive load, a condition which is not encountered during normal extrusion processes. Hence the authors' use of the flat-punch analogy appears to be more valid than that of an extrusion analogy.

[4] Assistant Professor of Mechanical Engineering, Massachusetts Institute of Technology, Cambridge, Mass.

[5] "The Extrusion of Metals," by C. E. Pearson, John Wiley & Sons, Inc., New York, N. Y., 1944.

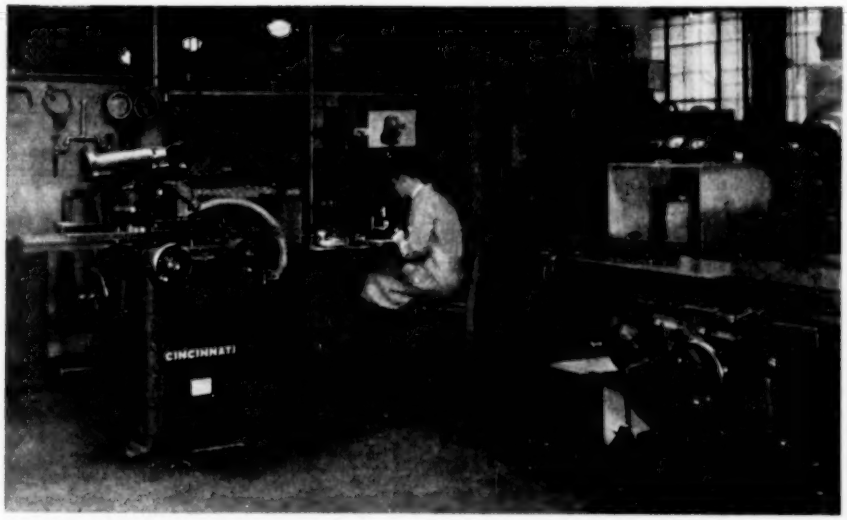

FIG. 1 GENERAL VIEW OF THE EQUIPMENT USED IN THE MILLING OF CAST-IRON TESTS

(Cutter grinder is at left, desk with inspection and wear-measuring microscopes in the center, and wattmeter, profilometer, and milling machine at right. A typical unmachined bar of cast iron is shown on table of machine.)

Cutter Life for Face-Milling Cast Iron

BY W. W. GILBERT,[1] O. W. BOSTON,[2] AND H. J. SIEKMANN[3]

This is a second paper[4] to give the results of a series of tests to face-mill a variety of metals with cutters of various materials. The work was sponsored by the War Production Board under the auspices of the Office of Production Research and Development, through the Manufacturing Engineering Committee of The American Society of Mechanical Engineers. A great deal of data was obtained which, as yet, has not been published. An extensive series of tool-life and power tests were made under controlled laboratory conditions, to evaluate the capacity of sintered-carbide, cast nonferrous metal, and high-speed-steel face-milling cutters when milling several classes of cast iron. The variables reported here consist of the following: Grade of cast iron, tool material, feed, depth, width of bar, number of teeth in cutter, and the cutting speed. The effect of each variable was evaluated by making tool-life tests at several speeds to obtain cutting-speed tool-life curves ($VT^n = C$). All of these variables are finally summarized in a nomograph which shows the importance of each variable and predicts the tool life.

[1] Professor of Production Engineering, University of Michigan, Ann Arbor, Mich. Mem. ASME.

[2] Professor of Mechanical and Production Engineering, and Chairman, Department of Production Engineering, University of Michigan. Fellow, ASME.

[3] Engineer, Carboloy Department, General Electric Company, Detroit, Mich. Assoc. Mem. ASME.

[4] The First Paper, "Power Required by Carbide-Tipped Face-Milling Cutters," by W. W. Gilbert, O. W. Boston, and H. J. Siekmann, Trans. ASME, vol. 75, 1953, pp. 1087–1093.

Contributed by the Research Committee on Metal Processing and presented at the Annual Meeting, New York, N. Y., Nov. 29–Dec. 4, 1953, of THE AMERICAN SOCIETY OF MECHANICAL ENGINEERS.

CONDITIONS OF TESTS

IN these tests a No. 5 HM Kearney and Trecker Corporation, knee-type horizontal milling machine was used. It has a 20-hp-motor which drives the spindle, and a 5-hp motor to provide the feed and rapid traverse to the table. A number of types of face-milling cutters were used providing different cutting-tool materials and different effective diameters of the cutters. Most of the work, however, was done with a 9-in-diam face-milling cutter using only one inserted blade. The 4-in-wide and 18-in-long cast-iron bars were mounted on a rigid fixture and were held on the center line of the cutter as shown in Fig. 1. The nomenclature and angles of a sintered-carbide and a high-speed steel tooth are shown in Fig. 1(*a*).

A recording wattmeter was attached to the 20-hp driving motor to determine the gross horsepower, hp_g, as developed under full cut, and the tare horsepower, hp_t, as developed by the machine running with speed and feed gears engaged but not cutting the work. The net horsepower, hp_n, was obtained by subtracting the tare horsepower from the gross. The wear on the flank of the tool was measured either by a microscope provided with a Filar micrometer eyepiece, or by a toolmaker's microscope. The cutters were run until a flank wear of 0.030 in. below the side cutting edge was obtained. When this wear occurred, the net power had increased about 100 per cent and the tool was considered failed. This same procedure was used for determining the life of cutters of high-speed steel and cast nonferrous metals.

The machining time required to produce this 0.030-in. wear was

NOTE: Statements and opinions advanced in papers are to be understood as individual expressions of their authors and not those of the Society. Manuscript received at ASME Headquarters, October 8, 1953. Paper No. 53—A-149.

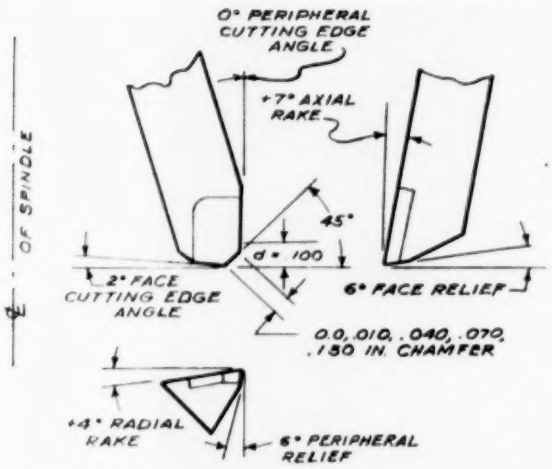

FIG. 1(a) NOMENCLATURE OF SINGLE TOOTH OF FACE-MILLING CUTTER WITH FORM DESIGNATION

(Angles shown were used on all tool materials in all tests unless otherwise specified.)

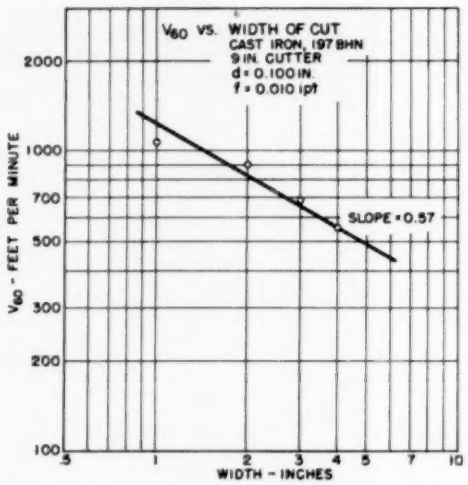

FIG. 3 RELATIONSHIP BETWEEN CUTTING SPEED FOR 60-MIN TOOL LIFE, V_{60}, AND WIDTH OF CUT WHEN FACE-MILLING CAST IRON OF 197 BHN WITH A SINGLE CARBIDE-TIPPED TOOTH CUTTER FOR CONDITIONS SHOWN

obtained by stopping the test periodically to measure the wear, and plotting the results to determine the exact time of failure. Although the rate of flank wear was slower during the first part of the life of high-speed-steel tools, the 0.030-in. flank wear method was found to be a reliable index of tool life.

In each series of tests involving a single variable, a relationship was determined between the cutting speed and tool life. The tool life for several cutting speeds was plotted on log-log paper so that the equation $VT^n = C$ could be determined. All of the tool-life data was analyzed and reduced to a basis of cutting speed for a 60-min tool life, V_{60}. It is presented so that V_{60} can be read from the several charts for any of the cutting conditions.

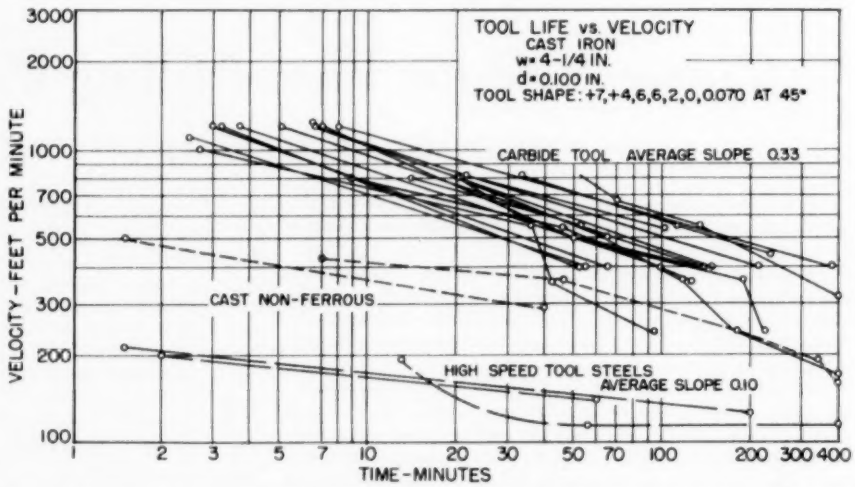
TOOL LIFE VS. VELOCITY
CAST IRON
w = 4-1/4 IN.
d = 0.100 IN.
TOOL SHAPE: +7, +4, 6, 6, 2, 0, 0.070 AT 45°
CARBIDE TOOL AVERAGE SLOPE 0.33
CAST NON-FERROUS
HIGH SPEED TOOL STEELS
AVERAGE SLOPE 0.10
VELOCITY - FEET PER MINUTE
TIME - MINUTES

FIG. 2 RESULTS OF CUTTING-SPEED TOOL LIFE TESTS WHEN FACE-MILLING SEVERAL CAST IRONS OF VARIOUS STRENGTHS WITH SINTERED CARBIDE, CAST NONFERROUS METAL, AND HIGH-SPEED STEEL TOOLS

(Width of cut, 4¼ in.; depth, 0.100 in.; feed 0.010 ipt. A single-tooth cutter was used with shape shown in figure for all tool materials.)

RESULTS OF TESTS

Effect of Cutting Speed and Tool Material. Fig. 2 shows the results of cutting-speed-tool-life tests when machining a variety of cast irons with several tool materials of the shape indicated in Fig. 1(a). All tests were made using a width of cut of 4¼ in., a depth of 0.100 in., and a feed per tooth of 0.010 in. The sintered-carbide grades of tools tested were "Carboloy 55A, 44A, 883, and 905," and "Kennametal K28." The cutting speed for a 60-min tool life, V_{60}, which is used as the criterion of machinability, averaged 530 fpm. The tool-life-cutting-speed equation was $VT^{0.33} = 1800$ when cutting the 40,000-psi "Meehanite" cast iron with these sintered-carbide tools.

The cast nonferrous metal tools, "Crobalt 138" and "Rexalloy," had a cutting speed V_{60}, of 300 fpm and a tool-life equation of $VT^{0.17} = 550$ when face-milling the 40,000-psi cast iron as shown by the two short-dashed lines in the center of Fig. 2.

The 6-6 molybdenum high-speed-steel tools were tested by face-milling 20,000 and 40,000-psi cast iron and the resulting tool-life curves, shown at the bottom of Fig. 2, indicated a cutting speed V_{60} of 120 to 150 fpm and an average tool-life equation of $VT^{0.1} = 220$. The relative cutting speeds for the three tool materials were approximately 1 for high-speed steel, 2 for cast nonferrous, and 4 for sintered-carbide tools.

Nine grades of cast irons were face-milled with the K28 and 44A sintered-carbide tools as shown in the top of Fig. 2. These cast irons varied from a low strength 20,000 psi, 143 Bhn, cast

iron which had a cutting speed V_{60} of 680 fpm, to a high-strength alloyed cast iron with 50,000 psi, 229 Bhn, which had a cutting speed V_{60}, of 390 fpm. (The hardness of the metals as influencing the tool life is discussed further in connection with Fig. 5.)

Effect of Width of Cut. Doubling the width of cut reduced the cutting speed V_{60} 32 per cent, when all other factors of face-milling were kept constant, as shown in Fig. 3. The equation for the effect when using sintered-carbide tools was

$$V_{60}w^{0.57} = 1250$$

where w = width of cut, in.

These data were plotted in Fig. 4 to show the effect of width of cut on the "cubic inches of metal removed per tool grind." If a 60-min tool life were desired, the 4-in-wide bar could be cut at 550 fpm and a total of 56 cu in. of metal removed as shown in Table 1. If the width of bar was decreased to 1 in., the cutting speed could be increased to 1070 fpm but only 26 cu in. of metal would be removed. This indicated that a larger volume of metal can be removed when cutting wider bars even though the cutting speed must be reduced to keep the tool life constant.

TABLE 1 EFFECT OF WIDTH OF BAR ON METAL REMOVAL

(Face-milling "Meehanite" cast iron, 197 Bhn, with a 9-in-diam single-tooth carbide-tipped face-milling cutter using a depth of cut of 0.100 in. and a feed of 0.010 ipt.)

Width of bar in., w	Cutting speed for 60-min life, V_{60}	Cu in. per grind T = 60 min	Cutting speed for 100 cu in. per grind
1	1070 (1250)[a]	27	690
2	890 (830)	45	680
3	680 (660)	52	520
4	550 (550)	56	460

[a] From line in Fig. 3.

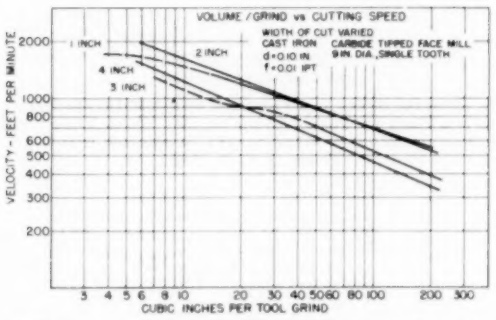

FIG. 4 RELATIONSHIP BETWEEN CUTTING SPEED AND CUBIC INCHES OF METAL REMOVED PER TOOL GRIND FOR FOUR SPECIFIC WIDTHS OF CUT

$$\text{Cu in. per grind} = Twdf \text{ no } N = \frac{Twdf \text{ no } 12v}{\pi D}$$

For a 4-in-width of bar, a tool life of 60 min, a depth of 0.100 in., and a feed of 0.010 ipt, the cutting speed was 550 fpm with the single-tooth 9-in-diam face-milling cutter. The volume of metal removed was

$$\text{Cu in. per grind} = \frac{60 \times 4 \times 0.1 \times 0.01 \times 1 \times 12 \times 550}{\pi 9} = 56$$

If it is desired to remove a definite volume of metal, then the cutting speed must be reduced as the bar width increases, as shown in Table 1. Increasing the bar width from 1 to 4 in. required that the cutting speed be reduced from 690 to 460 fpm when removing 100 cubic inches of metal.

Effect of Brinell Hardness. Increasing the Brinell hardness reduces the cutting speed significantly. The scattered results of tests are shown in Fig. 5. The equation of the straight line drawn to represent the relation of Brinell hardness to the cutting speed for a 60-min tool life is

$$V_{60}\,\text{Bhn}^{1.32} = \text{const}$$

where Bhn = Brinell hardness number.

The value of V_{60} is generally reduced as the hardness is increased. A 33 per cent increase in Brinell hardness caused a 32 per cent decrease in cutting speed for the 60-min tool life. The majority of these data was obtained using sintered-carbide cutting tools, but the indications are that the same slope was applicable to high-speed-steel cutters as well.

Effect of Number of Teeth. Increasing the number of teeth in a face-milling cutting requires a slight reduction in the cutting speed to maintain the same tool life but increases the rate of

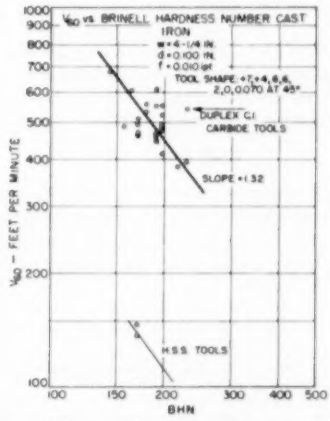

FIG. 5 VALUES OF V_{60} AS A FUNCTION OF BRINELL HARDNESS NUMBER WHEN FACE-MILLING VARIETY OF CAST IRONS UNDER CONDITIONS SHOWN

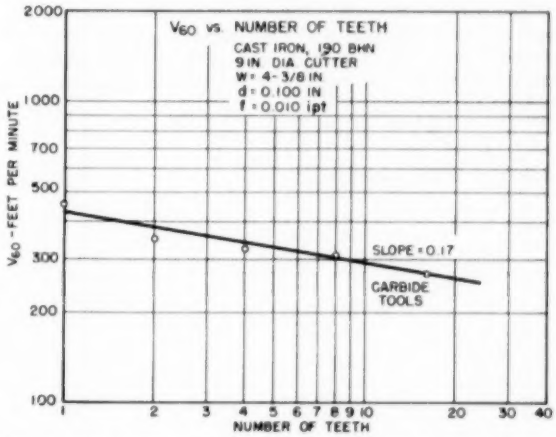

FIG. 6 RELATIONSHIP OF V_{60} TO NUMBER OF CARBIDE-TIPPED TEETH IN 9-IN-DIAM FACE-MILLING CUTTER WHEN MILLING CAST IRON OF 190 BHN

metal removed. Stated in another way, for a constant feed per tooth and a constant speed, doubling the number of teeth will reduce the cutter life, as shown in Fig. 6. A relation between the number of teeth and V_{60} may be expressed by the following equation for the conditions in Fig. 6

$$V_{60}\,no^{0.17} = 430$$

where no = number of teeth in the cutter.

The more teeth used, the higher the rate of metal removal as shown in Table 2, where the cu in. per grind was increased from 50.5 to 484 by changing from 1 to 16 teeth. This is the principal advantage of using cutters with more teeth.

TABLE 2 EFFECT OF NUMBER OF TEETH ON RATE OF METAL REMOVED

(Face-milling 4½-in-wide "Meehanite" cast iron, 190 Bhn, with a 9-in-diam face-milling cutter with sintered-carbide-tipped teeth. Depth 0.100 in., feed 0.010 ipt.)

No. of teeth, no	Cutting speed for 60-min life, V_{60}	Cu in. per grind at V_{60}	Cu in. per min at V_{60}
1	450 (430)[a]	50.5	0.84
2	350 (385)	78	1.30
4	325 (345)	130	2.16
8	310 (305)	278	4.63
16	270 (270)	484	8.10

[a] Values taken from the curve of Fig. 6.

Effect of Depth of Cut. There is little change in tool life but a definite increase in rate of metal removed because of an increase in depth of cut as shown in Fig. 7. The tests showed that the following equation represents the relation

$$V_{60}d^{0.08} = \text{const}$$

where d = depth of cut, in.

These data are plotted in Fig. 8 to show cutting speed versus cubic inches removed per grind, for each of four depths of cut. A relation between the depth of cut V_{60} and the cubic inches per grind is given in Table 3.

TABLE 3 EFFECT OF DEPTH OF CUT ON CUTTING SPEED AND RATE OF METAL REMOVAL

(Face-milling 4½-in-wide, 190 Bhn "Meehanite" cast iron with 9-in-diam single-tooth carbide-tipped cutter. Depth of cut 0.100 in., feed 0.010 ipt.)

Depth of cut, in., d	Cutting speed for 60-min life, V_{60}	Cu in. per grind at V_{60}	Cu in. per min at V_{60}
0.025	540	15	0.25
0.050	515	29	0.48
0.100	480	54	0.90
0.200	460	103	1.72

Effect of Feed Per Tooth. The effect of increasing the feed per tooth is to reduce slightly the cutting speed V_{60}, as the feed is increased, but the rate of metal removal is decidedly increased, as shown in Table 4. The results in Fig. 9 show the relationship of feed and V_{60} as follows:

$$V_{60}f^{0.16} = \text{const}$$

where f = feed per tooth, in

TABLE 4 EFFECT OF FEED PER TOOTH ON RATE OF METAL REMOVAL

(Face-milling 4½-in-wide, 190 Bhn, "Meehanite" cast iron with a single-tooth 9-in-diam carbide-tipped face-milling cutter using a depth of cut of 0.100 in.)

Feed, in. per tooth, f	Cutting speed for 60-min life from tests	Cu in. per grind at V_{60}	Cu in. per min at V_{60}
0.0025	770	21.5	0.36
0.005	690	38	0.63
0.010	610	67	1.12
0.020	550	122	2.05
0.030	520	170	2.85

NOTE: $V_{60}f^{0.16}$ = const.

Table 4 shows that when the feed is increased from 0.0025 to 0.030 ipt it is necessary to decrease the cutting speed only from 770 fpm to 520 fpm, keeping the tool life constant at 60 min. Even though the cutting speed is reduced, the cubic inches per grind are increased from 21.5 to 170 for this feed increase of 0.0025 to 0.030 ipt, Fig. 10. This is one of the most important methods of increasing the rate of metal cutting. The largest feed gives the highest rate of metal removal, the upper limit of feed being governed by the chipping of the carbide teeth which is a function of the rigidity of the setup. In these particular tests, feeds of more than 0.020 ipt often caused chipping. Larger values of feed usually cause rougher surface finish but this objection can be overcome either by special cutter designs or by care in cutter grinding.

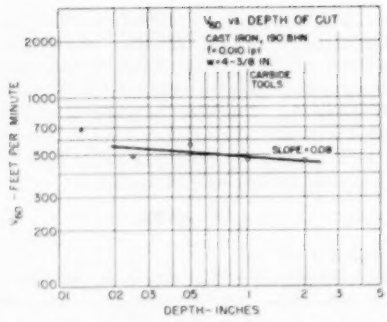

FIG. 7 RELATIONSHIP OF V_{60} TO DEPTH OF CUT WHEN FACE-MILLING CAST IRON WITH SINTERED-CARBIDE, SINGLE-TOOTH 9-IN-DIAM FACE MILL

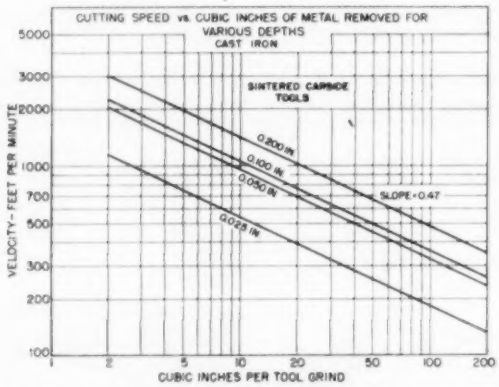
CUTTING SPEED vs. CUBIC INCHES OF METAL REMOVED FOR VARIOUS DEPTHS CAST IRON
SINTERED CARBIDE TOOLS
0.200 IN.
0.100 IN.
0.050 IN.
0.025 IN.
SLOPE = 0.47
VELOCITY - FEET PER MINUTE
CUBIC INCHES PER TOOL GRIND

FIG. 8 CUTTING SPEED AS A FUNCTION OF CUBIC INCHES PER TOOL GRIND FOR EACH OF FOUR DEPTHS OF CUT WHEN FACE-MILLING CAST IRON OF 190 BHN WITH SINGLE SINTERED-CARBIDE-TIPPED TOOTH IN FACE MILL

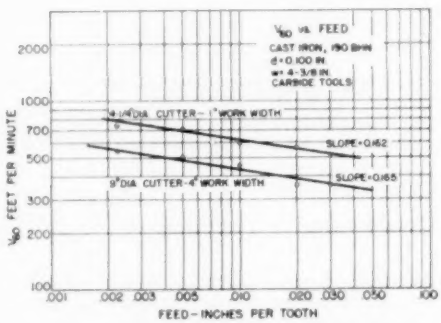
V_{60} vs. FEED
CAST IRON, 190 BHN
d = 0.100 IN.
w = 4-3/8 IN.
CARBIDE TOOLS
9" DIA CUTTER - 1" WORK WIDTH
SLOPE = 0.62
9" DIA CUTTER - 4" WORK WIDTH
SLOPE = 0.65
V_{60} - FEET PER MINUTE
FEED - INCHES PER TOOTH

FIG. 9 VALUES OF V_{60} AS A FUNCTION OF FEED PER TOOTH OF TWO FACE MILLS OF DIFFERENT DIAMETERS WHEN MACHINING CAST IRON OF 190 BHN

(A single carbide-tipped tooth was used in each cutter.)

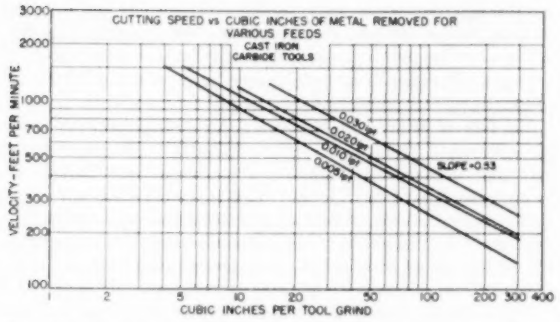
CUTTING SPEED vs CUBIC INCHES OF METAL REMOVED FOR VARIOUS FEEDS
CAST IRON
CARBIDE TOOLS
VELOCITY - FEET PER MINUTE
CUBIC INCHES PER TOOL GRIND
SLOPE = 0.53

FIG. 10 VALUES OF CUTTING SPEED AS A FUNCTION OF CUBIC INCHES PER TOOL GRIND FOR EACH OF FOUR VALUES OF FEED PER TOOTH WHEN FACE-MILLING CAST IRON OF 190 BHN
(Cutter had a single carbide-tipped tooth.)

Diameter of Cutter. The actual time of cutting T_A is smaller than the machine operating time T_M and is a function of the relative values of the bar width w and the cutter diameter D

$$\frac{T_A}{T_M} = \frac{\theta}{360}$$

where $\sin \theta/2 = w/D$, and θ = angle of contact of cutter and work in degrees.

Most of the tests reviewed in this paper were made when cutting $4^1/_4$-in-wide bars with 9-in-diam cutters, Fig. 9. This is taken as the standard condition with $w/D = 0.47$ and $T_A/T_M = 0.156$. When larger bars are face-milled and the w/D ratio increases the T_A/T_M also increases as shown in Table 5. The effect of this increase in T_A is to decrease the cutting speed. The equation $VT^{0.33} = C$ is used to compute the necessary cutting-speed reduction shown in Table 5. The cutting speeds indicated on the

TABLE 5 CUTTING-SPEED MULTIPLIERS FOR w/D RATIOS

w/D	Contact angle, θ	$\frac{T_A}{T_M}$	w/D Cutting-speed multiplier
1.0	180	0.5	0.68
0.8	106	0.295	0.81
0.6	74	0.205	0.915
0.5	60	0.166	0.98
0.47	56	0.156	1.00
0.4	47	0.130	1.03
0.3	35	0.098	1.17
0.2	23	0.064	1.34
0.1	11.5	0.032	1.69

nomograph should be multiplied by the "w/D cutting-speed multiplier" in Table 5 to determine the correct operating speed.

The Nomograph. The effect of each variable has been shown independently but these all can be represented collectively by

$$VT^n f^a d^b w^c \text{no}^x \text{Bhn}^y = C_1 \quad \ldots\ldots[1]$$

where no = number of teeth in cutter

$$\text{Since } T = \frac{\text{cu in. per tool grind} \times \pi D}{12 V f \text{ no } wd}$$

Equation 1 also may be stated as

$$V \text{ (cu in. per grind)}^{\frac{n}{1-n}} f^{\frac{a}{1-n}} d^{\frac{b}{1-n}} w^{\frac{c}{1-n}} \text{no}^{\frac{x}{1-n}} \text{Bhn}^{\frac{y}{1-n}} = C_2 \quad \ldots\ldots[2]$$

The average exponents of Equation [1] have been presented individually and, for carbide-tipped face-milling cutters milling cast iron, give the equation

$$VT^{0.33} f^{0.16} d^{0.06} w^{0.57} \text{no}^{0.17} \text{Bhn}^{1.32} = 1.9 \times 10^8 \quad \ldots\ldots[3]$$

When it is desired to use this equation in the form of Equation [2] it becomes

$$V \text{ (cu in. per grind)}^{0.49} f^{0.24} d^{0.12} w^{0.86} \text{no}^{0.26} \text{Bhn}^{1.97} = 9.12 \times 10^7 \quad \ldots\ldots[4]$$

This equation may be used for high-speed-steel cutters with

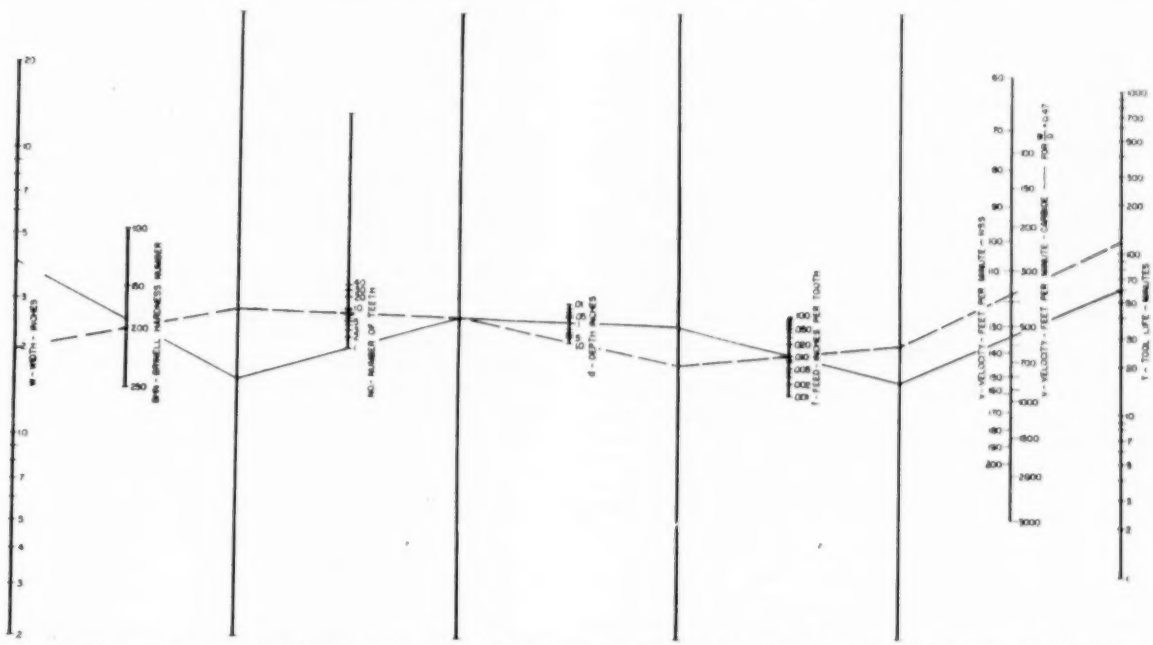
W - WIDTH - INCHES
BHN - BRINELL HARDNESS NUMBER
NO - NUMBER OF TEETH
d - DEPTH INCHES
f - FEED - INCHES PER TOOTH
v - VELOCITY - FEET PER MINUTE - HSS
v - VELOCITY - FEET PER MINUTE - CARBIDE
T - TOOL LIFE - MINUTES

FIG. 11 NOMOGRAPH FOR FACE-MILLING A CAST IRON WITH SINTERED-CARBIDE AND HIGH-SPEED-STEEL CUTTERS TO CO-ORDINATE WIDTH OF CUT, BRINELL HARDNESS OF THE CAST IRON, NUMBER OF TEETH IN THE CUTTER, DEPTH OF CUT, FEED PER TOOTH, CUTTING SPEED, AND TOOL LIFE

fair accuracy by changing the relation between cutting speed and tool life as shown in Fig. 2.

The nomograph, Fig. 11, is based on Equation [3] to show graphically the relation between each variable and the solution of any problem by drawing five straight lines.

An example of the use of the nomograph is the determination shown in heavy dashed lines of the desired cutting speed when face-milling 2-in-wide bars of cast iron of 200 Bhn, using an 8-tooth, 6-in-diam cutter with a feed of 0.010 ipt, and a depth of cut of $^3/_4$ in. If a tool life of 2 hr is desired the cutting speed would be 370 fpm as indicated in Fig. 11. If it were desired to change the tool life to 8 hr (480 min) the cutting speed should be reduced to 230 fpm. Using Equation [3] this problem could be solved as

$$V = \frac{1.9 \times 10^6}{T^{0.33} f^{0.16} d^{0.08} w^{0.57} n o^{0.17} \text{Bhn}^{1.32}}$$

$$V = \frac{1.9 \times 10^6}{120^{0.33} \times 0.010^{0.16} \times 0.75^{0.08} \times 2^{0.57} \times 8^{0.17} \times 200^{1.32}}$$

$$V = \frac{1.9 \times 10^6}{4.85 \times 0.479 \times 0.977 \times 1.485 \times 1.415 \times 1120}$$

$V = 356$ fpm compared to 370 determined from the nomograph

The solid line in Fig. 11 represents a second example in which a 6 Mo 6 W type of high-speed-steel blade was used in the face-milling cutter. The 4-in. width of bar of cast iron of 190 Bhn was machined with a single-tooth 9-in-diam cutter, with depth of cut of 0.100 in., a feed of 0.010 in. ipt. For a 60-min tool life the cutting speed is shown to be 134 fpm.

Caution. The data and the nomograph are based on closely controlled test conditions and probably represent "better than average" shop conditions. It is known, however, that better tool shapes, improved grades of carbide, and better cutter bodies may result in longer tool life. On the other hand, if scale is present on the cast bars, or the rigidity is not so good as used in these tests, there will be a decrease in tool life.

Acknowledgments

This work is part of an extensive investigation on the milling of various cast irons and cast steels with cutters of sintered carbide, cast nonferrous metal, and high-speed steel. This work was done in the Department of Production Engineering, University of Michigan, as an Engineering Research Project. Many of these data have never been published and for this reason are being collected and analyzed to give general results of use to industry.

Walter Noffke, now with Air Reduction Corporation, did much of the experimental and analytical work. H. J. Siekmann and C. H. Good analyzed and further correlated the data, as student assistants on a Graduate School, Faculty Research Fund. Both are now with the Carboloy Department of General Electric Co.

Discussion

Hans Ernst.[8] This paper is a welcome addition to the one presented in December, 1952, by the same authors and covering other aspects of the data gathered in the carbide-milling investigation of 1944–1945. Restudies of old data, such as these, in the light of present knowledge, often lead to the discovery of new facts.

One fact of interest presented by the authors appears under the subheading "Effect of Number of Teeth." Here it is stated that the "cubic in. per grind was increased from 50.5 to 484 by changing from 1 to 16 teeth. This is the principal advantage of using cutters with more teeth." Actually, these figures disclose the fact (which also has been observed by others) that cutters appear to become less effective, in terms of cubic inches per grind, as the number of teeth is increased. If each tooth of the 16-tooth cutter had removed as much metal per grind as the one tooth of the single-tooth cutter, the former would have removed 16×50.5, or 808 cu in. instead of only 484.

No satisfactory explanation has yet been presented for this finding. It may be speculated that, as the number of teeth in a cutter is increased (for a given cutting speed), the time between successive tooth contacts is decreased; hence the temperature of the metal engaged by each tooth is higher. This would result in a somewhat higher temperature at the chip-tooth interface and possibly therefore a higher rate of wear. It also may be speculated that, with a single-tooth cutter, any vibration of the workpiece excited by the engagement of the cutter tooth and work would have had time to die out before the tooth again entered, while in the case of a multitooth cutter a vibration excited by any tooth might be sustained or reinforced by succeeding teeth.

It has been observed that high-frequency vibration, at even low energy levels, may decrease cutter life appreciably. A careful investigation should be made to remove this question from the realm of speculation.

Authors' Closure

The authors are grateful, indeed, to Mr. Ernst for his comments on this paper. His analysis of the effect of multiple-tooth face milling agrees with those of the authors in that we do not, at this time, clearly understand the reason for the reduced life per tooth as the number of teeth are increased in a face-milling cutter. It may be vibration caused by several teeth cutting simultaneously, or with others entering and leaving the work, causing a shock, or it may be a temperature effect. The latter doesn't seem to be so logical as the former as most of the heat of cutting is removed in the chip, rather than being left in the work. This theory might, however, apply to the use of cutting fluids in face milling with carbide tools, as we have also found that when cutting dry the life is longest. When cutting with an oil, it is slightly shorter, and when cutting with a more severe coolant, such as an emulsion, it is still shorter. This appears to be a case of thermal shock.

I am sure that Mr. Ernst, as well as the authors, have in mind the continuation of these studies, with the hope that eventually these, and many other points of metal cutting, may be more clearly understood.

[8] Director of Research, The Cincinnati Milling Machine Company, Cincinnati, Ohio. Fellow ASME.

Measurement of Stresses Imposed on Wheels in Diesel-Locomotive Service

By L. L. OLSON,[1] CHICAGO, ILL.

The dieselization of railroads has been accompanied by many reports of locomotive-wheel failures. Laboratory tests by wheel manufacturers have been helpful but inadequate, since actual operating conditions were not duplicated. This paper describes a test program, now in its preliminary stages, which will undertake to secure necessary data. The objectives, test procedures, and instrumentation of the proposed program are outlined.

Introduction

THE extensive dieselization program being carried on by the railroads has reached a point where wheel failures in this type of service have indicated the desirability of obtaining data on the service stresses they encounter. These failures are different from wheel failures which have been experienced previously in other types of service and generally are characterized by (1) progressive shattering of rims (oyster-shell fractures), (2) progressive failures occurring through stamping on the rims, and (3) circumferential plate fractures. While the incidence of these failures is low, the occurrence of these types of failures in sufficient numbers has led to the implication that when operating under actual service conditions, diesel locomotives may produce service stresses that are different from those which would be anticipated from the knowledge of weight and other recognized characteristics of this type of equipment.

Laboratory tests carried on by the wheel manufacturers have yielded valuable data but thus far have proved inadequate in so far as being able to duplicate conditions experienced in actual service, for the simple reason that these conditions are not known. It thus became apparent that tests made on locomotives under field conditions would be necessary to secure the type of data needed for an understanding of the forces and stresses imposed on a diesel wheel. A program designed to secure the data necessary for this understanding has been set up by the Association of American Railroads (AAR). This program is being participated in jointly by the AAR, the Technical Board of the Wrought Steel Wheel Industry, and the Electro-Motive Division of the General Motors Corporation.

At the present time this program is in the preliminary stage and as such, no actual test data has been taken in the field other than data necessary to evaluate the performance of special instrumentation developed for these tests. However, considerable work has been done to advance this program to the point at which techniques of measurement procedure and development of instrumentation will make it possible to secure the type of data desired. This research program has presented many difficulties especially from the measurement standpoint; that is, (1) the determination of what should be measured to give us the necessary data for an accurate understanding of what is happening to the diesel wheel in service, and (2) the development of instrumentation to enable us to make such measurements.

This paper will attempt to give a brief description of the objectives and scope of the research program, the test equipment and instrumentation used, the problems involved in carrying out the program, the solutions to date of such problems, and the work that has been done up to the time this paper was written. Of course it is impossible at this time to draw any conclusions. However, we hope that the information presented herein will be of value to all interested in the subject, if for no other reason than to stimulate thinking along the lines of this test program. It purposely has been made flexible in nature so as to allow deviation from any fixed line of attack, should such deviation be justified by test results.

Objectives and Scope of Research Program

The objectives of this program can be stated as follows:

1 The determination of forces and loads subjected to diesel-locomotive wheels and the resultant stresses and temperatures produced therein under service conditions.

2 The application of the information obtained toward the development of more serviceable and safer diesel-locomotive wheels.

3 Analysis of data to determine whether anything in the operation or design of the locomotive is a contributing factor in the failure of diesel wheels.

To accomplish these objectives it was realized fully that a comprehensive test program would be necessary. Also, since no work has been done up to the present time on dynamic measurement in service of stresses in diesel-locomotive wheels, it was further evident that some amount of exploratory work would be necessary to enable proper placement of strain gages. The test procedure as contemplated will consist of both laboratory and field work. Static loading of a wheel under laboratory conditions has proved to be of definite aid in determining strain-gage location, as will be discussed later in this paper.

In order to obtain the necessary type of data it is planned to make the road-test part of the program comprehensive in nature which will involve measurements over a wide range of operating conditions. Much valuable information can be obtained by placing an instrument test car in a train in regular scheduled service, although it is contemplated that some controlled testing will be necessary to duplicate test conditions and speeds to enable correlation of various test data. Controlled testing as referred to here means testing in which a special train is operated on a definite speed schedule so as to enable runs to be duplicated under the same test conditions.

In outlining an investigation of this type it is not possible to anticipate the exact work involved as to the location and number of test runs. There are several railroads where operating conditions and profile will make it possible to obtain the desired test variables. It will not be difficult to obtain permission from a railroad to make test runs where an instrument car can be placed in a train in regular scheduled service, such as mentioned

[1] Electrical Engineer, Central Research Laboratory, Association of American Railroads—Mechanical Division.

Contributed by the Railroad Division and presented at a joint session of the Railroad Division and the American Society for Testing Materials at the Annual Meeting, New York, N. Y., November 29–December 4, 1953, of The American Society of Mechanical Engineers.

Note: Statements and opinions advanced in papers are to be understood as individual expressions of their authors and not those of the Society. Manuscript received at ASME Headquarters, July 31, 1953. Paper No. 53—A-114.

previously. This will be done in the exploratory phase of the investigation. At the present time it is planned to make test runs that will include the following test conditions and will involve the following measurements:

1 Tests of operating conditions including variables such as grade, track curvatures and elevation, and speed. The amount of any combination of variables, such as grade or curvature and speed, in a specific test will be fixed, of course, by such factors as type of service, whether passenger or freight, locomotive design and speed limitations fixed by the participating railroad. However, it is planned to utilize test sites and operating conditions which will make it possible to include test variables up to a maximum of 3 per cent grade, 10-deg curvature, and 100 mph speed.

2 Measurements on wheels of 36 in., 40 in., and possibly 42 in. diam of the type used in diesel-locomotive road service.

3 Wheel measurements to determine (*a*) stresses due to vertical and lateral loading, (*b*) forces due to torques and stresses resulting from pulling and braking, and (*c*) temperature gradient.

4 Measurements of magnitudes of stresses or loads with particular emphasis on the frequency of occurrence over any given distance of track. Special instrumentation will make it possible to obtain a continuous record, registered on automatic counters.

5 Particular emphasis on measurements of stresses or loads and temperatures imposed on the wheel plate and rim due to (*a*) severe braking such as is encountered when a stop is made from high speed and (*b*) long continued brake applications such as are encountered in controlling the speed of a train down a long grade.

It is realized that any one set of test conditions, such as (*a*) type of locomotive, (*b*) type of wheel, (*c*) track variable, and (*d*) speed, may not give results considered to be of significance. In such cases it would be advisable to devote more time to some other set of test conditions. In other words, this research program is planned to be sufficiently elastic, as mentioned previously, as to allow deviation from any given test procedure should such deviation be justified by test results.

Test Equipment and Instrumentation

A special test car is being used in these tests which carries all of the recording instrumentation. This test car, which is the chassis of a diesel unit, is the property of the Electro-Motive Division of the General Motors Corporation. It contains commercially available instrumentation such as recording oscillograph equipment, temperature and pressure recorders, as well as special instrumentation designed and built by the staff of Electro-Motive. This special instrumentation consists of automatic speed recorders accurate to 0.1 mph, automatic mile-post recorder which eliminates the need for an observer, and automatic counters, which through associated circuits can be energized from the output of strain gages.

These automatic counting circuits are expected to be of considerable value in the test program because running continuously they can record the occurrence of certain magnitudes of the phenomena being measured. For example, if vertical loading of the wheel is being measured, the counters can be set up to respond to values of, say, 5, 10, 15, and 20,000 lb. Thus, regardless of the length of the test run, whether it be 1 mile or 1000 miles, these recorders will count the number of times any one of the selected values of load is reached. Where it is desired to obtain the wave shape of the phenomena being measured, the recording oscillographs can be operated simultaneously with the counters. A further advantage of the counters is that the record is always visible and immediately available. This makes it possible to note and correlate unusually high stresses or loads with track or other instigating factors.

In addition to the measurements made directly off the wheel, lateral forces can be measured by means of a weigh-bar arrangement. This weigh bar is essentially a steel plate to which electric-resistance strain gages are attached and which has been calibrated in a test machine. It is so located as a part of the journal box that movement of the axle due to lateral thrust will result in deflection of the weigh bar. It is expected that the data derived from the use of the weigh bar will provide for some correlation between lateral thrust loads and wheel stresses.

Other features of the EMD test car, certainly important in so far as the test crew are concerned, are the sleeping and eating accomodations. The test car carries two Pullman sections, a shower stall, a small refrigerator, and eating facilities for a crew of four.

Problems of Instrumentation

One of the biggest problems in this research program involved a method for taking a signal from a strain gage located on a revolving wheel and transferring it, free of noise, to the recording equipment located in the test car. Of course, this called for a slip-ring assembly of some sort and the obvious location for such an assembly was some place on the axle. However, an axle location was impossible because it was realized that a very important part of the test program would be necessarily measurements on diesel wheels mounted on driven axles, and the presence of the traction motor did not allow any room for a slip-ring assembly. Therefore the journal box appeared to be a likely spot to house this assembly. In earlier work involving axle-stress measurements, Electro-Motive had utilized a drilled axle through which wire leads from the strain gages on the axle were passed to a mercury slip-ring assembly, especially designed for this purpose, which worked off one end of the axle and was located in the journal box. However, while some measure of success was enjoyed, maintenance of the slip-ring assembly was very difficult and it was subjected to a high level of shock and vibration, which eventually resulted in abandonment of this arrangement. After a considerable period of development work by Electro-Motive, a new slip-ring assembly has been designed which permits the slip ring and brushes to be shock-mounted on the truck frame where they can be maintained easily. Leads from the strain gages on the wheel are passed through a drilled hole in the axle to the end of the journal where, through a gear and flexible-shaft arrangement, the leads and rotation of motion of the axle are transmitted to the slip-ring assembly. This arrangement has been road-tested and thus far has appeared to be satisfactory.

Other problems of major concern involve the use of strain gages on the wheel. It would be a simple matter if a strain gage could be placed on a wheel at random and used to measure strain from which stress in the wheel at that point could be computed. However, unfortunately, it is not that simple, as measured strain multiplied by the modulus of elasticity of steel, except under very special conditions, would not give a value of stress which would be indicative of the true stress-strain relationship existing in the wheel. Without getting too deep in this subject which can easily become very involved, let it suffice to say that in a complex structure such as a wheel, strain in any given direction at the point of location of the strain gage is usually due to stresses acting in other directions as well as in the direction of the measured strain. Under service conditions a wheel is subjected to lateral or thrust as well as vertical forces which may occur simultaneously. Obviously then, considerable discretion has to be exercised in the location of strain gages if we are to get the type of data we desire.

Strain Distribution

In order to secure information on strain distribution in a wheel under vertical and lateral loading conditions, a series of laboratory

tests have been made on a standard A-40 and a standard F-36 wheel. As shown in Fig. 1, three different loading conditions were applied to each wheel as follows:

1 A vertical load of 60,000 lb applied against the tread at a point $^5/_8$ in. from the outside face of the rim.

2 A vertical load of 60,000 lb applied against the tread at a point $3^1/_2$ in. from the outside face of the rim.

3 A lateral load of 20,000 lb applied against the flange.

Fig. 2 shows the laboratory setup used for applying the vertical loads, and Fig. 3 shows the method used to apply the lateral loads.

To measure strain under these loading conditions, a total of approximately 112 electric-resistance-type strain gages were applied to the rim, plate, and hub in both radial and tangential

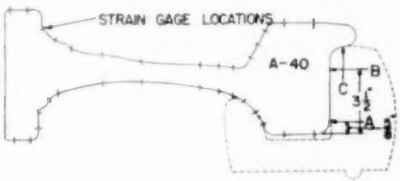

Fig. 1 View Showing Strain-Gage Distribution and Points of Applied Loads

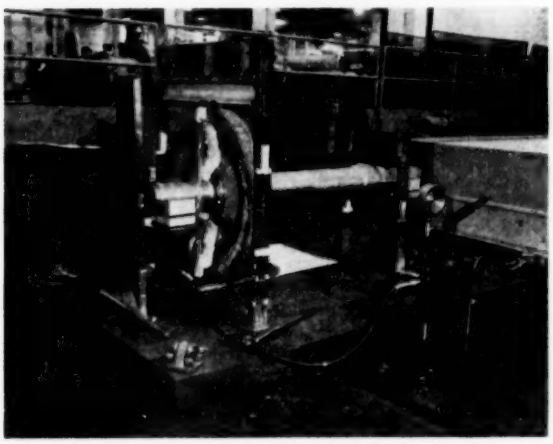

Fig. 2 Laboratory Setup Used to Apply Vertical Load

Fig. 3 Laboratory Setup Used to Apply Lateral Load

Fig. 4 Strain Gages on Outside Face of A-40 Wheel

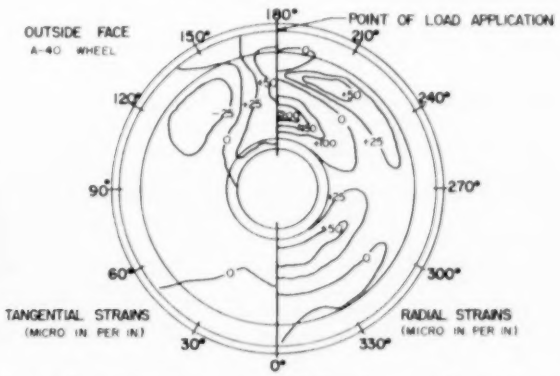

Fig. 5 Strain Distribution for 30-Ton Vertical Load Applied 3.5 In. From Outside Face of Rim

positions along two radial lines 180 deg apart on both sides of each wheel. Fig. 1 shows the distribution of the strain gages over the inside and outside faces of a standard A-40 wheel, while Fig. 4 shows an actual view of the strain gages on the outside face of the same wheel. In order to obtain the strain pattern over the entire wheel for each condition of applied load, the wheel was rotated through 360 deg and the strain gages read at 16 different angles with respect to the load. This procedure has resulted in an accumulation of a considerable amount of data which gives a relatively complete picture of the strain distribution over the entire inside and outside face of the wheel. It is not the purpose of this paper to discuss in detail the complete results of the laboratory work to date. However, it is of interest to note the strain distribution as plotted for the A-40 wheel.

Fig. 5 shows the isostrain lines, both radial and tangential, as determined for the outside face of the wheel for the conditions of an applied vertical load of 60,000 lb at point B (see Fig. 1) on the tread.

Due to the limitation of slip-ring capacity as well as other limitations, it is, of course, impossible to place a large number of strain gages on a wheel, such as was done under static laboratory conditions, and make simultaneous measurements. A study of the laboratory data taken to date has indicated that it may be possible to group certain strain gages in an electrical bridge circuit in such a manner that the resultant output multiplied by some constant would be an indication of the loading applied to

the wheel. If such a relationship can be established definitely it then may be possible to measure the loads applied to a wheel in the field and with such data simulate these loads in the laboratory and determine the resultant stresses. The logic of such a method, and the variables that may affect it, are being studied rigorously and, therefore, no conclusions regarding its feasibility can be given at this time.

Summary

This paper has attempted to present briefly a picture of the research program now in progress that has been set up to measure stresses imposed on wheels in diesel-locomotive service. This program has necessitated the development of special instrumentation and has required the formulation and evaluation of special measuring techniques. At the present time the test work is in a very early stage; some problems which have arisen have been solved while many others still remain to be solved. It is expected that the near future will advance this research program to the point where it will be possible to realize the objectives as set forth in the body of this paper.

1.5 Per Cent Carbon Cast-Steel Railroad-Car Wheels

By N. A. MATTHEWS[1] and R. A. FLINN[2]

A 1.5 per cent carbon cast-steel wheel, designated AARX-2, has been developed for freight-car service after 12 years of research and 6 years of evaluation by numerous laboratory and field-service tests. Pilot-plant production has been initiated to prove the economics of the process of manufacture. On the basis of two-and-a-half million car miles of service under typical and severe conditions, wear rate is comparable to that of one-wear wrought wheels. Little tendency for abnormal flange wear has been observed, and a minimum of "shellout" conditions are expected. Dynamometer and service tests have demonstrated conclusively that the wheel overcomes the thermal-checking problem which results from brake-shoe action. Ductility at the 1.5 per cent carbon level is achieved by a combination of close analysis control and a two-stage heat-treatment which produces a pearlitic structure with carbides favorably dispersed. The excess carbide promotes improved wear resistance at a given hardness level.

Introduction

In 1941, research was instituted under the sponsorship of the Association of Manufacturers of Chilled Car Wheels to develop an improved cast car wheel for freight-car service. The formulation of the research program and its supervision were responsibilities of a Technical Committee which held meetings at frequent intervals to review the research results and plan subsequent phases of the investigation. The Association's studies indicated that the tread surface of chilled wheels was of such a nature that thermal checking as a result of brake-shoe action could not be overcome by modifications in chemistry or treatment without seriously impairing wear resistance or other desirable attributes of the chilled-iron wheel.

The chilled-iron car wheel performs well in conventional freight-car service but it has limitations mainly as to flange strength and resistance to thermal checking resulting from brake-shoe action. The limited flange strength becomes important in the case of heavily loaded cars such as 70-ton covered hopper cars on curved track or under other conditions imposing severe side thrusts on wheel flanges. Similarly, the brake-burning problem becomes significant only in the case of runs involving severe braking such as refrigerator service.

With the trend to heavier loads and more severe braking, it became apparent that a cast wheel was desirable which would perform more satisfactorily in the most severe types of freight-car service.

[1] Assistant Chief Metallurgist, American Brake Shoe Company, Mahwah, N. J.

[2] Professor of Metallurgical and Production Engineering, University of Michigan, Ann Arbor, Mich.

Contributed by the Railroad Division and presented at a joint session of the Railroad Division, Research Committee on Metal Processing, and the American Society for Testing Materials at the Annual Meeting, New York, N. Y., November 29–December 4, 1953, of The American Society of Mechanical Engineers.

Note: Statements and opinions advanced in papers are to be understood as individual expressions of their authors and not those of the Society. Manuscript received at ASME Headquarters, July 31, 1953. Paper No. 53—A-118.

Experimental Wheel Types

Gray-Iron Wheels. The original experiments were directed at investigating the service performance of heat-treated gray-iron wheels. This material was selected as being likely to avoid the thermal-checking problem and production techniques were sufficiently similar to chilled-iron wheels so that standard melting, molding, and pouring facilities could be utilized. Griffin Wheel Company and American Brake Shoe Company facilities were utilized for production and preliminary evaluation of the wheels augmented by the Chilled Wheel Association physical-testing facilities.

Before experimental wheels can be tested under railroad cars, exhaustive laboratory-evaluation tests must be conducted to insure that the wheels are safe. The tests involved on the initial experimental wheels included:

(*a*) Soundness tests, principally fracture and sectioning, later including x-ray and magnetic-particle techniques.

(*b*) Thermal tests involving pouring a band of molten iron around the tread periphery to determine whether or not cracking is induced by the thermal upsetting while hot and resultant circumferential tensile stresses as the tread cools.

(*c*) Rim-impact tests, involving the impact of falling weights on the tread of the wheel as positioned vertically, weight striking 1 in. from rim face.

(*d*) Static plate and flange tests evaluating the resistance to fracture of the wheel under transverse applied loads.

(*e*) Residual-stress measurements.

(*f*) Drag and multiple-stop tests based on AAR test practices on dynamometer equipment to investigate degree of stress build-up in wheels and resistance to thermal checking under brake-shoe action.

After considerable experimentation with heat-treatment variables, a practice was evolved that produced water-quenched gray-iron wheels which successfully withstood the series of tests just enumerated and resulted in a high tread hardness approximating 350 Brinell (Bhn). This hardness level was chosen as the maximum which could be achieved in conjunction with a satisfactory residual-stress distribution. Lower hardnesses in the tread area were not considered because of the probability that higher wear rates would result as indicated by metal-to-metal wear-test results.

These quenched gray-iron wheels were installed under a locomotive tender of the Bangor and Aroostook Railroad and immediate evidence developed that wear rates caused by rail and brake-shoe action were excessive. There also was evidence of minute spalling tendencies associated with the graphite flakes. Subsequent laboratory examination of the worn tread areas confirmed that plastic flow under the high-contact stresses was promoted by the graphite flakes, leading to minute ruptures and spalling of the tread surface. It was concluded immediately that the tread structures containing appreciable flake graphite could not be expected to provide satisfactory wear resistance.

Malleable-Iron Wheels. The second phase of the investigation was devoted to malleable-iron wheels achieved by standard casting techniques and subsequent malleableizing heat-treatments applied directly after hot shakeout. It was postulated that the

graphite present in temper carbon form (roughly spheroidal shapes) would be less likely to cause high wear rates and still provide improved resistance to thermal checking under brake-shoe applications. Wheels were produced for service tests after heat-treatment practices were developed yielding 320 Bhn in the tread area and satisfactory stress distributions to pass thermal and drop tests. Malleable-iron wheels at the two carbon levels of 3.5 and 2.5 per cent were involved. Wear behavior under freight cars was disappointing, although from the standpoint of thermal checking the malleable-iron wheels gave outstanding performance. Here again, the presence of an excessive amount of graphite, even though in spheroidal form, resulted in high rates of wear.

Composite Steel-Tread Wheels. Considerable effort during 1944 to 1946 was devoted to developing pilot practices for the production of a steel-tread wheel with gray-iron plate and hub. The steel tread consisted of a $^3/_4$-in. to 1-in-thick band of 0.75 per cent carbon steel cast centrifugally in a vertical-axis machine. After pouring and solidification of the steel tread, the machine was stopped and the balance of the mold cavity filled with molten cast iron. Two major problems developed which ultimately discouraged further pursuit of this composite-wheel concept and both relate to production-control problems affecting the integrity of the bond between the steel and iron components. Incomplete bonding due to inadequate fusion appeared to be avoidable with precise timing of pouring operations and precise temperature control. However, a more insidious obstacle involved the effects of intermixing of the steel and cast-iron components at the interface. Intermixing resulted in a narrow band at the interface which was brittle and could not accommodate the thermal and mechanical stresses transmitted through the strong and ductile steel-tread layer. Although wheels were made and tested which eliminated this deficiency in the interface zone, it was concluded that there were no practical inspection techniques which would permit adequate control of production with respect to absence of the brittle structure at the interface zone.

By 1945, it was apparent that the search for improved cast car wheels should include the investigation of materials other than cast iron. Continued research was left in the hands of Griffin Wheel Company and American Brake Shoe Company which, with assistance from the Chilled Wheel Association, developed a co-operative research program involving the production and treatment of experimental wheels, laboratory-evaluation tests, and service testing. During the past few years the Brake Shoe Company effort has been applied primarily to the 1.5 per cent carbon cast-steel wheel whereas Griffin has concentrated on the 0.75 per cent carbon-graphite mold wheel.

Development of the 1.5 Per Cent Carbon-Steel Car Wheel

Initial Analysis Variations. By 1946, experiments had indicated that sound cast wheels could be produced in a 1.5 per cent carbon steel. Heat-treatment variables were studied and wheels processed which exhibited excellent combinations of strength and ductility and successfully passed the battery of evaluation tests listed in the foregoing. Two varieties were tested with a structure variable introduced by heat treatment. Brinell hardness ranged from 200 to 240 and graphitic carbon to the extent of 0.50 per cent in temper carbon form in the tread area resulted from the combination of chemical composition employed and heat-treatment necessary to achieve ductility and satisfactory performance in thermal and drop tests. Again, service tests under freight cars loaded to 10.5 tons per wheel produced disappointing wear results. Wear rates compared to one-wear wrought-steel wheels ranged from 2.9–4.4 to 1. Better wear resistance was necessary, but wheels made from these steels performed satisfactorily in all other respects. It had become crystal clear that appreciable graphitic carbon could not be tolerated in the tread area if satisfactory wear rates were to be achieved.

Metallurgical Problem. No prior commercial experience was available on a graphite-free 1.5 per cent carbon steel. The metallurgical problem was to develop an analysis so balanced that graphite could be avoided and yet amenable to practical heat-treating cycles to produce appreciable ductility in cast metal at this carbon level. The 1.5 per cent carbon level was established early based upon:

(*a*) Evidence that the excess carbide volume at higher carbon levels prevented adequate ductility with practical heat-treatment.

(*b*) A tendency for lower carbon levels to detract from wear resistance and exaggerate the problem of obtaining clean, sound castings in sand molds.

Preliminary exploration of the effects of chemical-analysis variations and heat-treatments were carried out on small pieces cut from the experimental wheels and evaluated on the basis of metallographic structure and mechanical properties. A combination of analysis and dual-stage heat-treatment was developed which eliminated the as-cast brittle-carbide network, avoided graphite, and produced combinations of strength and ductility promising for wheel service. Typical structures as-cast and after each stage of the heat-treatment, together with corresponding physical properties, are shown in Fig. 1.

The next problem involved achieving these physical properties in wheels reproducibly in conjunction with a proper stress distribution. Fortunately, prior experience with gray and malleable-iron wheels had delineated the general principles. Residual radial-compression stresses in the front-hub fillet had been shown to be desirable in conjunction with low circumferential stresses in the tread area. A controlled hub-cooling technique was accordingly applied by which the wheel is cooled from the final heat-treating temperature in air, but cooling of the heavy hub zone is accelerated by air flow through the bore so that it cools ahead of the less massive tread producing the residual-stress levels depicted in Fig. 2.

Laboratory Testing of 1.5 Per Cent Carbon Wheel. The first wheels representing the current practice went into experimental test service on the Bangor and Aroostook Railroad in the middle of 1947, on a car especially assigned for the purpose. It was soon apparent that excellent wear rates were to be expected in this service which was selected because of (1) availability of car for regular inspection, (2) rapid accumulation of mileage, (3) maximum wheel loading, and (4) the severe action of a nonresilient frozen roadbed during winter months. Specifically, the test car provided accelerated conditions attributable to the 5000 miles per month of travel and the wheel loading of 10.5 tons. This test location on one or two cars continued through March, 1953, and during the 10 years over which tests were conducted, 40 experimental wheels, representing eight materials, were tested without an accident, attesting to the adequacy of the preliminary tests which were depended upon to determine whether or not a wheel is considered safe for service testing.

An extensive physical test and evaluation program was instituted on a number of wheels of 600 and 750 lb. These data are summarized in Table 1. It will be noted that the hardness and physical properties reflect the improved combination of strength and ductility.

The 1.5 per cent carbon cast-steel wheel machines similarly to wrought wheels. Hub hardnesses are considerably higher than chilled-iron wheels so that machinability of the two types of cast wheels is not comparable. Conventional tooling is satisfactory with speeds and feeds comparable to those used in machining wrought wheels.

The modulus of elasticity of the 1.5 per cent carbon cast steel is

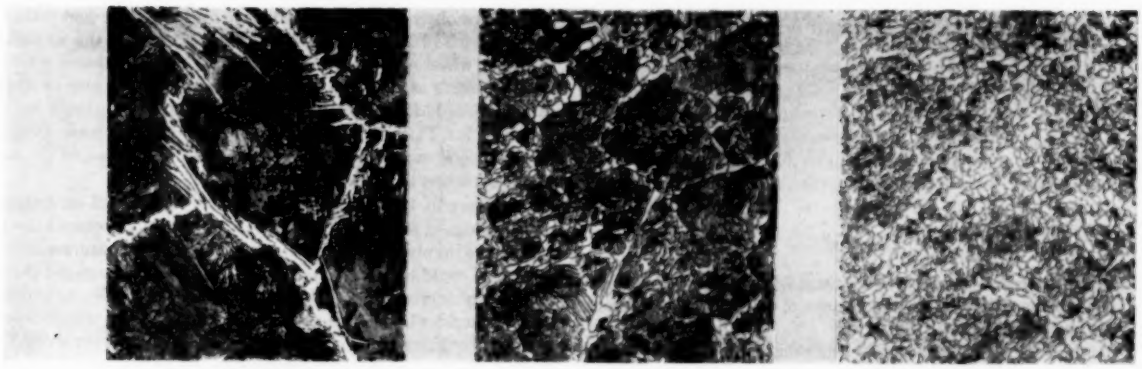

	500X As Cast Pearlite matrix with iron carbide as grain boundary network.	1000X 1700°F.-2 hours-air cool Pearlite matrix, refined grain size, with grain boundary carbides partially dispersed.	1000X 1700°F.-2 hours-air cool 1450°F.-5 hours-air cool Pearlite matrix with grain boundary carbides dispersed.
Tensile Str., psi	60-70,000	90-100,000	100-120,000
Percent Elongation	0	1.0-2.0	4.0-6.0
Brinell Hardness	320-340	245-255	245-255

FIG. 1 MICROSTRUCTURES AND PHYSICAL PROPERTIES OF 1.5 PER CENT CARBON CAST-STEEL WHEEL AS INFLUENCED BY HEAT-TREATMENT

FIG. 2 SIGNIFICANT RESIDUAL STRESSES IN 1.5 PER CENT CARBON CAST-STEEL WHEEL

comparable to wrought steel. Accordingly, similar mounting tolerances are recommended and similar mounting pressures result. An allowance of 0.001 in. per in. of bore has been adopted. Mounting pressures range from 75 to 110 tons for light weight and from 80 to 120 tons for heavy wheels. Tests have been performed on wheels experimentally bored with excessive tolerance of up to 180 per cent of normal, with correspondingly higher pressures, and bore micrometer measurements have shown no plastic deformation.

Braking Tests. An extensive series of brake-shoe tests was

TABLE 1 MECHANICAL PROPERTIES AND DESTRUCTIVE TESTS ON WHEELS

	1.5 per cent carbon	
Type wheel	600 lb	750 lb
Flange strength, lb	200000	300000
	390000	460000
Rim impact, 400-lb weight	broken	not broken
	7 to 10 ft	10 ft
Plate strength, lb: Back hub up	850000 to over 1000000[a]	over 1000000
Front hub up	over 1000000	over 1000000
Tensile strength, psi	110000	110000
Yield strength, psi, 0.2 per cent offset	64000	64000
Elongation in 2 in., per cent	4	4
Elastic modulus, psi × 10^6	30.0	30.0
Brinell hardness	255	255

[a] Capacity limit of testing equipment = 1000000 lb

carried out on the 1.5 per cent carbon wheel on the American Brake Shoe Company dynamometer located at the Sargent Laboratory, Mahwah, N. J. Drag and multiple stopping tests simulating freight-car conditions were applied to a number of wheels of each weight. No cracking was induced under repeated trials.

Drag tests involved four series of 48-min runs simulating 25 mph and a brake-shoe load of 3000 lb. On several wheels, tested with standard analysis and heat-treatment, no cracks or other manifestations of failure were observed, although circumferential tensile stresses in the tread area approaching 20,000 psi were developed.

In addition to drag tests, a test simulating tender-stopping conditions was utilized involving stops from 8 mph with a high wheel load of 40,150 lb and a brake-shoe load of 7548 lb. No cracks or other adverse effects were observed.

A series of wheels representing the standard analysis and heat-treatment in 600 and 750-lb sizes were subjected to 100 stops each from 40 and 60 mph under conditions simulating freight emergency stops. The tread of the wheel was water-cooled to below

TABLE 2 COMPARATIVE WEAR RATES ON BANGOR AND AROOSTOOK RAILROAD; LOADING 10.5 TONS PER WHEEL

Type wheel	Number axle pairs involved	Over-all average wear rate per 1000 miles	Over-all rating[a]
1.5 per cent carbon cast steel	6	0.0012	1.0
One-wear steel:			
Over-all	5	0.0019	1.6
Winter	.	0.0036	3.0
Summer	.	0.0017	1.4
Chilled iron	3	0.0035	2.9

[a] Rate of 1.5 per cent carbon steel as 1.0.

125 F after each stop. Wheel load was 24,500 lb and the brake-shoe load was 6340 lb. No cracks developed in any of the wheels tested in this manner.

In summary, the laboratory-testing program has indicated that the 1.5 per cent carbon cast-steel wheel is not subject to thermal checking under conditions to be expected in freight service. Maximum radial plate stress observed as a result of the most severe braking applied was 18,000 psi or less than one third the yield strength of the material.

Balance Tests. In view of the general interest in dynamic balance of rotating parts in railroad equipment, a group of 1.5 per cent carbon wheels of light and heavyweight designs, in both as cast and machined conditions were tested on a Bear balancing machine to investigate degree of unbalance. All wheels tested showed an average out-of-balance of 15 oz with individual wheels ranging from a minimum of $3^1/_4$ oz to a maximum of $1^1/_4$ lb. The low degree of unbalance observed in these tests reflects the close adherence to design dimensions achieved by the casting process.

Service Experience. The longest wear experience with the new wheel is in northern Maine on the Bangor and Aroostook Railroad. The Bangor and Aroostook performance is particularly pertinent since it involves a consistent high loading of 10.5 tons per wheel and incorporates the added severity associated with the lack of resiliency of a frozen roadbed during 4 months of the year. The consolidated experience is shown in Table 2 comparing the 1.5 per cent carbon-steel wheel with the chilled-iron wheel and the wrought-type one-wear wheel.

It will be observed that the wear rate for the 1.5 per cent carbon cast-steel wheel is approximately 63 per cent that of the wrought one-wear wheel and 35 per cent of that of the chilled-iron wheel. An interesting aspect of these wear figures is the increase in wear rate observed during winter months on wrought wheels by a factor of 2. This change, consistent on wrought wheels during several years' experience, was not observed in the case of the 1.5 per cent carbon or chilled-iron cast wheels.

Beginning in 1948, field-service tests were initiated on freight cars in assigned service under a variety of conditions where known loads were involved, and periodic inspections for measurement of wear rate could be made. The field-test wheels were gaged carefully from reference points along with the companion new one-wear wrought wheels. The 1.5 per cent carbon cast wheels were installed by pairs on an alternating basis with one-wear wrought wheels. In some cases the cast wheels were on nos. 1 and 4 axles whereas under other cars the reverse arrangement was used. Each truck had one pair of each type wheel in all cases. During the first year of operation, inspections were made at approximately monthly intervals, whereas during subsequent service, inspections have been made when advisable, usually at 3 to 6-month intervals. Inspection data obtained on these occasions included tread-wear measurements and tread contours for the purpose of determining flange wear.

As of June 1, 1953, thirty-one wheel-test cars had accumulated more than 10,000 miles each, of which fifteen had exceeded 60,000 miles each, seven had exceeded 100,000 miles, and one pair had averaged over 200,000 miles. Wear rates per 1000 miles have varied extensively with the service from a high of 0.0047 in. per 1000 miles with an average wheel loading of 8.75 tons, to a low of 0.0006 in. per 1000 miles on cars involving a wheel loading averaging 4.0 tons. The detailed data on the test installations which have exceeded 10,000 miles are shown in Table 3.

It will be observed that the cumulative experience representing over 120 wheels each of the 1.5 per cent carbon cast-steel and one-wear wrought types indicates an equivalent wear rate averaging 0.0018 in. per 1000 miles. Although this experience represents a small sample, it is certainly an indication of results to be ex-

TABLE 3 ASSIGNED SERVICE FIELD TESTS[a]

Railroad	Type car	Average wheel loading, tons	Mileage[c]	Wear rate, in./1000 Mi[b] 1.5% carbon cast steel	Wear rate, in./1000 Mi[b] One-wear wrought
Seaboard	auxiliary water and fuel oil	6.0	60049	0.0021	0.0019
			58943	0.0021	0.0017
Atlantic Coast Line	auxiliary water	6.9	66895	0.0030	0.0042[d]
			60188	0.0033	0.0036
Fruit Growers Express	brine-tank refrigerator	4.8	41684	0.0020	0.0019
			34289	0.0023	0.0019
			40049	0.0018	0.0015
Northern Refrigerator	refrigerator	5.75	127195	0.0011	0.0015
			136518	0.0014	0.0017
			121077	0.0018	0.0019
Erie	LCL box cars	3.7	176126	0.0008	0.0006
			224804	0.0008	0.0007
Virginian	auxiliary water tank	8.75	100950	0.0037[e]	0.0030
			109730	0.0044	0.0039
Wabash	covered hopper	6.0	41250	0.0020	0.0021
			46876	0.0019	0.0025
B&O	box, express	5.3	10900	0.0024	0.0023
			12341	0.0027	0.0024
Santa Fe	refrigerator	6.6	94840	0.0013	0.0012
Merchants Dispatch	refrigerator	6.6	80051	0.0014	0.0013
			89580	0.0015	0.0011
			101410	0.0014	0.0013
NYNH & H	flat car	4.0	64723	0.0005	0.0008
			48637	0.0008	0.0011
Fruit Growers Express	mechanical refrigerator	5.5	47847	0.0011	0.0012
			39658	0.0011	0.0011
Gen'l. American	tank car	6.3	33838	0.0011	0.0013
			31714	0.0011	0.0014
Erie	box cars	3.7	14491	0.0005	0.0007
			10889	0.0009	0.0014
Over-all average wear rate, in. per 1000 miles				0.0018	0.0018

[a] Tests listed in order of installation.
[b] Wear figures represent cumulative wear rate per 1000 miles for average of four wheels of each type per car.
[c] Mileage figures at last inspection during second quarter 1953.
[d] One pair one-wear wrought wheels removed at last inspection for vertical flange.
[e] Cast-steel wheels remachined and reinstalled at 60,000 miles.

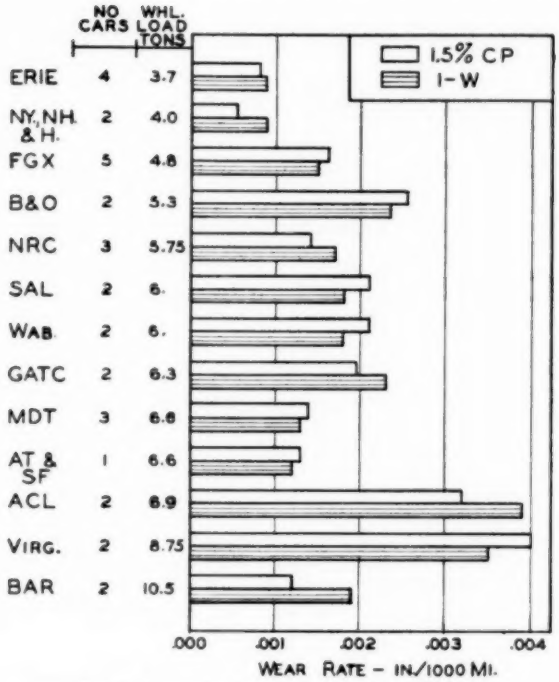

FIG. 3 ASSIGNED SERVICE FIELD-TEST RESULTS

pected in general service. Flange wear will be the limiting factor in most types of service and surveys of flange contours indicate an average rate of flange wear of 0.001 in. per 1000 miles.

In all cases, test wheels have shown higher wear rates during the first few thousand miles than those shown in Table 3. However, after the run-in period, wear rates have remained remarkably constant. The sole exception involves Northern Refrigerator cars where an increased wear rate was observed on wrought wheels during winter months attributable to the frozen-roadbed condition prevalent over a substantial part of the route traveled by these cars. This observation substantiates earlier experience on the Bangor and Aroostook Railroad.

The wear data tabulated in Table 3 have been plotted in Fig. 3. From this, nominal wear-rate expectancy for these types of wheels can be approximated as a function of wheel loading. This, of course, does not take into account the braking variable which certainly promotes the scatter observed. In heavily loaded cars without appreciable breaking, the wear-rate expectancy based on Bangor and Aroostook tests is 0.0012 and 0.0019 in. per 1000 miles for cast and one-wear wheels, respectively, whereas the Atlantic Coast Line and Virginian experience exceeds these rates by ratios of 2 to 4. This discrepancy in wear rate is attributed to effects of braking.

SUMMARY

Summarizing the service experience, the following may be concluded:

(*a*) In general service involving typical wheel loadings and average breaking, the 1.5 per cent carbon steel and one-wear wrought wheels wear at similar rates.

(*b*) In heavily loaded service involving light braking, the cast wheel will show a superiority.

(*c*) In heavily loaded service involving moderate to heavy braking, the data to date are inconclusive but suggest no substantial difference in performance of the two wheels.

(*d*) No thermal checking of wheel treads is expected.

(*e*) Early removals due to "shellouts" on the tread are not expected at normal wheel loadings. Under maximum wheel loadings in high-capacity cars minor "shellouts" may occur in both types of wheel which grow at exceedingly slow rates.

(*f*) Service experience suggests that the wheels are safe throughout their life.

The foregoing conclusions are based on 6½ years of running the cast-steel wheel in actual test service. In standard types of freight equipment the accumulated experience suggests that the new-type wheel holds great promise in assuring new railroad-operating economies.

ACKNOWLEDGMENT

The authors are indebted to many colleagues who have worked on the car-wheel problem during the 12-year period, principally Mr. R. H. Schaefer, Vice-President; Mr. R. J. Ely and Mr. R. W. Kraft, Jr., of the Brake Shoe Research Center. Appreciation is also expressed to Mr. Eads Johnson, Jr., President of the Southern Wheel Division, for permission to publish the paper and for his assistance in its preparation, and to Mr. Robert A. Gow for his guidance and assistance in accumulating the field-test data.

Better Yield Through Dimensional Control in Small-Sawmill Operation

By J. S. BETHEL,[1] RALEIGH, N. C.

Small sawmills often are criticized on the lack of dimensional control in their products. The opportunities presented for increasing yields by control are discussed in this paper together with the realization of increased profit to the operator.

Introduction

ONE of the adverse criticisms most frequently leveled at that portion of the lumber industry which produces its product on small sawmills is that the product is not uniform in dimension. Lumber which is inaccurately manufactured from the standpoint of thickness has much less utility than has well-manufactured lumber. Thick and thin boards create problems at the planing mill as well as for the ultimate user. One of the most serious consequences of inaccurate manufacture, however, is that it contributes to low yields and, consequently, high costs and much waste.

Sawmill Specifications

It is customary, at least in southeast United States, for planing mills which are buying 4/4 lumber from small sawmills to specify that the lumber shall be $1^1/_4$ in. in thickness and to reject all boards that fall below 1 in. in thickness. The planing mill operator dislikes boards that are too thick because they overload his surfacing equipment and increase his waste problem. He is more concerned though with boards that are too thin because to quote one of these operators, "You can take it off but you can't put it on." As a consequence, the specification given to the small-sawmill operator includes a minimum tolerance but usually not a maximum tolerance. It is the sawmill operator's problem then to assure that no appreciable part of his lumber exceeds the minimum tolerance.

Small sawmills, in common with all other pieces of manufacturing equipment, do not produce successive pieces of 4/4 lumber with precisely the same thickness. No matter how well maintained nor how well operated the sawmill is, the thickness of 4/4 boards which it produces will vary. If it is in fact, well constructed, maintained, and operated, it will operate in a state of statistical control and the 4/4 lumber thicknesses normally will be distributed about an average thickness.

Fig. 1 illustrates the distribution of lumber thicknesses from such a sawmill. Fig. 2 shows a quality-control chart for a sawmill operating with reasonably good control. If the sawmill is not well constructed, maintained, or operated it may be out of control and the variation in thickness of boards produced will far exceed that characteristic of the product of a sawmill operating in control. Fig. 3 illustrates a control chart for a sawmill which exhibits lack of control.

Operating In Control

The problem faced by the sawmill operator is that of setting his sawmill to cut the smallest average board thickness that will not yield an excessive number of boards below the minimum thickness acceptable to his customers. If the sawmill is operating in control it is possible to predict with a high degree of precision what that average board thickness ought to be. The dispersion of board thicknesses about the nominal thickness for sawmills operating in control can be expressed in terms of the standard deviation of the appropriate normal distribution. This is a measure of the machine capability or the basic accuracy of the sawmill as a piece of manufacturing equipment.

Three sawmills which the author recently had occasion to investigate showed standard deviations of 0.05, 0.06, and 0.07 in. Differences in the standard deviations from controlled sawmill operations reflect differences in quality of the original sawmill construction, age, and state of maintenance. If it is possible to accept as a reasonable basis for operation a condition in which boards thinner than 1.00 in. will not be produced more frequently than once in every 100 boards,[2] then the average thickness which should be set for each of the three sawmills previously referred to would be as shown in Table 1.

TABLE 1 AVERAGE THICKNESSES OF BOARDS FROM THREE SAWMILLS

Sawmill	Standard deviation of board thickness, in.	Average thickness of board required, in.
A	0.05	1.11
B	0.06	1.14
C	0.07	1.17

Mill A will give better lumber yields than will mill C since on the average the 4/4 boards produced by mill A will contain 5.1 per cent less lumber than will the 4/4 boards produced by mill C. It is sometimes argued that this extra lumber actually will not be captured unless the log is of sufficient size to permit it to be accumulated into an additional board. Telford[3] indicates that this is illogical and states, "It can be demonstrated diagramatically that an increase of approximately $2^1/_2$ per cent in softwood footage results from each $^1/_{32}$-in. decrease in saw kerf, and a comparable saving results from improved precision in sizing." It is apparent then that even where sawmills are operated in a state of statistical control there is a real advantage from a yield standpoint to operating a mill which has a high degree of basic accuracy. Good machine capability in a small sawmill results from use of good materials in its manufacture, careful machining and fitting of individual parts, and facilities for accurate adjustment in use. It is also essential that the sawmill be set up, maintained, and

---

[1] Director, Wood Products Laboratory, North Carolina State College.

Contributed by the Wood Industries Division and presented at the Annual Meeting, New York, N. Y., November 29–December 4, 1953, of The American Society of Mechanical Engineers.

Note: Statements and opinions advanced in papers are to be understood as individual expressions of their authors and not those of the Society. Manuscript received at ASME Headquarters, September 16, 1953. Paper No. 53—A-199.

[2] "Quality Control in Lumber Manufacture," by J. S. Bethel, A. C. Barefoot, and D. A. Stecher, Proceedings Forest Products Research Society, Madison, Wis., 1951. It might appear that one thin board out of every 100 boards would be an excessively liberal allowance. These authors, however, found after examining 100 successive shipments of lumber received at a concentration yard from 24 different suppliers that the average percentage of thin boards per shipment was 4.5 per cent, that only 5 per cent of the shipments contained no thin boards, and that 80 per cent of the shipments contained more than 1 per cent of thin boards.

[3] "Small Sawmill Operators' Manual," by C. J. Telford, U.S.D.A. Agriculture Handbook No. 27, Washington, D. C., January, 1952.

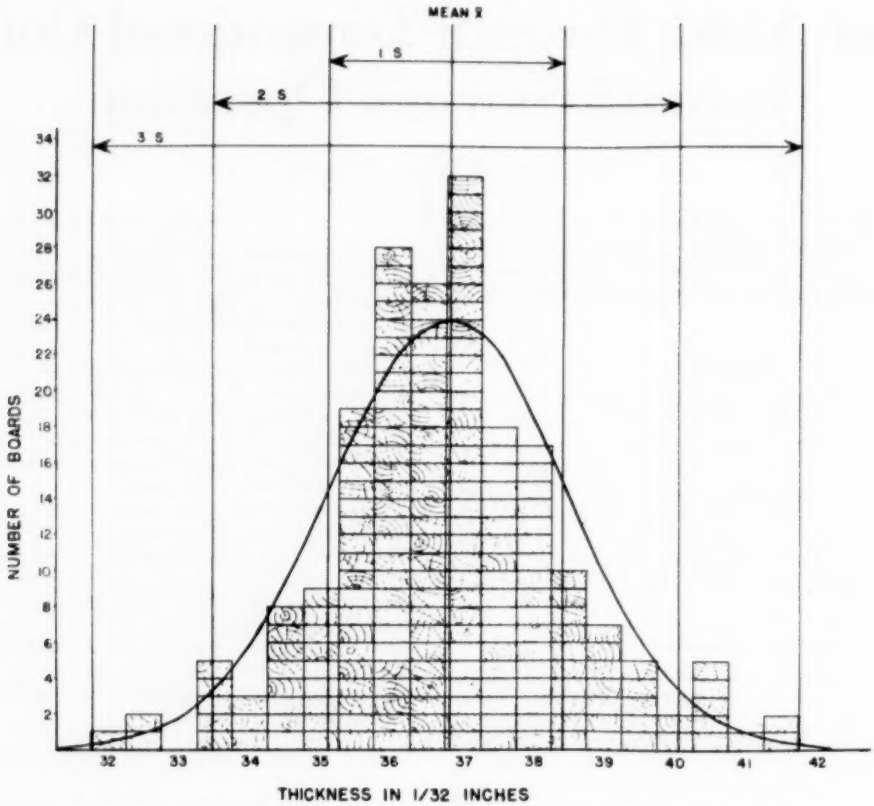

FIG. 1 DISTRIBUTION OF LUMBER THICKNESSES FROM A SAWMILL OPERATING IN CONTROL
(A normal curve has been fitted to the frequency histogram.)

operated properly by the user. A sawmill which has a high basic accuracy when new will show a reduction in this accuracy if worn parts are not replaced.

OPERATING OUT OF CONTROL

When a sawmill is operating out of control it is necessary for the sawyer to set his mill to cut an average board much thicker than that cut by the same mill operated in control. This is necessitated to insure that the boards which are out of control on the low side are not thinner than the minimum specification requirement. Furthermore, when a sawmill is out of control there is no basis for predicting what the target average thickness should be or what percentage of boards will be outside the specification limit for any given target average thickness.

Figs. 2 and 3 represent control charts for two sawmills which have very nearly the same machine capabilities. Therefore, it would be presumed that the target average thickness would be about the same for the two mills if they were attempting to produce lumber to comply with the same specification of minimum thickness. In actual fact, the mill which was operating badly out of control had an average board thickness which was 0.11 in. thicker than that of the mill which was operating in control. The 4/4 boards from the mill operating in control contained on the average 8.7 per cent less lumber than did the boards from the mill operating out of control. Over a period of several weeks the actual difference in yield between these two mills was somewhat less than this value because at the start of the study both mills were out of control. The sawmill represented by Fig. 2 was brought into control by the operator, thus permitting a change to a smaller target thickness.

It is sometimes said that it is unrealistic to be concerned with what appears to be relatively small differences in average board thickness. With the small profit-margin characteristic of most small-sawmill operations, differences in yield of the order of magnitude of 5 to 9 per cent easily may represent the difference between a profitable and a submarginal operation. This is particularly true since the evidence currently available suggests that it is no more costly to operate a sawmill with good machine capability in a state of control than it is to operate a poor mill out of control.

IMPROVING CONTROL

If a sawmill operator is to gain the maximum yield through improving control of dimension the followng steps are required:

1 Bring the lumber-manufacturing process into a state of statistical control.

2 Improve the basic accuracy or capability of the sawmill.

Bringing the process into control means creating a condition in which the variation among boards represents a stable system of chance causes. The most frequent causes of lack of control have been found to be, poor mill setup, inadequate power, improper saw lead, poor saw maintenance, improper carriage alignment, careless setting, improper calculation of cut, and inadequate dogging. Correction of these defects usually can be accomplished by a tightening up of the operating organization. Close and intelligent supervision of the enterprise during mill setup and

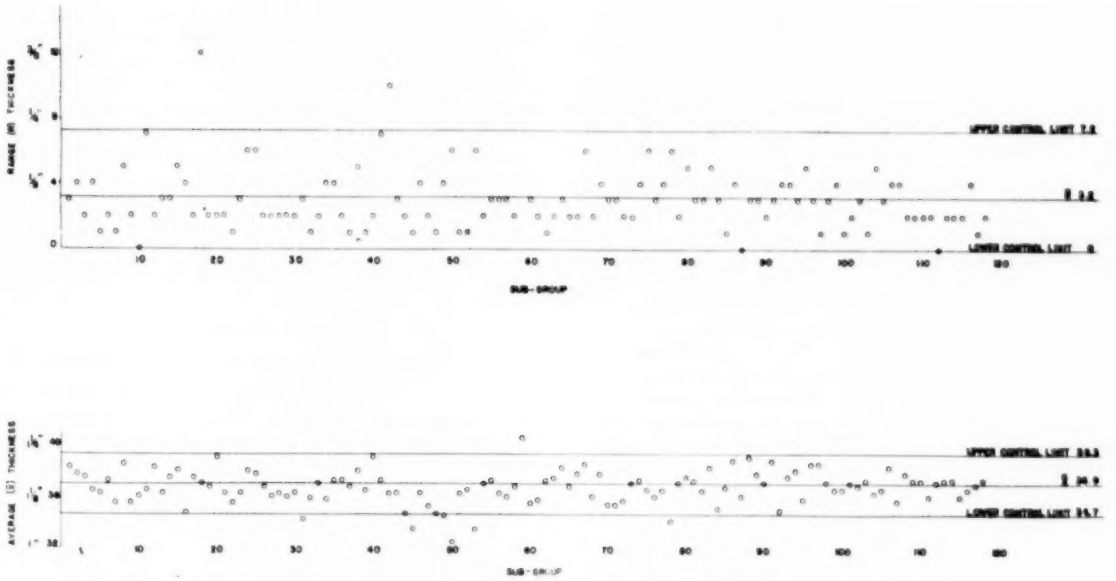

FIG. 2 CONTROL CHART FOR A SAWMILL WHICH SHOWS A REASONABLY GOOD CONTROL OF LUMBER THICKNESS

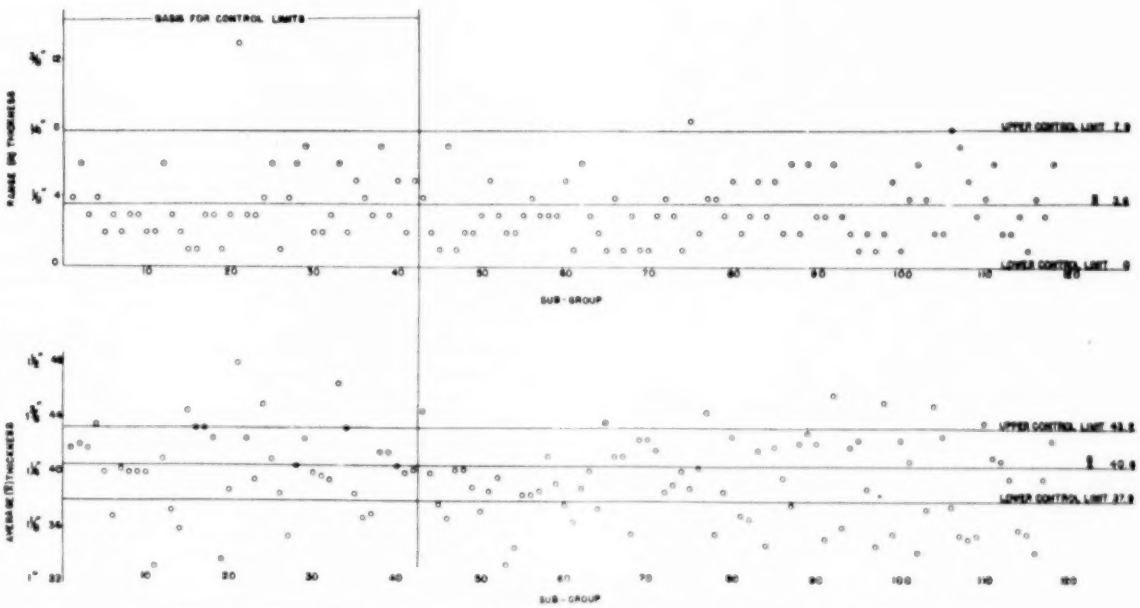

FIG. 3 CONTROL CHART FOR A SAWMILL WHICH SHOWS POOR CONTROL OF LUMBER THICKNESS

operation can result in correction of most of the assignable causes for lack of control.

Improving the basic accuracy or capability of the sawmill usually involves a more fundamental change in the equipment. It may mean the replacement of the sawmill with a new one. At the least it is likely to mean replacement of worn, damaged, or misfit parts.

CONCLUSION

The opportunities for increasing yields through better dimensional control are great. The increased profits which can be expected to accompany such increased yields recommend this action to the small-sawmill operator.

Discussion

GREGORY BAKER[4] Anyone who has been associated intimately with small sawmills becomes very conscious of miscut lumber and the variations in thickness—variations which occur both between boards and within the same board. The author has come up with a very useful method of pin-pointing this trouble and of indicating ways for its elimination. The writer believes this would be a potent educational tool in the hands of an inspector or buyer concerned with the product of several small mills. It could be used to point out in tangible form ("pictures," if you like) the difference between good and poor product. It would have been most welcome to the writer 20 years ago when he was concerned with acceptance inspection of lumber from a number of small contracting sawmills.

[4] Professor of Forestry, University of Maine, Orono, Me.

A Concept of Fatigue Damage

By S. M. MARCO[1] and W. L. STARKEY,[2] COLUMBUS, OHIO

An experimental investigation was conducted to study the effects of cumulative fatigue damage on endurance life. Stepwise-varying stress sequences were applied to rotating-cantilever-beam specimens. Typical curves of fatigue damage versus cycle ratio were deduced. The effect of scatter in the test results was evaluated.

Nomenclature

The following nomenclature is used in the paper:

D = fraction of damage; at failure, $D = 1$
i = particular step in sequence of steps of different stress amplitudes in sequential-load test
m = number of steps in sequence of steps of different stress amplitudes in sequential-load test
n_i = number of cycles of operation under conditions of ith step of sequence
N_i = number of cycles required to produce failure under conditions of ith step of sequence
σ_1 = stress amplitude for first step of sequence
σ_i = stress amplitude for ith step of sequence
σ_m = stress amplitude for last step of sequence

Introduction

The fatigue failure of machine parts has been the subject of study by numerous investigators. There are many aspects of this phase of design which require a great deal of investigation before satisfactory design methods can be developed. The problems involved are extremely complex. Any attempt to describe the behavior of materials subjected to fluctuating loads involves a large number of variables. As with most design procedures, it is desirable to attempt to express the complex behavior of machine parts under actual operating conditions in terms of the behavior of laboratory test specimens of relatively simple geometry under simple loading conditions. The realization of this desire will depend upon the degree of understanding which can be developed regarding the fundamental nature of fatigue failure and fatigue damage.

Most fatigue failures in the laboratory have been produced by subjecting a test specimen to a number of stress cycles in which the stress varies approximately sinusoidally with time and in which the stress amplitude is maintained at a constant value throughout the life of the specimen. In contrast to this, many machine parts are subjected to stress-time cycles in which the maximum and minimum stresses vary at random throughout the life of the part. If data from laboratory tests are to be used for predicting the behavior of actual machine parts, it is apparent that some theory must be developed which will describe the effect of subjecting a material to stress cycles of varying amplitude.

[1] Professor and Chairman of Mechanical Engineering, The Ohio State University. Assoc. Mem. ASME.
[2] Assistant Professor of Mechanical Engineering, The Ohio State University. Assoc. Mem. ASME.
Contributed by the Machine Design Division and presented at the Annual Meeting, New York, N. Y., November 29–December 4, 1953, of The American Society of Mechanical Engineers.
Note: Statements and opinions advanced in papers are to be understood as individual expressions of their authors and not those of the Society. Manuscript received at ASME Headquarters, September 1, 1953. Paper No. 53—A-143.

Damage Theories

In recent years a number of investigators have studied this varying-load aspect of fatigue by subjecting test specimens to a sequence of stress cycles in which the amplitude and mean stress were maintained at one set of values for a fraction of the life, then at another set of values for another fraction of the life, and so on until failure resulted. In each case a limited number of tests has been run. Usually only one specimen has been tested for a given stress pattern.

These investigators have proposed several theories of damage based upon the results of their tests. In some of the proposed theories, an attempt has been made to relate some concept of damage to the life of a material subjected to a complex stress pattern. In functional form these theories may be expressed by

$$D = f(n_i/N_i) \quad [1]$$

where n_i/N_i is the cycle ratio.

The theories of Miner,[3] Langer,[4] and others, for example, assume that Equation [1] has the linear form

$$D = n_i/N_i \quad [2]$$

for any stress pattern. Equation [2] leads to the conclusion that the amount of damage done is exactly equal to the cycle ratio. A plot of Equation [2] is shown in Fig. 1. In this figure it may be

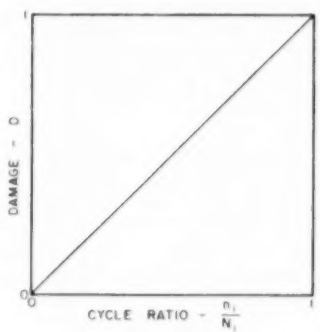

Fig. 1 Cycle Ratio Versus Damage Curve for $D = n_i/N_i$

seen that if a sequence of stress cycles of different amplitudes is applied to a specimen until failure ($D = 1$) is accomplished, the sum of the cycle ratios for the various stress levels used in the sequence should be unity. In equation form this may be expressed as

$$\sum_{i\,=\,1,\,2,\,\cdots,\,m} (n_i/N_i) = 1 \quad [3]$$

This concept of damage assumes that if a certain fraction of the life $n_1/N_1 = z$ is consumed at stress level σ_1, there remains a usable life of $n_2/N_2 = (1 - z)$ at any stress level σ_2. According to this concept of damage it makes no difference if σ_2 is larger or smaller than σ_1.

[3] "Cumulative Damage in Fatigue," by M. A. Miner, Trans. ASME, vol. 67, 1945, pp. A-159–A-164.
[4] "Fatigue Failure From Stress Cycles of Varying Amplitude," by B. F. Langer, Trans. ASME, vol. 59, 1937, p. A-160.

Experimental Investigations

On the basis of tests of single specimens for each sequence of loading, consisting of two, three, or four steps in the sequence, Miner[3] reports that the range of values for $\Sigma(n_i/N_i)$ was from 0.61 to 1.49, with an average value close to unity. Newmark[5] reports that on the basis of tests by Dolan, Richart, and Work,[6] a much larger range of values for $\Sigma(n_i/N_i)$ resulted. However, he also reports that an average value of approximately unity is indicated by these tests.

Kibbey[7] reports the testing of rotating-beam specimens subjected to sequences of ascending stress amplitudes and sequences of descending stress amplitudes. Here again single specimens were tested with 2, 3, 4, 5, 6, and 7 steps in the sequences. The average value for $\Sigma(n_i/N_i)$ for ascending loadings, based on the mean S-N curve, was found to be 1.49, while the average value of $\Sigma(n_i/N_i)$ for descending loadings was found to be 0.78.

In view of the wide range of values reported by these investigators and the uncertainty regarding the effect of the order in which the steps in a sequence of loading are applied, a series of tests was conducted by the authors. This test program attempted to determine if the number of steps in a sequence, or the order of application of the steps, would affect the value of $\Sigma(n_i/N_i)$. The results reported in this paper were determined through work conducted on a project of The Ohio State University Research Foundation sponsored by the Air Force under Contract No. AF 33(038)-12393. A complete description of the work with all data obtained was included in two reports submitted to the Air Research and Development Command, dated June 1, 1951, and October 9, 1951.

Experimental Equipment and Testing Procedures

Testing Machines and Specimens. All fatigue tests were made on three Krouse rotating-cantilever-beam machines having maximum operating speeds of 10,000 rpm. One series of tests was conducted with specimens of 76S-T61 aluminum alloy. Another series of tests was conducted with specimens of SAE 4340 steel alloy. The steel specimens were heat-treated to within the Rockwell

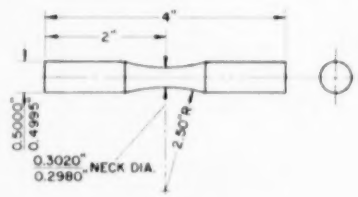

Fig. 2 Dimensions of Fatigue-Test Specimens

hardness range C28 to C32. The shape of the test specimens used is shown in Fig. 2. Great care was exercised in the roughing, finish-turning, and polishing operations. The final polish marks were parallel to the axis of the specimen. The roughness of the final surface was of the order of 4 microin. Tests of hardness, yield point, and ultimate strength were conducted to control the properties of the specimens used in the investigations.

Sequential-Load Tests. For the sequential-load study, about 6 specimens were tested for each sequence of stress amplitudes. Each stress pattern in the sequence for any specimen was such that the mean stress was zero. Each specimen was subjected successively to n_i cycles at stress amplitude σ_i, where $i = 1, 2, \ldots, m$. The value of σ_i for the ith step in a sequence was determined by

$$\sigma_i = \sigma_1 + (\sigma_m - \sigma_1)\left(\frac{i-1}{m-1}\right) \quad \ldots\ldots\ldots [4]$$

The value n_i for each step in the sequence except the last was determined by

$$n_i = N_i/m \quad \ldots\ldots\ldots [5]$$

where N_i is the number of cycles at stress amplitude σ_i which would produce failure according to the mean S-N curve. The value of n_m was determined by counting the number of cycles required to produce failure during the last step in the sequence. In case failure occurred before the last step in the planned sequence, say the step $i = f$, then, of course, $n_m = n_{m-1} = n_{m-2} = \ldots = n_{f+1} = 0$, and n_f = cycles of operation at σ_f before failure.

Simple Reversed-Stress Endurance Tests. The simple reversed-stress endurance properties were determined for the 76S-T61 aluminum alloy and for the SAE 4340 steel alloy. A total of 59 specimens was tested to determine the S-N curve for the aluminum alloy. For the steel alloy, 40 specimens were tested. Although the results of these tests are of interest and of significance in themselves, they were conducted primarily as a supplement necessary to the interpretation of the results of the sequential-load tests.

Test Results

Sequential-Load Tests. The results of the sequential-load tests are summarized in Table 1. It will be observed that in most cases at least 6 specimens were tested for each set of values of σ_1, σ_m, and m. The column marked σ_1 indicates the first stress amplitude used in the sequence. The column marked σ_m indicates the last stress amplitude used in the planned sequence. The value of $\Sigma(n_i/N_i)_{avg}$ gives the average for all the specimens tested under a particular set of values of σ_1, σ_m, and m. The value of $\Sigma(n_i/N_i)_{max}$ was computed for the one specimen of the set which showed the longest total life. The value of $\Sigma(n_i/N_i)_{min}$ was computed for the one specimen which showed the shortest total life. All values of $\Sigma(n_i/N_i)$ shown in Table 1 were computed by using the mean value of N_i as determined from the S-N curves for the materials tested.

Simple Reversed-Stress Endurance Tests. The S-N curves for the two materials tested are shown in Figs. 3 and 4. It will be noted that for the aluminum alloy 10 specimens were tested at a stress level of 50,000 psi and 10 others were tested at 25,000 psi. Similar multiple tests were conducted with the steel alloy. These tests were performed to study the effect of scatter.

Fracture-Appearance Observations. An examination of the specimens tested in determining the S-N characteristics of the two alloys showed that the fractures could be classified into three types on the basis of appearance and geometry of the ruptured surfaces. For convenience these may be called type-S (side), type-R (ring), and type-J (jagged) fractures. In the type-S fracture, a crack usually started at only one point on the side of the specimen and progressed across the specimen to a point at the opposite side before final separation. Fig. 5 shows a typical fracture of this kind.

In the type-R fracture, cracks started at a great many points around the circumference and progressed uniformly toward the center where final rupture occurred. This crack did not progress more than a few hundredths of an inch before complete separation occurred. Fig. 6 is an example of this type of fracture.

In the type-J fracture, the surface was extremely jagged and it

[5] "A Review of Cumulative Damage in Fatigue," by N. M. Newmark, Fatigue and Fracture of Metals Symposium held at the Massachusetts Institute of Technology, June 19–22, 1950, pp. 197–227.

[6] "The Influence of Fluctuations in Stress Amplitude on the Fatigue of Metals," by T. J. Dolan, F. E. Richart, Jr., and C. E. Work, Proc. ASTE, vol. 49, 1949, pp. 664–682.

[7] "Cumulative Damage in Fatigue in Steel," by D. R. Kibbey, thesis in mechanical engineering, The Ohio State University, 1949.

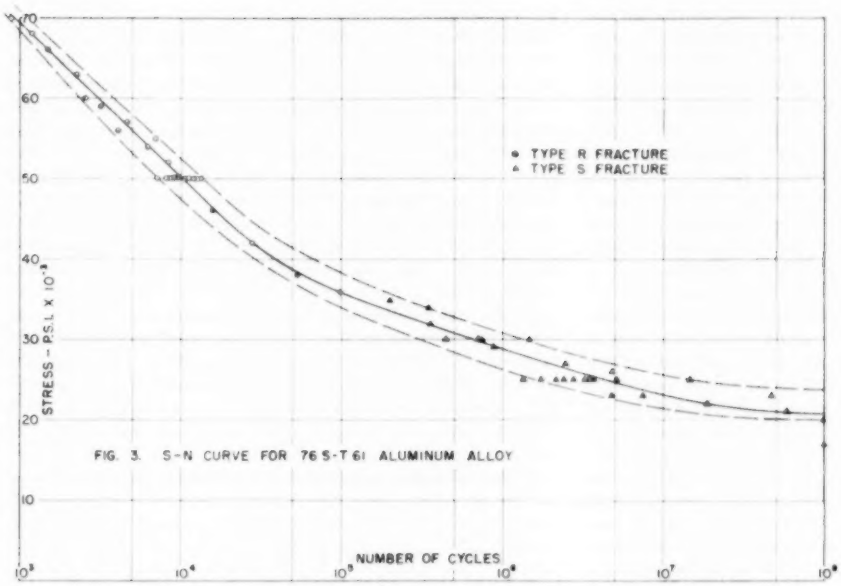

FIG. 3 (*left*) *S-N* CURVE FOR 76S-T61 ALUMINUM ALLOY

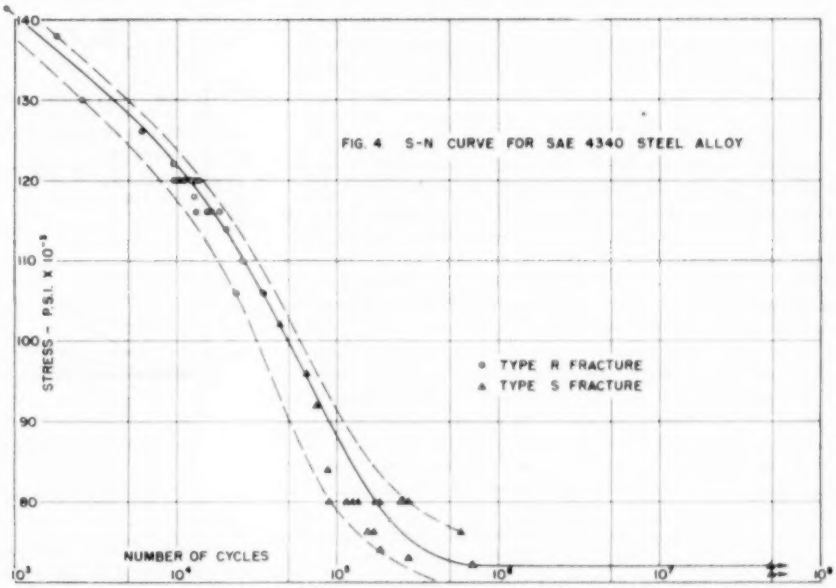

FIG. 4 (*right*) *S-N* CURVE FOR SAE 4340 STEEL ALLOY

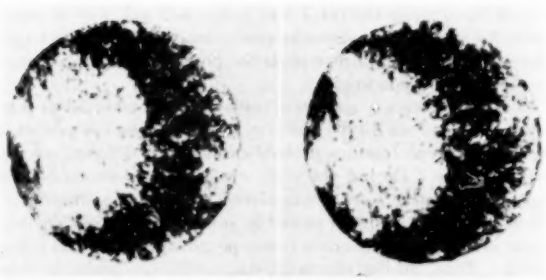

FIG. 5 TYPE-S FATIGUE FRACTURE OF 76S-T61 ALUMINUM ALLOY

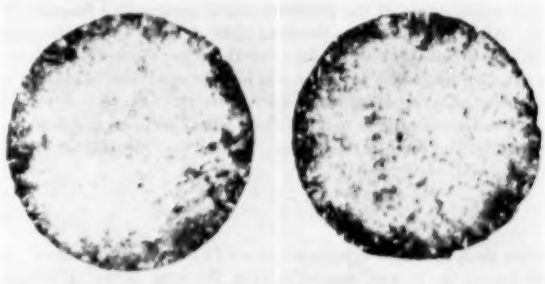

FIG. 6 TYPE-R FATIGUE FRACTURE OF 76S-T61 ALUMINUM ALLOY

was not possible to distinguish where the fracture had started nor how it had progressed. This type of fracture was observed in only a few of the large number of specimens tested. Of the 59 aluminum-alloy specimens tested in determining the S-N curve, only 4 showed a type-J fracture, and of the 40 steel specimens tested, none of the fractures was of type J.

In Figs. 3 and 4, the type fracture observed for each specimen is indicated. It will be noted that for each of the alloys there is a stress amplitude above which only type-R fractures were found and below which only type-S fractures were observed. For the aluminum alloy this stress amplitude was approximately 35,000 psi; for the steel alloy it was approximately 105,000 psi.

These observations appear to indicate that fatigue failure is caused by cracks which progress from some stress risers or fatigue nuclei. It is possible that these nuclei existed before any stress was applied. Apparently the likelihood of a crack developing is a function of the seriousness of individual nuclei with respect to the stresses applied. Each individual nucleus, therefore, has its own threshold of susceptibility and there is a wide variation of susceptibility in any aggregate of such nuclei. At low stress levels, the effect of this variation is more pronounced than at high stress levels and, therefore, only a small number of these nuclei (usually one) are sufficiently serious to develop into progressive cracks, and a type-S failure results. At high stress levels, on the other hand, many of the nuclei are serious enough to produce cracks, and a type-R failure occurs. Furthermore, an examination of the R-type fractures clearly reveals that there is a correlation between stress level and the number of fatigue nuclei which result in independent cracks. At the higher stress levels the larger number of cracks are observed.

Interpretation of Results

Fatigue damage is a difficult term to define precisely or quantitatively. It may be defined qualitatively as that which is experienced by a material subjected to cyclic stressing which reduces the number of cycles of stress the material will yet withstand before final failure. Fatigue damage is probably a function of the following physical variables: The number of independent fatigue nuclei or progressive-fracture cracks which are operative, the sizes and shapes of these cracks, the cold-working effect on the material adjacent to the crack surfaces, and a possible thermal-recrystallization effect in the same material. For the purposes of this paper, fatigue damage is assumed to be representable by term D, which is zero when no cyclic-stress history exists in a specimen and is unity when the specimen has finally broken into two pieces under the influence of cyclic stressing. It is assumed that damage may be expressed quantitatively as a function of the cycle ratio number, n_i/N_i. Thus $D = f(n_i/N_i)$.

Some clue as to the form of this functional relationship in the range, $0 < D < 1$, may be deduced from the results of the sequential-load tests recorded in Table 1, and also from observations which can be made relative to the physical appearance of fractured specimens and the phenomenon of progressive fracture itself. Although the sequential-load tests of Table 1 offer the most conclusive substantiation for the damage concepts proposed herein, the secondary evidence will be discussed first, since it is of value as background information.

Several observations may be cited which seem to suggest that the functional form of Equation [1] may be represented by the exponential relationship

$$D = (n_i/N_i)^{x_i},\ x_i > 1 \qquad [6]$$

rather than the linear equation assumed by Miner and others. In the foregoing, it was suggested that the rate at which fatigue damage is accumulated in a specimen at any given time is a function of the number of fatigue cracks in progress and the sizes and shapes of these cracks. It seems reasonable to assume that the rate of damage must increase as the crack sizes increase, and as the shapes of the cracks change in such a manner as to result in larger stress-concentration factors. As a fatigue crack progresses through a material it is apparent that the size of the crack increases and also the stress-concentration factor increases. Hence, it may be concluded that the form of Equation [6] must be such as to result in a plot of D versus (n_i/N_i), which is concave upward and to the left on co-ordinates similar to those of Fig. 1. Such a relationship may be expressed by the exponential Equation [6]. Fig. 7 shows several curves representing equations of this form.

A study of the S-type and R-type fractures gives a clue regarding the correlation which might be expected between values of x_i and σ_i. The S (side)-type fractures, which usually involved only one fatigue crack, were consistently found at low stress levels. It is reasonable to suspect that fatigue damage in a specimen which was stressed at low level took place very slowly during the

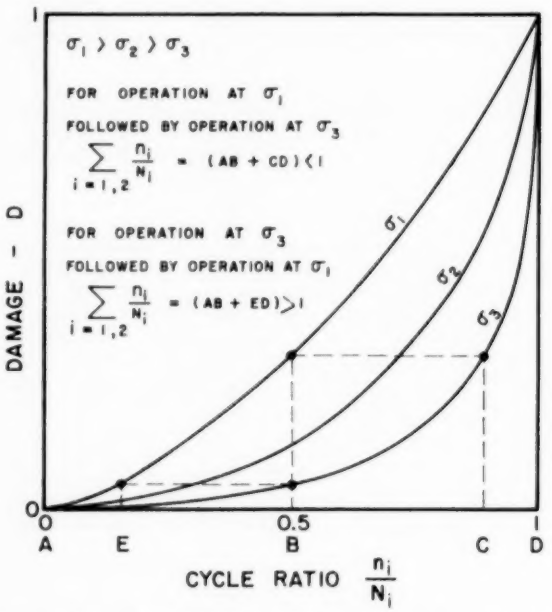

Fig. 7 Cycle Ratio Versus Damage Curves for $D = (n_i/N_i)^{x_i}$

early cycles of its life, since during that period only one crack was in operation and the size of that crack and its stress-concentration effect were relatively small. On the other hand, the rate of damage was probably very high during the latter stages of the life of the specimen when the crack had progressed half way or more across the neck, and the stress-concentration factor was very large. The curve of σ_3 in Fig. 7 represents the progress of fatigue damage in a low-stressed specimen.

In contrast with a specimen tested at low-stress level, and which exhibited an S-type fracture, a specimen which exhibited an R (ring)-type fracture probably followed a different-shaped damage curve. During the early cycles of a specimen of this type, many cracks were accumulating damage simultaneously. Various susceptible nuclei probably started and developed into larger cracks by a chain-reaction-type process of mutual interaction. Thus, during the early stages, damage probably progressed more rapidly than in the corresponding period of the S-

type specimen. However, owing to the size and shape of the ring of cracks in the highly stressed specimen, the increase in damage rate at later life stages was probably not so great as the increase suggested for the low-stress specimen. The damage curve of σ_1 in Fig. 7 represents the likely rate of damage for a highly stressed specimen.

It may be concluded from this discussion that the relationship, $D = (n_i/N_i)^{x_i}$, $x_i > 1$, shown in Equation [6], probably quite closely expressed fatigue-damage accumulation during progressive fracture. It also may be concluded that in Equation [6] large exponents x_i probably correspond to large values of stress amplitude σ_i.

Impressive substantiation for the type damage curves proposed in the foregoing is contained in the sequential-load test results of Table 1. An examination of Table 1 clearly establishes one significant fact. In every series of tests in which the stress amplitude was increased from a low value to a high value, the number $\Sigma(n_i/N_i)_{avg}$ was greater than unity, while in every series of tests in which the stress amplitude was decreased from a high value to a low value, the number $\Sigma(n_i/N_i)_{avg}$ was less than unity. From this, it may be deduced that at low stress levels very little damage was done during the early cycles, but close to the end of the endurance life the damage rate increased to a very large value. On the other hand, at high stress levels the damage rate was high during the initial stages of life but did not increase greatly during the latter stages. Thus it would seem that damage curves, of the type shown in Fig. 7, are substantiated by the sequential-load tests. For further clarification of this statement a two-step illustration is given in Fig. 7.

Curves of the type shown in Fig. 7 have been used with success by the authors to predict results of tests using various numbers of steps in ascending and descending increments. Such damage curves or their equations may be used to predict endurance lives for any combination of stresses induced by sequential loading.

Effect of Scatter

It will be noted from Fig. 3, that for the aluminum alloy the 10 specimens tested at a stress amplitude of 50,000 psi indicate a life range from 7.2×10^3 cycles to 14×10^3 cycles. The longest life was approximately 2 times the shortest life for these specimens. At the lower amplitude of 25,000 psi the life varied from 13.5×10^6 cycles for the shortest life to 14.5×10^7 for the longest life. This covers a range of approximately 10 to 1. The scatter found by testing 10 specimens at each of two stress levels for the steel specimens was somewhat smaller. At a high stress amplitude of 120,000 psi the life ranged from 9.6×10^3 cycles to 13.5×10^3 cycles, while at the lower stress amplitude of 80,000 psi the life ranged from 9×10^4 to 27×10^4 cycles.

While the testing of only 10 specimens at one stress level is far from conclusive, it is significant to note that in each case the scatter increases as the stress amplitude decreases. The testing of 10 specimens at one stress amplitude gives an indication of the order of magnitude of variation in life, but the number of specimens is too small to attempt to draw probability curves. At the present time, the authors are conducting tests in which 100 specimens are tested at each of three different stress amplitudes for the purpose of determining life-distribution curves. The results of these tests will be reported in a later paper.

Since there is considerable scatter in life values for a group of specimens tested at a given stress amplitude, it is not possible to state a true value of N_i for any particular specimen subjected to sequential-loading tests. For this reason, conclusions regarding the effect of sequential loading must be based upon average values for groups of specimens.

The actual magnitude of the scatter to be expected in sequential-load tests may be illustrated by performing calculations using the values in line 1 of Table 1, and using the maximum and minimum values of life from the reversed-stress endurance curves at the two stress levels indicated.

Table 2 shows the results of such calculations for the two specimens which showed the largest and smallest values for $\Sigma(n_i/N_i)$ based on the average values of N_i.

Table 2 indicates that if the sequential-load specimen which showed the greatest total life had reversed-stress endurance lives corresponding to the minimum values of the S-N scatter band, the value of $\Sigma(n_i/N_i)$ would have been 2.63. If the same specimen had values of N_i corresponding to the maximum values of the S-N scatter band, $\Sigma(n_i/N_i)$ would have been 1.19. For the second

TABLE 1 SEQUENTIAL-LOAD TESTS[a]

Material	$\sigma_1 \times 10^{-3}$	$\sigma_m \times 10^{-3}$	n_1	$\Sigma\left(\frac{n_i}{N_i}\right)_{avg}$	$\Sigma\left(\frac{n_i}{N_i}\right)_{max}$	$\Sigma\left(\frac{n_i}{N_i}\right)_{min}$	No. of specimens
SAE 4340	80	120	2	1.14	1.51	0.71	10
	80	120	4	1.13	1.43	0.70	10
	80	120	6	1.14	1.40	1.00	6
	80	120	10	1.17	1.66	0.77	13
	80	120	15	1.10	1.27	1.00	3
	80	120	20	1.05	1.40	0.90	6
	120	80	2	0.73	0.84	0.64	6
	120	80	4	0.74	0.84	0.61	6
	120	80	6	0.76	0.86	0.65	6
	120	80	10	0.81	0.84	0.78	6
	120	80	15	0.73	0.79	0.60	9
	120	80	20	0.69	0.79	0.57	13
76S-T61	25	50	2	1.45	1.61	1.00	6
	25	50	4	1.46	1.70	1.00	6
	25	50	6	1.51	1.66	0.92	6
	25	50	10	1.52	1.77	1.34	6
	50	25	2	0.63	0.71	0.58	6
	50	25	4	0.71	0.86	0.56	6
	50	25	6	0.79	0.91	0.92	3
	50	25	10	0.94	0.96	0.92	3

[a] Value of N_i for each step in sequence is determined from the S-N curve for reversed stress (Fig. 3 or Fig. 4).

TABLE 2 EFFECT OF SCATTER

Specimen	i	Stress amplitude	$N_{i(max)}$	$N_{i(mean)}$	$N_{i(min)}$	n_i	$\left(\frac{n_i}{N_{i\,max}}\right)$	$\left(\frac{n_i}{N_{i\,mean}}\right)$	$\left(\frac{n_i}{N_{i\,min}}\right)$
Longest lived	1	80×10^3	2.80×10^6	1.80×10^6	0.90×10^6	0.90×10^6	0.32	0.50	1.00
	2	120×10^3	0.15×10^6	0.13×10^6	0.08×10^6	0.13×10^6	0.87	1.00	1.63
						Totals	1.19	1.5	2.63
Shortest lived	1	80×10^3	2.80×10^6	1.80×10^6	0.90×10^6	0.90×10^6	0.32	0.50	1.00
	2	120×10^3	0.15×10^6	0.10×10^6	0.08×10^6	0.027×10^6	0.18	0.21	0.34
						Totals	0.50	0.71	1.34

specimen, which showed a smaller total life, the corresponding values for $\Sigma(n_i/N_i)$ would be 1.34 and 0.50.

It is probable that the specimen which showed the greatest total life had values of N_i corresponding to the maximum values of the scatter band, whereas the specimen which showed the lowest total life had values of N_i corresponding to the minimum values of the scatter band. Thus, the most likely values of $\Sigma(n_i/N_i)$ for these two specimens are probably between 1.19 and 1.34. It is significant that for this sequence the average value of $\Sigma(n_i/N_i)$, computed by taking N_i from the mean of the S-N curve and applying it to all 10 of the specimens tested, was 1.14.

Thus, it is not possible to arrive at unique quantitative evaluations of the effects of stress amplitude, direction of stress-amplitude change, and number of steps, since each particular test specimen or each machine member has its own individual S-N curve which may be quite different from any average S-N curve which may be determined for a particular material. For design purposes, therefore, it will be necessary to introduce a factor of probability into any mathematical expression which attempts to relate damage to cycle ratio or which attempts to describe the total life in terms of the properties under simple loading conditions.

Conclusions

In conclusion, it appears that a closer approach may be made to an accurate prediction of endurance life by utilizing a concept of fatigue damage similar to that upon which the curves of Fig. 7 have been based. It should be pointed out, however, that the validity of predictions of total life for machine members subjected to complex stress-cycle patterns must depend upon a theory of damage that takes into account the statistical aspect of fatigue failures.

Linkage Design—A Note on One Method

By A. S. HALL, JR.,[1] and D. C. TAO[2]

A graphical procedure, using velocity-vector diagrams, is suggested for determining the coefficients $\partial S/\partial p_n$, where S represents the output displacement of a linkage and p_n are parameters (dimensions) of the linkage. These coefficients appear in a design procedure used by Svoboda[3] on the 4-bar linkage. It is suggested that his procedure may prove useful in the design of more complex linkages.

Introduction

FOR a large class of problems in the size synthesis of linkages, the desired kinematic performance of the linkage to be designed can be reduced to a functional relation between the displacements of the output and input links

$$S_o = \phi_d(S_i) \quad [1]$$

The designer must make a tentative selection of the type of linkage to be employed. The selected linkage will be characterized by disposable parameters (linear or angular dimensions) p_1, p_2, . . . p_n, ... p_k, and will generate a function

$$S = \phi_g(p_1, p_2, \ldots p_n, \ldots p_k, S_i) \quad [2]$$

The design problem then lies in determining the parameters p_n such that, within specified tolerances, the generated function S will equal the desired function S_o at all values of S_i.

There are several techniques available for attacking the problem just formulated. If the specifications call for close agreement of S and S_o at a small number of values of S_i, with no limitations elsewhere, then an exact geometric solution may be feasible. If the specifications are quite stringent in the immediate vicinity of one value of S_i but loose elsewhere, then some of the theory of point-path curvature and polode (centrode) curvature may give a direct solution. Sieker[4] has presented some excellent work along these lines.

Another common situation is that in which the tolerances on the output S_o, over the full range of input S_i, are large enough to make a practical design reasonably possible but small enough to preclude finding a solution by "hit-and-miss" methods. This situation is encountered, for example, in designing linkages for computing mechanisms. Svoboda[3] has developed some practical methods for handling this problem in regard to the slider-crank and four-bar linkages.

One feature of Svoboda's design process seems especially worthy of further study with a view to extending its application to more complex linkages. The feature referred to is the method of adjusting the linkage parameters to improve a design which is close to that desired but is not yet within specified tolerances. The basic idea of the adjusting method is as follows:

Let p_n be the disposable parameters of the tentative design.

Let e be the difference between the desired displacement of the output link and the displacement produced by the tentative design

$$e = S_o - S \quad [3]$$

Let Δp_n represent small changes to be made in the parameters p_n to improve the design. Then we may write, approximately

$$e = \sum_{n=1}^{n=k} \frac{\partial S}{\partial p_n} \Delta p_n \quad [4]$$

If there are k disposable parameters then Equation [4] may be written for k selected values of S_i. The resulting set of equations may then be solved simultaneously for values of the parameter changes, Δp_n. The new design, characterized by adjusted parameters, $p_n + \Delta p_n$, may, with a number of reservations, be expected to show an improved performance.

There are several difficulties in the use of this procedure. It does not guarantee arriving at a design which is within the specifications, but it does show promise of being a useful tool for the designer's collection.

One of the tedious steps in the use of the process just described is evaluation of the coefficients $\partial S/\partial p_n$. It is the primary purpose of this paper to point out a graphical means for doing this.

Coefficients as Velocity Ratios

The coefficient $\partial S/\partial p_n$, where p is a particular parameter of the linkage, expresses the rate at which the displacement of the output link changes with a change in parameter p for a particular value of S_i and with all other parameters constant. If, in Equation [2], all parameters except p_1, for example, are held constant, and if p_1 is permitted to vary with time t, then for a particular value of S_i

$$\frac{\partial S}{\partial p_1} = \frac{dS/dt}{dp_1/dt} \quad [5]$$

It thus appears that $\partial S/\partial p_1$ can be expressed as the ratio of two velocities and hence can be evaluated by any of the several means for analyzing velocity relationships in linkages. A simple example will make this more clear.

Slider-Crank Example. Consider the slider-crank linkage in

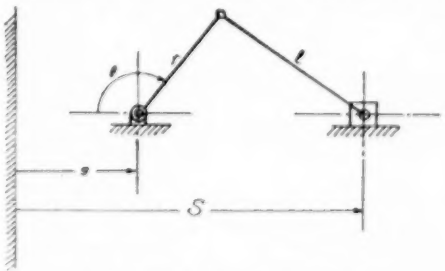

Fig. 1 Slider Crank; Variables S and θ (Parameters g, r, and l.)

Fig. 1. Let the slider be the output link and the crank the input link. The linkage generates a function

$$S = \phi(r, l, g, \theta) \quad [6]$$

in which r, l, and g are parameters of the linkage, θ is the displacement (angular) of the input link, and S is the displacement

---

[1] Professor of Mechanical Engineering, Purdue University, Lafayette, Ind. Mem. ASME.

[2] Chief Engineer, Portage Machine Company, Akron, Ohio.

[3] "Computing Mechanisms and Linkages," by A. Svoboda, McGraw-Hill Book Company, Inc., New York, N. Y., 1948, pp. 199–222.

[4] "Ermittlung von Gelenkvierecken aus den Krummungs-halbmessern der Polbahnen und deren Anderungen," by K. H. Sieker, *Die Technik*, vol. 3, April, 1948, pp. 170–174.

Contributed by the Machine Design Division and presented at the Annual Meeting, New York, N. Y., November 29–December 4, 1953, of The American Society of Mechanical Engineers.

Note: Statements and opinions advanced in papers are to be understood as individual expressions of their authors and not those of the Society. Manuscript received at ASME Headquarters, June 23, 1952. Paper No. 53—A-142.

(linear) of the output link. Equation [5] applied to the crank length r becomes

$$\frac{\partial S}{\partial r} = \frac{dS/dt}{dr/dt} \quad \ldots\ldots [7]$$

Fig. 2 illustrates the meaning of Equation [7] in terms of velocity vectors. The crank is allowed to stretch with a velocity represented by the vector dr/dt. With g, l, and θ constant the slider will then move with a velocity represented by the vector dS/dt. The ratio of the lengths of these vectors, drawn to any convenient scale, gives the coefficient $\partial S/\partial r$ for the particular value of θ.

To determine $\partial S/\partial l$ the connecting rod is stretched with a velocity represented in Fig. 3 by the vector dl/dt, resulting in movement of the slider at a velocity represented by the vector dS/dt. Changing parameter g merely shifts the entire linkage with respect to the reference for S. Hence $\partial S/\partial g = 1$ for all values of θ. The three coefficients, $\partial S/\partial r$, $\partial S/\partial l$, and $\partial S/\partial g$, have been plotted in Fig. 4 for the full range of input crank angle, θ. For more complex linkages such curves may yield valuable hints as to which parameters can most fruitfully be changed to improve the design.

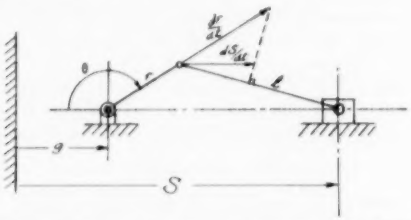

Fig. 2 Slider Crank; Velocity Vectors for Determining $\partial S/\partial r$

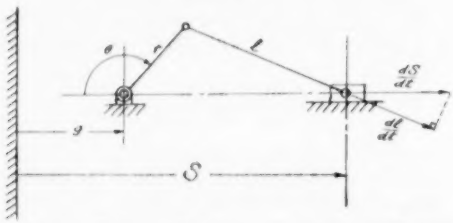

Fig. 3 Slider Crank; Velocity Vectors for Determining $\partial S/\partial l$

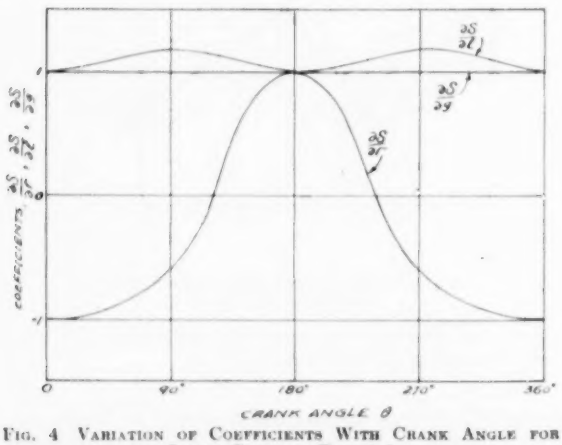

Fig. 4 Variation of Coefficients With Crank Angle for Slider Crank of Figs. 1–3

Four-Bar-Linkage Example. For another example, consider the 4-bar linkage in Fig. 5. Let the left crank AD be the input link and the right crank BC the output link. The fixed link CD is of unit

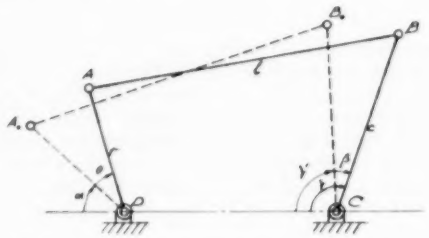

Fig. 5 4-Bar Linkage; Variables β and θ; Parameters r, l, c, and α

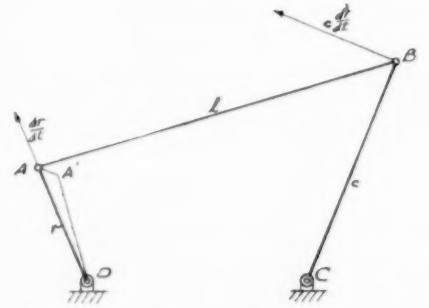

Fig. 6 4-Bar Linkage; Graphical Determination of $d\gamma/dt$ for Assumed dr/dt

length and connecting rod AB is l. The initial position is A_0B_0DC, with A_0D at an angle α with CD. The disposable parameters are r, l, c, and α. Thus the angular displacement β of the output link BC measured from its initial position B_0C can be expressed as a function of r, l, c, α, and θ, i.e.

$$\beta = \phi(r, l, c, \alpha, \theta) \quad \ldots\ldots [8]$$

where θ is the angular displacement of the input link AD from its initial position A_0D.

Equation [5] applied to the crank lengths r, c, connecting-rod length l, and α becomes

$$\partial\beta/\partial r = (d\beta/dt)/(dr/dt) \quad \ldots\ldots [9]$$

$$\partial\beta/\partial c = (d\beta/dt)/(dc/dt) \quad \ldots\ldots [10]$$

$$\partial\beta/\partial l = (d\beta/dt)/(dl/dt) \quad \ldots\ldots [11]$$

$$\partial\beta/\partial\alpha = (d\beta/dt)/(d\alpha/dt) \quad \ldots\ldots [12]$$

If we express the angular displacements of the output link BC and its initial position B_0C from the fixed link CD as γ and γ', respectively, then $\beta = \gamma - \gamma'$ and the foregoing equations become

$$\partial\beta/\partial r = (d\gamma/dt)/(dr/dt) - (d\gamma'/dt)/(dr/dt) \quad \ldots\ldots [9a]$$

$$\partial\beta/\partial c = (d\gamma/dt)/(dc/dt) - (d\gamma'/dt)/(dc/dt) \quad \ldots\ldots [10a]$$

$$\partial\beta/\partial l = (d\gamma/dt)/(dl/dt) - (d\gamma'/dt)/(dl/dt) \quad \ldots\ldots [11a]$$

$$\partial\beta/\partial\alpha = (d\gamma/dt)/(d\alpha/dt) - (d\gamma'/dt)/(d\alpha/dt) \quad \ldots\ldots [12a]$$

Fig. 6 illustrates the graphical solution of $(d\gamma/dt)/(dr/dt)$ in terms of velocity vectors. The left crank is allowed to stretch with a velocity represented by the vector dr/dt. At that position,

with l, c, α, and θ constant, the right crankpin B will move with a velocity represented by the vector $c(d\gamma/dt)$. If we use $[AD]$ to represent dr/dt and draw AA' perpendicular to BC and $A'D$ perpendicular to AB, then $[AA']/[AD]$ will represent

$$c\,\frac{d\gamma}{dt}\Big/\frac{dr}{dt}$$

hence

$$(d\gamma/dt)/(dr/dt) = [AA']/c[AD]$$

Similarly, Fig. 7 illustrates the solution of

$$\frac{d\gamma}{dt}\Big/\frac{dc}{dt}$$

in terms of velocity vectors. If we hold α, θ, r, and l constant

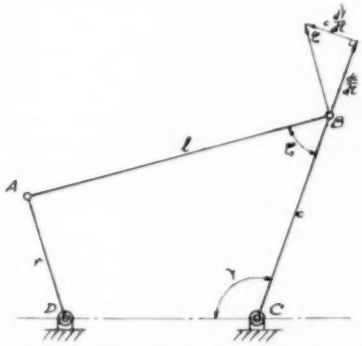

FIG. 7 4-BAR LINKAGE; GRAPHICAL DETERMINATION OF $d\gamma/dt$ FOR ASSUMED dc/dt

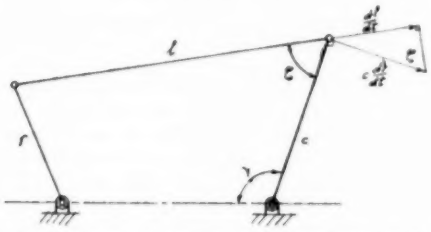

FIG. 8 4-BAR LINKAGE; GRAPHICAL DETERMINATION OF $d\gamma/dt$ FOR ASSUMED dl/dt

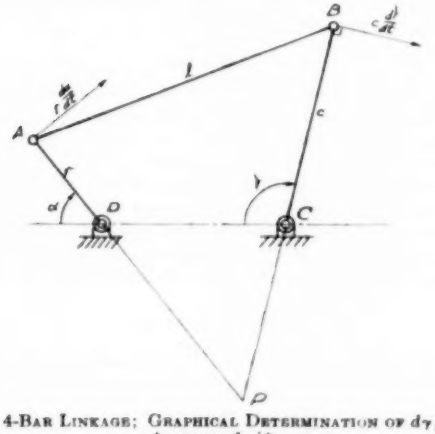

FIG. 9 4-BAR LINKAGE; GRAPHICAL DETERMINATION OF $d\gamma/dt$ FOR ASSUMED $d\alpha/dt$

and stretch BC with a velocity dc/dt, $c(d\gamma/dt)$ can be found easily as shown

$$\frac{d\gamma}{dt}\Big/\frac{dc}{dt} = c\,\frac{d\gamma}{dt}\Big/c\,\frac{dc}{dt} = \frac{1}{c}\cot\zeta$$

where ζ is the angle formed by AB and BC.

To determine

$$\frac{d\gamma}{dt}\Big/\frac{dl}{dt}$$

the connecting rod is stretched with a velocity represented in Fig. 8 by the vector dl/dt while α, θ, r, and c are held constant. Consequently

$$\frac{d\gamma}{dt}\Big/\frac{dl}{dt} = c\,\frac{d\gamma}{dt}\Big/c\,\frac{dl}{dt} = \frac{1}{c}\csc\zeta$$

In order to find $(d\gamma/dt)/(d\alpha/dt)$ in Equation [12a], $(d\gamma/dt)/(d\alpha/dt)$ can be transformed into

$$\frac{r}{c}\left(\frac{c\,\dfrac{d}{dt}}{r\,\dfrac{d}{dt}}\right) = \frac{r}{c}\,\frac{[PB]}{[PA]}$$

as shown in Fig. 9.

In Equations [9a to 12a], the values of

$$\frac{d\gamma'}{dt}\Big/\frac{dr}{dt},\quad \frac{d\gamma'}{dt}\Big/\frac{dc}{dt},\quad \frac{d\gamma'}{dt}\Big/\frac{dl}{dt},\text{ and }\frac{d\gamma'}{dt}\Big/\frac{d\alpha}{dt}$$

can be found in the same way as just described but with the linkage at its initial position with A_0D making an angle α with CD.

PARAMETERS OTHER THAN LINK DIMENSIONS

Frequently, in designing a linkage, certain conditions may be imposed at the start, such that functional relations are established between several of the linkage dimensions. If these conditions are to be preserved then it will not be possible to vary independently all the linkage dimensions, and some parameter other than a link dimension may be more conveniently used. To illustrate this situation consider the offset slider crank shown in Fig. 10. In this linkage the slider displacement S is a function of the crank displacement θ, the crank pivot location g, the offset h, the crank length r, and the rod length, l

$$S = \phi(\theta, g, h, r, l) \qquad [13]$$

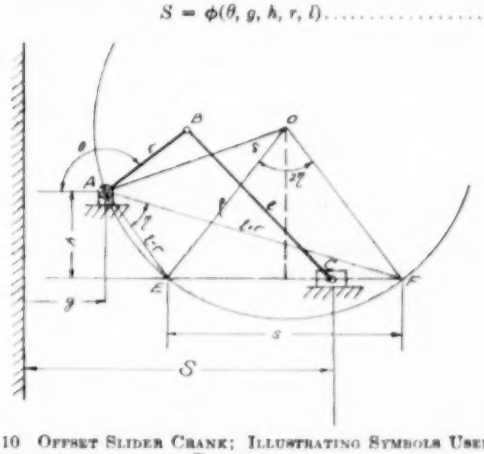

FIG. 10 OFFSET SLIDER CRANK; ILLUSTRATING SYMBOLS USED IN DISCUSSION

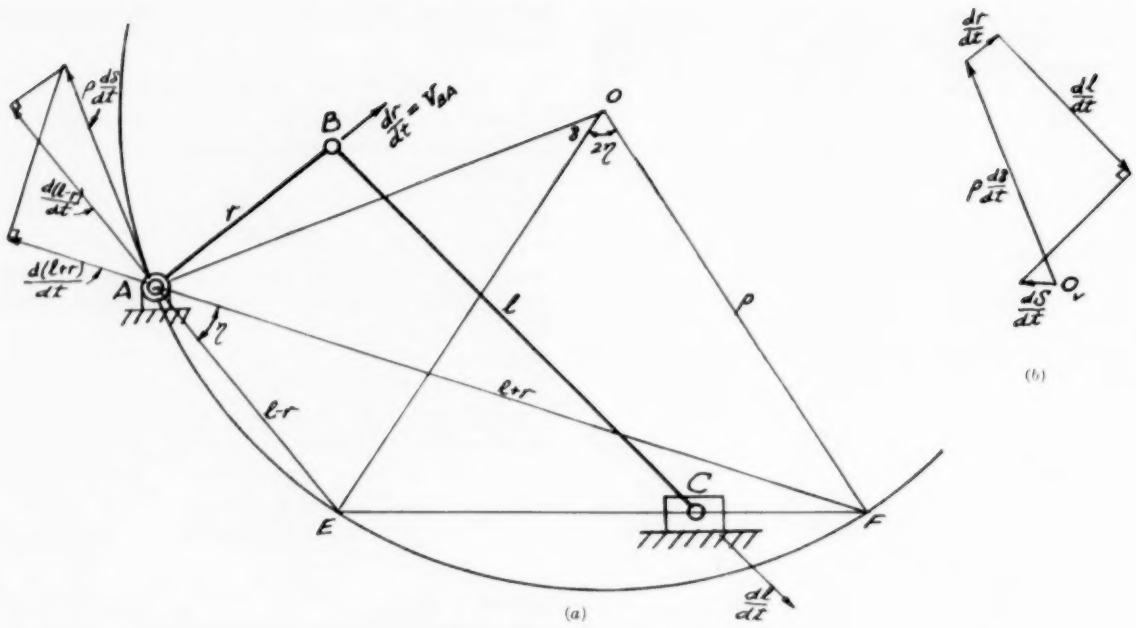

FIG. 11 OFFSET SLIDER CRANK

(a, Determination of dr/dt and dl/dt for assumed $d\delta/dt$; b, velocity-vector diagram used to determine dS/dt for crank position shown in a.)

The stroke length of the slider is s and the time ratio of slow to fast strokes (for constant angular velocity of the crank) is $(180 + \eta)/(180 - \eta)$. By inspecting Fig. 10 we find

$$s = [(l + r)^2 - h^2]^{1/2} - [(l - r)^2 - h^2]^{1/2} \quad [14]$$

and

$$\eta = \text{arc cos}[h/(l + r)] - \text{arc cos}[h/(l - r)] \quad [15]$$

Now let us suppose that we are adjusting the dimensions of such a linkage but we require that the values of s and η be not disturbed. Dimensions r, l, and h may be changed, but only in such a way that Equations [14] and [15] will still be satisfied with the desired values of s and η. This means that in Equation [13], instead of four adjustable parameters (g, r, l, h) we have only two (g and either r, l, or h). However, neither r, l, nor h is necessarily the most convenient parameter to use. Again referring to Fig. 10, we find that the restrictions placed on s and η mean that possible locations of the pivot A for the crank are restricted to points on the circle passing through the ends of the slider stroke (points E and F). This suggests using the position of A, as measured by the angle δ, for one parameter instead of either r, l, or h. If we do this, then

$$S = \phi(g, \delta, \theta) \quad [16]$$

and we will wish to evaluate $\partial S/\partial g$ and $\partial S/\partial \delta$ for different values of θ.

The value of $\partial S/\partial g = 1$ for all values of θ, simply because a change in g results in an equal change in S.

The procedure for evaluating $\partial S/\partial \delta$ is illustrated in Fig. 11. First write

$$\partial S/\partial \delta = \rho[(dS/dt)/\rho(d\delta/dt)] \quad [17]$$

We imagine point A to be moving in a direction tangent to the circle (center at O) with a velocity $\rho(d\delta/dt)$, while the crank and connecting rod are stretched with corresponding velocities dr/dt and dl/dt. In Fig. 11(a) we see that the component of $\rho(d\delta/dt)$ on line AF is $d(l + r)/dt$, and the component on line AE is $d(l - r)/dt$. Hence, by the following equations, we can find the velocities with which crank and rod are stretched

$$dr/dt = \frac{1}{2}[d(l + r)/dt - d(l - r)/dt] \quad [18]$$

$$dl/dt = \frac{1}{2}[d(l + r)/dt + d(l - r)/dt] \quad [19]$$

It should be noticed that dr/dt and dl/dt are not dependent on crank displacement θ and therefore must be evaluated only once in a particular problem.

Now the value of dS/dt for a particular value of θ can be found by the vector sum of the velocity of point A ($= \rho d\delta/dt$), the velocity of B relative to A ($= dr/dt$), and the velocity of C relative to B ($= dl/dt$ plus a component perpendicular to line BC). The construction of this vector diagram is shown in Fig. 11(b) for the particular crank position shown in Fig. 11(a).

CONCLUSION

The authors wish to emphasize that this paper is not intended to be at all comprehensive of linkage design problems, but merely to make a suggestion concerning one design procedure which seems to show enough promise to justify further study.

Equation [4] is approximate in that it contains only the first-order terms in a Taylor-series expansion. Should it ever appear desirable to consider the second-order terms, the coefficients could be determined by the general method outlined here, but including acceleration relations in addition to velocities.

Discussion

A. E. RICHARD DE JONGE.[5] This paper advocates one of Svoboda's (footnote 3 of the paper) design procedures in which he

[5] Mechanical Engineer and Consultant, Reeves Instrument Corporation, New York, N. Y. Mem. ASME.

establishes the error term between the actual value of a function and the value obtained from the mechanism by which it is to be represented, in form of a Taylor series expansion of which the authors have considered the first-order term only.

In this term the quotient $\partial S/\partial p_n$ occurs, where $p_1, p_2, \ldots p_n$ are the various parameters. Thus n expressions will result. These quotients, in general, are difficult to evaluate. It is to the credit of the authors that they have shown in a simple way how this can be accomplished graphically. In order to do this, they transform these ratios into velocity ratios and then proceed to evaluate the latter by means of velocity diagrams.

As examples, they present the slider-crank mechanism and the four-link mechanism. In the case of the former, the analysis is relatively straightforward. In the case of the latter, however, it is not quite so simple but still can be handled by differences of velocity ratios.

This brings up the important question how accurate the drawing work has to be in order to give accurate results, since, with differences, especially when they are small, extreme accuracy is essential. As a general rule, it may be stated that solutions based on differences of two terms should be avoided as far as possible, because a great number of digits frequently is required in numerical determinations if the two terms of the difference are of nearly the same magnitude.

In the case of parameters other than link dimensions, the authors give an analysis which, while correct, requires clearer explanations than those presented in the paper in order to make it understandable to the average engineer.

Although the authors claim no more than to have shown a geometrical method for evaluating rather simply the ratios $\partial S/\partial p_n$, it should be realized that short cuts such as the one they have made are often most desirable. They should be commended heartily for having suggested this rather simple way.

There are a few points regarding terminology which the writer would like to mention. Having advocated some 12 years ago a resumption of the study of mechanisms and kinematics in this country, he is, naturally, most gratified to see that Professor Hall has adopted, in his writings, some of the simple terms advocated by the writer in one of his papers[6] and in his discussion of a paper by Candee,[7] such as "size synthesis," "polodes," and so on. On the other hand, the authors call the two links of a four-bar mechanism, which are hinged to the frame, as shown in their Figs. 5 to 9, the "two cranks." As the writer has pointed out in a previous discussion, this is incorrect, as a "crank" is a link that can make complete revolutions continuously while the link that cannot make a full revolution, but performs only an oscillating motion, should be called "lever" or "oscillating link."

The writer deems it essential that we here in the United States should not succumb to the pitfalls that German kinematicians have, who have created almost as many terms for the same kinematic element, and even for entire mechanisms, as there have been writers. Only recently they were obliged to discuss at a meeting of the section for "Getriebelehre" (Science of Mechanisms and Kinematics) of the Verein deutscher Ingenieure (VDI) the question of how to establish a uniform and standard terminology. The writer hopes that here in the United States we may learn from their mistakes and avoid the use of loose terms and, in general, of a loose terminology by calling the various items by proper and carefully established names. Thus, for example, the term "linkage" should simply be a synonym for "kinematic chain" and not stand for "mechanism," because linkage implies an assembly of links without preference for any one of them, such as for that which forms the frame in the case of a mechanism.

The writer hopes that agreement on a fundamental terminology may be reached, and he suggests that this Society should take the initiative in bringing this about. His advice and assistance are always at the disposal of the Society.

Authors' Closure

The authors appreciate Mr. de Jonge's comments and are fully in agreement with his suggestions concerning the desirability of standardizing terminology in the field of mechanisms and kinematics.

Mr. de Jonge brings up the question of accuracy required in the graphical work, pointing out that the example problem on the four-bar mechanism involves differences of graphically determined quantities. This is certainly an important question in any problem. No blanket statement can be made concerning the per cent accuracy attainable, as this will vary in any one problem from one position of the mechanism to the next. Perhaps the most important thing, in so far as this paper is concerned, is that determination of the coefficients $\partial S/\partial p_n$ by velocity analysis as suggested will give results to one more significant figure, than would determination of the same coefficients by measurements of small displacements. Should the graphical determination of these coefficients not be sufficiently accurate for a particular problem, the velocity diagrams can still be a great help in setting up the necessary procedure for calculating the coefficients.

[6] "A Brief Account of Modern Kinematics," by A. E. Richard de Jonge, Trans. ASME, vol. 65, 1943, pp. 663–675.

[7] "Kinematics of Disk Cam and Flat Follower," by A. H. Candee, Trans. ASME, vol. 69, 1947, pp. 718–722.

Thermal-Shocking Austenitic Stainless Steels With Molten Metals

By R. A. TIDBALL[1] and M. M. SHRUT,[2] CALLERY, PA.

Specimens of AISI 347 pipe and pipe welds have been subjected to repeated thermal shocks by quenching the inner surface with cool sodium-potassium alloy. The equipment used and a method of measuring the transient fluid and wall temperatures are described. Temperature changes encountered during tests and resulting stresses are shown. The effects of 2500 transient thermal cycles on one specimen are discussed.

Nomenclature

The following nomenclature is used in the paper:

E = Young's modulus
m = constant
NaK = sodium-potassium alloy
T = temperature, deg F
α = coefficient of thermal expansion, in/in. deg F
σ = stress, psi
μ = Poissons ratio

Subscripts:

i = inside surface
l = longitudinal
m = mean
o = outside

Introduction

Thermal shock and fatigue resulting from thermal cycling must be considered in the design of high-temperature heat-transfer systems using molten metals as heat-transfer fluids. Rapid temperature changes of the fluid can be caused by sudden loss of either heating or cooling, causing stresses in excess of the yield point of the container material.

These high stresses under thermal shock are inherent because of the relatively low thermal resistance of the interface of molten metals and the container wall. For example, sodium flowing at 10 fps through 8-in. schedule-40 pipe at 850 F has a heat-transfer coefficient of approximately 3000 Btu/(hr)(sq ft)(deg F), or a thermal resistance of 0.00033. This is roughly equivalent to the thermal resistance of 0.050 in. of austenitic stainless steel.

It is evident, owing to these low thermal resistances, that the temperature at the inner surface of the piping containing sodium would vary with the temperature of the liquid metal.

During rapid temperature changes, stress patterns are set up in three directions—radially outward from the center, tangentially, and longitudinally along the wall. The tangential and longitudinal stresses reach maximum values at the inner and outer fibers of the pipe wall. The radial stress attains a maximum at the center of the pipe wall. These are shown in Fig. 1.

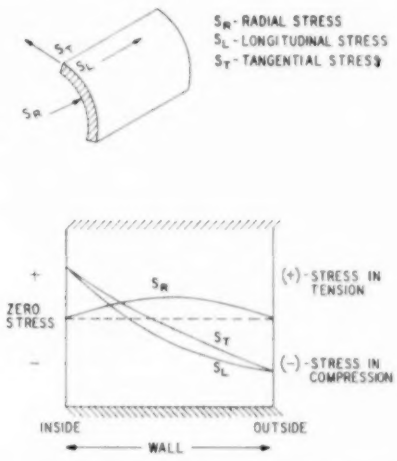

Fig. 1 Stress Pattern—External Heating or Internal Cooling

It can be seen from this figure that maximum stresses will occur at the inner and outer fibers of the wall during a rapid temperature change and the radial-stress value will not need to be considered.

If the temperatures at the inside and outside fibers of the wall are known, and if a linear temperature variation is assumed, the longitudinal stress across the wall may be calculated from

$$\sigma_i = \frac{\alpha E(T_o - T_i)}{2(1-\mu)}\left(1 - \frac{m}{3}\right)$$

where α, E, and μ are known constants for the metal used over the range of temperatures from T_o to T_i, and m is a constant for the pipe geometry.[3] For 8-in. schedule-40 pipe, $1 - m/3 = 0.975$. If the temperature profile across the wall is known the mean temperature of the wall may be found and the maximum stress may be calculated from

$$\sigma_i(\max) = \frac{\alpha E(T_m - T_i)}{(1-\mu)}$$

At the request of the Nuclear Power Division of the Bureau of Ships, Navy Department, a test program was arranged between Knolls Atomic Power Laboratory of the General Electric Company, and the authors' company to subject a series of austenitic stainless-steel specimens of large size to thermal shock to determine its effect on welding techniques and procedure. Each specimen was to be shocked 2500 times by quenching the heated test section from 850 F with cool NaK (sodium-potassium alloy). The minimum rate of temperature change was designated at 100 deg F per sec on the inner fiber of the wall. The temperatures of 850 F and the rate of 100 deg F per sec were chosen as the first representative temperatures by which satisfactory shocking conditions

[1] Mine Safety Appliances Company. Mem. ASME.

[2] Mine Safety Appliances Company.

Contributed by the Metals Engineering Division and presented at a joint session with the Applied Mechanics Division at the Annual Meeting, New York, N. Y., November 29–December 4, 1953, of The American Society of Mechanical Engineers.

Note: Statements and opinions advanced in papers are to be understood as individual expressions of their authors and not those of the Society. Manuscript received at ASME Headquarters, September 8, 1953. Paper No. 53—A-179.

[3] "Theory of Elasticity," by S. Timoshenko and J. W. Goodier, McGraw-Hill Book Company, Inc., New York, N. Y., second edition, 1951, p. 414.

could be produced easily and which would produce results that would be a representative cross section of performance.

Description of Equipment

All materials of construction which contacted the NaK were of AISI types 304 and 347 stainless steels.

The apparatus, shown in Fig. 2, consisted of three 350-gal tanks, an electromagnetic pump, a magnetic flowmeter, a test section,

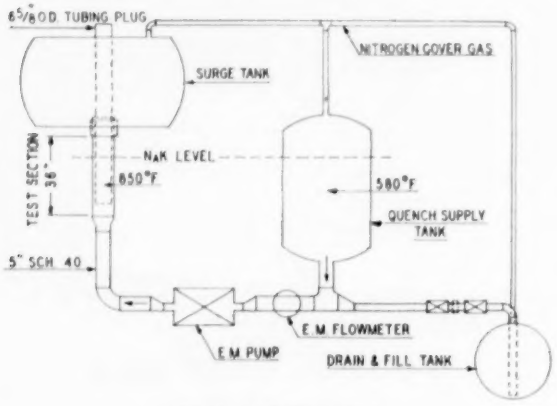

Fig. 2 Test Apparatus

and interconnecting pipe. The three tanks, each 3 ft diam, 4 ft long, with dished heads were fabricated from ¼-in-thick stainless-steel plates. One tank, holding the quench supply, was mounted vertically inside a furnace and heated by gas. The rate of firing was controlled by the temperature of the NaK in the tank. A second tank was employed as a surge tank to collect the NaK above the test section during the thermal-shock cycle. The third tank was an emergency drain tank which also held the NaK charge during shutdown periods.

The electromagnetic pump[4] was a 500-gpm, 15-psi, a-c conduction-type pump built by the authors' company. The pumping section was a 36-in. piece of formed 3-in. schedule-40 AISI type 304 stainless steel. The magnetic flowmeter[4] was calibrated in operation in the system.

A 6-ft length of 6⅝-in-OD tubing was set inside the test specimen, extending through the surge tank, and capped on the lower end. This plug served to increase the NaK velocity inside the test section by decreasing the free-flow area.

The interconnecting piping was 5-in. schedule-40 stainless-steel pipe. The free surfaces of the NaK were protected by nitrogen gas. The nitrogen atmosphere was common to all tanks to equalize pressure during shocking and draining.

A typical test specimen consisted of three sections of 8-in. schedule-40 AISI type 347 piping connected by three girth welds as shown in Fig. 3. Rigid specifications on the welding procedures and testing were followed. Each pass was checked for flaws using oil-penetrant tests and each weld was radiographed upon completion. A duplicate test section was fabricated which was examined for imperfections in the unshocked condition.

Since microfissures sometimes are found at the joint of the backing ring, the parent metal, and the weld metal, it was decided to fabricate test specimens as follows: Duplicate welds were used on each specimen; after the welding was completed one backing ring was removed prior to test and the area covered by the ring undercut 0.030 in. It was felt that this undercut would remove all root fissures and that any cracking observed after test would be due to thermal stresses without the added notch effect caused by the presence of the root fissures.

Heating of the test section and piping, when necessary, was provided by the use of electrical-resistance heaters strapped to the outside of the piping. In cases where a more severe shock was desired, the piping between the quench tank and the specimen was unheated, uninsulated, and further cooled by air blasts.

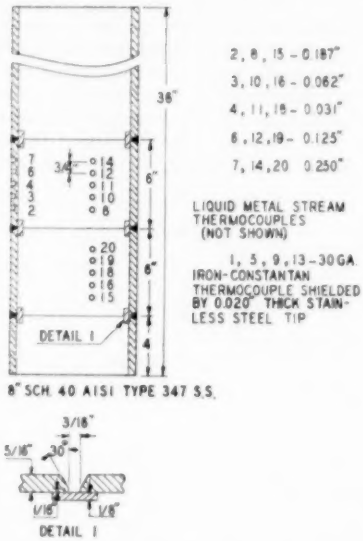

Fig. 3 Typical Test Specimen

Specimen wall temperatures were measured at points 0.031, 0.062, 0.125, 0.187, and 0.250 in. from the inner surface. Two groups of thermocouple holes 5/64 in. diam were drilled in the walls of the test specimen. The thickness of the wall and the depth of the thermocouple holes were measured with an accuracy of 2 mils. The depth of these holes was determined to permit an accurate temperature-gradient measurement across the wall during the thermal-shock cycle and to permit extrapolation of the gradient to the inner surface of the wall.

The temperature of the NaK stream inside the test section was measured by shielded thermocouples. These thermocouples were installed in wells made of ¼-in-OD stainless tubing, extending downward through the surge tank and test section to the same level as the wall thermocouples. The tips of these wells, as shown in Fig. 4, were designed to have a minimum thermal capacity consistent with fabrication techniques. Thermal contact between the thermocouple junction and the thermowell or the test-section wall was assured by welding the thermocouple junction to the tip or wall with a capacitor-discharge welder developed for the purpose.

Operation

Approximately 250 gal of NaK was charged into the thoroughly dried system reaching a level slightly above the test section and filling over half of the quench-supply tank. Heat was then applied to the test specimen electrically and to the quench-supply tank by the gas burners. When the temperature of the NaK in the test specimen and the quench-supply tank reached 850 F and 600 F, respectively, a series of relays locked out the test-specimen heaters and energized the pump. The pump remained on for 15

[4] "Liquid Metals Handbook," (NAVEXOS D-733 revised) Atomic Energy Commission, Department of the Navy, Washington, D. C., U. S. Government Printing Office.

sec during which time the liquid metal flowed from the quench-supply tank, through the flowmeter, through the pump, through the test specimen at 10 fps, and into the surge tank. When the pump shut off, the NaK returned to the original level by gravity. The test-section heaters were turned on and, when necessary, the gas input to the furnace was increased.

When the shock was not severe enough, several blowers were operated to cool the piping between the quench-supply tank and the test specimen. Since this piping contained less than a 2-sec supply of NaK at the 500-gpm pumping rate, the initial and most severe rate of shock was determined by the temperatures of this piping. The following NaK from the quench tank then, in effect, soaked the test section for the remaining 13 sec. Specimens were shocked 2500 times at the rate of 4 cycles per hr in this manner. After testing, the specimen was removed, examined for surface defects, radiographed, and sectioned for metallographic studies.

Instrumentation

Throughout the entire testing period, a high-speed, single-point, electronic potentiometer was used to record the temperature of a

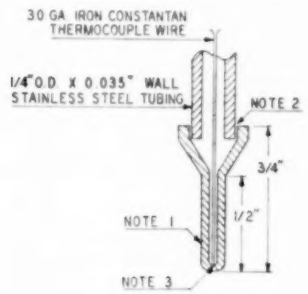

NOTE 1 WALL ALONG SIDE & END OF TIP - 0.020" THICK

NOTE 2 TIP HELIARC WELDED TO THERMOWELL

NOTE 3 THERMOCOUPLE WIRE BONDED TO TIP BY CAPACITOR DISCHARGE WELDING

Fig. 4 NaK-Stream Thermocouple Assembly

NaK-stream thermocouple, Fig. 4, which also controlled the time when the shocking cycle started. Indicating controlling potentiometers were utilized to control the heat input to the test section and quench-supply tank and indicate the wall temperature of the cooled interconnecting piping. Since the test specimen was heated externally, the controlling potentiometer was so set that a short soaking period, during which time the electrical heaters were shut off, permitted the test-section wall and the included liquid to approach a common temperature before the start of each shock cycle.

At least twice during each series of tests, transient temperatures were measured more precisely than was possible using the electronic potentiometer. All the thermocouples used in the wall of the test section and the NaK-stream wells were made of 30-gage iron-constantan wires. The output signal of these thermocouples was converted to 60-cycle alternating current, amplified 1000 times and fed to dual-beam oscilloscopes. The oscilloscope trace was photographed as a sine wave on 35-mm strip film. An additional signal input to the camera was energized at the instant the pump started. This established the start of the shock cycle.

The amplitude of the sine wave on the film was related directly to the temperature. This relationship was established on the heating cycle by calibrating the amplitude of the sine wave against the electronic potentiometer over the range of temperatures encountered during the shock cycle. The time during shocking was established by counting the peaks of the 60-cycle sine wave. Since the amplitude of the oscilloscope was limited to 1 in., the cold junction of the thermocouples was maintained at 400 F to increase the accuracy of the data. Two dual-beam oscilloscopes were used so that one NaK-stream thermocouple was recorded simultaneously with three wall immersion couples. Repeated measurements following this procedure indicated a precision wherein temperature measurements varied no more than ±10 deg F for all tests.

The time lag of the measuring instruments was determined by causing a dead short at the input to the amplifiers while filming the output of a thermocouple on the oscilloscope. The result is shown in Fig. 5 and can be seen to be approximately 5 cycles, or less than 0.1 sec for the entire reaction. By heating a bare thermocouple to 500 F and quenching in cold water, a film has shown that it requires 0.1 sec for the thermocouple to reach water temperature. This includes the time lag in the amplifier and the

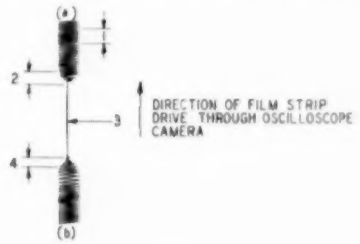

A (a) & (b) INDICATE START & FINISH OF TEST

B TIME INTERVAL "1" (6 CYCLES) EQUIVALENT TO 0.1 SECONDS

C TIME INTERVAL "2" IS TIME OF RESPONSE TO DEAD SHORT AT INPUT TO AMPLIFER (5 CYCLES-1/12 SECOND)

D DURING TIME INTERVAL "3" INPUT TO OSCILLOSCOPE IS ZERO

E TIME INTERVAL "4" IS TIME OF RESPONSE UPON REMOVING DEAD SHORT TO AMPLIFER (4 CYCLES 1/15 SECOND)

Fig. 5 Typical Oscilloscope Trace Showing Time Lag in Recording Equipment

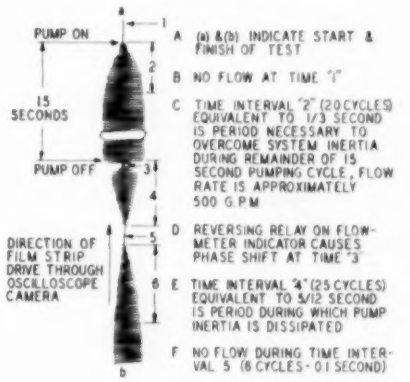

A (a) &(b) INDICATE START & FINISH OF TEST

B NO FLOW AT TIME "1"

C TIME INTERVAL "2" (20 CYCLES) EQUIVALENT TO 1/3 SECOND IS PERIOD NECESSARY TO OVERCOME SYSTEM INERTIA DURING REMAINDER OF 15 SECOND PUMPING CYCLE, FLOW RATE IS APPROXIMATELY 500 G.P.M.

D REVERSING RELAY ON FLOW-METER INDICATOR CAUSES PHASE SHIFT AT TIME "3"

E TIME INTERVAL "4" (25 CYCLES) EQUIVALENT TO 5/12 SECOND IS PERIOD DURING WHICH PUMP INERTIA IS DISSIPATED

F NO FLOW DURING TIME INTERVAL 5 (6 CYCLES - 0.1 SECOND)

G TIME INTERVAL 6 (30 CYCLES) EQUIVALENT TO 0.5 SECOND IS START OF GRAVITY RETURN FLOW CYCLE REQUIRING APPROXIMATELY 35 SECONDS TO REACH NORMAL LIQUID LEVEL IN SYSTEM

Fig. 6 Oscilloscope Trace Showing Typical Flow Pattern During Shock

oscilloscope. The shielded NaK thermocouples require nearly 0.2 sec. before response to the quench. The output of the magnetic flowmeter also was fed to the oscilloscope circuit to determine the time required to overcome the system inertia. This, according to Fig. 6, was found to be 0.3 sec.

Results

The films of the oscilloscope trace were read for each 0.1-sec time interval by projecting the film on a grid. The transient temperatures measured were plotted against time, Fig. 7, to determine the temperature-time relationship of the NaK stream and pipe-wall thermocouples. These curves were used to obtain values to make temperature-profile curves. Although the entire shock cycle consumed 15 sec, the largest gradients across the test-specimen wall and the most severe stresses occurred at 1.5 sec.

Temperature profiles were plotted for conditions existing at 0.5, 0.75, 1.0, 1.25, 1.5, 2.0, 2.5, and 3.0 sec and 1 sec intervals through 8.0 sec. Fig. 8 contains temperature profiles for a test showing wall temperatures at various times. By using the NaK-stream temperature and the calculated rate of heat transfer, these curves for the gradient may be extrapolated to determine the temperature at the inner surface of the wall.

These profiles were then used to determine the maximum stress occurring during the thermal shock. This was done by drawing a horizontal line through the profile to determine the mean wall temperature by the method of equal areas as shown in Fig. 9.

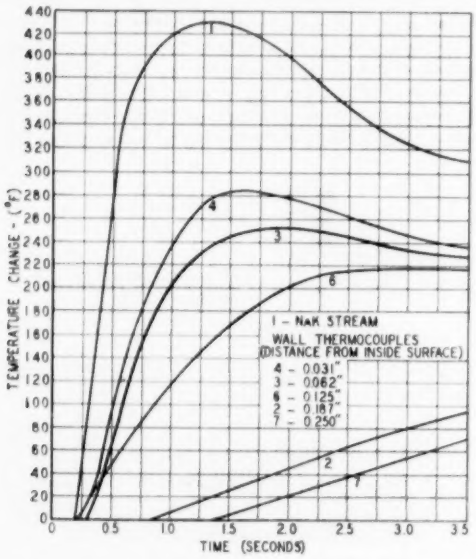

Fig. 7 Transient Temperatures During Shock

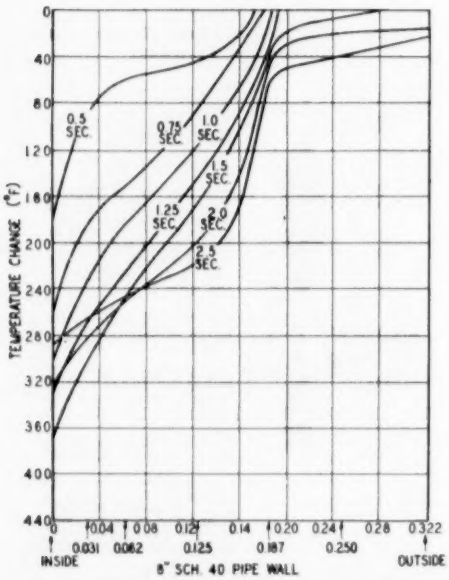

Fig. 8 Temperature Variation in Pipe Wall During Shock

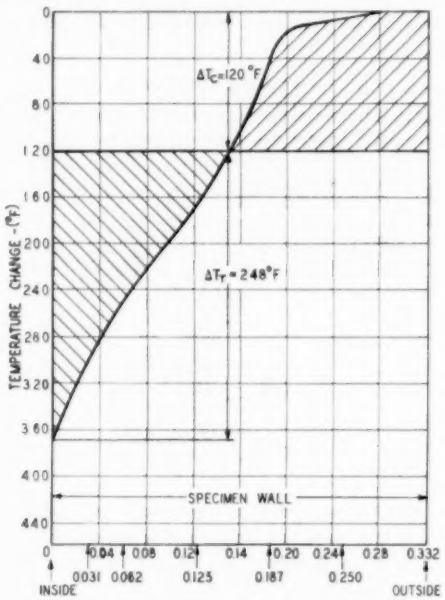

Fig. 9 Temperature Profile at 1.5 Sec

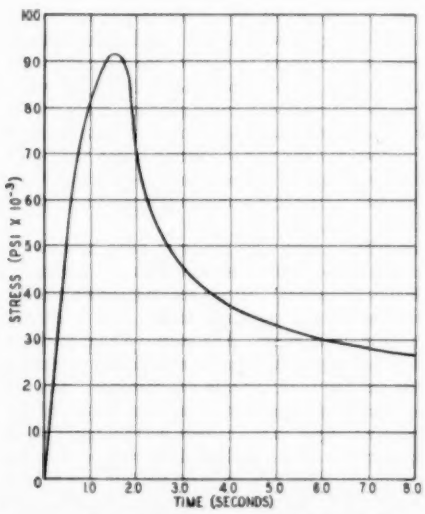

Fig. 10 Maximum Tensile Stress Versus Time

The difference between this mean temperature and the extrapolated temperature at the inner surface of the wall was used to calculate the maximum tensile stress at the inner wall.

A plot of the maximum tensile stress versus time (assuming no plastic flow) is shown in Fig. 10. The stress is shown to increase rapidly to 92,000 psi at 1.5 sec and decrease as the wall temperatures become more uniform to 27,000 psi at 8 sec.

Since the rapid cooling originated on the inside of the pipe, the area from the inner fibers of the wall out to the point designated as the mean temperature of the wall were considered in tension. The remainder of the pipe wall was in compression since the cooling of this sector had lagged owing to the thermal resistance of the metal. The forces in tension occurring on the inner part of the wall were much greater than the compressive forces acting on the outer sector of the wall. In fact, the stress in tension at, for example, time of 1.5 sec, was more than double the yield strength of AISI type 347 stainless steel. This transient stress and resultant strain probably caused plastic deformation of the inner fibers of the pipe wall on the first cycle. This deformation became a permanent set and was not affected by future reheating or shocking. Although the same temperature profile and stress would be observed for the second run, the net strain on the test-section wall would be reduced below the critical point and no further plastic deformation occurred.

Metallographic examination of the unshocked duplicate test specimen indicated that failure to remove the backing ring after welding had permitted cracks several microinches in length to remain in the root pass. Inspection of the test section after 2500 shocks revealed that these cracks had increased to twice the original size (based on examination of the unshocked specimen). However, no evidence was present which showed that any new cracks had been formed during the thermal-shock cycling. On similar test specimens, the initial root-pass cracks were eliminated by machining out the backing rings. Inspection of the shocked test piece again indicated that no new cracks were formed.

Each test specimen also was checked for possible distortion due to thermal shocking. Measurements for the outer diameter of the 8-in. test section were made before and after testing using a pair of micrometer calipers. Although these measurements indicated possible distortion, the magnitude was so small that the results are not conclusive.

Conclusions

While much more work on other alloys, geometries, and temperature changes is needed to evaluate truly the problems incurred by thermal-shocking piping in liquid-metal systems, it seems safe to use current design methods where stresses caused by thermal shock are not in excess of those reported here. The most serious problem is to eliminate the microfissures in the root pass by better weld techniques.

Acknowledgments

The authors thank the Office of Naval Research under whose auspices this program was carried out and the Nuclear Power Division of the Bureau of Ships of the Navy Department for aid, technical assistance, and valued discussions in this program. They also thank W. L. Fleischman, R. J. Fritz, and D. R. Miller of the Knolls Atomic Power Laboratory, for their co-operation in preparing and examining the samples.

Heat-Treatments of Welded Structures for Relief of Residual Stresses With Particular Reference to Type 347 Stainless-Steel Weldments

By W. L. FLEISCHMANN,[1] SCHENECTADY, N. Y.

Welded ring samples of Type 347 stainless steel were given a number of different thermal treatments to study their effectiveness in relieving residual stresses. Treatment at temperatures of 1650 F and above caused complete relaxation. At lower temperatures the amount of relaxation obtainable in reasonable periods depended upon the magnitude of the residual stresses. Experiments conducted on twisted Type 347 stainless-steel wire showed that relaxation occurred at low temperatures. A treatment at 1100 F produced some untwisting and established a pattern of residual stresses that did not cause any further movement when the wire was cycled from room temperature at 850 F. High-temperature treatments produce metallurgical changes which may be of greater importance in conditioning the weld for the intended service than the fact that residual welding stresses were relieved. To emphasize the over-all effect of heat-treatments of welded structures, the use of the term "thermal-conditioning" is suggested in place of "stress-relieving."

Introduction

OPINION prevails that beneficial results are obtained by stress-relieving welded structures. The reason for this generally held opinion is probably traceable to the fact that most of our metallurgical-shop practices are based on the behavior of carbon and low-alloy steels. In that class of alloys, welding produces within the heat-affected zone a region of greater hardness than either the base metal or the weld deposit. A tendency toward brittleness may also exist, depending upon the type of electrodes used. Therefore, under conditions that cause plastic deformations in the neighborhood of the weld, local yielding may occur along the line of the steepest hardness gradient. Thus a stress concentration is created which, in a future stress cycle, may cause fracture. Hence, the purpose of stress relief is to establish uniform yielding behavior—a requisite to pass the bend tests—and to overcome the embrittling effect from the hydrogen-rich atmosphere of certain classes of electrodes.

The hardness variations and hydrogen embrittlement that occur in carbon and low-alloy steels upon welding are not found in austenitic steels. Therefore that aspect of stress relieving has no validity. The Boiler Code Committee in Section VIII of the Boiler Code (1)[2] recognized this fact and eliminated the clause which made stress-relieving of welded austenitic-steel vessels mandatory. Naturally, there exist other reasons which necessitate changes in the stress pattern set up by welding; for instance, avoidance of stress corrosion and the maintenance of close dimensional tolerances. Although there are several ways to modify the stress pattern by processes which deform the weld plastically (overloading—autofrettage or locally by peening), it has been the general experience that stresses introduced into the structure below its operating temperature will relieve themselves in service and may cause dimensional instability. Therefore, a thermal treatment above intended operating temperatures is necessary if strict requirements for dimensional stability are to be met.

The mechanism by which residual stresses are relaxed is controlled by the stress-relief temperature. Complete and fast relaxation occurs in the austenitic steels at temperatures above 1650 F. However, annealing of fabricated Type 347 stainless-steel structures at high temperatures has been reported to cause weld-cracking. One reference (2) even goes so far as to state that cracks after a 1350 F stress-relief treatment are not unexpected and seem to be characteristic of 18-8 welds when they are stress-relieved. Arrested heating cycles (800 to 1000 F) prior to going to the full high temperature have been suggested as a partial palliative (3). The intention of that intermediate step in the heat-treatment is relaxation of peak stresses which otherwise might cause fracture at a higher temperature at which the weld deposit or weld heat-affected zone might be brittle.

The experiments described in this paper were undertaken to determine whether relaxation actually would occur in a heat-resistant alloy, such as the columbium-stabilized Type 347 stainless steel, at the relatively low temperature of 1100 F. Also if relaxation should occur at 1100 F, it would be of interest to know whether such a treatment would be useful by itself in assuring dimensional stability of the structure operating over a range whose upper temperature was below that of the stress-relieving treatment.

Tests on Welded Rings

Because the over-all response of a welded Type 347 stainless-steel structure to a low-temperature stress-relief treatment might be different from that of the base metal or weld deposit, it was decided to study the stress-relaxation behavior of a simple welded specimen. The basic specimens were sections of two different pipe sizes (5-in. OD with $^1/_2$-in. wall and 9$^1/_2$-in. OD with 1$^1/_2$-in. wall). After making one longitudinal cut in the pipe and machining the cut to a standard weld preparation, the section was annealed to remove any residual stresses. After that the slot in the pipe was welded, Fig. 1(A). The stresses set up by welding were

---

[1] Metallurgical Engineer, Materials and Metallurgy Section, Knolls Atomic Power Laboratory, operated for the United States Atomic Energy Commission by the General Electric Company under Contract No. W-31-109. Eng.—52. Mem. ASME.

Contributed by the Metals Engineering Division and presented at a joint session with the Applied Mechanics Division at the Annual Meeting, New York, N. Y., November 29–December 4, 1953, of The American Society of Mechanical Engineers.

Note: Statements and opinions advanced in papers are to be understood as individual expressions of their authors and not those of the Society. Manuscript received at ASME Headquarters, October 16, 1953. This paper was not preprinted.

[2] Numbers in parentheses refer to Bibliography at end of paper.

TABLE 1 STRESSES IN WELDED 5-IN-OD PIPE, TYPE 347 STAINLESS STEEL, ANNEALED PRIOR TO WELDING

Location	Circumferential stress, psi	Longitudinal stress, psi
4 in. from end A	23000	11000
4 in. from end B	27000	11800
9 in. from end A	22100	22000
18 in. (center)	21000	22600

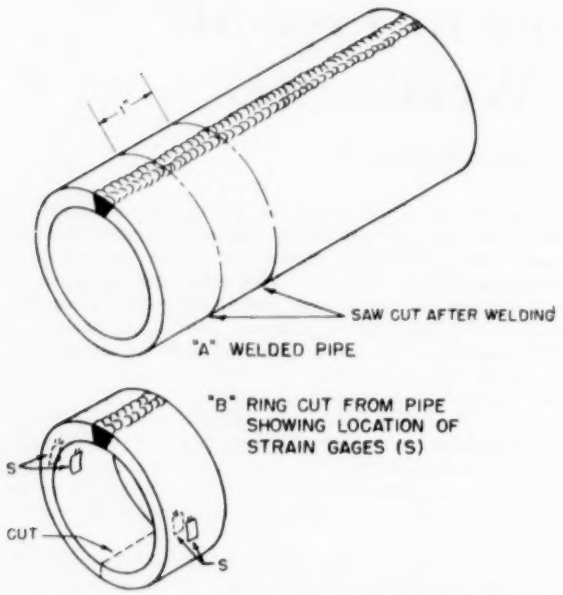

FIG. 1 TEST FOR MEASURING HOOP STRESS IN WELDED RING

determined in the 5-in-OD pipe, which was 36 in. long. These stresses are given in Table 1.

The data obtained in the subsequent tests refer solely to stresses measured in an average section, not in the region of the weld or weld heat-affected zone. Fig. 1(B) shows how the welded pipe was cut into 1-in-wide rings on which strain gages were mounted on the inside and outside 90 deg from the weld to determine the residual stress after the heat-treatments. These strain gages measured the movement of the segments as a result of slitting the ring opposite the weld. Because the circumferential stress varied from the free end of the welded pipe to the center, only every alternate ring was given a heat-treatment, so that the adjacent ring which did not receive a heat-treatment would represent the initial stress existing prior to the heat-treatment. The results of stress relaxation for the 5-in-OD rings are given in Table 2.

The hoop stress in the "as-welded" rings, which were cut from the pipe, was lower than the measured hoop stress in the pipe after welding, as part of the residual stress was relieved by the cutting operation. The differences in the tensile and compressive stress at each point of the slit ring arose from the bending of the curved surfaces following slitting.[3]

The 1650 and 1850 F treatment caused complete relaxation. In the range of 4 to 36 hr, the length of the exposure to 1200 F did not affect the amount of stress reduced, which was small in all cases. However, because of the low level of the original residual stress in the rings, not much relaxation at 1200 F and even less at 1100 F was expected.

To study the effectiveness of the 1100 F treatment, more highly stressed specimens were needed. Sections from a tube with $1^1/_2$-in. wall thickness, $9^1/_2$-in. OD, of Type 347 stainless steel was obtained. This pipe and the specimens cut from this pipe were processed in the same manner as the 5-in. pipe. To compare results with those of the lighter pipe, some rings were heat-treated at 1200 F. Table 3 gives the results of the tests on the $1^1/_2$-in-thick pipe.

[3] For a discussion on stress distribution in curved bars, see, for example, reference (4).

TABLE 2 RESULTS OF RESIDUAL-STRESS MEASUREMENTS ON WELDED RINGS FROM 5-IN-OD, 4-IN-ID PIPE

($^1/_2$-In. Wall Thickness)

Ring No.	Heat-treatment	Outer surface, psi	Inner surface, psi
3	12 hr at 1200 F	+13200	—16000
4	12 hr at 1200 F	+11800	—16700
5	As-welded	+15000	—18500
6	36 hr at 1200 F	[a]	[a]
7	36 hr at 1200 F	+11500	—15600
8	As-welded	+13000	—14700
9	4 hr at 1200 F	+11600	—13700
10	4 hr at 1200 F	+11800	—13700
11	As-welded	+15000	—17500
12		[a]	[a]
13	2 hr at 1650 F	0	0
14		[a]	[a]
15	4 hr at 1200 F	+12500	—15300
16	4 hr at 1200 F	+11000	—13500
17	As-welded	+13100	—16200
18	2 hr at 1650 F	0	0
19	1 hr at 1850 F	0	0
20	As-welded	+13000	—15000
21	1 hr at 1850 F	0	0

[a] Strain gages failed.

TABLE 3 RESULTS OF RESIDUAL STRESS MEASUREMENTS ON WELDED RINGS FROM $9^1/_2$-IN-OD, $6^1/_2$-IN-ID PIPE

($1^1/_2$ In. Wall Thickness)

Ring No.	Heat-treatment	Outer surface, psi	Inner surface, psi
1	16 hr at 1100 F	+14600	—20000
2		[a]	[a]
3	4 hr at 1200 F	+15000	—21500
4	As-welded	+17800	—30000
5	48 hr at 1100 F	+16200	—22000
6		[a]	[a]
7	4 hr at 1200 F	+15650	—24000
8	As-welded	+18200	—30000
9	72 hr at 1100 F	+17000	—23000
10	As-welded	+18400	—25700

[a] Strain gages failed.

The results obtained on rings cut from the heavy pipe confirm the data from the tests with rings from the thinner walled pipe (Table 2); namely, at the low stress level of 18,000 psi, not much relaxation was caused by a 1200 F treatment. The 1100 F treatment was about as effective, although the exposure times used were slightly longer. However, increasing exposure times at 1100 F did not yield a greater amount of stress relaxation.

Generalizing, the data from the residual-stress measurements on the welded-ring samples showed that some stress relief occurred at 1100 and 1200 F, but they did not demonstrate whether the welded assembly was dimensionally stable over a number of heating and cooling cycles at slow temperature changes.

TWISTED WIRE TESTS

To determine whether dimensional stability could be obtained by a low-temperature stress-relief treatment, a separate experiment was devised, studying the movement of a twisted wire during heating and cooling.[4]

For this test an annealed Type 347 stainless-steel wire, 10 in. long and 0.018 in. diam, was twisted 100 turns. This produces a surface strain of about 60 per cent. The wire was hung in a vertical furnace which had a nitrogen atmosphere. The upper end of the wire was gripped firmly and the lower end left free to twist or untwist as the temperature was raised. A quartz rod with a mirror was attached to the free end so that the motion of the wire could be followed by observing the movement of a reflected spot of light.

[4] These tests were conducted by A. Gatti of the Metallurgy Research Department of the General Electric Research Laboratory.

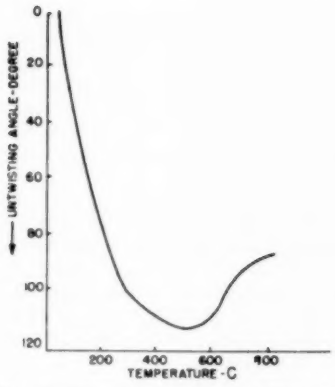

FIG. 2 MOVEMENT OF TWISTED TYPE 347 WIRE; HEATING RATE—200 DEG C PER HR

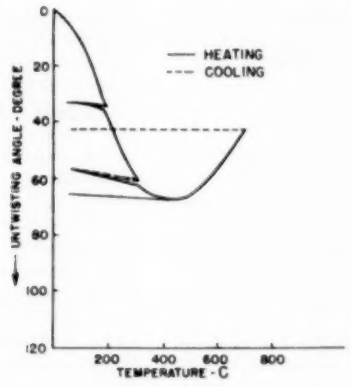

FIG. 3 MOVEMENT OF TWISTED TYPE 347 WIRE ON HEATING AND INTERMITTENT COOLING

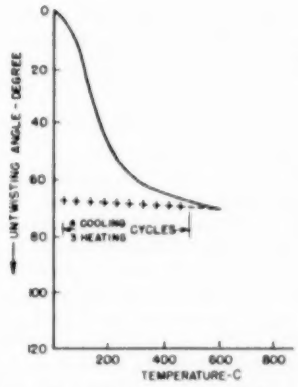

FIG. 4 STABILIZATION OF TWIST DURING HEAT-CYCLING—ROOM TEMPERATURE TO 480 C—AFTER HIGH-TEMPERATURE EXPOSURE—600 C

The twisted wire may be considered a model of a welded structure in which a balanced system of internal stresses exists. Since a heat-treatment will cause a change in the stress level, this experiment was designed to demonstrate whether the residual-stress system, established as a consequence of a high-temperature treatment, was stable at a lower temperature.

In the first test of this type, the wire was heated at a rate of 360 F per hr (200 C per hr) as linearly as possible. Following the movement of the wire by the reflected beam of light, untwisting occurred up to 932 F (500 C), followed by a reversal to twisting above that temperature, Fig. 2.

The untwisting indicated relaxation of the residual stresses. The reversal can be explained by the rapid creep of the highly stressed incremental layers which caused a stress of opposite signs in the regions of lower stress. At the higher temperatures, the newly established stress pattern began to relax, and since it was created in opposition to the earlier stress system, it relaxed by creep in the opposite direction; that is, it twisted.

The second test was made to determine the effect of intermediate temperature cycling on the movement of the wire. Fig. 3 shows that the untwisting and twisting followed the same pattern as in the first test. However, a slight dimensional instability conceivably might be indicated by the spread between the cooling and reheating lines of the first two cycles.

In order to provide additional information for determining whether a low-temperature stress-relief treatment would give dimensional stability, a third twisted wire was heated to 1122 F (600 C). This was followed by three cooling and heating cycles to 896 F (480 C)—two cycles about 4 hr at temperature and the third cycle 24 hr at temperature. In between the heating cycles the wire was at room temperature for at least 12 hr. Fig. 4 indicates that dimensional stability is obtained by this low-temperature treatment in which the so-called "stress-relief" temperature was above the operating temperature.

DISCUSSION OF TEST RESULTS

The stresses in the as-welded condition were caused by the contraction of the weld metal over its cooling range. The difference between the tensile and compressive stresses was caused by the nonlinear stress distribution existing in heavy tubes.

The effectiveness of high temperatures in obtaining stress relief was shown in the tests conducted at 1650 F (900 C) and 1850 F (1010 C) in which the samples were completely relaxed. Stress relief at 1100 F (590 C) and 1200 F (650 C) was partial. The amount of relief obtainable depended on the stress level.

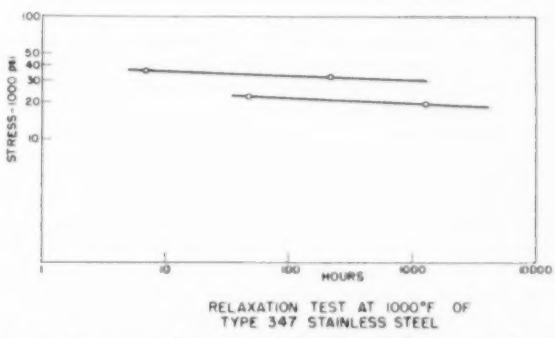

FIG. 5 RELAXATION TEST AT 1000 F OF TYPE 347 STAINLESS STEEL

At the relatively low stress levels locked up in the $^1/_2$-in. wall, 5-in-OD pipe, it is not surprising to find only a very slight effect of the thermal treatment. At the high stress level which was obtained in welding the thick $1^1/_2$-in. wall, 9-in-OD pipe, considerable relaxation took place.

Table 4 gives a summary of the tests reported in Tables 2 and 3. They are reported here as the arithmetic average in which are included all tests conducted at one temperature, regardless of length of exposure to the heat-treatment.

TABLE 4 RESIDUAL STRESSES IN PIPES BEFORE AND AFTER LOW-TEMPERATURE ANNEAL

Pipe	Condition	Outer surface, psi	Inner surface, psi
5 in. OD	As-welded	+14000	—16000
	1200 F	+12000	—15000
$9^1/_2$ in. OD	As-welded	+18000	—28500
	1100 F	+16000	—22000
	1200 F	+14000	—22500

The stress level of about 20,000 psi reached in the heavy-walled ring after an 1100 F thermal treatment was in a range where hardly any further relaxation should take place at 850 F. This was confirmed by two relaxation tests at 1000 F, Fig. 5. Even at the 150 F higher temperature, only a very slow relaxation took place at a 20,000 to 30,000-psi stress level.

The experiments performed on the twisted wire also showed that stressed metal relaxes rapidly. They demonstrated qualitatively that dimensional stability can result from a stress-relief treatment at 1100 F. Other experience, such as the heat-stabilizing of turbine rotors (5) where a heat-treatment above the

service temperature was found to make the shafting maintain its balance in operation, adds considerable assurance that dimensional stability is obtainable by a thermal treatment at 1100 F if the operating temperature is around 850 F.

General Discussion of Thermal Treatments

A discussion of these data would not be complete without a word of caution against a too general application of such a low-temperature heat-treatment of welded Type 347 stainless steel.

During the welding cycle, a narrow region adjacent to the fusion zone is heated high enough in temperature so that even in the relatively short period of the welding cycle, the columbium carbides are dissolved in the austenitic matrix (6). Upon reheating in a range from about 950 to 1550 F, carbides are precipitated at the boundaries of those austenitic grains into which the carbon and columbium atoms had diffused during the welding cycle. The reaction of this region to exposure of certain corrosive agents is identical with that of the sensitized, unstabilized, 18-8 stainless steel (6). Hence, where welds have to withstand boiling nitric-acid tests or equilivalent service, this low-temperature treatment is not recommended for stress-relieving Type 347 stainless steel.

Both the high-temperature heat-treatments—1650 and 1850 F—gave complete stress relief. For high-temperature applications the 1850 F postweld heat-treatment has been accepted for the following metallurgical reasons (7):

To make a fissure-free Type 347 stainless-steel weld, the composition of the deposit is adjusted to contain a small percentage of ferrite. Upon extended exposure to elevated temperatures, this ferrite transforms into the sigma phase, embrittling the weld. The postweld treatment of 1850 F and above causes transformation of ferrite to austenite; thus, with a lowered ferrite content, the embrittling process is delayed. Practical applications of this heat-treatment have been made in the power industry (8).

The investigation of the effect of low-temperature heat-treatment covered solely a problem in plastic flow. The role residual stresses play in the failure of welded structures is still a matter of conjecture because of the difficulty of combining analytically the applied stresses with the complex residual stresses caused by welding.

By eliminating the mandatory stress relief for austenitic stainless steels, the code authority has accepted the point of view that residual welding stresses do not contribute to the fracture of welded structures. An explanation of this noncontribution or neutral effect is given by Weck (9).

Residual stresses must form a self-balancing system which in all probability is different from a system of external loads, so they are never additive. Hence, the collapse load under static loading would be unaffected, for progressively more load could be carried by the understressed sections. As a matter of fact, loading high enough to cause plastic flow will establish a new residual-stress system which will be entirely different from the stress system caused by welding.

The importance of residual welding stresses in ship failure, even though carbon steel is involved, has been de-emphasized by a report of the "Committee on Welding in Marine Construction" (10). They state that of primary concern are (*a*) design, (*b*) impact transition temperature of the material, and (*c*) workmanship.

Under conditions of dynamic loading, however (and here transient thermal cycling is included), a stress pattern can be thought of which superimposes additional tensile stresses upon the weld, causing a premature fatigue failure. In such cases stress relief might be desirable.

Thermal postweld treatments relieve residual stresses and are necessary for the maintenance of close dimensional tolerances, freedom from stress corrosion-cracking, and possibly longer life under cyclic loading. They also cause metallurgical changes in the weld and weld heat-affected zone such as delay of sigma formation and re-establishment of corrosion resistance in the weld heat-affected zone which the code (11) recognizes as important considerations.

Hence, in the selection of a postweld treatment, mechanical as well as metallurgical factors have to be evaluated. By singling out stress relief as the major purpose of a heat-treatment, important metallurgical facts may be overlooked. To emphasize the value and purpose of the postweld heat-treatment, it is suggested that the term thermal-conditioning be used, as that is exactly what the postweld treatment does or should do—condition the weld for the intended service.

Conclusions

Thermal treatments, even at relatively low temperatures, cause a relief of residual stresses. The abolition of the mandatory stress-relief clause in the Boiler Code (1) is well justified in light of experiences with welded structures even other than Type 347 stainless steel. However, correctly selected thermal treatments produce metallurgical changes which result in more serviceable welded structures, irrespective of the simultaneously occurring stress relief. Therefore, it is suggested that the term thermal-conditioning be used in place of stress relief, which singles out one aspect of a thermal treatment.

Acknowledgment

The pros and cons of stress-relieving welded structures always invite many comments. The discussions the author had with Messrs. L. F. Coffin, Jr., W. E. Cooper, J. F. Eckel, R. J. Fritz, R. L. Fullman, R. F. Koenig, D. R. Miller, and L. Zickrick in planning these tests were most helpful. The assistance of Mr. R. F. Jordon of the Turbine Division Laboratory in making strain measurements to check our results is greatly appreciated. Special thanks are due Mr. A. Gatti of the General Electric Research Laboratory for the tests on the twisted stainless-steel wire.

BIBLIOGRAPHY

1 ASME Boiler and Pressure Vessel Code; Section VIII: Unfired Pressure Vessels, 1952; paragraph UHA 32, "Thermal Stress Relieving."

2 "A Report of the Metallurgy and Piping Subcommittee of the Prime Movers Committee," *Metallurgy and Piping* (1950), Edison Electric Institute Pub. No. 50-10, 1951.

3 "The Incidence of Cracking in the Welding of Type 347 Steels," by L. K. Poole, NYO-3494, May 22, 1952.

4 "Strength of Materials," Part II, by S. Timoshenko, second edition, D. Van Nostrand Company, Inc., New York, N. Y., 1940, p. 65.

5 "Stabilization of Steam Turbine Shafts," by S. H. Weaver, *General Electric Review*, vol. 44, 1941, p. 543.

6 "The Mechanism of Knife Line Attack in Welded Type 347 Stainless Steel," by M. L. Holzworth, F. H. Beck, and M. G. Fontana, *Corrosion*, vol. 7, 1951, p. 441.

7 "Welding High-Temperature Austenitic Steel Piping," by R. W. Emerson and M. Morrow, *Welding Journal*, vol. 30, 1951, pp. 15s-33s.

8 "Statement by Public Service Electric and Gas Company," *Metallurgy and Piping* (1952), Edison Electric Institute, Pub. No. 52-13, 1953.

9 "Residual Stresses Due to Welding," by R. Weck, *Symposium on Internal Stresses in Metals and Alloys*, Institute of Metals, London, England, 1948, p. 119.

10 "Report on Thermal Stresses and Shrinkage in Welded Ship Construction," American Welding Society, New York, N. Y., 1941.

11 ASME Boiler and Pressure Vessel Code; Section VIII: Unfired Pressure Vessels, 1952; nonmandatory appendix HA, p. 102.

Thermal Checking of Wrought-Steel Railway Wheel Material

By H. R. WETENKAMP,[1] URBANA, ILL.

The mechanism of the formation of small cracks (thermal checks) that are formed as a result of two heat cycles is discussed. These thermal checks were noted in the treads of car wheels and careful examination of the conditions which caused them to form led to the development of a method of producing these thermal checks in a small specimen under better-controlled conditions. The reasons for the checks forming more readily in higher plain-carbon steel are discussed. Basically, the contraction of martensite upon tempering seems to be the cause of the formation of thermal checks.

Introduction

In railway service, car wheels are, in general, required to fulfill two functions: (*a*) To act as a wheel which supports the weight of the car as it moves along the rails, and (*b*) to act as a brake drum. In this latter capacity the wheels, along with the brake shoes, are required to dissipate as heat the energy to be absorbed in stopping or controlling the speed of a train. The tread of the wheel which acts as one of the friction surfaces can be heated to temperatures well above the austenitizing temperature of the steel. This high temperature is usually accompanied by a very steep temperature gradient with corresponding steep stress gradients. These high stresses and temperatures permit plastic deformations to take place and thereby can cause excessive residual stresses when the wheel has cooled to a uniform temperature. If cracks of sufficient size are formed in the wheel, they may act as starting points for an explosive-type wheel fracture which may cause a derailment. The stresses that can cause wheel fracture and the stresses that cause cracks in the tread of the wheel are produced by the braking conditions imposed upon the wheel. Generally, the cracks are caused by a different type of braking condition than the braking condition that causes the stresses necessary for wheel fracture.

The University of Illinois, in co-operation with the Technical Board of the Wrought Steel Wheel Industry, has been studying the thermal damage of steel car wheels for many years. The study of thermal cracking of wrought-steel car wheels led to the discovery of cracks formed in wheel treads that had not been considered in previous tests at the University. Prior to this investigation the types of cracks noted and produced in the laboratory were detected easily by the naked eye and, furthermore, the formation of a crack always was accompanied by a "pinging" of the wheel caused by the relief of stress. This relatively large crack is referred to as a thermal crack. Thermal cracks were readily produced in the higher-carbon wheels when the wheels were subjected to full-stop tests.

[1] Research Assistant Professor, Department of Theoretical and Applied Mechanics, University of Illinois.

Contributed by the Metals Engineering Division and presented at a joint session with the Applied Mechanics Division at the Annual Meeting, New York, N. Y., November 29–December 4, 1953, of The American Society of Mechanical Engineers.

Note: Statements and opinions advanced in papers are to be understood as individual expressions of their authors and not those of the Society. Manuscript received at ASME Headquarters, August 10, 1953. Paper No. 53—A-72.

The wheel to be tested along with a flywheel, which is equivalent to 20,000 lb traveling at the same speed as the tread of the test wheel, was rotated at 1074 rpm (115 mph) and then stopped by forcing two brake shoes against the tread of the wheel with a force of 20,000 lb on each brake shoe. The exact mechanism of thermal cracking was not known and in an effort to learn more about thermal cracking, the testing procedure was changed. It was found by releasing the brakes when only a small percentage of the total energy had been absorbed that many small cracks formed. The cracks (thermal checks) invariably were located where the edge of a heated zone fell within a heated zone produced by a prior braking cycle. When first formed, the checks were very fine and often could not be seen without a magnaflux inspection. Thermal cracks and thermal checks may have the same external appearance; however, the thermal crack is usually longer and invariably deeper than the thermal check. The mechanism of formation is the real difference between the two types of cracks and, furthermore, the thermal check is probably not a serious defect in a wheel as it seems to have a maximum depth of approximately $^1/_8$ in. and does not seem to grow with subsequent tests. The thermal check will open slightly in width with subsequent heating cycles and, therefore, may have the same appearance as a thermal crack; however, the actual length and depth are probably unchanged.

From examining the location of thermal checks relative to the location of "hot spots" and examining the cracked area under the microscope, the general conditions required for the formation of the thermal checks were determined. Once these conditions were noted, it was possible to produce thermal checks under controlled conditions in small specimens. This way the study of the problem was greatly simplified.

Simulated Tests on Small Specimens

General. The production of thermal checks in railway-car wheels appeared to be a function of the generated heat and its absorption, unavoidably accompanied by local structural transformations of the steel in the tread of the wheel. An intensive study of the physical location and nature of thermal checking in the wheels was undertaken. After each test, the tread of the wheel was covered with a strip of onion-skin paper and a tracing was made showing the location of all hot spots and checks. After a series of tests were completed, these tracings were studied with a view toward correlating the location of thermal checks with respect to hot spots. The inference drawn from these results was that at least 2 heat cycles were required to produce the type of check being studied. The first cycle produced a hardened zone, while the second cycle provided an overlapping hot spot which apparently tempered a portion of the originally hardened zone. If such an overlapping of hot spots occurred, the usual result was a thermal check. This study led to the development of a test in which a specimen was heated by means of an oxyacetylene torch.

Equipment and Procedure. The equipment used for subjecting a specimen to a heating cycle consisted of a specimen holder which oscillated under a torch while a jet of water was directed on the under surface of the specimen.

The cooling water on the under side of the specimen was to simulate the mass effect of the rim material beneath the tread surface of a wheel. The source of heat was an oxyacetylene torch with a No. 11 tip mounted on a pivot which permitted the torch to be ignited before being lowered to a definite height above the specimen. The time that the torch was in the first heating position was controlled mechanically. For the second heating cycle, the specimen was fixed at the extreme end of its stroke. The duration of this heating cycle (tempering) was controlled by a time-delay relay which in turn controlled an electric solenoid. Reproducibility of the torch flame was obtained by using mercury manometers to measure the oxygen and acetylene pressures.

Preliminary experiments to determine a practical size and shape of a specimen were conducted. The results indicated that a specimen approximately $2^1/_2$ in. $\times$ $2^1/_2$ in. $\times$ $^1/_2$ in. ground with parallel faces was suitable.

The specimens were placed in the oscillating fixture and the torch stop adjusted so that the tip of the torch was $^1/_2$ in. above the surface of the specimen. Cooling water was directed on the bottom of the specimen before igniting the torch and left running throughout the entire test. The torch was ignited in the up position with the control valves at the torch fully open and with the oxygen and acetylene pressures at the regulator valve adjusted to 15 in. and 20 in. Hg, respectively. These pressures gave a slightly oxidizing flame. Before bringing the torch down, the mechanism for oscillating the specimen through a $^1/_2$-in. stroke and operating the timing cam was put into motion. When the timing cam released the torch from its up position, the torch rotated about its pivot and snapped into its heating position where it remained until the cam again released it to return to its up position. The duration of heating was about 13.5 sec. Approximately 50 sec were allowed for the specimen to cool before the second heating, or tempering cycle, was applied. With the specimen stationary and at the extreme end of its stroke, the torch was lowered. The tip of the torch was kept $^1/_2$ in. above the specimen by the magnetic effect between a bar clamped to the torch and the adjustable core of a solenoid. After a predetermined time interval, the solenoid released the torch. A time-delay relay was used to vary the duration of tempering from 0.5 to 4.0 sec. The foregoing conditions are referred to as standard conditions.

Relative Resistance of Wheel Material to Thermal Checking. Six car-wheel steels were tested as listed in Table 1.

Thirteen groups of tests, each containing one specimen of analysis 1, 2, 3, 4, and 6 were run so that any variation in test procedure would be more equally distributed among the different analyses. In addition, five groups of tests of analyses 2, 3, and 5 were run. The initial heating cycle was the same for all specimens but the tempering time was changed.

In Fig. 1 are plotted the six analyses of wheel steel with the carbon content as the abscissa and the time required for the specimen to crack, after completion of the test, as the ordinate. The data in Fig. 1 indicate two interesting trends: (*a*) Increasing carbon content rendered the steels tested more susceptible to checking; and (*b*) increasing tempering times rendered the steel less susceptible to checking. The latter trend was of questionable importance yet appeared interesting. It will be noted that frequently a specimen did check after a long (2-sec) temper though a matter of hours may have elapsed prior to failure. This trend could possibly be associated with creep and relaxation effects.

Another trend, not indicated in Fig. 1, was the location of the crack with respect to the tempering spot, i.e., the heat-affected zone formed during the tempering cycle. As the tempering time was decreased, the crack formed in a zone closer to the heat-affected zone formed during tempering. For a tempering time of 1 sec, the crack formed approximately $^1/_4$ in. from the tempering spot, and for a 0.6-sec time it was located about $^1/_8$ in. from the tempering spot. The external appearance of a specimen after it has been subjected to a test is shown in Fig. 2.

There are several explanations of why higher carbon steels were more sensitive to thermal checking than steels of lower carbon content: (*a*) The lower carbon steels must be heated to a higher temperature before becoming completely austenitic; (*b*) the lower carbon steels must be quenched more drastically to produce a martensitic structure; and (*c*) the transformation of austenite to martensite is accompanied by a larger increase in volume in the higher carbon steels. The higher carbon steels also decrease more in volume upon the tempering of the martensite.

According to Cohen (1)[3] the *a*, *b*, and *c* parameters of martensite, extrapolated to zero carbon, are equal, i.e., about 2.86 AU. With increasing carbon, the parameters are changed, and at about 0.8 per cent carbon the value of *c* is approximately 2.96 AU and that of *a* and *b* are approximately 2.85 AU. This would give a volume change of approximately 3.5 per cent. The changes in parameter are linear with increasing carbon; therefore the amount of lattice distortion increases with carbon. The martensite of higher carbon content has a greater degree of

TABLE 1 CAR-WHEEL STEELS TESTED

		Class of material	Carbon, per cent
1	High carbon	C	0.83
2	High carbon	C	0.75
3	High carbon	B	0.67
4	High carbon	B	0.60
5	High carbon	A	0.54
6	Low carbon	A	0.45

[3] Numbers in parentheses refer to the Bibliography at the end of the paper.

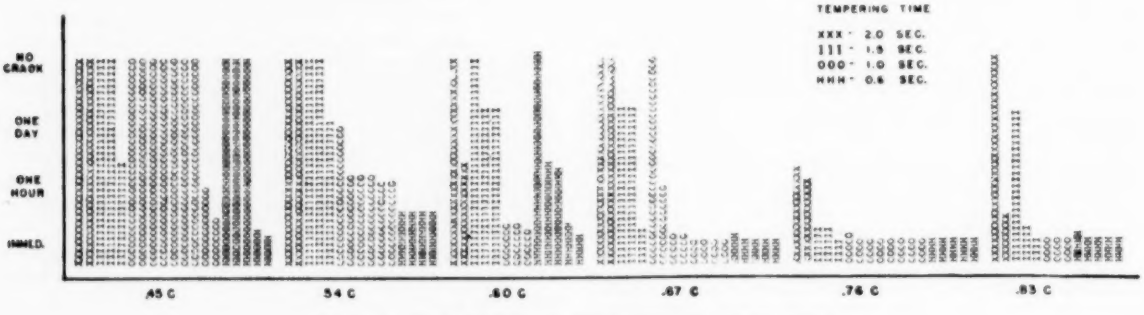

FIG. 1 CARBON VERSUS CRACKING TIME IN WHEEL STEEL

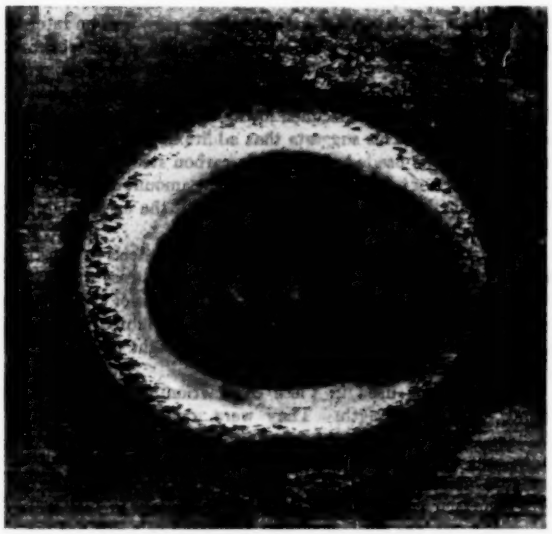

FIG. 2 THERMAL CHECK IN TEST SPECIMEN

tetragonality, a lower Ms, and less ductility. High transformation stresses as well as microcracks accompany a lower Ms temperature (2).

Microscopic Examination. The microstructure of the heated zones of the test specimens tested under standard conditions was virtually 100 per cent martensitic. Microscopic examination of the specimens showed that the cracks formed at the boundaries of the prior austenitic grains. It is proposed that the grain boundaries contained either a brittle or a very weak material which failed under the stress imposed by the tempering of the martensitic matrix. The brittle material could have been the "martensitic spines" studied by Grossman (3). Actual microscopic examination of specimens did indicate the possibility of this phase being present, but no positive identification was made. A possibility exists also of minute amounts of ferrite and transformation products being present at the grain boundaries. With the exception of the Class-A steel, these products were not noted. Also it is proposed that the cracks initiate in a coarse-grained region in the center of the heat-affected zone formed by the hardening cycle.

To permit a better study of the intergranular crack, it was decided to alter the standard conditions of testing in such a manner as to produce martensitic grains with nodular pearlite and free ferrite outlining the boundaries of prior austenite. This type of microstructure is justified because frequently thermal checks in wheels are located in areas of 20 to 50 per cent martensite. Actually, microstructural variations in wheels under service conditions are almost limitless due to lack of control of the extent and location of the heat-affected zones on the wheel tread by action of the brake shoes. A considerable number of tests were conducted using conditions other than standard. These tests maintained all the standard conditions with the exception that the specimen was not quenched continuously from the underside. Instead, the quenching jet was opened at some predetermined time after completion of the 13.5-sec hardening cycle. Quenching was then continued through the tempering cycle. As would be expected, this procedure altered the microstructure from almost 100 per cent martensite to a combination of martensite with varying amounts of nodular pearlite and free ferrite at the grain boundaries. Fig. 3 illustrates portions of the center of a heat-affected zone resulting from a delayed quench.

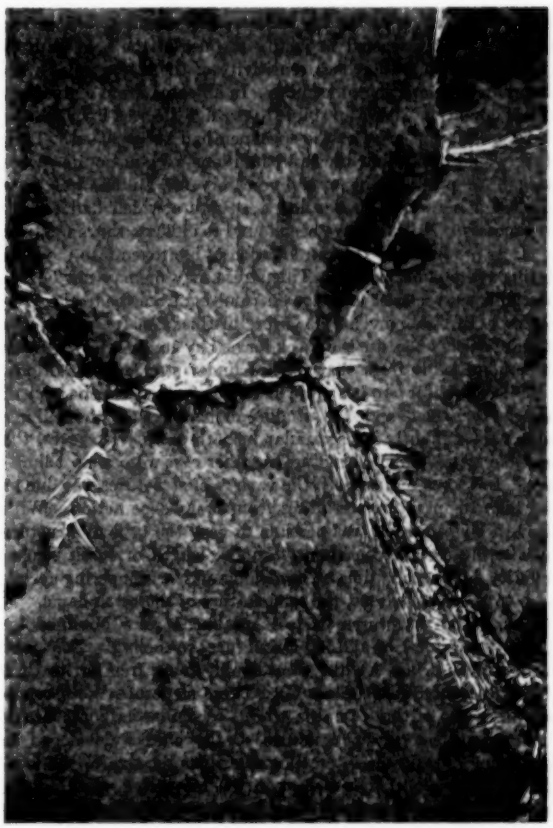

FIG. 3 PORTION OF A THERMAL CHECK FORMED IN A CLASS-C SPECIMEN SUBJECTED TO A DELAYED QUENCH OF 7 SEC; CRACK PROPAGATED ALONG GRAIN BOUNDARIES

If the mechanism of check formation was assumed to be the same under both the standard and delayed-quench conditions, then the mechanism of check formation was somewhat easier to study under the delayed-quench conditions because the prior austenitic-grain size was well delineated by nodular pearlite. The pearlite nucleated at the boundaries of austenite. Free ferrite was also noted within the grain boundaries. Fig. 3 reveals quite clearly that cracks in the delayed-quench series apparently initiated and progressed along grain boundaries. Another interesting observation of this work was that if the quench was delayed for 8 sec or more after the completion of the hardening cycle, the specimen would not crack with subsequent treatment. This effect was probably due to the presence of relatively soft and ductile material compared to the microstructure formed using standard conditions.

Further testing was concerned with the uniform furnace tempering of specimens after the application of the initial (hardening) cycle and prior to the application of the tempering cycle. As a rule the uniform tempered specimens did not check after being subjected to the spot-tempering cycle; therefore it was necessary to induce checking by placing them in an etch-crack solution of 15 per cent sulphuric acid at room temperature for periods of 10 min. The first signs of checking were usually noted before this time limit had elapsed.[3]

[3] For an explanation of the mechanism of the etching solution and a discussion of its use, the reader is referred to the work of Brophy (4) and Tarasov (5).

The very nature of the check formed by etching, its location and appearance, seemed to justify the use of the acid bath to qualitatively gage the check sensitivity of the steels tested with the uniform tempering procedure. In all cases, from a given set of test conditions, it was possible to predict the area in which the check would appear after the specimen had been etched. This, then, would imply that the test conditions were not quite severe enough to produce the stress necessary for failure, but were of such a nature as to develop a structure which had certain weaknesses. No data have been found to indicate the magnitude of stress produced by the introduction of hydrogen into the steel during the etching period. This stress may or may not be appreciable with respect to the stress resulting from the testing procedure. In either event, however, justification for use of the etchant existed because the check formed by etching was virtually indistinguishable from that formed under standard conditions.

Metallographic studies were made of test specimens and of wheel specimens, and the studies indicated that the failures were predominantly intergranular in both cases. However, the possible types of microstructure in either case were almost limitless. In the case of wheels, the variety of structures was due to the high temperatures resulting from brake-shoe action. With the test equipment it was possible to vary the type of structure by altering certain conditions, that is, length of torch stroke, severity of quench, time of hardening and/or tempering cycles, and, to a limited extent, the temperature of the torch flame.

The initial structures in test specimens were obtained by austenitizing for 1 hr at 1550 F and furnace cooling. The lower carbon steel (Class A) had considerably more free ferrite than the high-carbon steel (Class C). These structures were representative also of that found in wheels of similar carbon content.

Hardness Survey. The nature of the checks developed in specimens raises some interesting questions relative to the location of the checks with respect to the tempering spots. Inasmuch as the location of the check varied somewhat with tempering time, it was assumed that a hardness survey would be of value in indicating a line of attack toward studying the nature of the material around the check.

Actual observation of check propagation after subjecting specimens to heating cycles showed that the checks initiated on or near, and at right angles to, the longitudinal axis of the heat-affected zone formed during the hardening cycle. This axis was the center line of the specimen oscillation with respect to the tip of the oxyacetylene torch.

The data obtained from Rockwell A surface-hardness readings indicated that for a given class of steel there existed a hardness range which favored checking. The upper and lower limits of this range showed a weak but definite tendency to be higher for the higher carbon steels.

An interesting feature of the hardness range was supplied by data of specimens that did not check when tested under conditions different from standard. These specimens were checked by immersion in the etch-crack solution discussed previously. Subsequent hardness surveys showed that the check occurred within the same hardness range observed for specimens which had checked upon testing with standard conditions.

The results of the hardness survey would indicate that the critical hardness range does vary slightly with the chemistry of the steel being investigated.

Fig. 4 shows a comparison of hardness through the depth of hardened, untempered zones of a wheel subjected to two 30 per cent energy-absorption tests and a specimen subjected to the initial hardening cycle. The curves appear to be in very good agreement. The data were obtained by taking Tukon microhardness (136-deg diamond pyramid indenter and a 1-kg load) readings 0.02 in. apart, starting 0.02 in. from the edge of the specimen. The first reading for each specimen may well be in error because the indentations were close to the edge of the specimen.

Determination of Contraction of Martensite on Tempering. Information obtained from the hardness-survey tests indicated that the failure of the specimen always occurred within a given hardness range. This suggests that additional information of a basic nature was needed of the plain carbon steels being tested. One such piece of information would be the amount of contraction of martensite, which is known to vary with the carbon content of the various steels tested.

If the contraction curves were known for the steels in question, it might be possible to estimate the maximum stress that would occur with tempering; although the distribution of stress in the block specimens or in railway-car wheels is undoubtedly complex, a knowledge of the amount of contraction might be useful in a qualitative sense.

The specimens used in these contraction tests were $^1/_4$-in. rounds, 5 in. in length. They were austenitized and then quenched in water. After hardening, the rounds were cut to 3-in. lengths and the ends were ground parallel.

Initial measurements were then made at room temperature with a surface gage with the dial reading directly to 1/10,000 in. Following this, the specimens were tempered in a salt pot for 30 sec at 100-deg F intervals from 300 F to 1100 F. The final measurements were made in the same manner as initially.

The test results for steels of different carbon contents are shown plotted in Fig. 5. A trend of an increasing amount of contraction with increasing carbon was definitely noted. This work was in good agreement with results obtained by Grossman (3).

Determination of Residual Stress in the Heat-Affected Zone. The production of checks in specimens tested quite naturally led to the belief that an area of high-tensile stress existed at the surface of the specimens. The data obtained from the tests for determining the amount of contraction upon the tempering of martensite lent support to this belief, especially in view of the fact that the amount of contraction noted would give rise to a tensile stress of 120,000 psi, assuming the theory of elasticity and a biaxial state of stress.

The physical nature of the $2^1/_2$-in-square specimens used posed a serious problem for obtaining reliable residual-stress information within the heated area. The procedure finally adopted made use of a Tukon microhardness testing machine.

It was recognized that experimental data were necessary to prove or disprove the presence of a tensile condition, and to this end the procedure described was developed.

Specimens were spot-hardened in the usual manner, then about 0.010 in. of material was removed from the surface of the specimens around the heated area leaving an unrelieved circular area about 1 in. in diam. Narrow bands of material at the corners of the specimens were retained as an aid in keeping the specimens flat during polishing. After polishing and etching to examine the surface microscopically, the etch was removed and strain rosettes marked on the specimens by a 136-deg diamond pyramid indenter of a Tukon microhardness testing machine. The gage lines of the rosettes were measured in the same machine.

When the measurements of a rosette were completed, the heat-affected area was removed from the rest of the specimen by cutting around the 1-in-diam portion while the specimen was mounted in a lathe. The relieved portion of the specimen, containing the strain rosette, was approximately the diameter and thickness of a 25-cent piece and the rosette was then remeasured in the same manner.

In addition, specimens of Class-A steel (low carbon) were given a 13.5-sec hardening cycle followed by a 2-sec temper in the

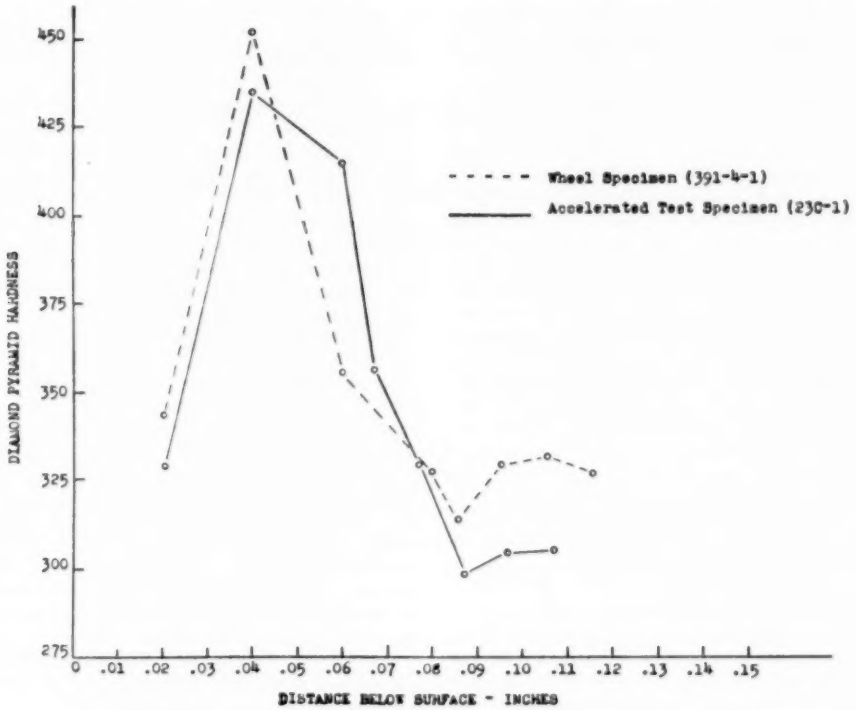

FIG. 4 COMPARISON OF HARDNESS VERSUS DEPTH FOR HARDENED ZONE OF A WHEEL AND AN ACCELERATED-TEST SPECIMEN

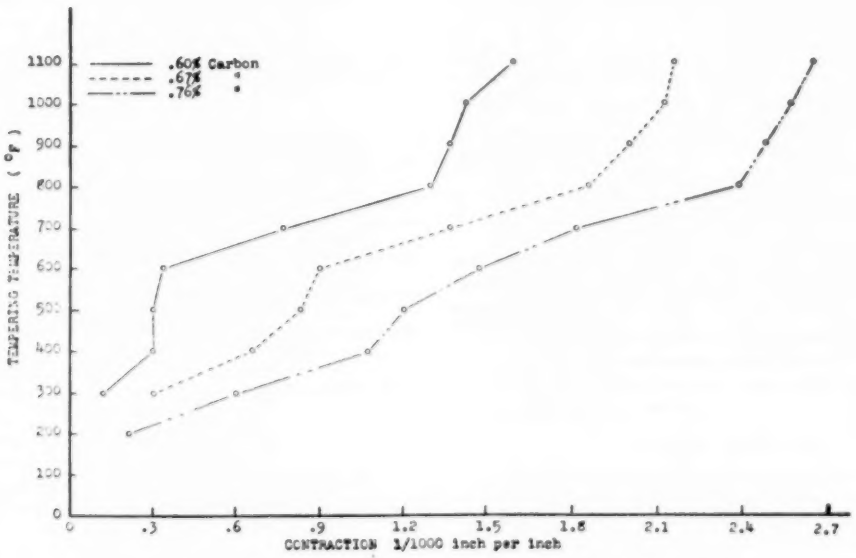

FIG. 5 CONTRACTION ON TEMPERING OF QUENCHED PLAIN-CARBON STEELS

center of the heat-affected area. The residual stresses were then determined by the previously described method.

During the heating cycle the locally heated zone is "hot-upset." This would lead to a residual tensile stress upon cooling if no phase transformation occurred. However, specimens subjected only to the 13.5-sec hardening cycle were under a compressive stress of 40,000 to 80,000 psi. The presence of compression indicated that the stress resulting from the expansion of the austenite to martensite transformation was greater than the contraction due to thermal effects. Specimens which were spot-tempered after the hardening cycle were found to be in tension with a stress of 60,000 to 85,000 psi. This stress had to be the result of thermal stresses and the stress resulting from the contraction of martensite upon tempering. The resultant tensile stress after tempering was in agreement with the magnitude of stress calculated for the maximum amount of contraction of martensite upon tempering as determined experimentally. Perfect agreement could not be expected because the stress system in the test specimens was probably complex and not perfectly restrained at its boundaries as assumed in calculations of theoretical stress values.

The data obtained from this test led to the conclusion that the hardened areas of test specimens initially were subjected to a high compressive stress which was reversed as a result of tempering to a tensile stress of the same order of magnitude.

Summary and Conclusion

In the laboratory investigations conducted to study thermal checking in railway-car wheel steel, five compositions of steel were investigated. Tests were designed (*a*) to give a measure of check sensitivity of wheel steels; (*b*) to study microscopically the area in which the check initiates; (*c*) to determine the critical hardness range of the material in which the check initiated; (*d*) to determine the amount of contraction of martensite upon tempering fully hardened specimens of wheel steel; and (*e*) to determine the sign and magnitude of the residual stresses resulting from the test procedure.

The thermal-check sensitivity was found to increase with increase in carbon content within the range of carbon content considered. The results are in accord with the tests on full-size car wheels tested in the wheel-testing machine.

Hardness surveys showed that for a given class of steel the thermal checks initiated within a hardness range which was reasonably constant. As the carbon content of the steel was increased, there was a shift to progressively higher values of the limits of the hardness range, where checks initiated.

The data obtained from residual-stress determinations were qualitative in nature. The heat-affected zone of the specimens subjected to the initial hardening cycle was found to be under a compressive stress of 40,000 to 80,000 psi. Similar studies of specimens subjected to both cycles, with conditions such that checking was impending, indicated tensile stresses ranging from 60,000 to 85,000 psi.

Determination of the contraction of martensite upon tempering resulted in data that were in good agreement with the work of Grossman (3). The theoretical maximum stress that could be caused by contraction of martensite was found to be of the order of 120,000 psi, assuming perfect restraint of the material and a biaxial state of stress. This calculated value agrees reasonably well with the difference of residual stresses noted in hardened specimens and hardened and tempered specimens.

Microscopic examinations seemed to indicate that the checks were intergranular. The microstructure varied from tempered martensite to nodular pearlite.

The following theory of thermal-check formation is presented:

The initial heating or hardening cycle raises the temperature of the specimen locally to a high value, possibly in the range of 2000 F. At this temperature, coarse grains are formed and plastic deformation takes place because of the high compressive stresses caused by thermal expansion. The quenching phase of the cycle causes the microstructure to consist of an area of coarse grains which are virtually 100 per cent martensitic, or some lower percentage of martensite plus varying amounts of nodular pearlite, bainite and free ferrite depending upon the conditions of testing. The transformation products tend to nucleate at the boundaries of the prior austenitic grains and the free ferrite is found along the grain boundaries. The quenching of the material to martensite causes an expansion which counteracts the tensile stress which would be produced if no transformation products were formed and results in the material being under a compressive stress.

The tempering cycle causes a contraction of the martensite which in turn causes tensile stresses. This tensile stress may be sufficient to initiate a check if sites of weakness or stress concentrations exist.

Acknowledgment

The author wishes to thank Mr. Roy M. Brodnick for his capable assistance in conducting this investigation.

BIBLIOGRAPHY

1 "Retained Austenite," by M. Cohen, Trans. ASM, vol. 41, 1949, pp. 35–94.

2 "The Influence of Metallurgical Factors on the Mechanical Properties of Steel," by S. A. Heeres and C. H. Lorig, Trans. ASM, vol. 40, 1948, pp. 774–807.

3 "Toughness and Fracture of Hardened Steels," by M. A. Grossman, Trans. AIME, vol. 167, 1946, pp. 39–79.

4 "Stresses and Cracks in Hardened and Ground Steel," by G. R. Brophy, Trans. ASST, vol. 18, 1930, p. 423.

5 "Detection, Causes, and Prevention of Injury in Ground Surfaces," by L. P. Tarasov, Trans. ASM, vol. 36, 1946, p. 389.

A Short Method for the Evaluation of the Effect of Some Thermal-Cycle Variations on Steam-Turbine Heat Rates

By S. D. FULTON,[1] PHILADELPHIA, PA.

The purpose of this paper is to present a short method of evaluating the effect of several thermal-cycle variations on steam-turbine heat rates, utilizing the data given in a heat balance. The method is based on the fact that the product of the input to a cycle and its thermal efficiency equals the output. To use this fact a method for determining the thermal efficiency from any extraction point to the turbine exhaust is presented. Equations derived for the various changes in the cycle make determination of heat-rate changes quite simple. A high order of accuracy is obtained by computing only changes in input and output.

Nomenclature

The following nomenclature is used in the paper:

- A = enthalpy difference between drains leaving a heater and feedwater entering that heater, Btu/lb
- a = subscript, the higher of two extraction points principally affected by a cycle change
- b = subscript, the lower of two extraction points principally affected by a cycle change
- ΔBtu = change in heat supplied to a cycle, Btu/hr
- c = subscript, condenser, condenser hot well
- D = feedwater drains leaving a heater, lb/hr
- d = heater drains enthalpy, Btu/lb
- E = extracted steam, lb/hr
- ΔE = change in extracted steam, lb/hr
- e = subscript, evaporator
- F = heat given up by drains in a feedwater heater, Btu/lb
- G = gain in thermal efficiency for infinite heater cycle, per cent
- H = heater, extraction point, steam enthalpy, Btu/lb
- H_r = heat added in reheater, Btu/lb
- h = feedwater enthalpy, Btu/lb
- HR = gross turbine heat rate, Btu per kwhr
- ΔHR = change in gross turbine heat rate, Btu per kwhr
- KW = kilowatts at generator terminals
- ΔKW = change in kilowatts at generator terminals
- M = evaporator feed, lb/hr
- n = subscript, highest of a series of extraction points (heaters)
- P = fraction of theoretical gain
- p = subscript, boiler feed pump
- R = feedwater enthalpy rise in a single heater, Btu/lb
- U = used energy from an extraction point to the next lower extraction point (to turbine exhaust for lowest extraction point), Btu/lb
- ΔU = change in used energy, Btu/lb
- W = boiler feedwater, lb/hr
- 1, 2, etc. = subscript, extraction point, heater
- η = thermal efficiency, regenerative cycle—with a, b, n, or a numerical subscript from extraction point designated to exhaust
- η_o = generator efficiency (if not known assume 0.985)
- η_N = nonextraction thermal efficiency
- Δ = prefix to indicate a finite change
- $'$ = (prime) superscript indicating changed state

Introduction

The need for a quick and accurate method of determining the effect of minor changes in the steam-turbine cycle on the heat rate is well known to those who are concerned with steam-station performance. A method giving the required degree of accuracy using only slide-rule calculations is desirable. Such a method is feasible if calculations involve only differences and the necessity for a complete set of heater calculations is avoided. These calculations can be avoided by considering the secondary effects of a cycle change as constituting a complete cycle with a given heat input. Calculations of the change in shaft work and the heat input can be made easily by this method. The change in heat rate is fixed by these changes.

Equations are derived for determining the effect on the turbine heat rate of:

1 Change in the distribution of liquid enthalpy rise between two adjacent heaters.
2 Change in pressure drop of extracted steam.
3 Change in heater-terminal difference.
4 Change in drain-cooler approach.
5 Effect of compressibility on liquid enthalpy.
6 Inclusion or omission of an evaporator condenser.
7 Changes in liquid enthalpy of boiler feedwater from an external heat source.
8 Change in final feedwater enthalpy.
9 Inclusion or omission of an evaporator.
10 Change from a flashed or drain-cooler heater to a contact or pumped heater or vice versa.

Basis of the Method

Gross turbine heat rate is defined as the heat-energy input to the turbine divided by the kilowatt output at the generator terminals. Therefore, determination of the change in kilowatt output and the heat-energy input permits evaluation of the change in heat rate. For small changes in turbine output there are no appreciable changes in engine, electrical, or mechanical efficiency. This simplifies the evaluation of output changes. If the throttle flow is held constant, changes in heat-energy input are eliminated except from changes in reheater flow, changes in final feed enthalpy, or changes in heat supplied to the cycle from an external source other than the steam generator.

[1] Engineer, Steam Division, Westinghouse Electric Corporation. Mem. ASME.

Contributed by the Power Division and presented at a joint meeting with the Joint Research Committee on Boiler Feedwater Studies at the Annual Meeting, New York, N. Y., November 29–December 4, 1953, of The American Society of Mechanical Engineers.

Note: Statements and opinions advanced in papers are to be understood as individual expressions of their authors and not those of the Society. Manuscript received at ASME Headquarters, August 5, 1953. Paper No. 53—A-97.

Since, for the cycle variations under consideration, the change in kilowatts is very small in comparison to the kilowatt output, the equation for the change in heat rate is

$$\text{Change in heat rate} = -\frac{\text{heat rate} \times \text{change in KW}}{\text{KW output}} + \frac{\text{Btu input change}}{\text{KW output}}$$

or

$$\Delta HR = -\frac{HR \times \Delta KW}{KW} + \frac{\Delta Btu}{KW}, \quad \text{Btu/kwhr} \ldots [1]$$

Fig. 1 represents a cycle having four heaters heating the feedwater to the saturation enthalpy corresponding to the throttle pressure. If there is K Btu per hr of heat units available and the thermal efficiency is η, then the shaft work $= \eta K$, Btu per hr.

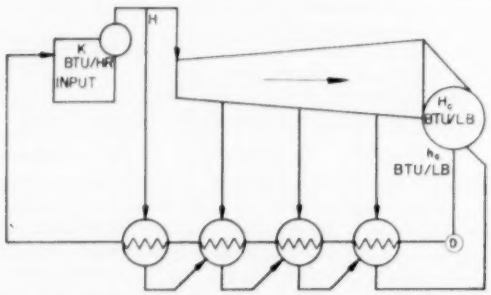

FIG. 1 FOUR-HEATER CYCLE HEATING FEEDWATER TO SATURATION LIQUID ENTHALPY CORRESPONDING TO INITIAL STEAM PRESSURE

Fig. 1 may represent a complete cycle or only a part of a cycle. The change in work output may be calculated from the change in heat supplied. Determination of a change in heat supplied, or heat available, together with the cycle efficiency fixes the change in work output.

In the regenerative feed-heating cycle the heat chargeable to the turbine is assumed to equal the steam flow times the steam enthalpy minus the corresponding boiler-feed enthalpy. At the throttle the boiler-feed enthalpy is taken as the final feed enthalpy. At any extraction point the feed enthalpy is taken as the feedwater enthalpy out of the heater at that extraction point. For zero pressure drop and zero terminal difference the feed enthalpy is taken as the liquid enthalpy corresponding to the saturation pressure. This relationship would permit setting up a heat balance from any extraction point to the exhaust. Fortunately, this is not necessary since the change in heat supplied times the thermal efficiency of a regenerative cycle, heating the feed to the enthalpy corresponding to the saturation enthalpy, equals the change in shaft work. The algebraic sum of the changes in shaft work equals the net change in shaft work.

Since the throttle flow is constant, a change in the heat supplied to the turbine can come only from a change in the reheater flow, a change in the final feed enthalpy, or from an external heat source such as hydrogen coolers. A change in the heat rejected to the condenser in the heater drains is handled as a change in heat from an external source.

Mechanical losses are constant and therefore do not enter into the computations.

DETERMINATION OF CYCLE THERMAL EFFICIENCY

The cycle efficiency, Fig. 1, from any extraction point to the turbine exhaust is determined as follows

$$\text{Nonextraction cycle efficiency} = \frac{H - H_e}{H - h_e} = \eta_N \ldots [2]$$

Note that H_e includes the turbine-exhaust loss. The theoretical gain G, in thermal efficiency, when heating the feed in an infinite number of contact heaters from the saturated liquid enthalpy corresponding to the exhaust pressure to the saturated liquid enthalpy corresponding to the extracted steam pressure, is determined from Fig. 2. The values of Fig. 2 were computed by the method developed by Salisbury.[2] Table 1 gives the fraction of

TABLE 1 FRACTION OF THEORETICAL GAIN IN NONEXTRACTION THERMAL-CYCLE EFFICIENCY REALIZABLE WITH A FINITE NUMBER OF HEATERS HAVING PRESSURE DROP, TERMINAL DIFFERENCE, ARRANGEMENT, AND DISTRIBUTION LOSSES

Number of heaters	—P (fraction of gain)— Below reheat	Above reheat
1	0	..
2	0.50	..
3	0.70	..
4	0.80	..
5	0.85	0.70
6	0.88	0.70
7	0.89	0.70
8		0.70

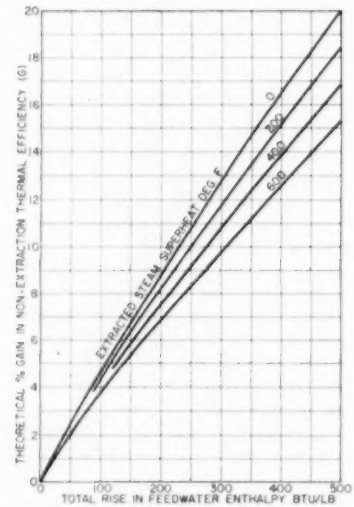

FIG. 2 THEORETICAL GAIN IN NONEXTRACTION CYCLE THERMAL EFFICIENCY FROM HEATING FEEDWATER IN INFINITE NUMBER OF HEATERS FROM THE SATURATED LIQUID ENTHALPY CORRESPONDING TO THE EXHAUST PRESSURE TO SATURATED LIQUID ENTHALPY CORRESPONDING TO EXTRACTION PRESSURE

the theoretical gain P, which can be realized with a finite number of heaters having pressure drop, terminal difference, arrangement, and distribution losses. The values in this table are average as determined from actual heat balances. The maximum error will occur at the top heater of a series of flashed heaters and will not exceed 2 percentage points in the realizable gain. The change in heat rate will be even less. No attempt has been made to reduce this possible error since to do so would unnecessarily complicate the method. The cycle efficiency is then

$$\eta_a = \eta_N \left(1 + \frac{GP}{100}\right) \ldots [3]$$

For a method of determining the thermal efficiency at the

[2] "The Steam-Turbine Regenerative Cycle—An Analytical Approach," by J. K. Salisbury, Trans. ASME, vol. 64, 1942, pp. 228-229.

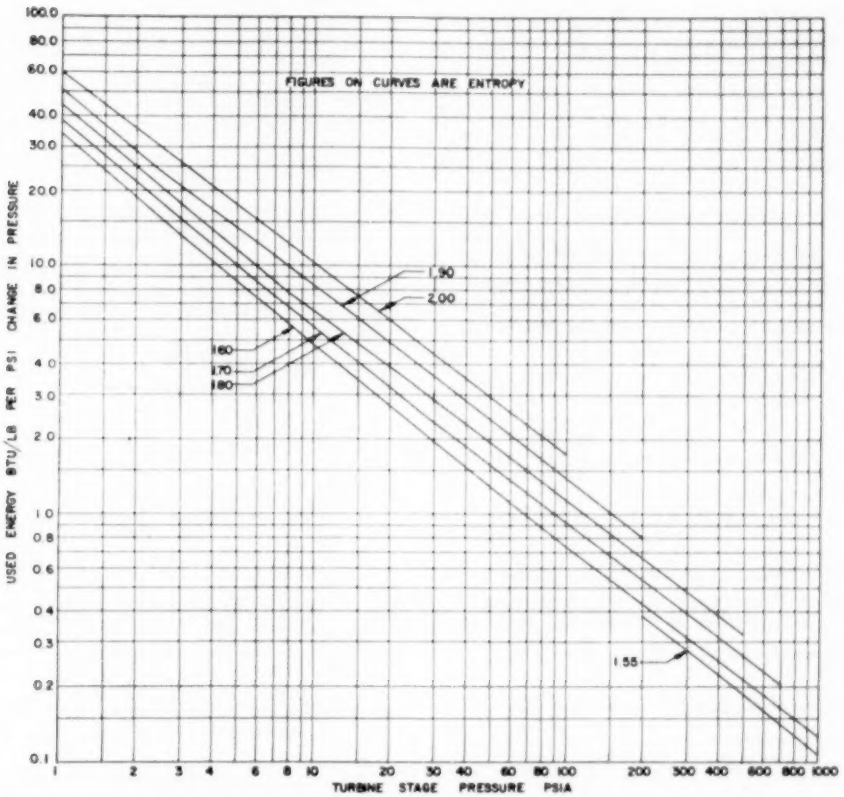

FIG. 3 USED ENERGY, BTU PER LB. PER PSI DIFFERENCE IN PRESSURE ON THE TURBINE STATE LINE

highest extraction point accurately, refer to the Appendix, Equation [35] under derivation of Equation [19].

In Fig. 3, used energy, Btu per lb per psi difference in pressure on the turbine state line (the difference in enthalpy of extracted steam per psi difference in pressure) is plotted against the turbine-stage pressure with entropy as a parameter. These curves are prepared on the basis of 90 per cent incremental turbine-stage efficiency with a reduction of 1.2 per cent for each average per cent of moisture. The curves provide a means for determining the difference in extraction enthalpy for a given difference in extraction pressure. For small differences in extraction pressure, the difference in enthalpy may be read at the mean of the old and new pressures but for large pressure differences the enthalpy change should be taken as the average of the values read at the old and new pressures. Table 2 is a tabulation of these values.

TABLE 2 USED ENERGY BTU PER LB PER PSI CHANGE IN PRESSURE

Turbine stage pressure, psia	Entropy					
	1.55	1.60	1.70	1.80	1.90	2.00
1	...	33.8	38.2	44.0	50.8	59.5
2	...	18.7	21.4	24.8	28.5	35.0
3	...	13.2	15.2	17.5	20.7	25.6
5	...	8.55	9.95	11.4	14.1	17.3
7	...	6.45	7.50	8.60	10.8	13.4
10	...	4.79	5.63	6.50	8.30	10.2
20	...	2.70	3.20	3.90	4.85	6.00
30	...	1.94	2.33	2.87	3.55	4.37
50	...	1.28	1.57	1.94	2.40	2.95
70	...	0.98	1.22	1.50	1.84	2.28
100	...	0.74	0.920	1.13	1.39	1.74
200	0.385	0.43	0.540	0.660	0.805	...
300	0.280	0.314	0.393	0.480	...	...
500	0.187	0.212	0.265	0.321	...	...
700	0.143	0.165	0.205	...	...	...
1000	0.107	0.126	...	...	...	...

APPLICATION OF METHOD

Derivations of equations suitable for application of this method to evaluation of the heat-rate changes resulting from cycle variations listed are given in the following paragraphs and in the Appendix.

Change in Distribution of Liquid Enthalpy Rise Between Two Adjacent Heaters. Fig. 4 illustrates the case where the liquid enthalpy rise between heaters H_a and H_b has been changed so that the extraction point for heater H_b is at H_b'. All other conditions of the cycle including the throttle flow remain unchanged.

The following changes take place:

The extraction point H_b moves to H_b' with an increase in the extracted steam enthalpy of ΔU_b Btu per lb.

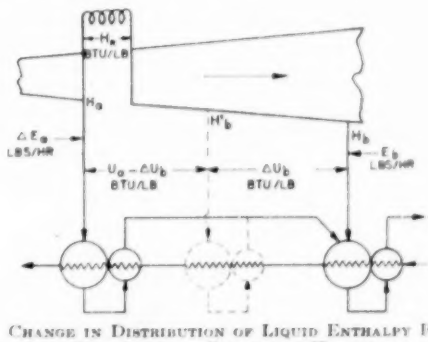

FIG. 4 CHANGE IN DISTRIBUTION OF LIQUID ENTHALPY RISE BETWEEN TWO ADJACENT FEEDWATER HEATERS

The quantity of steam extracted E_a decreases ΔE_a lb per hr (calculated by usual methods).

The reheater flow increases ΔE_a lb per hr when the extracted steam E_a decreases ΔE_a lb per hr.

The increased heat added in the reheater equals

$$\Delta E_a H_r \text{ Btu/hr} \quad \ldots\ldots [4]$$

This is also the change in heat supplied to the cycle, ΔBtu.

The shaft work from H_a to H_b' increases by $\Delta E_a(U_a - \Delta U_b)$ Btu per hr. The shaft work from H_b' to H_b decreases by $E_b \Delta U_b$ Btu/hr.

Then the change in heat available at H_b' equals

$$E_b \Delta U_b + \Delta E_a(U_a - \Delta U_b) - \Delta E_a H_r, \text{ Btu/hr}$$

The change in shaft work from H_b' to the exhaust equals

$$\eta_b'[E_b \Delta U_b + \Delta E_a(U_a - \Delta U_b) - \Delta E_a H_r], \text{ Btu/hr}$$

The total change in shaft work equals

$$-\Delta E_a(U_a - \Delta U_b) - E_b \Delta U_b + \eta_b'[E_b \Delta U_b + \Delta E_a(U_a - \Delta U_b) - \Delta E_a H_r], \text{ Btu/hr}$$

also

$$-(1 - \eta_b')\,[\Delta E_a(U_a - \Delta U_b) + E_b \Delta U_b] - \eta_b' \Delta E_a H_r, \text{ Btu/hr} \quad \ldots\ldots [5]$$

$$\Delta \text{KW} = \frac{\eta_g}{3413}\{-(1 - \eta_b')\,[\Delta E_a(U_a - \Delta U_b) + E_b \Delta U_b] - \eta_b' \Delta E_a H_r\} \quad \ldots\ldots [6]$$

Substituting Equations [4] and [6] in [1]

$$\Delta \text{HR} = \frac{\text{HR}\eta_g}{3413\ \text{KW}}\{(1 - \eta_b')\,[\Delta E_a(U_a - \Delta U_b) + E_b \Delta U_b] + \eta_b' \Delta E_a H_r\} - \frac{\Delta E_a H_r}{\text{KW}}, \text{ Btu/kwhr} \quad \ldots\ldots [7]$$

If there is no reheat between extraction points H_a and H_b, $H_r = 0$ and Equation [7] becomes

$$\Delta \text{HR} = \frac{\text{HR}\eta_g}{3413\ \text{KW}}[(1 - \eta_b')\Delta E_a(U_a - \Delta U_b) + E_b \Delta U_b], \text{ Btu/kwhr} \quad \ldots\ldots [8]$$

Equation [7] can be used to determine the change in turbine heat rate for cycle changes involving any of the following:

(*a*) Distribution of liquid enthalpy rise between two adjacent heaters. (Cutting a heater out of service is a special case where the entire rise of the heater cut out is taken by the next higher heater.)

(*b*) Pressure drop (except top heater).

(*c*) Terminal difference (except top heater).

(*d*) Drain-cooler approach (except bottom heater).

(*e*) Effect of compressibility on liquid enthalpy (except top heater.)

(*f*) Addition or elimination of evaporator condenser.

Since items (*b*), (*c*), (*d*), (*e*), and (*f*) have the effect of shifting the extraction quantity between two adjacent extraction points they are special cases of (*a*). In these cases

$$\Delta U_b = 0$$

since there is no change in the extraction point for the heater. The equation then becomes

$$\Delta \text{HR} = \frac{\text{HR}\eta_g}{3413\ \text{KW}}[(1 - \eta_b)\,\Delta E_a U_a + \eta_b \Delta E_a H_r] - \frac{\Delta E_a H_r}{\text{KW}}, \text{ Btu/kwhr} \quad \ldots\ldots [9]$$

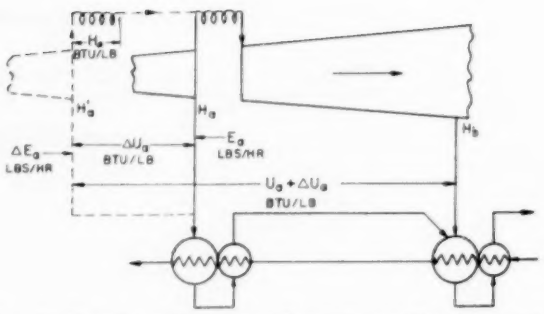

Fig. 5 Change in Extraction Pressure for Top Heater to Maintain Constant Final Feedwater Enthalpy With Change in Extraction Pressure Drop or Terminal Temperature Difference

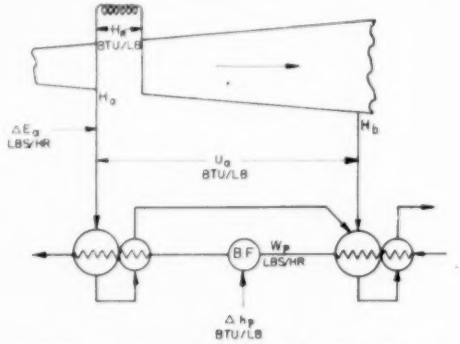

Fig. 6 Change in Boiler Feedwater Liquid Enthalpy From Enthalpy Rise in Boiler Feed Pump

If there is no reheat between extraction points H_a and H_b, $H_r = 0$ and the equation becomes

$$\Delta \text{HR} = \frac{\text{HR}\eta_g}{3413\ \text{KW}}[(1 - \eta_b)\,\Delta E_a U_a], \text{ Btu/kwhr} \quad \ldots\ldots [10]$$

Change in Pressure Drop, Terminal Difference, or Effect of Compressibility at Top Heater. Equation [9], with $(\Delta R_a W_a + \Delta E_a H_r)$ substituted for $\Delta E_a H_r$, could be used to obtain the change in heat rate for a change in pressure drop or terminal difference at the top heater except that, if the extraction point is fixed, the effect of a change in the final feed enthalpy is included in the result obtained. To avoid this difficulty and to obtain the true effect of the change in pressure drop or terminal difference a modification of Equation [7] is used.

Fig. 5 is a diagram of the portion of the cycle affected.

Following the steps used in deriving Equation [7],[3] the equation derived is

$$\Delta \text{HR} = \frac{\text{HR}\eta_g}{3413\ \text{KW}}\{(1 - \eta_b)\,[\Delta E_a(U_a + \Delta U_a) + E_a \Delta U_a] + \eta_b \Delta E_a H_r\} - \frac{\Delta E_a H_r}{\text{KW}}, \text{ Btu/kwhr} \quad \ldots\ldots [11]$$

Change in Liquid Enthalpy of Boiler Feedwater From an External Heat Source. The introduction of heat from an external source into a turbine heat cycle has the effect of reducing the quantity of steam extracted and hence increasing the kilowatt output. Let Fig. 6 represent a boiler feed pump raising the enthalpy of W_p lb per hr of boiler feedwater Δh_p Btu per lb.

Then the heat added to the cycle $= \Delta h_p W_p$ Btu per hr.

The change in the steam extracted to heater H_a, ΔE_a, lb/hr, can be determined in the usual manner. The change in reheater

[3] See Appendix for derivation.

flow = $-\Delta E_a$ lb/hr. The change in heat input in the reheater equals $-\Delta E_a H_r$ Btu/hr. The total change in heat added equals

$$\Delta h_p W_p - \Delta E_a H_r, \text{ Btu/hr} \quad [12]$$

In Equation [7] the term $-\Delta E_a H_r$, Btu/hr, represents the heat added. If

$$\Delta h_p W_p - \Delta E_a H_r, \text{ Btu/hr} \quad [13]$$

is substituted for $-\Delta E_a H_r$ inside the braces and $\Delta U_b = 0$, the equation covers the case of a change in liquid enthalpy of the boiler feedwater from an external source and reads

$$\Delta HR = \frac{HR\eta_g}{3413\ KW}\left[(1-\eta_b)\,\Delta E_a U_a - \eta_b(\Delta h_p W_p - \Delta E_a H_r\right] - \frac{\Delta E_a H_r}{KW}, \text{ Btu/kwhr} \quad [14]$$

Note that the term $\Delta E_a H_r/KW$, the additional heat supplied to the cycle, is unchanged since the enthalpy rise in the boiler feed pump is not charged to the turbine.

If there is no reheat between extraction points H_a and H_b or below H_b, H_r = zero and the equation becomes

$$\Delta HR = \frac{HR\eta_g}{3413\ KW}\left[(1-\eta_b)\,\Delta E_a U_a - \eta_b \Delta h_p W_p\right] \text{ Btu/kwhr} \quad [15]$$

If the steam is reheated below extraction point H_b, the change in flow through the reheater will be less than ΔE_a and therefore the change in heat added in the reheater will be less than $\Delta E_a H_r$. However, Equation [15] may be used with an error in ΔHR of less than 0.1 per cent.

Equations [14] and [15] are applicable for determining the change in heat rate due to a change in liquid enthalpy of the boiler feedwater above the lowest heater from an external heat source such as the boiler feed pump.

If the change in liquid enthalpy takes place below the lowest heater, the change in heat available at the lowest extraction point equals

$$\Delta h_1 W_1, \text{ Btu/hr} \quad [16]$$

The change in shaft work equals

$$\eta_t \Delta h_1 W_1, \text{ Btu/hr} \quad [17]$$

Substituting in Equation [1]

$$\Delta HR = -\frac{HR\eta_g}{3413\ KW}\left[\eta_t \Delta h_1 W_1\right], \text{ Btu/kwhr} \quad [18]$$

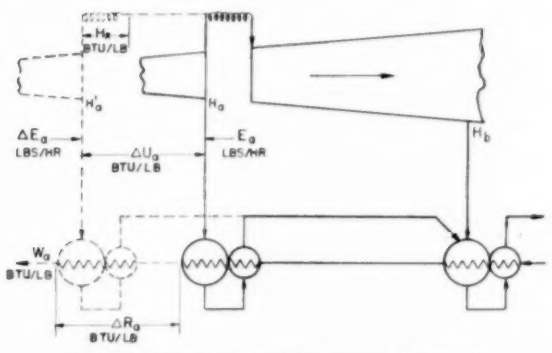

FIG. 7 CHANGE IN FINAL FEEDWATER ENTHALPY

Equation [18] is applicable for determining the change in heat rate due to a change in liquid enthalpy of the boiler feedwater below the lowest heater from (1) air-ejector condenser, (2) hydrogen coolers, (3) lubricating-oil coolers, (4) change in drain-cooler approach.

The effect of a change in the drain-cooler approach on the lowest heater is to increase or decrease rejection of heat from the cycle. Then $\eta_t D_1 \Delta d_1$ may be substituted for $\eta_t \Delta h_1 W_1$ in Equation [18].

Equation [10] may be used, instead of Equation [18] if the lowest heater is considered as H_a and $\eta_b = 0$.

Change in Final Feedwater Enthalpy. In Fig. 7 the enthalpy rise in the top feedwater heater has been increased by extracting steam at a higher pressure to give a higher final feedwater enthalpy. No other changes are made in the cycle.

Following the steps used in deriving Equation [7][3] the equation derived is

$$\Delta HR = \frac{HR\eta_g}{3413\ KW}\left[(1-\eta_a')E_a\Delta U_a + \eta_a'(\Delta R_a W_a + \Delta E_a H_r)\right] - \frac{\Delta R_a W_a + \Delta E_a H_r}{KW}, \text{ Btu/kwhr} \quad [19]$$

For accurate determination of η_a' see Equation [35].

Inclusion or Omission of Evaporator From Cycle. Fig. 8 illustrates a five-heater cycle with the evaporator between the third and fourth heaters.

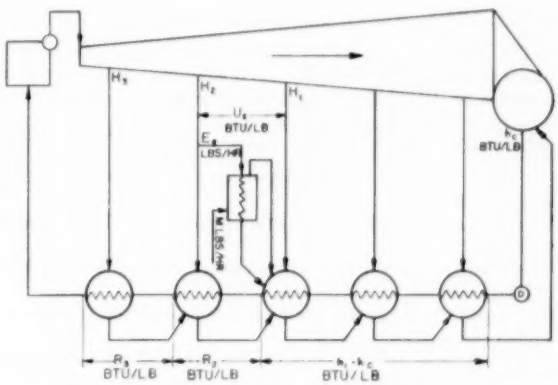

FIG. 8 FIVE-STAGE FEEDWATER HEATING CYCLE WITH MAKE-UP EVAPORATOR

Omission of the evaporator permits extracting E_a lb of steam per hr from extraction point H_1 instead of H_3. The gain in shaft work equals

$$E_a U_2, \text{ Btu/hr} \quad [20]$$

This reduces the heat available at H_1 by $E_a U_2$ Btu per hr. The additional steam extracted will reduce the shaft work to the exhaust by

$$\eta_t E_a U_2, \text{ Btu/hr} \quad [21]$$

The make-up is M lb per hr and since the evaporator is omitted the feedwater to be heated is reduced by this amount. This reduction of feed heated will increase the heat available at extraction point H_1 and each extraction point above it. The shaft work from these increases of heat available equals

$$\eta_1 M(h_1 - h_a) + \eta_1 MR_2 + \eta_2 MR_3 + \eta_3 MR_4 + \dots .$$

Then the total change in shaft work equals

$$E_a U_2 - \eta_1 E_a U_2 + M\,[\eta_1 (h_1 - h_a) + \eta_2 R_2 + \eta_3 R_3 + \eta_4 R_4 + \dots .], \text{ Btu/hr} \dots [22]$$

Substituting Equation [22] in Equation [1]

$$\Delta HR = -\frac{HR\eta_g}{3413\ KW}\{E_a U_2(1 - \eta_1) + M(\eta_1[h_1 - h_a] + \eta_2 R_2 + \eta_3 R_3 + \dots .)\}, \text{ Btu/kwhr} \dots [23]$$

The fact that the flow through the reheater will change, and consequently the heat added to the cycle, is disregarded since the error in ΔHR from this cause will be on the order of 0.25 per cent. It is improbable that extraction for the evaporator would be taken at or above the reheater-inlet pressure.

In Equation [23] the evaporator feed is heated to the final feedwater enthalpy. If the distillate or an equivalent quantity of feedwater is taken to storage at some lower enthalpy, the equation should be modified accordingly.

Changing From a Flashed or Drain-Cooler Heater to a Contact or Pumped Heater or Vice Versa. Fig. 9 illustrates a case where a heater is changed from a drain-cooler heater to a pumped heater. The equation for determination of the change in heat rate is[3]

$$\Delta HR = \frac{HR\eta_g D_a}{3413\ KW}\,[\eta_a A_a + \text{— — —} + \eta_1(R_1 - F_1)], \text{ Btu /kwhr} \dots [24]$$

Conclusion

This method of evaluating heat-rate differences should prove useful to power-plant designers and operators because it provides a means of determining heat-rate differences for various cycle changes with a minimum of work and a maximum of accuracy. It has the following advantages:

1 It is easily understood because usual heat-balance data and methods are used.

2 The operation is reduced to substitution of values in simple equations.

3 Nearly all of the values required are obtained directly from the heat balance.

4 With one exception, slide-rule calculations will give the required degree of accuracy.

5 Inspection of the equations gives considerable information about the effect of changes in different parts of the cycle.

Appendix

Derivation of Equation [11]

Change in Pressure Drop, Terminal Difference, or Effect of Compressibility at Top Heater. Fig. 5 illustrates the case where the extraction pressure of a top heater has been increased to maintain unchanged the final feed enthalpy after a change in extraction pressure drop, terminal difference, or the effect of compressibility.

The following changes take place: The extraction point moves from H_a to H_a' with an increase in extracted steam enthalpy of ΔU_a Btu per lb. The extracted steam decreases ΔE_a lb per hr. The reheater flow increases ΔE_a lb per hr. The heat added in the reheater increases

$$\Delta E_a H_r, \text{ Btu/hr} \dots [25]$$

The shaft work from H_a' to H_a decreases $E_a \Delta U_a$ Btu per hr. The shaft work, Btu/hr, from H_a' to H_b increases

$$\Delta E_a(U_a + \Delta U_a), \text{ Btu/hr} \dots [26]$$

The change in heat available at H_b equals

$$E_a \Delta U_a + \Delta E_a(U_a + \Delta U_a) - \Delta E_a H_r, \text{ Btu/hr} \dots [27]$$

The change in shaft work from H_b to the exhaust equals

$$\eta_b[E_a \Delta U_a + \Delta E_a(U_a + \Delta U_a) - \Delta E_a H_r], \text{ Btu/hr} \dots [28]$$

The total change in shaft work equals

$$-\Delta E_a(U_a + \Delta U_a) - E_a \Delta U_a + \eta_b[E_a \Delta U_a + \Delta E_a(U_a + \Delta U_a) - \Delta E_a H_r], \text{ Btu/hr}$$

also

$$-(1 - \eta_b)\,[\Delta E_a(U_a + \Delta U_a) + E_a \Delta U_a] - \eta_b \Delta E_a H_r, \text{ Btu/hr} \dots [29]$$

Then the change in kilowatt output

$$\Delta KW = -\frac{\eta_g}{3413}\{(1 - \eta_b)\,[\Delta E_a(U_a + \Delta U_a) + E_a \Delta U_a] + \eta_b \Delta E_a H_r\} \dots [30]$$

The change in the heat supplied to the cycle equals

$$-\Delta E_a H_r, \text{ Btu/hr} \dots [31]$$

Substituting in Equation [1]

$$\Delta HR = \frac{HR\eta_g}{3413\ KW}\{(1 - \eta_b)\,[\Delta E_a(U_a + \Delta U_a) + E_a \Delta U_a] + \eta_b \Delta E_a H_r\} - \frac{\Delta E_a H_r}{KW}, \text{ Btu/kwhr} \dots [11]$$

Derivation of Equation [19]

Change in Final Feedwater Enthalpy. In Fig. 7 the enthalpy rise in the top feedwater heater has been increased to give a higher final feedwater enthalpy by extracting steam at a higher pressure. No other changes are made in the cycle.

The following changes take place: The extraction point is moved from H_a to H_a' with an increase in the extracted steam enthalpy of ΔU_a, Btu/lb.

The extracted steam quantity increases ΔE_a, lb/hr. The shaft work from H_a' to H_a decreases $E_a \Delta U_a$, Btu/hr. The reheater flow decreases ΔE_a, lb/hr and the heat added in the reheater decreases by $\Delta E_a H_r$, Btu/hr.

The additional extraction reduces the heat available at H_a' by $\Delta R_a W_a$, Btu/hr.

The change in heat at H_a' equals

$$-\Delta R_a W_a - \Delta E_a H_r + E_a \Delta U_a, \text{ Btu/hr} \dots [32]$$

$$\Delta KW = \frac{\eta_g}{3413}\,[\eta_a'(-\Delta R_a W_a - \Delta E_a H_r + E_a \Delta U_a) - E_a \Delta U_a] \dots [33]$$

The reduction in heat supplied to the cycle equals

$$\Delta E_a H_r + \Delta R_a W_a, \text{ Btu/hr} \dots [34]$$

Substituting Equations [33] and [34] in Equation [1]

$$\Delta HR = \frac{HR\eta_g}{3413\ KW}\,[(1 - \eta_a')E_a \Delta U_a + \eta_a'(\Delta R_a W_a + \Delta E_a H_r)] - \frac{\Delta R_a W_a + \Delta E_a H_r}{KW}, \text{ Btu/kwhr} \dots [19]$$

Since the change in heat rate in this case is the difference between two nearly equal quantities, an accurate determination of the

thermal efficiency is necessary to obtain the desired degree of accuracy. Since the thermal efficiency required includes all of the heaters it can be determined quite easily from the heat-balance data

$$\text{Efficiency} = \frac{\text{Output}}{\text{Input}}$$

The thermal cycle required has a reduction of ΔKW, the kilowatts generated down to the first extraction point, and an identical reduction of the heat input to the cycle

$$\text{Efficiency} = \frac{\text{KW output} + \text{KW mech and elec losses} - \Delta\text{KW}}{\text{heat rate} \times \text{KW} + 3413 - \Delta\text{KW}} \quad \ldots\ldots [35]$$

This is efficiency η_a' of Equation [19].

Derivation of Equation [24]

Changing From a Flashed or Drain-Cooler Heater to a Contact or Pumped Heater or Vice Versa. Fig. 9 illustrates a four-heater cycle where the fourth heater is changed from a drain-cooler

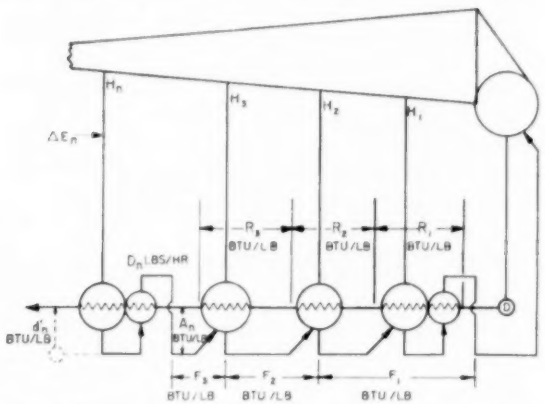

Fig. 9 Change From Drain-Cooler Heater to Pumped Heater

heater to a pumped heater. The extraction points above this heater are not affected. If the drains are pumped instead of cascaded through a drain cooler, D_nA_n Btu/hr additional will be available at H_n for heating the feedwater. This will result in ΔE_n lb/hr reduction in extraction at H_n and consequently D_nA_n Btu/hr additional available for conversion to shaft work at the thermal efficiency of the cycle from H_n to the exhaust. Then the additional shaft work from H_n to the exhaust equals

$$-\eta_n D_n A_n, \text{ Btu/hr} \quad \ldots\ldots [36]$$

Since the drains cascaded to heater 3 may give up more or less heat than necessary to heat the equivalent amount of feedwater there may be a change in the heat available for conversion to shaft work at extraction point H_3. This change in heat available at H_3 equals

$$-D_n(R_3 - F_3), \text{ Btu/hr}$$

and the change in shaft work from H_3 to the exhaust equals

$$-\eta_3 D_n(R_3 - F_3), \text{ Btu/hr} \quad \ldots\ldots [37]$$

Similarly, at extraction point H_2 the change in shaft work equals

$$-\eta_2 D_n(R_2 - F_2), \text{ Btu/hr} \quad \ldots\ldots [38]$$

and at extraction point H_1 the change in shaft work equals

$$-\eta_1 D_n(R_1 - F_1), \text{ Btu/hr} \quad \ldots\ldots [39]$$

Then the net change in shaft work is the sum of Equations [36], [37], [38], and [39]

$$\Delta\text{KW} = -[\eta_n D_n A_n + \eta_3 D_n(R_3 - F_3) + \eta_2 D_n(R_2 - F_2) + \eta_1 D_n(R_1 - F_1)]$$

This may be written

$$\Delta\text{KW} = -D_n[\eta_n A_n + \text{— — —} + \eta_1(R_1 - F_1)] \quad \ldots\ldots [40]$$

Substituting Equation [40] in Equation [1]

$$\Delta\text{HR} = \frac{\text{HR}\eta_g D_n}{3413\ \text{KW}}[\eta_n A_n + \text{— — —} + \eta_1(R_1 - F_1)], \text{ Btu/kwhr} \quad \ldots\ldots [24]$$

This equation is correct only when D_n represents the drains cascaded. If D_n represents drains pumped or mixed in a contact heater the use of $D_n' = D_n + \Delta E_n$ would be more accurate. However, it is questionable whether the improved accuracy justifies the additional complication. The error probably will not exceed 5 per cent of the change in heat rate in any case.

Examples of Use of Equations

Fig. 10 is a complete heat-balance diagram with all data shown. It will be used in illustrating the various cases. The method of establishing the nomenclature will be given in the first example. The same method will be used in all other examples and therefore will not be given. Reference should be made to the applicable diagram to follow the procedure.

Change in Distribution of Liquid Enthalpy Rise Between Two Adjacent Heaters. Heater 4 in Fig. 10 is to have a terminal difference of 0 deg F instead of 5 deg F. The feed temperature out becomes 374.8 F and the enthalpy 347.9 Btu/lb. The rise in heater 5 then becomes 347.9 — 342.5 = 5.4 Btu/lb less.

Equation [7] and Fig. 4 apply. Extraction points for heaters 5 and 4 in Fig. 10 are extraction points H_a and H_b, respectively, of Fig. 4

$$\Delta\text{HR} = \frac{\text{HR}\eta_g}{3413\ \text{KW}}\{(1 - \eta_b')[\Delta E_a(U_a - \Delta U_b) + E_b\Delta U_b] + \eta_b'\Delta E_a H_r\} - \frac{\Delta E_a H_r}{\text{KW}} \quad \ldots\ldots [7]$$

ΔE_a = 5.4 (change in rise) × 671,940 (feedwater flow through heater) ÷ 934.6 (Btu/lb of extracted steam given up to heater) = 3882 lb/hr.

HR = 8150 Btu/kwhr
η_g = 0.985 assumed
KW = 100,000

$$\eta_N = \frac{H_b - H_c}{H_b - h_c} = \frac{1431.7 - 1037.0}{1431.7 - 59.7} = 0.288$$

η_b' = 0.288 (1 + 0.103 × 0.80) = 0.312
G_b = 10.3 (SH at H_b = 435 deg approx)
P_b = 0.80

Total rise to H_b = 347.9 — 59.7 = 288.2 Btu/lb
ΔE_a = —3882 lb/hr
U_a = 1522.8 — 1431.7 = 91.1 Btu/lb
ΔU_b = 0
H_r = 1522.8 — 1361.1 = 161.7 Btu/lb

Substituting in Equation [7]

$$\Delta\text{HR} = \frac{8150 \times 0.985}{3413 \times 100{,}000}[(1 - 0.312)(-3882 \times 911)$$

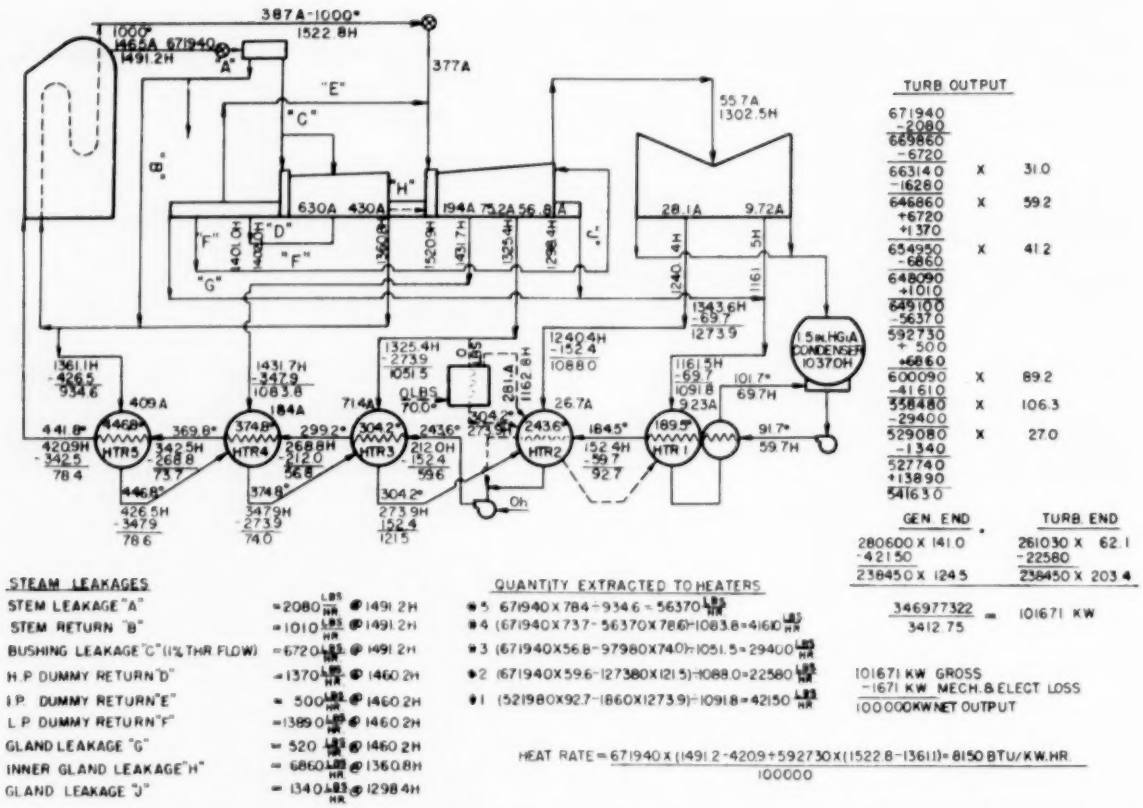

STEAM LEAKAGES

STEM LEAKAGE "A"	= 2080 lb/hr @ 1491.2H
STEM RETURN "B"	= 1010 lb/hr @ 1491.2H
BUSHING LEAKAGE "C" (1% THR FLOW)	= 6720 lb/hr @ 1491.2H
H.P DUMMY RETURN "D"	= 1370 lb/hr @ 1460.2H
I.P. DUMMY RETURN "E"	= 500 lb/hr @ 1460.2H
L.P DUMMY RETURN "F"	= 1389.0 lb/hr @ 1460.2H
GLAND LEAKAGE "G"	= 520 lb/hr @ 1460.2H
INNER GLAND LEAKAGE "H"	= 6860 lb/hr @ 1360.8H
GLAND LEAKAGE "J"	= 1340 lb/hr @ 1298.4H

QUANTITY EXTRACTED TO HEATERS

#5 671940 X 784 ÷ 9346 = 56370 lb/hr

#4 (671940 X 737 - 56370 X 786) ÷ 1083.8 = 41610 lb/hr

#3 (671940 X 56.8 - 97980 X 740) ÷ 1051.5 = 29400 lb/hr

#2 (671940 X 596 - 127380 X 121.5) ÷ 1088.0 = 22580 lb/hr

#1 (521980 X 92.7 - 18600 X 127.39) ÷ 1091.8 = 42150 lb/hr

$$\text{HEAT RATE} = \frac{671940 \times (1491.2 - 4209 + 592730 \times (1522.8 - 1361.1) = 8150 \text{ BTU/KW.HR}}{100000}$$

FIG. 10 HEAT-BALANCE DIAGRAM, 100 MW AIEE-ASME PREFERRED STANDARD TURBINE-GENERATOR UNIT, 1450 PSIG—1000/1000 F, 1.5 IN. HG ABS

$$+ 0.312 \times (-3882) \times 161.7] - \frac{(-)\,3882 \times 161.7}{100{,}000}$$

$$\Delta HR = \frac{2.351}{10^5}[-243{,}240 - 196{,}000] + 6.27$$

$$\Delta HR = -10.32 + 6.27 = -4.05 \text{ Btu/kwhr}$$

Change in Pressure Drop at Top Heater. Heater 5 in Fig. 10 is to have a pressure drop of 1 per cent instead of 5 per cent. The new extraction pressure will be at 413.1 psia. The difference between the old and new extraction pressures is 16.9 psia and the mean pressure is 421.6 psia. From Fig. 3 the difference in extraction enthalpy at 1.634 entropy is 0.262 Btu/lb per psi times 16.9 psi = 4.43 Btu per lb.

Equation [11] and Fig. 5 apply

$$\Delta HR = \frac{HR\eta_g}{3413 \text{ KW}}\{(1-\eta_b)[\Delta E_a(U_a + \Delta U_a) + E_a \Delta U_a] + \eta_b \Delta E_a H_r\} - \frac{\Delta E_a H_r}{KW} \quad \ldots\ldots [11]$$

HR = 8150 Btu/kwhr
η_g = 0.985 assumed
KW = 100,000
U_a = 1522.8 — 1431.7 = 91.1 Btu/lb
ΔU_a = (—) 4.43 Btu/lb
H_r = 1522.8 — 1361.1 = 161.7 Btu/lb
E_a = 56,370 lb/hr

$$\Delta E_a = \frac{56{,}370}{1} \times \frac{4.43}{930.2} = 268 \text{ lb/hr}$$

G_b = 10.3 (435 F SH, 282.8 Btu rise)
P_b = 0.80 (4 heaters)

$$\eta_b = \frac{1431.7 - 1037.0}{1431.7 - 59.7} \times (1 + 0.103 \times 0.80) = 0.312$$

$$\Delta HR = \frac{8150 \times 0.985}{3413 \times 100{,}000}\{(1 - 0.312)[268\,(91.1 - 4.43) - 56{,}370 \times 4.43] + 0.312 \times 268 \times 161.7\} - \frac{268 \times 161.7}{100{,}000}$$

$$\Delta HR = -3.78 \text{ Btu/kwhr}$$

Change in Liquid Enthalpy of Boiler Feedwater From an External Heat Source. In Fig. 10, if the rise in feedwater enthalpy in the boiler feed pump is assumed to be 7.8 Btu per lb, Equation [15] and Fig. 6 apply

$$\Delta HR = \frac{HR\eta_g}{3413 \text{ KW}}[(1-\eta_b)\,\Delta E_a U_a - \eta_b \Delta h_p W_p], \text{ Btu/kwhr} \quad \ldots\ldots [15]$$

HR = 8150 Btu/kwhr
η_g = 0.985 (assumed)
KW = 100,000
U_a = 85.0 Btu/lb
h_p = 7.8 Btu/lb
W_p = 671,940 lb/hr

$$\Delta E_a = -7.8 \times 671{,}940 \div 1051.5 = -4980 \text{ lb/hr}$$

$G_b = 0.065$ (155 F SH, 152.3 Btu rise)

$P_b = 0.50$ (2 heaters)

$$\eta_b = \frac{1240.4 - 1037.0}{1240.4 - 59.7}(1 + 0.065 \times 0.50) = 0.1777$$

$$\Delta HR = \frac{8150 \times 0.985}{3413 \times 100{,}000}[(1 - 0.1777) \times (-4980) \times 85.0 - 0.1777 \times 7.8 \times 671{,}940]$$

$\Delta HR = -30.1$ Btu/kwhr

Change in Final Feed Enthalpy. In Fig. 10, if the final feed enthalpy is increased 10 Btu/lb and other conditions are held constant, the conditions at heater 5 will be

Final feed enthalpy = 430.9 Btu/lb
Final feed temperature = 450.7 F
Saturation temperature in heater 5 = 455.7 F
Extraction steam pressure at heater 5 = 447.5 psia
Extraction steam pressure at turbine = 471 psia
Entropy at 430 psia and 1361.1 Btu/lb = 1.63
Used energy per psi difference at 430 psia = 0.245 Btu/psi
Used energy per psi difference at 471.0 psia = 0.230 Btu/psi
Difference in extraction enthalpy

$$= (471 - 430)\frac{(0.245 + 0.230)}{2} = 9.75 \text{ Btu/lb}$$

The new extraction point is at 471 psia and 1370.9 Btu/lb. Equation [19] and Fig. 7 apply

$$\Delta HR = \frac{HR\eta_g}{3413 \text{ KW}}[(1 - \eta_a')E_a\Delta U_a + \eta_a'(\Delta R_a W_a + \Delta E_a H_r)] - \frac{\Delta R_a W_a + \Delta E_a H_r}{\text{KW}}, \text{ Btu/kwhr} \quad [19]$$

HR = 8150 Btu/kwhr
$\eta_g = 0.985$ assumed
KW = 100,000
$\Delta U_a = 9.75$ Btu/lb
$H_r = 161.7$ Btu/lb
$\Delta R_a = 10.0$ Btu/lb
$E_a = 56{,}370$ lb/hr

$$\Delta E_a = \frac{56{,}370 \times 0.2}{934.4} + \frac{10 \times 671{,}940}{934.4} = 7203 \text{ lb/hr}$$

$W_a = 671{,}940$ lb/hr

Substituting in Equation [35] to get efficiency η_a'

$$\eta_a' = \frac{(100{,}000 + 1671)3413 - 663{,}140 \times 31.0 - 646{,}860 \times 59.2 - 654{,}950(41.2 - 9.75)}{100{,}000 \times 8150 - 663{,}140 \times 31.0 - 646{,}860 \times 59.2 - 654{,}950(41.2 - 9.75)} = 0.3637$$

$$\Delta HR = \frac{8150 \times 0.985}{100{,}000 \times 3413}[0.3637(10.0 \times 671{,}940 + 7203 \times 161.7) + (1 - 0.3637)(56{,}370 \times 9.75) - \frac{10.0 \times 671{,}940 + 7203 \times 161.7}{100{,}000}]$$

$\Delta HR = -3.17$ Btu/kwhr

Changing From a Contact Heater to a Flashed Heater. In Fig. 10 heater 2 is to be changed from a contact to a flashed heater with 0 deg F terminal difference.

Equation [24] and Fig. 9 apply

$$\Delta HR = \frac{HR\eta_g D_n}{3413 \text{ KW}}[\eta_n A_n + \ldots + \eta_1(R_1 - F_1)], \text{ Btu/kwhr} \quad [24]$$

HR = 8150 Btu/kwhr
$\eta_g = 0.985$ assumed
$D_n = 56{,}370 + 41{,}610 + 29{,}400 + 22{,}580 = 149{,}960$ lb/hr

$A_n = (212.0 - 152.4) = 59.6$ Btu/lb

$(R_1 - F_1) = (152.4 - 59.7) - (212.0 - 69.7) = -49.6$ Btu/lb

$G_n = 0.065$ (156 F SH at 152.3 Btu/lb rise)

$P_n = 0.50$

$$\eta_n = \frac{(1240.4 - 1037.0)}{(1240.4 - 59.7)}(1 + 0.065 \times 0.50) = 0.1777$$

$$\eta_1 = \frac{(1161.5 - 1037.0)}{(1161.5 - 59.7)}(1 + 0.042 \times 0.0) = 0.1129$$

$$\Delta HR = \frac{8150 \times 0.985}{3413 \times 100{,}000}[59.6 \times 149{,}960 \times 0.1777 + 0.1129 \times (-49.6) \times 149{,}960] \text{ Btu/kwhr}$$

$\Delta HR = 17.6$ Btu/kwhr

Discussion

W. F. Allen, Jr.[4] The method presented in this paper is a valuable addition to the existing procedures for solution of the effect of minor changes in the turbine-extraction feed-heating cycle.

Three other methods have been proposed in recent years for the solution of the effect of minor changes.[5,6,7] Two of these methods are analytical[5,6] and the third[7] is based on using mass-flow and enthalpy differences and simple arithmetic. The method proposed in the present paper is similar to the last reference,[7] in that only differences are employed and the change in extraction flow is computed for the heater principally affected, but differs in that the necessity of carrying out a complete set of heater calculations is obviated by the ingenious device of determining thermal efficiency for the remainder of the cycle.

Usually, an analytical approach to the problem of heat-cycle changes necessitates simplifying assumptions that render the method of little value for accurate evaluation, but the method given in this paper does not appear to suffer from this shortcoming. In this regard, the results given in Table 3, herewith, obtained by the methods given in the references cited[5,7] and by the proposed method for a change of 2 F in terminal difference on the closed heaters for the 60,000-kw AIEE-ASME Preferred Standard unit, steam conditions 850 psi gage, 900 F, may be of interest. The method given in reference[6] is somewhat less accurate than the other methods and has not been included. The first and third columns in Table 3 have been taken from reference[7], and the last column has been computed by the writer, using Equation [10] from the paper.

[4] Engineer, Mechanical Division, Stone & Webster Engineering Corporation, Boston, Mass. Assoc. Mem. ASME.

[5] "Power-Plant Cycle Evaluation," by J. K. Salisbury, Trans. ASME, vol. 71, 1949, pp. 593–604.

[6] "The Evaluation of Steam-Power-Plant Losses by Means of the Entropy-Balance Diagram," by Allen Keller, Trans. ASME, vol. 72, 1950, pp. 949–953.

[7] "Evaluation of the Effect of Terminal Difference and Pressure Drop on Steam-Power-Plant Heat Rate," by W. F. Allen, Jr., ASME Paper 51—F-28.

"Simple Figuring for Minor Feed Heating Cycle Changes," by W. F. Allen, Jr., *Power Engineering*, vol. 56, November, 1952, pp. 98–100, 102, and 104.

TABLE 3 CHANGE IN TURBINE HEAT RATE, BTU PER KWHR

Method	Reference[4]		Reference[7]	
Top heater	2.1	(2.0)[a]	3.3	3.3
Heater No. 2	2.1	(2.1)	2.6	2.6
Heater No. 3	2.2	(1.6)	3.0	2.9
Bottom heater	2.4	(3.1)	2.1	2.1
Total	8.8	8.8	11.0	10.9

[a] In a private communication to the writer, M. W. Larinoff pointed out that if each heater is analyzed individually by this method, the results are as shown in parentheses.

The accuracy of the reults given in reference[7] was within ±0.1 Btu per kwhr as checked by complete calculations.

The author states that Equation [10] should not be used to obtain the true effect of change in terminal difference on the top heater as it includes the effect of a change in final feedwater temperature. In the writer's experience, the steam power-plant design engineer is concerned with minor variations in the feed-heating cycle after turbine size, steam conditions, and location of extraction openings have been fixed. Specifically, the design engineer is not concerned with the theoretical effect of terminal difference but rather is interested in evaluating the cost of additional feedwater-heater surface for a terminal-difference change and the effect of this change in heater surface on heat rate. This includes the effect of change in final feedwater temperature.

The writer and his associates have performed many hundreds of heat-cycle calculations by the method of complete solution by differences given in reference[7]. In his opinion, the complete solution of heat-cycle variations by differences in some cases may be carried out by a skilled analyst in equal or less time than by substitution in the formulas given in the present paper, because of the fact that it is not necessary to read values from tables and charts. This applies particularly to cycle variations affecting either extreme of the heat cycle and where only a few variations of a particular type are studied at a time.

Author's Closure

The author appreciates Mr. Allen's comments, particularly the tabulation of comparative values of change in heat rate obtained by different methods of analysis.

The author agrees with Mr. Allen that determination of changes in heat rate resulting from cycle changes affecting only the lowest heater can be made as readily by reference (7) as by the author's method. In fact, if Equation [10] is used for determination of these changes, η_b becomes zero and the steps in determination of the change in heat rate are the same. The justification for use of an equation in this case is to obtain consistency.

The author stated that the effect on heat rate of a change in the final feed temperature should not be included with changes in heat rate caused by changes in pressure drop, or terminal difference. This statement is based on the assumption that the extraction point for the top heater has been selected to give a final feed temperature at or near the optimum when both the turbine and steam generator are considered. If this assumption is true, then small changes in final feed temperature will have no appreciable effect on the over-all plant heat rate even though they may have an appreciable effect on the turbine heat rate. To lump this effect in with pressure drop or terminal difference may lead to incorrect conclusions as to justifiable investments.

Obviously, not all cases will come under this classification but inclusion of Equation [11] does provide a ready means of determining the effect of changing pressure drop or terminal difference independent of the change in final feed temperature.

Experimental Superheater for Steam at 2000 Psi and 1250 F—Progress Report After 12,000 Hours of Operation

By F. EBERLE,[1] F. G. ELY,[2] AND J. A. DILLON,[3] ALLIANCE, OHIO

In order to supplement laboratory studies on certain new alloys developed in the past few years, a test element was constructed and installed in an operating boiler at the Twin Branch plant. Operation, which is similar to a small superheater, was started in March 1950. Experience with the unit for the first two years was described in a previous paper.[4] The present paper gives the record for the past two-year period and includes preliminary information derived from metallurgical examination of specimens removed from the element after nearly 7000 hr of operation.

Introduction

THE generation and use of steam at higher pressures and temperatures offers a direct and important means for improving power-plant cycle efficiency. Current practice is limited primarily by the materials available for construction of the high-temperature sections of superheaters and turbines, and can be advanced only as new materials become available which have superior strength properties in conjunction with stability and resistance to corrosion at the higher temperatures, with the further requirement that they be capable of commercial fabrication at reasonable cost.

Certain new alloys which were developed during and after World War II showed promising characteristics for extending steam temperatures beyond the 1050 F limit then prevailing.

In order to supplement the laboratory studies of these materials, and to obtain a practical and long-term demonstration of their suitability for superheater service, a test element was constructed and installed in an operating boiler at Twin Branch Plant where it could function as a small superheater, exposed to hot gases from pulverized-coal-firing, and receiving steam at 2000 psi 1000 F, which, by actual heat transfer, was increased to 1250 F at the outlet of the test element.

Field operation of this project was started in March, 1950. With certain interruptions, the test has continued successfully up to the present time, and shows favorable indications for eventual attainment of these steam conditions in commercial service.

An account of the experience gained during the first 2 years of operation was presented by the authors in a previous paper.[4] The present paper deals with the succeeding 2 years of operation, and includes preliminary information derived from metallurgical examination of a number of specimens removed from the element after approximately 7000 hr of operation.

Virtually all of the original materials are still in service in the operating element. Advantage has been taken of the opportunity to install specimens of a new experimental alloy and also to utilize the high-temperature steam produced in the system for corrosion tests of conventional superheater steels in order to extend the knowledge of the behavior of these materials.

Description of Equipment

As fully described in the earlier paper, the test element was constructed of 2-in -OD alloy tubes, in the form of four hairpin loops, connected in series, and arranged for semi-portable insertion through the rear wall of boiler No. 42 at the Twin Branch Plant. Its location in the boiler setting is shown in Fig. 1. At this location, it is swept by the gas stream approaching the main superheater at temperatures in the range of 2000 F, and is exposed to the action of a type IK soot blower operated on normal schedule. Steam from the main superheater outlet is supplied to the inlet of the test element, and flows through the four consecutive loops to a final outlet for disposal. Appearance of the element in the boiler setting is shown in Fig. 2.

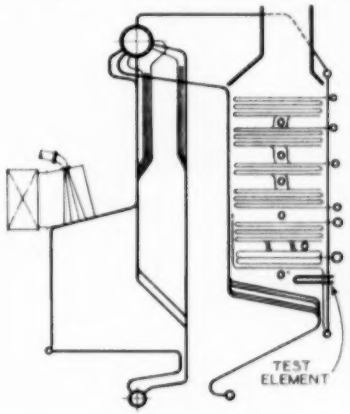

Fig. 1 Location of Superheater Test Element in Operating Boiler

General arrangement of the test element is shown schematically in Fig. 3. As described in the earlier paper, provision was made for supplying steam from any of the three sources indicated, but for most of the operating time, the supply has been taken from unit No. 5 at 2000 psi 1050 F. Rate of steam flow through the system is adjusted primarily by manual selection of the flow-control resistors in the discharge circuit. Since virtually all of

[1] Chief Metallurgical Engineer, Research Center, The Babcock & Wilcox Company.

[2] Consultant, Research Center, The Babcock & Wilcox Company. Mem. ASME.

[3] Test Engineer, Research Center, The Babcock & Wilcox Company.

[4] "Experimental Superheater for Steam at 2000 Psi and 1250 F—Progress Report of Field Operation," by F. G. Ely and F. Eberle Trans. ASME, vol. 74, 1952, pp. 803–812.

Contributed by the Research Committee on High-Temperature Steam Generation and presented at a joint session of the Petroleum and Power Divisions, Research Committee on High-Temperature Steam Generation, and Joint ASTM-ASME Committee on the Effect of Temperature on Properties of Metals at the Annual Meeting, New York, N. Y., November 29-December 4, 1953, of The American Society of Mechanical Engineers.

Note: Statements and opinions advanced in papers are to be understood as individual expressions of their authors and not those of the Society. Manuscript received at ASME Headquarters, August 10, 1953. Paper No. 53—A-90.

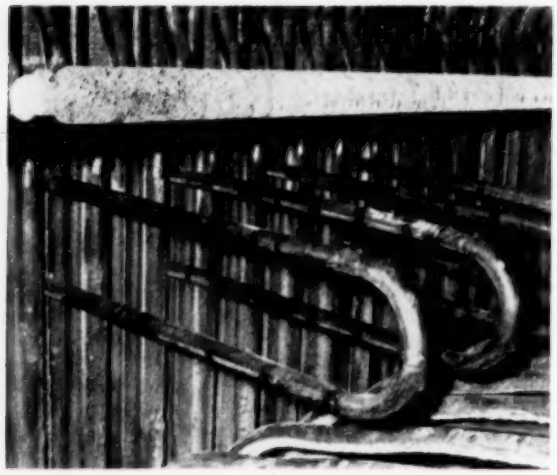

FIG. 2 APPEARANCE OF SUPERHEATER TEST ELEMENT IN BOILER SETTING

the pressure drop occurs in the resistors, the test element proper is maintained at substantially full operating pressure of 2000 psi.

MATERIALS OF CONSTRUCTION

The types of alloy materials used in the original construction are indicated in the diagram, Fig. 3(*a*), and are further described by the data given in Table 1. Several changes in arrangement of the test element, resulting from alterations and repairs, from the removal of specimens and from the introduction of new materials, are shown in successive portions of the figure. All of these modi-

TABLE 1 TUBE DATA AND CALCULATED STRESS VALUES FOR VARIOUS ALLOYS USED IN TEST ELEMENT

Material	Composition	Leg No.	OD (in.)	Min. Wall Thickness (in.)	Avg Metal Temp F(1)	Stress at Allowable(2) 2000 psig ASME (psi)	Working Stress (psi)
304	18CrBN1	3	2.00	.512	1279	1907	2786
304	18CrBN1	6	"	.492	1309	2053	2333
347	18CrBN1Cb	4	"	.395	1270	3025	2850
321	18CrBN1T1	5	"	.521	1314	1836	2004
316	16Cr13N13Mo	5	"	.504	1309	1970	3765
318	16Cr13N13MoCb	7	"	.509	1340	1932	2950(3)
Timken	16Cr25N16Mo	8	"	.273	1341	5330	3420(4)
Croloy 15-15-N	Experimental Alloy	8	"	.284	1341	5040	4320(4)
Armco	17Cr14N1CuMo	8	"	.258	1341	5460	5150(4)

(1) Average metal temperature corresponding to outlet steam temperature of 1250 F.

(2) The allowable working stresses are corrected for the average metal temperatures shown, with exception of those of Timken 16-25-6, 15-15-N, and Armco 17-14CuMo, for which the values at 1350 F are given.

(3) The allowable working stress for Type 318 material has been taken as equal to Type 316 material.

(4) The allowable working stresses for 16-25-6, 15-15-N, and Armco 17-14CuMo were taken as 60 per cent of their rupture stresses in 100,000 hr at 1350 F, i.e. 5700 psi for 16-25-6, 7200 psi for 15-15-N, and 8500 psi for Armco 17-14CuMo.

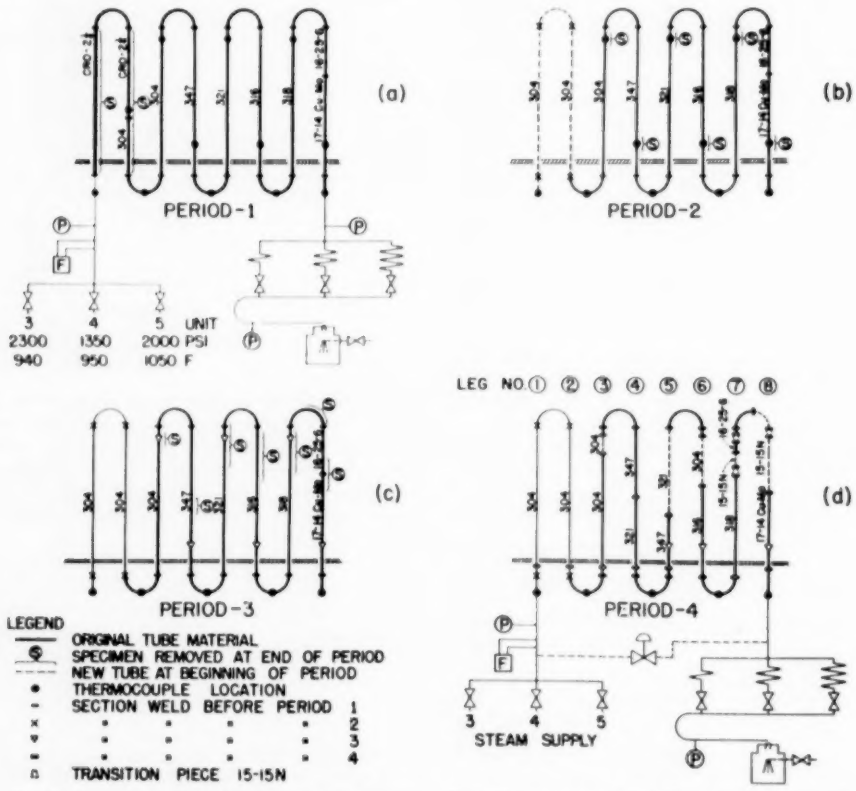

FIG. 3 SCHEMATIC ARRANGEMENT OF SUPERHEATER TEST ELEMENT FOR EACH PERIOD OF OPERATION

fications are related chronologically by the numbered operating periods designated in the summary plot of Fig. 4.

The initial operating period No. 1 was terminated in order to repair damaged internal parts of the discharge condenser and to restore the metal-temperature thermocouples which had failed in the first few weeks of operation. Ferritic tubes (Croloy $2^1/_4$) were removed from legs 1 and 2 of the element because their operating temperatures were found to be in excess of normal limits for this alloy.

Termination of period No. 2 was necessitated by a leak which developed at the special thermocouple weldment in leg No. 8, and subsequent inspection showed cracks in similar thermocouple weldments in other tubes. All of these weldments were cut out of the assembly after period No. 2.

During operating period No. 3, a slight, but progressive, enlargement of tube diameter was noted in the AISI-321 (18-8Ti) material at the hotter end of leg No. 5, as disclosed by measurements taken periodically on week-end outages of the boiler. Some concern was felt that this might reach the point of rupture prematurely, and it was decided to remove the element from service. Later examination of the 321 material showed that the original tube inadvertently had not been solution-treated, and substitution of the affected portion was made, using a new piece of tube of the same composition but produced from a different heat and with proper solution treatment at 2000 F. The unaffected portion of 321 alloy tube at the cooler end of leg No. 5 was retained for further service but was exchanged in location with part of the AISI-347 material originally used in leg No. 4.

A small circumferential stress-rupture type of crack was found in the 316 alloy tube bend preceding leg No. 8 at a section of maximum bending stress, where the wall thickness of the tube bend had been machined to match the thinner wall of Timken 16-25-6 alloy. Part of the tube bend was replaced by new 316 tubing.

New Materials

At the end of operating period No. 3, representing approximately 7000 hr of total service time, a number of major specimens were removed from the assembly for metallurgical examination, as indicated in Fig. 3(*c*). Some of these specimens included section weldments which were of equally vital interest in the study. For reassembly of the test element, several new sections of tubing were inserted.

A new piece of unstabilized 18-8 (AISI-304) tubing was installed at an advanced position in leg No. 6 where operating temperatures would be higher than in other specimens of this material.

A new piece of experimental superstrength alloy, Croloy 15-15N, was installed in leg No. 8, displacing the original piece of Timken 16-25-6, which was transferred to leg No. 7.

New transition pieces, machined from the experimental alloy, were introduced for connections between the thick-wall and thin-wall tube sections, where such joints occurred in legs No. 7 and No. 8.

Many new section weldments were made necessary by this rearrangement of tubing; however, in the choice of tube specimens for removal, care was taken to retain significant welds of the original construction for further operating service.

Coincident with the changes made before operating period No. 4, but forming a distinctly separate study of steam corrosion, a number of machined cylindrical test specimens of various superheater materials shrink-fitted on steel rods were inserted as cores in the sections of superheater tubing external to the boiler setting, where they would be exposed to the flow of steam at increments of temperature from 1000 F at the inlet to 1250 F at the outlet leg of the test element. These specimens are still in place, and eventually will be removed and examined for evaluation of relative steam-corrosion rates.

Service Record

A historical summary of the entire test is presented graphically in Fig. 4 for which the general range of outlet steam temperature has been used as a tracer. With the load demand on boiler No. 42 requiring full-load operation during the day, but with customary banked periods each night and complete outage on week ends, there resulted a daily cycle of temperature in test-element performance, ranging from the controlled value of 1250 F outlet-steam temperature during the operating hours, to something less than 1000 F during the banked hours, and cooling below saturation temperature when steam was shut off during the week-end outage. To date, there have been 607 cycles sustained by the element.

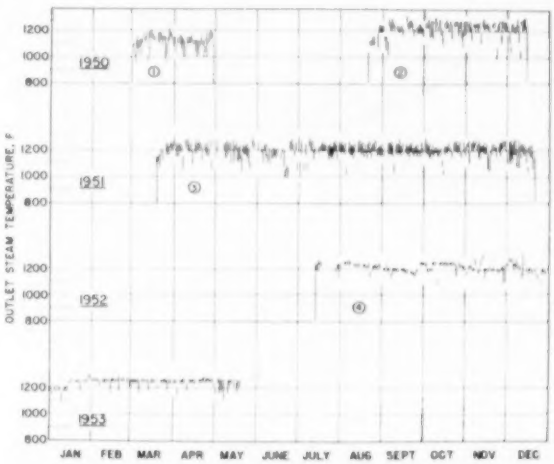

Fig. 4 Graphic Log of Test Element Operation

During periods Nos. 1, 2, and 3, the only available means of regulating steam flow was by manual selection of appropriate resistors in the outlet circuit. Prior to operating period No. 4, a by-pass was installed, as shown in Fig. 3(*d*), with automatic regulation of the control valve to proportion the flow between element and by-pass and maintain desired steam-outlet temperature. As a result of applying this control, the test project was relieved of much supervisory attendance and has yielded a higher return of service hours in the desired range of temperature above 1200 F. Typical chart records, which illustrate the functioning of the control during changes in boiler load, are shown in Fig. 5.

Based upon chart records, a summary of service hours is shown in Fig. 6, from which it will be noted that the element as a whole has now accumulated approximately 12,000 total service hours, of which more than 50 per cent is in the desired range above 1200 F outlet-steam temperature.

Data acquired previously during the life of metal-temperature thermocouples, as described in the earlier paper, permit an approximate evaluation of metal temperatures in the various sections of the element, as illustrated in Figs. 7 and 8.

Examination of Materials After 6950 Hr of Operation

The described alterations of the experimental superheater offered an opportunity to study the effect of the first 7000 hr of operation under cycling pressure and temperature conditions upon the alloys employed. The removed tube sections were

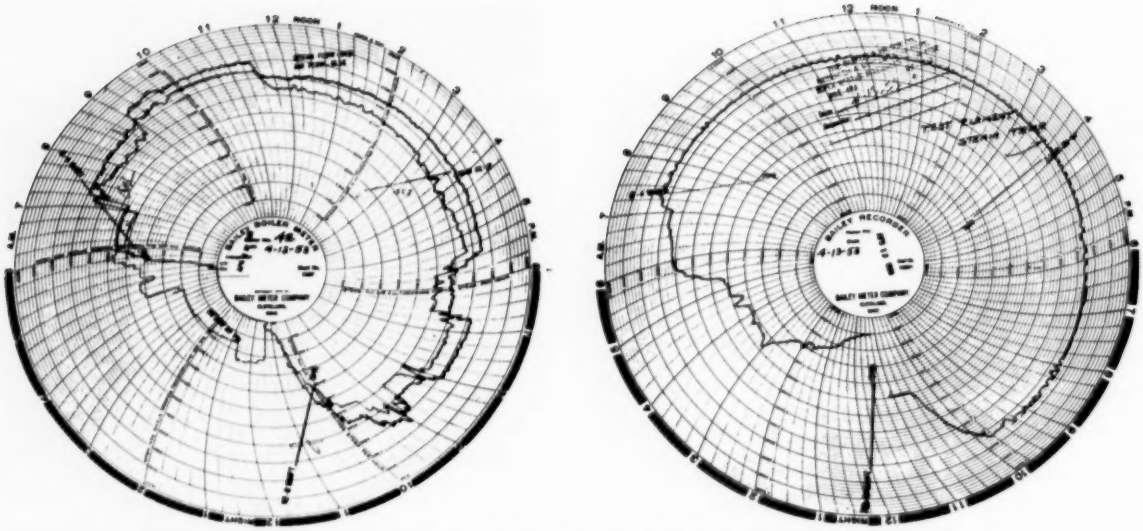

FIG. 5 TYPICAL CHART RECORDS OF BOILER LOAD AND OUTLET-STEAM TEMPERATURE—PERIOD NO. 4

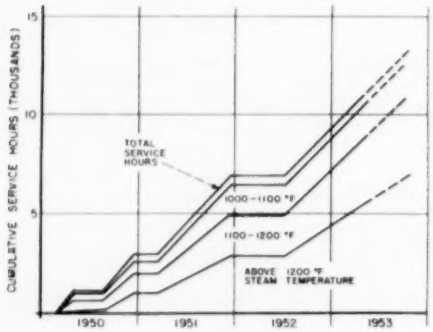

FIG. 6 SUMMARY OF SERVICE HOURS TO JUNE 1, 1953

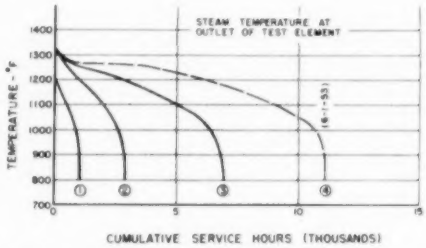

FIG. 7 OUTLET-STEAM-TEMPERATURE DURATION CURVE TO JUNE 1, 1953

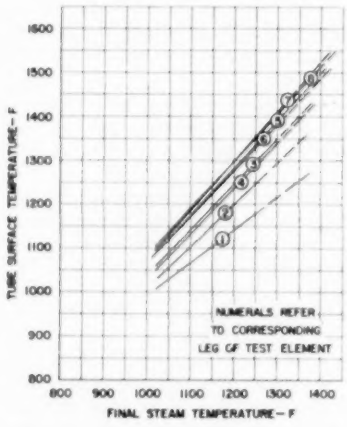

FIG. 8 RELATION OF TUBE-METAL TEMPERATURE TO OUTLET-STEAM TEMPERATURE FOR VARIOUS SECTIONS OF TEST ELEMENT

small, but sufficient to carry out tests for most of the significant properties and thereby obtain an insight into the changes which they had undergone in service. Of principal interest in this respect were the rate of attack upon the metals by the high-pressure steam and by the combustion gases from sulphur-bearing coal; undesirable microstructural changes, specifically formation of sigma phase; deterioration of mechanical properties at room temperature and at operating temperatures; and last, but not least, possible impairment of the load-carrying ability of the alloys.

HIGH-TEMPERATURE CORROSION BEHAVIOR

There has been some speculation as to whether high-pressure superheated steam at the high metal temperatures encountered might prove to be excessively corrosive, inasmuch as some investigators have shown by laboratory tests that corrosion rates in steam are higher than in air.[5] It has been suggested that this possibly might be due to the effect of hydrogen resulting from steam reaction at the hot metal surface, the released hydrogen supposedly loosening up the lattice structure of the protective oxide layer.

Great interest likewise was felt regarding the corrosive action of the combustion gases from coal containing up to about 3.8 per cent sulphur.

Sections of commercial tubing removed from service do not lend themselves to the determination of accurate corrosion rates, but for the present purpose, it is of interest to calculate the latter

[5] "Vorgänge beim Angriff hietzebeständiger Stähle in Heissen Gasen," by E. Houdremont and G. Bandel, *Arch. für Eisenhuttenwesen*, vol. 11, September, 1937, pp. 131–138.

TABLE 2 CORROSION RATES CALCULATED FROM AVERAGE MAXIMUM THICKNESS OF EXTERNAL AND INTERNAL SCALE FORMED DURING FIRST 6950 HR OF SERVICE

	Corrosion Rate, mils per year		
	Steam	Flue Gas	Air (1400 F)*
AISI-304	1.5	0.75	0.22
AISI-321	1.5	0.875	0.14
AISI-347	.375	0.875	0.32
AISI-316	6.0	2.0	0.13
AISI-318	0.5	1.25	0.14
16-25-6	0.5	4.0	0.15
17-14CuMo	.625	0.125	0.25

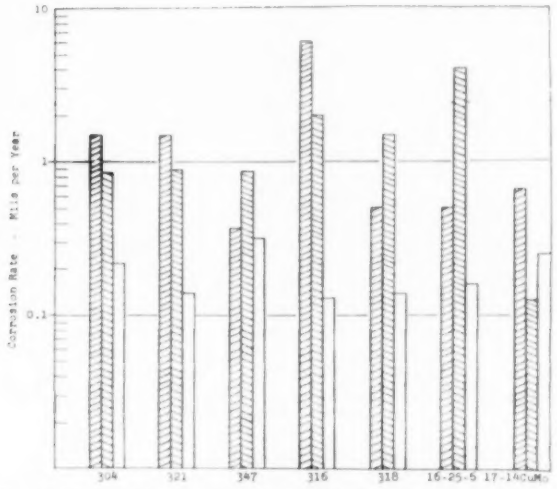

FIG. 9 CORROSION RATES FOR FIRST 6950 HR IN STEAM AND FLUE GAS AND FOR 1270 HR IN STILL AIR AT 1400 F—LABORATORY
(Left column—steam; center column—flue gas; right column—air.)

from the average maximum scale thickness on the internal and external surfaces of the tubing. The values thus obtained are given in Table 2 and are presented graphically in Fig. 9. As a matter of general interest, the oxidation rates of the alloys in still air at 1400 F likewise were determined by holding $^1/_4$-in-diam × 1-in-long specimens machined from the original tubing in weighed porcelain crucibles in an electric muffle furnace for 1270 hr and calculating the oxidation rates from the weight increases resulting from oxygen absorption.

The general corrosion rates for steam and combustion gases, obtained by these determinations, do not appear to be excessive and probably will diminish with increasing time in service.

AISI-Type 316 alloy displayed the highest corrosion rate, and this alloy also shows evidence of incipient intergranular surface attack. This is believed to be due to the relatively low chromium content of this alloy and to chromium removal from the matrix by carbide precipitation. Indication of intergranular surface oxidation also was noted on the outside of the 16-25-6 alloy which showed the second highest scaling rate. The corrosion rates in steam appear in the majority of cases to be slightly higher than those in the combustion gases, and both these corrosion rates are somewhat higher than those in air at 1400 F. The mode of surface attack which occurred in the seven alloys is illustrated in Figs. 10 and 11. The relatively mild effect of the combustion gases from coal containing up to 3.8 per cent sulphur finds an explanation in the analysis of the fly ash found on the outside of the test element. Three such analyses, representing layers of various thicknesses, are given in Table 3, from which it is evident that the sulphur has been converted to calcium sulphate and thereby rendered innocuous.

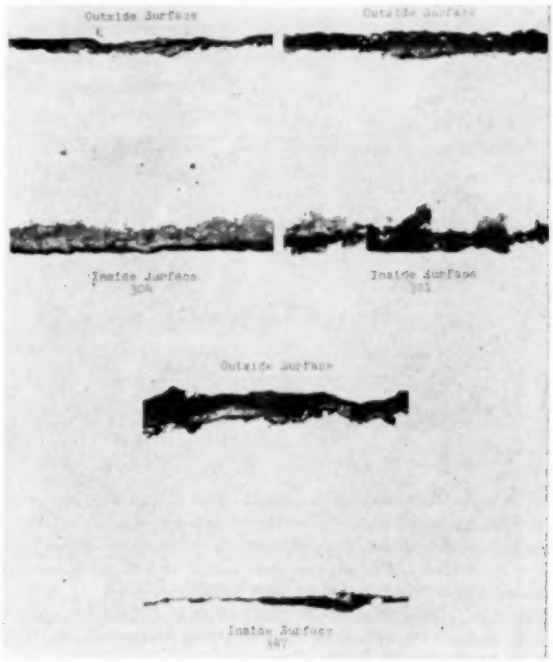

FIG. 10 SCALE FORMED DURING 6950 HR OF SERVICE; ×250

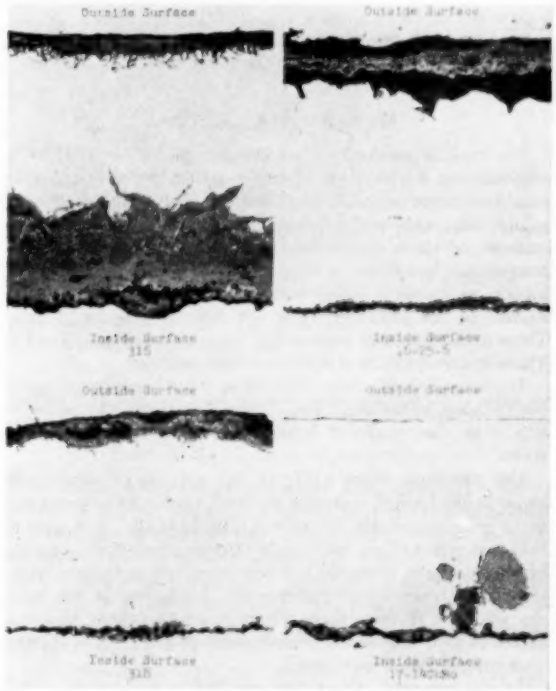

FIG. 11 SCALE FORMED DURING 6950 HR OF SERVICE; ×250

TABLE 3 ANALYSIS OF FLY-ASH DEPOSIT ON EXPERIMENTAL SUPERHEATER

(a) Spectrographic Quantitative Analysis			
Si as SiO_2	50.0 per cent	25.0	16.0
Al as Al_2O_3	22.0	11.0	8.4
Fe as Fe_2O_3	20.5	43.0	53.0
Ti as TiO_2	1.5	0.7	0.6
Ca as CaO	2.0	11.0	12.5
Mg as MgO	0.6	0.6	0.5
Na as Na_2O	0.3	0.7	0.2
K as K_2O	1.7	1.3	1.1
(b) Chemical Analysis			
S as SO_3	2.9	8.7	10.1
(c) X-Ray Diffraction Analysis			
Major Crystalline Constituent	Fe_2O_3	Fe_2O_3 $CaSO_4$	Fe_2O_3 $CaSO_4$
Minor Crystalline Constituents	$CaSO_4$ SiO_2	Fe_3O_4 $3Al_2O_3 \cdot 2SiO_2$ (Mullite)	Fe_3O_4

In examining the surface condition of the tubing, special attention was paid to the possible occurrence of scale exfoliation due to the repeated heating and cooling cycles to which the tubing was subjected during service, but visual as well as microscopic examination failed to reveal any definite evidence of such occurrence. Internal seams or ball scratches and similar unavoidable surface imperfections resulting from tube manufacturing were found to have increased in depth and size, but their transgranular path and rate of propagation do not give cause for concern. An illustration of the growth of such surface imperfections is given in Fig. 12.

In summary, it may be stated that the corrosion rates observed after the first 6950 hr of operation do not appear to be prohibitive, but warrant further study.

Microstructural Changes

The type of microstructural changes which occurred in the alloys during service were, of course, known and anticipated and consisted principally of precipitation of carbides and other compounds; some alloys formed sigma phase. The mode of occurrence of these compounds under the cycling conditions of temperature and stress as compared to their precipitation or formation at constant temperatures at which they are generally studied in the laboratory was not without practical interest. These microstructural changes are illustrated in Figs. 13 and 14. There was no evidence of significant deteriorations.

The nonstabilized alloys AISI-304 and 316 experienced carbide precipitation at the grain boundaries, but there was no indication that they suffered intercrystalline corrosion attack by steam.

The stabilized alloys AISI-321, 347, and 318 displayed sigma phase in the form of scattered particles, predominantly occurring at the grain boundaries, as shown in Figs. 13 to 15. It is generally held that sigma phase has a slight adverse effect upon the creep-rupture strength, especially if it occurs in chain or stringer form in the grain boundaries. Sigma-phase formation is an innate characteristic of these three alloys, which of course, also is reflected in their established creep-rupture properties and therefore does not give cause for concern.

As was expected, Types 304 and 316 as well as the 16-25-6 alloy were found free of any visible evidence of sigma phase, but a

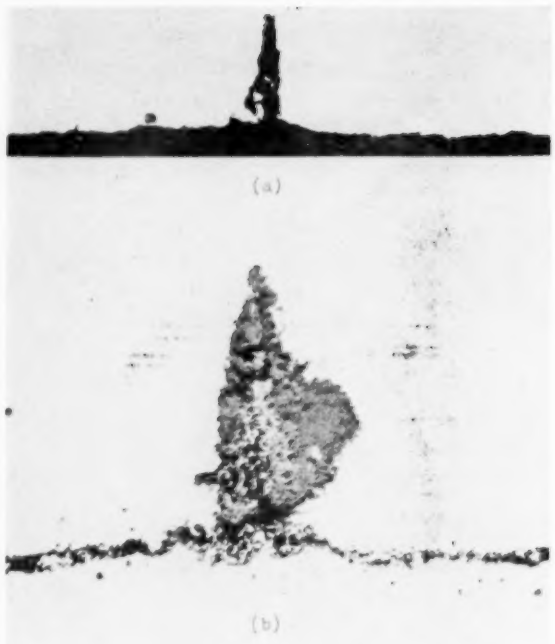

Fig. 12 Enlargement of Internal Surface Seams in 347 Alloy During 6950 Hr of Operation

(a, Section through representative seam before service. b, Similar type of seam after 6950 hr; ×500.)

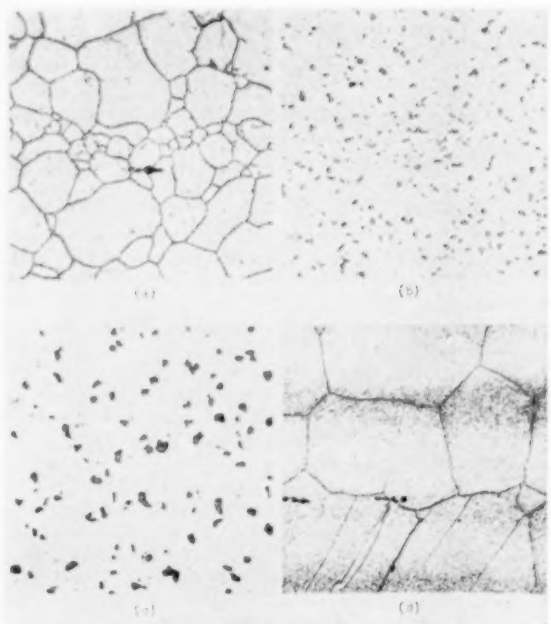

Fig. 13 Significant Microstructures of Alloys After 6950 Hr of Service

(a, Type 304, Villela's reagent; ×500. b, Type 321, concentrated Murakami's reagent; ×500. c, Type 347, concentrated Murakami's reagent ×500. d, Type 316, Glyceregia; ×500.)

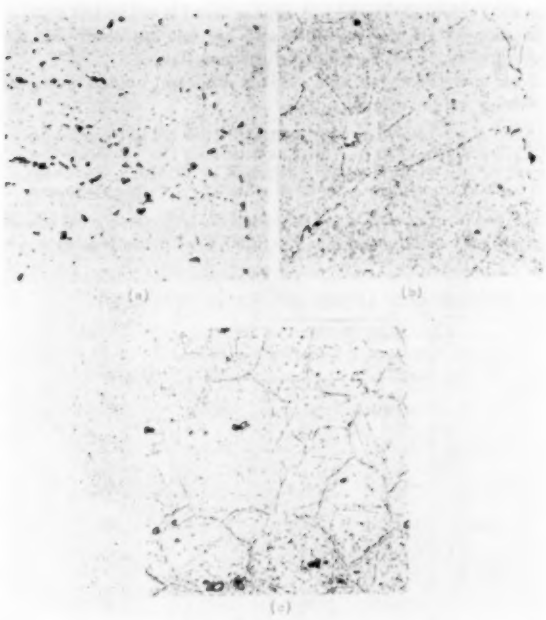

FIG. 14 SIGNIFICANT MICROSTRUCTURES OF ALLOYS AFTER 6950 HR OF SERVICE

(*a*, Type 318, concentrated Murakami's reagent; ×500. *b*, 16-25-6 alloy, Murakami's reagent; ×500. *c*, 17-14 CuMo alloy, Glyceregia; ×500.)

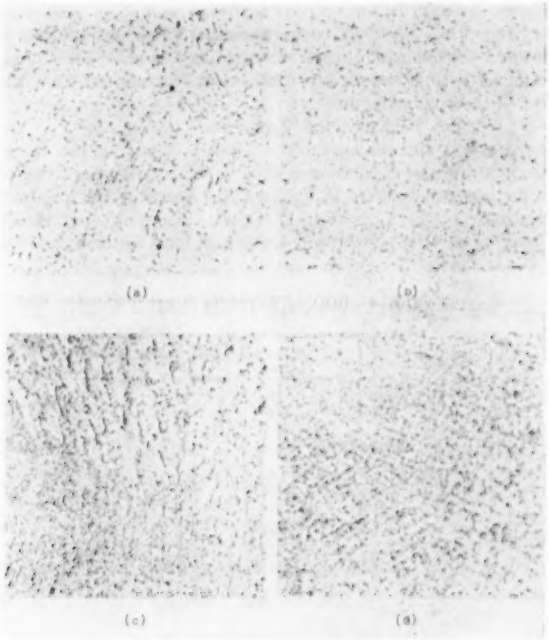

FIG. 16 SIGMA PHASE IN WELD METALS

(*a*, 19-9 Cb after 4000 hr of service. *b*, 19-9 Cb after 4000 hr of service. *c*, 18-12 MoCb after 4000 hr of service. *d*, 17-14 CuMo after 6950 hr of service. Concentrated Murakami's etch; ×250.)

FIG. 15 SIGMA PHASE IN TUBING MATERIALS AFTER 6950 HR OF OPERATION

(*a*, Type 321. *b*, Type 347. *c*, Type 318—concentrated Murakami's etch; ×100.)

few scattered small particles of sigma were believed to have been observed in the 17-14 CuMo alloy. However, their identification was predominantly based on the angular shape of some of the particles and therefore is far from positive. Furthermore, their occurrence would not be significant.

The 16-25-6 and 17-14 CuMo alloys formed a heavy matrix precipitate of carbides and other compounds, which is a characteristic feature of their microstructures. Apart from the scaling attack by steam and flue gases, there were no indications of microstructural surface deterioration in any of these alloys.

Among the samples removed from the experimental superheater after 6950 hr of service were weldments made with Types 347, 318, and 17-14 CuMo electrodes. All these weld metals formed notable amounts of sigma phase, as illustrated in Fig. 16.

Summarily, it may be said that all seven alloys stood up well microstructurally and in this respect, likewise, gave no cause for concern.

CHANGES IN MECHANICAL PROPERTIES

The microstructural changes which high-temperature alloys undergo in service, influence, of course, their creep-rupture characteristics and their short-time mechanical properties at room temperature as well as at elevated temperatures. The following tests therefore were performed, in so far as the available material permitted, on retained sections of the original tubing and on the tube sections removed from the experimental superheater after 6950 hr of service:

(*a*) *Stress-Rupture Tests at 1350 F.* The 18-8 Ti (Type 321) tubing, which had shown a certain amount of circumferential creep during the third operating period, displayed a subnormal

rupture strength in the original condition as well as after 6950 service hours. However, a short solution treatment at 2000 F restored the nominal rupture strength, as was subsequently determined with stress-rupture tests on specimens cut from the wall of the original tubing.

(*b*) *Tensile Tests at Room Temperature and at 1350 F.* The changes in mechanical properties brought about by the stress-temperature-time conditions of 6950 hr of operation are reflected in the test results listed in Tables 4 and 5, and in the graphical illustrations shown in Figs. 17 to 20. The yield and tensile strengths at room temperature are seen to have increased and the ductility values decreased. A similar trend is evident at 1350 F. The changes are not excessive and are not apt to impair the structural load-carrying ability of the materials.

Four of the removed tube sections contained weldments of the following combinations:

AISI-304	welded to AISI-304 with 19-9 Cb	electrodes
AISI-321	welded to AISI-321 with 19-9 Cb	electrodes
AISI-318	welded to AISI-318 with 18-12 Mo	electrodes
17-14 CuMo	welded to 16-25-6 with 17-14 CuMo	electrodes

These weldments also were subjected to transverse weld tensile tests at room temperature and at 1350 F with the results shown

TABLE 4 ROOM-TEMPERATURE TENSILE PROPERTIES BEFORE AND AFTER 6950 HR OF SERVICE

	Before Service				After Service			
	Yield Str. psi	Tensile Str. psi	Elong 1.5" %	Red.of Area %	Yield Str. psi	Tensile Str. psi	Elong 1.5" %	Red.of Area %
AISI-304	39,000	82,000	66.0	80.0	39,200	90,900	53.3	69.2
AISI-321	35,900	80,100	57.3	79.2	36,300	89,000	42.0	58.4
AISI-347	41,800	91,800	46.0	76.8	64,200	126,900	22.7	36.5
AISI-316	38,900	80,600	63.3	79.1	43,200	96,700	40.7	54.2
AISI-318	41,000	86,300	52.0	73.7	43,100	99,600	33.3	48.0
16-25-6	51,300	109,100	50.0	72.5	70,600	132,000	22.7	30.7
17-14CuMo	40,900	84,900	50.7	66.3	45,800	92,500	39.3	52.5

TABLE 5 TENSILE PROPERTIES AT 1350 F BEFORE AND AFTER 6950 HR OF SERVICE

	Before Service				After Service			
	Yield Str. psi	Tensile Str. psi	Elong 1.5" %	Red.of Area %	Yield Str. psi	Tensile Str. psi	Elong 1.5" %	Red.of Area %
AISI-304	19,600	35,500	60.0	71.5	21,600	35,900	64.7	75.2
AISI-321	23,900	34,900	58.0	67.1	20,100	33,100	68.0	66.9
AISI-347	21,800	37,600	78.0	72.9	25,200	35,700	57.3	67.0
AISI-316	19,400	38,300	60.0	67.1	23,000	38,700	62.7	66.0
AISI-318	22,800	45,100	40.7	45.8	23,600*	40,200*	64.0*	52.4*
16-25-6	28,600*	55,100*	18.0*	22.0*	38,900	54,500	56.0	57.6
17-14CuMo	27,400	46,000	33.3	45.4	29,300	41,400	34.7	32.0

* Rupture through gage mark.

TABLE 6 TRANSVERSE WELD TENSILE TESTS ON WELDMENTS AT ROOM TEMPERATURE AND AT 1350 F AFTER 6950 HR OF SERVICE

	At Room Temperature				At 1350 F			
	Yield Str. psi	Tensile Str. psi	Elong 1.5" %	R.A. %	Yield Str. psi	Tensile Str. psi	Elong 1.5" %	R.A. %
304/304 Electrode 19-9Cb	45,000	93,600	40.0	68.8	25,200**	38,900	18.7**	71.2
321/321 Electrode 19-9Cb	39,700	91,200	31.3	58.2	21,700**	34,600	29.3**	56.0
318/318 Electrode 18-12MoCb	47,100	99,600	27.3	48.6	25,600	42,000	37.3	60.4
17-14CuMo/16-25-6* Electrode 17-14CuMo	41,700	74,400	9.3*	32.8*	26,200**	36,400	8.0**	40.4

* Fracture in 17-14CuMo Weld Metal Induced by entrapped slag.

** Rupture through gage mark.

Note: Failure occurred in the weld-unaffected base metal with the exception of the 17-14CuMo/16-25-6 weldment which failed in the 17-14CuMo weld metal.

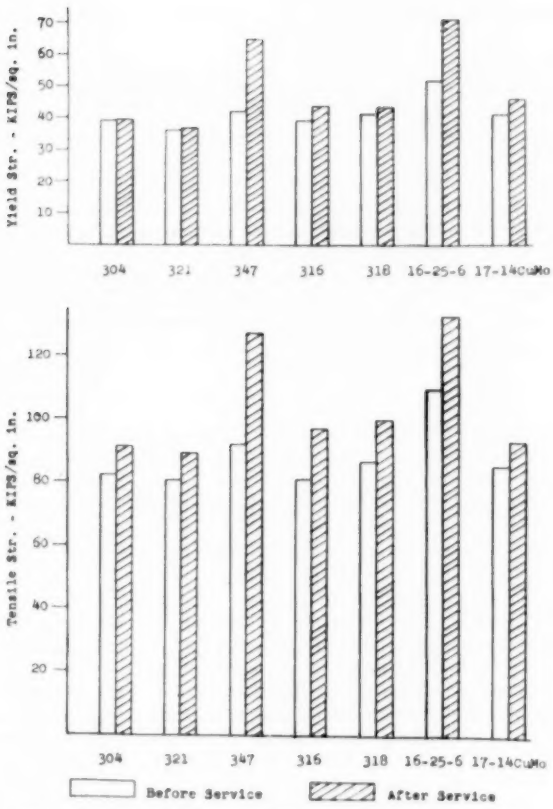

FIG. 17 YIELD AND TENSILE STRENGTHS BEFORE AND AFTER SERVICE
(Room-temperature tests.)

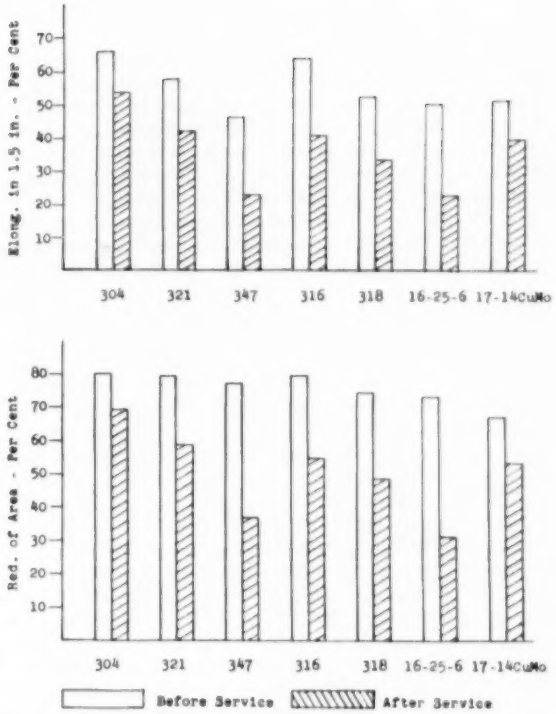

FIG. 18 ROOM-TEMPERATURE DUCTILITY BEFORE AND AFTER SERVICE

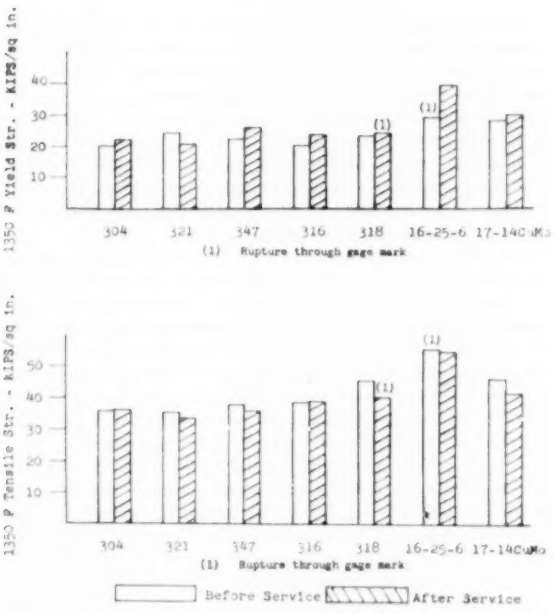

FIG. 19 YIELD AND TENSILE STRENGTHS AT 1350 F BEFORE AND AFTER SERVICE

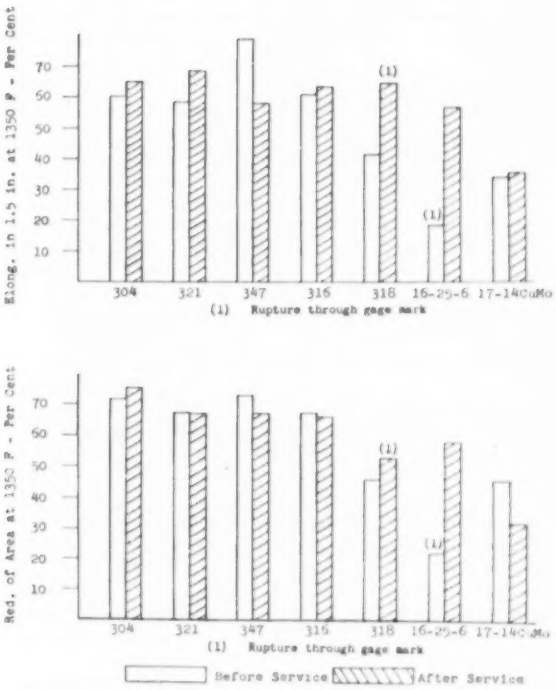

FIG. 20 HOT DUCTILITY AT 1350 F BEFORE AND AFTER SERVICE

in Table 6. With the exception of the 17-14 CuMo/16-25-6 weldment which broke in the weld metal due to entrapped slag, all these weld tensile tests failed in the unaffected base metal. The properties compare favorably with those obtained on the unwelded base metals after service and indicate that the weld joints are structurally as satisfactory as the unwelded tubing. The greater strength of the weld metals deserves attention.

(c) *Charpy Impact Tests at Room Temperature.* These tests were made to reveal notch sensitivity or a significant decrease in shock resistance which the alloys might have suffered as a result of microstructural changes. Of particular interest in this respect were alloys 321, 347, and 318 which are known to form sigma phase. The tests were performed on half-width Charpy specimens since some of the tube-wall thicknesses were not heavy enough and the available material not sufficient to permit the use of full-size specimens. However, in order to demonstrate the relative effect of half-width versus full-size specimens, tests with both types were made on the pre-service materials of alloys 304, 321, 316, and 318. The test results are presented in Table 7 and are graphically illustrated in Fig. 21 (bottom).

TABLE 7 CHARPY IMPACT PROPERTIES AT ROOM TEMPERATURE BEFORE AND AFTER 6950 HR OF SERVICE

	Before Service		After Service	
	Full-Size Specimens ft-lb	Half-Width Specimens ft-lb	Full-Size Specimens ft-lb	Half-Width Specimens ft-lb
AISI-304	93	55.0	-	29
	97.25	58.0	-	21
	92.75	56.0	-	24.5
	avg 94.3	avg 56.3	-	avg 24.66
AISI-321	95	52.0	-	14
	89.5	52.0	-	15
	91.5	53.9	-	15.25
			-	14
	avg 92	avg 52.3		avg 14.56
AISI-347	-	38	-	20.5
	-	41	-	18.5
	-	46.5	-	16.75
	-	avg 41.8	-	18.5
				avg 10.56
AISI-316	89.5	48.0	-	17.5
	93	50.0	-	19.25
	83	48.5	-	17.5
	avg 88.5	avg 48.8	-	16.25
				avg 17.62
AISI-318	77	45.0	-	10
	80	44.5	-	7.75
	79.5	41.0	-	8
	avg 85.5	avg 43.5	-	10
				avg 8.94
16-25-6	-	37	-	6
	-	35	-	6
	-	34	-	6.5
		avg 35.3	-	5.5
				avg 6
17-14CuMo	-	24.5	-	13
	-	25	-	13.5
	-	24.5	-	13.5
		avg 24.66	-	13.25
				avg 13.31

TABLE 8 ROOM-TEMPERATURE CHARPY IMPACT TESTS ON WELDMENTS AFTER 6950 HR OF SERVICE

Weldment	Ft-Lb	Location of Fracture	Size of Specimen
304/304 19-9Cb Electrodes	25.5	Root Half of Weld	Full Size
	16	Top Half of Weld	Full Size
	5.5	Root Half of Weld	Half Width
	10.5	Top Half of Weld	Half Width
321/321 19-9Cb Electrodes	10.25	Root Half of Weld	Full Size
	7	Top Half of Weld	Half Width
	3.5	Top Half of Weld	Half Width
	4	Radial Plane of Weld	Half Width
318/318 18-12MoCb Electrodes	1.5	Root Half of Weld	Half Width
	2	Root Half of Weld	Half Width
	1.25	Top Half of Weld	Half Width
	3	Top Half of Weld	Half Width
17-14CuMo/16-25-6 17-14CuMo Electrodes	1	Radial Plane of Weld	Half Width
	1	Radial Plane of Weld	Half Width
	1	Radial Plane of Weld	Half Width
	1	Radial Plane of Weld	Half Width

Location of Keyhole Notch with Respect to Weld Geometry:

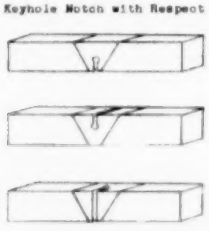

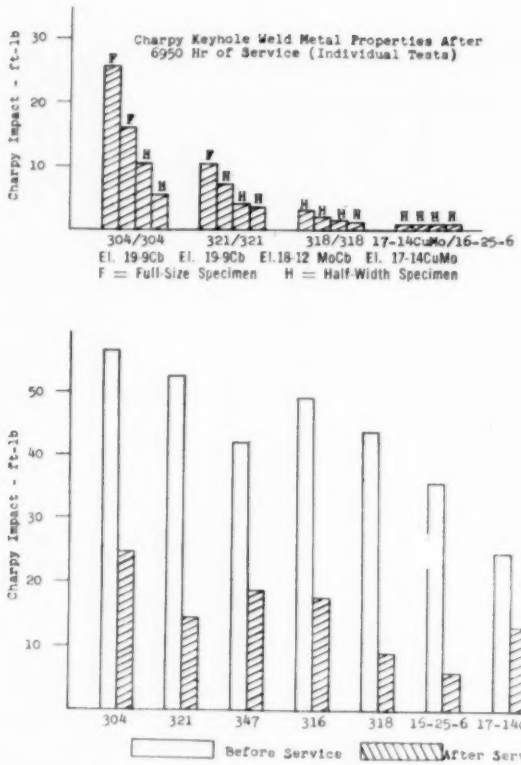

FIG. 21 ROOM-TEMPERATURE CHARPY OR KEYHOLE IMPACT PROPERTIES BEFORE AND AFTER 6950 HR OF SERVICE
(Half-width specimens.)

The loss in impact strength is considerable for all materials, but the remaining notch toughness appears to be adequate for superheater service if there is no further significant decrease. Of interest is the much larger decline in notch ductility of the Type 318 alloy as compared to that of AISI-316, which is undoubtedly due to the formation of sigma phase in the former.

In view of these results, it appeared to be of particular interest to investigate the impact behavior of the four available weld metals. The test results are listed in Table 8 and graphically presented in Fig. 21 (top), from which will be noted that 19-9 Cb weld metal had retained a measure of impact strength, whereas 18-12 Mo and 17-14 CuMo weld metals are markedly embrittled. Just what the permissible limit from an operating standpoint is in this respect, is difficult to say. In the absence of mechanical shock, low impact values may possibly be tolerated.

CONCLUSION

In conclusion, the examination of tube sections removed from the experimental superheater after 6950 hr of operation has

shown that no serious impairment of essential properties has occurred in any of the seven alloys employed. Among the weld metals, 18-12 Mo and 17-14 CuMo have suffered considerable impact embrittlement. However, there is reason to believe that an improved 18-12 Mo electrode can be developed which will deposit weld metal free of dangerous embrittling tendency. An improved 17-14 CuMo electrode is already commercially available.

In view of the satisfactory behavior of the tubing materials, it may not be unrealistic to envisage the commercial use of superheaters operating with steam above 1200 F in the not-too-distant future. In the meantime, the authors intend to continue the operation of the experimental superheater in order to accumulate further test data and also to try out new materials of construction.

ACKNOWLEDGMENTS

The authors wish to express their appreciation of the sustained interest and vital assistance contributed by numerous members of the American Gas & Electric Company system toward the successful continuation of this project at Twin Branch Plant.

Discussion

R. C. FITZGERALD.[6] The authors and the co-operating companies are to be congratulated for the conception and execution of a research program of such practical significance to industry.

The present paper is a progress report on a continuing test of superheater-tube materials the arrangement and testing environment of which closely approach those of a practical superheater installation. Biaxial pressure stresses are present along with the corrosive action of steam on the inside of the tube and the products of combustion on the outside of the tube. An ingenious method of blocking the area of the tube permits the use of steam-flow rates over the inside surfaces of the tubes in accordance with accepted design practices. All of these factors make the data from this test program more acceptable for direct application to superheater design.

In addition to temperature variation resulting from variations in boiler loading, the test element is subjected to the thermal shock resulting from soot blowing. It would be valuable if data on thermal shock could be developed in these tests which would serve as a guide in the design of soot-blowing systems tolerable to materials operating at steam temperature of 1250 F and metal surface temperatures of 1350 F. Apparently no deterioration attributable to thermal shock was observed but the question is raised whether or not this may have been a factor in the rupture failure of the type 316 bend which occurred during the third operating period.

From the excessive creep rate of the type 321 loop which had not been solution-treated it appears that this treatment is necessary for adequate high temperature strength. Freeman et al.[7] report low creep properties at 1300 F for similar material air-cooled from 2050 F. It seems that the water quench employed in the treatment of the tube material in the present tests is the principal difference. Water-quenching of fabricated superheater loops might pose something of a problem for designers and fabricators.

In the section of the paper dealing with corrosion behavior it is observed that the corrosion rate will diminish with the formation of a protective oxide coating. This is in accord with experience and is generally true; however, it is felt that this note of optimism is not justified for some of the materials when the thickness of oxide scale, shown in Figs. 10 and 11 of the paper, are compared with thicknesses listed in the author's paper of 1951 on the same subject. It is felt that the intergranular oxidation and oxide penetration shown in Fig. 11, for the type 316 and the 16-25-6 material are particularly significant in determining their suitability for 1250F steam service.

The mechanical properties of samples removed after 6950 hr of service show little change. Loss in ductility is reflected mostly in notch toughness of the materials.

The notched-bar impact test is an excellent method for demonstrating loss of ductility and the formation of sigma phase but its correlation with service requirements is as the authors have suggested a difficult matter. In this writer's experience, room-temperature ductility of superheater materials is a matter of concern only when it is necessary to make repairs to individual superheater elements and the elements themselves must be spread for working room. This, of course, assumes a reasonable degree of flexibility in the loops of the elements so that cooling and heating incidental to operating the boiler does not impose stresses in the plastic range. It appears from the tensile ductility of both the tube materials and weld metal at room temperature that there is plenty of stretch left for both of these requirements. It is becoming increasingly evident that satisfactory high-temperature properties and low-temperature ductility are often incompatible. It behooves both the designer and the user to take cognizance of this in the design of the equipment and the way it is handled so that "unforeseen" room-temperature failures are minimized.

With reference again to the incipient intergranular attack noted in the type 316 material, it would be of great interest to operating people to know the margin of strength remaining in the tube when this strength would be influenced by surface conditions. If it were practical to make tubular stress-rupture tests on samples removed from the experimental superheater in the manner previously performed and reported by the author's associates, such information could be obtained.

It is to be expected that this program not only will select suitable materials for service at 1350 F but also will determine the life expectancy of such an installation. Life expectancy is, of course, of considerable interest to operating companies who will have to justify the cost by the increased thermal efficiency derived from these temperatures.

Future progress reports on this worthy project will be awaited with great interest.

G. E. LIEN.[8] In behalf of the American Gas and Electric Company System, we wish to congratulate the authors on their excellent paper, and their company for publishing these important findings on the performance of superheater materials at high temperatures.

We have been pleased to be hosts at the Twin Branch Plant to the test installation which has been so efficiently run. The findings of this test are also of great interest to us because of engineering work now being done on Philo Unit No. 6 which will utilize steam at 4500 psi and 1150 F.

If this test program had not been initiated 3 years ago, information on service characteristics of suitable superheater materials for our high-temperature unit would be lacking. Service-test programs of this type to supplement laboratory findings are most effective in making correct evaluations of materials to be used under new conditions.

[6] Senior Engineer, Consolidated Gas Electric Light and Power Company, Baltimore, Md. Mem. ASME.

[7] "Rupture and Creep Characteristics of Titanium—Stabilized Stainless Steel at 1100 to 1300 F," by J. W. Freeman, G. F. Comstock, and A. E. White, Trans. ASME, vol. 74, 1952, pp. 793–801.

[8] Mechanical Engineering Division, American Gas and Electric Service Corporation, New York, N. Y. Mem. ASME.

M. A. Scheil.[9] The author mentions the use of unstabilized 18-8 stainless steel as one of the tube materials. It would appear that for this temperature of service there might be an advantage in the use of Type 304L material with carbon limited to 0.030 per cent maximum. Reference was made to a Type 304 weld metal deposited from a 19 Cr-9 Ni electrode. It would be of interest to users of this electrode in steam power-plant service to know the percentage of ferrite deposited in the joints that were prepared and discussed in this paper. Also, it would be of interest to know what conversion of this ferrite to sigma was obtained after the reported 12,000 hr of operation.

It has been somewhat general practice to use a low-ferrite content of say 3–4 per cent in weld metal for steam power-plant service rather than 6–8 per cent ferrite which is more normal for the lower temperature applications of stainless-steel weld metal.

In connection with the reported low keyhole notch-bar values for various weld metals shown in Table 8 of the paper, it is indicated that the embrittlement obtained possibly has been due to the long-time temperature service. This is indicated by the presence of sigma in the etched microstructures of the weld-metal deposits.

It would be of interest to determine when material is available, similar keyhole notch-bar values on the weld metal at the service temperature as it has been variously reported in the literature that the presence of sigma at some elevated temperatures is not harmful to reducing the notch-bar value. There also is a good question to be answered on the relative susceptibility to stress corrosion-cracking for the alloys used in this experiment. Apparently, there has been no observation of stress corrosion-cracking effects shown to date in the experiments performed. However, the writer would appreciate the opinion of the authors as to the relative susceptibility to this phenomena for the various alloys and weld metals in test.

Finally, the writer would like to inquire whether examination of the various materials has been made at the junction line of the weld metal and parent metal. In some types of service elevated temperature for extended periods of time has produced grain growth at the junction line in the parent metal. A sample of this is shown in an article by the writer,[10] where an illustration is given of 4-6 Cr, $^1/_2$ Mo steel welded with 25 Cr, 20 Ni and exposed to 10,000 hr heated at 1290F. In this illustration extraordinarily large grains were developed in the parent metal between 5000 and 10,000 hr exposure. The writer is calling this to the attention of the authors and would appreciate if they would comment on the joints which they have under examination.

The writer would suggest that possibly a little more detail as to the welding procedures used for the various joints under examination would benefit many interested in this subject.

Authors' Closure

The authors greatly appreciate the stimulating and profitable comments presented by Messrs. R. C. Fitzgerald, G. E. Lien, and Dr. M. A. Scheil.

Mr. Fitzgerald has emphasized the desirability of obtaining information on the thermal-shock behavior of the stainless and superalloys under soot-blowing conditions. Since the test element is directly exposed to the action of an IK-soot blower operating on normal schedule, no better test could have been devised. It is, indeed, reassuring that none of the materials has shown any indications of adverse effects due to thermal shocks after 7000 hours of operation. Such adverse effects manifest themselves as surface craze cracking which is readily detected by a competent metallurgist. The surface area of the Type 316 bend in which the reported circumferential stress-rupture crack occurred was entirely free from craze cracking or surface oxide notching characteristic of quench effects as produced by harmful soot blowing. There is no doubt that the failure of this bend was caused by bending stresses and not by pressure stresses and/or quenching effects.

Mr. Fitzgerald has furthermore expressed the thought that solution heat-treatments involving water quenching of fabricated loops might pose a problem for designers and fabricators. The answer to this suggestion is that the tubing is generally solution-treated prior to fabrication and that the fabrication processes and procedures do not significantly impair the creep-rupture strength obtained by a prior solution treatment. A high-temperature heat-treatment of these materials is necessary to eliminate the varying hot-working effects imposed upon the materials during tube fabrication.

The authors agree with Mr. Fitzgerald that the surface-grain boundary attack observed in the Type 316 and 16-25-6 alloys warrants further study, and they have said so in the paper. However, the authors feel that it is premature to consider the corrosion resistance of these alloys as inadequate. The observed surface-grain boundary oxide notching of these two alloys may possibly have been brought about or promoted by previous hot finishing and pickling operations. Only further service can tell whether this condition will aggravate with time.

It seems to the authors that Mr. Fitzgerald is ascribing too much importance to the surface-grain boundary notching of the Type 316 and 16-25-6 alloys. This condition is only one to two grains deep and therefore much too shallow to be evaluated by tubular stress-rupture tests as suggested. This surface notching should not be mistaken for the type of intercrystalline deterioration which initiates stress-rupture failures.

Mr. Fitzgerald's authoritative discussion of shock resistance versus superheater service requirements is a most helpful and valuable contribution. There has been much uncertainty as to whether a superheater material must possess an appreciable amount of shock resistance in long-time service. It appears from Mr. Fitzgerald's discussion that bending or tension ductility, rather than shock resistance, is the dominant requirement, although it is, of course, understood that superheater materials must not become outright brittle.

Mr. Lien's remarks are greatly appreciated by the authors and their company. The progressive attitude and helpful co-operation of the American Gas & Electric Company have significantly contributed to this investigation.

Dr. Scheil has raised some pertinent questions. As to the possible use of Type 304L with 0.03 per cent max carbon, the authors feel that this material would not offer any advantage over the higher-carbon regular Type 304 material if the latter, as the test has shown so far, is not susceptible to intergranular attack in this type of service.

As far as the weldments are concerned, they were all made with 3/32-in-diameter electrodes, using a back-up ring and no preheating or postweld treatment. Each weld deposit was examined for fissuring and crater cracking. The first 19-9 Cb weld metal listed in Table 8 (joining Type 304 to Type 304 material) had a ferrite content of about 2 per cent; the second 19-9 Cb weld metal (joining Type 321 to Type 321 material), a ferrite content of about 5 per cent; and the 18-12 MoCb weld metal (joining Type 318 to Type 318 material) a ferrite content of about 2 per cent. The Armco 17-14 CuMo weld metal was fully austenitic. As far as the small-particle size permitted identification, all of the ferrite appeared to have been converted to sigma phase after 4000 hours at operating temperature. The lower residual room-temperature impact strength of the 19-9 Cb weld

[9] Director, Metallurgical Research, A. O. Smith Corporation, Milwaukee, Wis. Mem. ASME.

[10] "Migration of Cr and C in a Weld in Type 502," by M. A. Scheil, *Metal Progress*, vol. 64, September, 1953, pp. 108 and 110.

metal joining the two 18-8 Ti materials may be explained by the higher operating temperature as well as by the higher initial ferrite content of the weld metal. As the authors have pointed out, there was not enough material available for determining the impact properties of these weld metals at the operating temperatures. The hot and cold embrittling tendencies of the 18-8 type alloys and of their corresponding weld metals have been the subject of a separate study in the authors' laboratories, which will be published in the near future.

Dr. Scheil's inquiry regarding the relative susceptibility of the alloys to stress-corrosion cracking was not unexpected by the authors. It is assumed that Dr. Scheil refers to stress corrosion in condensate during off or starting-up periods. Some few years ago one of the authors conducted stress-corrosion tests in synthetic chloride-bearing boiling condensate solutions with unwelded and welded horseshoe-type specimens of all the 18-8 type alloys stressed to the yield point at the apex. Summarily, it may be said that the stabilized as well as the nonstabilized alloys were found under these conditions to be susceptible to stress-corrosion cracking in dilute as well as in more concentrated solutions. However, it must be borne in mind that the internal surface of a superheater tubing is in compression after it has cooled down from the operating temperatures and a surface under compression is not susceptible to stress-corrosion cracking, as the tests in the authors' laboratory have indicated.

Dr. Scheil finally inquired whether any of the materials has shown grain growth in the weld-affected parent metal adjacent to the weld-fusion interface. No grain growth was displayed by any of these austenitic alloys. However, studies of ferritic-austenitic weldments conducted in the authors' laboratories have shown that grain growth does occur in the low-alloy member of such dissimilar welds when they are exposed to high enough temperatures for sufficiently long times. In all these cases, grain growth was preceded by carbon migration from the ferritic low-alloy steel into the austenitic weld metal, and grain growth occurred only in the visibly decarburized zone adjacent to the fusion interface. There is no justification for assuming that this phenomenon may occur in austenitic alloys.

Interface Extension Versus Upper Limiting Time-Mean Energy-Release Rates of Constant-Pressure Steady-State Combustion Process

By W. J. WOHLENBERG,[1] NEW HAVEN, CONN.

The concepts of size and distribution of the mass elements sheared out by turbulence are added to the interface theory. This enables inclusion of the parameter interface extension in terms of the surface-volume ratio of such mass elements. The reciprocal of this ratio is the hydraulic mean depth of the mass elements which, in turn, is of the same order of magnitude as is the thickness of gaseous layer of the tail-end thermal diffusion process which is always present in the combustion process just prior to the major portion of the terminal chemical or molecular collision phases of the reaction. In applying this theory, it is found that, for the higher levels of energy-release rate, the mass elements must be so small, in order to provide the necessary interface extension, that the possible magnitude of tail-end diffusion is so small as to preclude any possibility that it could exercise a major influence in control over the reaction rate. This now resides in the terminal chemical phases of the reaction. The quantitative aspects of the preceding statement are based on results of an application of the theory to dodecane, the theory being generally applicable to second-order reactions but the accuracy of such results appears for the present as limited to their orders of magnitude. The disclosed quantitative aspects should not be far from the real facts for the cases considered, provided the deduced mass-element sizes are actually realized.

Introduction

THIS paper is a further development of the interface theory[2] and brings together the essential parts of two preceding papers[3, 4] and a discussion,[4] each of which deals with separate phases of the theory. An important addition to the original theory is the time-mean size-shape characteristic of the fuel and air-side mass elements of which the mixture is composed. This has made it possible to evaluate the dependence of the upper limiting interface extension and hence of upper limiting energy-release rates, per unit mixture volume, on the size of such elements, the size being expressed in terms of the volume-surface ratios of the elements and thereby demonstrating this to be a most influential physical property of the mixture with respect to its capacity for volume-based rate of energy release.

The content of the air-side mass elements enters, of course, in the gaseous state, whereas that of the fuel-side elements may enter in either the solid, liquid, or gaseous state. The theoretical development and the results of their application to a given fuel (included later in the paper) assume the fuel as introduced in the gaseous state. Quantitative results shown are thus applicable only to this case and then only as to the order of magnitude of such results for reasons which will become evident later on. However, from a qualitative point of view, there are some features of the combustion process which may be considered as in common for all three cases—gaseous, solid, or liquid states of fuel induction. A brief discussion of these and also of points of difference between them will serve to clarify the problem, at least in a qualitative sense.

Solid or Liquid Fuels in Suspension

With fuels in suspension in the form of particles, either solid or liquid, there will be at least two classes of fuel-side mass elements. One of these consists of the particle enclosed in a gaseous envelope, a part of the latter stemming from the volatile portion of the particle itself. The other class of such elements also stems from the volatile portion of the particle and may be visualized as a trail of small mass elements in gaseous or vapor state, which is discharged from the particles. The fraction of the mixture volume which is occupied by the two classes of elements depends on the kind and size of particle and on temperature, pressure, and turbulence histories to which the particle and its immediate vicinity have been submitted.

Note now that for both classes of fuel mass elements a reaction interface may be imagined in the gaseous or vaporous zone, where fuel and air-side mass elements impinge. It is here that the chief chemical phases of the reaction occur by means of the molecular-collision mechanisms engaged in by the fuel and oxygen molecules which are transported into this zone—the fuel molecules from within the fuel-side mass elements, and oxygen molecules from within the air-side mass elements. Also, for both classes of fuel-side zones, the final stage of the approach journey toward the imaginary reaction interface is through the process of thermal diffusion. Turbulence is too coarse-grained ever to toss individual molecules directly into chemical reaction with each other. A diffusion stage, designated henceforth as tail-end diffusion, is always interposed between the turbulent or mass transfer toward the reaction interface and the terminal chemical stages of the combustion process occurring in flames.

This, of course, applies to the approach journeys toward the

---

[1] Dean, Yale University, School of Engineering. Fellow ASME.

[2] "The Influence of Reaction Interface Extension in the Combustion of Gaseous Fuel Constituents," by W. J. Wohlenberg. Trans. ASME, vol. 70, 1948, pp. 143–160.

[3] "Minimum Depth of Flame Front for Stable Combustion . . . ," by W. J. Wohlenberg, Fourth Symposium (International) on Combustion, Massachusetts Institute of Technology, Cambridge, Mass., September, 1952.

[4] "Interface Extension, Tail End Diffusion . . . ," by W. J. Wohlenberg, Fourth Symposium (International), Massachusetts Institute of Technology, September, 1952.

Contributed by the Fuels Division and presented at the Annual Meeting, New York, N. Y., November 29–December 4, 1953, of The American Society of Mechanical Engineers.

Note: Statements and opinions advanced in papers are to be understood as individual expressions of their authors and not those of the Society. Manuscript received at ASME Headquarters, March 18, 1953. Paper No. 53—A-103.

imaginary reaction interface of both fuel and oxygen molecules, and it applies for all three cases, solid, liquid, or gaseous state of the fuel being induced. Since this is true, then per unit area of reaction interface the magnitude of the energy-release rate should be about the same for all three cases. However, this statement does not hold when the energy-release rate is referred to a unit volume of the mixture because, as will become evident later, the interface extent on a volume base is proportional to the fraction α of mixture volume which is occupied by the fuel-side (or of air-side mass elements, whichever is the lesser of the two), and the magnitude of this fraction is strongly influenced by physical state of the induced fuel. Roughly, it varies inversely with the density of the induced fuel.

The complex nature of the dependence of energy-release rate on the physical or geometrical aspects of the burning mixture, where particles are in suspension, thus becomes obvious. Large particles moving with low relative velocity in the mixture provide for small interface extension on two counts: (*a*) Because of their high density, particles plus their gas envelopes occupy but a small fraction α_1 of the mixture volume and so can contribute only small interface extension; and (*b*), the trailing fuel mass elements in the gaseous state may be relatively few in number per particle for this case. For smaller particles, the contribution to interface extension, of the system composed of particles plus their envelopes, increases over that of the coarse particles for obvious reasons. If such particles are moving with high relative velocities, then the trailing gaseous fuel mass elements also may be large in number per particle. However, as the particles become small, their velocity relative to the gases soon decreases to a small value. Now, the frequency with which trailing gaseous mass elements are washed from the particle is decreased materially, and so the number formed per particle in its flight through the flame is again low.

Whatever the foregoing relationships, the upper limiting extent of reaction interface for a given average size of mass element with a given fuel requires that both fuel and air-side mass elements be in the gaseous state and that they be in uniform macroscopic distribution with respect to each other. This, then, is the basic condition assumed to exist for the mixture under consideration. It is the mixture state which for a given set of the other combustion parameters, i.e., fuel, air-fuel ratio, pressure, and temperature, results in the maximum energy-release rate per unit volume for a given time-mean size of mass elements. As previously indicated, one of the relations sought is that which shows how the upper limiting value of the volume-based energy-release rate depends on the time-mean size of the mass element—no questions being asked at this time concerning the intensity and duration of turbulence, or of premixing, which may be required to create the mass-element sizes necessary to the energy result.

The answers to such questions, when found, will, of course, relate theory to practice. In this connection, there also arises the question as to whether or not fuel injected at high velocity in the form of particles within a certain range as to size (i.e., for some liquid fuels) may not be the most effective way in which to achieve gaseous mass-element sizes in the smaller ranges and hence of realizing high interface extension in the most effective practical manner. This does not concern us at present. It is simply the influence of the size of this element which is under investigation. This, by itself, provides a new basic position from which to view the physical reality of the combustion process.

Unmixedness Factor

At this point it may be appropriate to refer briefly to the concept "unmixedness factor," developed by Hawthorne, Weddell, and Hottel.[8] It is applicable to turbulence-controlled combustion and expresses the root-mean-square value of the deviation from its local time-mean value of the local composition of the mixture. This is shown to be an index of the local distribution of the mixture composition—the greater the value of the factor, the less intimate the mixing. Interface extension is also an index of the mixture distribution but in a direct proportion to it; i.e., the greater its value, the more intimate is the mixture and the closer the distribution is to that of a molecularly uniform mixture. It thus appears that eventually it may be possible to translate a value of the unmixedness factor into the value of interface extension which should be associated with it.

With this in mind, it is noted that, although unmixedness indicates a state of mixture distribution, the definition of this state is not in sufficient detail to indicate how it should be fitted into that portion of the reaction equation which represents reaction progress subsequent to the attainment of this state. But the definition of interface extension does exactly this, with reference to the states of mixture distribution represented by it. Is it not logical, therefore, to consider that, except for the still missing gap between the two, the interface theory begins where the unmixedness theory leaves off? This in spite of the fact that direct experimental verification of interface extension is impossible unless by some device it becomes feasible to measure the effective size and distribution of the mass elements which determine its value. It is still an essential dimension of the process and, for a given case, its magnitude is indirectly ascertainable from experimental evidence. Furthermore, values may be assigned to it; i.e., as to the size and distribution of the mass elements in the attempt to evaluate the influence of such conditions of energy results which, as previously stated, is the chief objective of this analysis. It is developed with reference to concentration patterns for which combustion progress is one-dimensional.

The Mass Elements and Upper Limiting Interface Extension

Considering both fuel and air mass elements, as in the gaseous state, a section cut out of the burning mixture might appear as represented in Fig. 1. The interzone (to which chemical phases

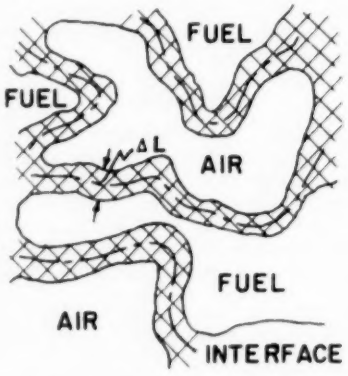

Fig. 1 Nonuniform Mixture

of the reaction are chiefly confined) is represented by the cross-hatched regions and the trace of the imaginary reaction interface by the dot-and-dash line running through it. The interface extension[9] is thus the lateral extent, per unit of mixture volume, of the imaginary interface. Symbol ΔL represents the depth of this interzone. Later this symbol and also Δl were restricted to represent its minimum depth for stable combustion,[9] both symbols having been employed inadvertently to represent the same thing.

[8] "Mixing and Combustion in Turbulent Gas Jets," by Hawthorne, Weddell, and Hottel, Third Symposium on Combustion, Flame, and Explosion Phenomena. Williams & Wilkins Co., Baltimore, Md., 1949.

For a given cross section through which the burning mixture flows, i.e., for a given point along the path of combustion progress, let

v_1 = volume of average fuel mass element
a_1 = surface area of average fuel mass element
α_1 = partial mixture volume occupied by fuel mass elements
A_1 = upper limiting value of interface extension as computed from fuel-side mass elements

Then

$$A_1 = \alpha_1 (a_1/v_1) \quad [1]$$

and similarly for the air-side elements, the upper limiting value is

$$A_2 = \alpha_2 (a_2/v_2) \quad [2]$$

where subscript 2 indicates the air side.

The real upper limiting value, for the mixture under observation, will then be whichever of the two, A_1 or A_2, is the smaller, since the true extent of it obviously cannot exceed the possible contribution of the smaller of the two to that which is common to both classes of mass elements. Furthermore, this higher limiting value will be obtained only if the fuel and air mass elements are distributed uniformly among each other; i.e., the distribution is macroscopically uniform.

With fuels fired as solids or as liquids in suspension $\alpha_1 << \alpha_2$ but even when fired in the gaseous state $\alpha_1 < \alpha_2$ for many fuels, and so the upper limiting value in interface extension is A_1 in all of such cases unless the ultimate mass element on the fuel side should be much smaller than that on the air side. This question bears investigation.

The surface attacked by the shearing forces of turbulence per unit volume of gas in this instance is, of course, numerically equal to the surface-volume ratio. This shearing action per unit volume of mass elements on the two sides is resisted chiefly by viscosities μ_1 and μ_2 of the fluids. Where air elements impinge on fuel elements, the shearing forces are generated by resistances between the two. Hence, in such areas the shearing force acting per unit of common contact area between the two elements is identically the same force. This contact area per unit volume is (a_D/v_D), the latter ratio being equal to $1/l_D$, where l_D is the hydraulic mean depth of the mass elements. This must therefore approach a limiting value such that

$$\frac{l_{D1}}{l_{D2}} = \frac{\mu_1}{\mu_2} = \left(\frac{\sigma_2}{\sigma_1}\right)^2 \left(\frac{m_1}{m_2}\right)^{1/2} \quad [3]$$

Thus the limiting hydraulic mean depths of the two classes of elements become proportional to their viscosities. The last group on the right is obtained from the kinetic theory of gases. In it, σ and m are respectively the molecular diameter and weight. The subscript D has been attached in order to distinguish l_D from l, the latter symbol being employed in the following to represent the depth of the reaction interzone to be defined presently.

Specification of Mass Element in Terms of Its Diffusion Core and Its Interzone Boundary Layer

Reference is made to Fig. 2 where the fuel-side mass element is represented in more detail. It is now considered as composed of a core of volume v_{D1} surrounded by an interzone of depth l, the latter containing an interface area a_i. If, as before, the mixture volume fractions (mol fractions, gaseous state) are designated, respectively, as α_1 and α_2 for fuel and air, then interface a_i to be associated with the fuel-side zone encloses a total volume

$$v_i = v_{D1} + \alpha_1 \, l \, a_i \quad [3a]$$

Here $\alpha_1 \, l \, a_i$ is the portion of the interzone to be associated with the fuel zone. The remainder of the interzone, or $(1 - \alpha_1) \, l \, a_i$, is thus that associated with the air zone. This leads to the relation

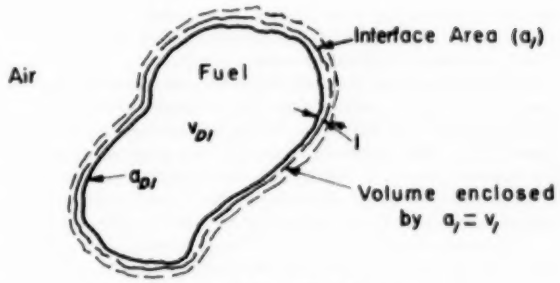

Fig. 2 Fuel Zone With Interzone

$$A_1 = \alpha_1 \frac{a_1}{v_1} = \frac{\alpha_1}{l_{D1} + (l_{A1} - l_{D1})} \cong \frac{\alpha_1}{l_{D1} + \alpha_1 l} \quad [4]$$

Here l_{A1} is interpreted as the hydraulic mean depth to interface surface a_1, the difference $(l_{A1} - l_{D1})$ being approximated by the product $\alpha_1 \, l$. This approximation is close to the real difference when $\alpha_1 \, l$ is small compared to the hydraulic mean depth of the core volume v_{D1}. When the two become of the same order of magnitude, the macroscopic is merging into the molecularly uniform state of distribution. It is noted that as l_{D1} approaches zero, A_1 approaches $(1/l)$. This is the equivalent interface-extension value of the molecularly uniform mixture since now the total mixture volume is in the reaction interzone. When l_{D1} is infinite, A_1 is zero—the interface extension of the infinite body. Equation [4] thus approaches the correct limits.

Conditions in Interzone and Energy Equation

Concentration gradients which exist across boundary layers of impinging fuel and air mass elements or zones are illustrated in Fig. 3. Here, as before, subscripts 1 and 2 are attached, respectively, to properties or positions to be associated with fuel and air-side mass elements. Hence l_{D1} and l_{D2} represent depths of tail-end diffusion boundary layers, respectively, on fuel and air sides,

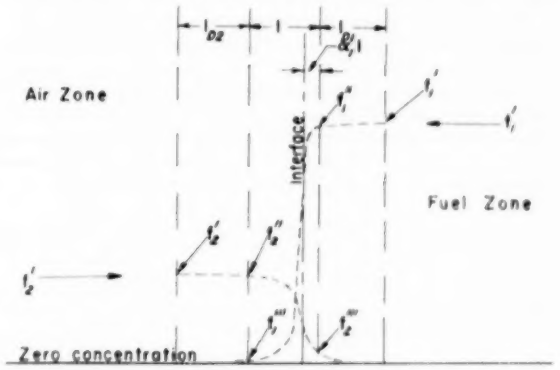

Interzone and Diffusion Layers

$l = \Delta l$ for uniform mixtures
$\alpha_1 l = \alpha_1 \Delta l$ " " "
$l_{D1} = l_{D2} =$ zero " " "

Concentrations are constant across Δl for uniform mixtures

Fig. 3 Interzone and Diffusion Layers

the total interzone of depth l being the common meeting ground where oxygen and fuel molecules impinge on each other by means of the molecular collision mechanism.

With the foregoing in mind, the combustion process is as follows: Referring to the fuel side, fuel molecules are transported from within the fuel-side mass elements to the interzone at their boundaries. This results in concentration gradient $f_1' - f_1''$, the concentration f_1' being that in the center of volume of the mass elements, its magnitude being a function of the state of combustion progress. With combustion occurring in the interzone, the fuel concentration decreases from its value f_1'' at entrance to f_1''' at the opposite interzone boundary. Changing subscripts from 1 to 2, the foregoing description applies to the oxygen molecules applied from the air side.

If the time-mean rate of the reaction is steady at a given point along the path, then the time mean of the foregoing concentration gradients are steady, and so the time-mean rates of diffusion per unit area of interface may be represented as

$$\frac{dV_1}{d\theta} = D_1\left(\frac{-df_1'}{dl}\right) \quad [5]$$

$$\frac{dV_2}{D\theta} = D_2\left(\frac{-df_2'}{dl}\right) \quad [6]$$

where the following definitions apply:

V = volume, cu ft
D = coefficient of diffusion, sq ft per sec
θ = time, sec

Now let $f'' = \chi f'$. Then

$$\left(\frac{-df_1'}{dl}\right) \cong \frac{(1-\chi_1)f_1'}{l_{D1}} \quad [7]$$

$$\left(\frac{-df_2'}{dl}\right) \cong \frac{(1-\chi_2)f_2'}{l_{D2}} \quad [8]$$

where the order of magnitude of layer depths l_{D1} and l_{D2} is the same as that of the hydraulic mean depths, respectively, of the fuel and air-side mass elements. But the hydraulic mean depths of these elements are exactly the reciprocals of their interface extension.

This, then, comprises the specification of the mixture characteristics which, when included in the energy equation, make it possible to arrive at quantitative relations between size of mass element and upper limiting energy-release rates. It enables, also, an evaluation of the variation of the effect of tail-end diffusion on reaction rate with variation in size of the mass elements.

For later reference, it is noted in passing that the pressure-temperature dependence of D is found from self-diffusion to be

$$D = \frac{\mu}{\rho} = D_0\frac{P_0}{P}\left(\frac{T}{T_0}\right)^{n'+1} \quad [9]$$

where ρ represents density and subscript 0 refers to standard conditions. Both D_0 and n' are assumed as constants, the values of which depend on the gas composition.

Energy-Release Rates Supported by Diffusion

Equations [5] and [6] express the volume rate of diffusion per unit area of interface. The energy-release rate equivalent of this, referred to the same base, is expressed as

$$\frac{1}{A}\left(\frac{dH}{d\theta}\right)_{D_1} = \frac{dV_1}{d\theta}Q_f \quad [10]$$

$$\frac{1}{A}\left(\frac{dH}{d\theta}\right)_{D_2} = \frac{dV_2}{d\theta}\frac{Q_f}{n_2} \quad [11]$$

where

$$Q_f = Q_{0f}\frac{P}{P_0}\frac{T_0}{T}\ (\text{Btu/ft}^3) \quad [12]$$

Q_{0f} = calorific content (Btu/ft³) of fuel, the fuel being considered in gaseous state (for reasons before noted) and at standard conditions P_0, T_0
n_2 = mols oxygen per mol fuel in reaction as assumed to occur in collision zone, i.e., interzone

Inserting Equations [7] and [8] in Equations [5] and [6], respectively, and the latter two with Equations [9] and [12] in Equations [10] and [11], respectively, the results are

$$\frac{1}{A}\left(\frac{dH}{d\theta}\right)_D = D_{01}Q_{0f}\left(\frac{T}{T_0}\right)^{n_1'}\frac{(1-\chi_1)f_1'}{l_{D1}}\frac{\text{Btu}}{(\text{sec})(\text{ft}^2)} \quad [13]$$

$$\frac{1}{A}\left(\frac{dH}{d\theta}\right)_D = D_{02}\frac{Q_{0f}}{n_2}\left(\frac{T}{T_0}\right)^{n_2'}\frac{(1-\chi_2)f_2'}{l_{D2}}\frac{\text{Btu}}{(\text{sec})(\text{ft}^2)} \quad [14]$$

These are the diffusion equations on the energy basis. They state the energy-release rate which may be supported per unit area of interface by the diffusion process. For a time-mean steady state, these rates are equal to the release rate in the collision zone when referred to the same base.

The Complete Energy Equation

The foregoing is the approach branch of this equation. The collision branch, as applied to a molecularly uniform mixture distribution, has been developed[2] and is reproduced in the following, when stated on the basis of energy-release rate per unit of volume

$$\left(\frac{dH}{d\theta}\right)_\chi = \frac{X\,(P/P_0)^2\,(T_0/T)^{3/2}\,Q_{0f}\,f_1\,f_2}{0.47\times10^{-10}\,N_{12}\sqrt{m}\,R_\lambda}\frac{\text{Btu}}{(\text{ft}^3)(\text{sec})} \quad [14a]$$

Here subscript χ has been attached to indicate that it applies to the chemical reaction or collision zone. Other new symbols are defined as follows:

X = fraction of potentially releasable energy which is free, i.e., unbound in so far as dissociation is concerned
f_1 = concentration of unburned fuel in interzone, at point under observation, considering molecularly uniform distribution of gases present in the vicinity of that point
f_2 = same as f_1, only for oxygen in this case
N_{12} = collision number = $e^{E/RT}$
E = energy of activation Btu/lb mol
m = molecular weight of fuel molecule
R_λ = ratio of mean free-path length of the fuel molecules when present in furnace gases to that of hydrogen molecule in hydrogen gas, both gaseous systems being considered at standard conditions (P_0, T_0)
R = universal gas constant = 1.985 Btu/(mol)(deg)

For the case of molecularly uniform distribution, fuel and oxygen molecules are everywhere in the most favorable time-mean position with respect to each other, in so far as the chemical reaction is concerned. The requisite supply of each is at hand everywhere for favorable air-fuel ratios and it requires no diffusion to get them into position to react chemically. Diffusion has accomplished this task in advance. Under these conditions, concentrations of fuel and oxygen molecules are level across each and every collision-zone depth of the mixture, that depth being represented by Δl for the case of the molecularly uniform mixture distribution.

Let it be assumed, for the moment, that such a state could exist across depth l, of the interzone of the macroscopic mixture; i.e., the distribution within the interzone is molecularly uniform, and

the composition of its contents is that of a molecularly uniform mixture of the contents of the adjacent fuel and air mass elements for the state of combustion progress under observation. Then the factors χ_1 and χ_2 will be the ratios of concentrations of the foregoing molecularly uniform distributions to those, f_1' and f_2', existing in the cores of the adjacent fuel and air-mass elements. The concentrations f_1 and f_2 in the interzone, at any point of combustion progress, are thus assumed constant across l, respectively, at $\chi_1 f_1'$ and $\chi_2 f_2'$, and the product $f_1 f_2$ of Equation [14a] has the value

$$f_1 f_2 = \chi_1 \chi_2 f_1' f_2' \quad \ldots\ldots [15]$$

With this value of $f_1 f_2$ included in its collision branch, i.e., in Equation [14a], the complete energy equation may be applied to solve for that depth l_D of the tail-end diffusion layer which would satisfy the conditions outlined in the preceding paragraph. This is its maximum permissible depth when the energy-release rate per unit area of interface of the macroscopic state is equal to that which would occur there per unit area of interface, should the molecular concentrations in the interzone be those which would exist if the contents of the impinging fuel and air mass elements were in molecularly uniform distribution among each other.

In general, however, concentration gradients do exist across the interzone of the macroscopic-mixture state while combustion is occurring. Therefore, it is desirable to view the foregoing special condition in the light of the more general conditions prior to further development of the special case.

Under those favorable circumstances where oxygen and fuel flow into the interzone counter to each other in stoichiometric proportions, a gradient such as is illustrated in Fig. 3 by $f_1' \rightarrow f_1'' \rightarrow f_1'''$ would exist on the fuel side. The reaction is now completed across the interzone, and the concentrations f_1''' and f_2''' at escape from this zone would each closely approach the limit zero. The mean values of concentrations across the zone may then be shown to be approximately

$$\left.\begin{aligned} \bar{f}_1 &= \alpha_1 \chi_{D1} f_1' \\ \bar{f}_2 &= \alpha_2 \chi_{D2} f_2' \end{aligned}\right\} \quad \ldots\ldots [15a]$$

and the effective value of the product $f_1 f_2$ across l becomes

$$\bar{f}_1 \bar{f}_2 = \alpha_1 \alpha_2 \chi_{D1} \chi_{D2} f_1' f_2' \quad \ldots\ldots [15b]$$

It will be shown later that $\alpha_1 = \chi_1$ and $\alpha_2 = \chi_2$ when the composition and distribution within the interzone of the macroscopic state satisfies the foregoing assumed state. Substituting these values in Equation [15] yields

$$f_1 f_2 = \alpha_1 \alpha_2 f_1' f_2' \quad \ldots\ldots [15c]$$

when on comparison of Equations [15b] and [15c]

$$\bar{f}_1 \bar{f}_2 = f_1 f_2 \chi_{D1} \chi_{D2} \quad \ldots\ldots [16]$$

where the product $\chi_{D1} \chi_{D2}$ approaches unity as the diffusion layers l_{D1} and l_{D2} approach zero.

The release rate per unit area of interface is proportional to the mean value of the concentration product across the depth of the interzone times this depth, since the latter has the same value as the volume of interzone per unit area of interface. Note now, from Equation [16], that the ratio of effective mean values of the concentration product for the macroscopic to that of the molecularly uniform mixture is

$$\bar{f}_1 \bar{f}_2 / f_1 f_2 = \chi_{D1} \chi_{D2} \quad \ldots\ldots [16a]$$

It follows that, for a given release rate per unit area of interface, it will require an interzone depth l for the macroscopic state which is about $(1/\chi_{D1}\chi_{D2})$ times the depth Δl of the collision zone of the molecularly uniform distribution which yields this given release rate per unit area of interface.

This is a consequence of the counterflow molecular-supply arrangement inherent to the interzone of the macroscopic state of distribution. As the mass elements of the macroscopic distribution decrease in size and approach molecular dimensions, each of the factors χ_{D1} and χ_{D2} approaches unity, and so, in the limit, Equation [16] merges into Equation [15].

In the subsequent investigation of the order of magnitude of the effect of tail-end diffusion, the base of operations is the release rate per unit area of interface for the molecularly uniform mixture distribution. The interzone side of the equation will thus be that for this distribution state, and the depth factor of the zone is Δl. The equivalent counterflow interzone of the macroscopic state yielding the same release rate per unit of interface would thus have a depth approximately equal to

$$l = \Delta l / \chi_{D1} \chi_{D2} \quad \ldots\ldots [16b]$$

It is noted in passing that this relation is necessary to the development, later on, of Equation [31] which expresses the ratio of the upper limiting interface extension of the macroscopic to that of the molecularly uniform mixture—a factor involved in determination of the upper limiting energy-release rate per unit volume of the macroscopic-mixture state.

With these preliminaries out of the way, reference is again made to the particular application of the energy equation, previously outlined, which is to lead to quantitative results for the maximum permissible thickness l_D of the tail-end diffusion layer when the release rate per unit area of interface of the macroscopic-mixture state is equal to that which would exist if the molecular concentrations in the interzone were those resulting from a molecularly uniform distribution within the interzone of the contents of the adjacent fuel and air mass elements for the state of combustion progress at the point under observation.

It is now known that, when these conditions are satisfied, then the ratio of depth $(l/\Delta l)$ of macroscopic to molecularly uniform interzones will be in accord with Equation [16b]. This particular knowledge is interesting but not necessary in the determination of maximum permissible l_D versus release rate per unit of interface. It is, of course, a condition associated with the result.

What is necessary, is to return to the point where Equation [15] is substituted in Equation [14a]—the point at which the development was interrupted for the sake of gaining more background information relative to interzone conditions. Making this substitution and introducing the multiplying factor $(1/A)$ in order to have the release rate stated per unit of interface area then yields

$$\frac{1}{A}\left(\frac{dH}{d\theta}\right)_x = \Delta l \, \frac{X \left(\frac{P}{P_0}\right)^2 \left(\frac{T}{T_0}\right)^{s/2} Q_{0f} \, \chi_1 \chi_2 f_1' f_2'}{0.47 \times 10^{-10} N_{12} \sqrt{m_1} R_\lambda} \quad \frac{\text{Btu}}{(\text{ft}^2)\,(\text{sec})} \quad \ldots\ldots [17]$$

where $\Delta l = 1/A$ $(\text{ft}^3/\text{ft}^2)$ represents the collision-zone volume per unit of interface area. Then, equating the right-hand side of Equation [14] to that of Equation [17] and solving

$$\Delta l \, l_{D2} = \frac{0.47 \times 10^{-10}}{X f_1'} \frac{D_{02}}{n_2} \frac{N_{12} \sqrt{m_1} R_\lambda}{\left(\frac{P}{P_0}\right)^2 \left(\frac{T_0}{T}\right)^{(s/2 + n')}} \frac{1 - \chi_2}{\chi_1 \chi_2} \, (\text{ft}^2) \quad \ldots\ldots [18]$$

From Equation [13] of reference[3] after correction to ft from cm and replacement of f_2 by $\chi_2 f_2'$

$$\Delta l = 0.292 \times 10^{-6} R_\lambda \left(\frac{\bar{N}_{12}}{\chi_2 f_2'}\right)^{1/3} \frac{P_0}{P} \frac{T}{T_0}, \text{ ft or } (\text{ft}^3/\text{ft}^2) \quad [19]$$

Note that on the basis of its development in reference[3] the collision-zone volume and area elements to be associated with Δl are respectively $V = (\Delta l)^3$ and $(\Delta l)^2$. On this basis Δl is not only the depth of the zone but also its volume referred to unit area of interface. It thus has the dimensions $(\text{ft}^3/\text{ft}^2)$, and the interface extension becomes $(1/\Delta l)$ ft^2/ft^3.

Dividing Equation [18] by Equation [19]

$$l_{D2} = \frac{1.61 \times 10^{-4}}{X} \frac{D_{02}}{n_2} \frac{(f_2')^{1/3}}{f_1'} \frac{(\bar{N}_{12})^{2/3} \sqrt{m_1}}{\frac{P}{P_0}\left(\frac{T_0}{T}\right)^{(1/3+n_2')}} \frac{1-\chi_2}{\chi_1' \chi_2^{2/3}} (\text{ft}^3/\text{ft}^2) \quad [20]$$

Noting that $n_2' = 0.75$, and dividing Equation [20] by Equation [19]

$$\frac{l_{D2}}{\Delta l} = \frac{5.5 \times 10^3}{X R_\lambda} \frac{D_{02}}{n_2} \frac{(f_2')^{2/3}}{f_1'} (\bar{N}_{12})^{1/3} \sqrt{m_1} \left(\frac{1-\chi_2}{\chi_1 \chi_2^{1/3}}\right) \quad [21]$$

It is noted that l_{D2} varies inversely with pressure and is independent of R_λ while for the ratio $l_{D2}/\Delta l$ just the reverse is true, the latter being independent of temperature also.

Finally, equating the right sides of Equations [12] and [13] and solving

$$l_{D1}/l_{D2} = \frac{n_2}{n_1} \frac{D_{01}}{D_{02}} \frac{f_1'}{f_2'} \left(\frac{T_0}{T}\right)^{(n_2'-n_1')} \left(\frac{1-\chi_1}{\chi_1 \chi_2}\right) \quad [22]$$

This equation permits solving for the maximum permissible value of l_{D1} as based on the diffusion limitations, l_{D2} having been solved for from Equation [20]. Equation [3] shows how the two are related on the basis of turbulent shearing forces and viscosities. If l_{D1} from Equation [22] is greater than l_{D1} from Equation [3], there is no bottleneck on the fuel side. If the contrary, then the fuel side contains the bottleneck to the reaction rate.

Equations [19], [20], [22] together with Equation [3] thus enable solutions for the principal thickness dimensions of the important elements of which the system is considered as composed. What they mean is, as before implied, a matter of interpretation. In this analysis, the point of view is that, for reasons previously stated, they represent the order of magnitude of the hydraulic mean depth of the elements. Any attempt at more refinement than this in the interpretation involves details of the flow, concentration, and shape patterns not available generally. Inspection of foregoing equations indicates that the values of terms such as concentrations, for example, depend on combustion progress. Such functions are now investigated.

Concentrations f^1 Mixture Fractions α and Concentration Ratios χ as Functions of Combustion Progress

With fuel induced in the gaseous state α_1 and α_2 are mol fractions. A point along the path of combustion progress is stated in terms of burned fraction x of the fuel. On this basis, the concentrations of the uniform mixture become

$$\left.\begin{aligned} f_1 &= (1-x)/\beta \\ f_2 &= 0.21N(y-x)/\beta f \end{aligned}\right\} \quad [23]$$

where

f = fraction combustible in fuel as supplied
y = actual/stoichiometric air supply
$\beta = (\beta_0 + x f \Delta)/f$ = volume of products per unit volume of combustible in entering fuel, both at same (P, T)
$\beta_0 = yN + 1$ = entering air plus fuel gas per unit volume of fuel gas supplied
N = stoichiometric air/fuel (by volume)
Δ = mol change[6] in reaction per mol fuel supplied

Assume that the fractional change in volume Δ of the reaction is distributed between fuel and air sides in proportion[7] to the mixture fractions α on fuel and air sides. It is then found

$$\alpha_1 = 1/\beta_0 \qquad \alpha_2 = (1-\alpha_1) = yN/\beta_0$$

$$\left.\begin{aligned} f_1^1 &= \frac{(1-x)f}{1+\frac{xf\Delta}{\beta_0}} \\ f_2^1 &= \frac{0.21(y-x)}{y\left(1+\frac{xf\Delta}{\beta_0}\right)} \\ \frac{f_2^1}{f_1^1} &= \frac{0.21(y-x)}{y(1-x)f} \end{aligned}\right\} \quad [24]$$

Recalling that for assumed molecularly uniform distribution in a collision zone associated with diffusion layers

$$\chi_1 = f_1/f_1^1 \text{ and } \chi_2 = f_2/f_2^1$$

it is found by substituting from Equations [23] and [24]

$$\left.\begin{aligned} \chi_1 &= 1/\beta_0 = \alpha_1 \\ \chi_2 &= yN/\beta_0 = \alpha_2 \end{aligned}\right\} \quad [25]$$

The latter thus lead to the special values of χ which have been employed in the attempt, which follows, to estimate the order of magnitude of the influence of tail-end diffusion on the reaction rate.

Application of Preceding Equations to a Case

The fuel is dodecane ($C_{12}H_{26}$), to which the following values apply:

$D_{02} = 1.7 \times 10^{-4}$ ft^2/sec	$m_1 = 170$
$D_{01} = 0.88 \times 10^{-4}$ ft^2/sec	$m_2 = 32$
$n_1^1 = 1.00$ (ref.[3])	$f = 1.00$
$n_2^1 = 0.75$ (ref.[3])	$N = 88.1$ ft^3/ft^3
$R_\lambda = 0.125$	$\Delta = +5.5$ ft^3/ft^3
$X = 1.00$	$n_2 = 18.5$ ft^3/ft^3
	$P = P_0 = 1$ atm

With these conditions included, Equation [19] reduces to

$$\Delta l = 3.65 \times 10^{-7} \left(\frac{\bar{N}_{12}}{\chi_2 f_2'}\right)^{1/3} \left(\frac{T}{T_0}\right) \text{ft}^3/\text{ft}^2 \quad [26]$$

Equation [20] to

$$l_{D2} = 1.93 \times 10^{-3} \frac{(f_2')^{1/3}}{f_1'} \frac{T}{T_0} (\bar{N}_{12})^{2/3} \left(\frac{1-\chi_2}{\chi_1 \chi_2^{2/3}}\right) \text{ft}^3/\text{ft}^2 \quad [27]$$

and Equation [22] to

$$\frac{l_{D1}}{l_{D2}} = 9.66 \frac{f_1'}{f_2'} \left(\frac{T}{T_0}\right)^{0.25} \left(\frac{1-\chi_1}{1-\chi_2}\right) \quad [28]$$

Let $y = 1.1$ with $E = 90{,}000$ Btu/lb mol. Then from Fig. 3 (reference[3]) the time-mean release rate over the interval $x = 0$ to $x = 0.99$ is found to be about 16.3 million Btu/(ft^3) (hr), with

[6] In reference[3] this was designated as ΔV.
[7] This differs from that made in closure in reference[3].

zero heat loss from the flame. The temperature of combustion is 4000 R. The time-mean value $\overline{\Delta l}$ of Δl is about 4×10^{-4} ft. Hence, the time-mean interface extension $(1/\overline{\Delta l})$ is about 2.5×10^{4} ft²/ft³, and the time-mean release rate per unit of interface is approximately 660 Btu/(ft²) (hr).

We shall investigate the magnitudes involved in the tail-end diffusion process as combustion begins ($x = 0$) and where gases escape from the cavity with $x = 0.99$ for the conditions outlined in the preceding discussion; i.e., when rates of combustion at the interface are those for which the foregoing time-mean release rate results.

Applying Equations [25] to the foregoing case, it is found

$$\left.\begin{array}{ll} \chi_1 = \alpha_1 = 0.0102 & \dfrac{1-\chi_2}{\chi_1 \chi_2^{1/4}} = 1.02 \\ \chi_2 = \alpha_2 = 0.9498 & \\ \dfrac{1-\chi_1}{1-\chi_2} = 90 & \dfrac{1-\chi_2}{\chi_1 \chi_2^{3/4}} = 0.987 \end{array}\right\} \quad \ldots\ldots [29]$$

Applying the data which are now available in preceding equations yields results shown in Table 1.

TABLE 1

For E = 90,000 Btu/lb mol = 50,000 cal/gram mol

$\Delta l = 2.25 \times 10^{-4}$ (ft³/ft²) or 6.55×10^{-4} (cm³/cm²) at $x = 0$
$\Delta l = 4.94 \times 10^{-4}$ (ft³/ft²) or 15.10×10^{-4} (cm³/cm²) at $x = 0.99$
$l_{D1} = 1.77 \times 10^{-4}$ (ft³/ft²) or 5.4×10^{-4} (cm³/cm²) at $x = 0$
$l_{D2} = 85.0 \times 10^{-4}$ (ft³/ft²) or 260×10^{-4} (cm³/cm²) at $x = 0.99$
$(l_{D2}/\Delta l) = 7.85$ at $x = 0$ and $= 172$ at $x = 0.99$
From Equation [28] $\{l_{D1}/l_{D2} = 7.04 \times 10^{2}$ at $x = 0$
$\{l_{D1}/l_{D2} = 69.3 \ldots$ at $x = 0.99$
From Equation [3] $l_{D1}/l_{D2} = 0.56$ for all (x)

For E = 59,600 Btu/lb mol = 33,000 cal/gram mol

$\Delta l = 0.627 \times 10^{-4}$ (ft³/ft²) or 1.91×10^{-4} (cm³/cm²) at $x = 0$
$\Delta l = 1.38 \times 10^{-4}$ (ft³/ft²) or 4.21×10^{-4} (cm³/cm²) at $x = 0.99$
$l_{D2} = 1.08 \times 10^{-4}$ (ft³/ft²) or 3.30×10^{-4} (cm³/cm²) at $x = 0$
$l_{D1} = 51.8 \times 10^{-4}$ (ft³/ft²) or 158.0×10^{-4} (cm³/cm²) at $x = 0.99$
From Equation [3] $l_{D1}/l_{D2} = 0.56$ for all x

Approximate Time-Mean Values $0 - x$

For $E = 90{,}000$:
$\overline{\Delta l} = 4.14 \times 10^{-4}$ (ft³/ft²) $= 1.26 \times 10^{-3}$ (cm³/cm²)
$\overline{l_{D1}} = 339 \times 10^{-4}$ (ft³/ft²) $= 123 \times 10^{-3}$ (cm³/cm²)
$\overline{l_{D2}} = 605 \times 10^{-4}$ (ft³/ft²) $= 183 \times 10^{-3}$ (cm³/cm²)

For $E = 59{,}600$:
$\overline{\Delta l} = 1.17 \times 10^{-4}$ (ft³/ft²) $= 0.36 \times 10^{-3}$ (cm³/cm²)
$\overline{l_{D1}} = 21.2 \times 10^{-4}$ (ft³/ft²) $= 7.74 \times 10^{-3}$ (cm³/cm²)
$\overline{l_{D2}} = 38 \times 10^{-4}$ (ft³/ft²) $= 11.5 \times 10^{-3}$ (cm³/cm²)

Discussion of Results

Since the maximum permissible l_{D1} based on the diffusion requirements of Equation [28], Table 1, is many times the maximum permissible l_{D2} and since l_{D1} from Equation [3] based on the effect of turbulence versus viscosity is much less than this, it is obvious that, for the case investigated—dodecane—diffusion conditions on the fuel side are free and easy as compared with those on the oxygen side. For the latter, results indicate the following time-mean values

$$\left.\begin{array}{l} \overline{l_{D2}} = 0.183 \text{ (cm}^3\text{/cm}^2\text{) at } E = 90{,}000 \text{ Btu/lb mol} \\ \overline{l_{D2}} = 0.0115 \text{ (cm}^3\text{/cm}^2\text{) at } E = 59{,}600 \text{ Btu/lb mol} \end{array}\right\} \quad [30]$$

If the ultimate mass elements should be thin extended slabs, the foregoing values indicate their thickness. If they are spherical, the diameters of the spheres would be 6 times the foregoing values. In any event, the foregoing is the order of magnitude of the maximum permissible depth of the diffusion layer on the oxygen side for conditions previously specified.

This means that the oxygen molecules must have a free ride by turbulence to within the foregoing distances of the terminal collision zone. Or, to state it otherwise, turbulence on the oxygen side must force a steady time-mean penetration to within the foregoing distances of the collision zone for all points on the boundary of a fuel zone. The latter obviously could be insured only if the ultimate mass elements, into which turbulence shears the air elements, themselves possess volume-surface ratios l_D of the foregoing orders of magnitude, and then only if collision-zone boundaries are kept in continuous contact with such elements. This requires a uniform distribution of the ultimate fuel and air-side mass elements among each other. This comparison is thus really between the results of macroscopically versus molecularly uniform states of distribution.

Simultaneously with the foregoing, the maximum permissible dimension l_{D1} of mass elements on the fuel side may, as previously stated, be much larger than is that of the foregoing air elements, while actually turbulence causes it to be smaller.

Although relatively large fuel-side mass elements might be maintained in diffusion flames or in the initial stages of turbulent firing, they would result in a decrease of the interface extension, thus limiting release rates on a volume basis to low values. It boils down to this: Large interface extension requires small mass elements, usually on the fuel side, because the fraction of fuel volume in the mixture is small. High energy-release rates on the volume basis require not only large interface extent but simultaneously small diffusion resistance on the oxygen side. Realization of the latter is possible only with small mass elements on the air side. A comparison of the potential for volume release rates of the macroscopically versus the molecularly uniform mixture distribution is now in order.

Relative Potential for Volume Release Rate of Macroscopic Mixtures

This is readily evaluated by means of the interface extensions existing or assigned in the two cases. For molecular uniformity, it is definite at the limiting value $(1/\Delta l)$. For the macroscopic mixture, it is represented by Equation [4] which, together with Equation [16b] for l, leads directly to

$$R_D = \frac{\alpha_1 \Delta l}{l_{D1} + \alpha_1 \Delta l / \chi_{D1}'' \chi_{D2}} \quad \ldots\ldots [31]$$

Here R_D is the ratio of the interface extension of the macroscopically uniform to that of the molecularly uniform distribution. On the basis of its development, it represents also the ratio of their volume release rates for a given temperature and pressure. It is noted that in the limit of a molecularly uniform distribution l_{D1} = zero, $\chi_{D1}\chi_{D2} = 1.00$, and R_D = unity, as it should be. Note also that for large ultimate mass elements $\alpha_1 \cong \chi_1$ and $\alpha_2 \cong \chi_2 \cong (1 - \alpha_1)$. Hence, for this case

$$\alpha_1 \Delta l / \chi_{D1}\chi_{D2} = \Delta l / \alpha_2 \quad \ldots\ldots [32]$$

For very small elements $\chi_{D1} \cong \chi_{D2} \cong 1.00$ and

$$\alpha_1 \Delta l / \chi_{D1}\chi_{D2} = \alpha_1 \Delta l \quad \ldots\ldots [33]$$

But for large masses, i.e., when l_{D1} is large compared to Δl, terms [32] and [33] have a relatively small influence on the result of Equation [31]. This is self-evident with reference to Equation [33] and becomes so with reference to Equation [32] when noting that $\alpha_2 > 0.50$ and closer to 0.90 for most hydrocarbon fuels. It is assumed, therefore, that in the computations leading to values of R_D, the product $\chi_{D1}\chi_{D2}$ may be taken at unity throughout. This assumption certainly will not disturb the order of magnitude of the result by as much as one power of ten for the large elements and should be quite close to the true facts for the small elements.

Application of the equation with these conditions then yields the results shown in Table 2. Consider the second line. The ultimate fuel mass element here has a time mean l_{D1} equal to

$$\bar{l}_{D1} = 21.2 \times 10^{-4} \text{ (ft}^3\text{/ft}^2\text{)} = 0.65 \times 10^{-3} \text{ (cm}^3\text{/cm}^3\text{)} \quad [34]$$

If these elements should be compact shapes, such as spheres or symmetrical crystals, their mean diameters would be 6 times the

TABLE 2 VALUES OF l_{D1} VERSUS R_D AND RELEASE RATES FOR DODECANE FIRED WITH 10 PER CENT EXCESS AIR

$P = 1$ atm $T = 4000$ R

$\overline{\Delta l} = 4.14 \times 10^{-5} \frac{\text{ft}^3}{\text{ft}^2}$ at $E = 90{,}000$ Btu/lb mol

$\overline{\Delta l} = 1.17 \times 10^{-6} \frac{\text{ft}^3}{\text{ft}^2}$ at $E = 59{,}600$ Btu/lb mol

Energy-release rates of uniform mixture are

16.3×10^6 for $E = 90{,}000$ Btu/lb mol
700×10^6 for $E = 59{,}600$ Btu/lb mol

Maximum permissible time-mean values of l_{D1} when release rate per unit of interface is that of uniform mixture, are

$\bar{l}_{D1} = 339 \times 10^{-5}$ ft^3/ft^2 at $E = 90{,}000$ Btu/lb mol
$\bar{l}_{D1} = 21.2 \times 10^{-5}$ ft^3/ft^2 at $E = 59{,}600$ Btu/lb mol
$\alpha_1 = 0.0102$
λ = mean free molecular-path length

$\bar{l}_{D1}$ (ft³)/(ft²) × 10⁻⁵	$\bar{l}_{D1}/\overline{\Delta l}$		$\bar{l}_{D1}$	R_D		Btu/(ft³)(hr)	
	$E = 90{,}000$	$E = 59{,}600$	λ	$E = 90{,}000$	$E = 59{,}600$	$E = 90{,}000$	$E = 59{,}600$
339.00	82.0	290	$>10^5$	1.25×10^{-4}		2.03×10^3	
21.2	5.12	18.5	10^4	1.88×10^{-3}	5.62×10^{-4}	3.07×10^4	3.93×10^3
2.12	0.512	1.85	10^3	1.95×10^{-2}	5.62×10^{-3}	3.18×10^5	3.93×10^4
0.212	0.051	0.185	10^2	1.65×10^{-1}	5.33×10^{-2}	2.70×10^6	37.3×10^4
0.0212	0.005	0.018	10	0.65	0.36	10.7×10^6	252×10^4

foregoing values, or about 0.50×10^{-2} cm. This still appears to be a very small mass element. The interface extension on the fuel side for the foregoing l_{D1}, as found from Equation [4], is of the order of 48 ft³/ft², which puts another light on the problem. That of the uniform mixture is

$$\left.\begin{aligned} A &= 2.4 \times 10^4 \text{ ft}^2/\text{ft}^3 \text{ at } E = 90{,}000 \text{ Btu/lb mol} \\ A &= 8.5 \times 10^4 \text{ ft}^2/\text{ft}^3 \text{ at } E = 59{,}600 \text{ Btu/lb mol} \end{aligned}\right\} \quad [35]$$

The energy-release rates are

$$\left.\begin{aligned} &3.07 \times 10^4 \text{ Btu/ft}^3 \times \text{hr at } E = 90{,}000 \text{ Btu/lb mol} \\ &3.93 \times 10^3 \text{ Btu/ft}^3 \times \text{hr at } E = 59{,}600 \text{ Btu/lb mol} \end{aligned}\right\} \quad [36]$$

The former appears ridiculously low. It may thus be concluded that the energy of activation for that case is too high. A recent investigation of this value for weak mixtures of kerosene in pure air leads to the result 45,500 cal/mol = 81,900 Btu/lb mol. This would yield a release rate of about 8.3×10^4 Btu/(ft³) (hr) for the conditions of the second line of Table 2, which still seems low. In this connection it is noted that the foregoing value $E = 59{,}600$ is that reported as applicable by the research laboratory of a prominent oil company, and that energy-release rates of the order of 4×10^6 Btu/(ft³) (hr) have been reported as attained in practice. If the fraction burned was 0.99, as assumed for Table 2, then the ultimate mass elements could not have been much larger than shown in the third line of this table or of the order 0.50×10^{-3} cm, which seems very small. The correct value of E thus appears to lie between the two stated values.

But for the release rates per unit of interface on which these computations are based, it has been found, in so far as tail-end diffusion limitations are concerned, that the maximum permissible l_{D1} is of the order of 21.2×10^{-5} (ft³/ft²), or it is 10 times the value which leads to the foregoing release rate of 4.6×10^6 Btu/(ft³) (lb). It is thus necessary to shrink up l_{D1} to $^1/_{10}$ of its permissible value in order to provide the interface extension required. Then, since the release rate per unit of interface remains practically unaltered with this increase, it follows that the diffusion resistance has but $^1/_{10}$ of its maximum permissible magnitude. Hence, for release rates of the order of 10^6 Btu/(ft³)(lb), tail-end diffusion takes but a negligible part in control over the reaction rate. This now rests primarily with the collision zone itself. It depends, thus, chiefly on the required magnitude of the energy of activation. The foregoing result is based on $E = 59{,}600$ Btu/lb mol. If the correct value of the latter should be 90,000 Btu/lb mol, then reference to Table 2 shows that the preceding remarks apply to energy-release rates of the order of 10^8 Btu/(ft³) (lb).

Summary

In arriving at foregoing results, conditions in the molecularly uniform mixture have been employed as a basis of reference. In particular, the release rate per unit of interface extent has served as a connecting link between the macroscopically and molecularly uniform states. These unit rates are the same in the two cases when the temperature, pressure, and air-fuel ratios are the same, the interzone depth of the macroscopic state being approximately $1/\chi_{D1}\ \chi_{D2}$ times that of the molecularly uniform state under these conditions. It is then found:

1 That the potential for release rate, on a volume basis, of the macroscopically uniform state is equal to that of the molecularly uniform mixture times the ratio of their respective interface extensions.

2 For the macroscopic case, this extension is determined by the size of the ultimate mass elements, of which the mixture is composed, and by the mol fraction α_1 or α_2 of the mixture, whichever is smaller.

3 The smaller the elements, the lower is the tail-end diffusion resistance to the reactions and the greater is the interface extent of the mixture.

4 For high release rates, the element must be so small in order to meet the needs of interface extent that the resistance offered by its tail-end diffusion to the reaction rate becomes negligible. The reaction is then primarily under control of the chemical forces at work in the collision zone. This is true for release rates of the order 10^5 and 10^6 Btu/(ft³)(lb), with energies of activation, respectively, at 90,000 and 59,000 Btu/lb mol.

5 Since the results are based on a macroscopically uniform distribution, they represent the upper limits which may be approached in practice for the conditions shown.

6 Although the results are based on dodecane, the equations employed are generally applicable to fuels involving reactions of the second order, providing $y \geq 1.00$.

7 From the point of view of largest permissible mass element, the ideal case is that in which $\alpha_1 = \alpha_2$. This permits closest approach to the potential release rate of the molecularly uniform mixture by the macroscopically uniform mixture for any given size of mass element, since it provides the greatest interface extension for a given size mass element. It is noted that in this scale dodecane ranks low, since for it $\alpha_1 = 0.01$ with $y = 1.1$. Methane, for which $\alpha_1 = 0.087$ with $y = 1.1$, thus ranks much higher.

8 In setting up conditions for comparisons which have been made, the flame temperature has been considered as constant throughout volume, thus reducing thermal conduction between interzone and diffusion layers to zero and thereby avoiding the necessity of inclusion of a special term to represent this process. Investigation of the influence of such thermal conduction[3] as may exist indicates that the assumption which reduces it to zero

will not disturb the order of magnitude of the results disclosed.

This concludes the general review and leads to a few additional comments concerning the mass elements themselves.

Special Characteristics of the Mass Elements

It has been shown how the size l_D of a mass element may be related to the potential of the macroscopic mixture volume for energy-release rate. But nothing has been said about certain special kinds of elements such as, for example, vortex motion at the boundaries of the interzone. The latter could show up only as its effects on l_D in this analysis. A free vortex would, no doubt, have a relatively small tail-end diffusion thickness l_D, since now molecular transport from within it must be strongly aided by the interior turbulence existing within the element itself. This, of course, would tend to speed up the reaction rate by reducing the resistance in the tail-end diffusion and possibly also by increasing the interface extent—a considerably more powerful effect.

As to most probable shape of element, it must lie between that of a sphere and a thin extended slab. Whatever it may be, the order of magnitude of its effect is included by l_D, the latter being interpreted as the hydraulic mean depth of the element.

As implied, there is a range of sizes as to element below which the state of uniform distribution is imminent. Equation [2*d*] of reference[3] may provide a clue to this. This formula, as set up, states the rate of volume traversed by a molecule. Although developed with reference to a uniform distribution for dodecane in furnace gases, it may be applied to dodecane in the fuel mass element itself by including the value of R_λ for this case. It then represents the rate of volume traverse of a dodecane molecule in dodecane. The time required to traverse the fuel mass element is thus

$$\Delta\theta_D = v_D/\Delta V \text{ sec} \quad [37]$$

where v_D is the volume of the fuel mass element and ΔV the volume from Equation [2*d*] of reference[3] for time $\Delta\theta$ equal to 1 sec. Then $\Delta\theta_D$ is the average time required for a molecule to traverse volume v_D of the element. On this basis it is found for cubical v_D

$$\left.\begin{aligned} \theta_D &= 10^2 \text{ sec for } l_{D1} = 6.5 \times 10^{-2} \text{ (cm}^3\text{/cm}^2\text{)} \\ \theta_D &= 10^{-1} \text{ sec for } l_{D1} = 6.5 \times 10^{-3} \text{ (cm}^3\text{/cm}^2\text{)} \\ \theta_D &= 10^{-4} \text{ sec for } l_D = 6.5 \times 10^{-4} \text{ (cm}^3\text{/cm}^3\text{)} \\ \theta_D &= 10^{-7} \text{ sec for } l_{D1} = 6.5 \times 10^{-5} \text{ (cm}^3\text{/cm}^2\text{)} \end{aligned}\right\} \quad [38]$$

Thus it appears that, with respect to most combustion processes, a molecularly uniform mixture is imminent when

$$\bar{l}_{D1} \cong 6.5 \times 10^{-4} \text{ (cm}^3\text{/cm}^2\text{)} = 2.12 \times 10^{-5} \text{ (ft}^3\text{/ft}^2\text{)}. \quad [39]$$

Reference to Table 2 indicates this to be when $\bar{l}_{D1}$ is of the same order of magnitude as is Δl for the conditions of this problem. The results indicate also that an element requiring 10^2 sec is not large; i.e., about 0.065 cm for l_D, thus indicating the large amount of time which would be required for diffusion alone to attain a uniform distribution from large-scale mass elements.

Finally, it may be of interest to call attention to the distribution pattern illustrated in Fig. 4(B), where fuel elements shown in Fig. 4(A) have, in some manner, managed to distribute themselves between ultimate air elements as shown, even though α_1 might have been much less than α_2. The interface extension is now of the same magnitude with respect to either fuel or air mass elements; i.e., $A_1 = A_2$. The question is: What, if any, special conditions could make this possible? Comparison of Equation [7] with its companion for air elements leads to the result

$$A_1 = A_2 \text{ when } l_{D1}/l_{D2} = \frac{\alpha_1}{\alpha_2} \quad [40]$$

and reference to Equation [3] shows that this requirement is met when

$$\mu_1/\mu_2 = \alpha_1/\alpha_2 \quad [41]$$

This, then, is a necessary condition for $A_1 = A_2$. Reference to the second term on the right of Equation [3] indicates almost at a glance the probability of ever satisfying this condition to be very low when $\alpha_1 << \alpha_2$ or when $\alpha_2 << \alpha_1$. As an example, for dodecane $\alpha_1/\alpha_2 \cong 0.01$, whereas $\mu_1/\mu_2 \cong 0.50$. It would thus appear as though the distribution shown Fig. 4(B) is in the nature of an accident which may never occur.

A special case of the foregoing is that where

$$\mu_1 = \mu_2 \text{ and } \alpha_1 = \alpha_2 \quad [42]$$

Under these conditions, the distribution pattern would be as shown in Fig. 4(B), but the volumes occupied by air and fuel elements would be equal to each other. This is an upper limiting ideal-distribution pattern with reference to the potential for volume release rates expressed as a fraction of that possible for the molecularly uniform mixture.

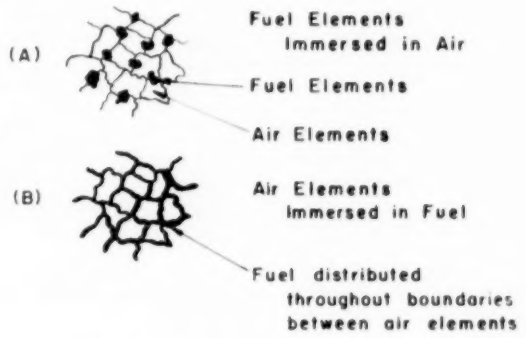

Fig. 4 Possible Distribution Pattern for $\mu_1/\mu_2 = \alpha_1/\alpha_2$

Finally, it is pointed out that when $\alpha_1 \cong \alpha_2$, the question of interference for contacts between a given mass element and those of the other class by contact between the given elements and others of its own class may have an appreciable effect on the result. In the foregoing discussion, it has been assumed that this factor is negligible. It no doubt is so when either is small compared to unity. However, if $\alpha_1 = \alpha_2$, it appears reasonable that a given mass element will have its potential interzone boundary occupied about one half of the time by other elements of its own class. Hence, the time-mean value of the interface extension of an otherwise uniform macroscopic distribution would, in such cases, be one half that which has been assumed; i.e., one half that which would be possible if the element distribution were considered frozen in a distribution containing no such interference.

From the foregoing point of view, the free fraction (multiplying factor) is, in general, equal to $(1 - \alpha)$ where α is the smaller of the two mixture fractions. But the smaller α varies between 0 and 0.50 and so the limits of variations of $(1 - \alpha)$ are from 0.50 to unity. Thus it is seen that omission of this effect does not disturb the order of magnitude of the results. There is, of course, no good reason why it should not be included, since it is so simple both as to itself and as to its application. For the case investigated, dodecane with $y = 1.1$, its value is $(1 - 0.01) = 0.99$. Considering the nature of the results, the departure from unity is in this case, of course, quite insignificant.

Discussion

F. W. Bailey.[8] The concept of reaction interface extension as developed by the author permits a useful and interesting insight into technical combustion problems. This analysis emphasizes the parameters of importance in combustion-chamber design and indicates the limiting performance of a combustion chamber when the size of its mass elements is prescribed. The method of analysis which the author has formulated may incorporate other refinements which eventually develop from studies of combustion kinetics and turbulent flow. At the present stage of the combustion-chamber art, however, an extensive study of this type is woefully needed to bring the various facets of the problem into proper focus and to assist in the design of future experiments.

[8] Research Division, Curtiss-Wright Corporation, Wood-Ridge, N. J.

Author's Closure

The author is indebted to Mr. Bailey for his generous evaluation of the possible importance of the parameters disclosed in the paper. It may be appropriate at this time to say that two other investigators who are well versed in combustion theory and experiment have expressed themselves along similar lines, in letters on the subject, addressed to the authors.

Pulverized-Coal-Fired Gasifier for Production of Carbon Monoxide and Hydrogen

By P. R. GROSSMAN[1] and R. W. CURTIS,[2] ALLIANCE, OHIO

This paper describes a pilot-plant pulverized-coal gasifier installed at the Morgantown Station of the Bureau of Mines and a semicommercial gasifier of similar design installed at the E. I. du Pont de Nemours & Company, Inc., Belle, West Virginia. A brief summary of the operating data obtained from these two units is presented and material requirements are given for this method of coal gasification. A large size unit of this design is now under construction and will go into operation next year. This will be the first commercial application of the process in this country. Details of the design that provide for handling of coal ash of widely varying fusing temperatures are given in an effort to point out those features which have contributed to continuous uninterrupted operation. Included also is a discussion of heat flow within the gasification unit to illustrate the factors involved in obtaining an economical process.

Introduction

With present-day demands for large quantities of ammonia, methanol, nylon, and many other chemicals, as well as future needs for synthetic-liquid fuels, it is essential that an efficient and economical method be developed for supplying synthesis gas, the basic raw material for these products. The term "synthesis gas," as used in this paper, refers to a gaseous mixture composed of carbon monoxide and hydrogen in varying proportions. This gas may be obtained by the partial combustion of various hydrocarbons. Of all the available hydrocarbons that are suitable for this application, coal alone appears to be in plentiful supply at low cost in the sections of the country where synthesis gas is required. For this reason, considerable effort has been expended to develop an efficient and economical process using coal as the base material for its production. The use of coal for the production of gas is not new since coke ovens and water-gas sets have been operated for this purpose for many years. However, the process has been costly because of the large capital expenditures for coke ovens and the fact that in this method two separate stages are required to produce synthesis gas.

In recent years many investigations have been carried on in an effort to develop a continuous process that will use coal and produce carbon monoxide and hydrogen inexpensively. These investigations have led to the development of the B&W pulverized-coal gasifier in which pulverized coal reacts with oxygen and steam in a continuous process to produce synthesis gas. This is a new application of pulverized-coal combustion, which uses a number of the basic fundamentals from a wide experience in pulverized-coal-firing of slag-tap steam-boiler furnaces.

In comparing the conventional pulverized-coal furnace to the gasifier it will be seen that while there are some points of similarity, there also are outstanding differences. In both applications carbon reacts with oxygen; however, the processes operate with different oxygen-carbon ratios. The normal combustion process uses some excess oxygen while gasification operates with excess carbon. In both cases it is desired to keep the excess constituent to a minimum, but there are practical limitations of the extent to which this can be accomplished. Since furnace-temperature conditions are similar in each type of combustion, it has been possible to adapt, for use in the gasifier, the fundamental principles of ash handling of a conventional slag tap pulverized-coal furnace.

With tonnage oxygen now available to industry at a reasonable cost there is every reason to believe that the pulverized-coal-fired gasifier will be able to produce synthesis gas at a cost much lower than the present cost of water gas. At the same time pulverized-coal gasification will extend the range of coal suitable for this production because the coking properties of the coal will not be a limiting factor. These statements are based on experience gained during extensive pilot-plant testing with the pulverized-coal-fired gasifier.

Pilot-Plant Experience

The first pilot plant shown in Fig. 1 was designed and constructed by the authors' company and was erected at the Bureau

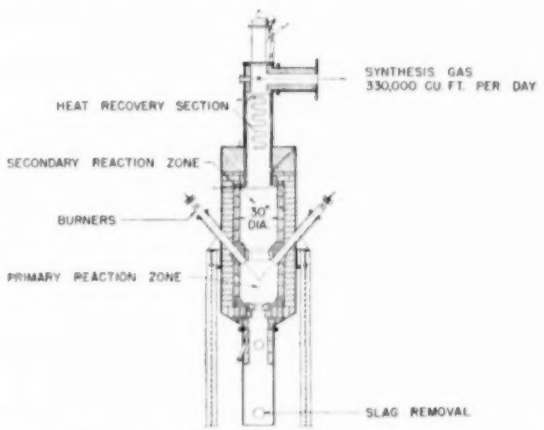

Fig. 1 Pulverized-Coal Gasifier Pilot Plant at U. S. Bureau of Mines, Morgantown, W. Va.

of Mines' Station at Morgantown, West Virginia. This unit went into service in the summer of 1951 and since that date has been operated on a co-operative basis with the Bureau of Mines. It has a nominal rating of 500 lb of coal per hr, producing about 330,000 cu ft of carbon monoxide and hydrogen per 24-hr day. Up to the present time it has produced gas for a total of about 1200 hr. Most of the tests have been of short duration for the purpose of investigating a large number of variables; however, one test of 296-hr duration has been made. The operation of this

[1] Superintendent, Product Development, The Babcock & Wilcox Company, Research Center. Assoc. Mem. ASME.

[2] Test Engineer, Product Development, The Babcock & Wilcox Company, Research Center.

Contributed by the Fuels Division and presented at a joint session of the Fuels and Oil and Gas Power Divisions at the Annual Meeting, New York, N. Y., November 29–December 4, 1953, of The American Society of Mechanical Engineers.

Note: Statements and opinions advanced in papers are to be understood as individual expressions of their authors and not those of the Society. Manuscript received at ASME Headquarters, July 1, 1953. Paper No. 53—A-49.

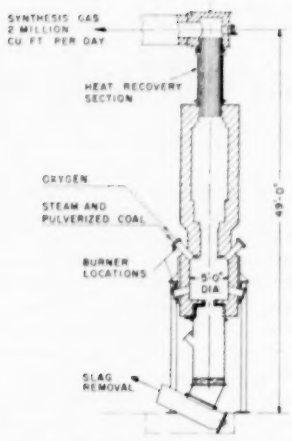

FIG. 2 PULVERIZED-COAL GASIFIER PILOT PLANT AT E. I. DU PONT COMPANY, INC., BELLE, W. VA.

gasifier has been highly successful and a large amount of performance data has been obtained. These data have been presented[2] by the Bureau of Mines and will be published as a "Report of Investigations."

A larger size, semiplant-scale unit of B&W design has been installed by the du Pont Company at its Belle Works in West Virginia. This gasifier, shown in Fig. 2, went into service in October, 1951, and has operated for more than 5000 hr, during most of which it produced gas utilized in the operation of the Belle Works. The unit has a rating of approximately 3000 lb of coal per hr and will produce over 2,000,000 cu ft of carbon monoxide and hydrogen per 24-hr day. As far as we now know, this plant is the largest pulverized-coal gasifier that has been installed in this country and is the first unit that has operated continuously for an extended period of time.

The Bureau of Mines and the du Pont units are quite similar, each being fired with two burners, through which pulverized coal, oxygen, and superheated steam are introduced into a refractory-lined furnace. The combustion chamber is divided into a primary and a secondary zone. In the lower or primary zone the temperatures are sufficiently high to melt the coal ash, and molten slag is continuously tapped from the bottom of the chamber. This molten slag drops into a water tank where it is solidified and fractured into small-size particles which are then removed by suitable conveying equipment. The secondary zone is designed for lower gas temperatures and the accommodation of ash in a semiplastic state. A small heat-recovery section has been installed at the top of the unit to simulate a waste-heat boiler. This arrangement makes it possible to study thoroughly the nature and characteristics of the ash deposits.

The dry-gas analysis from these units normally consists of about 40 per cent hydrogen, 40 per cent carbon monoxide, 15 per cent carbon dioxide, less than 1 per cent methane, and approximately 4 per cent inerts. This analysis will vary slightly with changes in operating conditions.

OPERATING CHARACTERISTICS

As a result of the experience gained on these pilot plants, the general operating characteristics of a pulverized-coal gasifier of the type shown have been established. Table 1 shows the wide range of coal that has been tested. It will be seen that coal of various ranks from anthracite through bituminous and subbituminous has been used. This coal has come from widely scattered sections of the country and represents wide ranges in ash-fusing temperatures, volatile matter, and fixed carbon content. From operating experience it is quite evident that the use of the gasifier need not be restricted to any one section of the country where a specific type of coal is available, but may be adapted to fire practically any coal, with the exception of extremely high-ash-fusing temperature coal found in some locations.

TABLE 1 RANGE OF COAL TESTED IN B&W PULVERIZED-COAL GASIFIERS

Types of coal	Ash-fusing temp, deg F — Oxidizing	Ash-fusing temp, deg F — Reducing	Volatile matter, per cent	Total carbon per cent
Anthracite:				
Pennsylvania	2620	2550	7.2	83.4
Bituminous:				
West Virginia—medium volatile, high fusing	2900 +	2840	33.5	71.3
Western Kentucky—medium volatile, medium fusing	2340	2235	34.1	58.7
Washington—high volatile, medium fusing	2340	2290	39.1	72.7
Subbituminous or lignite:				
Wyoming	2230	2070	42.2	64

TABLE 2 TYPICAL OPERATING RESULTS

Coal fired	Morgantown gasifier — Sewickley Seam W. Va.	du Pont gasifier — Valley Camp Coal Company No. 2 Gas Seam W. Va.
Ultimate analysis, per cent:		
C	71.7	80.7
H_2	4.7	5.4
O_2 (by diff)	6.2	8.2
N_2	1.3	1.6
S	1.5	0.8
Ash	14.6	3.3
Coal rate, lb/hr	467	2620
Oxygen rate, cfh	4100	26100
Steam rate lb/hr	270	2290
Oxygen-coal ratio cu ft/lb	8.7	9.95
Steam-coal ratio, lb/lb	0.58	0.88
Oxygen inlet temp, F	516	95
Steam inlet temp, F	516	325
Coal inlet temp, F	292	325
Gas analysis, per cent by vol dry basis:		
CO_2	14.8	16.2
CO	44.2	40.2
H_2	38.7	39.4
CH_4	0.4	0.7
O_2	0.1	0.2
Ill	0.5	0.4
N_2 (by diff)	1.3	2.9
Per cent C gasified	85.2	84.1
Requirements/1000 cu ft CO + H_2:		
Coal, lb	39.6	33.9
Oxygen, cu ft	338	337

All gas volumes calculated at 60 F and 29.92 in. Hg.

Typical operating results for these two gasifiers are shown in Table 2 for the particular coal listed. It will be seen that the results from the two gasifiers are similar. The percentage of carbon gasified in each case is approximately the same since the testing was done at a carbon gasification near the optimum point. The amount of oxygen required per thousand cubic feet of carbon monoxide and hydrogen is almost identical. The coal requirements, however, are different. Since this difference is due almost entirely to the carbon content of the two kinds of coal, on an equivalent carbon basis the requirements would be very nearly the same.

A review of the work of others[4] in pulverized-coal gasification has indicated that difficulty has been experienced in handling coal with widely varying ash-fusing temperatures. For this reason it will be worth while to examine here the features of the B&W gasifier that have enabled it to operate successfully as a slag-tap type of furnace.

[2] "The Gasification of Pulverized Coal With Steam and Oxygen at Atmospheric Pressure," by G. R. Strimbeck, et al., presented before the American Gas Association Production and Chemical Conference, New York, N. Y., May 25, 1953.

[4] Bureau of Mines Information Circular No. 7415, November, 1947.

The gasification process operates with a temperature-time relationship as shown in Fig. 3. It will be seen that the temperature immediately adjacent to the burner tip rises sharply in the zone where the reactions are predominantly exothermic and then falls off quite rapidly because of the preponderance of endothermic reactions. This curve is not meant to show exact temperatures throughout the reactor but to indicate that the temperature is above the ash-fusing point during most of the process. It should be remembered that the gasifier operates under reducing conditions where the ash-fusing temperature may be as much as 400 F lower than it would be under oxidizing conditions. Fig. 4 illustrates this point by showing a plot of fusing temperatures for a wide range of coal ash of varying iron content. It will be seen that the iron content of coal ash is a major cause in lowering the ash-fusing temperature under reducing conditions. The two factors of temperature level required for the process and fusing temperature of the coal ash both point to the slag-tap type of operation as most suitable for handling the coal ash. Operation of the pilot units also has indicated that the most economical production of synthesis gas is obtained with highest temperatures in the primary reaction zone of the gasifier.

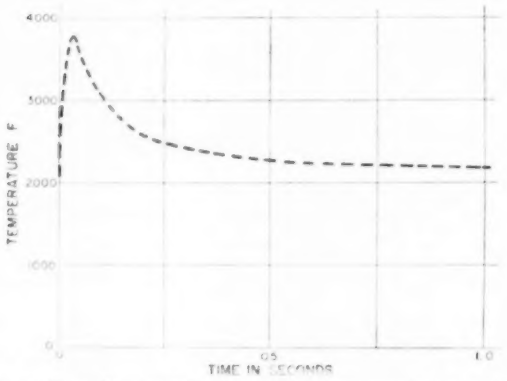

FIG. 3 TIME VERSUS TEMPERATURE FOR PULVERIZED-COAL GASIFICATION

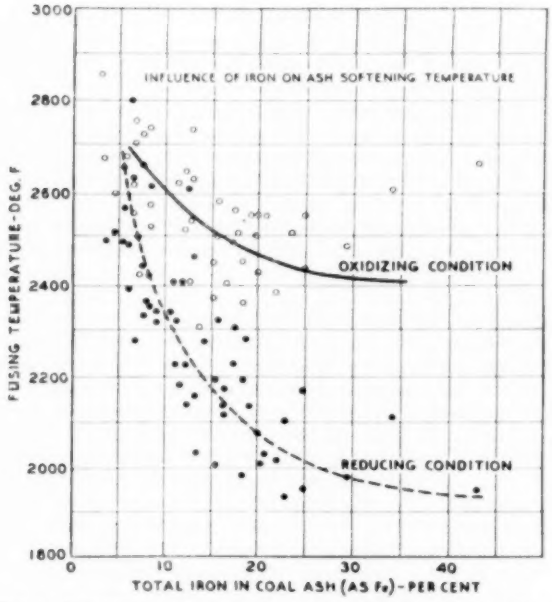

FIG. 4 INFLUENCE OF IRON ON COAL ASH-SOFTENING TEMPERATURE

Another factor to be considered in the production of a high-quality synthesis gas is the distribution of heat within the process. Heat is required to raise the incoming reactants to the optimum temperature level for the gas-making reactions. Most of this heat is produced by the exothermic reaction between carbon and oxygen to make carbon dioxide which usually would be considered as an impurity in the product gas. Obviously, it is therefore economically desirable to reduce the need for this exothermic reaction as much as possible. This is a major point of contrast to the normal boiler furnace where it is desired to convert all of the energy of the fuel into sensible heat in the product gas and then convert this sensible heat into steam.

In the modern boiler furnace about half of the heat in the fuel is absorbed by the furnace. This corresponds to a heat absorption of 5000 to 7000 Btu per lb of coal. Most of this heat is transferred from the products of combustion to the furnace walls in the temperature range above 2000 F. In the gasifier it is in this range that the endothermic reactions take place and it is here that the maximum heat utilization is required for the gas-making process and a minimum heat loss to the walls is desirable.

Fig. 5 shows the increased costs of the process when heat is lost by radiation to the walls of the reaction chamber. It can be seen that a heat loss of 1000 Btu per lb of coal will increase the material costs per 1000 cu ft of synthesis gas by more than 25 per cent. It is this high cost of heat loss that necessitates the use of a refractory-lined furnace to keep heat absorption to a minimum. It is expected that a full-scale gasifier will operate with a heat loss to the furnace walls of about 200 Btu per lb of coal. In order to insure this low heat loss a refractory lining is used in both the primary and secondary zones of the gasifier. This use of refractory presents a wear problem and periodic replacement will be required. Nevertheless its use is economically justified on the basis of material costs as shown in Fig. 5.

Heat distribution within the gasification process is an important factor in the economy of the operation and in this respect

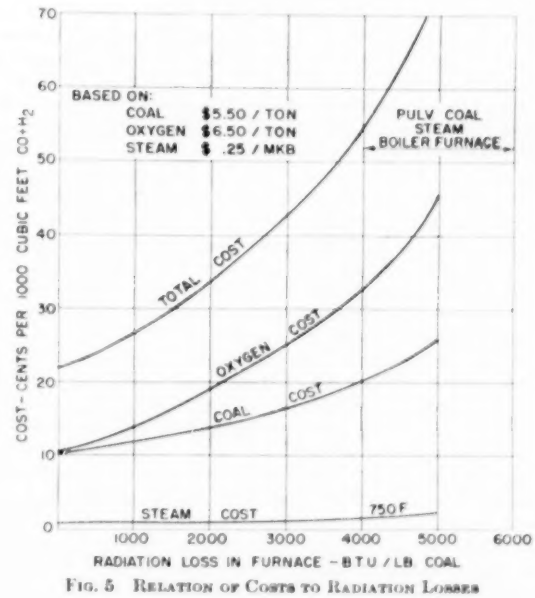

FIG. 5 RELATION OF COSTS TO RADIATION LOSSES

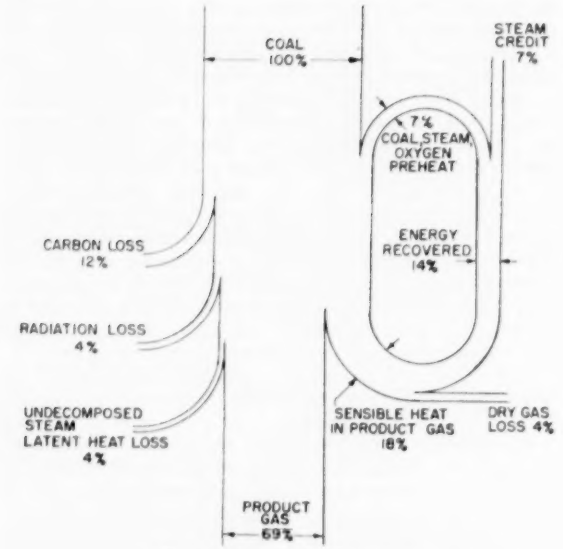

FIG. 6 HEAT-FLOW DIAGRAM

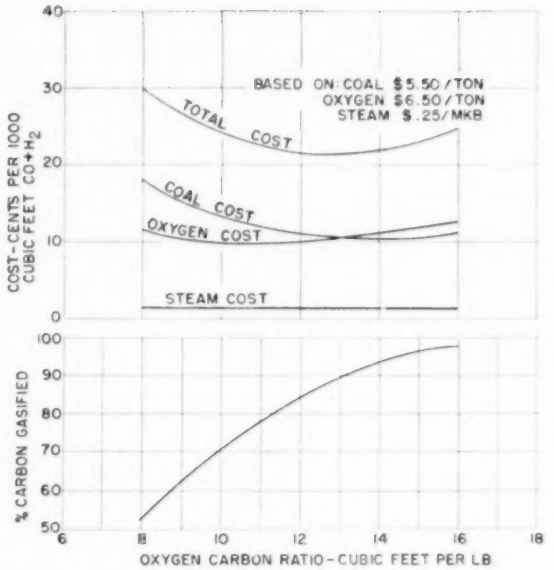

FIG. 7 PULVERIZED-COAL GASIFICATION OPERATING CHARACTERISTICS

it differs from the conventional water-gas process. Fig. 6 is a plot of heat flow within the process. It will be seen that a cold-gas efficiency of about 69 per cent can be expected. This means that 69 per cent of the coal heating value is obtained in the calorific content of the product gas. Sensible heat in the product gas represents 18 per cent of the heat in the coal. Of this, 14 per cent can be recovered in a waste heat boiler and the remaining 4 per cent is lost in the water-scrubbing operation that follows the gasifier. Of the 14 per cent recovered, about 7 per cent is recycled to the process in the form of heated coal, steam, and oxygen. These values are based on practical temperature levels of 300 F for coal, 750 F for steam, and 500 F for oxygen. The remaining 7 per cent of the heat leaves the process as steam that is available for use elsewhere in the plant.

The inherent losses consist of three major items; i.e. (1) latent heat in the unreacted steam, (2) radiation loss, (3) carbon loss. In order to obtain an efficient steam-carbon reaction and at the same time control temperature within the reactor, an excess of process steam is supplied. The portion of this steam that does not enter into the reaction leaves the gasifier at a higher temperature than it had upon entering. This represents a heat loss to the process. This loss could be reduced by using less process steam; however this also would reduce the amount of the steam-carbon gas-making reaction. The optimum steam requirement has been found to be about 0.6 lb of steam per lb of coal. Since the steam-coal ratio also can affect the hydrogen-carbon monoxide ratio and the temperature level within the gasifier, in certain applications it may be found desirable to vary this ratio to meet special operating requirements.

The 12 per cent carbon loss appears to be high at first glance, but actually it can be varied and may range from 5 to 15 per cent. The determining factor with regard to carbon loss is a question of economics. Fig. 7 shows the percentage of carbon gasified and the material cost per 1000 cu ft of $CO + H_2$ plotted against the oxygen-carbon ratio. It may be seen that for the cost figures chosen ($5.50 per ton for coal, $6.50 per ton for oxygen, and $0.25 per million Btu for steam) the minimum total material cost occurs at about 88 per cent carbon gasified. It is evident that by increasing the oxygen-carbon ratio the per cent carbon gasified may be increased but it is usually not economical to do so. The curves show that the material costs are divided roughly into 50 per cent for coal, 45 per cent for oxygen, and 5 per cent for steam. For different unit costs for these materials the optimum point may shift slightly but in general it will lie between 80 and 95 per cent carbon gasified for most conditions.

The 4 per cent radiation loss would appear to be insignificant to the over-all process, but, since heat loss in any form is an important factor in gasification, we shall consider in detail that portion of the total heat loss that is due to radiation, even though it is relatively small. This loss is made up of radiation from the casing, loss to water-cooled burners, slag coils, and so on. Since heat can be added to the process to offset any loss, consideration was given to various methods by which this could be accomplished. One of these is by preheating the incoming reactants. There are, however, economical limits to the extent to which this is practical. In order to investigate the economics of using superheated steam to furnish heat to the process, the Bureau of Mines at the Morgantown Station used steam ranging from 240 F to 2900 F.[4] Fig. 8 shows the material cost of the constituents at four different temperatures. It is evident that the most economical operation is obtained when steam is heated to approximately 1000 F. The reason for this is that when higher steam temperatures are used it is necessary to use a clean fuel with a more expensive heat exchanger of alloy or refractory construction. Thus, the savings realized in oxygen and coal consumption are outweighed by the increase in steam cost.

In designing the gasifier an effort has been made to attain the utmost process economy while at the same time making the gasifier itself reliable and inexpensive. It was pointed out previously in Fig. 3, that the exit-gas temperature from the gasification chamber is 2000–2400 F. This temperature range corresponds closely to that leaving a boiler furnace and for that reason the convection surfaces of the two types of units are similar.

Fig. 9 shows a sectional view of a slag-tap boiler furnace and typical temperature contours are indicated. It will be seen that

[4] Bureau of Mines Report of Investigations Number 4733, "Pilot-Plant Gasification of Pulverized Coal With Oxygen and Highly Superheated Steam," by G. R. Strimbeck, et al.

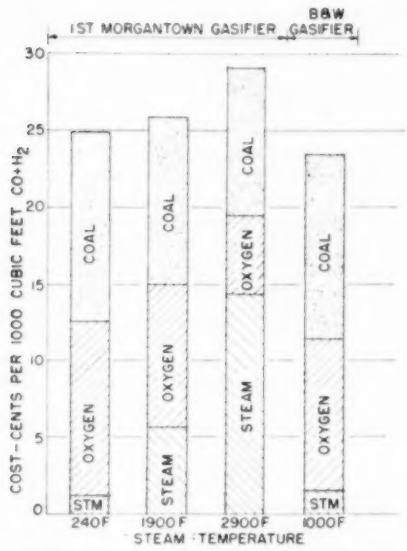

FIG. 8 COST OF CONSTITUENTS AT VARIOUS STEAM TEMPERATURES

the temperature entering the convection bank is about 2000 F. It also should be noted that the furnace is divided into primary and secondary zones to facilitate slag-tapping from the primary furnace. In this arrangement the burners are located near to and fire in the general direction of, the tap hole. This has been found to be essential if trouble-free operation of the slag-tap type of furnace is to be obtained. It is for this reason that the gasifier was constructed with the same general arrangement of divided furnace with burners located near the tap hole.

FULL-SCALE PLANT DESIGN

Fig. 10 shows a schematic layout of a full-scale gasification plant with a capacity of about 17 tons of coal per hr and capable of producing 25,000,000 cu ft of carbon monoxide and hydrogen per 24-hr day. The layout shown includes the equipment to handle coal, oxygen, and boiler feedwater for the production of synthesis gas and excess steam. The auxiliary equipment for coal and ash handling such as coal scales, feeders, rotary seals, pulverizers, and slag-removal equipment are all standard pieces of equipment that are in use on central-station boilers. One variation from normal boiler practice is the use of steam to sweep the pulverizer instead of the customary primary air. Steam for drying the coal within the pulverizer and conveying it to the burners has been tried and gives equal or better performance than does the use of air.

The gasifier itself is of circular cross section and consists of the reaction chambers, waste-heat boiler, superheater, and economizer. The convection surfaces are in no way different from those normally employed in a boiler although their arrangement may be varied somewhat. The reaction chambers themselves do differ from normal boiler furnaces in that they are refractory-lined. In addition, their design is such that maximum usage can be made of the furnace volume and slag may be handled in a satisfactory manner. The lower or primary zone operates with a layer of liquid slag covering the refractory surfaces and is therefore subject to the chemical and erosive action of this slag. Because a gradual loss of brickwork does occur, periodic replacement is necessary. However, this is confined to the primary reaction zone and might well be restricted to only a portion of it. Since refractory wear is present it is necessary that a durable structure be built to withstand these erosive conditions in the event of complete refractory failure in some zone. To accomplish this the generator is constructed of boiler tubes with metal studs and plastic chrome ore applied as a monolithic structure. This type of construction has been widely used in boiler furnaces and has been capable of withstanding continuous operation with slag flowing over the chrome-ore surface. The entire gasifier is encased in a pressure casing to prevent any leakage of product gas from the unit.

The convection bank of the boiler consists of a simple two-drum crossflow boiler with no baffling. This is a well-proved design that is not subject to build up of flyash and carbon since there are no baffles. The boiler is integral with and located at the top of the generator. At the temperature which exists at the exit of the reaction zone, the ash may be in the transition state between fluid and solid and for this reason the convection surfaces are arranged so that any deposits will be shed by gravity or can be blown by sootblowers back into the high-temperature melting zone where they can be tapped as slag.

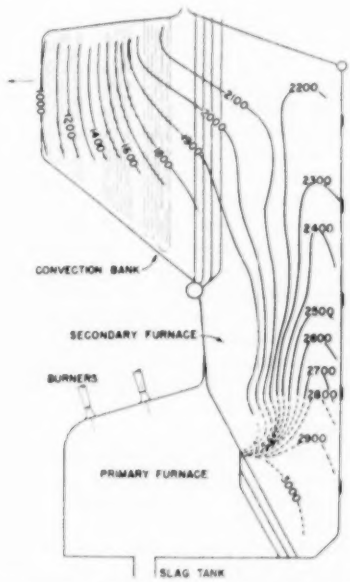

FIG. 9 TEMPERATURE GRADIENTS IN SLAG-TAP BOILER FURNACE

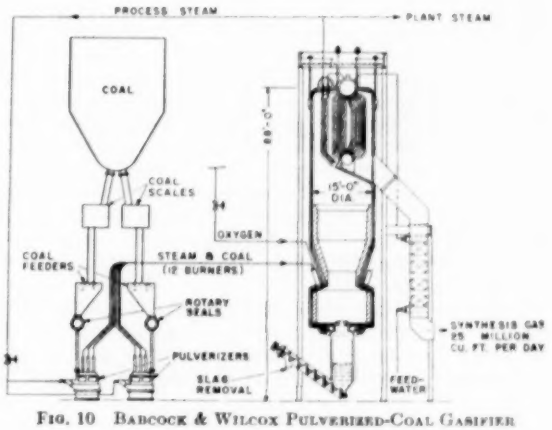

FIG. 10 BABCOCK & WILCOX PULVERIZED-COAL GASIFIER

The design of this unit incorporates fundamental principles of pulverized-coal combustion under a wide variety of conditions. The successful operation of the pilot plants is proof that the design is sound and should provide a method of coal utilization that will expand greatly the usage of coal as an economic raw material for many products. This can be done only by providing reliable service at low operating and material cost. We have every reason to believe that this design will meet these conditions and that the pulverized-coal gasifier will find acceptance in industry in the same manner as pulverized-coal-fired central-station boilers.

Acknowledgment

The information presented in this paper includes data from the U. S. Bureau of Mines and from the E. I. du Pont de Nemours & Company, Inc. To these organizations the authors wish to express appreciation. Technical contributions were made by a number of our associates within The Babcock & Wilcox Company and their contributions are gratefully acknowledged.

Discussion

Fred Denig.[6] The pulverized-coal gasifier promises to become one of the most important developments of this decade inasmuch as it will make available blue gas made economically from the so-called low grades of coal. This blue gas, or synthesis gas, as it is sometimes called, is a building block for several important chemicals, and it also may find extensive uses in reduction of ores or for manufacture of substitutes for natural gas as natural-gas supplies dry up or become excessively expensive.

The pulverized-coal gasifier came into being because of the European necessity to find a method of gasifying lignite, brown coal, and similar low-grade fuels, largely in connection with manufacture of synthetic liquid fuels or synthetic ammonia.

The development work of the German firm Koppers GmbH was brought to America by The Koppers Company of Pittsburgh, who, in turn, built in 1949 the world's first semicommercial plant for the U. S. Bureau of Mines at Louisiana, Mo., for all to see and study. The first hours of operation demonstrated that gas could be produced successfully by this technique. Later studies on this unit indicated some of the slag problems that the authors discuss. The experience at Louisiana has been useful to all students of total gasification and it is to be regretted that the Bureau of Mines did not follow up a more vigorous policy of operating the Lamo Plant for months at a time.

The German Koppers firm has built an installation at Oulu, Finland, consisting of three gasifiers, each of which will gasify 60 tons of coal per day, whose ash-fusion point is approximately 2130 F. The Koppers system allows such ash as will to leave the generator in dust form where it is removed by adequate means. The heavier particles that fall to the bottom are taken out as a quenched slag through a water layer. Thus it can be seen that Koppers system will handle high or low-fusion-ash coal with equal effectiveness. The Oulu plant operates with great ease and it has now over a year's experience. Two other such plants are now under construction outside of America. The Oulu plant encountered some refractory trouble but it is believed that these problems are now solved and the Oulu management has ordered two more Koppers-Totzek gasifiers in order to double their synthetic-ammonia capacity.

There are two differences in the total gasification plants offered by B&W and Koppers. First, as near as can be determined from the public expressions of the author and his associates, they plan to throw down as much ash as possible in the bottom of the gasifier and remove it either in the molten form or in the granulated form. On the other hand, Koppers allows the fine ash either to drop down and become a granulated slag in a water pit or as much as will can go out with the gas stream and be removed in the following equipment.

The second main difference is even more important and probably will prove governing as time goes on. It is Koppers' philosophy to blow the coal into the gasifier with the entire oxygen stream and only a small amount of steam, the bulk of the steam being added separately to the gasification flame, resulting in a better quality of gas. By better quality is meant the Koppers gas is free from methane and unsaturates. This is exceedingly important in high-pressure chemical work since the unsaturates will probably interfere with the catalytic process, and also, the volume of residual methane and unsaturates will build up and necessitate a heavy bleedoff in the recycle stream. The analysis in Table 3, herewith, will indicate the difference.

TABLE 3 COMPARATIVE GAS ANALYSES

	B&W at Du Pont	Koppers at Oulu
CO_2	16.2	12.6
CO	40.2	51.1
H_2	39.4	34.0
CH_4	.7	<0.1 to 0.0
O_2	.2	Trace
Ill	0.4	None
N_2	2.9	1.9
Per C gasified	84.1	85.0

Several questions present themselves to our minds as we follow this paper:

1 What is the pulverization of the coal used in the B&W gasifier?

2 What is the pressure and temperature within the pulverizer?

3 Is all of the gasifier steam requirement put through the pulverizer?

4 What quality of refractory is used in the primary cooler?

5 Is limestone or some other material mixed with the coal in order to render the slag more fluid?

6 Is any carbon carried out with the liquid slag or is the carbon particle falling on the molten slag gasified at once?

7 What is the screen size of the entrained coal residue leaving the unit and is the unconsumed carbon finally taken out with water, and if so, what is the settling time?

Wilhelm Gumz.[7] This paper is greatly appreciated as a firsthand account on a semicommercial-scale pulverized-coal gasifier, and as an opportunity to check on a method of calculation published recently.[8] By a series of calculations the "reaction temperatures" (as defined in reference[8]) were found to be 622 and 1170 C, respectively. With these reference temperatures, gas composition as well as coal, steam, and oxygen requirements were found in reasonable agreement with experimental data and within the limits of accuracy to be expected, Table 4, herewith. Deviation of methane content and the presence of illuminants are supposed to be caused by delayed devolatilization of the coarsest particles.

In evaluating these results, a higher reaction temperature seems to be advisable which could be obtained easily by a higher oxygen-steam ratio without increasing oxygen consumption per SCF of CO + H_2. Higher operating temperatures, however, possibly would decrease life expectancy of the lining which is

[6] Vice-President, Koppers Company, Pittsburgh, Pa. Mem. ASME.

[7] Steinkohlenbergbauverein, Essen, Germany. Mem. ASME.

[8] "A Critical Survey of Methods of Making a High BTU Gas From Coal," by Wilhelm Gumz and J. F. Fosher, Research Bulletin No. 6, The Gas Production Committee, American Gas Association, New York, N. Y., July, 1953.

TABLE 4 COMPARISON OF CALCULATED AND EXPERIMENTAL DATA

(Pilot Plant at E. I. du Pont Company, Inc., Belle, W. Va.)

Gas composition (dry basis), per cent	Calculated	Experimental	
		As reported	O_2-Ill-free basis
CO	40.59	40.2	40.5
CO_2	16.82	16.2	16.3
H_2	39.68	39.4	39.6
CH_4	0.07	0.7	0.7
H_2S	0.21	...	..
COS	0.01	...	..
N_2	2.62	2.9	2.9
Ill	...	0.4	..
O_2	...	0.2	..
Requirements per 1000 SCF CO + H_2			
Coal, lb	34.3	33.9	
Oxygen (100%), SCF	350	337	
Steam, lb	30.7	29.8	

one of the main reasons why pulverized-coal gasification is recommended for large units only, since efficient cooling does not affect gas quality and yield adversely in units gasifying 10 tons per hr or more.

Authors' Closure

The authors wish to thank Mr. Denig and Mr. Gumz for their review and discussion of the paper. Both of these gentlemen have had wide experience in total gasification and are well qualified in this field. With the many schemes being proposed for conversion of coal to synthesis gas, it is very encouraging to have these two authorities agree that total gasification of pulverized coal with steam and oxygen has real promise for the future.

Mr. Denig has pointed out the differences between the designs of the B&W and the Koppers' units. The B&W unit is designed for slag-tap operation, while the Koppers' unit handles the ash in dry form. Slag-tap furnaces invariably have less ash carryover with the product gas, as has been demonstrated by boiler practice, however, this factor is not the predominant one in our selection of the slag-tap type of operation. Reaction kinetics of gasification require a high temperature in the zone immediately adjacent to the burner, and we feel that the maximum flexibility for handling all types of coal ash, will be obtained with the slag-tap operation. To obtain the best conversion of sensible heat of the gas into latent heat of the product gas, it is our opinion that a definite segregation of the high-temperature zone near the burners from the lower temperature zone at the gas outlet is advantageous. This is the reason for the two-zone arrangement of the two units described.

As to the difference in gas analysis between the two gasifiers, we have observed a variation in methane content between 0.1 and 1.0 per cent and a variation in illuminants between 0.0 and 0.6 per cent during 130 tests. However, gas analysis alone does not present a complete or accurate picture of the operation of a gasifier. The real criterion is the quantity of oxygen and coal required to produce a unit quantity of carbon monoxide and hydrogen. On this basis it has been determined that the desired operating condition has a corresponding gas analysis on the order of that given in Table 2 of the paper. It is true that other hydrocarbons cannot be ignored, but certainly the over-all material requirements per unit of CO + H_2 must be given proper consideration.

The questions posed in Mr. Denig's discussion are answered in order below:

1 The coal used normally has been pulverized to 70 per cent through 200 mesh. Finer pulverization has been tried but significant improvements in gasification rate were not discernible.

2 The pulverizer operates at a pressure slightly higher than does the reaction chamber in order to compensate for the pressure drop in conveying the steam-coal mixture from the pulverizer to the reactor. The pulverizer normally is fed with 750 F steam and the steam-coal mixture leaves at some temperature below this, depending upon the steam-to-coal ratio and the amount of moisture in the coal. For the tests reported, the exit temperature was normally about 350 F.

3 All of the process steam is circulated through the pulverizer in order to provide the heat necessary to dry coal of the moisture content usually encountered. This amount of steam could be reduced and other arrangements made if it were found necessary or desirable.

4 The refractory used in the primary reaction zone has been a super-duty cast alumina brick which has a high resistance to fluid-slag penetration and chemical attack from the slags thus far encountered.

5 Fluxing of the coal ash to reduce its viscosity has not been found necessary, nor is it desirable because of the danger of simultaneously fluxing the refractories.

6 Carbon loss with the slag is negligible. This is also true with slag-tap boiler furnaces.

7 The entrained residue leaving the gasifier with the gas stream is very fine. The method of removal of this dust depends upon the operator's preference, though normally water-scrubbing is employed. The settling time required to clarify this water in all probability would be rather long, owing to the fine size of the residue.

In regard to the comments by Mr. Gumz, it is encouraging to note that experimental results were verified by an independent calculation procedure. It should be noted, however, that one of the most important factors in determining gasification performance is the determination of exit temperature from the process. We have found that this varies with fuel rank and coal reactivity. The latter is difficult to define and it is still necessary to rely on actual performance tests to establish the exit temperature.

The higher temperatures which Mr. Gumz mentions confirms our basic concept that the total gasification process must be operated at high temperatures in order to obtain the desired process economy.

Mr. Gumz's comments about refractory wear in large-scale units are well taken, and we are in agreement with the expectation that refractory wear will be minimized in larger size gasifiers.

AN ASME PAPER

Its Preparation, Submission and Publication, and Presentation

To a large degree the papers prepared and presented under the ASME sponsorship are evidence by which its professional standing and leadership are judged. It follows, therefore, that to qualify for ASME sponsorship, a paper must not only present suitable subject matter, but it must be well written and conform to recognized standards of good English and literary style.

The pamphlet on "AN ASME PAPER" is designed to aid authors in meeting these requirements and to acquaint them with rules of the Society relating to the preparation and submission of manuscripts and accompanying illustrations. It also includes suggestions for the presentation of papers before Society meetings.

CONTENTS

PREPARATION OF A PAPER—

General Information—Style, Preferred Spelling, Length Limitation, Approvals and Clearances.

Contents of the Paper—Title, Author's Name, Abstract, Body of Paper, Appendixes, Acknowledgments, Bibliographies, Tables, Captions, Photographs, Other Illustrations.

Writing the Paper—Outline Tabulations, Tables, Graphs, Charts for Computation, Drawings, Mathematics, Accuracy, Headings and Numbering, Lantern Slides, Motion Pictures, Typing, Number of Copies.

SUBMISSION AND PUBLICATION OF A PAPER—

Intention to Submit Paper Required in Advance, Meeting Dates, Due Dates for Manuscript, Discussers, Review and Acceptance, Proofs, Advance Copies and Reprints, Discussion and Closure, Publication by Others.

PRESENTATION OF A PAPER—

Time Limit, Addressing Your Audience, Public Address Systems, Use of Slides.

REFERENCES—

References on Writing and Speaking, Engineering Standards.

Price 40¢. No discount allowed. *A remittance must accompany all orders for $5.00 or less. U. S. Postage Stamps are acceptable.*

THE AMERICAN SOCIETY OF MECHANICAL ENGINEERS

29 West 39th Street, New York 18, N. Y.

A SELECTED LIST OF STANDARDS

published by the ASME, 29 W. 39th St., New York 18

BOILER AND PRESSURE VESSEL CODE

Selection of Material, Construction, Maintenance, Welding

Power Boiler Code (Sec. I) 1952	$3.00
Material Specifications (Sec. II) 1952	$7.50
Boilers of Locomotives (Sec. III) 1952	$1.25
Low-Pressure Heating Boiler Code (Sec. IV) 1952	$1.25
Miniature Boiler Code (Sec. V) 1952	$1.00
Suggested Rules for Care of Power Boilers (Sec. VII) 1954	$3.00
Unfired Pressure Vessel Code (Sec. VIII) 1952	$4.50
Welding Qualifications (Sec. IX) 1953	$1.75

AMERICAN STANDARDS

Dimensions, Specifications, Terminology and Definitions

BOLTS, NUTS, RIVETS

Large Rivets (½ Inch Diameter and Larger), B18.4—1950	80¢
Small Solid Rivets, B18.1—1953	$1.00
Plow Bolts, B18.9—1950	55¢
Track Bolts and Nuts, B18.10—1952	$1.00
Round Head Bolts, B18.5—1952	$1.00
Square and Hexagon Bolts and Nuts, B18.2—1952	$2.00
High-Strength, High-Temperature Internal Wrenching Bolts, B18.8—1950	50¢

GEARS

Spur Gear Tooth Form, B6.1—1932	55¢
Gear Tolerances and Inspection, B6.6—1946	80¢
20-Degree Involute Fine-Pitch System for Spur and Helical Gears, B6.7—1950	$1.50
Fine-Pitch Straight Bevel Gears, B6.8—1950	$1.00
Design for Fine-Pitch Worm Gearing, B6.9—1950	$1.50
Inspection of Fine-Pitch Gears, B6.11—1951	$2.50
Letter Symbols for Gear Engineering, B6.5—1949	50¢
Gear Nomenclature, B6.10—1950	$1.50

PIPE AND PIPE FITTINGS

Brass or Bronze Flanges and Flanged Fittings—150 and 300 Lb, B16.24—1953	$1.00
Brass or Bronze Screwed Fittings—125 Lb, B16.15—1947. (R1952)	65¢
Brass or Bronze Screwed Fittings—250 Lb, B16.17—1949. (R1953)	50¢
C I Pipe Flanges and Flanged Fittings:	
25 Lb PSI, B16b2—1931. (R1952)	50¢
Class 125, B16.1—1948	65¢
Class 250, B16b—1944	55¢
800 Lb Hydraulic Pressure, B16b1—1931. (R1952)	50¢
Refrigerant Piping—Class 300, B16.16—1948. (R1952)	50¢
C I Screwed Drainage Fittings, B16.12—1953	$1.00
C I Screwed Fittings—125 and 250 Lb, B16.4—1949. (R1953)	60¢
Malleable-Iron Screwed Fittings—150 Lb, B16.3—1951	$1.00
Malleable-Iron Screwed Fittings—300 Lb, B16.19—1951	75¢
Steel Pipe Flanges and Flanged Fittings, B16.5—1953	$3.00
Steel Butt-Welding Fittings, B16.9—1951	75¢
Steel-Socket Welding Fittings, B16.11—1946. (R1952)	60¢
Face-to-Face Dimensions of Ferrous Flanged and Welding End Valves, B16.10—1947	65¢
Ferrous Plugs, Bushings, and Locknuts with Pipe Threads, B16.14—1949	50¢
Nonmetallic Gaskets for Pipe Flanges, B16.21—1951	$1.00
Ring-Joint Gaskets and Grooves for Steel Pipe Flanges, B16.20—1952	$1.00
Cast-Brass Solder-Joint Fittings, B16.18—1950	75¢
Cast-Brass Solder-Joint Drainage Fittings, B16.23—1953	$1.00

SCREW THREADS

Acme Screw Threads, B1.5—1952	$2.25
Stub Acme Screw Threads, B1.8—1952	$1.25
Buttress Screw Threads, B1.9—1953	$1.00
Unified and American Screw Threads Standard B1.1—1949	$3.00
Screw Thread Gages and Gaging, B1.2—1951	$4.00
Screw Threads for High-Strength Bolting, B1.4—1945	50¢
Limits and Fits in Engineering and Manufacturing B4.1—1947	50¢

AMERICAN STANDARDS

SMALL TOOLS AND MACHINE TOOL ELEMENTS

Accuracy of Engine and Tool Room Lathes, B5.16—1952	$1.00
Adjustable Adapters, B5.11—1937	60¢
Chucks and Chuck Jaws, B5.8—1954	$1.00
Circular and Dovetailed Forming Tool Blanks, B5.7—1948	75¢
Drill Drivers (Split-Sleeve, Collet-Type), B5.27—1951	50¢
Involute Splines, B5.15—1950	$2.00
Involute Serrations, B5.26—1950	$1.00
Involute Splines, Serration Gages and Gaging, B5.31—1953	$1.25
Jig Bushings, B5.6—1949	50¢
Knurling, B5.30—1953	$1.00
Machine Pins, B5.20—1947	50¢
Punch and Die Sets for 2-Post Punch Press Tools, B5.25—1950	75¢
Rotating Air-Cylinders and Adapters, B5.5—1954	$1.00
Single-Point Tools and Tool Posts, B5.22—1950	$1.25
Spindle Noses for Tool Room Lathes, B5.9—1948	85¢
Spindle-Noses and Arbors for Milling Machines, B5.18—1953	$1.00
Straight-Cut-Off Blades for Lathes and Screw Machines, B5.21—1949	50¢
T-Slots, Their Bolts, Nuts, Tongues, and Cutters, B5.1—1949	50¢
Life Tests of Single-Point Tools, B5.19—1946	55¢
Twist Drills, B5.12—1950	75¢
Machine Tapers, B5.10—1953	$1.00
Milling Cutters, B5.3—1950	$2.25
Reamers, B5.14—1949	$1.50
Taps—Cut and Ground Threads, B5.4—1948	$1.50
Markings for Grinding Wheels, B5.17—1949	50¢
Mounting Dimensions of Lubricating and Coolant Pumps for Machine Tools, B5.28—1952	$1.00
Designation and Working Ranges of Grinding Machines, B5.32 and 33—1953	$1.00

SAFETY CODES

Construction, Installation, Maintenance

Pressure Piping, B31.1—1951 with Supplement B31.1a—1953	$4.00
Gas Transmission and Distribution Piping System B31.1.8—1952	$1.25
Conveyers, Cableways, and Related Equipment, B20.1—1947	90¢
Cranes, Hoists, Derricks, B30.2—1943	$1.80
Industrial Power Trucks, B56.1—1950	85¢
Private-Residence Elevators, A17.1.5—1953	$1.00
Elevators Escalators, and Dumbwaiters, A17.1—1937, Including 1942 Supplement	$1.50
Elevator Inspectors' Manual, A17.2—1945	$1.50
Manlifts, A90.1—1949	55¢
Mechanical Power Transmission Apparatus, B15.1—1953	$1.00

POWER TEST CODES

Methods for Successful Performance Testing of Equipment

Centrifugal, Mixed-Flow and Axial Flow Compressors and Exhausters, Pub. 1949	$1.50
Centrifugal Pumps, Pub. 1954	$1.50
Coal Pulverizer, Pub. 1944	85¢
Displacement Compressors, Vacuum Pumps and Blowers, Pub. 1954	$2.00
Dust Separating Apparatus, Pub. 1941	90¢
Evaporating Apparatus, Pub. 1941	60¢
Fans, Pub. 1945	$1.00
Feedwater Heaters, Pub. 1954	$1.00
Gas Producers, Pub. 1928	65¢
Gaseous Fuels, Pub. 1944	90¢
Gas Turbine Power Plants, Pub. 1953	$1.50
Hydraulic Prime Movers, Pub. 1949	85¢
Internal-Combustion Engines, Pub. 1949	$1.50
Reciprocating Steam-Driven Displacement Pumps, Pub. 1949	80¢
Reciprocating Steam Engines, Pub. 1935. (R1949)	80¢
Solid Fuels, Pub. 1954	$2.50
Stationary Steam-Generating Units, Pub. 1946	75¢
Steam Condensing Apparatus, Pub. 1954	$2.00
Steam Locomotives, Pub. 1941	65¢
Steam Turbines, Pub. 1949	$2.00
Appendix to Test Code for Steam Turbine, Pub. 1949	$2.00

20% Discount to ASME Members